Sovereign risk exploration in times of crisis : a look at financial contagion

Marc-Henri Thoumin

▶ **To cite this version:**

Marc-Henri Thoumin. Sovereign risk exploration in times of crisis : a look at financial contagion. Economics and Finance. Université Paris sciences et lettres, 2017. English. NNT : 2017PSLEM039 . tel-01780245

HAL Id: tel-01780245
https://pastel.hal.science/tel-01780245

Submitted on 27 Apr 2018

HAL is a multi-disciplinary open access archive for the deposit and dissemination of scientific research documents, whether they are published or not. The documents may come from teaching and research institutions in France or abroad, or from public or private research centers.

L'archive ouverte pluridisciplinaire **HAL**, est destinée au dépôt et à la diffusion de documents scientifiques de niveau recherche, publiés ou non, émanant des établissements d'enseignement et de recherche français ou étrangers, des laboratoires publics ou privés.

THÈSE DE DOCTORAT

de l'Université de recherche Paris Sciences et Lettres
PSL Research University

Préparée à MINES ParisTech

Sovereign Risk Exploration in Times of Crisis: A look at Financial Contagion

Le risque souverain en période de crise financière: Une analyse du phénomène de contagion sur les marchés de taux

Ecole doctorale n°396

ECONOMIE, ORGANISATION, SOCIETE

Soutenue par Marc-Henri THOUMIN le 21 Décembre 2017

Dirigée par **M. Alain GALLI**

COMPOSITION DU JURY:

M. Bernard LAPEYRE
Ecole des Ponts ParisTech
Président du jury

Mme Delphine LAUTIER
Université de Paris Dauphine
Rapporteur

M. Siem Jan KOOPMAN
Vrije Universiteit Amsterdam School of Business and Economics
Rapporteur

Mme Margaret ARMSTRONG
Fundaçao Getulio Vargas (FGV) Rio de Janeiro
Examinatrice

Mme Sandrine UNGARI
SGCIB London
Examinatrice

M. Alain GALLI
MINES ParisTech
Examinateur

Acknowldedgments

Firstly, I would like to express my sincere gratitude to my advisor M. Alain Galli for the continuous support of my Ph.D study and related research, for his patience, motivation, and very deep expertise. His guidance helped me in all the time of research and writing of this thesis.

Besides my advisor, I would like to thank the rest of my thesis committee: M. Bernard Lapeyre, Mme Delphine Lautier, M. Siem Jan Koopman, Mme Margaret Armstrong, and Mme Sandrine Ungari for their insightful comments and encouragement, but also for their questions which helped me widen my research from various perspectives.

I am also very grateful to Sésaria Ferreira for her valuable help and support over all these years, which spared me significant pain at many levels.

Last but not the least, I would like to thank my family: my wife, parents, brother and sisters for supporting me spiritually throughout writing this thesis and my my life in general.

Marc-Henri Thoumin

Table of Contents

Introduction 4

Sovereign Risk: State of the Art and context 6

Copula: The Framework 24

Generalized Hyperbolic (Skewed) t-Student distributions 32

Chapter I. A multivariate model to explore joint dependencies in sovereign CDS spreads 35

- Univariate analysis: calibration of the marginals 37
  - Empirical analysis of the data 37
  - The GAS framework 41
  - Estimating the conditional Marginals 43
  - The un-temporal Marginals 54
- Multivariate calibration of the model 67
- An estimator of the joint reaction to shocks 73
- Conclusion 91
- References 92

Chapter II. Deriving contagion from stress tests 98

- Literature Review 100
- Deriving the probability of default out of CDS prices 121
- Implementing stress tests on European asset swap spreads 125
  - How to define a shock/scenario 125
- A non-temporal approach to financial contagion 129
  - Influence of the univariate volatility 135
  - The multivariate contagion 153
- Practical applications of the model 182
  - Global Minimum Variance, Risk Budgeting, and Most Diversified Portfolios 183
  - Forecasting volatility using the GAS method 189
  - A view on optimal portfolio rebalancing 194
  - A novel optimization procedure based on mean reversion 205
- Conclusion 212
- References 213

Chapter III. Price discovery in bond options 217
Literature review and context 219
Separating the (continuous) wheat from the (jumpy) chaff 223
Mutually Exciting Jump Diffusion 224
Mean Reversion-based jump intensities 225
Distribution of the jump amplitude 226
Calibration Procedure 227
The univariate calibration 228
A measure of the empirical skewness 228
Calibrating the remaining unknowns 230
Results 231
Monte Carlo simulations 232
A model exclusively based on jumps 237
Formalisation of the problem, univariate case 237
Dataset and calibration of the univariate model 242
The multivariate version of the model 252
Construction of the risk-index 258
Calibration of the multivariate model 261
Pricing zero coupon bond options 269
Deriving implied volatility from characteristic functions 272
A lack of data 273
Results 273
The shape of the distribution 278
Conclusion 280

General conclusion 281
Appendix 285
References 295

Introduction

The 2011/2012 sovereign crisis in Europe has raised considerable uncertainties on the sustainability of the monetary union. This ultimately led to a partial default of Greece in 2012 which in effect, helped restrain the visible confidence crisis in financial markets. While the peak is now behind us, troubled economies in Europe are still facing some headwinds, partly because persistently low inflation and limited growth, on the back of still excessive debt levels, have made the environment somewhat challenging as to implement meaningful structural reforms. While austerity has been promoted as a logical curative to curtail unsustainably high indebtedness, an effort towards further European integration in the past years also helped make risk-sharing among sovereign entities more efficient. This led to the creation of the Banking Union (for instance) and the introduction of tougher regulations on financial institutions.

Although the prudential aspect of regulatory supervisions has undoubtedly become more efficient as a result, this made little as to curb other potent sources of financial distress. Italian banks for instance still have to deal with a substantial amount of non-performing-loans (although we saw notable progress in 2017). And as the detention of domestic sovereign debt by banks has increased in peripheral countries throughout the recent crises, the risk of contagion from banks into sovereign securities remains a meaningful threat. Still on the negative side, risk-sharing also creates obvious moral hazards, and while austerity is market-friendly, it is much less appreciated by tax payers. As a consequence, all this translated into a rising appeal for Euro-sceptic political parties in many jurisdictions, even in countries where default is not a palpable threat (like France, the Netherlands and the UK).

Unconventional monetary policy has been a mantra in Japan/US and UK during years of abnormally low inflation. In Europe though, the ECB has been 'historically' more reluctant to go beyond its original mandate of just jugulating high inflation. But this changed in 1Q 2015, when Mr. Draghi launched an ambitious Quantitative Easing (QE) program. ECB QE effectively pushed interest rates in sovereign and credit spaces to extremely low levels, much below fundamentals-based fair values. While this decoupling between extraordinarily low interest rates and recovering fundamentals has proved a bargain for debt issuers, this exceptional support from the central bank will not last forever.

Sovereign risk reflects the probability that a sovereign entity does not meet its future debt repayment. While there is no exclusive quantification of this risk, its perception is primarily influenced by fundamental indicators like debt levels, growth and inflation. Sovereign interest rates (or more commonly sovereign 'bond yields') are the more natural illustration of how sovereign risk is appreciated: the risk-premium incorporated in bond yields is supposed to be a fair reflection of whether default is more or less likely in the future. Interest rates however, are not driven by sovereign risk exclusively, and other drivers tend to interfere on bond valuations; sometimes causing notable distortions in risk-premia. Central bank policy, and expectations of future policies in particular, are potent drivers of bond prices in general. These forces have been especially powerful during the past decade as central banks (including the ECB) embraced aggressively non-conventional policies. And since bond yields were reaching new lows in the process, sovereign risk has been perceived as having massively fallen. But in the end, stretched valuations due to substantial QE have just been hiding persistent structural concerns at the political/economic level, with the actual credit worthiness in sovereigns being possibly less robust than suggested by marked-to-market valuations.

As debt restructuring induces considerable losses, getting a reliable estimate of sovereign risk is of crucial importance from a risk management perspective. And even before default effectively occurs, the behaviour of financial securities tends to be sharply impacted by the underlying deterioration of credit worthiness as empirical observations show that correlations usually inflate as a result of mounting risk aversion. This in turn, tends to exacerbate risk propagation between financial securities, and ultimately leads to a wide-spread sell-off in every asset class. Financial contagion characterises cross-asset risk propagation. While empirical correlation is a fair estimator of bilateral connections in 'standard' market conditions, it gives very little information on the expected contagion when financial markets are subject to abnormally large price variations. This is because empirical methods usually do not allow for the presence of fat tails in the data and this flaw usually leads to a visble underestimate of the joint price deterioration in extreme scenarios. On the other side, overestimating contagion and maximising prudence in investments is at the cost of curtailing returns – something that portfolio managers try to avoid as well.

As the behaviour of financial securities under heavy contagion is not naturally observable, there is a case for further exploration of contagion. A comprehensive quantification of this phenomenon via appropriate and sophisticated statistical models should also deliver sensible information for portfolio managers, although we are mindful that complex calculations can prove a drag for high-frequency manipulations of the model. In this dissertation, we explore the joint behaviour of sovereign securities and we develop a novel approach to financial contagion. We also put an emphasis on simplicity, e.g. in the different ways the model is manipulated. This could help disseminate our methodology to traders and investors, especially to those with limited quant resources. As the main innovation, we offer a comprehensive view on the expected market reaction to shocks in general, and we design new risk management procedures as to apprehend periods of financial distress.

In Chapter I, we explore a probabilistic approach to the distribution of sovereign CDS price variations since January 2008. We consider Generalized Hyperbolic distributions and a time-varying volatility. While the calibration offers an outstanding fit, the distributions we get are conditional on historical realisations. This tends to make any manipulation of the model a bit cumbersome. We thus consider a more convenient formulation of the model, as an alternative. Finally, we explore the calibration of multivariate distributions. These are supposed to reflect bivariate correlations, taking into account fat tails in the data. We also calculate a preliminary estimator of cross-asset contagion, which offers an interesting view on the non-linear aspect of the market reaction to shocks.

In Chapter II, we use our probabilistic model to derive new procedures for risk management purposes. We undertake VaR-based stress tests that deliver a generalised view on the expected market reaction to shocks. We also explore the forecast-aptitude of our time varying volatility estimator and we consider the relevance of incorporating this forecast in popular portfolio optimisation procedures. Finally, we design a novel approach to portfolio optimisation, based on our indicators of expected contagion. Our allocation strategy shows outstanding results, and seems to offer efficient protection in times of crisis, and interesting returns when risk appetite is prevailing.

In Chapter III, we consider that risk aversion favours the emergence of sizeable discontinuities in market prices. We explore the relevance of stochastic models with jumps as a means to apprehend these periods of pronounced volatility, and we focus in particular on Hawkes processes. This category of models incorporates a self-exciting loop which helps replicate the observed persistence

of jumps, in terms of both amplitude and frequency, during prolonged periods of risk aversion. Finally, we investigate the pricing of zero coupon bond options, and we compare the implied volatility resulting from univariate versus multivariate jump models.

Sovereign Risk: State of the Art and Context

Sovereign risk is supposed to reflect the repayment capability of a borrowing sovereign entity. To a large extent, sovereign risk is therefore an appreciation of the underlying macroeconomic situation. Debt ratios for instance, in light of GDP growth and inflation, may be a reliable illustration of the credit worthiness. But this is not enough information to get a robust opinion: Japan for instance shows a remarkably high level of gross debt, at about 240% of GDP. Since interest rates have reached unprecedented lows in this jurisdiction of late, sovereign risk looks still very muted in Japan. In practice, sovereign risk is also driven by factors exogenous to the sovereign entity. General demand for sovereign debt, liquidity conditions in Fixed Income securities or the access to funding via repurchase agreements (repo); all this also has major implications on bond valuations. Plus, monetary policy is recognised as having encouraged stretched valuations in bonds since the introduction of negative interest rates and the implementation of large quantitative easing programs over the past decade. In the end, estimating sovereign risk has proved a challenging exercise for portfolio managers, partly due to the diversity of these drivers that are responsible for the price-formation in bonds.

The appetite for Fixed Income securities is primarily driven by how debt products position themselves in the global picture of all asset classes. Higher growth and inflation in particular tend to favour higher interest rates, partly as investors want to be rewarded for greater inflation risks. Rising interest rates in this context mean that bond prices are on a decline. This usually results into substantial outflows, from bonds into equities. The greater appetite for equities is then bolstered by the view that risk-premia are protected by supportive fundamentals (e.g. better growth favours stronger earnings). After Mr. Trump's election in end-2016 for instance, a generalised increase in expectations that further growth-friendly policies in the US would boost global inflation led to a pronounced sell-off in US Treasuries. Aside from this dynamics, flows indicators over this period also helped identify a rising interest to reallocate from bonds and into equities (although inflation, ex-post, remained very low). In contrast to this momentum that tends to describe periods of improving fundamentals; a recession is marked by disappointing economic growth and declining inflation (in the early stage of the recession at least). As a result, central banks are keen to deliver more inflationarist policies, e.g. by lowering key interest rates. As a consequence of a reduced reward on deposits at the central bank, investment banks are left with bigger liquidity, and this is supposed to make the credit channels to corporates more efficient. In this context, market sentiment is turning more favourable for Fixed Income securities, in comparison to equities. First and foremost, because equities are meant to perform poorly when the macroeconomic picture is deteriorating. But also because falling interest rates (resulting from lower key rates) imply a gain in marked to market valuations for bond holders; a momentum that portfolio managers seek to take advantage of. Tracking global investment flows helps understand the underlying appetite/reluctance for sovereign debt in comparison to other asset classes (like equities or credit). These flows effectively, have been

frequently involved in the context of sovereign debt exploration. Longstaff and Singleton (2007) for instance consider the net flows (inflow minus outflow) to mutual funds, principally invested in international bonds and equity (data obtained from the Investment Company Institute). The authors in particular show that global-bond-flow and equity-flow variables are relevant explanatory variables for credit risk. Capital flows can also be used to explore the effect of a shift in investors' confidence and their willingness to supply capital, like in Sinyagina-Woodruff (2003). They explore in particular the dynamics led by the 'herd behaviour' of market participants. Gapen, Gray et al. (2008) also design an interesting framework that tends to quantify the degree of positive/negative implications that result from massive inflows/outflows, expressed as a function of the accommodative response from policymakers. The analysis focuses on emerging economies and conclusions highlight a tight connection between capital flows and the sovereign's default probability. Sensitivity measures between market valuations and capital flows also markedly increase when outflows become more and more intense.

When periods of depressed fundamentals tend to endure over a prolonged period of time ('secular stagnation' in Summers (2014a), (2014b), (2016)), central banks may be prompt to deploy non-conventional measures as an additional means to curb the downward spiral. Regardless of the form it takes, the goal is to push sovereign and corporate interest rates at lower levels. In developed economies, Quantitative Easing (QE) is one of the most common initiative, whereby the central bank becomes a buyer of financial securities (in effect mostly Fixed Income securities), usually for a substantial amount. By creating 'synthetic' demand on adequate securities like bonds, QE tends to boost the appetite for rates products, and consequently this helps decrease interest rates. Another tool, specific to the ECB is LTRO/TLTRO[1] operations. These consist of providing ample and long term liquidity to banks at a very competitive cost, all in the hopes that it will be re-invested in the economy via loans to corporate, or via larger demand (from banks) for high-yield debt. Such an approach helped push Euro-denominated interest rates to extremely low levels in the last five years. Negative interest rates in stronger economies also raised the opportunity for national Treasuries (and corporate debt issuers) to get their annual funding programme achieved at a substantially cheaper level than usual. This overall favoured a large recovery in equities: overall the non-conventional initiatives, launched by the ECB since 2012, significantly contributed to restore investors' confidence in Europe. By and large, stretched valuations in rates market have been the engine of recovering financial markets. A bit less enticing, liquidity in bonds is still significantly smaller than in the pre-crisis environment. To some extent, this could leave financial markets more exposed to risk aversion than it used to be.

A recession is also marked by recurring periods of intense uncertainties. These overall favour larger risk-premia, ie. higher interest rates in general. So while accommodative central banks favour lower interest rates, persistent uncertainties at the macro/political levels tend to push interest rates higher. The reaction in rates is all the more pronounced that higher levels are supposed to compensate investors for the greater risk of default in a context of persistently troubled fundamentals. While the loss of confidence remained relatively contained for core and soft-core economies in 2011-2012, it caused a substantial rise in peripheral interest rates (Spain, Italy, Portugal, Greece). Reasoning in terms of interest rate differential, the spread composed of 10Y Spanish versus German interest rates (ie. SPGB versus Bund spread) reached a high of 640bp (ie.

[1] https://www.ecb.europa.eu/mopo/implement/omo/html/index.en.html https://www.ecb.europa.eu/mopo/implement/omo/tltro/html/index.en.html https://www.ecb.europa.eu/explainers/tell-me/html/tltro.en.html

6.4%) in July 2012. In comparison, it was trading at just 180bp in March 2011. Risk aversion largely encouraged this sharp differentiation between safer German bonds and the more exposed peripheral debt. The 10Y SPGB/Bund spread then moved back to a very reasonable 120bp by end-2016; this is another sign that accommodative policies from the ECB have had a wide-scale impact on bond valuations since end-2012. Interestingly, the notion of spread is already an indicator of sovereign risk, as the higher premium paid by the Spanish Treasury – in comparison to Germany – is meant to compensate investors for the greater risk of default. Sovereign risk is definitely a meaningful driver of the 'spread complex' in Europe (ie. the relative picture of interest rates). As a result, understanding sovereign crisis is critical for those who want to invest in European sovereign debt outside of safe haven, ie. in soft-core and non-core credits as any emergence of risk aversion, in this case, will logically induce a loss. German bonds in contrast tend to rally in risk averse markets because of their safe-haven nature. Considering the spread complex in Europe, risk aversion logically translates into wider spreads (implicitly against German Bunds). In contrast, risk appetite will favour convergence and therefore some spread tightening.

Aside from the risk-aversion/risk-appetite paradigm, contagion is a key feature as well. Contagion qualifies the joint price depreciation that ensues from the emergence of risk aversion. In a world of reasonable volatility, risk aversion will favour a sell-off in riskier assets (more or less pronounced depending on the credit quality), accompanied by a rally in the safest securities (like German Bunds). And while there might be just one epicentre of risk aversion (e.g. emanating from a domestic 'bad news'), risk propagation will hit all entities that could potentially be affected by the corresponding piece of news, via a joint price depreciation. In the case of Greece for instance, risk aversion from expectations of a potential default also caused substantial losses in Portugal given its similarity with Greece in terms of macroeconomic fundamentals (at the fore of the crisis). But contagion is not always rational: beyond a certain level of stress, empirical observations indicate that cross-asset connections are stronger. In this case, risk aversion leads to hefty losses, spread out on a broader range of financial securities, for instance impacting sovereign securities that are still 'rationally' beyond the scope of the situation. Even before the advent of the GFC, Longstaff, Singleton (2007) noted that: "*shifts in the relative liquidity of markets over time as shocks induce investors to reallocate capital across different asset classes [...] could create correlations between asset class prices even in the absence of correlated fundamentals"*. More recently, at the peak of the sovereign crisis, and as a default in Greece turned to be more and more certain, a confidence crisis emerged in H2 2011 and caused a major and generalised rise in European sovereign interest rates, even in countries regarded as relatively sound in terms of their credit quality (e.g. France, Belgium, the Netherlands, see Apostolakisa and Papadopoulos (2014) and Tsai (2014)). As a result of contagion, correlations between the main asset classes became exceptionally large, causing wide-spread losses. Many studies (e.g. Arghyrou and Kontonikas (2011), Bernoth and Erdogan, (2012)) have also emphasized that financial markets are more sensitive to the fiscal situation during episodes of intense contagion, with the price action systematically penalizing bad fiscal positions. This illustrates already the notable transformation led by risk aversion, as well as its dramatic implications at the State level: fire sales in bonds ultimately make bond issuance a very uncertain process, thereby rising risks on the achievement of the annual funding programme. **In the end, there is a certain threshold beyond which financial distress leads to a harsh amplification of the joint market reaction to shocks.** This threshold is barely observable with empirical methods: first because contagion relates to 'tail events', which are uncommon by definition. Plus the 'global' dimension of contagion makes

these thresholds difficult to estimate as they are potentially impacted by a wide range of parameters. In this analysis, we develop a novel way to quantify contagion risk. This is based on observations of CDS price variations during the sovereign crisis, and shows a threshold, common to each sovereign, beyond which contagion is seen as causing major damages – namely below the 20% and beyond the 80% percentiles on the distribution.

The European spread complex is probably one of the most basic illustrations of any financial stress in financial markets (Allen, Moessner (2013)). While there was little differentiation of sovereign bond yields just following the creation of the Euro Area (Spanish and German 10Y rates were trading at similar levels until mid-2007), the emergence of the sovereign crisis led to a major desynchronisation in sovereign interest rates. Risk aversion on one side, favoured the more resilient countries like Germany, Finland and the Netherlands. And in contrast, intense selling-off pressures propelled interest rates to remarkably high levels in the periphery. As Kilponen, Laakkonen, Vilmunen (2012) note, this occasioned a noticeable thematic rotation in the literature, from exploring the former convergence in rates towards explaining the more recent decoupling. At SocGen, we have developed an empirical approach to estimating sovereign risk. Essentially, we calculate a score for each liquid and tradable country, based on several macroeconomic indicators. For a given country, each indicator is given a score from 1 to 10 (1 is best, 10 is worst), that reflects the percentile position of the measured value relative to the range admissible between the minimum and maximum measurements. Then we take the average score as the final rating. We consider 12 variables, exclusively domestic. We categorize them into three groups:

*** **1) Debt criteria.** Budget deficits, gross debt, the ratio of government interest payments to revenue (supplied by Moody's), and Current Account positions.

*** **2). Economic criteria.** Change in unemployment (2016-2017), GNP per capita, impact of demographics on net government debt (% GDP, S&P[2], 2030 forecast), along with a competitiveness indicator "ULC in total economy deflated" (OECD[3]) as well as Household consumption per capita ($k) and Government effectiveness (World Bank).

*** **3). Bank criteria.** Contingent financial liabilities (Eurostat)and Banking Industry Country Risk Assessment (BICRA, from S&P).

Table 1. 12 variables compose SG's proprietary Sovereign Scoring

	Debt				Economy						Bank	
Denomination	Public Deficit (% GDP)	Gross debt (% of GDP)	Gen.Gov. Int.Pymt / Gen.Gov. Revenue	Current Account (% GDP)	% Change in Unemployment Rates (2016-2017)	GNP per capita ($k)	Impact of demographics on net governemnt debt - No Policy Change	Real harmonised competitiveness indicator ULC in total economy deflated	Household consumption per capita ($k)	Government effectiveness	BICRA*	Government Contingent Liabilities (% GDP)
Germany	2	1	2	1	2	2	1	1	1	2	1	1
France	10	4	3	10	7	3	5	6	3	3	2	1
Netherlands	3	1	1	1	2	1	2	5	3	1	2	1
Finland	8	1	1	9	5	1	1	5	1	1	1	4
Austria	5	2	4	5	10	1	2	4	1	3	2	4
Spain	10	4	7	7	2	8	3	9	8	3	4	6
Ireland	4	2	9	1	3	1	1	5	3	2	6	6
Belgium	9	5	4	8	6	2	6	5	3	3	1	4
Portugal	9	7	10	7	1	10	5	8	10	5	7	2
Italy	9	7	8	6	8	6	5	8	5	9	6	1
Greece	1	10	8	8	1	10	10	10	9	10	10	10

[2] http://www.nact.org/resources/2013_NACT_Global_Aging.pdf from Table 8, page 43
[3] http://stats.oecd.org/Index.aspx?DataSetCode=ULC_EEQ

Results show that Germany is well ensconced at the top end of the ranking; its score has continued to improve from 2.67 to 1.42 since the last update of the model in 2016. Then we see the Netherlands at 1.92, still improving from 2.92 on encouraging prospects in terms of public deficit and on the back of lower unemployment. Finland is in third place (still), with a better score of 3.17, from 3.75. But the country is still struggling to boost growth, with the significant exposure to Russia proving a drag for the economy. Austria remains in fifth place, with a slightly better score of 3.58 by end-2016, compared to 4.67 one year ago. A better outlook on demographic indicators and apparently lower contingent liabilities justify the better score. The exposure to Eastern Europe remains a long-term concern though. Spain continues to outperform Italy, with a score consistently improving compared to the last updates of the model. Italy is still in ninth place with an unchanged score of 6.50. And ahead of Greece, Portugal is at 6.92, relatively unchanged to 2015 numbers (6.75). Employment forecasts have improved, but wealth criteria are still weak compared to other countries. Greece, finally, has seen no particular progress in our model since last year, with an unchanged score of 8.08, and it remains last in the ranking. That said, the model identifies some improvements in terms of public deficit, partly offset by tough numbers in terms of competitiveness. Overall, the score reflects a challenging environment for implementing reforms in Greece, with limited upside in the near term. Then we match the results to asset swaps spreads (ASW) and CDS prices (Graph 1, Graph 2). Overall, a higher country's score is associated with wider ASW or CDS levels. This looks coherent with the fact that troubled countries have to face higher risk-premia compared to more robust economies. Interestingly, a second order interpolation function provides a decent fit against market valuations, suggesting overall that the premium effectively sees a non-linear acceleration when the score is large (ie. for Spain, Italy, Portugal, Greece).

Graph 1. SG Scoring vs 10-year ASW

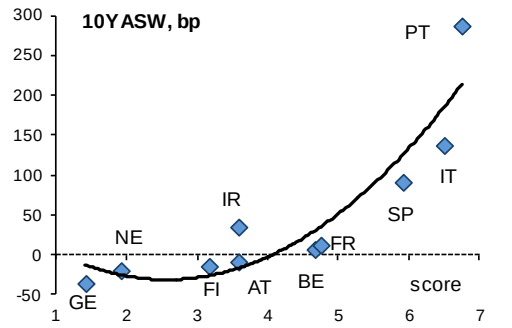

Graph 2. SG Scoring vs 5y CDS

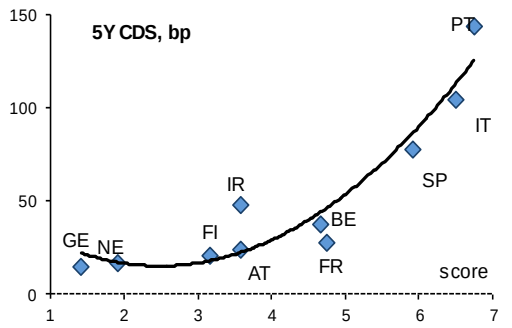

Table 2.SG sovereign Scoring, results by country

	EMU-12	
	Average Score	Ranking
Germany	1.42	1
Netherlands	1.92	2
Finland	3.17	3
Ireland	3.58	4
Austria	3.58	4
Belgium	4.67	6
France	4.75	7
Spain	5.92	8
Italy	6.50	9
Portugal	6.75	10
Greece	8.08	11

Graph 3. National GDP contribution to the EA GDP(or 'capital key')

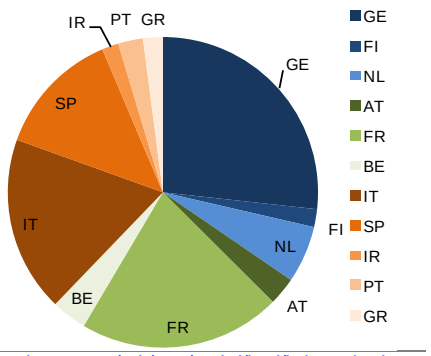

https://www.ecb.europa.eu/ecb/orga/capital/html/index.en.html

Overall this categorisation reflects the general understanding of sovereign risk in Europe: Germany, Finland and the Netherlands, usually denominated as 'core', are the most resilient EU countries. Then Austria, France, Belgium are seen as 'semi-core' or 'soft-core' economies; while Ireland, Spain, Italy, Portugal and Greece constitute the category of 'peripheral' (or 'non-core') countries. 'Peripheral countries' is a bigger category but the distribution by category is more equally spread when we look at the GDP contribution of each country to the whole Euro Area (EA) GDP: 34% is core, 27% is made of soft-core economies and peripheral countries amount to 37% of the total EA GDP (Graph 3). It is also worth noting that the model does not take political risk into account (e.g. uncertainties surrounding elections and risks surrounding the formation of governments). This is a notable caveat; Savona and Vezzoli (2011) for instance identifies political risk as a meaningful subcomponent of sovereign risk.

Contingent claims are another domestic indicator that can be explored for the purpose of credit risk estimation. This variable has been extensively involved to evaluate credit risk in corporates, for example in Black and Scholes (1973), Merton (1973 and 1998), McQuown (1993), Sobehart and Stein (2000), as well as in Crouhy, Galai, and Mark (2000), and Cossin and Pirotte(2001); or to estimate risk in the financial sector like in Merton (1977), Kupiec (2002), and Chan-Lau, Jobert, and Kong (2004). Contingent claims specifically applied to sovereign debt exploration is less recurrent in the literature, but Gapen, Gray et al. (2008) for instance offer interesting insight on that matter, on the basis of a ground-breaking framework. They note in particular that contingent claims offer insightful information for risk management as it helps identify existing balance sheet mismatches, while reflecting uncertainties inherent to balance sheet components. In the end, conclusions suggest that contingent claims analysis can offer sensible guidelines in two promising areas for sovereign risk mitigation: reserve management and debt sustainability. The framework can be used to derive an appropriate target for reserve adequacy, where the respect of the acceptance level for reserves is supposed to keep credit risk indicators above a specified threshold (or below, in the case of default probability). Hayri (2000), Gibson and Sundaresan (2001), Westphalen (2002), and Andrade (2009) extend this framework and draw fair values on sovereign interest rates in the context of contingent claims exploration. This approach looks valuable as to understand 'when' default is meant to happen.

Ratings provided by official agencies like Moody's, S&P, Fitch and DBRS are also highly-regarded information, as they are supposed to illustrate credit quality (Table 3). As publicly available estimations of the credit worthiness, a change of rating can have meaningful implications on financial markets. At the central bank level for instance, the ECB estimates the probability of default inherent to debt securities as a function of its credit rating. As a consequence, a bond involved as collateral in monetary policy operations will face a greater haircut if its rating does not fall in the best category[4]. Institutional investors also usually face strict limitations in terms of the credit quality of the bonds they are allowed to detain. As a consequence, investors will be forced to clear long positions on sovereign bonds if a downgrade puts the sovereign entity under the authorised level of rating. This obviously tends to magnify the market reaction surrounding rating downgrades. As ratings agencies are potent drivers of market sentiment, the acceleration of rating downgrades in Europe during the sovereign crisis has been an effective source of risk aversion. The downgrade of

[4] https://www.ecb.europa.eu/paym/coll/risk/ecaf/html/index.en.html
https://www.ecb.europa.eu/paym/coll/risk/liquidity/html/index.en.html

the United States by S&P on 5 August 2011 (ie. at the fore of the sovereign crisis) also led to sizeable volatility in many asset classes. On that ground, rating agencies cannot be regarded just as providing an illustration of sovereign risk, as admittedly they contribute to shape the general sentiment in financial markets. The methodology surrounding the assessment by rating organisations is primarily based on the observations of macro/financial/debt variables. The market access to funding, sustainability of debt, and investors' confidence are also key variables. All this makes ratings rather relevant in the context of sovereign risk exploration (Manganelli and Wolswijk, 2009). **But while this input is valuable to understand the present-state of credit risk, rating agencies have proved relatively unable to predict credit crunch.** As an example, Moody's, S&P, and Fitch all maintained at least an A rating on AIG and Lehman Brothers up until mid-September 2008: Lehman Brothers declared bankruptcy on 15 September, while the federal government provided AIG with its first multibillion dollar bailouts (out of four) on the following day. And as ratings are supposed to reflect domestic risk exclusively, they have also proven to be relatively unable to reflect potential contagion. These little forecasting skills surely did not help apprehend recent financial crises.

Table 3. Current ratings; European countries

	Moody's	Markit Scale		**S&P**	Markit Scale		**Fitch**	Markit Scale	
USA	Aaa	1	Sta	AA+	2	Sta	AAA	1	Sta
Japan	A1	5	Sta	A+	5	Sta	A	6.0	Sta
UK	Aa2	3.0	Sta	AA	3.3	Neg	AA	3.3	Neg
Germany	Aaa	1	Sta	AAA	1	Sta	AAA	1	Sta
Netherlands	Aaa	1	Sta	AAA	1	Sta	AAA	1	Sta
Austria	Aa1	2	Sta	AA+	2	Sta	AA+	2	Sta
Finland	Aa1	2	Sta	AA+	2	Sta	AA+	2	Sta
France	Aa2	3	Sta	AA	3.0	Sta	AA	3	Sta
Belgium	Aa3	4	Sta	AA	3	Sta	AA-	4	Sta
Ireland	A2	6.0	Sta	A+	5	Sta	A	6	Sta
Slovakia	A2	6	Pos	A+	5	Sta	A+	5	Sta
Slovenia	Baa1	8	Sta	A+	5	Pos	A-	7	Sta
Spain	Baa2	9	Sta	BBB+	8	Pos	BBB+	8	Pos
Italy	Baa2	9	Neg	BBB	10	Sta	BBB	9	Sta
Portugal	Ba1	11	Pos	BBB-	10	Sta	BB+	11	Pos
Cyprus	Ba3	13	Pos	BB+	10.7	Pos	BB-	12.7	Pos
Greece	Caa2	18	Pos	B-	16	Pos	B-	16	Pos

While endogenous variables deliver insightful information on the repayment capability, exogenous factors too, have meaningful implications on the determination of risk premia. In a confidence crisis for instance, evaporating demand on the primary markets tends to make debt issuance more and more challenging. This ultimately can raise substantial threats on debt rollover and future debt repayment, and so regardless of the underlying fundamentals. In this case, investors' behaviour is key. Variables linked to the distribution of debt holdings may give interesting insights too. Arslanap and Tsuda (2012) in particular have explored the change in portfolio allocation strategies during the sovereign crisis out of a comprehensive database of debt holdings by investors' type. Their analysis tends to discriminate the behaviour of investors, depending on their geographical location (domestic versus foreign) and the type of institution they work for (central bank, investment banks, nonbanks, official sector). They highlight key trends through and post crisis, and oppose two estimators: 'government refinancing' risk on one side, which is supposed to reflect selling pressure in bonds. This obviously becomes a powerful driver on the emergence of a confidence crisis. On the other side, the

authors quantify risks to the 'domestic financial stability', which is meant to illustrate the resilience of domestic investors as to offset a rise in sovereign rates. An observation is that the share of foreign investors has consistently risen for most European sovereigns over the years preceding the crisis, though this was less pronounced for higher yielding credits like Portugal, Ireland and Spain. Then exploring the consequences of funding shocks and sudden outflows, the analysis reveals a notable differentiation as to how foreign investors changed their holdings during the GFC (2008-2009) and during the euro area debt crisis (starting in 2010): during the euro area sovereign crisis, foreign investors operated a reallocation of their holdings (in the benefit of safer credits) much faster than in 2008. As the authors note, this was the effect of a transition from interest rates risk to credit risk combined with large-scale sovereign downgrades. The unusually high volatility in yields also contributed to fan the selling-off trend in peripheral markets. Results also show significant macro-financial risks emanating from holdings of sovereign debt held by banks. Effectively, the bank/sovereign nexus is prompt to exacerbate contagion when sovereign debt held by domestic banks is not properly diversified (Erce (2015)). The close relationship between the perceived solvency of governments and the solvency of domestic banks is also stressed in Allen, Moessner (2013). More generally, sovereign debt composition has also been investigated by Ali Abbas, Blattner, de Broeck (2014). Their dataset delivered insightful observations on investors' behaviour from a broader historical perspective, since 1900.

Liquidity is another exogenous key component, which has notable consequences on the perception of credit risk in general (Calomiris, Heider, Hoerova (2015), Arghyrou and Kontonikas (2011), Attinasi et al. (2009), Barrios et al. (2009), Favero et al. (2010), Gerlach et al. (2010), Gómez-Puig (2009); Manganelli and Wolswijk, (2009), Sgherri and Zoli, (2009), Schwartz, 2009). But this is a vast subject and liquidity operates at different levels. Foucault, Pagano, and Röell (2013) in particular see three different definitions of liquidity: First, ***market liquidity*** refers to the ease with which financial assets can be traded close to their fundamental price. Second, the closely related concept of funding liquidity refers to the ***ready availability of cash*** and the ease with which financial intermediaries can obtain funding. The third liquidity dimension is ***central bank liquidity***, which refers to banknotes, coins and reserves held with the central bank. In investment banks, 'market makers' are 'liquidity providers' and as such they are meant to nurture market liquidity by serving investors at fair price. Their role has become more and more challenging over the past decade. First the sovereign crisis has raised sizeable threats on the solvency of banks in general, partly because of palpable consanguinity with sovereigns. Plus the emergence of tough regulations in the most recent years has also made any balance sheet expansion much more expensive than before. In the end, while helping financial stability in general, recent regulations have also contributed to reduce the amount of liquidity that trading desks in banks are able to provide. Allen, Moessner (2013) explore the distortion in terms of liquidity that resulted from the sovereign crisis. As the authors note, Libor versus OIS spreads and bank CDS are relevant illustrations of financial stress in the banking sector. Wider levels in 2011-2012 (Graph 4) and the major decoupling with US bank CDS (Graph 5) suggest that financial distress was quite intense during the sovereign crisis. As Panetta (2011) explains, sovereign securities are used extensively by banks as collateral to secure wholesale funding from central banks, private repo markets, and the issuance of covered bonds, as well as in order to back over-the-counter (OTC) derivative positions. Inflating sovereign risk therefore naturally reduces the availability or eligibility

of collateral, and hence banks' funding capacity. Effectively, while liquidity risk and funding risks are given two different definitions[5], these risks are closely interrelated.

Graph 4. Three-month Libor-OIS spreads (bp)

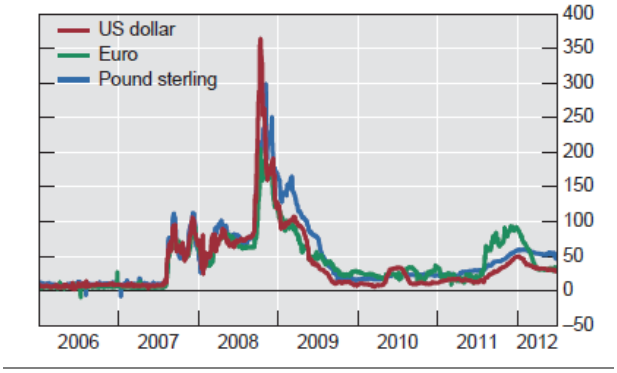

Graph 5. Bank CDS spreads (bp)

Five-year on-the-run credit default swap spreads. Simple average across leading banks

Graph 6. Net euro-denominated claims by banks in Germany vis-à-vis banks abroad (Loans and advances minus liabilities to foreign banks) - Amount outstanding, in billions of euros

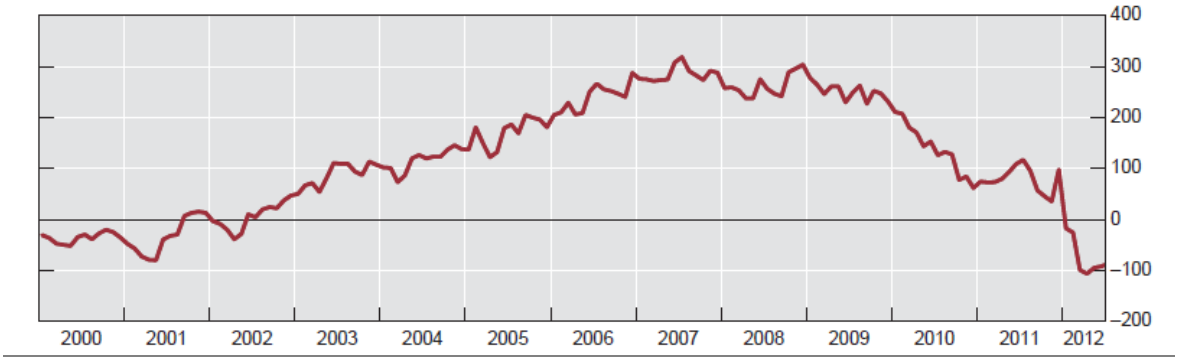

Source: Deutsche Bundesbank, BIS calculations.

Allen, Moessner (2013) delivers interesting insight too. The authors examine the balance sheet of European banks from 2008 to 2012 (from ECB's statistics and BIS databases). First they note that from mid-2010 to mid-2011 inter-commercial bank loans fell by €487bn. In comparison, this trend was less pronounced during the GFC, therefore suggesting that the mutual loss of confidence among euro area commercial banks was more serious than in 2008. Plus, external assets contracted by a large €283bn during this period, while in proportion, the more liquid assets also sharply increased (within the set of external assets). And as external liabilities fell by even more, it clearly appears that the deleveraging of euro area banks fell disproportionately on external rather than domestic assets (Graph 6). Another interesting point is that banks had a substantial amount of debt maturing in 2012. And in contrast to this trend, gross issuance saw a sharp decline in 2011, and fell below the level of bond redemptions. Overall this reflected deteriorating funding conditions. Commercial banks also experienced a slowdown in the growth of deposits from non-MFIs[6] in H2 2011 (Graph 7), suggesting that depositors began to share concerns that were afflicting financial markets. In the end, the launch of non-conventional measures in end-2011/early 2012 by the ECB via Long Term Refinancing

[5] Liquidity risk is the *"ability to finance cash outflows at any given point in time"*, while funding risk *"refers to a bank's ability to raise funds in the desired amount on an ongoing basis"* (King, 2013b, p. 4145).
[6] Monetary Financial Institutions

Operations[7] (LTRO) helped ease this liquidity problem quite significantly by providing successively €489bn and €529bn loans to banks for a three-year horizon, on 22 December 2011 and 1 March 2012.

Graph 7. Deposits of domestic residents with depository corporations

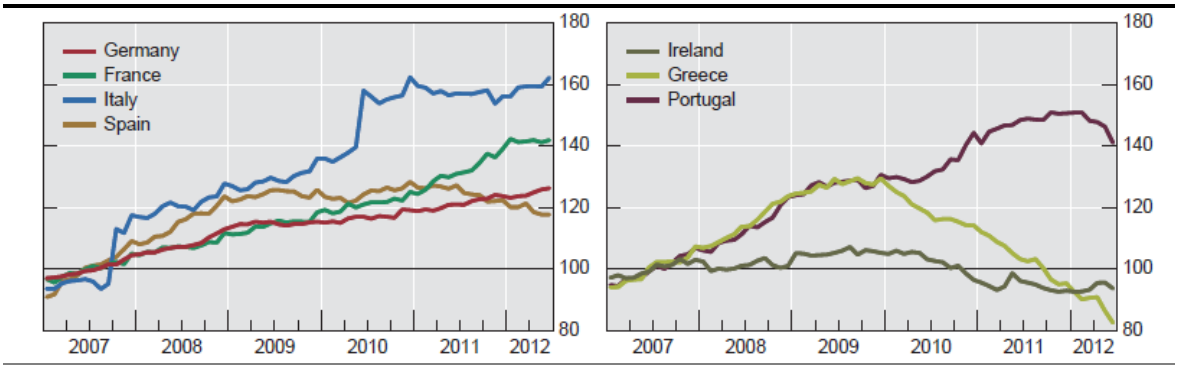

Demand deposits and other deposits; rebased to 2007 average = 100; excluding central banks.

Graph 8. Bid-ask spread on a selected Portuguese bond

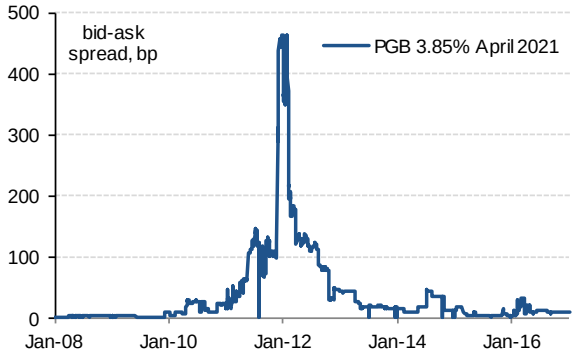

Graph 9. Cross-currency basis against the US dollar (bp), EURUSD basis (red), JPYUSD basis (blue)

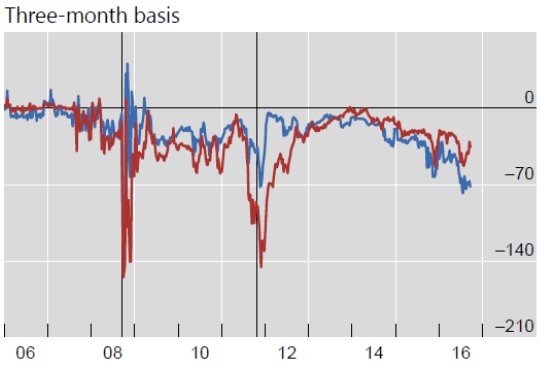

The vertical lines indicate 15 September 2008 (Lehman Brothers file for Chapter 11 bankruptcy protection) and 26 October 2011 (euro area authorities agree on debt relief for Greece, leveraging of the European Financial Stability Facility and the recapitalisation of banks).

Bank funding was reportedly contracting during the sovereign crisis. And as a consequence, market makers were left with limited room to hedge their positions. This naturally amplified the supply/demand imbalance when portfolio managers were rushing to diversify their risk. An illustration of reduced liquidity overall is the substantial widening in bid-ask spreads in sovereign debt markets. 10Y Portuguese bonds (PGB) for instance showed a massive widening in bid-ask spreads, from 2.5bp on average before 2010 up to 450bp in Q1 2012 (Graph 8). Needless to say, no-one was trading at these abnormally large levels. Portfolio managers exposed to Portugal had consequently no choice but to keep their positions as the gridlock on Greece intensified. In the literature, bid-ask spreads are effectively seen as a relevant picture of liquidity risk (Aßmann and Boysen-Hogrefe (2011), Fontana and Scheicher (2010), Abad, Chuliá, Gómez-Puig (2010)). Other approaches also consider the size of the government bond markets (Arghyrou and Kontonikas (2011), Bernoth et al. (2012), Abad, Chuliá, Gómez-Puig (2010), Haugh et al. (2009), Attinasi et al.

[7] https://www.ecb.europa.eu/mopo/implement/omo/html/index.en.html
https://www.ecb.europa.eu/explainers/tell-me/html/tltro.en.html

(2009)), or other measures like interest rate differentials against a specific benchmark: Schwartz (2009) for instance gauge liquidity risk as the interest rate differential between by bonds issued by KfW and by Germany (Bunds).

A key objective of banking regulation is to make individual banks (micro-prudential) and the banking sector as a whole (macro-prudential) more resilient to sudden changes in economic and financial conditions. The first two rounds of concerted international banking regulation, Basel I and II, which came into effect in 1988 and 2007 respectively, largely centred on capital regulation with a focus on credit risk and the solvency of banks. Before that, liquidity risk and liquidity crises, it was believed, could be addressed by a combination of banks' individual liquidity management, deposit insurance schemes and access to central bank funding. However, following the GFC and the sovereign crisis, the common idea that a well capitalized bank would always be able to raise funds became weak: banks, despite meeting the regulatory capital requirements, experienced serious funding difficulties owing to their excessive reliance on unstable, low quality sources of funding, erroneous asset-liability management and risky off-balance sheet positions (ECB (2013), Simion, Rogoni (2016), Santos and Elliot (2012), Calomiris, Heider, Hoerova (2015)). In response to this observation, the Basel Committee on Banking Supervision (BCBS) designed a new framework for banking regulation, known as Basel III (full implementation scheduled for 2019). **For the first time since the inception of global banking regulation in 1988, Basel III introduced explicit mandatory rules for liquidity regulation.** The cornerstone of this new framework is the introduction of two balance sheet ratios: the Liquidity Coverage Ratio (LCR) and the Net Stable Funding Ratio (NFSR), intended to regulate bank's liquidity risk. These changes significantly broaden the scope of global banking regulations. First, the liquidity coverage ratio (LCR) requires banks to hold a buffer of sufficient high-quality liquid assets (HQLA) to cover their total net cash outflows over a 30-day stress scenario. Second, the net stable funding ratio (NSFR) requires banks' amount of stable funding to exceed a required minimum amount. In the end, the LCR and NSFR seek to lower liquidity risk by forcing banks to reduce their maturity mismatch, thereby making it easier for them to meet their liabilities in due time. As Koenig, Pothier (2016) explain, a key challenge in the design of the LCR was determining what constitutes HQLA. The required feature of these assets is that they can be converted into cash at little or no loss of value. Regulators see four essential specifications: (1) low risk, (2) easy to valuate, (3) have a low correlation with other risky assets, and (4) the asset has to be listed on a recognized exchange (BCBS (2013)). Importantly, high quality liquid assets used as collateral to secure lending from the central bank do not count towards the LCR. Setting an appropriate level of requirements is critical: set too low, the liquidity requirements may fail to provide the desired level of insurance; set too high, the banking sector may reduce its lending and investment power. While the plus-value in terms of how this framework makes banks more resilient is indisputable, some investigations reveal notable caveats in the way Basel III is implemented. Koenig, Pothier (2016) first, tend to question whether the respect of both ratios, LCR and NSFR, is an absolute necessity, or if being compliant on just one could be sufficient. In particular, the authors raise the point that high quality liquid assets should not be considered to be liquid when LCR requirement is binding. Another limitation, identified in Malherbe (2014) is the fact that liquidity requirement is an incentive for banks to hoard liquidity during times of financial distress. This accumulation and retention may paradoxically lead to a substantial reduction in market liquidity. Another possible threat is that LCR may increase demand for central bank money, thereby pushing short-term interest rates down towards the floor of the central bank's corridor. This could ultimately affect monetary policy implementation (Keister, Todd,

and Morten L. Bech (2012)). In addition to limiting the ability of the central bank to steer overnight rates, the new liquidity ratios may also affect the composition of assets used as collateral in central bank operations. Since these assets cannot qualify for the LCR, the share of non-HQLA collateral posted at the central bank may increase as banks will want to freeze the use of HQLA assets. **This could squeeze demand for non-HQLA collateral securities; something that would occasion notable price distortions**. Bucalossi et. al. (2016) in particular observes that for banks with more than 70% non-HQLA in their asset pools effectively, the share of non-HQLA assets pledged as collateral to the ECB increased significantly between 2011 and 2015. **Capital regulations emanating from the Basel III framework are in fact already regarded as being responsible for some price exuberance in liquid and tradable markets.** The persistent deviation from Covered Interest Parity (CIP) for instance is usually presented as an illustration of the greater cost of balance sheet expansion for banks now (Caruana (2016), Shin (2016), Borio et al. (2016), Du et al. (2016)). CIP states that the interest rate differential between two currencies in the cash market should equal the differential between forward and spot rates in FX. This relationship broke down for the US dollar during the GFC, and the gap between these two measures consistently widened since mid-2014, overall encouraging a deviation of cross currency basis swaps towards more negative levels (Graph 9). The ensuing violation of CIP means that an investor could borrow at a low interest rate and lend out at a higher interest rate (either via FX or cross currency basis swaps). This arbitrage was not possible before 2008, as cross currency bases were consistently trading at zero. Essentially, any deviation from zero was systematically faded by trading desks in banks (amongst other). And while valuations have notably recovered in bonds and CDS prices since end-2012, CIP in contrast is set to remain 'open' for a prolonged period of time (see Du, Tepper and Verdelhan (2016)). The persistence of the gap in particular suggests that banks cannot exploit opportunities raised from the violation of CIP. As Caruana (2016) argues, they are putting such a high price on the use of their balance sheet that the trade becomes uneconomical. This is an illustration that the greater cost of balance sheet expansion for banks resulting from tighter regulations tends to impact market valuations and to some extent the overall market liquidity. In terms of reputation, the promotion of tighter regulations is also an incentive for banks to demonstrate their greater robustness, as market participants are now prompter to penalize the more troubled institutions. Caruana (2016) notes that consequently the cushion of capital that banks 'feel they have to hold' is in practice much above the minimum Basel III requirements, at around 5% points above the required 7% capital ratio. This presumably helps secure stress test results while keeping risks of rating downgrades or future supervisory constraints at bay. But this also tends to magnify the cost of balance sheet expansion, and thus supports further regulation-led price distortions. This undergoing transformation at the bank level, incentivised by the need for tighter regulations is meaningful information when exploring sovereign risk: on one side the more recent upgrades in regulations undoubtedly contribute to make banks more robust in the sense that the regulatory framework is more demanding. This can help relax the level of consanguinity between banks and sovereigns, which is a positive. **But this is a double-hedged sword too, as there is tangible evidence that the cost of capital for banks is occasioning the emergence of market failures. And these discrepancies could possibly feed the propagation of financial distress in an environment marked by mounting risk aversion, thereby exacerbating fire sales on sovereign securities.** Simion, Rigoni et al. (2016) look at how the market reacted to the regulatory announcements surrounding the implementation of Basel III. The authors note that investors' reaction was mixed, suggesting that new liquidity rules were regarded as increasing the banks'

probability of default. **This overall corroborates the risk that this new framework eventually demonstrates only limited effectiveness as to reduce contagion from banks.**

More global variables may also be added to the list of exogenous factors that are relevant to the exploration of sovereign risk in Europe. Longstaff et al. (2011) and Remolona et al. (2008) for instance show that a significant portion of the variations in European sovereign securities is attributable to the momentum from other jurisdictions like the United States. The authors tend to quantify implications on sovereign credit spreads from four different set of drivers: local economic variables, global financial market variables, global risk premia measures, and net investment flows into global funds. In the end, they note that "Sovereign credit spreads are generally more related to the U.S. stock and high-yield bond markets, global risk premia, and capital flows than they are to their own local economic measures". And coincidently they also conclude that: "country-specific variation represents only a minority fraction of the total variation in sovereign credit spreads". A principal component analysis also highlights that 30% of the variations in sovereign CDS spreads is explained by a single factor that is common to all countries in the sample. And this factor is fairly correlated to US stocks and the VIX index. In the end, the authors provide clear evidences that risk-premia in general, and therefore the perception of sovereign risk, are influenced by global considerations to a greater extent than by idiosyncratic developments. Other analyses like Kamin and von Kleist (1999), Eichengreen and Mody (2000), Geyer, Kossmeier, and Pichler (2004), Rozada and Yeyati (2005), and Remolona, Scatigna, and Wu (2007) lead to similar conclusions. However, it is worth to note that this literature mostly focuses on periods preceding the GFC (and the sovereign crisis): Longstaff et al. (2011) for instance focuses on the period 2000 to 2007. Their conclusions look therefore much valuable as to understand the dynamics of financial markets in the context of a standard volatility regime. Following the recent financial crises, the more recent literature has switched to a different verdict on the influence of international/global drivers on sovereign securities. Jeanneret (2012) for instance explores the fundamental drivers of sovereign credit spreads during the crisis. The authors incorporate market-related factors in their approach to explaining sovereign credit spreads. In particular they consider variations in the VIX index, S&P 500's returns, the 5-year US Treasury (UST) interest rate, and the slope of the US term structure calculated as the interest rate differential between the 30-year and the 3-month UST rates. As local variables, the model explores the connection between sovereign credit spreads and the soundness of the local stock market. The authors also include additional descriptive variables like 10Y German interest rate (in the same vein, Fontana and Scheicher (2010), Oliveira et al. (2012) involve 'risk-free' interest rates), government indebtedness and an indicator of macroeconomic risk. In contrast to what we mention above, conclusions this time point to a reduced influence from international market-wide indicators. Consequently, sovereign risk looks as primarily driven by country-specific information. As an explanation for this divergence of opinion, Jeanneret (2012) notes that Longstaff et al. (2011) includes small and illiquid countries in its sample. And valuations in those countries effectively may be more sensitive to global considerations. In our view, this also reflects the fact that economic and political developments within the euro area moved to the front stage in newswires during the sovereign crisis. This subsequently led to a greater attention from investors than before the crisis; hence justifying the bigger role played by domestic drivers on the price formation of sovereign securities during this period. In the end, the authors note that "forward-looking information on firm income in a country, as embedded in local stock market prices, helps explain an important part of the time-variation in sovereign credit spreads; in particular for large sovereign debt issuers with

liquid credit and equity markets." On our side, we have explored sovereign risk on the basis of sovereign CDS prices and asset swap spreads exclusively. We agree on the fact the global factors tend to become less relevant when the overall volatility is originating from domestic developments. This was admittedly the case during the sovereign crisis. Plus the data we explore is made of price variations of relatively liquid assets. A consequence of decent liquidity is that any contagion from other jurisdictions is quickly integrated in prices. This mostly motivates our choice to focus on Euro-based securities exclusively.

Although there are a multitude of factors that contribute to the price discovery in bonds, there is a common factor that reflects investors' changing attitude as risk sentiment sharply deteriorates: risk aversion systematically leads to a decline in the appetite for risk exposure in portfolios, while it enhances demand for safer assets. This obviously translates into a notable outperformance of safe-havens in general, ie. a richening of these securities that relate to 'core' European countries in the context of this report. Securities referring to peripheral countries, in contrast, will experience a price deterioration in the process, as a result of the ensuing flight to quality (Arghyrou and Kontonikas (2011), Barrios et al. (2009), Favero et al. (2010), Manganelli and Wolswijk (2009), Pozzi and Woslwijk (2012), Sgrerri and Zoli (2009)). As we noted in the previous paragraphs, the basket of descriptive variables that refer to sovereign risk is virtually boundless. And for any selected variable, models indicate that there are always some caveats attached to it: the degree of relevance may vary as time goes by (e.g. valid only for specific periods like pre-EMU, pre-GFC or post-crises), or may depend on market sentiment (some variables are less influential in risk averse market conditions), or on the country itself (small economies/illiquid securities versus more liquid assets). Barbosa and Costa (2010), Caceres et al. (2010) even suggest that there were two or three apparent regime shifts in correlations/market drivers during the GFC. Eventually, this makes the selection of a relevant set of descriptive variables for sovereign risk exploration a challenging process. Plus, redundancy between the selected variables is a risk to face an extra cost in terms of complexity/computational burden for very limited gains. For better clarity, the literature identifies three main 'core' risk factors as the main determinants surrounding the price formation in sovereign bonds (and CDS spreads): credit risk, liquidity risk and the general risk appetite. This interpretation can be found in Bettendorf (2016), ECB Banking Supervision (2016), Das, Oliva, and Tsuda (2012), Arghyrou and Kontonikas (2011). We already described the estimation of credit risk and liquidity risk in the paragraphs above (macro variables, ratings, regulations...). And while it is well accepted that the general risk attitude (or risk appetite) of portfolio managers has meaningful implications on market valuations, this risk factor is a bit more difficult to estimate. This is because investors' risk appetite/aversion mostly comes from the assessment of the two other risk factors (credit risk and liquidity risk) and this interconnection makes the isolation of a proper descriptor of risk appetite relatively complex. While macroeconomic and fiscal variables give little information on general risk appetite, market-based data like bond yields or CDS spreads presumably incorporate it as a core determinant (Kilponen, Laakkonen, Vilmunen (2012), Arghyrou and Kontonikas (2011)). This is a strong incentive to prefer market-based information as the main input for the exploration of sovereign risk and contagion in Europe. Plus, CDS spreads and bond yields offer high frequency data as they are continuously quoted for developed economies. This makes the implementation of sophisticated econometric models particularly convenient. Investment flows are another descriptor of the general risk attitude (see Gapen, Gray et al. (2008), Arslanap and Tsuda (2012)). But these indicators are usually released with a lag of several months, and at a low frequency, which, if anything, makes them less suitable for a

day-to-day re-assessment of sovereign risk. Volatility indicators like the VIX can also be regarded as an illustration of risk appetite: Bekaert et al. (2010) in particular offers a decomposition of the VIX into risk appetite and uncertainty factors. That said, liquid sovereign securities are also meant to reflect the general market volatility, so there is a risk of redundancy when adding the VIX to a sample of sovereign bond yields or CDS prices. Our analysis is founded on market-based data exclusively, namely 5Y sovereign CDS spreads and 10Y asset swap spreads – and so for the reasons we just mentioned - plus the fact that CDS spreads are admittedly allowing for cross border financial linkages (Kallestrup et al. (2012)).

By definition, sovereign risk is not a multivariate quantity. Rating agencies for instance focus on domestic risk, estimated on the basis of local variables. While this delivers a sound fair value of the credit worthiness in normal market conditions, the approach does not allow for the potentially sharp deterioration in credit quality that would result from an external shock. In this report we focus on the dynamics of financial markets in periods marked by mounting risk aversion. And we explore in particular the acceleration of the joint price depreciation – and the abnormally large volatility – that usually ensues from contagion (Diebold et al. (2012), Yilmaz et al. (2010), Zhou et al. (2012)). Since contagion relates to risk propagation through risk assets, there is a multivariate angle that is naturally attached to it. And this multivariate aspect needs to be addressed properly; in particular there is a wide acceptation that the dynamics of contagion is mostly non-linear (Ahnert and Bertsch (2013), Forbes and Rigobon (2002), Bekaert et al. (2014), Favero and Giavazzi (2012)). Plus there is the complication that episodes of intense contagion are relatively infrequent. Observed contagion is consequently just a small portion of all available market observations, and this makes the generalisation of its behaviour and future predictions somewhat challenging. Looking at the structural approach to sovereign exploration, we see mostly two kind of approaches: on one side those who seek to quantify the underlying robustness of sovereign entities and possibly to track it as time goes by; and on the other side those who try to understand the impact of contagion in terms of price variation and potential losses in portfolios. Both purposes are quite different. In the first category there is an implicit goal of drawing macro-prudential guidelines on how to avoid or how to detect a situation where deteriorated fundamentals could justify the emergence of severe contagion (Lane (2010), Angelini, Grande, Panetta (2014), Gros (2013), Acharya and Steffen (2013), Battistini, Pagano and Simonelli (2013), ESRB (2015)). The other way round, in the second approach, contagion is assumed as a given fact and the analysis tends to derive the expected shortfall in portfolios, and usually explores ways to hedge the resulting volatility (Angelini, Grande, Panetta (2014), Angeloni and Wolff (2012), Gapen, Gray et al. (2008)). While in theory both approaches could be based on similar dataset and explanatory models, there are notable divergences in practice. First, those who want to gauge sovereign credit quality are more inclined to consider a dataset of fundamental domestic data; mostly macroeconomic (e.g. Yue (2010)). Market prices in contrast are generally a less preferred option for the dataset. The analytical approach then seeks to illustrate the negative feedback loop between deteriorated fundamentals and the emergence of contagion. Conclusions may reveal a quantification of the dynamics that would relate credit worthiness to macroeconomic fundamentals – sometimes by focusing on the probably of default (Ratovomirija, 2015, Gapen, Gray et al. (2008), Lagi, Bar-Yam (2012)). Macro prudential guidelines are then drawn from these observations, with the authors usually emphasizing either a greater impact from certain variables, or some relevant thresholds beyond which sovereign risk is supposed to become a serious concern. In terms of calculations, these papers usually involve slightly less sophisticated models than the second

approach does: linear regressions/correlations or basic interpolation methods are generally sufficient to deliver sensible results. In fact, the argumentation is usually oriented as to stress the special upside resulting from the dataset itself rather than from the exploration of convoluted analytical models: the authors usually pride themselves on considering a sensible set of variables that offers exhaustive and sufficiently diversified information to conclude on the robustness of the sovereign entity. We reckon that picking up appropriate descriptive variables is a tough challenge indeed given the breadth of the topic. To illustrate this first category of papers, Arslanap and Tsuda (2012) seeks to distinguish the different components of sovereign risk. The authors in particular break it down into three specific indices: the Sovereign Funding Shock Scenario (FSS), the Investor Base risk Index (IRI) and the Foreign investor position index (FIPI). FSS is a framework to simulate forward-looking sovereign funding shock scenarios to assess the vulnerability of a country to sudden foreign outflows. This index highlights the ability of a sovereign entity to rely on its domestic institutional investors and banking sector as alternative investors. The analysis also examines implications of a withdrawal of foreign investors from the sovereign debt market on the domestic financial stability. Three parameters describe investment decisions of foreign private investors, namely: (i) their contribution to funding of the global fiscal deficit over the next year. (ii) The rollover of short-term government debt that will be redeemed next year. (iii) The fire sale of long-term government debt. The model envisages three shock scenarios. In each scenario, foreign investors strategies are varying, thereby affecting demand for debt. Results are measured in terms of foreign outflows on the balance sheet of domestic banks. The IRI is meant to illustrate the likelihood of sudden outflows by different types of investor in the sovereign investor base. The index takes a value from 0 to 100 with a higher score suggesting that the country is prompt to face a sudden investor outflow. The index can be seen as complementary to the FSS. While the FSS aims to assess the vulnerability of a country in a hypothetical sudden investor outflow scenario, the IRI seeks to reflect the likelihood of such an event materializing. The index is mostly built on the basis of historical correlations between log-variations in investor holdings against log-variations in sovereign bond yields. Finally, the authors assign an aggregate risk score to each country. And accordingly, a country whose debt is fully held by its domestic central bank would have a score of 0, while another country whose debt is fully owned by foreign nonbanks would have 100. Finally, the FIPI aims to qualify the share of foreign investors compared to other investors, with respect to the outstanding debt portfolio of each country. The goal is to explore to which extent foreign investors may initiate a sharp rise in interest rates or may exacerbate market volatility through a huge sell-off of sovereign bonds if risk conditions deteriorate. This time again the procedure is based on simple data aggregation procedures as the authors mostly look at the dynamics of the portion of foreign investors, expressed as a share of the total debt outstanding. The quantitative framework is relatively basic and this helps make the results very comprehensible. Overall it is relatively clear that the data itself - based on investment flows - is already priceless information, as in essence it is a very difficult exercise to find neat and reliable information on these flows. In contrast to this approach, models in the second category are extensively based on market valuations (Duffie, Pedersen, and Singleton (2003), Pan and Singleton (2008), Bodie, Gray and Merton (2007), Gapen, Gray et al (2008), Doshi et al. (2011), Brutti, Sauré (2012), Erce (2015)). This is mainly because asset prices reflect the switch in market sentiment that is usually attributable to the emergence of contagion. Beyond a certain point in particular, a confidence crisis coming up would lead to a disproportionate sell-off, through fire sales. The resulting price action, in turn, usually proves very much de-synchronised with underlying fundamentals that would call for a more contained market reaction (Jones et al. (1984),

Eom et al. (2004)). This is a sound reason to prefer market-based information to more fundamental indicators in this context of contagion exploration. Aside from this difference, analyses in the second category of models usually rely on relatively more sophisticated frameworks. The notion of multivariate dependence in particular is a key component when apprehending the joint price depreciation arising from contagion. And since contagion occurs on extreme occasions, a proper review of this phenomenon is virtually not possible by empirical means. As we already mentioned, contagion is usually seen as causing a non-linear acceleration of the joint price depreciation (Zhang et al. (2009)). And because the dataset is supposed to encompass periods of palpable contagion (the algorithm is supposed to 'learn' from these episodes), contagion is usually regarded as being responsible for the fat tails in the data. A common challenge is therefore to capture multivariate dependence within the tails, with the 'fat' aspect making things slightly more complex as it tends to disqualify a lot of common probabilistic approaches (Harvey, Luati (2014), Harvey (2013), Janus, Koopman, Lucas (2014), Zhang, Creal, Koopman, Lucas (2012a)). The erratic aspect of the volatility is another meaningful concern when seizing the cost of mounting contagion. In this case though, volatility models applied to time series exploration like GARCH (Harvey, Luati (2014), Harvey (2013)) and its variations could provide much satisfactory results. This is all the more interesting as there is notable autocorrelation within the volatility (Creal, Koopman, Lucas (2009), Zhang, Schwaab, Lucas (2012)). This feature is worth to focus on as it helps understand the persistence of momentums in the volatility. Periods of very low volatility for instance, usually prove somewhat resilient to shocks as they show only a gradual deterioration when risk aversion is hitting the market. And in contrast, very volatile periods will remain turbulent for a while, even after we observe a stabilisation of the newsflow - thereby illustrating the persistence of momentums in the volatility and presumably some autocorrelation. In these papers, we also note a recurrent usage of copulas (Bernardi, Catania (2015), Fei Fei, Fuertesy, Kalotychou (2013), Dalla Valle, De Giuli et al. (2014), Armstrong, Galli (2002), Totouom Tangho, Armstrong (2007a), and Totouom Tangho, Armstrong (2007b)). These are versatile multivariate statistical models that offer great flexibility, especially in the context of estimating non-linear multivariate correlations and fat tails (Embrechts et al. (2001)). The higher frequency of market prices (compared to more fundamentals variables like macroeconomic indicators) is also rather convenient for the implementation of more sophisticated statistical frameworks. Arellano (2008) and Yue (2010) for instance consider dynamic stochastic equilibrium models, while Longstaff et al. (2011) is based on a principal component analysis. In the same vein, Hilscher and Nosbusch (2010) promotes a panel-based approach. From a probabilistic point of view, many analysis also promote Generalized Hyperbolic distributions as a relevant choice to address heavy tails in the data (like Zhang, Schwaab, Lucas (2012), Creal, Koopman, Lucas (2011), Creal, Koopman, Lucas (2013), Creal, Koopman, Lucas, Zamojski (2016)). These distributions can also be combined with Markov switching regime techniques like in (Fei Fei, Fuertesy, Kalotychou (2013), Eyigungor (2006)). Vector Autoregressive Models (VAR) also tend to provide sensible results when applied to sovereign risk exploration (Brutti, Sauré (2012)). In these papers, the prudential aspect moves to the level of portfolio managers: the quantification of the expected losses when contagion arises is supposed to improve risk diversification in portfolios during periods of risk aversion. Finally, we note that a decent part of the literature also tends to make a bridge between these two main approaches. Diebold and Yilmaz (2014) in particular design an interesting dependence estimator that helps differentiate 'fundamentals-based' periods from other periods marked by 'pure contagion'. Other papers have implemented different variations to this framework like Awartania et al. (2013),

Lee and Chang (2013), Chau and Deesomsak (2014) and Cronin (2014), Narayan et al. (2014), Duncan and Kabundi (2013).

In this report, we explore sovereign risk from the perspective of risk management. In the first chapter, we consider European sovereign CDS spreads from January 2008 to December 2016 as the only input of the model, and we implement a somewhat sophisticated multivariate statistical framework, inspired by the foundational works of Creal, Koopman, Lucas (2009), Zhang, Schwaab, Lucas (2012). Essentially, we combine the use of heavy-tailed probability distributions with the implementation a versatile volatility model, the Generalised Autoregressive Score model (GAS), derived from the GARCH theory (Zhang, Creal, Koopman, Lucas (2012a), Zhang, Creal, Koopman, Lucas (2012b), Creal, Koopman, Lucas (2011), Creal, Koopman, Lucas (2013), Creal, Koopman, Lucas, Zamojski (2016)). Overall this proves a successful combination as to address the sharp variations in market sentiment, and the resulting modifications to the market structure that occurred during the period we explore. Episodes of large risk aversion in particular, are marked by an erratic price action and abnormally large volatilities. This overall tends to make the calibration of probabilistic models fairly complicated. While our model is inspired to a large extent by the available literature, we also implement noticeable variations to existing models. In the end, our multivariate framework highlights 'hidden' market dependencies between CDS spreads, especially these supposed to materialise when contagion is looming. Based on the aforementioned categorisation of models, and because we seek to quantify 'the cost of contagion' in a portfolio of sovereign CDS spreads, our approach belongs to the second category of sovereign risk models. Our conclusions are complementary to the available literature from many angles. First we offer a comprehensive understanding of the dynamics of contagion when risk aversion gradually increases. The high degree of granularity in the scenarios we explore enables us to establish an accurate profile of different regimes in the market reaction to shocks. Overall, the quantification of these different phases is insightful information from a risk management perspective, as it helps drawing guidelines on the expected volatility in the case of a sudden deterioration in market sentiment. Our results, from that perspective, also contribute to enlarge the existing literature on financial contagion. While our model delivers a temporal (and conditional) exploration of market prices in a first instance, we also explore another formulation which helps generalising the market reaction to shocks. Our generalised model makes sense from a statistical point of view and offers great ease-of-use for a high-frequency manipulation of the framework. A benefit of using the temporal model in contrast, is its embedded forecasting capability. We explore this feature (amongst others) in Chapter II.

Copula: the framework

The model we explore in the first chapter is largely inspired from the theory of copulas introduced in Sklar (1959). **Copula is a statistical framework that is supposed to unveil multivariate non-linear dependencies.** This approach is based on the foundational work of Sklar (1959), where the author demonstrates the existence of copulas for every set of univariate marginals $(F_1, \dots, F_n)$ attached to a sample of multivariate random variables $(x_1, \dots, x_n)$. Sklar's theorem (eq. (1)) also qualifies the multivariate joint dynamics F as a function of the univariate marginals F_i: **the formulation shows that copulas undertake a transformation of the initial data x_k into a new frame where it is more manageable to capture the multivariate dependencies** (ie. where the calibration of the multivariate distribution c, and its cumulative version C, is feasible)**.** Using the cumulative distributions F_k in this transformation (as indicated in eq. (1)), makes the conversion into the new frame very much convenient. This transformation is sometimes denominated as an anamorphosis (Amezcua, van Leeuwen (2014)).

Sklar's theorem. Let $F \in \Im(F_1, \dots, F_n)$ be an n-dimensional distribution function with marginals $F_1, \dots, F_n$. Then there exists a copula $\mathbb{C} \in \Im(U, \dots, U)$ with uniform marginals such that

$$F(x_1, \dots, x_n) = C\big(F_1(x_1), \dots, F_n(x_n)\big) \qquad (1)$$

The common approach to copulas involves a two-step calibration of the model. First the algorithm estimates the univariate density of the variables $(x, y, z$ for instance). Then the data is transformed into uniformly distributed variables (u, v, w) on $[0,1]$ using the corresponding cumulative density function U_i. The second stage involves calibrating the multivariate distribution $G(x, y, z)$, such that $C(u, v, w) \overset{\text{def}}{=} G(U_1^{-1}(x), U_1^{-1}(y), U_1^{-1}(z))$, where $\mathbb{C}$ denotes the copula. An interesting feature of this multivariate distribution is the covariance matrix as it illustrates the multivariate dependencies. **In our analysis, we explore a relatively similar framework, which also involves time-varying volatility parameters. This proves a tractable approach as to capture the dynamics of historical volatilities, though obviously at a certain cost of greater computational complexity.**

Graph 10. 3-dimensional dataset with different empirical distributions

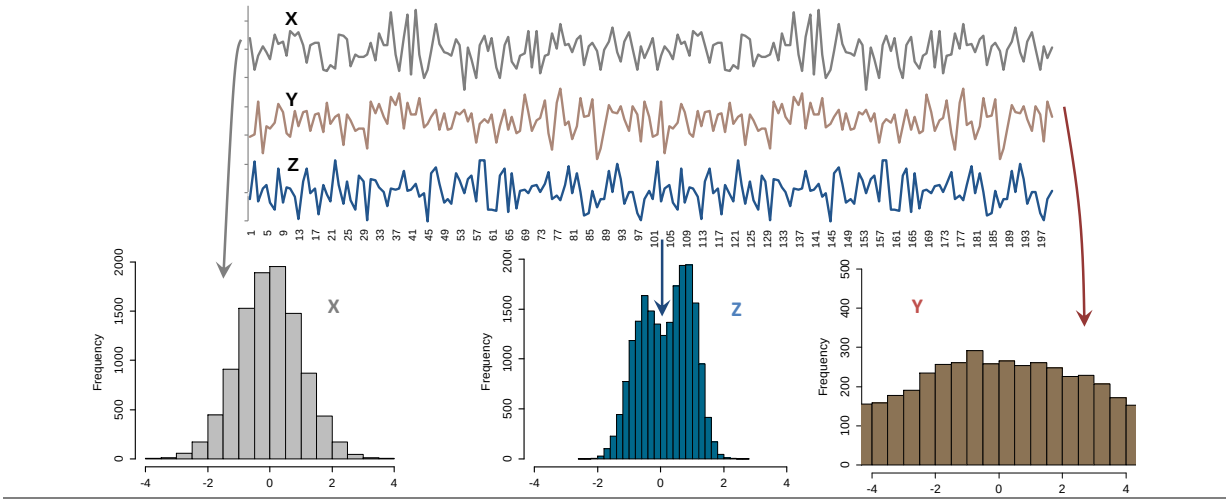

A meaningful benefit when working with copulas is that the dataset can be composed of time series with much dissimilar densities (ie. different standard deviations, kurtosis or skewness like in Graph 10). This dissimilarity usually is a drag as common correlation measures prove unable to reflect

underlying non-linear linkages between each series. **Copulas in contrast offer interesting insight on that front, and help overcome this limitation:** assuming that the copula is properly calibrated, it becomes a powerful tool to assess the links that tie series altogether. While there are no theoretical boundaries on the dimension of the sample, a problem of higher dimension leads to a non-linear expansion of the calculation time – ultimately this could turn to be an obstacle to frequent recalibrations of the model.

The various stages for copula calibration are listed below; the steps are detailed in the following paragraphs:

1) **Choice of the model for the marginal distribution**
2) **Calibration of the univariate distributions**
3) **Assess the quality of the calibrated marginals**
4) **Standardization of the data into uniformly distributed variables**
5) **The multivariate analysis.**
6) **Assess the quality of the calibrated multidimensional distribution**
7) **How to use the copula: an event oriented tool**.

As to improve clarity, let us consider a basket of three random variables X, Y, Z. Our aim is to understand the joint behaviour of these three series as time t goes by:

$$\begin{Bmatrix} X_1 & Y_1 & Z_1 \\ X_2 & Y_2 & Z_2 \\ \vdots & \vdots & \vdots \\ X_L & Y_L & Z_L \end{Bmatrix} \quad (t = 1 \ldots L \text{ in this example})$$

1) Choice of a distribution function for the marginals. The first step in copula estimation is to look at each time series separately, and to calibrate the corresponding univariate probability density functions (denoted f_i, with the cumulative version F_i). In practice, one has to find the most appropriate analytic expression of the density for every time series, so that the selected distribution function offers a satisfactory calibration against the empirical observations. Classical densities like the Gaussian, t-Student, mixed Gaussians, exponentials... are usual candidates that may fit the data sufficiently well. However, one may have to fulfil specific needs like the presence of a large skewness or a peculiar shape at some places of the distribution. Observing the empirical distribution of the sample in this context can help make an appropriate choice, which sometimes necessitates more complex formulations than common distributions. **In this paper we compare various candidates for the univariate probability function. Better results have been obtained with Generalized Hyperbolic t-Student functions that proved particularly efficient to capture fat tails in the dataset.**

2) Calibration of the univariate distributions. Once the potential candidates for the univariate probability distribution function have been chosen, the calibration of each distribution will deliver the set of optimal parameters (variance, skewness, average value...). But before that, another crucial choice must be done: do we assume fixed or time varying parameters? Both methods have their own benefits and limitations, that we explore below.

Graph 11. Fixed parameter univariate distributions

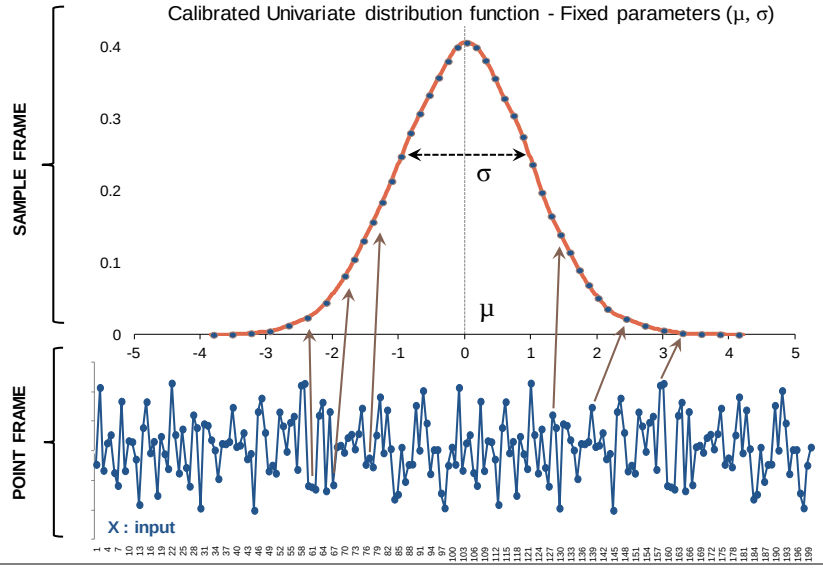

The first scenario assumes fixed parameters. In this case the calibration is more straightforward; overall this is an easy way to estimate the dynamics of the data. And since the parameters are valid descriptors for the whole dataset, we are usually left with a limited number of unknowns to calibrate. That ensures lighter computational needs and therefore a faster calibration. Moreover, fixed parameters reduce the complexity of the algorithm, by the use of adequate approximations e.g. relative to the calculation of statistical moments. This may also allow us to use higher dimensional copulas. Less engaging, fixed parameters are much less flexible than a time-varying approach: the data must follow the assumed dynamics, with very limited room for any deviation from the expected shape. This can be seen also in the fact that the parameters within the distribution remain unchanged regardless of the period under consideration in the sample. In other words, the microstructure of the input has to be relatively stable regardless of time and independently of the sample size. This assumption may be a challenge, especially when exploring the price action in financial markets through the recent episodes of crises. This scenario implies considering every point in the sample as belonging to the same distribution (Graph 11).

In comparison, allowing for time varying parameters offers greater flexibility. Adaptive parameters have proved an interesting way to capture the changing dynamics as time goes by. For instance periods with jumps in the volatility are more effectively captured when the variance parameter is time-varying. But the complexity of the calibration also rises meanwhile, as the dynamics of the volatility (in this case) needs to be modelled, for instance via a GARCH/ARCH or a VAR model. This usually adds a few unknowns to the problem, with the risk of making convergence more difficult to reach during the calibration. The overall benefit all the same is that a properly calibrated volatility model must be able to fit periods of very dissimilar volatility in the sample, hence the greater flexibility than before (Totouom Tangho, Armstrong (2007a), and Totouom Tangho, Armstrong (2007b).

Graph 12. Conditional distributions with time varying parameter

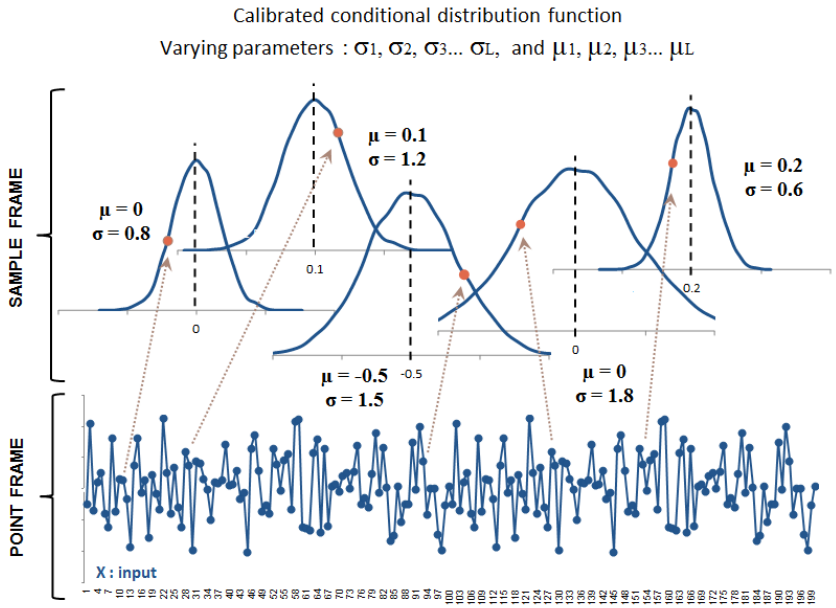

Other kind of volatility models may also be chosen, like kernels, regime switching models, filtering techniques (Javaheri, Lautier, Galli (2003)), or probabilistic distributions (e.g. one can assume the distribution of the parameter in the sample). **Under varying parameters, every point in the data is seen as belonging to its own and particular distribution, based on the respective value of each parameter, only valid at this specific place in the sample** (Graph 12). While calibrating time-varying parameters, the calibration algorithm also looks at the global fit that the assumed marginal offers, and obviously tends to minimize the error. In this scenario, the higher computational burden may restrict the dimension of the copula as the calibration is much more demanding in terms of calculations compared to fixed parameter models. **The probabilistic model we explore in this report belongs to this category of models as we assume a time-varying volatility. And because our volatility estimator involves an autogressive coefficient, the probability distribution function we obtain is actually conditional on the immediate realisation in the past. We thus denote is** $p(x|x_{i-1})$.

3) Assess the quality of the calibrated marginals. The calibration of the univariate marginals is supposed to deliver the optimal combination of parameters, ie. those that provide the best fit to the empirical observations. In practice, there is a significant risk for the calibrated parameters to be just a "local" optimum, instead of a "global" solution to the minimisation problem. In this case, there may be other combinations for these parameters that would deliver a smaller error. To avoid being stuck in such a local extremum we ran the calibration 20 times with different initial values, and this increased the chance of getting a global solution. Out of the resulting 20 combinations of optimal parameters, we then selected the distribution that offers the best fit. Our decision relies on three estimators of the goodness of fit: first we consider two statistical tests, the Anderson Darling criterion (ADC) and the Probability Integral Transform (PIT). Finally we take a look at the deviation between the calibrated variance and the rolling standard deviation of the data.

PIT and ADC which are relatively similar tests. These estimators look at the values of the calibrated cumulative distribution function F (see eq. (1)) evaluated on the sample points $(x_1, .. x_L)$. **If the calibrated distribution properly fits the data, the set composed of** $\{F(x_1), F(x_2), \dots, F(x_L)\}$ **must**

be uniformly distributed (eq.(2) and eq. (3)). The PIT and the ADC tend to observe and quantify the deviation from this assumption. In the case of conditional distributions, the PIT test is known as CPIT (Conditional Probability Integral Transform).

Non conditional case – Univariate marginal: $F(x_i) = \int_{-\infty}^{x_i} p(x)\,dx$ (2)

Conditional case – Univariate marginal: $F(x_i|x_{i-1}) = \int_{-\infty}^{x_i} p(x|x_{i-1})\,dx$ (3)

Graph 13. Understanding the PIT and CPIT histogram test

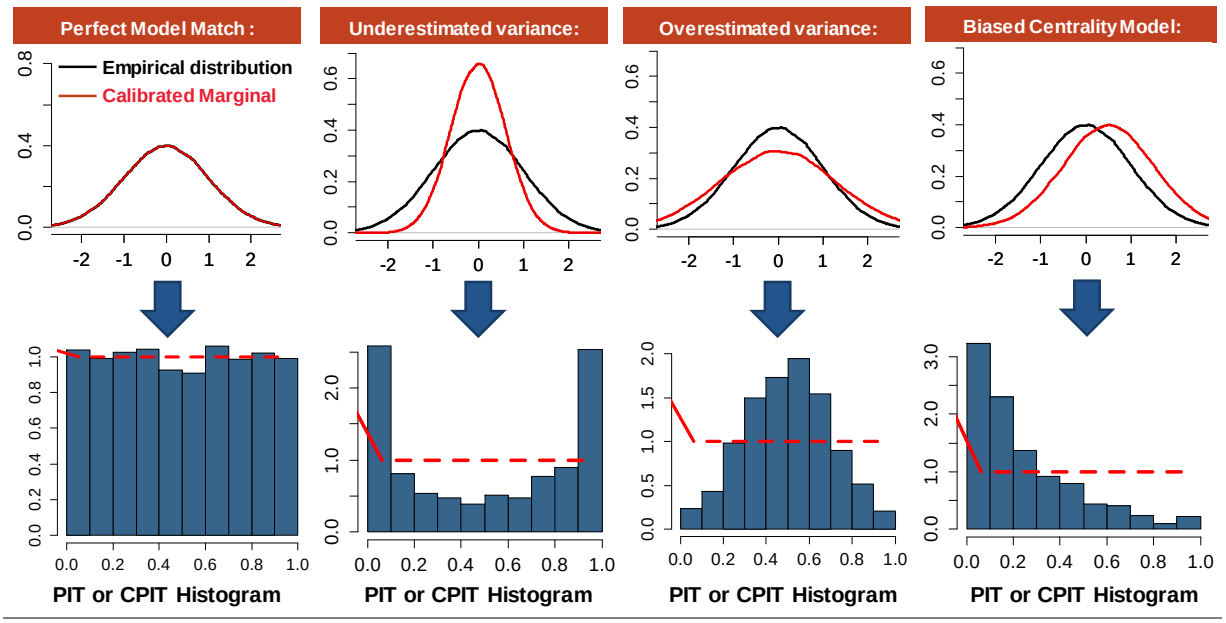

The PIT or CPIT is a bar chart exhibiting the distribution of $\{F(x_1), F(x_2), \dots, F(x_L)\}$. As we mentioned above, the points – if properly calibrated - should be uniformly distributed. So any deviation in the bar chart from the expected uniform distribution (red dashed line in Graph 13) **illustrates some error in the calibration of the univariate distribution.** This is a powerful and refined assessment of the goodness of fit as the user can precisely identify the areas where the error is more substantial. In particular the PIT (or CPIT) are very convenient to understand whether the error tends to be concentrated more in the centre of the distribution or, in a worst case given the context of this analysis, in the tails of the distribution. An interesting point too is that the PIT/CPIT reveals if the error consists of an underestimate or an overestimate of the density in the concerned areas - Graph 13 shows the related methodology. Singular errors could also be rapidly identified via this approach, like an asymmetric error that could be spread on just one side of the distribution. In this case the PIT could suggest that some skewness in the dataset has not been captured by the calibration (Graph 13). In comparison, most of statistical tests supposed to measure the goodness of fit are usually not able to deliver such accurate information on the fit.

In addition to this graphical assessment, we consider the Anderson-Darling criterion (ADC). This statistical test involves $\{F(x_1), F(x_2), \dots, F(x_L)\}$ too, and the resulting p-value is a quantification of the deviation from the (expected) uniform distribution. The special benefit of using the ADC resides in the fact that the test gives a much bigger weight to the tail regions in comparison to the centre of the distribution. The higher sensitivity in the tails is a notable upside in the context of sovereign risk exploration given that contagion is essentially at work in the tails of the distribution. The equation

(4) displays the calculation of the ADC (Anderson and Darling (1952), Press et al. (1991), and Elliott (1998)):

$$ADC^2 = -L - \frac{1}{L}\sum_{j=1}^{L}(2j-1)(ln\, V_j + ln(1 - V_{L-j+1})) \quad (4)$$

where $\{V_j\}$ is the sorted version of $\{F(x_j)\}$, in ascending order. The hypothesis that the marginal is uniformly distributed must then be rejected if this resulting p-value is too high. So far, we considered a criterion of 2.5 as an acceptable threshold for rejection. This corresponds to a significance level of about 5% and thus looks reasonable (Table 34).

Table 4. Significance level with respect to the p-value resulting from the Anderson-Darling test

Significance Levels	Critical Values
0.10	1.933
0.05	2.492
0.01	3.857

We also consider an additional test based on the variance of the resulting marginal. Intuitively, we consider the two-week rolling standard deviation as a benchmark for the expected volatility coefficient. We thus take the distance between both indicators as a measure of the volatility error. This proved helpful to establish how much the estimated marginal effectively captures the dynamics of the empirical volatility. **Using these three observations of the goodness of fit, we can select the best marginal function out of the 20 calibrations.**

4) Standardization of the data into uniformly distributed variables.

The success of copula is largely attributable to its capacity to seize non-linear multivariate dependencies. These dependencies are said to be 'non linear' because the procedure involves a non-linear 'change of frame' of the original data into a new frame where it is assumed that it is more convenient to capture the multivariate dependencies. Usually, the transformation is made such that each time series is distributed according to the same distribution g in the new frame, as indicated in eq. (5). In this case G is the cumulative distribution function of the density g. In this analysis specifically, the whole transformation is just a standardisation of the dataset, as G is the standard (and centred) version of Generalised Hyperbolic t-Student distributions.

$$z_t = G^{-1}\big(F(x_t)\big) \quad (5)$$

Table 5 summarizes the different steps of the calibration procedure, including the aforementioned 'change of frame' (standardisation in our case). **This step completes the univariate analysis.** In what follows we consider the new dataset $(\theta, \varphi, \gamma)$ that results from this transformation(see Table 5).

Table 5. Summary of the standardization process that transforms the original dataset into a standard frame

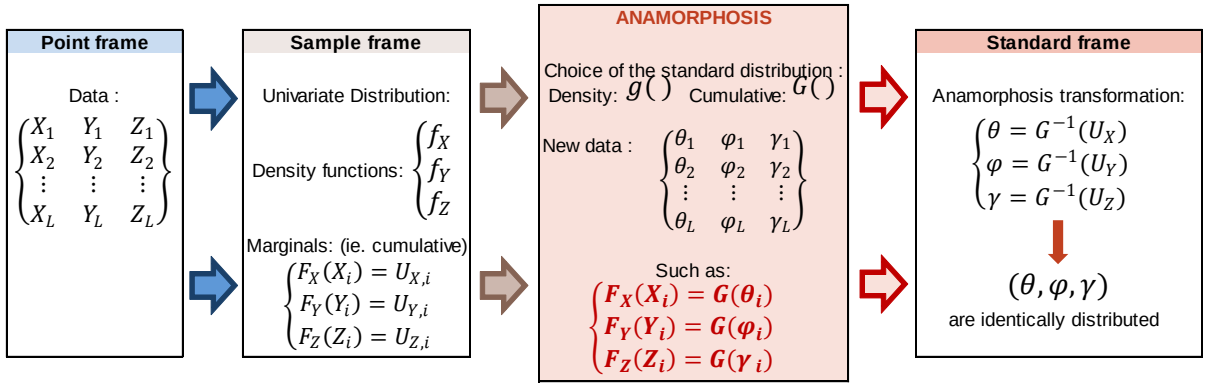

5) The multivariate analysis. Since the data was standardized in the last step of the univariate analysis, the resulting series are distributed according to a standard distribution, which is known. This is helpful information obviously as the multivariate distribution that is supposed to describe the joint behaviour, is assumed to be of the same kind. **We now seek to calibrate the multivariate distribution.** The main purpose of the multivariate calibration is to provide an adequate estimation of the multivariate dependencies. And in particular a parameter that requires extensive care is the covariance matrix. Once again, the covariance matrix can be formulated either as a fixed or time-varying parameter (Graph 14).

Graph 14. Multivariate calibration with varying parameters – example based on a 2-dimensional copula

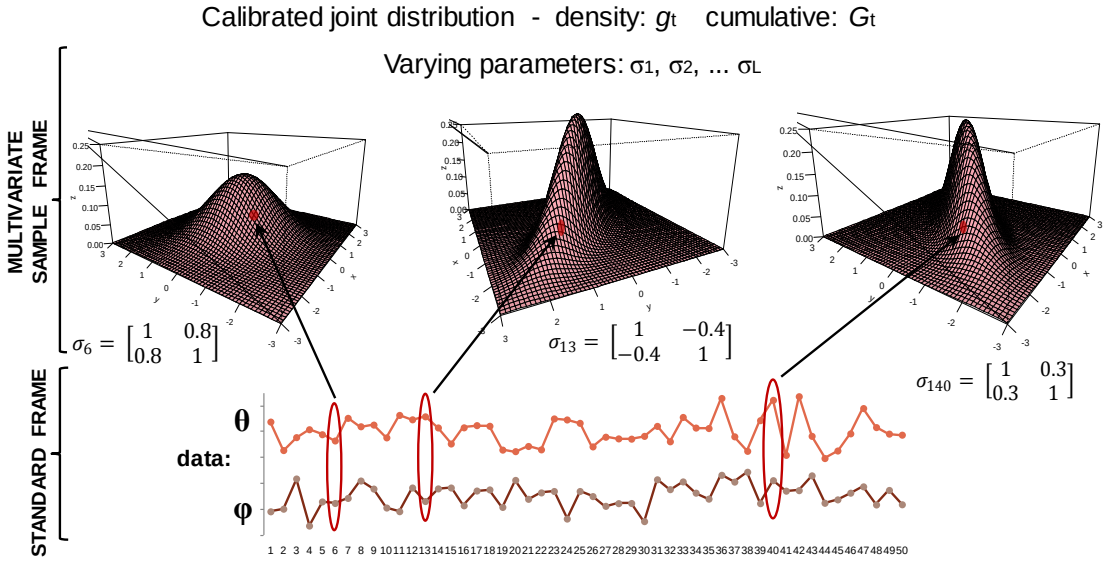

Although our approach assumes a time-varying covariance matrix, we will meet both cases in the following analysis. For better clarity, Graph 14 summarizes the steps of the multivariate calibration under time-varying parameters for a bivariate copula. Since the data has been previously standardised, we can write that $Var(\theta) = Var(\varphi) = Var(\gamma) = 1$. **So in this specific case, the covariance matrix is in fact a measure of multivariate correlations.**

6) Assess the quality of the calibrated multivariate distribution. Like in step 3) we ran the calibration procedure 20 times to avoid selecting parameters that only refer to a local optimum. In order to identify the best combination, we consider the PIT and ADC again as relevant measures of the goodness of fit. **Based on the same rules as in the univariate analysis, the two tests indicate which combination provides the best fit. In the end, a copula is entirely characterized by both univariate marginals and the corresponding multivariate distribution.**

Generalized Hyperbolic distributions

Our analysis relies to a great extent on Generalized Hyperbolic t-Student distributions. These are extensively investigated in Rachev (2003), Bibby, Sorensen (2003), Eberlein & Keller (1995), Bibby & Sorensen (1997), Hurst (1997), Eberlein, Keller & Prause (1998), Rydberg (1999), Kuchler et al. (1999), Jiang (2000), and Barndor-Nielsen & Shephard (2001). In this report we explore a multivariate model on 5-year European sovereign CDS spreads. At both univariate and multivariate levels, we assume that our variables are distributed according to Generalized Hyperbolic (GH) t-Student distributions. We explore their formulation in the next paragraphs.

Generalized Hyperbolic (Skewed) t-Student

Definition. Generalized Hyperbolic distributions were introduced in Barndorff-Nielsen (1977) as a novel means to illustrate empirical findings in geology. As the tail behaviour of the whole class of GH distributions spans a large range, from Gaussian tails via exponential tails to the power tails of the t-distributions, these distributions became increasingly popular, especially in finance due to their ability to capture tail events. In our analysis, we will focus on t-Student GH distribution which is a subset of all GH distributions, regarded as an appropriate choice for credit risk exploration (see Zhang, Schwaab, Lucas (2012a), Zhang, Schwaab, Lucas (2012b), Creal, Koopman, Lucas (2009)).

A multivariate vector X of k random variables is said to follow a multivariate GH distribution if:

$$X = \mu + W.\gamma + \sqrt{W}.A.Z \tag{6}$$

Where: $Z \sim N_k(0, I_k)$ with $N_k(0, I_k)$ referring to the k-dimensional standard Gaussian.

$A \in \mathbb{R}^{d \times k}$

$\mu, \gamma \in \mathbb{R}^d$

$W \geq 0$ is a scalar-valued random variable which is independent of Z and W, which admits a Generalized Inverse Gaussian distribution $GIG(\lambda, \chi, \psi)$. Based on Breymann, Luthi (2013), there are at least five other alternative definitions of the GH distributions.

Parameters describing a GH distribution have the following statistical meaning:

- λ, χ, ψ determine the shape of the distribution. These parameters determine the weight assigned to the tails and to the central part. The larger these numbers the closer the distribution is to the normal distribution.
- μ is the location (or mean) parameter.
- $\Sigma = A.A^T$ is the dispersion matrix.
- γ is the skewness parameter. If $\gamma = 0$ then the distribution is symmetric around μ.

It is also worth noting that the conditional distribution of $X|W = w$ is normal:

$$X|W = w \sim N_d(\mu + w, w\Sigma) \quad \text{with} \quad \Sigma = A.A^T$$

Descriptive statistics. The expected value and the variance are given by:

$$\mathbb{E}[X] = \mu + \mathbb{E}[W].\gamma$$

$$Var(X) = \mathbb{E}[cov(X|W)] + cov(\mathbb{E}[X|W]) = var(W).\gamma.\gamma^T + \mathbb{E}[W].\Sigma \tag{7}$$

Density. The GH density function is derived on the fact that the conditional distribution of X given W is Gaussian with mean $\mu + W \times \gamma$ and variance $W \times \Sigma$:

$$p_X(x) = \int_0^\infty f_{X|W}(x|w) f_W(w) dw = \int_0^\infty \frac{e^{(x-\mu)^T \Sigma^{-1} \gamma}}{(2\pi)^{\frac{d}{2}} |\Sigma|^{\frac{1}{2}} w^{\frac{d}{2}}} \exp\left(-\frac{Q(x)}{2w} - \frac{\gamma^T \Sigma^{-1} \gamma}{\frac{2}{w}} \right) f_W(w)\, dw$$

$$= \frac{\left(\sqrt{\frac{\psi}{\chi}}\right)^\lambda (\psi + \gamma^T \Sigma^{-1} \gamma)^{\frac{d}{2}-\lambda}}{(2.\pi)^{\frac{d}{2}} |\Sigma|^{\frac{1}{2}} K_\lambda(\sqrt{\chi.\psi})} \times \frac{K_{\lambda-\frac{d}{2}}\left(\sqrt{(\chi + Q(x)).(\psi + \gamma^T \Sigma^{-1} \gamma)} \right) e^{(x-\mu)^T \Sigma^{-1} \gamma}}{\left(\sqrt{(\chi + Q(x))(\psi + \gamma^T \Sigma^{-1} \gamma)} \right)^{\frac{d}{2}-\lambda}}$$

Where K_λ is the modified Bessel function of the third kind and $Q(x)$ denotes the Mahalanobis distance.

$$Q(x) = (x - \mu)^T \Sigma^{-1} (x - \mu)$$

Special cases of the GH distributions. The properties of GH distributions tend to vary depending on the value of each parameter. A few particular cases are worth to mention:

- If $\lambda = \frac{d+1}{2}$ the probability function loses its *generalized* characteristics to become only "hyperbolic" distributions. That said, the univariate margins are still GH distributed. Conversely, when $\lambda = 1$ we get a multivariate GH distribution with hyperbolic margins.
- If $\lambda = -\frac{1}{2}$ the distribution simplifies into a *Normal Inverse Gaussian* (NIG).
- $\chi = 0$ and $\lambda > 0$ is a particular parametrization of the GH distributions, known as Variance Gamma (VG) distribution.
- If $\psi = 0$ and $\lambda < 0$ one obtains a Generalized Hyperbolic Student-t distribution, possibly skewed. Our copula model merely relies on this particular expression. Let us now take a look at the parameterization of this specific sub-category of distributions.

Generalized Hyperbolic Student-t distributions. Based on the properties of the third order Bessel function, it can be shown that when $\psi \to 0$ and $\lambda < 0$ the density of a GH distribution is:

$$p_X(x) = \frac{\chi^{-\lambda} (\gamma^T \Sigma^{-1} \gamma)^{\frac{d}{2}-\lambda}}{(2.\pi)^{\frac{d}{2}} |\Sigma|^{\frac{1}{2}} \Gamma(-\lambda).\, 2^{-\lambda-1}} \times \frac{K_{\lambda-\frac{d}{2}}\left(\sqrt{(\chi + Q(x)).\gamma^T \Sigma^{-1} \gamma} \right) e^{(x-\mu)^T \Sigma^{-1} \gamma}}{\left(\sqrt{(\chi + Q(x))(\gamma^T \Sigma^{-1} \gamma)} \right)^{\frac{d}{2}-\lambda}}$$

When $\gamma \to 0$ we obtain the symmetric multivariate Student-t density:

$$p_X(x) = \frac{\chi^{-\lambda}.\, \Gamma\left(-\lambda + \frac{d}{2}\right)}{\pi^{\frac{d}{2}} |\Sigma|^{\frac{1}{2}} \Gamma(-\lambda)} \times \left(\chi + Q(x)\right)^{\lambda - \frac{d}{2}}$$

We then switch to the Student-t parameterization (CITA.) and set the degree of freedom $\nu = -2\lambda^2$. Because $\psi = 0$ the transformation of $\overline{\alpha}$ to χ and ψ reduces to:

$$\chi = \overline{\alpha} \frac{K_\lambda(\overline{\alpha})}{K_{\lambda+1}(\overline{\alpha})} \xrightarrow{\overline{\alpha} \to 0} 2(-\lambda - 1) = \nu - 2$$

Plugging in the values for λ and ν, one finally obtains the formulation of the **skewed version** of Generalized Hyperbolic Student-t distributions (that we shorten as 'GHST'):

$$p_X(x) = \frac{(\nu-2)^{\frac{\nu}{2}}(\gamma^T\Sigma^{-1}\gamma)^{\frac{\nu+d}{2}}}{(2.\pi)^{\frac{d}{2}}|\Sigma|^{\frac{1}{2}}\Gamma\left(\frac{\nu}{2}\right).2^{\frac{\nu}{2}-1}} \times \frac{K_{\frac{\nu+d}{2}}\left(\sqrt{(\nu-2+Q(x)).\gamma^T\Sigma^{-1}\gamma}\right)e^{(x-\mu)^T\Sigma^{-1}\gamma}}{\left(\sqrt{(\nu-2+Q(x))(\gamma^T\Sigma^{-1}\gamma)}\right)^{\frac{\nu+d}{2}}} \quad (8)$$

And for the symmetric case, which does not allow for the skewness ($\gamma \to 0$) we obtain:

$$p_X(x) = \frac{(\nu-2)^{\frac{\nu}{2}}.\Gamma\left(\frac{\nu+d}{2}\right)}{\pi^{\frac{d}{2}}|\Sigma|^{\frac{1}{2}}\Gamma\left(\frac{\nu}{2}\right)(\nu-2+Q(x))^{\frac{\nu+d}{2}}} \quad (9)$$

In this case we denote it 'GHT'.

It is worth to note that the variance of GHT and GHST distributions exists only if the degrees of freedom parameter is higher than 4. In what follows we set $\nu = 5$.

Both distributions in eq. (8) and eq. (9) are those we explored in depth in this dissertation. We describe in particular the calibration of the required parameters, and we observe the benefits of using such distributions in the context of sovereign risk exploration.

Chapter I.

Joint dependencies within European sovereign CDS spreads

Résumé du Chapitre I

Le Chapitre I est dédié à la compréhension de la dynamique générale des obligations souveraines Européennes. Notre approche implique un échantillon incorporant à la fois des épisodes de crises et donc d'aversion au risque intense, ainsi que de périodes marquées par un fort appétit pour le risque.

Nous considérons un modèle probabiliste impliquant des distributions à queues lourdes comme les distributions généralisées hyperboliques, de type t-Student. Afin de capturer la dynamique temporelle de la volatilité, notre modèle se base sur la méthode du score généralisé autorégressif (GAS) introduit par Creal, Koopman, Lucas (2011). Cette approche découle de la théorie des modèles GARCH et implique un terme d'ajustement supplémentaire qui rend le modèle particulièrement flexible.

L'ajustement obtenu avec les distributions Hyperboliques Généralisées est robuste, et les résultats laissent penser que notre approche est particulièrement efficace durant les périodes marquées par une volatilité erratique. Dans un but de simplification, nous décrivons la mise en place d'un estimateur de volatilité intemporel, sensé refléter la volatilité intrinsèque de chaque obligation. Cet estimateur suggère que la volatilité croît de manière quadratique lorsque celle-ci est exprimée en fonction de la fonction de répartition des variations de rendements. Dans un second temps nous explorons une version bivariée du modèle. La calibration, robuste, met en valeur les corrélations entre chaque obligation. En guise d'observation générale, notre analyse confirme que les distributions à queues épaisses sont tout à fait appropriées pour l'exploration des prix de marché en période de crise financière.

Introduction

Risk aversion, by nature, translates into both a depreciation of risky assets and a richening of these securities, perceived as safer. However, empirical observations indicate that this general behaviour does not hold when financial distress exceeds a certain degree of intensity: in this case, the flight to safety is so high that it tends to alters investors' perception quite significantly. This usually leads to a disproportionate loss of confidence, which translates into a generalised liquidation of long positions in portfolios, including on assets that look logically disconnected from shocks that gave rise to the crisis. Herd behaviour amongst investors is also extremely fierce under such circumstances, and this reinforces the global nature of the liquidation, thus favouring a general squeeze of the market liquidity. In the end, the global dimension of the observed price deterioration indicates that correlations during the sell-off are remarkably stronger than in more normal market conditions. The natural resilience of safe-haven securities in particular, is usually questioned during these periods, as financial contagion, beyond a certain level, tends to propagate into all marketable asset classes.

In this chapter, we describe the calibration of a multivariate statistical framework dedicated to the exploration of financial contagion during the European sovereign crisis. The model involves Generalised Hyperbolic distributions, on the basis that these distributions are able to capture fat tails in the data. Plus we consider an adjusted version of the Generalised Autoregressive Score (GAS) method to model the dynamics of the volatility. Our goodness-of-fit estimator puts a special emphasis on the tail regions of the distribution; this helps ensure that the specific behaviour of financial securities under heavy contagion is properly addressed in our methodology.

While the GAS method proves sufficiently flexible to capture the sharp variations in the volatility throughout the period, the resulting coefficient is conditional on immediate realisations in the past. This makes a high-frequency manipulation of the model relatively cumbersome; so we design a non-temporal volatility estimator that simplifies the calculations. The resulting non-conditional distributions make sense from a statistical point of view, and we show that intrinsic volatilities accelerate in a parabolic fashion when risk aversion intensifies.

Finally, we explore the market response to financial shocks. The high degree of granularity helps us identify a threshold – common to all sovereigns - beyond which the price reaction is sharply non-linear. This illustrates the confidence crisis taking over, and the price deterioration one can expect in such a configuration.

Univariate analysis: calibration of the marginals

Our dataset is made of daily price variations of 5-year European sovereign CDS spreads for the period from 1 January 2008 to 31 December 2016 (2230 points, Graph 15). This includes Germany, Finland, the Netherlands, Austria, France, Belgium, Italy, Spain, Ireland, Portugal and the UK. Because of no CDS prices around the default in 2012, as well as between March and May 2013, Greece is not involved in the first part of the analysis. The very low liquidity on Greek CDS during the period also makes the data very challenging to exploit; another reason to exclude Greece in this first chapter. That said, Greece is a very interesting candidate for sovereign risk exploration, so we introduce it in the second chapter, where we consider asset swaps spreads (instead of CDS spreads).

Graph 15. Our dataset of 5Y sovereign European CDS spreads

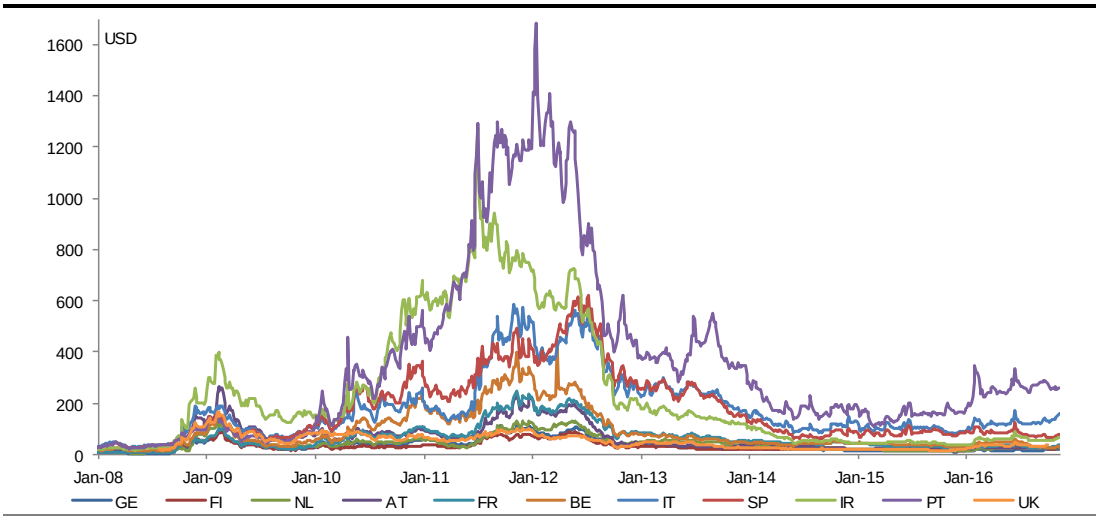

Empirical analysis of the data

Table 6 shows the descriptive statistics of the sample. The standard deviation first, consistently increases as the credit quality deteriorates, ie. from Germany to Portugal, with the UK very comparable to core countries. The sample mean is also very small (less than 1% of standard dev), **and it looks reasonable to assume that our series are centred on zero.**

The third and fourth order moments, in Table 6, show that the excess kurtosis is larger for non-core countries. This suggests that the tails of the distribution are bigger for these more volatile countries. **The skewness parameter highlights just very little asymmetry** in general, slightly positive for most of the countries. If anything, this points to a slightly higher concentration of points on the lower part of the distribution, ie. for $x_{i,t} \leq 0$

Table 6. Descriptive Statistics of the data (CDS daily changes from Jan-2008 to Dec-2016)

Original CDS Changes	Germany	Finland	Netherlands	Austria	France	Belgium	Italy	Spain	Ireland	Portugal	UK
Mean	0.007	0.008	0.009	0.011	0.013	0.009	0.062	0.029	0.024	0.106	0.018
Standard deviation	1.8	1.4	2.3	3.8	3.3	7.2	10.1	9.1	13.2	19.4	2.1
Excess Kurtosis	10.3	13.3	19.5	26.8	13.5	13.5	30.7	27.5	32.0	28.5	11.9
Skewness	0.1	0.7	1.1	1.4	-0.2	2.3	0.3	-0.4	0.2	0.2	0.8

Graph 16. Similar kurtosis within the core countries.

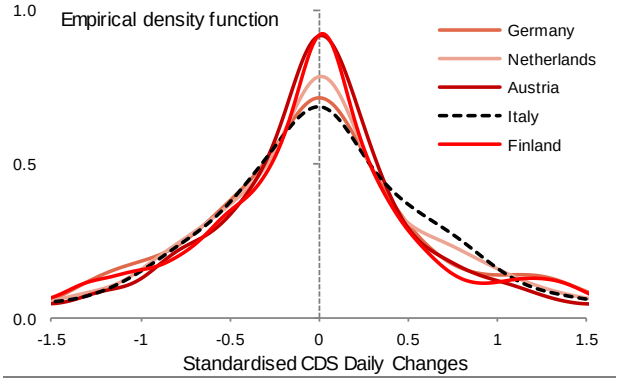

Graph 17. Soft core and non core data

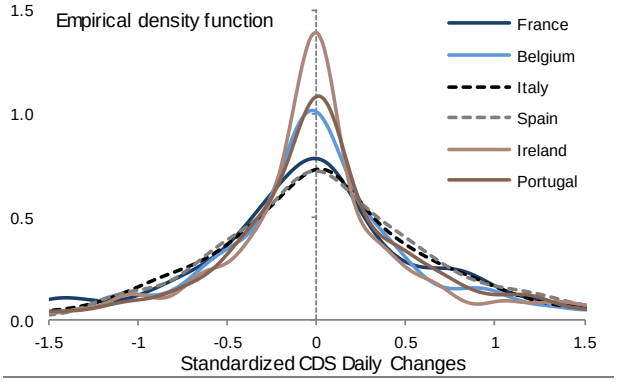

As to observe these dissimilarities in terms of skewness and kurtosis, we plot a standardised version of the empirical densities in Graph 16 and Graph 17. Graph 16 shows that effectively core CDS are very similar in terms of probability distribution functions. Then in Graph 17, the larger kurtosis in soft-and non-core countries translates into a larger density at the centre of the distribution, and in the tails as well. We also compute a series of **Kolmogorov tests,** supposed to reflect the degree of similarity between empirical distributions and the more common distribution functions: Uniform, Normal, Poisson, t-Student, Exponential, Gamma, Beta, Cauchy, Chi-2, Weibull, Lognormale, and Logistic laws. **As Table 7 shows, we got significant p-values for t-Student and Cauchy distributions only**.

Table 7. p-values of the Kolmogorov tests relative to common distributions

	Germany	*Netherlands*	*Austria*	*France*	*Belgium*	*Italy*	*Spain*	*Portugal*	*Ireland*
Student	0.27	0.03	3.65	0.01	0.11	0.60	0.58	0.13	0.04
Cauchy	0.17	0.33	0.66	0.31	0.13	0.08	0.06	0.47	0.50

As a means to gauge stationarity, we compute the acf and pacf for each country. We see a fast convergence towards zero in the bars, which is a sign that the data is stationary. Bars are all below 0.15, except at the lag 1**,** for which we get a peak at 0.2 in Graph 18 and Graph 19. ➔ **This suggests that there is potentially a first order autocorrelation** ($\Delta t = 1$)**, overall illustrating the persistence of momentums in the volatility.** The augmented Dickey-Fuller (DF) test also confirms the rejection of the unit-root hypothesis, and so for every country (Table 8).

Table 8. Augmented Dickey-Fuller statistics are largely negative, confirming no unit root

	Germany	*Netherlands*	*Austria*	*France*	*Belgium*	*Italy*	*Spain*	*Portugal*	*Ireland*	*UK*
DF Statistics	-7.17	-7.87	-7.18	-7.71	-6.46	-7.51	-7.85	-6.06	-6.06	-6.22

Graph 18. Autocorrelogram (acf) of Germany

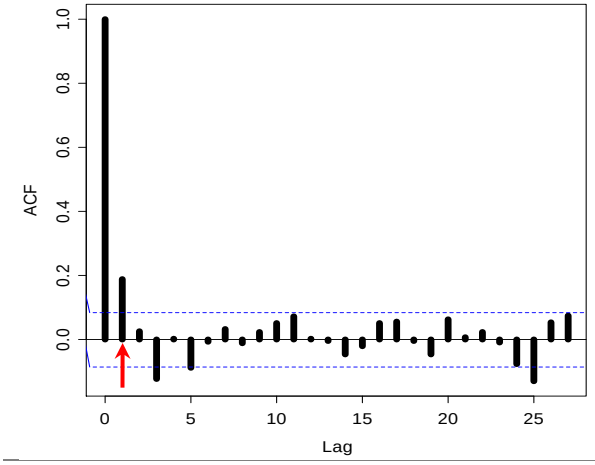

Graph 19. Partial autocorrelogram (pacf) of Germany

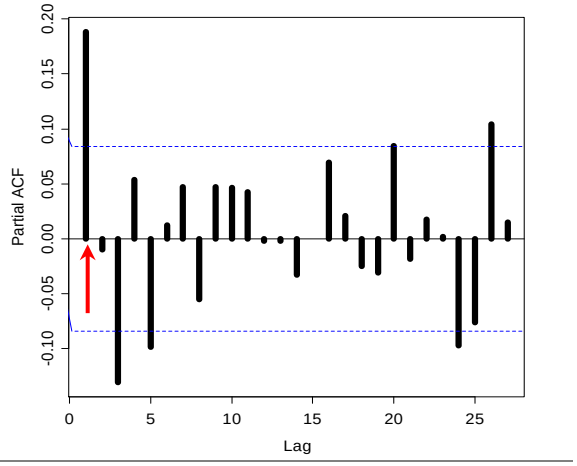

To get a basic understanding of the multivariate interdependencies, we also calculate the sample correlation matrix (Pearson Product-moment) defined as:

$$\rho^{i,j} = \widehat{\mathrm{Cor}}(z^i, z^j) = E(z^i . z^j) - E(z^i).E(z^j) \qquad (10)$$

Where E is the sample mean.

Table 9. Empirical correlation $\rho^{i,j}$

$\rho^{i,j}$	COUNTRY 1										
COUNTRY 2	GE	FI	NL	AT	FR	BE	IT	SP	IR	PT	UK
GE		0.71	0.70	0.68	0.80	0.72	0.62	0.61	0.51	0.46	0.64
FI	0.71		0.67	0.68	0.68	0.67	0.60	0.60	0.55	0.48	0.64
NL	0.70	0.67		0.69	0.69	0.70	0.62	0.58	0.55	0.42	0.60
AT	0.68	0.68	0.69		0.74	0.74	0.62	0.64	0.60	0.45	0.61
FR	0.80	0.68	0.69	0.74		0.76	0.66	0.65	0.59	0.50	0.61
BE	0.72	0.67	0.70	0.74	0.76		0.73	0.75	0.60	0.54	0.63
IT	0.62	0.60	0.62	0.62	0.66	0.73		0.87	0.63	0.63	0.59
SP	0.61	0.60	0.58	0.64	0.65	0.75	0.87		0.64	0.66	0.58
IR	0.51	0.55	0.55	0.60	0.59	0.60	0.63	0.64		0.58	0.54
PT	0.46	0.48	0.42	0.45	0.50	0.54	0.63	0.66	0.58		0.39
UK	0.64	0.64	0.60	0.61	0.61	0.63	0.59	0.58	0.54	0.39	

Table 24 shows the resulting coefficient. A first observation is that the correlation is more important for core and soft-core than peripherals countries and the UK. Portugal in particular exhibits just 0.51 correlation with other countries, on average, while this amounts to 0.65 and 0.67 for Germany and France in comparison.

As we argue in the literature review, the empirical correlation coefficient $\rho^{i,j}$ experience some limitations. First, the correlation coefficient $\rho^{i,j}$ is constrained if the data does not have a normal distribution (see Hsu (2012)). This is a recurring caveat when working with financial returns given the presence of fat tails that make the data non-Gaussian (Ang and Chen (2002); Boyer et al. (1999); Kolari et al. (2008)). In this case, $\rho^{i,j}$ tends to undermine the actual level of correlation. Drawing correlation estimators out of Generalized Hyperbolic distributions is a possible means to address this limitation; something that we explore in great details in this report.

Another drawback of the sample correlation is relative to the volatility: the coefficient is no longer reliable when the volatility undertakes tough regime changes; and in particular when the variance

approaches infinity (McNeil, Frey, Embrechts (2005)). This can prove a serious burden as hedging these periods of very high volatility is critical for portfolio managers.

Rank correlations can prove an interesting alternative to the Pearson coefficient. These coefficients involve the order (or the "rank") of the points, as obtained once the sample is sorted (McNeil, Frey, Embrechts (2005)). Rank correlation also has the property of invariance under monotonic transformations as any transformation of that kind (including an anamorphosis) keep the rank of the points unchanged. Kendal Tau (ρ_τ) and Spearman Rho (ρ_S) are the most common indicators of rank correlations.

Kendall Tau, is a correlation estimator which measures the degree of concordance between two random variables z_t and $\tilde{z}_t$. Two pairs of observations in $\mathbb{R}^2$, denoted by (z_t^i, z_t^j) and $(\tilde{z}_t^i, \tilde{z}_t^j)$, are said to be concordant if $(z_t^i - z_t^i)(\tilde{z}_t^j - \tilde{z}_t^j) > 0$, and to be disconcordant if $(z_t^i - z_t^i)(\tilde{z}_t^j - \tilde{z}_t^j) < 0$. In the end we just compare the observed probability of concordance to the probability of discordance:

$$\rho_\tau^{i,j}(z_t^i, z_t^j) = P\left((z_t^i - \tilde{z}_t^i)(z_t^j - \tilde{z}_t^j) > 0\right) - P\left((z_t^i - \tilde{z}_t^i)(z_t^j - \tilde{z}_t^j) < 0\right) \quad (11)$$

This can also be expressed as an expectation:

$$\rho_\tau^{i,j}(z_t^i, z_t^j) = E\left(\text{sign}\left((z_t^i - \tilde{z}_t^i)(z_t^j - \tilde{z}_t^j)\right)\right) \quad (12)$$

Spearman Rho is another useful estimator, based on rank correlation as well. This estimator involves the rank of the data, as provided by its cumulative distribution function:

$$Rank_t^i = F(z_t^i) \quad (13)$$

Then the Spearman Rho is defined as the empirical correlation of the Ranks:

$$\rho_S^{i,j}(z_t^i, z_t^j) = \text{Corr}(Rank_t^i,\ Rank_t^j) = \text{Corr}\left(F(x_t^i), F(x_t^j)\right) \quad (14)$$

Both measures have many properties in common (Schmidt (2006)): obviously they take values in the range $[-1,1]$; both are equal to zero for independent variables. They return a value of 1 for the comonotonic case and -1 for the countermonotonic case.

We calculated Kendall's Tau and Spearman's Rho (eq. (11) and eq. (14)) on the sample; Table 10 and Table 11 show the results, with larger correlation in red, smaller in green and mild correlation in yellow. Both estimators return quite different values in absolute terms, with a significantly higher Spearman's Rho overall. Arguably, authors like in (Xu et al. (2010)) acknowledge that the three estimators $\rho^{i,j}, \rho_\tau, \rho_S$ are not equivalent in absolute terms. In particular they demonstrate that the following inequalities hold when the sample size becomes large (both are verified here):

$$\frac{3}{2}\rho_\tau - \frac{1}{2} \leq \rho_S \leq \frac{1}{2} + \rho_\tau - \frac{1}{2}\rho_\tau^2 \qquad \text{if } \rho_\tau \geq 0 \quad (15)$$

$$\frac{3}{2}\rho_\tau + \frac{1}{2} \geq \rho_S \geq \frac{1}{2}\rho_\tau^2 + \rho_\tau - \frac{1}{2} \qquad \text{if } \rho_\tau \geq 0 \quad (16)$$

Table 10. Kendall's Tau resulting from GHT distributions

$\rho_\tau^{i,j}$	COUNTRY 1 GE	FI	NL	AT	FR	BE	IT	SP	IR	PT	UK
GE		0.27	0.38	0.30	0.40	0.40	0.19	0.23	0.26	0.21	0.33
FI	0.27		0.29	0.28	0.28	0.32	0.29	0.24	0.30	0.17	0.23
NL	0.38	0.29		0.39	0.42	0.40	0.32	0.33	0.42	0.27	0.30
AT	0.30	0.28	0.39		0.37	0.50	0.37	0.37	0.37	0.30	0.26
FR	0.40	0.28	0.42	0.37		0.50	0.39	0.39	0.42	0.30	0.31
BE	0.40	0.32	0.40	0.50	0.50		0.36	0.35	0.40	0.25	0.30
IT	0.19	0.29	0.32	0.37	0.39	0.36		0.75	0.52	0.63	0.27
SP	0.23	0.24	0.33	0.37	0.39	0.35	0.75		0.50	0.63	0.25
IR	0.26	0.30	0.42	0.37	0.42	0.40	0.52	0.50		0.47	0.24
PT	0.21	0.17	0.27	0.30	0.30	0.25	0.63	0.63	0.47		0.25
UK	0.33	0.23	0.30	0.26	0.31	0.30	0.27	0.25	0.24	0.25	

(COUNTRY 2)

Table 11. Spearman's Rho as another estimate of dependencies

$\rho_S^{i,j}$	COUNTRY 1 GE	FI	NL	AT	FR	BE	IT	SP	IR	PT	UK
GE		0.69	0.71	0.73	0.81	0.71	0.64	0.62	0.56	0.51	0.67
FI	0.69		0.65	0.7	0.68	0.66	0.63	0.62	0.58	0.53	0.65
NL	0.71	0.65		0.71	0.71	0.69	0.62	0.59	0.56	0.51	0.6
AT	0.73	0.7	0.71		0.77	0.79	0.7	0.68	0.62	0.57	0.66
FR	0.81	0.68	0.71	0.77		0.79	0.7	0.68	0.63	0.59	0.64
BE	0.71	0.66	0.69	0.79	0.79		0.72	0.73	0.64	0.59	0.64
IT	0.64	0.63	0.62	0.7	0.7	0.72		0.89	0.7	0.72	0.58
SP	0.62	0.62	0.59	0.68	0.68	0.73	0.89		0.7	0.74	0.57
IR	0.56	0.58	0.56	0.62	0.63	0.64	0.7	0.7		0.69	0.51
PT	0.51	0.53	0.51	0.57	0.59	0.59	0.72	0.74	0.69		0.47
UK	0.67	0.65	0.6	0.66	0.64	0.64	0.58	0.57	0.51	0.47	

(COUNTRY 2)

Essentially, both Kendall Tau and Spearman Rho highlight **greater correlations for pairs of peripheral countries.** "Spain and Italy" in particular exhibits the largest Kendall Tau and Spearman Rho estimators, slightly above pairs involving Portugal with Italy or Spain. The Spearman Rho is also quite large for pairs of soft-core countries, but this is less pronounced for the Kendall Tau (Table 10). We also note that pairs involving countries of a more or less similar credit quality exhibit the largest correlations, something consistent with our observations of the market dynamics. The pair "France and Germany" also displays a large correlation in terms of Spearman Rho. This looks like an outlier as neighbouring pairs in Table 11 are less correlated.

Non-linear correlations are also much smaller for pairs that exhibit very disparate credit quality on each component. Non-core countries for instance are less correlated to core countries than they are with soft-core. **This probably illustrates a reduced risk of contagion into core countries.**

Liquidity may also be a potential driver of correlations. Finnish CDS for instance experience much tighter liquidity than Germany or the Netherlands. As Table 10 and Table 11 show, pairs involving Finnish CDS and another core country, show fewer correlations than other pairs involving core economies.

➔ **The empirical exploration of the data already reveals the presence of sizeable linear and non-linear correlations in the sample.**

The GAS framework

Assumptions of the univariate model

We consider the Generalized Autoregressive Score (GAS) method as a means to model the course of the volatility. This is a recent and innovative volatility model, that was introduced in (Zhang, Creal, Koopman, Lucas (2012a), Zhang, Creal, Koopman, Lucas (2012b), Creal, Koopman, Lucas (2013), Creal, Koopman, Lucas (2011), Creal, Koopman, Lucas, Zamojski (2016)). We explore the implementation of the GAS model in the following paragraphs, and the respective adjustments that we have made to fit the context of our analysis.

The Generalized Autoregressive Score dynamics for time varying volatility

The GAS method is based on the computation of a score f_t, which is a transformation of the volatility σ_t. Like in Creal, Koopman, Lucas (2012), we first explore the effectiveness of two different formulations for f_t:

$$f_t = \log(\sigma_t{}^2) \text{ and } f_t = \sigma_t{}^2$$

The relationship that relates the score f_t to the volatility σ_t is then defined as:

$$\begin{cases} f_t = \omega + A\, s_{t-1} + B\, f_{t-1} \\ s_{t-1} = S_{t-1}\nabla_{t-1} \end{cases} \quad \text{with} \quad \begin{cases} \nabla_{t-1} = \frac{\partial \log p(x_{t-1}|f_{t-1};\theta)}{\partial \sigma_{t-1}{}^2}\frac{\partial \sigma_{t-1}{}^2}{\partial f_{t-1}} \\ S_{t-1} = -\mathbb{E}_{t-2}[\nabla_{t-1}\nabla'_{t-1}]^{-1} \end{cases} \qquad (17)$$

Where: ω, A, B are constant parameters that we need to estimate, and $p(x_t|f_t;\theta)$ is the probability density function of the dataset, conditional on f_t. Finally, S_{t-1} is the Fisher information matrix (FIM).

Since the calculation of the volatility at time t involves values obtained at time $t-1$, (ie. σ_{t-1} and $p(x_{t-1}|f_{t-1};\theta)$), the estimation of the volatility is path-dependent. This is the reason for the conditionality embedded in p.

Calibrating the GAS model requires the estimation of three unknown parameters: ω, A, B. The calculation also involves the Fisher Information matrix, which can be regarded as an "average" illustration of the available information in the market. This coefficient proves useful when it comes to characterising long term trends, but the "average" aspect may also make the FIM rather insensitive to abrupt changes in market sentiment. And this could lead to an underestimate of the volatility in the tails when financial stress tends to sharply accelerate. As this coefficient could prove an obstacle in the context of our analysis, we prefer removing it. This is in line with Creal, Koopman, Lucas (2012) who argues that the $S_t = 1$ is an acceptable assumption.

As a result, we use an adjusted formulation of the GAS model:

$$\begin{cases} f_t = \omega + A\,.s_{t-1} + B.f_{t-1} \\ s_{t-1} = S_{t-1}.\nabla_{t-1} \end{cases} \quad \text{with} \quad \begin{cases} \nabla_{t-1} = \frac{\partial \log p(x_{t-1}|f_{t-1};\theta)}{\partial \sigma_{t-1}{}^2}\frac{\partial \sigma_{t-1}{}^2}{\partial f_{t-1}} \\ S_{t-1} = 1 \end{cases} \qquad (18)$$

Based on eq. (18), the volatility estimator is designed as:

- A constant intercept ω.
- A coefficient A, which indicates to what extent the derivatives of the marginal distribution with respect to the score s_{t-1}, evaluated at time $t-1$, is involved.
- An autoregressive coefficient B attached to the score f_{t-1}. B is fully dedicated to quantifying persistence in the volatility.

➔ **The GAS volatility estimator relies upon three unknowns: $\boldsymbol{\theta} = \{\boldsymbol{\omega}, \boldsymbol{A}, \boldsymbol{B}\}$.**

Since the value of f_t depends on the realisation at $t-1$, $\sigma_t$is conditional on x_{t-1}. This means that the probability distribution function p that involves σ_t will hold this conditionality. As a result, we denote it $p(x_t|x_{t-1};\theta)$. We also use the Levenberg-Marquardt optimisation procedure to achieve the maximisation of the likelihood function. This eventually delivers the calibrated values of ω, A, B. The optimisation algorithm is beyond the scope of this report; for those looking for deeper insight, please refer to a detailed description here[8].

[8] http://users.ics.forth.gr/~lourakis/levmar/

Estimating the conditional Marginals

In this section we describe the calibration of the univariate marginals with different assumptions on p. We then highlight the formulation that looks the most appropriate, and we take a look at the calibrated parameters. These are the different steps of the procedure:

1) **First we choose/assume an analytic expression for $\boldsymbol{p(x_t|x_{t-1};\ \theta)}$**. This goes from the basic Gaussian up to more sophisticated Generalised Hyperbolic t-Student skewed distributions. **In the end we show that Generalised Hyperbolic distributions outperform other formulations.** The presence of heavy tails in particularly makes this class of distributions especially adequate to describe the price action of CDS spreads.

2) We focus on the score f_t and we show that the calibration procedure is more effective when we consider $f_t = log\ ({\sigma_t}^2)$ rather than $f_t = {\sigma_t}^2$. ➔ **We retain $\boldsymbol{f_t = log\ ({\sigma_t}^2)}$ as the best formulation.**

3) We apply the GAS formula and we build the corresponding log likelihood equation Π as:

$$f_{t+1} = \omega + A\,.\,s_t + B.f_t \tag{19}$$

$$s_t = 1.\nabla_t \text{ with } \nabla_t = \frac{\partial\, log\, p(x_t|f_t;\theta)}{\partial {\sigma_t}^2}\frac{\partial {\sigma_t}^2}{\partial f_t} = \frac{\partial\, log\, p(x_t|x_{t-1};\theta)}{\partial {\sigma_t}^2}\frac{\partial {\sigma_t}^2}{\partial f_t}$$

From which we derive the log-likelihood function:

$$\Pi = \sum_t log[p(x_t|f_t;\ \theta)] = log\left[\prod_t p(x_t|f_t;\ \theta)\right]$$

with the convention that $p(x_1|x_0,\theta) = p(x_1,\theta)$.

4) **Calibration step.** We maximize the likelihood equation, using the Levenberg-Marquardt algorithm. As a result we obtain the optimal value of the three parameters ω, A, B plus additional variables when required (like the skewness γ). This step delivers an estimate of the conditional marginal $p(x_t|x_{t-1},\theta)$. As we already mentioned, we run the procedure 20 times to avoid being stuck in a local extremum.

5) Ascertain the relevance of the estimators. Then we need to select the best estimator, out of the 20 calibrations. We consider the Anderson-Darling criterion, and the RMSE of the GAS volatility against the empirical two-week rolling standard deviation as measures of the goodness of fit. We also look at the Conditional Probability Integral Transform (CPIT) as a graphical illustration of the error, that helps identify how the error positions itself on the distribution. We highlighted the approach in the section dedicated to the Copula framework, and emphasized that **the best estimator is chosen as the one which provides the smallest ADC and volatility error. This completes the univariate analysis.**

While we will later decide which distribution looks the best candidate to explore the dynamics of our dataset, we first have to decide which formulation of the score is the most relevant:

$$f_t = log\ ({\sigma_t}^2) \text{ or } f_t = {\sigma_t}^2\ ?$$

What is the best expression for f_t ?

We investigate the appropriateness of each formulation of the score synthetic data. Our tests are very similar to the approach of Lucas, Schwaab and Zhang (2012) that explores different variations of the GAS method. The authors in particular focus on these two formulations: $f_t = log\ ({\sigma_t}^2)$ and $f_t = {\sigma_t}^2$.

Our synthetic data was **generated as a series x_t of 2500 points following a standardised normal distribution** (mean $\mu = 0$; sample standard deviation at 1). This is a summary of the procedure:

- Data: synthetic sample with $x_t \sim N(0,1)$.
- We assume that the marginal p is a Gaussian distribution. We set $\mu = 0$ (mean) and we keep the standard deviation σ_t as a time varying unknown that needs to be estimated. The purpose of this simulation is to gauge to what extent the GAS algorithm is able to calibrate the volatility parameter σ_t around the targeted value of 1.
- We define the score: **First case** $f_t = \log\ ({\sigma_t}^2)$.
- We calculate the score functions based on Creal, Koopman and Lucas (2012):

$$\nabla_t = \frac{x_t^2}{2.\exp\ (f_t)} - \frac{1}{2}$$

$$S_t = -\mathbb{E}_{t-1}[\nabla_t \nabla'_t]^{-1} = 2$$

$$f_{t+1} = \omega + A.\left(\frac{x_t^2}{\exp(f_t)} - 1\right) + Bf_t$$

$$\sigma_{t+1}^2 = \exp\left(\omega + A.\left(\frac{x_t^2}{\sigma_t^2} - 1\right)\right)\sigma_t^{2B}$$

- We derive the corresponding log-likelihood equation:

$$\log\big(p(x_t|x_{t-1};\ \theta)\big) = -\frac{1}{2}\log(2\pi) - \frac{1}{2}\log(\sigma_t^2) - \frac{1}{2}\frac{x_t^2}{\sigma_t^2}$$

After running the calibration procedure, we obtain a fairly constant volatility as time goes by, centred on 1. ➔ **This is coherent, and confirms the ability of the model $\boldsymbol{f_t = \log\ (\sigma_t^2)}$ to approach the real value of $\boldsymbol{\sigma_t}$.**

Then we applied the same procedure to the second formulation $f_t = {\sigma_t}^2$. This time we get the following formulas (as in Creal, Koopman and Lucas (2012)):

$$\nabla_t = \frac{x_t^2}{2.f_t^2} - \frac{1}{2f_t}$$

$$S_t = -\mathbb{E}_{t-1}[\nabla_t \nabla'_t]^{-1} = 2f_t^2$$

$$f_{t+1} = \omega + A\ (x_t^2 - f_t) + Bf_t$$

The log-likelihood function remains unchanged. After the calibration, it appears that the estimated volatility is significantly larger than in the first case, with an average volatility at around 1.75, which is far from the true value. ➔ **Results are much less compelling this time, which suggest that $f_t = {\sigma_t}^2$ is not appropriate. In what follows we will thus exclusively focus on $f_t = \log\ ({\sigma_t}^2)$.**

We applied the GAS framework to our dataset of CDS price variations. We ran the calibration for several distribution functions: **Gaussian, Student-t, GHT and GHST**.

Technical aspects of the optimisation procedure. σ_t is initialised on its empirical value $\tilde{\sigma}_t$ (ie. the 2-week rolling standard deviation). We then run the calibration 20 times for each distribution, with varying initial values for $\{\omega, A, B\}$. Then we calculate the corresponding ADC, VOL error and we plot the CPIT. Based on this information we select the best set of parameters.

Empirical tests help us narrow the range of initial values for each coefficient. In the end we decide to take random values between $[-0.5, -0.1]$ for ω, $[0.05, 0.5]$ for A, $[0.1, 0.8]$ for B, and $[0.,0.1]$ for the skewness γ (when applicable). **For coherence we use identical initial values for each distribution.**

Inference and Results.

Here we compare the results obtained for each probability distribution function. For clarity, we only consider German CDS spreads – in fact most of the conclusions can be generalised to other countries. We conduct a more general review in the subsequent section.

First case: <u>normal Gaussian marginals.</u> First we consider the normal distribution. We get the following formulation:

pdf: $p(x_t|x_{t-1}) = \frac{1}{\sigma_t\sqrt{2\pi}}\exp\left(-\frac{x_t^2}{2\sigma_t^2}\right)$

$$\nabla_t = \frac{x_t^2}{2.\exp(f_t)} - \frac{1}{2}$$

$$S_t = 2$$

$$f_{t+1} = \omega + A.\left(\frac{x_t^2}{\exp(f_t)} - 1\right) + Bf_t$$

Log-likelihood:

$$\log\left(p(x_t|x_{t-1};\theta)\right) = -\frac{1}{2}\log(2\pi) - \frac{1}{2}\log(\sigma_t^2) - \frac{1}{2}\frac{x_t^2}{\sigma_t^2}$$

Results:

ADC: 3.8

VOL error: 0.307

The final ADC is rather disappointing at 2.8. Graph 20 shows that the error hit both, the centre and the tail regions of the distribution. In the same vein, the VOL error is huge at 0.8bp/day. In particular, Graph 21 shows that periods of very low volatility, ie. after Jan 2013, are not properly captured. ➔ **Gaussian distributions are not able to capture the actual behaviour in the tails, we reject them.**

Graph 20. CPIT with Gaussian marginals – ADC = 2.8

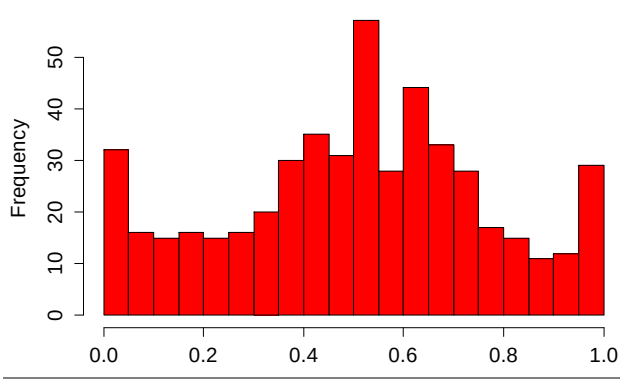

Graph 21. Poor volatility estimate with Gaussian marginals

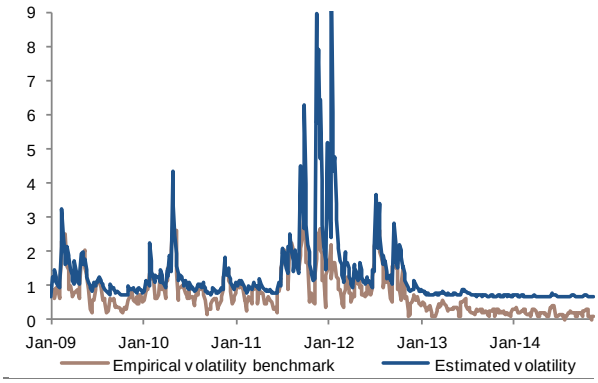

Second case: the t-Student distribution

Next we explore Student-t marginals. We follow the methodology of Creal, Koopman and Lucas (2012) (ν is the degrees of freedom, we set $\nu = 5$):

pdf: $p(x_t|x_{t-1}) = \frac{1}{\sqrt{\nu\pi}} \frac{\Gamma\left(\frac{\nu+1}{2}\right)}{\Gamma\left(\frac{\nu}{2}\right)} \left(1 + \frac{x_t^2}{\nu}\right)^{-\frac{\nu+1}{2}}$

$$\nabla_t = \frac{(\nu+1)}{2} \left(1 + \frac{x_t^2}{(\nu-2)\exp(f_t)}\right)^{-1} \frac{x_t^2}{(\nu-2)\exp(f_t)} - \frac{1}{2}$$

$$S_t = \frac{2(\nu+3)}{\nu}$$

$$f_{t+1} = \omega + A.\left[\frac{(\nu+3)}{\nu}\left(\left(1 + \frac{x_t^2}{\nu-2}\right)^{-1} \frac{(\nu+1)x_t^2}{(\nu-2)\exp(f_t)} - 1\right)\right] + Bf_t$$

Results:

ADC: 8.4

VOL error: 6.06

Log-likelihood:

$$\log\left(p(x_t|x_{t-1};\,\theta)\right) = \log\Gamma\left(\frac{\nu+1}{2}\right) - \log\Gamma\left(\frac{\nu}{2}\right) - \frac{1}{2}\log\pi - \frac{1}{2}\log(\nu-2) - \frac{1}{2}\log\sigma_t^2 - \frac{\nu+1}{2}\log\left(1 + \frac{x_t^2}{(\nu-2)\sigma_t^2}\right)$$

Results are even weaker than before. The ADC criterion is unacceptably poor at 8.4. Graph 22 also shows a very weak CPIT too, with nothing below 0.2 and above 0.75 in terms of percentile. Looking at the volatility, Graph 23 shows that the estimate of the variance is very much diverging from the actual value (5bp/day on average in 2012 vs. a benchmark at 1.5bp/day). ➔ **The Student-t law is definitely not an adequate distribution.**

Graph 22. CPIT with Student-t marginals – ADC = 8.4

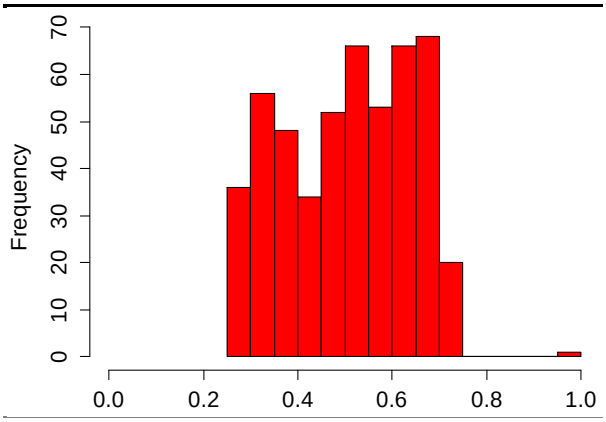

Graph 23. Volatility is poorly estimated with Student-t marginals

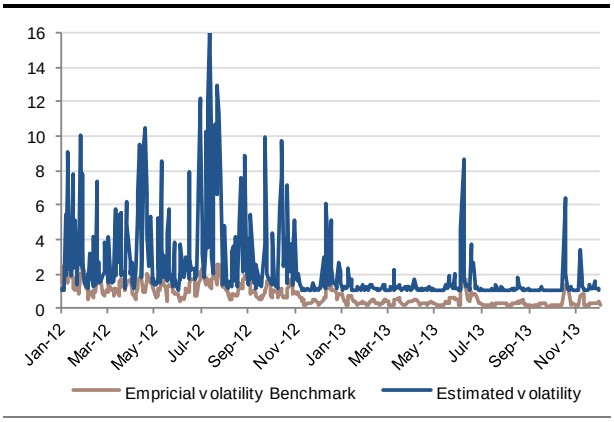

Third case: the Generalized Hyperbolic t-Student distribution(GHT)

We carried out the same calculation with GHT marginals:

Pdf: $p(x_t|x_{t-1}) = \frac{(\upsilon-2)^{\upsilon/2}}{\pi^{1/2}\sigma_t} \frac{\Gamma(\frac{\upsilon+1}{2})}{\Gamma\left(\frac{\upsilon}{2}\right)(\upsilon-2+\frac{x^2}{\sigma_t{}^2})^{\frac{\upsilon+1}{2}}}$ with $\upsilon = d.o.f. = 5$

$$\nabla_t = \frac{\partial f_X(x)}{\partial \ln(\sigma_t{}^2)} = -\frac{1}{2} + \frac{x^2(\upsilon+1)}{2\sigma^3(\upsilon-2+\frac{x^2}{\sigma_t{}^2})}$$ and we used: $S_t = 1$

Results:

ADC: 1.51

VOL error: 0.11

Graph 24. CPIT with GHT distribution – ADC = 1. 51

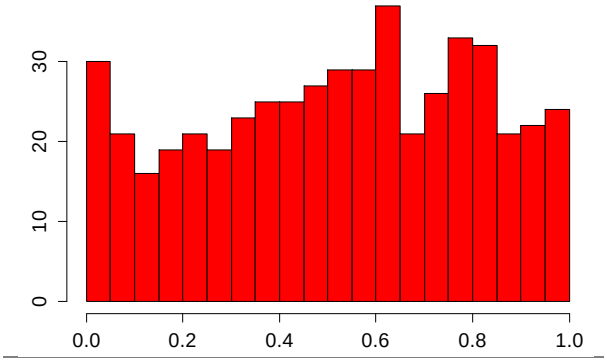

Graph 25. Better estimate with GHT distributions

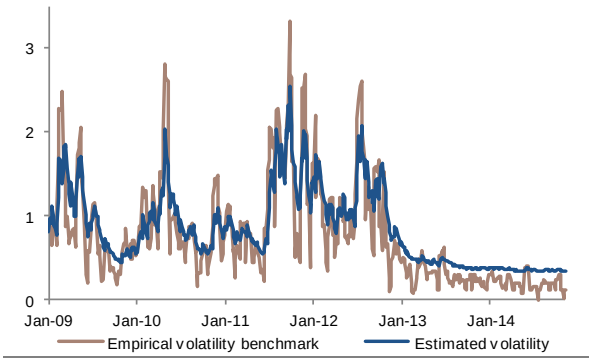

Results are much better than before. The ADC criterion shows a robust 1.51, which is much more satisfactory than what we had before. Graph 24 also shows a very good CPIT, where both the tails and the belly look fairly well calibrated, while the estimated volatility in Graph 25 is really close to the empirical value. That said, we note that the model tends to moderately overestimate the volatility during periods of very low volatility. **We conclude that GHT distribution functions offer a very good fit to the empirical data. ➔ GHT distributions are good candidates to model the univariate conditional distribution p.**

Fourth case: <u>the Generalized Hyperbolic Skewed Student-t distribution (GHST):</u>

We consider the same distribution as just before, but with the addition of a skewness coefficient γ - which is supposed to reflect a possible asymmetry in the data. We got the following equations:

$$p(x_t|x_{t-1}) = \frac{(\upsilon-2)^{\frac{\upsilon}{2}}.(\frac{\gamma^2}{\sigma_t{}^2})^{\frac{\upsilon+1}{2}}}{(2\pi)^{\frac{1}{2}}.\sigma_t.\Gamma\left(\frac{\upsilon}{2}\right).2^{\frac{\upsilon}{2}-1}} \frac{K_{\frac{\upsilon+1}{2}}(\sqrt{\left(\upsilon-2+\frac{(x+\gamma)^2}{\sigma_t{}^2}\right)(\frac{\gamma^2}{\sigma_t{}^2})})}{\sqrt{\left(\upsilon-2+\frac{(x+\gamma)^2}{\sigma_t{}^2}\right)(\frac{\gamma^2}{\sigma_t{}^2})}^{\frac{\upsilon+1}{2}}} e^{\frac{(x+\gamma)\gamma}{\sigma_t{}^2}}$$

$$\nabla_t = \frac{\partial f_X(x)}{\partial \ln(\sigma^2)} = (E+F+G+H).\frac{\partial \sigma^2}{\partial \ln(\sigma^2)}$$

With :

$$F = \frac{\partial\left[K_{\frac{\upsilon+1}{2}}(\sqrt{\left(\upsilon-2+\frac{(x+\gamma)^2}{\sigma_t{}^2}\right)(\frac{\gamma^2}{\sigma_t{}^2})})\right]}{\partial\left[\sqrt{\left(\upsilon-2+\frac{(x+\gamma)^2}{\sigma_t{}^2}\right)(\frac{\gamma^2}{\sigma_t{}^2})}\right]} \frac{\frac{-\gamma^2}{\sigma_t{}^2}2(x+\gamma)^2-(\upsilon-2)\frac{\gamma^2}{\sigma_t{}^4}}{2\sqrt{(\upsilon-2+\frac{(x+\gamma)^2}{\sigma_t{}^2})(\frac{\gamma^2}{\sigma_t{}^2})}} \frac{1}{K_{\frac{\upsilon+1}{2}}(\sqrt{\left(\upsilon-2+\frac{(x+\gamma)^2}{\sigma_t{}^2}\right)(\frac{\gamma^2}{\sigma_t{}^2})})}$$

$$E = \frac{-(\upsilon+2)}{2\sigma_t{}^2} \qquad G = \frac{(\frac{\gamma^2}{\sigma_t{}^6}2(x+\gamma)^2+\frac{(\upsilon-2)\gamma^2}{\sigma_t{}^4})}{2((\upsilon-2+\frac{(x+\gamma)^2}{\sigma_t{}^2})(\frac{\gamma^2}{\sigma_t{}^2}))}\frac{(\upsilon+1)}{2} \qquad H = \frac{-(x+\gamma)\gamma}{\sigma_t{}^4}$$

Where $K_{\frac{\upsilon+1}{2}}()$ is the modified Bessel function of the second kind. So $\frac{\partial K_{\frac{\upsilon+1}{2}}()}{\partial[\ ]}$ is the first derivative of the Bessel function of the second kind.

Results:

ADC: 1.27

VOL error: 0.11

Graph 26. CPIT with GHST distribution – ADC = 1.27

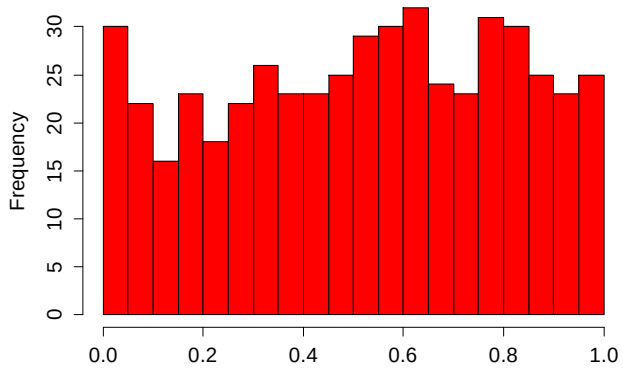

Graph 27. Better estimate with GHST distributions

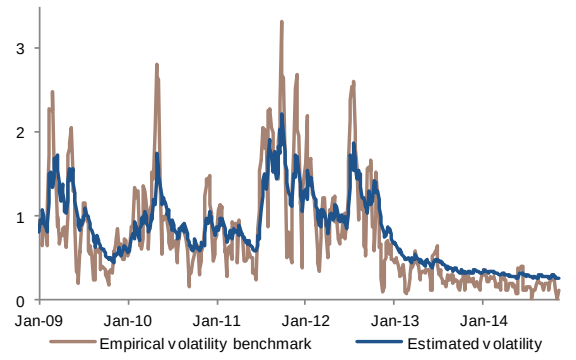

GHST distributions give results similar to the GHT. The ADC criterion is a bit smaller than with the GHT distribution and delivers an excellent score of 1.27. The CPIT in Graph 26 shows that the error mostly lies in the left tail (this is specific to Germany), and remains quite small. The VOL error is in line with GHT distributions (at 0.11, Graph 27). ➔ **Both GHT and GHST distributions are interesting ways to define the probability distribution function p of CDS returns**.

Table 12 shows the evolution of the VOL and ADC errors for each try. Here again, GHT and GHST distributions clearly outperform other distribution. For these two distributions, ADC are much satisfactory in almost all cases. ➔ **The optimisation algorithm is robust.**

Table 12. Volatility error and ADC for each type of distribution

Test number:		1	2	3	4	5	6	7	8	9	10
VOL	Gaussian:	3.73E+06	3.62E+06	2.90E+06	3.69E+06	3.12E+06	2.99E+06	2.94E+06	4.59E+06	4.10E+06	3.99E+06
	t-Student:	1.17E+02	7.63E+01	6.24E+02	2.11E+01	7.01E+81	2.02E+29	1.31E+04	2.79E+01	1.04E+02	9.01E+03
	GHT:	0.14	0.30	0.12	0.14	0.19	0.30	0.15	0.16	0.13	0.14
	GHST:	0.12	0.14	0.65	0.11	0.13	0.18	0.13	0.11	0.13	0.13
ADC	Gaussian:	6.11	6.11	6.09	6.11	6.10	6.09	6.09	6.12	6.11	6.12
	t-Student:	8.98	8.99	8.76	9.00	213.54	123.92	8.19	9.05	8.95	8.23
	GHT:	1.75	1.67	1.50	1.59	1.75	1.90	1.88	1.46	1.87	1.47
	GHST:	1.27	1.35	3.33	1.55	1.61	1.79	1.41	1.40	1.92	1.80

Test number:		11	12	13	14	15	16	17	18	19	20	AVERAGE
VOL	Gaussian:	3.06E+06	3.24E+06	2.93E+06	3.35E+06	4.65E+06	4.44E+06	3.15E+06	3.77E+06	4.46E+06	3.41E+06	3.61E+06
	t-Student:	3.32E+02	4.73E+01	1.18E+20	6.06E+00	5.86E+02	1.95E+01	3.35E+248	3.40E+54	5.29E+01	8.85E+02	1.67E+247
	GHT:	0.13	0.12	0.12	0.16	0.12	0.11	0.12	0.12	0.18	0.16	0.16
	GHST:	0.14	0.20	0.15	0.12	0.13	0.13	0.15	0.18	0.14	0.24	0.17
ADC	Gaussian:	6.09	6.10	6.08	6.10	6.12	6.12	6.10	6.11	6.13	6.11	6.11
	t-Student:	8.93	8.99	100.10	8.37	8.79	8.93	376.23	164.34	9.03	8.70	55.50
	GHT:	1.60	1.74	1.79	2.22	1.46	1.52	1.53	1.77	2.31	2.61	1.77
	GHST:	1.94	2.71	1.45	1.52	1.63	1.43	1.54	1.66	1.49	1.37	1.71

Final parameters

We now look at the resulting coefficients for $\{\omega, A, B\}$. Table 13 shows the coefficients of the 5 best calibrations, and the average value calculated out of the 20 calibrations. The autoregressive component B in particular is around 0.9 on average (for GH distributions), which is massive as it suggests that the calculation of σ_t is influenced by 90% of the market realisation at $t-1$. **This confirms the high-level of persistence in the volatility.** Interestingly, Gaussian and t-Student distributions deliver a much smaller coefficient B (average at 0.11, 0.54). ➔ **Gaussian and t-Student**

distributions are unable to capture autocorrelations in the volatility. This partly explains the poor results out of these two distributions.

The coefficient A takes a value around 0.45 – and this is regardless of the assumed distributions. The skewness parameter is also very small with an average value at around -0.01, and this is the case for all countries. ➔ **Overall, there is no need to consider the skewness coefficient as an additional unknown. We consider therefore the more parsimonious GHT distribution (compared to GHST) as the best descriptor of the data's behaviour.**

Table 13. Best estimators for each distribution

Coefficients	*AVERAGE*	*Five best calibrations*				
GHT						
ω	1.04	1.02	1.05	0.98	1.10	1.04
A	0.62	0.68	0.73	0.73	0.26	0.68
B	0.86	0.86	0.88	0.75	0.94	0.86
GHST						
ω	1.08	1.07	1.08	1.09	1.11	1.05
A	0.55	0.65	0.38	0.80	0.31	0.62
B	0.89	0.85	0.92	0.89	0.95	0.85
Skewness	0.07	0.06	0.08	0.08	0.06	0.07
Gaussian						
ω	-0.001					
A	0.40					
B	0.11					
Student						
ω	0.005					
A	0.64					
B	0.54					

Dispersion of the likelihood values

It is interesting to gauge the potential connection between the parameter values and the quality of the calibration. This helps understand the degree of complexity attached to each unknown as to reach a proper level of calibration, and the influence of each parameter on the overall quality of the calibration.

For this purpose, we conduct 200 calibrations with only one parameter left as a free variable, and we fix the two other unknowns at a level close to their optimum. Then **we look at the dispersion of the estimated values, that we plot against the resulting ADC** (Graph 28 to Graph 30). The graphs indicate that for each variable there is a wide range of (estimated) values that leads to satisfactory ADCs. Yet we also note that the very best ADC is reached in a much tighter range of values, thus suggesting that there is effectively a relationship between the optimum ADC and the parameters. In relative terms, Graph 29 shows that the parameters A are less sensitive to the quality of the calibration than the parameters ω and B (Graph 28, Graph 30). As a result, the "scope of validity" for B and ω is narrower compared to the dispersion of the points.

Validity scope of ω: $[1.05,1.1]$ Validity scope of A: $[0.3, 0.7]$ Validity scope of B: $[0.8, 0.95]$

➔ **B has a bigger effect on the goodness of fit than ω and A.** As we will see below, the "validity scopes" of A and B are very similar for all countries but we cannot generalise the behaviour of ω to other countries as this parameters is bigger for the more volatile credits.

Graph 28. ADC versus estimated ω

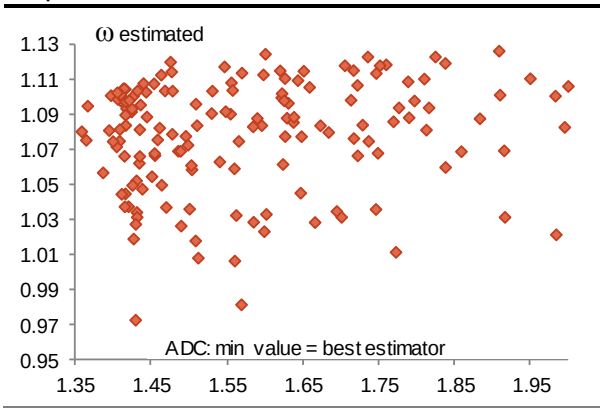

Graph 29. ADC versus estimated A

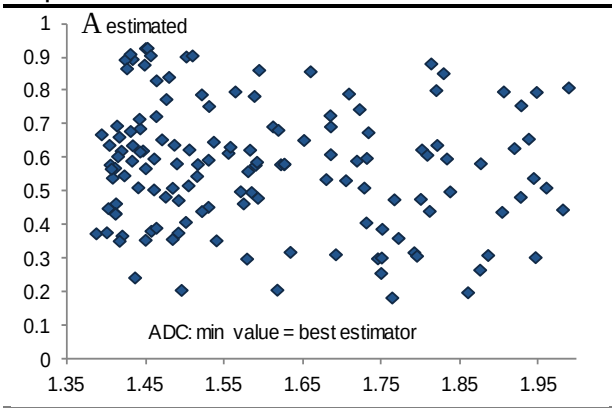

Graph 30. ADC versus estimated B

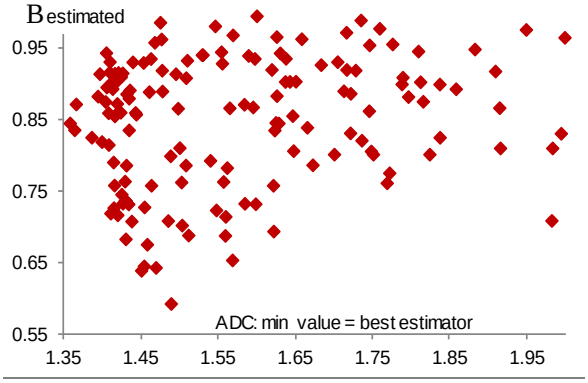

Graph 31. ADC vs. initial values of ω

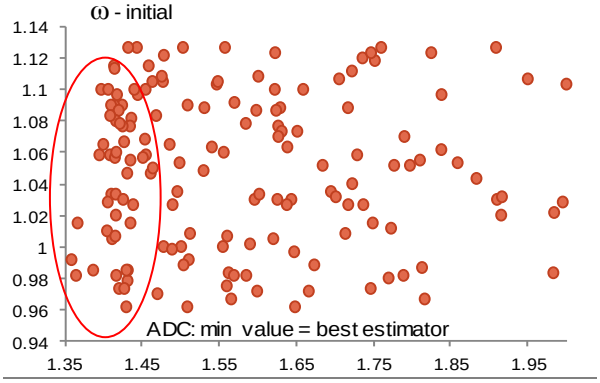

Have initial values a huge influence on the results?

Initial values may also have significant implications on the quality of the calibration. To get an idea on that, we explore the influence of initial values against the final ADC in Graph 31, Graph 32 and Graph 33.

Graph 32. Final ADC vs. the initial value of A

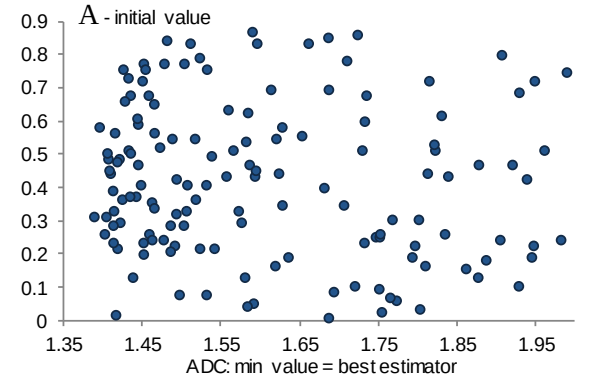

Graph 33. Final ADC vs. the initial value of B

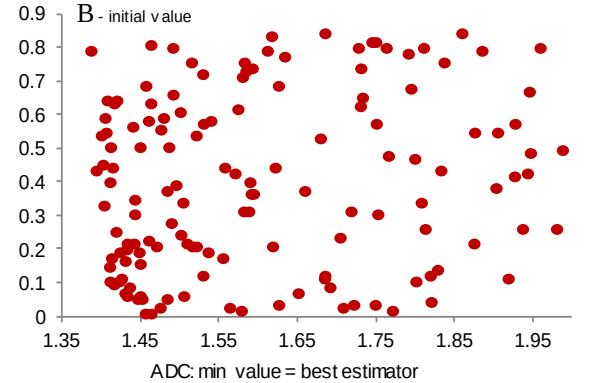

ω first, shows no particular pattern against the final ADC (Graph 31), suggesting that the success of the calibration is somewhat independent of initial values there. For A and B (Graph 32 and Graph 33), there is a relationship as initial values have to lie within a specific range, otherwise the calibration will is systematically not successful. As a consequence, we estimate the "validity scope"

for initial values as $[0.2, 0.6]$ for A, and $[0.1, 0.65]$ for B. These ranges are larger than the "validity scopes" we just calculated before.

➔ These observations help refine the range of generations for initial values. This time again, this range tends to vary from one country to another for ω, while it remains relatively unchanged for A and B.

How do parameters evolve around their best estimator?

When looking at the evolution of every parameter around their best estimator (Graph 34– Graph 36 below), the curve looks continuous and differentiable with a unique peak, at the best value for each parameter. **This confirms that the estimation is tractable and straightforward.**

Graph 34. Final likelihood as a function of ω

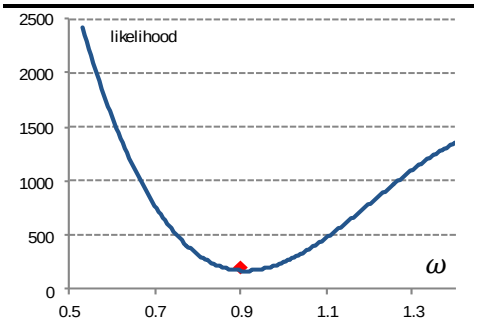

Graph 35. Final likelihood as a function of A

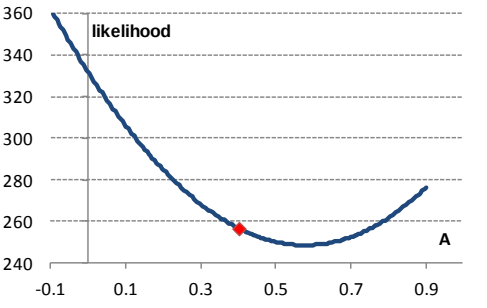

Graph 36. Final likelihood as a function of B

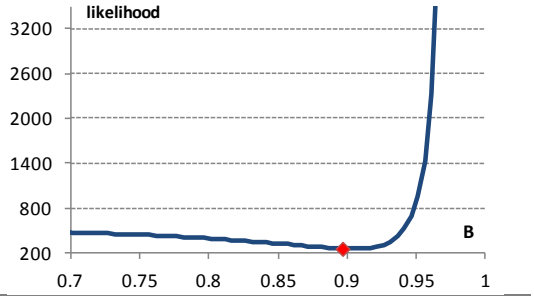

Cross country analysis

We conducted the same analysis on other CDS spreads, still involving both GHT and GHST distributions. Table 14 shows the value of the best estimators for each distribution, and **indicates that both approaches deliver excellent ADC while the VOL error remains very much contained**. And coefficients overall show that A and B are relatively stable for all countries, while ω moves in sync with the underlying standard deviation of the data – and thus reaches a peaks for Portugal at 5.8.

Graph 37 and Graph 38 display the corresponding CPIT for French and Spanish CDS as examples: the points are uniformly distributed. This confirms that GHT/GHST distributions are much appropriate to describe the behaviour of the data, and thus relevant choices for p. Even the large kurtosis of non-core countries does not cause particular deterioration.

Table 14. Cross country results for GHT and GHST conditional marginals

	GE	FI	NL	AT	FR	BE	IT	SP	IR	PT	UK
GHT											
ω	1.09	0.51	1.58	2.62	2.33	3.86	4.58	4.38	5.00	5.87	1.35
A	0.62	0.74	0.88	0.30	0.30	0.43	0.55	0.57	1.04	0.36	0.68
B	0.91	0.75	0.81	0.95	0.94	0.92	0.91	0.91	0.86	0.93	0.86
GHST											
ω	1.11	0.53	1.63	2.54	2.31	3.90	4.55	4.35	5.04	5.83	1.37
A	0.31	0.64	0.37	0.84	0.78	0.33	0.51	0.60	0.64	0.62	0.70
B	0.95	0.77	0.92	0.88	0.89	0.95	0.83	0.82	0.90	0.89	0.88
Skewness	0.06	0.03	0.05	0.10	0.08	0.04	0.00	0.00	0.06	0.02	0.01
VOL GHT	0.09	0.12	0.12	0.13	0.09	0.12	0.11	0.09	0.15	0.17	0.11
VOL GHST	0.11	0.12	0.14	0.19	0.11	0.13	0.13	0.11	0.09	0.13	0.11
ADC GHT	1.88	2.12	1.87	1.67	1.19	1.46	0.58	0.65	1.53	1.23	1.29
ADC GHST	1.74	2.14	1.85	1.57	1.03	1.28	0.63	0.67	1.14	1.17	1.31

Graph 37. Strong CPIT for France (GHT)

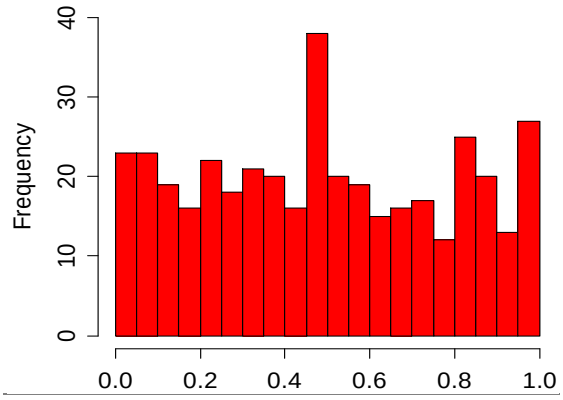

Graph 38. Strong CPIT for Spain (GHT)

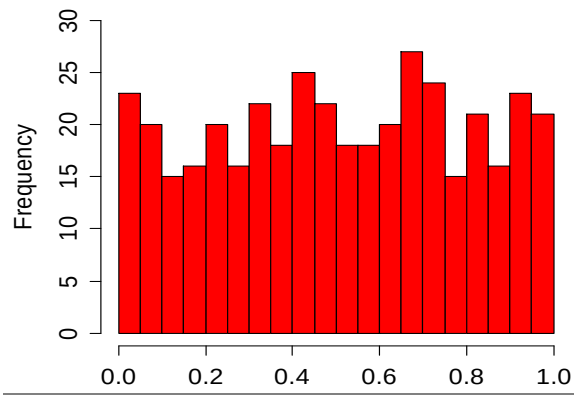

Graph 39. Good CPIT for Austria too (GHT)

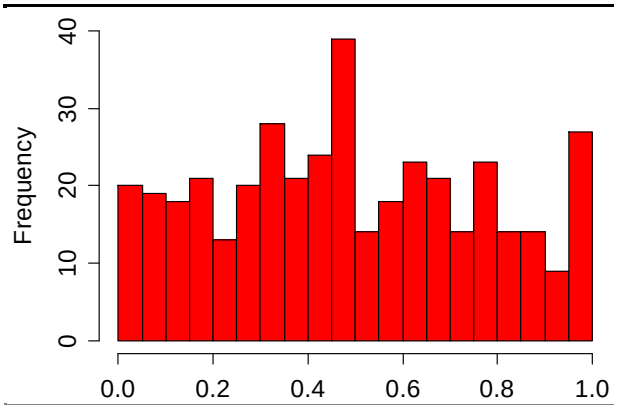

We look at Austria in Graph 40 as empirical indicators show a remarkably high kurtosis there too. Overall, the estimated volatility is very close to its empirical value. In the same vein, the CPIT of Austria in Graph 39 highlights only 10% of 'misplaced' points that diverge from the uniform distribution (mostly in the belly). ➔ **Results overall comfort our first observations that GHT/GHST distributions are relevant formulations to model the distribution of the data. These probability distribution functions are particularly flexible, and provide an outstanding fit, even to times series that exhibit a large kurtosis (and thus bigger tails).**

Other illustrations in Graph 41 and Graph 42 show the calibrated GHT volatility for France and Spain. The calibrated volatility provides an outstanding fit to the benchmark, even during periods of large volatility. ➔ **We see no particular distortion in our volatility estimator when market**

sentiment turns sharply risk averse. Our estimator is able to adjust itself to tough changes in the underlying volatility without bearish a loss of consistency. This is another sign of robustness in the whole procedure.

Other countries exhibit results as good as for Germany, with the quality of the GAS volatility remaining unaffected by the intrinsic credit worthiness in general (ie. no visible deterioration for peripheral countries). Overall, the GAS estimator remains fairly resilient to any turn in market sentiment. **In conclusion, it is correct to assume that our dataset is distributed according to GHT or GHST distributions. We prefer GHT distributions as there is no clear gain in adding skewness as an additional parameter.** ➔ The GAS method looks a relevant choice to estimate the time-varying volatility. Overall, results suggests that the model is remarkably agile - this will certainly prove much helpful to explore periods of erratic volatility.

Graph 43 also shows that the GHT volatility for Spanish CDS is correlated to the 10-year SPGB versus Bund yield spread (ie. Spanish sovereign spread against Germany). Part of this spread reflects the risk premium attached to Spanish interest rates, and therefore can be seen as a proxy for financial distress in Spain (a wider spread means greater differentiation between Germany and Spain in terms of credit quality). In the graph, periods of a wider SPGB/Bund spread are coincident with periods of larger volatility. This correlation between sovereign risk and the volatility suggests that any deviation in our GAS estimator against the true volatility could have dramatic implications when it comes to estimating sovereign risk (and more generally for risk management purposes). ➔ **In this context, the observed robustness of the GAS estimator is all the more valuable.**

Graph 40. Austria's volatility has been well calibrated

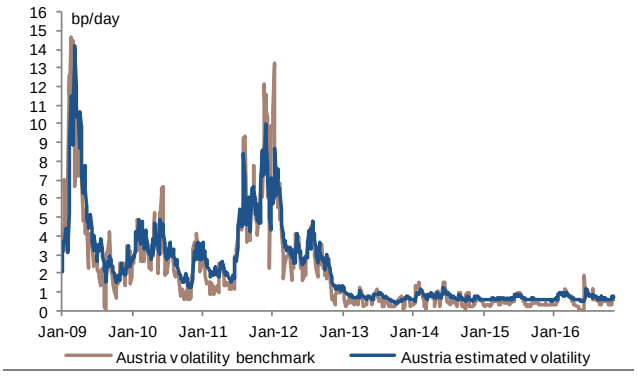

Graph 41. France's GHT volatility close to benchmark

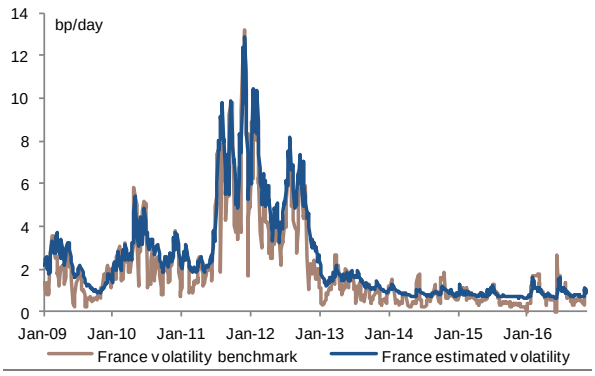

Graph 42. Spain's estimated volatility (GHT) close to benchmark

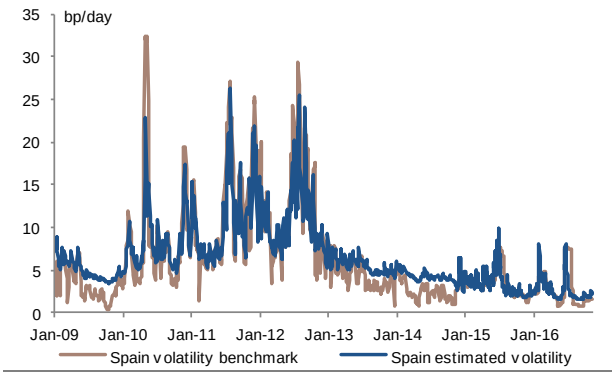

Graph 43. Volatility is a basic indicator of market stress

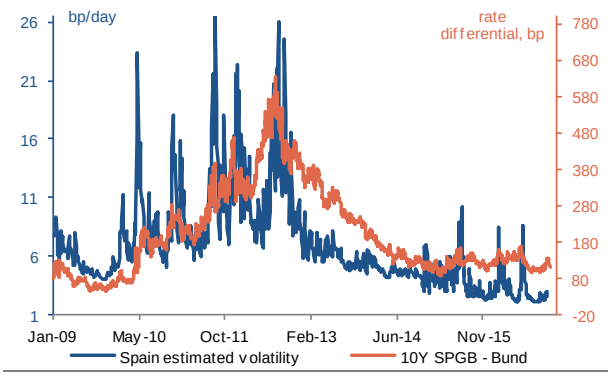

The un-temporal Marginals

The GAS method has provided a relevant descriptor of the conditional probability distributions function $p(x_t|x_{t-1})$ that characterises the behaviour of European sovereign CDS price variations. Let y be a series of real numbers that takes the actual historical realisations of $(x_t)_{t=1..N}$ as recorded in the dataset:

$$\text{For } t = 1,..,N \quad y(t) = x_t \quad \text{as measured in the data} \tag{20}$$

Based on this definition, y is not a random variable - in contrast to x.

At a given time t, $p(x_t|x_{t-1})$ is conditional on previous realisations $\{x_{t-1}, x_{t-2} \dots\}$. And this is because the calculation of the volatility coefficient σ_t involves parameters evaluated at $t-1$ (namely f_{t-1} and s_{t-1} in eq.(18)). While this helps seize the persistence of the volatility momentums, the conditionality also makes a high frequency manipulation of the model relatively cumbersome. At any time t in particular, evaluating the GAS estimator σ_t requires calculating all the series $\{\sigma_1, \dots, \sigma_{t-1}\}$. The time varying aspect of σ_t also means that $p(x_{t-1}|x_{t-2}) \neq p(x_t|x_{t-1})$: the model delivers a specific probability distribution function for every market realisation in the data. This tends to make any extrapolation outside the history more complicated (like the exploration of synthetic case studies). This sophistication could prove a drag for non-quantitative market participants, or in the context of a day to day use of the model, as in both cases the computational/mathematical burden can prove complex and time-consuming. The extension of the model on a broader set of time series could similarly be somewhat a heavy task, so it could be beneficial to consider a simpler version of the model instead.

A possible way to reduce complexity is to design a new volatility estimator, **independent of the historical path of market prices**. In this respect, removing the time conditionality in $p(x_t|x_{t-1})$ may be helpful. ➔ The new version of p has to be designed on the basis that the current-day price realisation y is enough information as to characterise the corresponding distribution function of x. As a result we denote this new probability distribution function $p_y(x)$.

We want to make $p(x_t)$ conditional on $y(t)$ instead of x_{t-1}. **And to do so, we now have to establish a new volatility estimator that has to be calculated out of y.** We denote this novel volatility estimator as $h(y)$, and we describe an empirical estimation of this coefficient in the next paragraphs. We also explore the soundness of this new indicator via the ADC and PIT applied to the resulting p_y. Finally we take a look at the potential ease of use that comes from this new model.

Grounds, assumptions and approximations relative to the volatility parameter h

For a given price realisation $y(t)$, we denote the novel volatility indicator as $h(y)$. And as in preceding paragraphs, σ_t refers to the conditional volatility obtained from the GAS model. **One assumption that we want to keep unchanged is that CDS changes are still distributed according to a GHT density.** We thus define p_y as a GHT density, whereby the volatility parameter σ has been replaced with its new version $h(y)$.

Since our calculation of $h(y)$ may jeopardize the normality constraint associated to probability density functions, we also add the required normalisation coefficient:

$$p_y(x) = \frac{(\nu-2)^{\nu/2}}{\pi^{\frac{1}{2}} h(y)} \quad \frac{\Gamma\left(\frac{\nu+1}{2}\right)}{\Gamma\left(\frac{\nu}{2}\right)\left(\nu-2+\frac{x^2}{h(y)^2}\right)^{\frac{\nu+1}{2}}} \times \frac{1}{\int_{-\infty}^{+\infty} p_y(w)dw} \tag{21}$$

Where ν is the degree of freedom that we set at $\nu = 5$.

The benefit of considering the cumulative distribution function

There is apparently no obvious connection between the GAS volatility σ_t and y, as plotting one against the other yields a very fuzzy scatterplot (Graph 44). The intense concentration of the points in the interval $y \in [-1,1]$ in particular makes the exploration of any pattern pointless. Plus y spans over different intervals for each country (CDS daily price changes span over $[-15,15]$ for France for instance, and $[-55,41]$ for Italy). This makes cross-country comparisons in the frame of x particularly challenging.

Because of these limitations, we prefer exploring the behaviour of σ_t as a function of the cumulative probability function of p_y, that we denote $F(x) = \int_{-\infty}^{x} p_y(x)\,dx$. Since we do not have an analytical expression of $F(x)$, we just consider its empirical version, calculated on the dataset (ie. for $x = y_t$). We denote this empirical indicator $\hat{F}(x)$, and we assume that $\hat{F}$ is a reliable descriptor of $\hat{F}$, ie. $\hat{F}(x) \sim F(x)$.

The bijective relationship between $\hat{F}$ and y (Graph 45) is an important feature, as it suggests that we could potentially express the volatility h as a function of $\hat{F}(x)$. This may be an interesting alternative to considering h as a function of x. A consequence however, is that h is estimated via empirical estimators in this case, and therefore needs to be adjusted to $\hat{h}$. In the end we get:

$$h(y) \sim \hat{h}(y) = \hat{h}\big(\hat{F}(y)\big)$$

Graph 46 is an illustration of the volatility's dynamics where we plot the conditional volatility σ_t against the empirical cumulative function $\hat{F}(y)$ (for Germany).

Graph 44. The vol σ is not a straightforward function of y

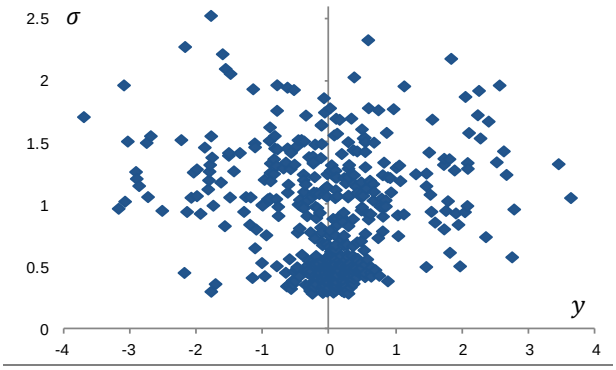

Graph 45. $\hat{F}(y)$ is the empirical cumulative function of x

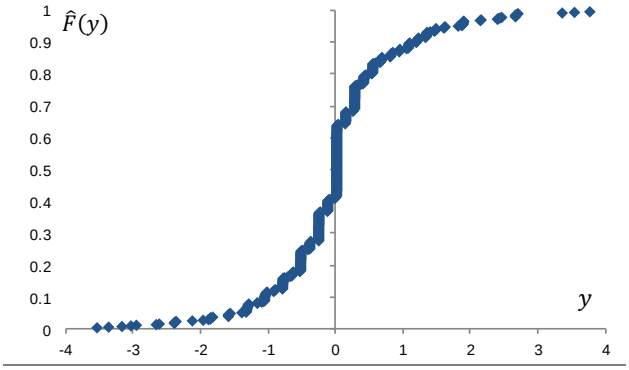

Considering h as $\hat{h}\big(\hat{F}(x)\big)$ also makes the calculation of probabilities relatively straightforward: Assuming two different events in terms of price realisations: $0 < x < K_1$ and $K_2 < x < 0$, with P_1 and P_2 be the respective probability that each event materialises (as per eq. (22)). The knowledge of $\hat{u} = \hat{F}(x)$ is sufficient to calculate P_1 and P_2:

$$\begin{cases} P_1 = P(0 < x < K_1) = F(K_1) - F(0) \sim \hat{F}(K_1) - \hat{F}(0) \ \ for\ 0 < x < K_1 \\ P_2 = P(K_2 < x < 0) = F(0) - F(K_2) \sim \hat{F}(0) - \hat{F}(K_2) \ \ for\ K_2 < x < 0 \end{cases} \quad (22)$$

We already showed that the data is centred ($\bar{x} \sim 0$). We also assume that x admits a GHT distribution, and since this distribution is symmetrical, the average value $\bar{x}$ is concordant with its median, so we can note that $\hat{F}(\bar{x}) = \hat{F}(0) \sim 0.5$. As a result, $\hat{F} < 0.5$ refers to a negative CDS price variation ($x < 0$), while $\hat{F} > 0.5$ relates to an increase in CDS prices ($x > 0$). This will prove particularly straightforward to explore the implications of tail events. In particular when considering a limit $K > 0$ on the price variation x (this could be the maximum tolerated volatility), we derive the probability that x effectively exceeds this threshold as $1 - \hat{F}(K)$. The other way round, if $K < 0$ the probability of x moving below this threshold is given by $\hat{F}(K)$.

Graph 46. σ_t as a function of $\hat{F}$ is a more tractable approach

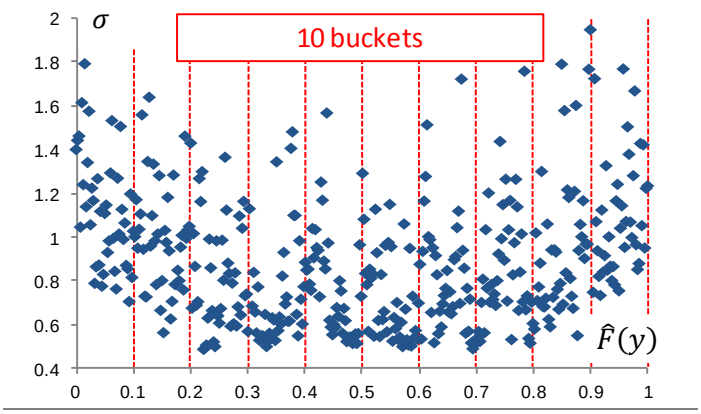

Calculating $h(y)$

In this chapter we describe the calculation of a new un-temporal volatility estimator $h(y)$, computed out of the cumulative distribution $\hat{F}$. We also gauge the soundness of this new estimator, by exploring the shape of the resulting probability distribution function p_y.

As an intuitive understanding of the un-temporal volatility, $\hat{h}$ can be regarded as an estimator of the average value of σ, given that $x = y$, at any time t. In other words, we think that it is sensible to understand $\hat{h}$ as an estimator of the expectation of σ, conditional on $x = y$:

$$\hat{h}(y) = \hat{\mathbb{E}}\left(\sigma | \hat{F}(x)\right) \quad (23)$$

We now describe an empirical procedure to estimate $\hat{\mathbb{E}}\left(\sigma | \hat{F}(x)\right)$. As shown in Graph 46, we first divide the values of $\hat{F}$ into 10 buckets; and we consider the points in every bucket as a measure of the volatility σ , conditional on $\hat{F} = \ centre\ \ of\ the\ bucket$.

Then we look at the distribution of σ in each bucket. As expected, the variance of σ is larger in the tails. In the upper tail for instance (Graph 47) the frequency of σ is larger, reaching $[0.8, 1.0]$. In comparison, σ is much smaller in the centre of the distribution (ie. $\hat{F} \sim 0.5$), where it takes values in the $[0.4, 0.6]$ according to Graph 48.

Graph 47. Empirical distribution of σ in the tails $\hat{F}(y)\sim 1$

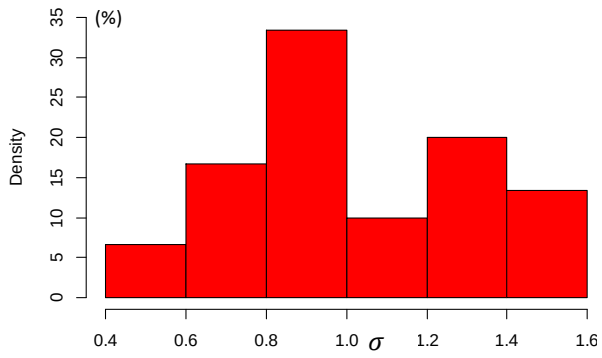

Graph 48. Empirical distribution of σ in the centre of the distribution, ie. $\hat{F}(y)\sim 0.5$

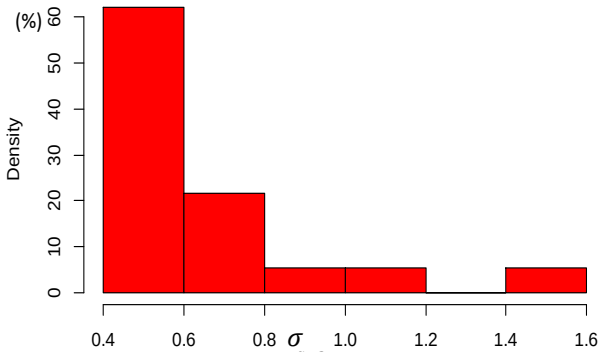

After having identified the probability distribution function of σ_t in each bucket, we now need to determine an empirical estimator of the corresponding average value (ie. $\hat{\mathbb{E}}(\sigma)$ in each bucket). Every bucket is composed of around 230 points, which is relatively small from a statistical point of view. As a consequence, the usual 'sample mean' coefficient may experience a significantly bias from the true value, perhaps a bigger bias than the 'sample median' does.

Reis, Botelho (2013) show that the sample median is generally a more robust statistical estimator than the sample mean. This becomes especially obvious when the sample size is reduced, in which case outliers in the sample can cause a substantial distortion on the sample mean – while this is less pronounced on the median estimator. The greater robustness of the median makes it a preferred estimator when there is only little data available. On that basis, we will explore both approaches separately (sample mean/median).

Graph 49. Median vs. Mean estimator for a given bucket located in the right tail

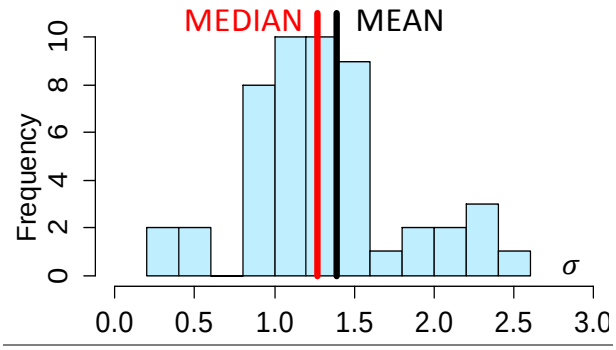

Graph 50. Median vs. Mean estimator for a given bucket located in the belly

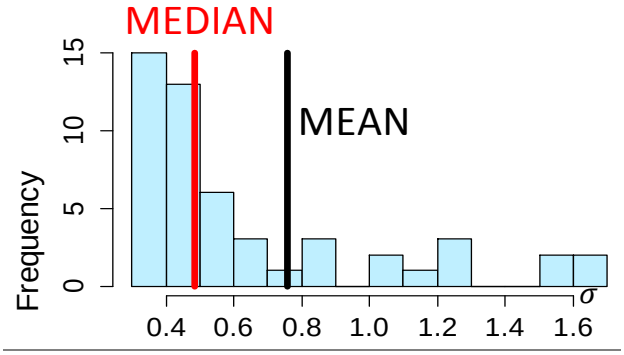

As an illustration of this difference, in terms of bias, between the median and the mean, we compared both estimators in the centre ($\hat{F}\sim 0.5$ in Graph 50) and in the tail regions of $\hat{F}$ ($\hat{F}\sim 1$, in Graph 49). There it appears that the sample mean (denoted $MEAN(\sigma)$) is relatively far from areas where the density of σ is particularly intense. And in contrast, the median estimator (ie. $MEDIAN(\sigma)$), is much more in line with these areas where the density of σ reaches a peak (red line in Graph 49 and Graph 50).

➔ **The median is potentially a better estimator to model the "expected value" of σ than the more typical sample mean.** We estimate two versions of $\hat{h}$, based on either the MEDIAN or the MEAN. This will help identify the best approach.

First we highlight results relative to the $MEDIAN$ estimator, in Graph 51 to Graph 54 (for different countries). Then we look at those relative to the $MEAN$ estimator in Graph 55 and Graph 56. For better clarity we denote $\hat{\mathbb{E}}_{MEDIAN}$ and $\hat{\mathbb{E}}_{MEAN}$ the two different operators, and $\hat{h}_1, \hat{h}_2$, the resulting volatility:

$$\begin{cases} \hat{h}_1(x) = \hat{\mathbb{E}}_{MEDIAN}\left(\sigma|\hat{F}(x)\right) \\ \hat{h}_2(x) = \hat{\mathbb{E}}_{MEAN}\left(\sigma|\hat{F}(x)\right) \end{cases}$$

We plot $\hat{h}_1$ against $\hat{F}$ in Graph 51 and Graph 52, and against y in Graph 53 and Graph 54. Then we do the same with $\hat{h}_2$ in Graph 55 and Graph 56.

Graph 51. $\hat{\mathbb{E}}_{MEDIAN}\left(\sigma|\hat{F}(x)\right)$ **as a function of** $\hat{F}$ **for core**

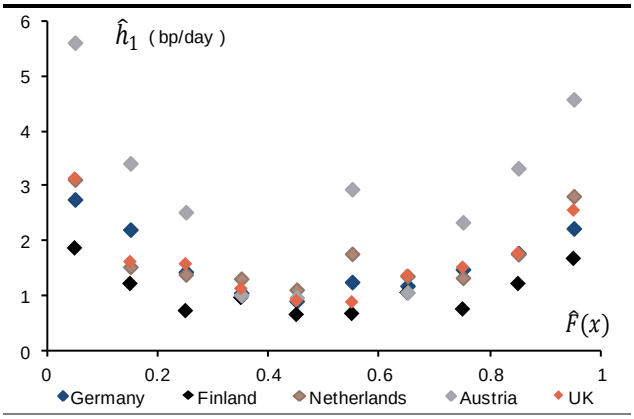

Graph 52. $\hat{\mathbb{E}}_{MEDIAN}\left(\sigma|\hat{F}(x)\right)$ **versus** $\hat{F}$ **in non-core**

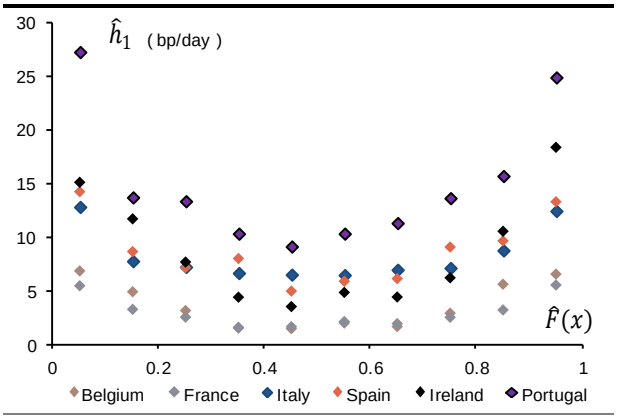

Graph 53. $\hat{\mathbb{E}}_{MEDIAN}\left(\sigma|\hat{F}(x)\right)$ **as a function of** x **for core**

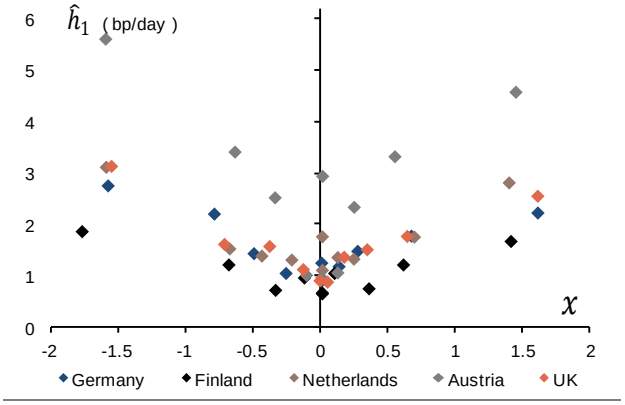

Graph 54. $\hat{\mathbb{E}}_{MEDIAN}\left(\sigma|\hat{F}(x)\right)$ **as function of** x **for non core**

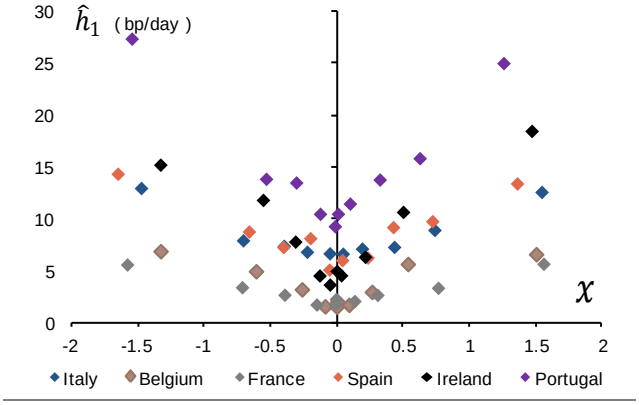

Graph 55. $\hat{\mathbb{E}}_{MEAN}\left(\sigma|\hat{F}(x)\right)$ **as a function of** x

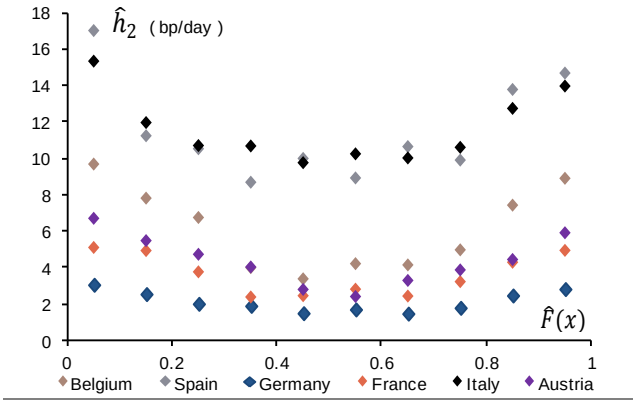

Graph 56. $\hat{\mathbb{E}}_{MEAN}\left(\sigma|\hat{F}(x)\right)$ **as a function of** x

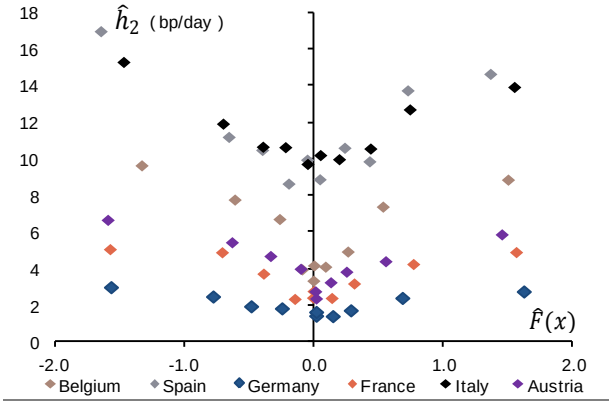

$\hat{h}_1$ and $\hat{h}_2$: from discrete to continuous variables

Because $\hat{F}$ was segmented into 10 buckets, we are now left with 10 values for $\hat{h}_1$ and $\hat{h}_2$. This already gives interesting insight, but we need to generalise these observations to other values of $\hat{F}$. Ideally, we would like to obtain a continuous expression of the volatility so that $\hat{h}$ could be evaluated for any $\hat{F}(y)$, as suggested in eq. (21). In this section, we explore how to extrapolate these preliminary results to all values of $\hat{F} \in [0,1]$, and we consider three different approaches:

- In a first attempt, we calculate $\hat{h}_1(\hat{F}(y))$ and $\hat{h}_2(\hat{F}(y))$ as a linear interpolation out of the two nearest neighbours, ie. the two closest centres of buckets ('nearest neighbour' type interpolation, that we denote NN). This is a very basic interpolation method, where the volatility $\hat{h}$ for every point is a linear combination of what we got for the two nearest buckets, using the Euclidean distance between the points. As the new points are derived from the "nearest information" only, this method usually provides a very nice fit to the dataset (with risks of overfitting in some circumstances). But this approach also fails to provide an analytical expression of the general behaviour of $\hat{h}(\hat{F}(y))$, and there is no way to extrapolate $\hat{h}$ outside of the measured range. This lack of tractability is a good reason for not retaining this interpolation method, but we will consider the resulting fit – supposed to be compelling - **as a benchmark to gauge the quality of other interpolation methods.** We denote the resulting series as $\hat{h}_{1,NN}$ and $\hat{h}_{2,NN}$.

- Secondly we explore a **second order polynomial interpolation** (noted **PI**). The second order polynomial behaviour implies calibrating three unknowns a_0, a_1, a_2, and we assume the following expression for the volatility $\hat{h}$: $\hat{h}\left(\hat{F}(y)\right) \sim a_0 \times \hat{F}(y)^2 + a_1 \times \hat{F}(y) + a_2$ We calibrate these three unknowns using the classical OLS approach. **We denote the resulting series as $\hat{h}_{1,PI}$ and $\hat{h}_{2,PI}$.**

- Thirdly, we consider **a logarithmic interpolation** (noted **LI**), on the basis that the logarithmic curvature may be more appropriate than the polynomial model to describe the acceleration of the volatility in the tails. We prefer calibrating this model directly on the full set of $\{\sigma_t, \hat{F}(y_t)\}$ instead of involving $\hat{h}_1$ and $\hat{h}_2$ separately.
First let us consider y_s a sorted version of y_t (increasing order). We then calibrate the logarithmic interpolation as per the following formula:

$$\begin{cases} \hat{h} \sim a_{0,1} \times \log\left(\frac{L}{2} - s\right) + a_{1,1} & if\ s < L/2 \\ \hat{h} \sim a_{0,2} \times \log\left(s - \frac{L}{2}\right) + a_{1,2} & if\ s > L/2 \end{cases}$$

where L is the sample size.

This means that we have to calibrate two unknowns in each subarea ($a_{0,1}$, $a_{1,1}$, and $a_{0,2}$, $a_{2,2}$ respectively). We denote the resulting volatility as $\hat{h}_{LI}$.

In the end we are left with 5 volatility estimators for each country: $\hat{h}_{1,NN}$, $\hat{h}_{1,PI}$, $\hat{h}_{2,NN}$, $\hat{h}_{2,PI}$, and $\hat{h}_{LI}$. Then for these five potential candidates, we consider the corresponding probability distribution function p_y, as defined in eq. (21):

$$p_y(x) \sim \hat{p}_y(x) = \frac{(\nu-2)^{\nu/2}}{\pi^{\frac{1}{2}}\hat{h}\left(\hat{F}(y)\right)} \frac{\Gamma\left(\frac{\nu+1}{2}\right)}{\Gamma\left(\frac{\nu}{2}\right)\left(\nu - 2 + \frac{x^2}{\hat{h}\left(\hat{F}(y)\right)^2}\right)^{\frac{\nu+1}{2}}} \times \frac{1}{\int_{-\infty}^{+\infty} \hat{p}_y(w)dw}$$

And we also consider the **corresponding cumulative distribution** function F:

$$F_y(x) = \int_{-\infty}^{x} p_y(l)dl \sim \int_{-\infty}^{x} \frac{(\nu-2)^{\nu/2}}{\pi^{\frac{1}{2}}\hat{h}\left(\hat{F}(y)\right)} \frac{\Gamma\left(\frac{\nu+1}{2}\right)}{\Gamma\left(\frac{\nu}{2}\right)\left(\nu-2+\frac{l^2}{\hat{h}\left(\hat{F}(y)\right)^2}\right)^{\frac{\nu+1}{2}}} dl \times \frac{1}{\int_{-\infty}^{+\infty} \hat{p}_{y_t}(w)dw} \quad (24)$$

Using the same notation as for $\hat{h}$ before, we calculate $p_y^{1,NN}(x)$, $p_y^{1,PI}(x)$, $p_y^{2,NN}(x)$, $p_y^{2,PI}(x)$, and $p_y^{LI}(x)$. We also calculate the corresponding cumulative distribution functions $F_y^{1,NN}(x)$, $F_y^{1,PI}(x)$, $F_y^{2,NN}(x)$, $F_y^{2,PI}(x)$ and $F_y^{LI}(x)$.

In order to assess the robustness of each version of $\hat{h}$, we consider the Anderson-Darling criterion, that we apply to the corresponding $\hat{F}_y$. Assuming a perfect calibration of $\hat{h}_i$, the series $\hat{F}_y(y)$ must be uniformly distributed. The ADC test quantifies the actual deviation against the uniform distribution. As a reminder, the smaller the ADC, the better the fit.

Table 15. Goodness of fit of the un-temporal cumulative distribution functions $F_y^i(y)$

Anderson Darling Criterion														
Interpolation Method		GE	FI	NL	AT	FR	BE	IT	SP	IR	PT	UK	Average	St. Dev.
Moving Average	$F_y^{1,NN}$	2.4	2.6	2.5	3.2	1.9	2.3	1.3	1.7	1.8	1.8	1.5	2.1	0.5
	$F_y^{2,NN}$	3.0	2.9	3.2	3.8	2.8	3.1	1.9	2.4	2.5	2.2	2.4	2.7	0.5
Polynomial Interpolation	$F_y^{1,PI}$	2.1	2.1	2.2	1.9	1.9	1.5	1.0	1.2	1.4	1.4	1.2	1.6	0.4
	$F_y^{2,PI}$	**2.9**	**2.7**	**3.0**	**2.6**	**4.2**	**2.7**	**2.3**	**2.4**	**2.4**	**2.4**	**2.3**	**2.7**	**0.5**
Logarithmic Interpolation	F_y^{LI}	3.8	3.4	3.8	4.2	3.8	3.5	2.5	2.8	2.1	3.1	2.0	3.2	0.7

Table 15 shows the resulting ADC; and helps conclude on the most appropriate volatility estimator:

- Logarithmic interpolation: worst results. As Graph 57 shows (for Germany), $\hat{h}_{LI}$ offers an acceptable fit against the volatility σ. The fit at least does not look particularly bad. However, ADCs relative to p_y^{LI} are much bigger than for other methodologies, suggesting that this probability distribution is not able to capture the actual dynamics of x. **As a consequence, the algorithmic interpolation cannot be regarded as an appropriate choice - we reject this option.**

Graph 57. Logarithmic volatility against σ The logarithmic model has a too large error in the belly of the distribution

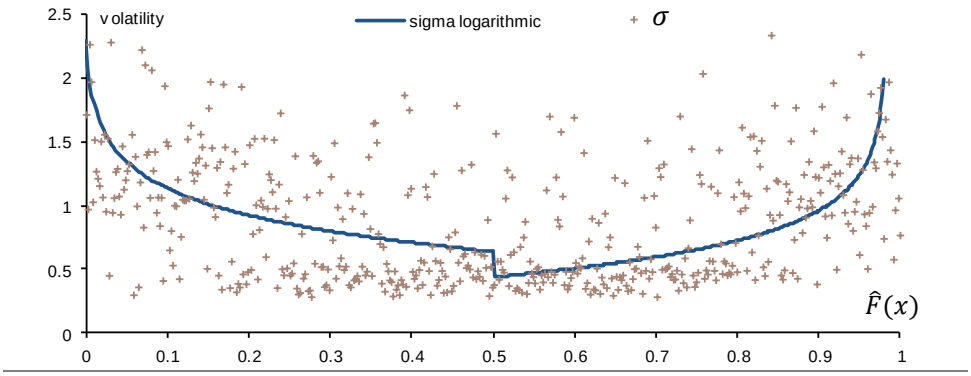

- Mean versus Median? Table 15 shows that ADCs are much better for distributions based on the median rather than on the mean, which is in line with our intuition. As a consequence, $F_y^{2,NN}$ and $F_y^{2,PI}$ are not acceptable descriptors of x, and so we disregard $\hat{h}_{2,NN}$ and $\hat{h}_{2,PI}$.

Graph 58. Nearest Neighbours volatility $\hat{h}_{1,NN}$ vs. $\hat{F}$ for Germany (left) and Spain (right)

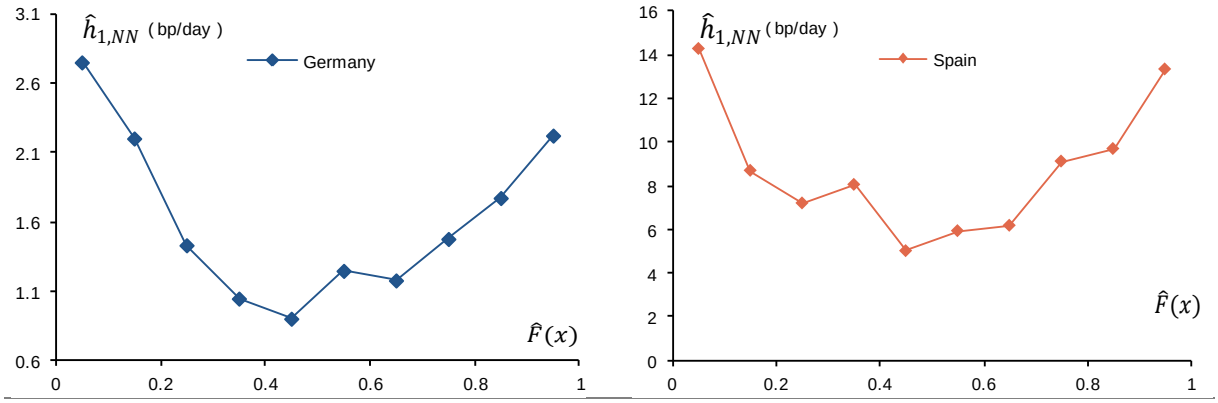

- Nearest Neighbour interpolation: Though $\hat{h}_{1,NN}$ provides a decent fit against the 10 measures of $\hat{h}_1$ in Graph 58, the ADC is relatively large, and in particular as big as 3.2 and 2.6 for Austria and Finland – thus beyond the acceptance level. As a consequence, $F_y^{1,NN}$ is not compelling and we reject $\hat{h}_{1,NN}$ as a fair estimator of the non-temporal volatility.

- Polynomial Interpolation: results are very good overall. $F_y^{1,PI}$ in particular exhibits an average criterion at just 1.6, **which is small enough to consider that $p_{1,PI}$ is properly calibrated.** As a result, **$\hat{h}_{1,PI}$ can be seen as an adequate estimator of the un-temporal volatility of x.** Arguably, the ADC is also smaller for peripheral countries, and a bit higher for core and soft-core countries. This suggests that the polynomial method is particularly appropriate to estimate the volatility of riskier assets – ie. of those who are the more subject to contagion. Graph 59 shows the dynamics of $\hat{h}_{1,PI}$ against the conditional volatility σ: we note that the acceleration of the volatility in the tail regions is a non-linear function of $\hat{F}$. This already hints at a remarkable acceleration of the market deterioration when financial distress tends to escalate.

Graph 59. Polynomial volatility $\hat{h}_{1,PI}$ against σ_t for Germany (left) and Italy (right)

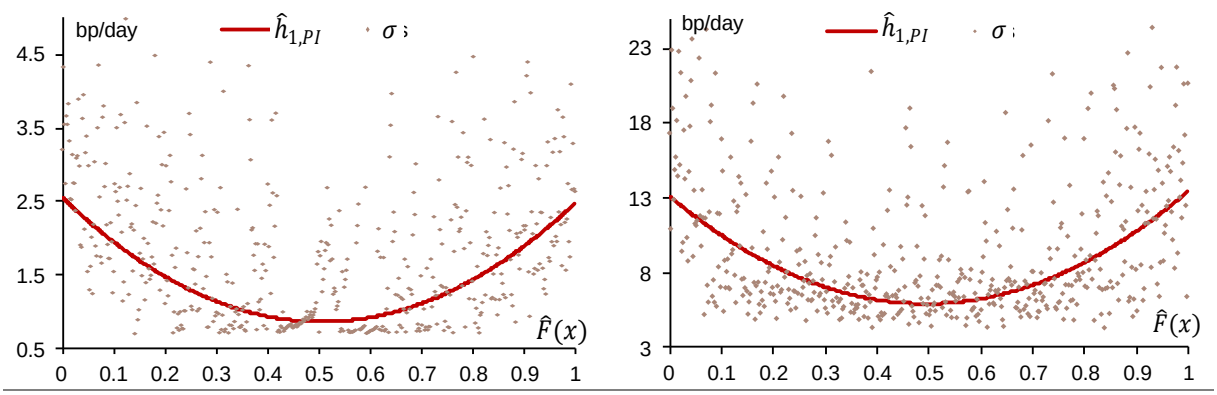

In conclusion, the polynomial model assorted with the sample median provides the best estimator of the un-temporal volatility $\hat{h}(y)$. Statistical tests confirm that the resulting un-temporal probability distribution function p_y offers an acceptable fit to the empirical data for every country. That said, we note that the Shapiro-Wilk normality test applied to the polynomial interpolation shows that residuals are not normally distributed, with the resulting statistics well below 5%.

The dynamics of the volatility indicator h

Considering the median estimator and the second order polynomial interpolation method, we finally obtained the following expression for the un-temporal volatility $\hat{h}$:

$$\hat{h}(y) \sim a_0 \times \hat{F}(y)^2 + a_1 \times \hat{F}(y_t) + a_2 \qquad (25)$$

With the following values for a_0, a_1, a_2:

Table 16. Estimated coefficients of the second order polynomial interpolation

	GE	FI	NL	AT	FR	BE	IT	SP	IR	PT	UK
a0	7.5	5.0	7.6	18.2	18.3	27.3	29.4	37.8	65.1	76.6	8.8
a1	-7.8	-5.1	-7.6	-18.7	-18.1	-27.1	-29.0	-37.5	-64.0	-76.4	-9.0
a2	3.1	2.0	3.0	6.1	6.0	8.2	13.1	14.9	19.1	27.8	3.2

In the end, we obtain the following non conditional univariate probability function $p_y(x)$:

$$\begin{cases} p_y(x) \sim \dfrac{(\nu-2)^{\nu/2}}{\pi^{1/2}} \times \dfrac{\Gamma\left(\dfrac{\nu+1}{2}\right)}{\Gamma\left(\dfrac{\nu}{2}\right) \times \left(\nu - 2 + \dfrac{x^2}{\hat{h}(y)^2}\right)^{\frac{\nu+1}{2}}} \\ \hat{h}(y) \sim a_0 \times \hat{F}(y)^2 + a_1 \times \hat{F}(y) + a_2 \\ \hat{F}(y) \sim \displaystyle\int_{-\infty}^{y} p(w)dw \end{cases}$$

Graph 60 to Graph 70 display the shape of $p_y(y)$ for all countries, ie. evaluated on values taken in the sample. We compare this against the empirical distribution of x; globally the fit is satisfying, therefore confirming the compelling ADC in Table 15.

Graph 60. Univariate density; GE

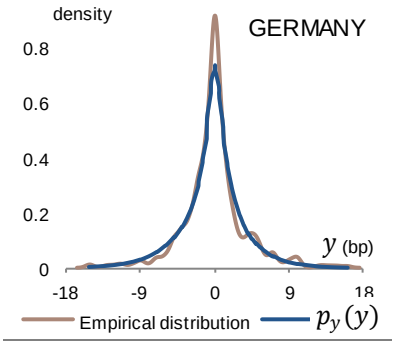

Graph 61. Univariate density; FI

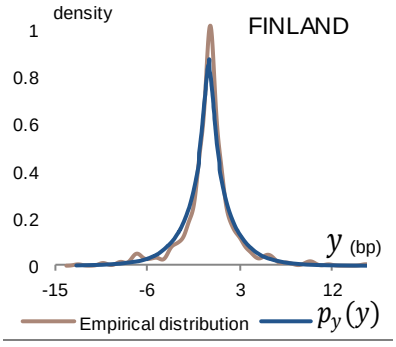

Graph 62. Univariate density; NE

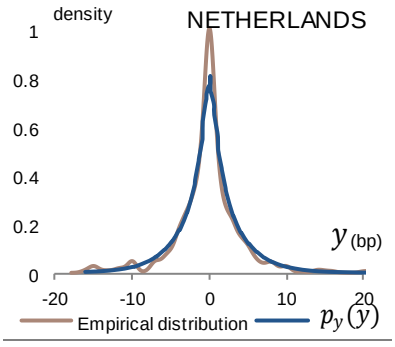

Graph 63. Univariate density; AT

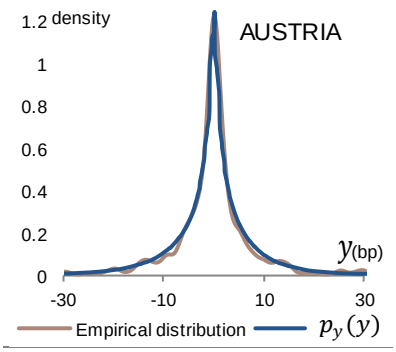

Graph 64. Univariate density; FR

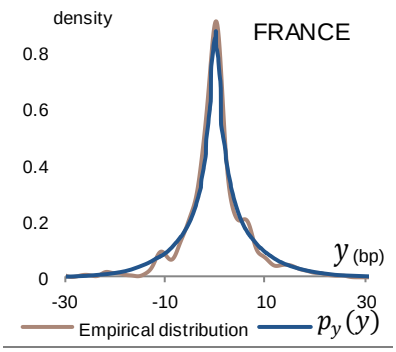

Graph 65. Univariate density; BE

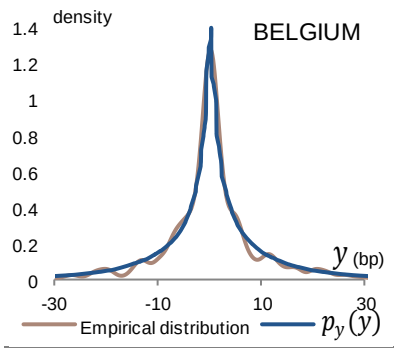

Graph 66. Univariate density; IT

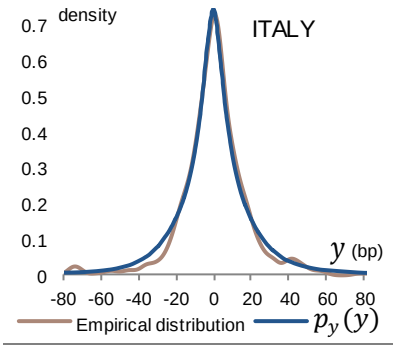

Graph 67. Univariate density; SP

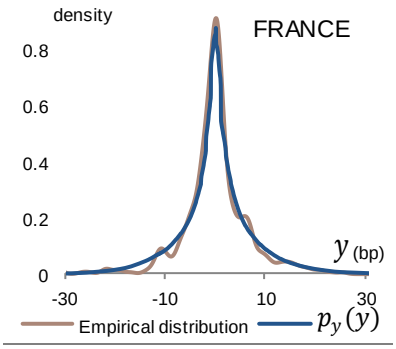

Graph 68. Univariate density; IR

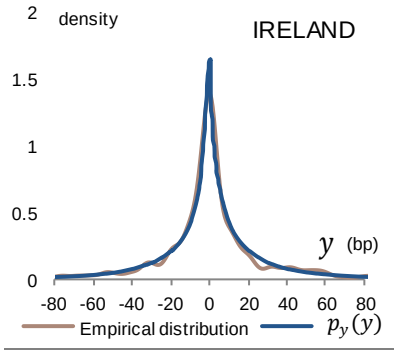

Graph 69. Univariate density; PT

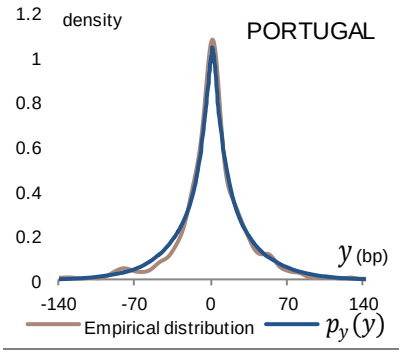

Graph 70. Univariate density; UK

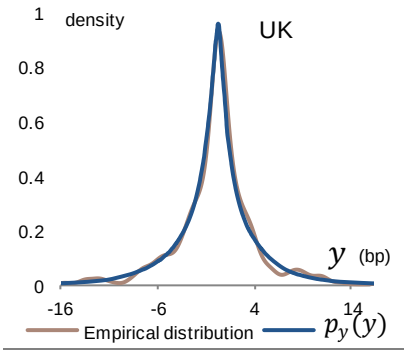

Graph 71. Volatility $\hat{h}$ in bp/day as a function of the empirical cumulative distribution

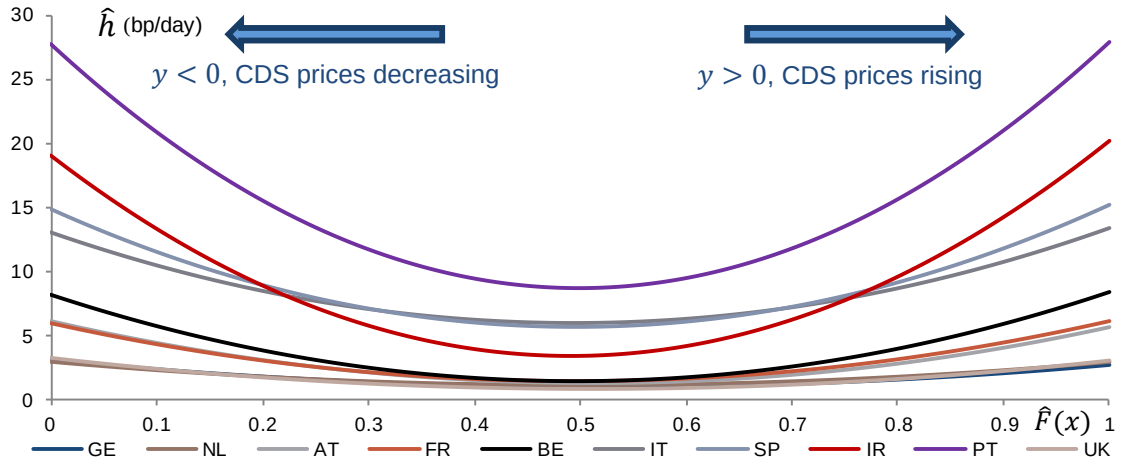

The volatility profile

Graph 71 shows the resulting volatility as a function of $\hat{F}$. Because of the polynomial interpolation, the volatility curves look like parabolas, which emphasizes the nonlinear increase in the volatility as we near the tail regions. Core countries overall exhibit little volatility, slightly less than soft-core countries do. In contrast, the volatility is much larger in peripheral countries. This is in line with empirical observations.

At the centre of the distribution, the market is very stable. This corresponds to a regime of very low volatility, whereby core and soft core countries show a comparable $\hat{h}$, at around $1bp/day$. $\hat{h}$ is much bigger in non-core countries, with e.g. Portugal showing the largest volatility in the sample, at $9bp/day$ just above Spain and Italy at $5.5bp/day$, and Ireland at $3.5bp/day$.

We also note that the parabola shape tends to magnify the differentiation between core/soft-core/non-core countries in the tail regions. The volatility in peripheral countries in particular rises much faster. Portugal and Ireland for instance are still the most exposed countries to a shock, with the idiosyncratic volatility rising to $28bp/day$ and $19bp/day$ respectively under extreme scenarios. ➔ **In a low volatility environment, Ireland is definitely more stable than other peripheral countries. But this does not hold when volatility is larger as the deterioration incurred by risk aversion leads to greater entropy in Ireland than in Spain or Italy.** In essence, Ireland's recovery since the sovereign crisis has favoured some convergence with soft-core economies. This is apparently more visible market conditions are more stable (ie. when volatility is muted). In more troubled situations though, the greater volatility in Ireland (compared to Spain and Italy) reflects still the marks of the sovereign crisis still.

Italy and Spain prove rather similar overall, except in the tails where Spanish CDS have a $2bp/day$ higher volatility than Italian CDS.

Soft-core countries prove much more resilient overall. Belgian CDS spreads for instance experience a volatility of $8bp/day$ in the tails, while the volatility on French and Austrian CDS is lower, around $6bp/day$. With no surprise, core countries are the more resilient, with a volatility of $3bp/day$ in the tails for Germany, the Netherlands and Finland.

Let us now explore the distribution of $\hat{h}$ within the dataset. Graph 72 shows the empirical distribution of the volatility $\hat{h}$ for Germany, France and Italy. These distributions give an idea of the risks relative to an unexpected surge in the volatility. We define in particular the "volatility risk" (VR) as the probability that $\hat{h}$ be equal to or higher than a given threshold $\hat{h}_{th}$. We then define our criterion VR as:

$VR(\hat{h}_{th}) = P(\hat{h} \geq \hat{h}_{th}) = 1 - \hat{F}_h(\hat{h}_{th})$ where $\hat{F}_h$ is the empirical cumulative distribution function of $\hat{h}$.

Graph 73 displays $VR(\hat{h}_{th})$ based on the same data as in Graph 72. This chart shows the probability that the volatility $\hat{h}$ tends to exceed the threshold $\hat{h}_{th}$ as indicated on the x-axis**.** For instance, it appears that there is a 10% risk that the volatility exceeds the threshold of $2.6bp/day$ in Germany, $5.2bp/day$ in France and $11.9bp/day$ in Italy. We generalize this approach to all countries in Table 17.

Graph 72. Empirical distribution of the volatility

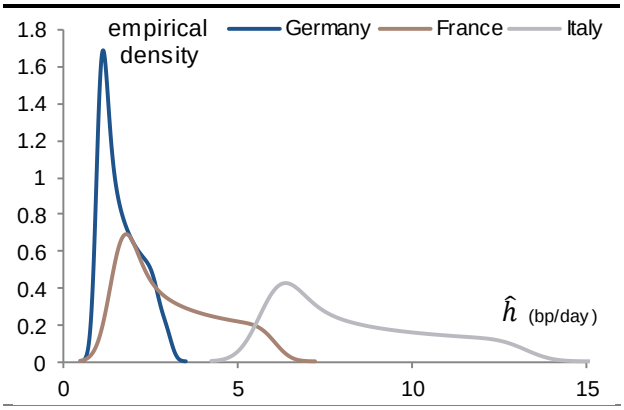

Graph 73. Empirical cumulative distribution of the volatility

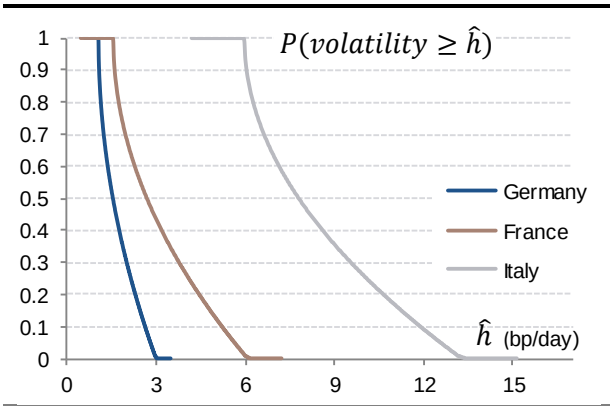

Table 17. Volatility Risk for EMU countries in bp/day

VR	GE	FI	NL	AT	FR	BE	IT	SP	IR	PT	UK
10%	2.6	1.7	2.6	5.1	5.2	7.0	11.9	13.3	16.8	24.0	2.7
20%	2.3	1.5	2.3	4.3	4.4	5.8	10.7	11.7	14.0	20.8	2.4
50%	1.5	1.0	1.6	2.5	2.7	3.2	7.8	8.0	7.6	13.5	1.5
80%	1.1	0.7	1.2	1.5	1.7	1.8	6.3	6.1	4.2	9.5	1.0
90%	1.1	0.7	1.1	1.4	1.6	1.6	6.1	5.8	3.7	9.0	0.9

We also express the volatility $\hat{h}$ as a function of the CDS daily price variations y (in basis points), in Graph 74. The picture is hard to exploit in this frame. In particular it is no longer possible to understand the risks associated to a given level of volatility. But there is additional insight though. We note for instance that Irish CDS are less volatile than equivalent Spanish or Italian CDS when the price variation on the x-axis is smaller or equal to $3bp$. This dynamics, however, does not hold beyond this threshold as Italian CDS are the more stable at the periphery, when the daily CDS price variation is larger than $3bp$. More generally, Graph 74 illustrate the structural differences between each security. In particular the contrast between and core/soft-core and non-core CDS spreads in terms of intrinsic volatility is fierce.

Graph 74. Polynomial volatility as a function of CDS price variations

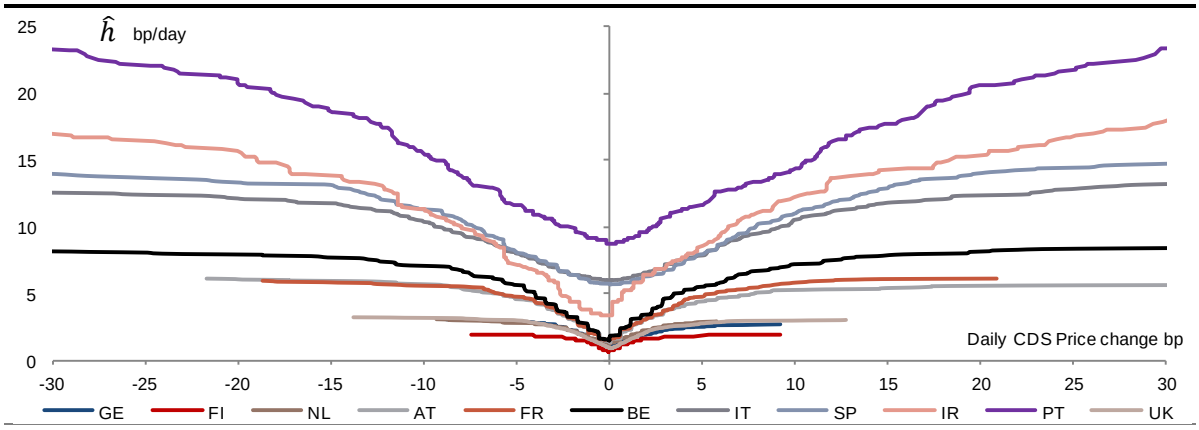

Conclusion to the univariate calibration

In this section we explored the calculation of an empirical estimator of the un-temporal volatility $\hat{h}$ of x. $\hat{h}$ is computed as an empirical extrapolation of the GAS volatility σ_t, from which we derived an expression of the un-temporal probability distribution function p_y of x.

In the end, $\hat{h}$ and p_y bring innovation in the sense that these parameters do not depend on the past realisations of x_t. This is therefore a time-independent extrapolation of the results obtained in the previous section. $\hat{h}$ and p_y are now more straightforward to calculate than σ_t and $p(x_t|x_{t-1})$. This makes a high-frequency use of the model more tractable, and more generally, this is a valuable innovation for market practitioners with limited quantitative tools at hand.

Because of the generalising nature of the conditional mean in eq. (23), our un-temporal estimator $\hat{h}$ may be less sensitive to short term variations in historical volatilities than the conditional estimators σ_t.

Multivariate calibration of the model

In this section we conduct a multivariate exploration of the dataset, which eventually highlights the strength of pair-wise connections between each asset. Our approach to the multivariate problem requires calibrating bivariate GHT distributions. We achieve this by using an adequate formulation of the GAS model, adjusted to the higher dimension now. Though preliminary results were disappointing, we consider additional tweaks to the method that deliver compelling results. Our approach is largely inspired by the methodology of copula estimations. The flexibility of copulas is valuable in risk management (Bernardi, Catania (2015), Fei Fei, Fuertesy, Kalotychou (2013), Dalla Valle, De Giuli et al. (2014)); this is something we take advantage of. In particular we conduct a standardised version of the dataset based on the GAS volatility estimator we previously estimated. On that basis, we now consider standardized bivariate GHT distributions as adequate functions to describe the multivariate distribution of the dataset at hand.

We conduct the standardisation by normalising the volatility, ie. by dividing the original dataset by the GAS volatility σ_t. We denote the resulting points as z_t^i, such that:

$$z_t^i = \frac{x_t^i}{\sigma_t} \tag{26}$$

Where i refers to the corresponding country, and σ_t is the GAS estimator previously calculated.

As a result of the standardisation, z_t^i can be seen as distributed according to standard GHT distributions. We denote the standard GHT probability density function as $g(z_t^i)$ and the corresponding cumulative distribution as $G(z_t^i)$.

One of the challenges raised by the multivariate calibrations is to deliver a reliable picture of the linear dependencies. In other words, the covariance matrix of the multivariate distribution needs to be properly estimated. Given two countries i and j, let Σ be the covariance matrix of the bivariate distribution related to the pair (i, j). Then isolating the non diagonal coefficient $\Sigma^{i,j}$, we have $\Sigma^{i,j} = \mathrm{Cov}(z_t^i, z_t^j)$. As the variance of z_t^i is now standardized at 1 (ie. $\sigma_{z,i} = \sigma_{z,j} = 1$), the covariance matrix $\Sigma^{i,j}$ (as per eq. $(27)(29)$) can be seen as a measure of the correlations between z_t^i and z_t^j:

$$\Sigma^{i,j} = \mathrm{Cov}(z_t^i, z_t^j) = \frac{\mathrm{Corr}(z_t^i, z_t^j)}{\sigma_{z,i} \times \sigma_{z,j}} = \mathrm{Corr}(z_t^i, z_t^j) \tag{27}$$

The multivariate GHT model:

Since the data follows a standard univariate GHT distribution, we consider this formulation as a relevant candidate to describe the multivariate dynamics. And we consider the multivariate version of the GAS method as to estimate the corresponding correlation matrix Σ. As detailed earlier, the GAS method assumes that the covariance matrix is a time-varying parameter. As a consequence we rename the correlation matrix $\Sigma^{i,j}$ as $\Sigma_t^{i,j}$.

We also denote the probability distribution function of the standard bivariate GHT distribution as q_t:

$$q_t(z_t) = \frac{(\nu-2)^{\frac{\nu}{2}}.\Gamma\left(\frac{\nu+n}{2}\right)}{\pi^{\frac{n}{2}}|\Sigma_t|^{\frac{1}{2}}.\Gamma\left(\frac{\nu}{2}\right)\left(\nu-2+(z_t-\mu).{\Sigma_t}^{-1}\,^T(z_t-\mu)\right)}\ ;\ \nu = \text{degree of feedom} = 5 \qquad (28)$$

$$\mu = \text{vector of the means of every column of } z_t \text{ (1 value per country)},$$

$$n\text{: dimension of the problem} = \text{number of countries we consider simultaneously}$$

By analogy with x_t, the vector z_t is centred on zero, so we intuitively constrain $\mu = 0$. In sum, there is thus only one variable left to be estimated: the covariance matrix $\sum_t$. We also denote $Q_t(z_t)$ the corresponding cumulative distribution function:

$$Q_t(z_t) = \int_{-\infty,-\infty}^{z_t^i,z_t^j} q_t(v^i,v)dv^i dv$$

The multivariate formulation of the GAS method involves an adjusted version of the vector f_t. Based on the methodology developed in (Zhang, Creal, Koopman, Lucas (2012a), Zhang, Creal, Koopman, Lucas (2012b)), f_t is now made of the correlation coefficients extracted from $\sum_t$, and expressed as hyperspherical coordinates. In comparison, we had $f_t = \log(\sigma_t)$ in the univariate analysis.

Calculation of the hyperspherical coordinates

The multivariate model assumes that f_t and $\sum_t$ are made of hyperspherical coordinates, ie. angles. In order to calibrate these two parameters, we first introduce L_t as the Cholesky decomposition of the correlation matrix $\sum_t$:

$$L_t^T * L_t = \sum_t$$

Then we assume:

$$L_t = \begin{pmatrix} 1 & c_{1,2,t} & c_{1,3,t} & \cdots & c_{1,n,t} \\ 0 & s_{1,2,t} & c_{2,3,t}.s_{1,3,t} & \cdots & c_{2,n,t}.s_{1,n,t} \\ 0 & 0 & s_{2,3,t}.s_{1,3,t} & \cdots & c_{3,n,t}.s_{2,n,t}.s_{1,n,t} \\ 0 & 0 & 0 & \cdots & c_{4,n,t}.s_{3,n,t}.s_{2,n,t}.s_{1,n,t} \\ \vdots & \vdots & \vdots & \vdots & \vdots \\ 0 & 0 & 0 & \cdots & c_{n-1,n,t}\prod_{l=1}^{n-2} s_{l,n,t} \\ 0 & 0 & 0 & \cdots & \prod_{l=1}^{n-1} s_{l,n,t} \end{pmatrix} \qquad (29)$$

With $\begin{cases} c_{i,j,t} = \cos(\phi_{i,j,t}) \\ s_{i,j,t} = \sin(\phi_{i,j,t}) \end{cases}$, and we obtain: $f_t = \begin{pmatrix} \phi_{1,2} \\ \phi_{1,3} \\ \phi_{2,3} \\ \phi_{1,4} \\ \cdots \\ \phi_{n-1,n} \end{pmatrix}$ → **Components of f_t are angles**.

Plus we keep the same definition of f_t as in the univariate case:

$$f_{t+1} = \omega + A * \frac{\partial \log(q_t(z_t))}{\partial f_t} + B * f_t \qquad (30)$$

Calculation of $\frac{\partial\, log\,(q_t(z_t))}{\partial f_t}$, formulas :

Using matrix derivation, we introduce the half-vectorization operator $vech$ such that:

If $\Sigma = \begin{pmatrix} a_{11} & a_{12} & a_{13} \\ a_{12} & a_{22} & a_{23} \\ a_{13} & a_{23} & a_{33} \end{pmatrix}$ then $vech(\Sigma) = \begin{pmatrix} a_{11} \\ a_{12} \\ a_{22} \\ a_{13} \\ a_{23} \\ a_{33} \end{pmatrix}$

So we obtain:

$$\frac{\partial \log\,(q_t(z_t))}{\partial f_t} = \frac{\partial\, vech(\sum_t)^T}{\partial\, f_t} * \frac{\partial \log\,(q_t(z_t))}{\partial\, vech\,(\sum_t)} \quad \text{with } * \text{ the matrix product.}$$

Replacing with eq. (28):

$$\frac{\partial\ log\,(q_t(z_t))}{\partial \sum_t} = -\frac{1}{2}\frac{\partial\, log(\det(\Sigma_t))}{\partial\, vech(\,\Sigma_t)} - \left(\frac{v+n}{2}\right)\frac{\partial \log\left(v-2+(x-\mu)^T\Sigma_t^{-1}(x-\mu)\right)}{\partial\, vech(\Sigma_t)}$$

Then

1) $$\frac{\partial\, log(\det(\Sigma_t))}{\partial\, vech\,(\,\Sigma_t)} = \frac{\frac{\partial\,(\det(\Sigma_t))}{\partial\ vech(\Sigma_t)}}{\det(\Sigma_t)} \text{ and:}$$

$$\frac{\partial\,(\det(\Sigma_t))}{\partial\ vech(\Sigma_t)} = vech\left[\left(\det(\Sigma_t)\ trace\left(\Sigma_t^{-1} * \frac{\partial\,\Sigma_t}{\partial\left(\Sigma_{t\,i,j}\right)}\right)\right)_{i,j}\right] \text{ (this one is tractable)}$$

2) $$\frac{\partial \log\left(v-2+(x-\mu)^T\Sigma_t^{-1}(x-\mu)\right)}{\partial\, vech(\Sigma_t)} = \frac{\frac{\partial(\,(x-\mu)^T\Sigma_t^{-1}(x-\mu))}{\partial\, vech(\Sigma_t)}}{v-2+(x-\mu)^T\Sigma_t^{-1}(x-\mu)} \quad \text{and:}$$

$$\frac{\partial(\,(x-\mu)^T\Sigma_t^{-1}(x-\mu))}{\partial\, vech(\Sigma_t)} = -I_{\frac{n(n+1)}{2},\frac{n(n+1)}{2}} \otimes (x-\mu)^T * I_{\frac{n(n+1)}{2},\frac{n(n+1)}{2}} \otimes (\Sigma_t^{-1}) * \frac{\partial\,\Sigma_t}{\partial\, vech(\Sigma_t)} * \Sigma_t^{-1} * (x-\mu)$$

Where $\otimes$ is the kronecker product, I is the identity matrix and n is the dimension of the problem.

Table 18. ADC for "Italy and another country" copula (μ=0)
Pink = poor calibration, Green = better results

	ITALY AND									
	GE	FI	NL	AT	FR	BE	SP	IR	PT	UK
ADC resulting from 20 tests	6.2	8.5	5.7	4.8	9.0	7.2	4.4	8.7	11.5	5.5
	6.1	6.4	5.9	6.5	5.2	8.8	4.8	9.6	9.8	6.7
	5.7	3.6	5.7	5.2	5.5	5.2	3.5	8.5	5.6	11.0
	6.8	7.1	7.0	5.8	8.2	5.9	4.1	7.4	9.7	12.4
	7.6	6.9	7.0	5.6	7.7	4.3	3.0	6.8	6.5	7.5
	7.6	8.2	9.0	5.4	8.1	5.7	5.8	9.5	6.3	6.4
	7.3	4.7	6.1	10.4	9.3	7.8	5.6	11.5	5.7	9.7
	6.6	6.5	6.6	6.5	5.3	8.3	4.4	10.4	8.1	7.1
	5.7	9.8	7.6	7.4	5.3	4.3	8.2	5.4	9.5	6.8
	6.9	12.4	6.2	9.8	6.5	7.6	3.4	9.5	4.9	4.2
	7.1	11.5	7.0	7.3	5.6	4.9	4.4	4.9	6.7	9.8
	7.3	10.1	8.9	7.7	6.6	4.8	3.2	5.8	6.2	7.4
	6.2	8.4	11.5	7.0	6.3	5.9	4.4	6.8	9.8	6.1
	5.6	9.2	9.5	8.6	7.2	7.0	3.8	9.7	6.8	9.5
	7.6	4.7	9.6	8.0	6.6	5.0	5.4	9.2	11.5	10.4
	6.3	5.8	7.1	4.8	5.6	5.1	6.5	11.4	12.4	11.0
	6.7	7.2	7.9	7.0	8.6	7.7	8.5	10.7	10.2	12.5
	7.5	6.3	7.0	5.8	4.9	6.3	4.2	8.7	9.7	7.0
	6.3	7.6	6.4	7.4	6.7	5.6	6.2	4.9	6.8	8.7
	7.1	6.6	5.5	6.0	9.3	9.2	6.4	7.4	7.8	10.5

Graph 75. The estimated correlation is too much erratic

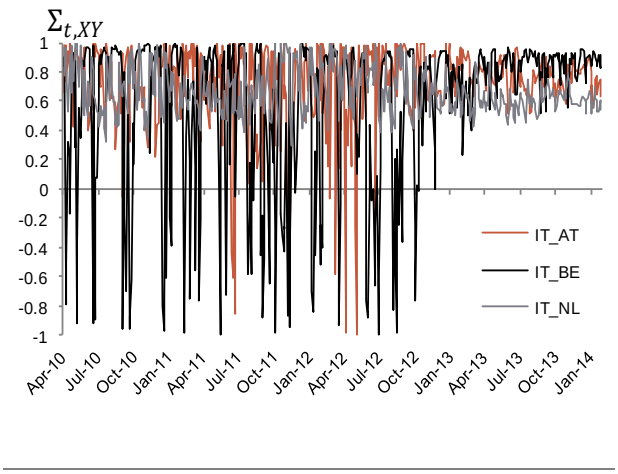

Results – Quality of the multivariate distribution

Similarly to the univariate analysis, **the calculation of the correlation matrix involves three unknown scalars ω, A and B that we calibrate with the Levenberg-Marquard algorithm.** For the sake of clarity, we first concentrate on pairs composed of Italian CDS as a fixed leg, and another European CDS, as a floating leg. In terms of terminology, we denote the selected pairs as e.g. "Italian and German CDS", "Italian and French CDS", etc... In a second stage we will extend the analysis to all the available pairs in the sample.

Every time, and in line with what we did in the univariate analysis, we ran the calibration 20 times. This helps reduce the risks to consider a faulty estimator, obtained on a local optimum only. Then we gauge the quality of the calibration via the same tools as before: **the PIT and the ADC test**.

Overall, results proved weak. An examination of the resulting distributions reveals two major issues: **Anderson Darling criterions are unacceptably high; and correlation coefficients are greatly instable.**

First, Anderson Darling criterions are not in the range of acceptable values. Table 18 shows that the ADC are much higher than before, with most of the values above 3.0. This is not acceptable and suggests that the multivariate calibration is not successful in most cases. Some empirical tests and generally a deeper investigation also shows that the constraint $\mu = 0$ is the main culprit for the disappointing results. We expected the mean vector to be fixed at $(0,0)$, **but in fact this assumption turns to be too restrictive.** As a consequence, we relaxed this condition, and we **left the mean coefficient μ as a free unknown variable.** Given the multivariate structure, μ is defined as a vector of two unknown (constant) values $[\mu_1, \mu_2]$. A few tests on initial conditions unveiled that μ is usually slightly negative, so μ_1 and μ_2 were initiated from random values taken within $[-0.5, 0]$.

The calibrated correlation coefficients $\Sigma^{i,j}$ (within the correlation matrix) **also proved remarkably volatile, probably too erratic to have a sensible meaning.** As Graph 75 shows, the correlation coefficients look very unstable. This is a meaningful caveat we believe, as the erratic aspect of these estimators tends to make correlation regimes within the dataset very unpredictable. Plus correlation metrics are usually regarded as long-term descriptors of the joint dynamics; which is in contrast to our instable estimator.

➔ **Results so far are not acceptable, and our estimate of the correlations is not a relevant picture of the actual dependencies.** We now explore some adjustments to the initial formulation of the multivariate GAS method that helped address these limitations.

An examination of each component in eq. (30) shows that the coefficient $A = \frac{\partial \log(q_t(z_t))}{\partial f_t}$ is responsible for most of the variance attached to the correlation coefficients. As a consequence, we decided to remove the coefficient A and we adjusted the formulation of the score f_t as:

$$f_t = \omega + B * f_{t-1} \qquad (31)$$

Obviously the model now takes less information into account. However, deleting A also helps offset the higher computational burden that resulted from the introduction of the unknowns μ_1 and μ_2. Keeping the mean vector μ as a free variable and removing the parameter A, we are left with four unknowns: μ (2 coefficients), ω, B .

Repeating the calibration, this new formulation delivered much better results this time. Table 19 highlights the ADC of the multivariate distributions for pairs involving Italian CDS: we see a lot of compelling values now, around or below 1.0, for many combinations. The pairs "Italy and Spain", "Italy and Belgium" and "Italy and France" yield a lot of green cells, a sign that the calibration was consistently successful among the 20 trials. In contrast, the pair "Italy and Portugal" was more difficult to calibrate, but the best ADC, all the same, is at a much acceptable 1.3. For every pair, we took the calibration with the smallest ADC as the best estimator.

With no surprise, the PIT is very strong as well; we plot a few examples in Graph 77, Graph 78 and Graph 79. ➔ **Results confirm the relevance and the tractability of the adjusted formulation of the GAS model that we consider here.**

On the front of correlation coefficients, Graph 76 shows that our estimators are now constant values – and so for all the combinations of countries. **This is obviously a surprise, and so far we see no obvious reason for this unexpected time-independence.**

The correlation coefficients, on average, are somewhat large (between 0.6 and 0.9). This suggests that cross-country linkages between Italian CDS spreads and the rest of Europe are intense. **Still based on Graph 76, both pairs "Italian and Finland" and "Italy and France" exhibit the smallest correlation coefficients, illustrating possibly greater resilience in Finland and France to a shock in Italy. In sharp contrast, Dutch and Irish CDS spreads show large correlation coefficients with Italian CDS.**

Since the correlation estimators $\Sigma_t^{i,j}$ do not depend on time, the resulting multivariate distributions do not depend on previous realisations. The time-independence in effect makes the exploration of these distributions relatively straightforward. In particular, it allows us to consider the points in the dataset regardless of their order of appearance – ie. similarly to our approach of the un-temporal volatility estimator. **We take advantage of this feature in the following paragraphs; in particular this will help us conclude on the strength of inter-dependencies between CDS spreads.**

Table 19. ADC of the distribution "Italy and another country" Pink = poor calibration, Green = better results

ADC resulting from 20 tests	ITALY AND									
	GE	FI	NL	AT	FR	BE	SP	IR	PT	UK
	2.8	3.2	1.5	3.9	2.9	3.8	1.4	5.6	1.3	2.1
	2.2	1.4	3.6	2.7	1.2	2.8	0.9	4.8	3.0	3.5
	2.5	2.4	2.6	1.5	1.4	2.0	1.5	4.6	1.7	4.2
	5.9	1.9	5.4	4.7	2.5	4.0	2.5	4.6	3.9	1.8
	4.2	2.1	3.8	4.3	3.5	2.4	2.6	5.0	4.4	2.4
	2.0	3.5	7.5	3.3	1.0	1.2	1.7	5.0	2.4	3.2
	1.6	3.2	4.4	1.4	1.9	1.4	1.2	4.0	5.5	3.4
	3.8	2.7	1.5	3.1	2.5	2.9	3.1	4.2	3.8	2.5
	3.8	1.8	3.4	3.4	3.2	4.0	2.2	1.4	4.8	2.1
	2.1	4.2	6.5	1.1	3.4	1.0	1.8	3.0	5.7	2.3
	3.2	3.0	1.6	1.5	1.1	1.2	4.2	2.1	2.1	1.1
	1.9	3.5	2.1	2.1	1.4	2.5	5.1	1.8	1.9	4.5
	4.1	1.2	3.5	2.5	3.0	1.4	1.4	2.5	3.4	5.1
	3.5	7.6	4.5	3.2	2.9	2.5	3.3	2.4	2.8	1.3
	2.8	2.0	2.1	1.9	3.1	3.1	2.0	1.8	4.2	1.5
	2.1	5.0	1.8	1.4	2.9	4.0	3.1	1.4	1.8	3.3
	1.7	2.6	2.4	2.5	1.8	2.8	3.2	2.8	3.4	1.1
	2.5	2.1	3.2	3.4	1.4	1.4	0.9	3.1	2.8	3.6
	1.8	3.6	2.7	2.1	6.6	1.9	1.0	4.2	2.4	2.6
	3.1	2.8	2.5	1.9	3.1	2.4	0.8	4.1	3.5	3.1

Graph 76. $\Sigma_t^{i,j}$ are now time-invariant

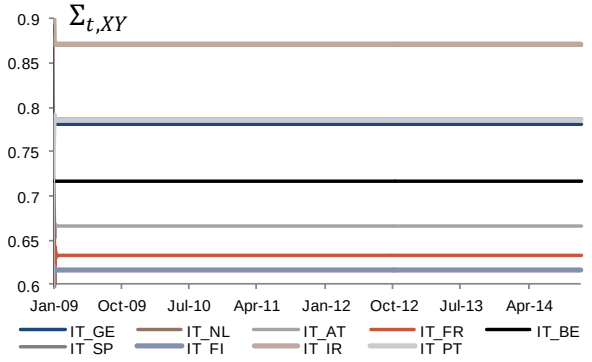

Graph 77. PIT of the IT_GE distribution

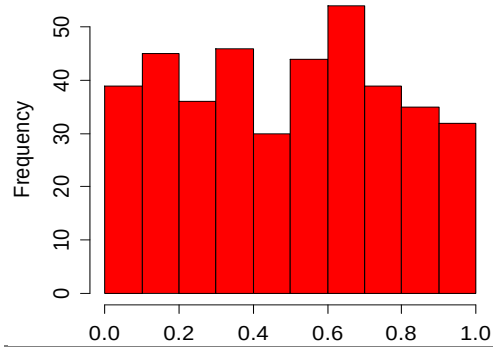

Graph 78. PIT of the IT_FR distribution

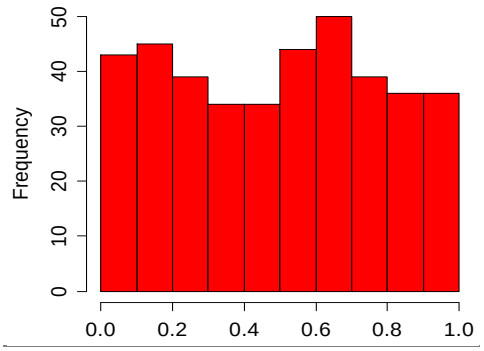

Graph 79. PIT of the IT_SP distribution

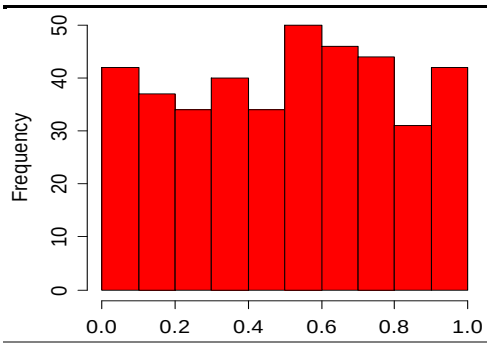

Enlarging the calibration to other pairs of European countries, results remain as compelling as before: the ADC is staying below 1.5 for most of the calibrations (Table 20). Arguably, the worst ADC is 2.2 for "Dutch and Finnish CDS" and 2.0 for "Belgian and Dutch CDS"; both are still acceptable yet.

Table 20. Multivariate ADC proved much satisfactory

ADC	COUNTRY 1										
COUNTRY 2	GE	FI	NL	AT	FR	BE	IT	SP	IR	PT	UK
GE		1.8	1.5	1.2	1.3	1.5	1.3	1.3	1.6	1.5	1.5
FI			2.2	1.4	1.8	1.6	1.4	1.3	1.9	1.4	1.6
NL				1.5	1.8	2.0	1.6	1.5	1.7	1.5	1.7
AT					1.4	1.1	1.4	1.1	1.3	1.2	1.5
FR						1.2	1.0	1.0	1.4	1.2	1.3
BE							1.0	1.0	1.5	1.3	1.6
IT								0.8	1.4	1.3	1.1
SP									1.5	1.3	1.2
IR										1.4	1.4
PT											1.3

➔ **Sound ADC and PIT tests, and a stable correlation profile are evidence that multivariate distributions have been successfully calibrated, and therefore provide a robust fit to the empirical data.**

In the next section we examine the mean and correlation parameters, and we look at the tails of the distributions as a baseline to quantify the expected joint price action when a shock materialises. Since our multivariate distributions are not conditional on past realisations, we can ignore the temporal aspect and thus we remove the index t. In particular, we replace $z_t^{i,j} = \left(z_t^i, z_t^j\right)$ by $z^{i,j} = \left(z^i, z^j\right)$, as well as q_t by q and Q_t by Q.

An estimator of the joint reaction to shocks

A deeper look at the multivariate distribution

As we mention above, we consider non-zero mean parameters $\mu = [\mu_1, \mu_2]$, with μ_1 referring to Country 1 (denoted $C1$ thereafter), and μ_2 to Country 2 ($C2$). Table 21 shows the calibrated μ coefficients.

For any pair $(C1, C2)$, the vector μ indicates the average value of each series, from a multivariate point of view. As Table 21 shows, this value tends to vary from one pair to another. For instance, Italian CDS display a negative mean of $\mu = -0.5$ when coupled with Germany, while this coefficient is closer to zero, at just -0.2, when Italy is combined with Finland or with the Netherlands.

Table 21. The mean vector μ highlight the asymmetric behaviour between core and non-core

COUNTRY 2	COUNTRY 1																			
	FI		NL		AT		FR		BE		IT		SP		IR		PT		UK	
	μ1	μ2	μ1	μ2	μ1	μ2	μ1	μ2	μ1	μ2	μ1	μ2	μ1	μ2	μ1	μ2	μ1	μ2	μ1	μ2
GE	-0.2	-0.5	-0.2	-0.5	-0.4	-0.4	-0.2	-0.5	-0.2	-0.5	-0.5	-0.3	-0.2	-0.5	-0.2	-0.5	-0.2	-0.5	-0.2	-0.5
FI			-0.2	-0.5	-0.2	-0.4	-0.3	-0.3	-0.2	-0.4	-0.2	-0.4	-0.5	-0.3	-0.2	-0.4	-0.5	-0.2	-0.2	-0.4
NL					-0.4	-0.3	-0.2	-0.5	-0.2	-0.5	-0.2	-0.5	-0.2	-0.5	-0.2	-0.5	-0.4	-0.3	-0.4	-0.3
AT							-0.4	-0.2	-0.3	-0.4	-0.4	-0.2	-0.5	-0.3	-0.3	-0.4	-0.5	-0.3	-0.4	-0.3
FR									-0.3	-0.4	-0.3	-0.4	-0.5	-0.3	-0.5	-0.3	-0.5	-0.3	-0.5	-0.3
BE											-0.3	-0.4	-0.3	-0.4	-0.3	-0.4	-0.3	-0.5	-0.3	-0.5
IT													-0.2	-0.3	-0.2	-0.3	-0.4	-0.1	-0.4	-0.1
SP															-0.2	-0.5	-0.3	-0.4	-0.3	-0.3
IR																	-0.4	-0.3	-0.4	-0.3
PT																			-0.4	-0.5

By definition, the mean vector μ indicates the area where the occurrence of the returns is higher. In other words, Italian CDS returns will be more negative "on average" when selected with German or with Austrian CDS (μ_1 is more negative in Table 21). In contrast, CDS returns in Italy are less negative on average when selected with Finnish or Dutch CDS (μ_1 is closer to zero).

A strong negative mean value on $C2$ CDS (ie. $\mu_2 < 0$) means that the multivariate framework identifies an asymmetry: negative prices variations have a greater occurrence than positive price variations. In this case, risk appetite (ie. lower CDS prices) is more frequent than risk aversion (higher CDS prices).

When comparing μ_1 and μ_2, Table 21 shows that for a selected pair, the more resilient credit usually gets a more negative mean coefficient than the other member of the pair. This difference is more palpable for pairs composed of very dissimilar assets in terms of credit quality: for "Italy and Finland" and "Ireland and Germany" for instance μ_2 is much more negative than μ_1. In contrast to this dynamics, pairs of securities that are relatively comparable in terms of credit quality exhibit closer μ_1 and μ_2. This is the case for the pairs "Belgium and France" or "Austria and the Netherlands" for instance.

➔ **This pattern suggests that a decline in core/soft-core CDS prices is an especially more likely outcome when taken as a pair against a peripheral country. This highlights greater resilience in core/soft-core sovereigns to financial distress emanating from peripheral countries.**

Let us now take a look at the shape of the multivariate distribution. As the general presentation in Graph 80 shows, we plot $q(z^i, z^j)$ as a function of the cumulative distribution function $G(z^i)$ and $G(z^j)$. This makes the results more convenient to exploit than looking at q against z^i and z^j.

On top of that, and since the data is centred, we can deduce the sign of z^i directly from G $z^i < 0$ for $G(z^i) < 0.5$ and $z^i > 0$ for $G(z^i) > 0.5$ (see Graph 80) - something also true for Country j. These graphical boundaries where z^i and z^j are either positive or negative makes the identification of risk-on ($z < 0$) and risk-off ($z > 0$) environments rather straightforward in Graph 80.

Graph 80. Plot of the multivariate density for countries i and j

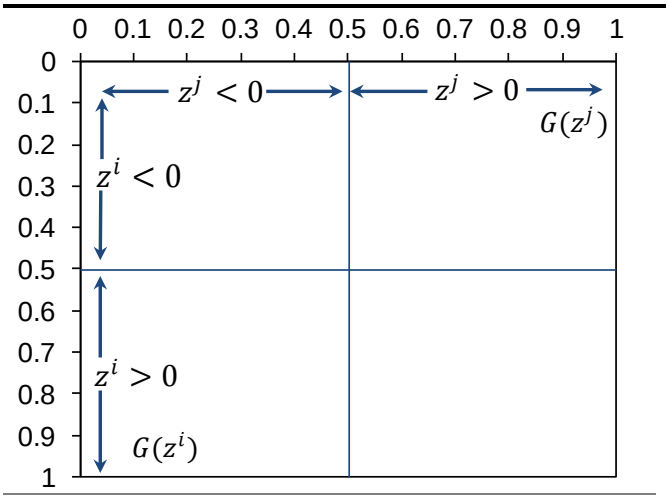

As examples, Graph 81 and Graph 82 highlight the values of q for "Italian and Belgian z_t" and "Italian and Dutch z_t". Colours in these Graphs evolve between green, yellow and pink. Green qualifies areas of a larger density, while pink refers to the lower values of the density and yellow is in the middle. Arguably, these two pairs have much different average values: $\mu = [-0.3, -0.4]$ for "Italian and Belgian z_t" while $\mu = [-0.2, -0.5]$ for "Italian and Dutch z_t".

As exposed above, the average coefficient μ has significant implications on the distribution of the points. In Graph 82 for instance, the very negative mean value $\mu = -0.5$ for the Netherlands causes a greater occurrence of the points in the domain $G(z^j) < 0.5$ (equivalent to $z^j < 0$). This is rather clear as most of the green points, ie. with the highest density, lie in the lower diagonal of the square, suggesting that there is a sizeable asymmetry in the joint behaviour of the data. In comparison, μ_1 and μ_2 are relatively similar for the pair "Belgian and Italian z_t" as $\mu = [-0.3, -0.4]$. **As a result, the distribution in Graph 81 looks much more balanced on each side of the diagonal, reflecting a more symmetric joint behaviour.**

Graph 81. Multivariate density q with i: SP and j: IT
Green cells: large density, salmon colored cells: small density

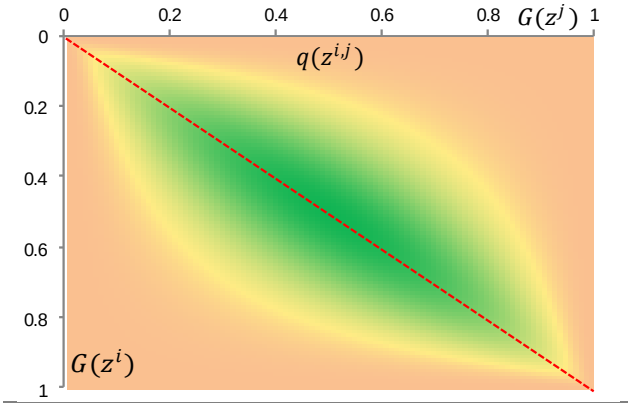

Graph 82. Multivariate density q with i: IT, j: NL
Green cells: large density, salmon cells: small density

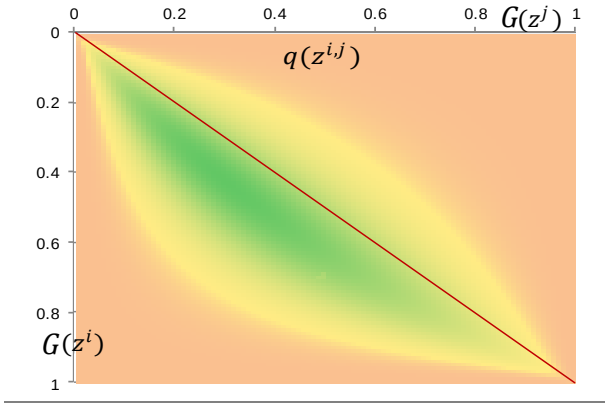

We also plot the parameters B and ω in Table 22 and Table 23. The dynamics is now quite different compared to the univariate analysis. As we mention above, the correlation coefficient is a constant value as time goes by. And since the score f_t is now time-independent: $f_{t-1} = f_t = f$.

Then from eq. (32) we can deduce that:

$$f = \frac{\omega}{1-B} \tag{32}$$

Using the hyperspherical coordinates, we also have:

$$\Sigma^{i,j} = \cos(f) = \cos\left(\frac{\omega}{1-B}\right) \tag{33}$$

Given the periodic aspect of the $cos()$ function in eq. (33), it is difficult to detect any relationship between ω, B and the correlation $\Sigma^{i,j}$. We just note that the correlation tends to increase when the ratio $\frac{\omega}{1-B}$ approaches zero. This is a change with the univariate analysis where a larger f_t used to be responsible for a larger volatility coefficient σ_t.

Table 22 shows that B remains rather small on average (around 0.1), with pairs involving France, Belgium, Spain and Italy showing slightly larger values, and thus bigger autocorrelations (see darker cells). Globally, ω remains within a tight range of $[-0.91, -0.26]$, with an average at -0.53. Interestingly, pairs involving "Belgium or Italy and the UK", and "Spain and Portugal" display the smallest ω. And because these pairs also show a small B coefficient, overall we can deduce that the correlation $\Sigma^{i,j}$ there is quite high (cf. eq. (33)).

Table 22. Calibrated parameter B

B	COUNTRY 1 FI	NL	AT	FR	BE	IT	SP	IR	PT	UK
COUNTRY 2 GE	0.1	0.1	-0.5	0.1	0.1	-0.4	0.1	0.1	0.1	0.1
FI		0.0	0.1	0.0	0.1	0.1	-0.1	0.1	0.0	0.1
NL			0.1	0.0	0.0	0.0	0.0	0.0	0.1	0.1
AT				0.0	-0.4	0.0	-0.2	-0.1	-0.1	0.0
FR					-0.5	-0.8	-0.3	-0.3	-0.2	-0.1
BE						-0.6	-0.6	-0.6	0.1	0.1
IT							-0.7	0.0	0.0	0.0
SP								0.1	0.1	-0.5
IR									0.0	0.0
PT										0.0

Table 23. Calibrated parameter ω

ω	COUNTRY 1 FI	NL	AT	FR	BE	IT	SP	IR	PT	UK
COUNTRY 2 GE	-0.4	-0.4	-0.9	-0.4	-0.4	-0.9	-0.4	-0.4	-0.4	-0.4
FI		-0.4	-0.4	-0.5	-0.4	-0.4	-0.7	-0.4	-0.7	-0.4
NL			-0.4	-0.4	-0.4	-0.4	-0.4	-0.4	-0.4	-0.4
AT				-0.4	-0.7	-0.4	-0.7	-0.5	-0.7	-0.7
FR					-0.8	-0.8	-0.8	-0.8	-0.8	-0.8
BE						-0.9	-0.9	-0.9	-0.3	-0.3
IT							-0.6	-0.4	-0.3	-0.3
SP								-0.4	-0.3	-0.8
IR									-0.4	-0.4
PT										-0.6

A closer look at the correlation coefficient $\Sigma^{i,j}$

The covariance matrix of the multivariate distribution is a picture of the bivariate interdependencies. As we already argued, the correlation we obtained from the calibration is time-invariant (Graph 76); and this is true for all pairs of CDS spreads.

Table 24. Correlation coefficients obtained out of the calibration

$\Sigma^{i,j}$	COUNTRY 1 GE	FI	NL	AT	FR	BE	IT	SP	IR	PT	UK
COUNTRY 2 GE		0.78	0.66	0.80	0.85	0.69	0.91	0.93	0.53	0.76	0.64
FI	0.78		0.82	0.80	0.85	0.61	0.91	0.93	0.87	0.87	0.64
NL	0.66	0.82		0.80	0.85	0.76	0.91	0.93	0.53	0.87	0.64
AT	0.80	0.80	0.80		0.85	0.78	0.91	0.93	0.68	0.87	0.64
FR	0.85	0.85	0.85	0.85		0.71	0.68	0.93	0.59	0.87	0.64
BE	0.69	0.61	0.76	0.78	0.71		0.70	0.93	0.57	0.87	0.64
IT	0.91	0.91	0.91	0.91	0.68	0.70		0.87	0.87	0.79	0.64
SP	0.93	0.93	0.93	0.93	0.93	0.93	0.87		0.79	0.74	0.58
IR	0.53	0.87	0.53	0.68	0.59	0.57	0.87	0.79		0.87	0.92
PT	0.76	0.87	0.87	0.87	0.87	0.87	0.79	0.74	0.87		0.64
UK	0.64	0.64	0.64	0.64	0.64	0.64	0.64	0.58	0.92	0.64	

Table 24 shows the calibrated values. Colour spans from red for large correlations to green for the smallest values. The first observation is that most of the combinations are intensively correlated,

with an average value at 0.77. Globally, there is no obvious pattern that could bind the credit quality to the level of correlation. We just note that France, Italy, Spain and Portugal exhibit larger correlations than other countries. Pairs involving the UK proved also less correlated, with an average correlation at just 0.64 (excluding UK/Ireland at 0.92).

We understand that time-independent correlation coefficients may be perceived as a caveat. The non-liner aspect of contagion in particular, as explored in (Ahnert and Bertsch (2013), Forbes and Rigobon (2002), Bekaert et al. (2014), Favero and Giavazzi (2012)) can be a reasonable justification to consider that contagion needs a reassessment of market correlations, that tends to yield much stronger numbers than in the normal course of financial markets. On that basis, our fixed estimator $\Sigma^{i,j}$ may look a bit too simplistic. However, we demonstrate later in this report that dependencies in fact tend to vary as we near the tail regions, regardless of the time-invariant dimension of the covariance matrix. Plus our correlation estimators are already large, and close to 1 in many cases. **This is a sign that a decent part of the tails may already be taken into account.**

With an average value of 0.77, the calibrated correlation $\Sigma^{i,j}$ looks large in comparison to the empirical sample correlation $\rho^{i,j}$ (0.66 on average in Table 9). Plus we see significant divergence between $\Sigma^{i,j}$ and $\rho^{i,j}$. The GAS correlation $\Sigma^{i,j}$ in particular is larger for peripheral countries than for core/soft-core sovereigns (e.g. 0.81 for Portugal versus 0.75 for Germany and 0.78 for France in Table 24). In contrast, $\rho^{i,j}$ detects much smaller correlations in non-core sovereigns (Table 9).

➔ **Overall, all this confirms that the empirical metric $\rho^{i,j}$ is greatly constrained. For time series that exhibit larger tails, like non-core CDS, the divergence between** $\Sigma^{i,j}$ and $\rho^{i,j}$ **is more pronounced: the much smaller $\rho^{i,j}$ indicates that empirical methods are not suitable to capture the actual cross-asset connections.**

A deeper look at multivariate dependencies

Risk propagation during periods of intense risk aversion can prove unexpectedly harmful for portfolio managers. This is because larger volatility regimes tend to amplify multivariate connections between financial securities. And while this is not observable with our time-independent correlation estimator $\Sigma^{i,j}$, the aforementioned acceleration of joint connections can be estimated via the coefficients of tail dependence λ_u and λ_l.

The shape of the calibrated distribution q delivers insightful information on the behaviour of financial securities. This is especially obvious in the tail regions. Fat or thin tails mean that the multivariate distribution is more or less prominent in both the upper-left and lower-right corners in Graph 81 and Graph 82. The coefficients of tail dependence, as described in Schmidt (2006), offer insightful information on the joint behaviour of financial securities when the price action reaches the tail regions of the distribution. As such, they are an illustration of the risk of a full 'joint' propagation of financial distress during periods of intense risk aversion. **These coefficients can prove particularly useful when it comes to estimating the shortfall in portfolios, ensuing from a sharp reversal in market sentiment.**

The upper-left corner of the distribution (Graph 81, Graph 82) refers to the domain of negative price variations, dependence there is thus denominated as 'lower tail dependence'. The lower-right corner in contrast refers to the domain of positive price variations . Any dependence here will be seen as 'upper tail dependence'.

Intuitively, the presence of some upper tail dependence means that there is a connection between both univariate cumulative distributions G^j and G^i in the sense that if G^j takes large values (ie. $G^j \to 1$), then G^i is likely to move in the same direction as well. In the same vein, some lower tail dependence means that the event $G^j \to 0$ will encourage the emergence of a similar price action on G^j. ➔ **Bigger tail dependence tends to exacerbate the joint reaction to shocks, and thus makes contagion a bigger risk in general.**

Coefficients of tail dependence are usually defined **as the risk that G^j exceeds a certain threshold v given that G^i has already exceeded v**. And as McNeil, Frey, Embrechts (2005) indicate, the limiting case when $v \to 1$ or $v \to 0$ is of particular interest as these highlight the specific behaviour of the tails (upper and lower tail respectively). McNeil, Frey, Embrechts (2005) also stress that this limit exists for hyperbolic and NIG distributions, thus including GHT distributions. In the end, the coefficients λ_u and λ_l of upper-and lower-tail dependence are defined as:

$$\lambda_u = \lim_{v \to 1} P\left(z^j \geq {G^{-1}}^j(v) | z^i \geq {G^{-1}}^i(v)\right)$$

$$\lambda_l = \lim_{v \to 0} P\left(z^j \leq {G^{-1}}^j(v) | z^i \leq {G^{-1}}^i(v)\right)$$

That we can re-write as:

$$\lambda_u = \lim_{v \to 1} \frac{P\left(z^j \geq {G^{-1}}^j(v) \cap z^i \geq {G^{-1}}^i(v)\right)}{P\left(z^i \geq {G^{-1}}^i(v)\right)} \quad \text{and} \quad \lambda_l = \lim_{v \to 1} \frac{P\left(z^j \leq {G^{-1}}^j(v) \cap z^i \leq {G^{-1}}^i(v)\right)}{P\left(z^i \leq {G^{-1}}^i(v)\right)}$$

With:

$$P\left(z^j \geq {G^{-1}}^j(v) \bigcap z^i \geq {G^{-1}}^i(v)\right) = \iint_{{G^{-1}}^i(v)\ {G^{-1}}^j(v)}^{+\infty\ +\infty} q(z^i, z^j) dz^i dz^j$$

And:

$$P\left(z^i \geq {G^{-1}}^i(v)\right) = \int_{G^{-1}(v)}^{+\infty} g^i(z^i)\, dz^i$$

So in the end we get:

$$\lambda_u = \lim_{v \to 1} \frac{\iint_{{G^{-1}}^i(v)\ {G^{-1}}^j(v)}^{+\infty\ +\infty} q\left(z^i, z^j\right) dz^i dz^j}{\int_{{G^{-1}}^i(v)}^{+\infty} g^i(z^i)\, dz^i} = 2 + \lim_{v \to 1} \frac{Q\left(G^{-1^i}(v), G^{-1^j}(v)\right) - 1}{1 - v} \tag{34}$$

$$\lambda_l = \lim_{v \to 1} \frac{\iint_{-\infty -\infty}^{{G^{-1}}^i(v)\ {G^{-1}}^j(v)} q\left(z^i, z^j\right) dz^i dz^j}{\int_{+\infty}^{{G^{-1}}^i(v)} g^i(z^i)\, dz^i} = \lim_{v \to 0} \frac{Q\left(G^{-1^i}(v), G^{-1^j}(v)\right)}{v} \tag{35}$$

Eq. (34) and eq. (35) show that λ_u and λ_l essentially look at the slope of the cumulative bivariate distribution, along the diagonal (drawn in Graph 81 and Graph 82), in the region approaching $(0, 0)$ and $(1, 1)$. **The greater the slope is, the larger the tail dependence.**

The tail dependence is a measure of probability, so λ_u and λ_l are bounded in the range $[0,1]$. In general terms, a non-zero value for λ_u or λ_l means that if Country i faces a shock of amplitude v, then there is a non-zero probability that Country j will face a shock of a similar or more severe amplitude. In this case, we consider that the initial shock on Country i has, at least partially, propagated onto Country j, **and therefore there is some tail dependence**. Otherwise, $\lambda_u = 0$ and $\lambda_l = 0$ indicate that Country j is relatively immune to developments on Country i, and therefore

there is no tail dependence (these series are said to be asymptotically independent). As (McNeil, Frey, Embrechts (2005)) explains, this is the case for Gaussian copulas.

Since λ_u, λ_l is a ratio of multivariate over univariate probabilities, these metrics can also be seen as a comparison between multivariate and univariate risks. A large tail dependence ($\lambda_u \sim 1$ $\lambda_l \sim 1$) in particular indicates that shocks at the univariate level are systematically transmitted via the multivariate structure. In this case a shock on one security within a portfolio can have dramatic implications onto the other members, hence reducing the efficiency of the sought after risk diversification. We would avoid holding these two securities at the same time when risk aversion becomes a palpable threat.

In contrast, fewer tail dependence ($\lambda_u \sim 0$ $\lambda_l \sim 0$) indicates that multivariate connections are less active. In this case, both securities prove relatively independent one from each other. From an investor perspective, holding this kind of securities helps achieve a more effective diversification of the risks, with limited danger that a shock will propagate from one member to another.

We calculated the coefficients λ_u and λ_l for all available pairs (Table 25 and Table 26). Larger values are displayed in red, and the smaller in green, with yellow cells in the middle. First, results highlight some asymmetry: upper tail dependence is higher than lower tail dependence, by around 18% (average dependence at 0.38 versus 0.31). Overall this makes sense: the upper tail dependence refers to risk averse market conditions (CDS prices rising), which are usually marked by mounting contagion. In contrast, the lower tail dependence qualifies an environment where risk appetite is prevailing, ie. where contagion is presumably less harmful. ➔ **The stronger contagion in the upper tail reflects larger multivariate connections in risk averse market conditions. This mostly justifies the general observation that $\lambda_u > \lambda_l$.**

As Table 25 and Table 26 show, tail dependences vary greatly from one sovereign to another. Pairs involving France, Italy, Spain and Portugal for instance exhibit the largest tail dependence. In contrast, pairs involving Ireland or the UK, along with some specific combinations like “Belgium and Germany or Finland”, ”Italy and France”, and “Italy and Belgium” show very little tail dependence, with a lower coefficient λ_l around 0.20. The UK also proves particularly disconnected from the rest of the sample, with very little tail coefficients overall. **This probably relates to the fact that this is the only non-Euro country in the sample.**

Looking at soft-and non-core countries, we note that France and Belgium are less exposed to a shock emanating from Italy than from Spain; there is also only less dependence between Ireland and Portugal than between Spain and Italy. **Interestingly, Italy and Spain appear as the most connected sovereigns to the rest of the sample. This suggests that these two countries are material drivers of global market sentiment in Europe, especially in Fixed Income markets**. Empirical observations of the market dynamics in recent years corroborate this pattern, as episodes of sizeable contagion into soft-core and core countries were mostly driven by Spain or Italy. Contagion into core and soft-core, from risk-off developments in Ireland and Portugal was less palpable in comparison.

Table 25. Lower tail dependence (average: 0.31)

λ_l	COUNTRY 1										
COUNTRY 2	GE	FI	NL	AT	FR	BE	IT	SP	IR	PT	UK
GE		0.29	0.21	0.31	0.36	0.23	0.46	0.49	0.15	0.27	0.20
FI	0.29		0.32	0.31	0.36	0.18	0.46	0.49	0.39	0.38	0.20
NL	0.21	0.32		0.31	0.36	0.27	0.46	0.49	0.15	0.38	0.20
AT	0.31	0.31	0.31		0.36	0.29	0.46	0.49	0.22	0.38	0.20
FR	0.36	0.36	0.36	0.36		0.31	0.22	0.49	0.18	0.38	0.20
BE	0.23	0.18	0.27	0.29	0.31		0.23	0.49	0.17	0.38	0.20
IT	0.46	0.46	0.46	0.46	0.22	0.23		0.38	0.39	0.29	0.20
SP	0.49	0.49	0.49	0.49	0.49	0.49	0.38		0.30	0.25	0.17
IR	0.15	0.39	0.15	0.22	0.18	0.17	0.39	0.30		0.38	0.48
PT	0.27	0.38	0.38	0.38	0.38	0.38	0.29	0.25	0.38		0.20
UK	0.20	0.20	0.20	0.20	0.20	0.20	0.20	0.17	0.48	0.20	

Table 26. Upper tail dependence (average: 0.38)

λ_u	COUNTRY 1										
COUNTRY 2	GE	FI	NL	AT	FR	BE	IT	SP	IR	PT	UK
GE		0.35	0.27	0.38	0.42	0.29	0.54	0.55	0.20	0.35	0.26
FI	0.35		0.38	0.38	0.42	0.23	0.54	0.55	0.47	0.46	0.25
NL	0.27	0.38		0.38	0.42	0.33	0.54	0.55	0.20	0.46	0.26
AT	0.38	0.38	0.38		0.42	0.35	0.54	0.55	0.28	0.46	0.25
FR	0.42	0.42	0.42	0.42		0.38	0.28	0.55	0.24	0.46	0.26
BE	0.29	0.23	0.33	0.35	0.38		0.29	0.55	0.22	0.46	0.25
IT	0.54	0.54	0.54	0.54	0.28	0.29		0.44	0.47	0.36	0.26
SP	0.55	0.55	0.55	0.55	0.55	0.55	0.44		0.37	0.32	0.22
IR	0.20	0.47	0.20	0.28	0.24	0.22	0.47	0.37		0.46	0.56
PT	0.35	0.46	0.46	0.46	0.46	0.46	0.36	0.32	0.46		0.26
UK	0.26	0.25	0.26	0.25	0.25	0.25	0.26	0.22	0.56	0.26	

➔ **Our analysis highlights sizeable tail dependence in many cases.** And while GHT distributions have proved particularly relevant to capture fat tails in the context of our analysis; McNeil, Frey, Embrechts (2005) paradoxically note that these multivariate distributions usually show less tail dependence than Student-t copulas. This can be seen in particular when looking at the upper and lower tail dependence coefficients associated to t-Student copulas:

$$\lambda_{u,t} = \lambda_{l,t} = \lambda_t = 2t_{v+1}\left(-\sqrt{\frac{(v+1)(1-\rho)}{1+\rho}}\right) \tag{36}$$

Where ρ is the sample correlation of the data and $v = 5$ is the degree of freedom.

Table 27. t-Student tail dependence λ_t (average at 0.51)

λ_t	COUNTRY 1										
COUNTYR 2	GE	FI	NL	AT	FR	BE	IT	SP	IR	PT	UK
GE		0.50	0.39	0.52	0.58	0.41	0.64	0.67	0.30	0.47	0.38
FI	0.50		0.54	0.52	0.58	0.35	0.64	0.67	0.60	0.59	0.37
NL	0.39	0.54		0.52	0.58	0.48	0.64	0.67	0.29	0.59	0.38
AT	0.52	0.52	0.52		0.58	0.50	0.64	0.67	0.41	0.59	0.37
FR	0.58	0.58	0.58	0.58		0.43	0.41	0.67	0.34	0.59	0.38
BE	0.41	0.35	0.48	0.50	0.43		0.43	0.67	0.32	0.59	0.38
IT	0.64	0.64	0.64	0.64	0.41	0.43		0.60	0.60	0.51	0.38
SP	0.67	0.67	0.67	0.67	0.67	0.67	0.60		0.52	0.46	0.33
IR	0.30	0.60	0.29	0.41	0.34	0.32	0.60	0.52		0.60	0.66
PT	0.47	0.59	0.59	0.59	0.59	0.59	0.51	0.46	0.60		0.38
UK	0.38	0.37	0.38	0.37	0.38	0.38	0.38	0.33	0.66	0.38	

Effectively, considering that $\rho \approx \Sigma^{i,j}$ leads to higher values for λ_t (Table 27) than what we got in Table 25 and Table 26. **That said, t-Student bivariate distributions would prove unable to capture the fat tails in our dataset**.

From a more general perspective, and in order to broaden our understanding of the multivariate dependencies, we can generalize the calculation of λ_u and λ_l to any level of v. This time, we express the dependence coefficient as a function of v, ie. it is seen as a function of the strength of the initial shock on Country i:

$$\lambda_u(v) = \frac{P\left(z^j \geq G^{-1}(v) \cap z^i \geq G^{-1}(v)\right)}{P\left(z^i \geq G^{-1}(v)\right)} = 2 + \frac{Q\left(G^{-1^i}(v), G^{-1^j}(v)\right) - 1}{1-v} \qquad \text{for } v > 0.5 \tag{37}$$

$$\lambda_l(v) = \frac{P\left(z^j \leq G^{-1}(v) \cap z^i \leq G^{-1}(v)\right)}{P\left(z^i \leq G^{-1}(v)\right)} = \frac{Q\left(G^{-1^i}(v), G^{-1^j}(v)\right)}{v} \qquad \text{for } v < 0.5 \tag{38}$$

As detailed in Venter (2002), the condition $\lambda_u > v$ or $\lambda_l > 1 - v$ is an indicator of the presence of some multivariate dependence. In this case effectively, there is an amplification of the risks v raised by the upfront shock $z^i \geq G^{-1^i}(v)$, which is partly attributable to the propagation of financial distress from CDS^i to CDS^j. In this case, the accrued risks on CDS^j reflects contagion at work, hence the presence of some cross-asset dependence.

Otherwise, $\lambda_u \leq v$ or $\lambda_l \leq 1 - v$ indicates that there is no amplification of the upfront shock. **This suggests little dependence, and thus relatively contained bivariate connections.**

We plot $\lambda_u(v)$ and $\lambda_l(v)$ for pairs involving soft-core countries in Graph 83, and for those involving non-core countries in Graph 84. Since v and $1 - v$ are the discriminating factors, we also add these variables in the respective region of the graph (black dashed line).

First and foremost, $\lambda_l(v)$ (resp. $\lambda_u(v)$) is always greater than v (resp. $1 - v$) in both graphs. ➔ **There is some dependence in all market conditions, not just in the tails.** In absolute term, dependence coefficients are bigger at the centre of the distribution, and then consistently decrease as we near the tail regions. On that basis, the tail coefficients λ_u and λ_l that we previously calculated for $v \to 0$ and $v \to 1$ correspond to the point where the dependence is the smallest on each side of the distribution.

Graph 83. Dependence coefficients $\lambda_u(v)$ and $\lambda_l(v)$ for pairs involving soft-core countries

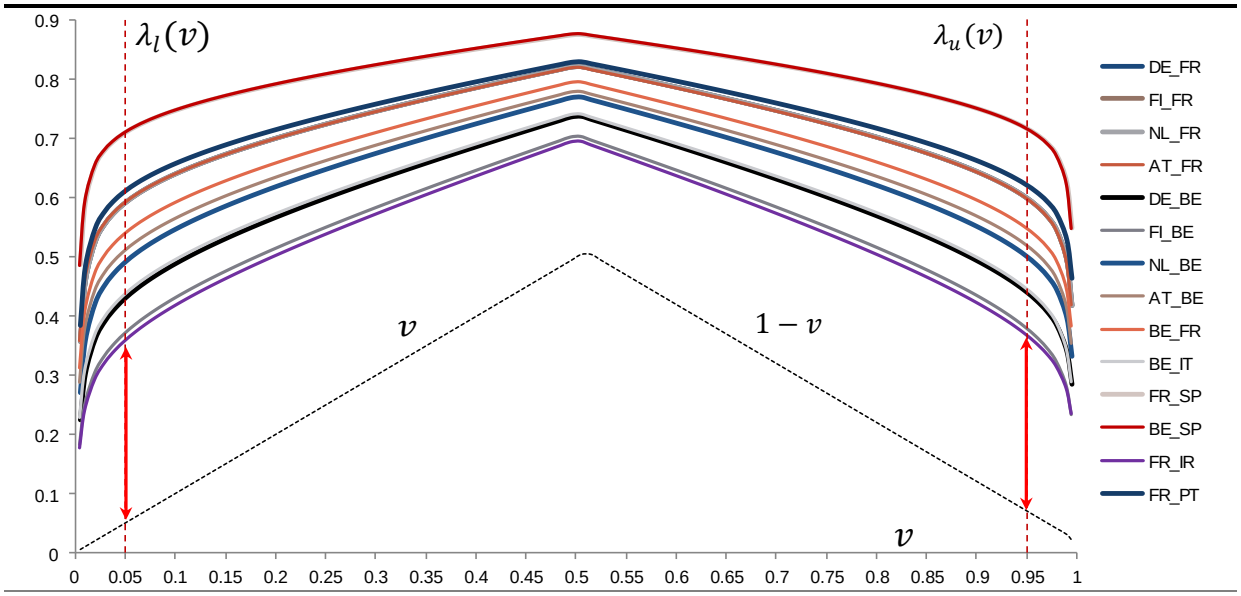

Graph 84. Dependence coefficients $\lambda_u(v)$ and $\lambda_l(v)$ for pairs involving non-core countries

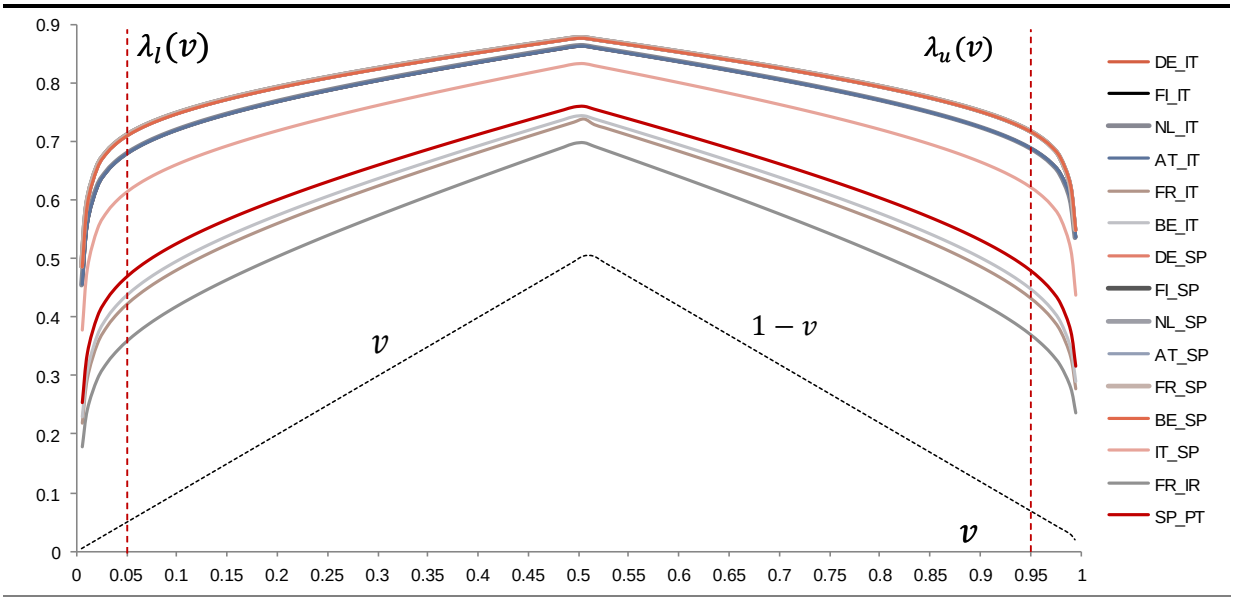

We see two main regimes for the dependence in Graph 83 and Graph 84: first, the coefficients decrease in a linear fashion, from their highest values at the centre. This linear regime is prevailing in the domain $0.05 \leq v \leq 0.5$ and $0.5 \leq v \leq 0.95$. The slope of the decay is apparently greater for pairs that display fewer dependencies in general. Secondly, we see an acceleration of the decline, with the dependence falling faster as we approach the tail regions ($v < 0.05$ and $v > 0.95$). ➔ **The linear regime is prevailing over a substantial portion of the distribution** (in the range $0.05 \leq v \leq 0.95$).

An interesting boundary is the 5% threshold in each tail, as it is the frontier between both regimes (see dashed lines in Graph 83 and Graph 84). **This is also the point where the difference $\lambda_l - v$ and $\lambda_u - (1-v)$ reach a peak (see red arrows in Graph 83): risk propagation is therefore more intense at this specific location, ie. at the 5% and 95% percentiles.**

We thus consider the dependence coefficients at the 5% and 95% level as additional indicators, that we denote as:

$$\lambda_{u,5\%} = \lambda_u(0.95) \text{ and } \lambda_{l,5\%} = \lambda_l(0.05) \qquad (39)$$

Results in Table 28 and Table 29 show a distribution of dependencies relatively similar to what we had with the tail dependence coefficients (Table 25, Table 26). More interestingly, the gap between the upper and the lower coefficients is now smaller than previously: there is now just 5% asymmetry between $\lambda_{u,5\%}$ and $\lambda_{l,5\%}$ on average, while in contrast λ_u is 18% bigger than λ_l in the tails. Since the linear regime is prevailing on most of the distribution, this observation is illustrative of the normal course of financial markets (ie. outside of the tails), which sees little asymmetry between the upper and the lower part of the distribution.

➔ **The more pronounced differentiation between λ_u and λ_l in the tail regions is not verified in other areas of the distribution. This illustrates the asymmetric impact of contagion, which is a specific component of the tail behaviour.**

$\Sigma^{i,j}$ gives little indication on the variations in correlations when we move along the distribution. λ_u and λ_l offer greater clarity on that front as both variables discriminate the strength of multivariate connections as a function of the percentile v. As a result, it appears that the risk of contagion reaches a peak at the 5% and 95% level.

Table 28. lower tail dependence at 5% level $\lambda_{l,5\%}$ (average at 0.51)

$\lambda_{l,5\%}$	COUNTRY 1										
COUTNRY 2	GE	FI	NL	AT	FR	BE	IT	SP	IR	PT	UK
GE		0.50	0.39	0.52	0.58	0.42	0.67	0.70	0.30	0.47	0.38
FI	0.50		0.54	0.52	0.58	0.35	0.67	0.70	0.61	0.60	0.38
NL	0.39	0.54		0.52	0.58	0.48	0.67	0.70	0.31	0.60	0.38
AT	0.52	0.52	0.52		0.58	0.50	0.67	0.70	0.41	0.60	0.38
FR	0.58	0.58	0.58	0.58		0.52	0.41	0.70	0.34	0.60	0.38
BE	0.42	0.35	0.48	0.50	0.52		0.42	0.70	0.33	0.60	0.37
IT	0.67	0.67	0.67	0.67	0.41	0.42		0.60	0.61	0.50	0.38
SP	0.70	0.70	0.70	0.70	0.70	0.70	0.60		0.51	0.45	0.33
IR	0.30	0.61	0.31	0.41	0.34	0.33	0.61	0.51		0.60	0.68
PT	0.47	0.60	0.60	0.60	0.60	0.60	0.50	0.45	0.60		0.38
UK	0.38	0.38	0.38	0.38	0.37	0.37	0.38	0.33	0.68	0.38	

Table 29. Upper tail dependence at 5% level $\lambda_{u,5\%}$ (average at 0.53)

$\lambda_{u,5\%}$	COUNTRY 1										
COUTNRY 2	GE	FI	NL	AT	FR	BE	IT	SP	IR	PT	UK
GE		0.51	0.40	0.53	0.59	0.43	0.68	0.71	0.31	0.49	0.39
FI	0.51		0.55	0.53	0.59	0.37	0.68	0.71	0.62	0.61	0.39
NL	0.40	0.55		0.53	0.59	0.49	0.68	0.71	0.32	0.61	0.39
AT	0.53	0.53	0.53		0.59	0.51	0.68	0.71	0.42	0.61	0.39
FR	0.59	0.59	0.59	0.59		0.54	0.42	0.71	0.36	0.61	0.39
BE	0.43	0.37	0.49	0.51	0.54		0.43	0.71	0.34	0.61	0.39
IT	0.68	0.68	0.68	0.68	0.42	0.43		0.61	0.62	0.51	0.39
SP	0.71	0.71	0.71	0.71	0.71	0.71	0.61		0.52	0.47	0.35
IR	0.31	0.62	0.32	0.42	0.36	0.34	0.62	0.52		0.61	0.70
PT	0.49	0.61	0.61	0.61	0.61	0.61	0.51	0.47	0.61		0.39
UK	0.39	0.39	0.39	0.39	0.39	0.39	0.39	0.35	0.70	0.39	

λ_u and λ_l have delivered some insight on the inter-connections between financial securities. In the next paragraph we derive an estimate of the joint market reaction to financial shocks based on these criterions, combined with our estimator of un-temporal volatility $\hat{h}$.

An estimate of the market reactions to shocks

Though larger tail dependence highlights a greater risk of simultaneous losses, λ_u and λ_l give little information on the magnitude of the resulting losses in portfolios. Covariance estimators in fact, could prove particularly interesting to explore this dimension, especially when it comes to identifying securities that are prompt to bear substantial losses. This is mostly because covariance reflects not just the binding forces of correlations, but also the idiosyncratic volatility of each entity. ➔ **Looking at λ_u and λ_l in light of the idiosyncratic univariate volatility could deliver insightful observations.**

For coherence, and because λ_l, λ_l are un-temporal estimators, the un-temporal coefficient $\hat{h}$ is a more adequate descriptor of the univariate voaltility than its temporal GAS version σ_t. As described in the dedicated section, the un-temporal volatility $\hat{h}$ is calculated as:

$$\hat{h}(x) \sim a_0 \times \hat{F}(x)^2 + a_1 \times \hat{F}(x) + a_2$$

We seek to estimate the amplitude of the reaction to a shock, from a multivariate perspective. For a given pair of random variable (x^i, x^j) of two different CDS spreads (CDS^i, CDS^j) that refer to the sovereign entities (i, j), we denote:

- $x_{shock}^{j|i}$ the amplitude of the market reaction on CDS^j after a shock of amplitude x_{shock}^i has materialised on CDS^i. (read "given that" a shock happened on CDS^i).

- $x_{shock}^{i|j}$ the amplitude of the market reaction on CDS^i after a shock of amplitude x_{shock}^j has materialised on CDS^j (respectively "given that" a shock happened on CDS^j).

$x_{shock}^{j|i}$ and $x_{shock}^{i|j}$ describe two different scenarios. The first scenario assumes that CDS^i is originally subject to a shock of magnitude x_{shock}^i. This situation can be expressed in terms of percentile, via

the empirical cumulative distribution $\hat{F}^i(x^i_{shock})$. We calculate the volatility $\hat{h}^i_{shock}$ that describes the entropy surrounding this shock as:

$$\hat{h}^i_{shock} \sim {a_0}^i \times \hat{F}^i(x^i_{shock})^2 + {a_1}^i \times \hat{F}^i(x^i_{shock}) + {a_2}^i$$

In the end, $\frac{x^i_{shock}}{\hat{h}^i_{shock}}$ appears to be a standardized measure of the intensity of the shock.

$x^{j|i}_{shock}$ denotes the price action on CDS^j in the immediate aftermath of the upfront shock x^i_{shock} on CDS^i. Assuming that there is a propagation of financial distress from CDS^i onto CDS^j (at least partially), part of $x^{j|i}_{shock}$ can be attributable to the contagion phenomenon.

We denote the market entropy on CDS^j surrounding the market reaction $x^{j|i}_{shock}$ as the volatility estimator $\hat{h}^{j|i}_{shock}$. In a worst case scenario, we assume that the shock is entirely transmitted, which means that CDS^j is hurt by a shock of a similar amplitude to the shock on CDS^i. This implies that $\hat{F}^j\left(x^{j|i}_{shock}\right) = \hat{F}^i(x^i_{shock})$, and as a result we derive $\hat{h}^{j|i}_{shock}$ as:

$$\hat{h}^{j|i}_{shock} \sim {a_0}^j \times \hat{F}^j\left(x^{j|i}_{shock}\right)^2 + {a_1}^j \times \hat{F}^j\left(x^{j|i}_{shock}\right) + {a_2}^j = {a_0}^j \times \hat{F}^i(x^i_{shock})^2 + {a_1}^j \times \hat{F}^i(x^i_{shock}) + {a_2}^j$$

Assuming that the whole shock propagates onto CDS^j, the product of the volatility $\hat{h}^{j|i}_{shock}$ by the standardized percentile $\frac{x^i_{shock}}{\hat{h}^i_{shock}}$, ie. $\frac{x^i_{shock}}{\hat{h}^i_{shock}} \times \hat{h}^{j|i}_{shock}$, can be regarded as an estimate of the market reaction $x^{j|i}_{shock}$. But this holds only if the shock propagates in full.

$\lambda_u\left(\hat{F}^i(x^i_{shock})\right)$ and $\lambda_l\left(\hat{F}^i(x^i_{shock})\right)$ reflect the probability that the shock x^i_{shock} leads to the emergence of another shock, of similar or more severe amplitude, onto CDS^j. Said differently, these two coefficients can be seen as illustrating the probability that the upfront shock propagates in full: **in essence they reflect the risk that the worst case scenario comes true.**

We prefer defining $x^{j|i}_{shock}$ as a positive coefficient, though this is not vital. This will just help make $x^{j|i}_{shock}$ easier to compare on each side of the distribution. As a result, we consider $abs(x^i_{shock})$ instead of x^i_{shock}.

In the end, we calculate the market reaction $x^{j|i}_{shock}$, that is supposed to arise from the shock x^i, as its expected value in the worst case scenario, ie. $\frac{abs(x^i_{shock})}{\hat{h}^i_{shock}} \times \hat{h}^{j|i}_{shock}$, moderated by its probability $\lambda_u\left(\hat{F}^i(x^i_{shock})\right)$ or $\lambda_l\left(\hat{F}^i(x^i_{shock})\right)$ that the assumed worst case scenario effectively turns up:

$$\begin{aligned} x^{j|i}_{shock} &= \frac{abs(x^i_{shock})}{\hat{h}^i_{shock}}\ \hat{h}^{j|i}_{shock} \times \lambda_l\left(\hat{F}^i(x^i_{shock})\right) \text{ for } \hat{F}^i(x^i_{shock}) < 0.5 \\ x^{j|i}_{shock} &= \frac{abs(x^i_{shock})}{\hat{h}^i_{shock}} \hat{h}^{j|i}_{shock} \times \lambda_u\left(\hat{F}^i(x^i_{shock})\right) \text{ for } \hat{F}^i(x^i_{shock}) > 0.5 \end{aligned} \quad (40)$$

Based on this definition, both a larger idiosyncratic volatility $\hat{h}^{j|i}_{shock}$ and larger dependence coefficients encourage a bigger market reaction to the upfront shock. And the other way round, a lower idiosyncratic volatility and less tail dependence favour less contagion.

Since the problem is symmetrical, we reciprocally define $x^{i|j}_{shock}$ as:

$$x_{shock}^{i|j} = \frac{abs(x_{shock}^{j})}{\hat{h}_{shock}^{j}} \hat{h}_{shock}^{i|j} \times \lambda_l \left(\hat{F}^j(x_{shock}^{j})\right) \text{ for } \hat{F}^j(x_{shock}^{j}) < 0.5 \quad (41)$$

$$x_{shock}^{i|j} = \frac{abs(x_{shock}^{j})}{\hat{h}_{shock}^{j}} \hat{h}_{shock}^{i|j} \times \lambda_u \left(\hat{F}^j(x_{shock}^{j})\right) \text{ for } \hat{F}^j(x_{shock}^{j}) > 0.5$$

$$\text{With: } \begin{cases} \hat{h}_{shock}^{j} \sim {a_0}^j \times \hat{F}^j(x_{shock}^{j})^2 + {a_1}^j \times \hat{F}^j(x_{shock}^{j}) + {a_2}^j \\ \hat{h}_{shock}^{i|j} \sim {a_0}^i \times \hat{F}^j(x_{shock}^{j})^2 + {a_1}^i \times \hat{F}^j(x_{shock}^{j}) + {a_2}^i \end{cases}$$

We calculated $x_{shock}^{i|j}$ for $x_{shock}^{j} = \hat{F}^{j^{-1}}(l)$ where l takes all possible values in the range $[0,1]$. Graph 85 and Graph 86 show the results relative to Spain and Italy. Obviously, larger values of $x_{shock}^{i|j}$ reflect a larger exposure to CDS^j, with a greater transmission of the shock.

Graph 85. Expected reaction to an upfront shock stemming from Spain and Italy, in basis points

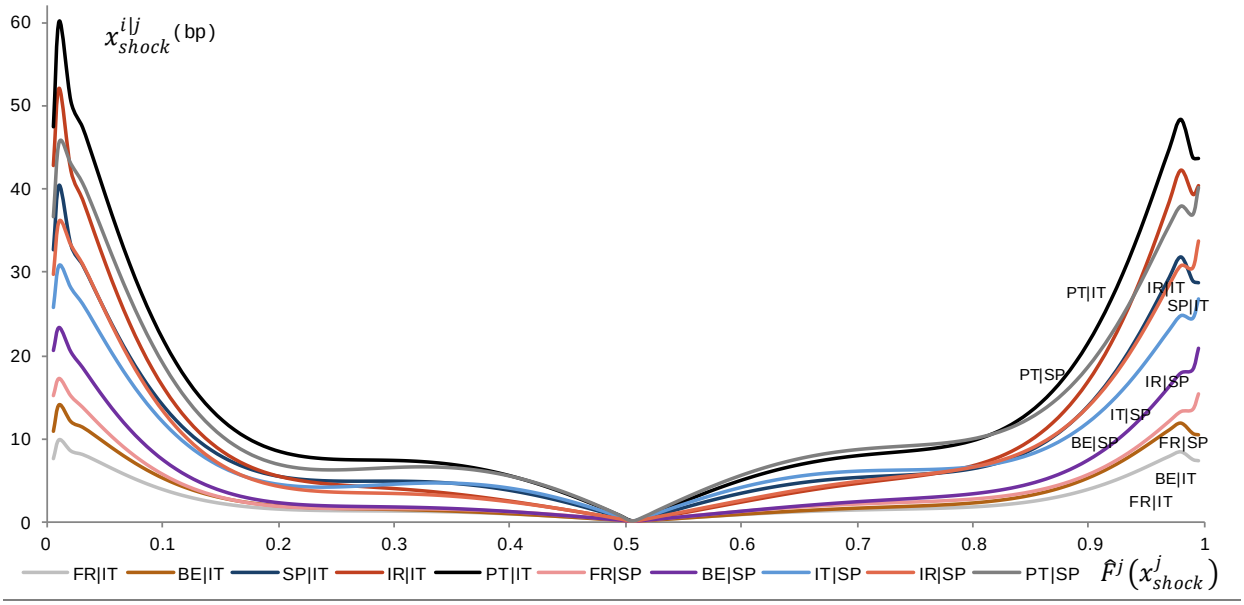

Graph 85 first, highlights the exposure of soft- and non-core countries to a shock coming from Spain and Italy. The y-axis describes the intensity of the expected market reaction $x_{shock}^{i|j}$ in basis points.

This time again we see the emergence of two regimes:

1) For shocks in the range $0.2 \leq \hat{F}^j(x_{shock}^{j}) \leq 0.8$ first (ie. small/moderate shocks overall); $x_{shock}^{i|j}$ remains relatively contained, below a maximum of $10bp$. **This is not a radical outcome per se, as for non-core sovereigns a variation of $x = 10bp$ corresponds to a percentile of $0.75 - 0.80$ on the cumulative distribution, which is not so high.** The rolling standard deviation for Spain in Graph 42 also shows that volatility can amount to more than $30bp/day$ during periods of risk aversion; $10bp$ market reaction looks relatively small in comparison. ➔ **In this first regime, the market reaction is not cataclysmic, and remains acceptably contained.**

2) For $\hat{F}^j(x_{shock}^{j}) \leq 0.2$ and $\hat{F}^j(x_{shock}^{j}) \geq 0.8$, ie. as we near the tails of the distribution, we now see a pronounced acceleration in the market reaction x_{shock}^{j}. This escalation illustrates that financial shocks become significantly more harmful beyond a certain level of severity. The non linear aspect of

the market response is noteworthy, as it suggests a fierce amplification of contagion into the tails. This overall corroborates the general observations of the contagion phenomenon in the literature (more in the literature review). In this domain, x_{shock}^{j} is much larger and reach values as high as $50bp$ for the pair PT|IT; more than $40bp$ for PT|SP or IR|IT; and more than $30bp$ for SP|IT or IR|IT.

As a general observation, $x_{shock}^{i|j}$ is seemingly reaching a peak around $\hat{F}^{j}(x_{shock}^{j})\sim 0.98$ in the upper tail, and $\hat{F}^{j}(x_{shock}^{j})\sim 0.01$ in the lower tail. Then $x_{shock}^{i|j}$ tends to decrease as we go farther in the tail. This reversal mostly reflects the decline observed in λ_u and λ_l at the very end of each tail: contagion is thus less stringent contagion in this area. To some extent, this may also be due to some numerical limitations in our calculations. Except in the tails, we see little differentiation on each side of the distribution.

The profile of $x_{shock}^{i|j}$ is in line with the general literature as authors usually distinguish a phase of mild contagion, followed by a non-linear acceleration of the market response to shocks. Here we offer a comprehensive quantification of this behaviour and the continuous aspect of the plot makes the identification of the transition between these two regimes relatively straightforward: the regime of mild contagion tends to reach saturation around $\hat{F}^{j}(x_{shock}^{j}) = 0.2$ and $\hat{F}^{j}(x_{shock}^{j}) = 0.8$, and then the non-linear acceleration comes into force.

The contagion effect becomes undoubtedly a bigger concern under larger shocks. Not surprisingly, Portugal and Ireland are the more exposed countries to shocks around, as we see the biggest market reactions on the pairs PT|IT, PT|SP, and IR|IT ($40 - 50bp$ reaction in the tails). IR|SP, SP|IT and IT|SP in comparison are a bit more resilient, with a maximal reaction at around $25 - 30bp$. This illustrates that for Ireland, Italy is a bigger source of contagion than Spain is. And in contrast to this dynamics, France and Belgium are less exposed to Italy than Spain, as BE|IT and FR|IT exhibit around $8 - 10bp$ reaction in the upper tail, while BE|SP and FR|SP reach $10 - 15bp$ reaction.

➔ **Italy is a more stringent source of contagion than Spain for other peripheral countries. In contrast, Spain is a bigger source of contagion than Italy for France and Belgium.** Comparing Italy and Spain one to each other, we note that SP|IT is slightly bigger than IT|SP though both countries are relatively equivalent in terms of credit quality ($30bp$ versus $25bp$ in the upper tail). This comforts the view that peripheral countries are hit by greater contagion when the upfront shock happens in Italy than in Spain.

Graph 86. Expected reaction to a shock on core- and soft-core countries from Italy and Spain, in basis points

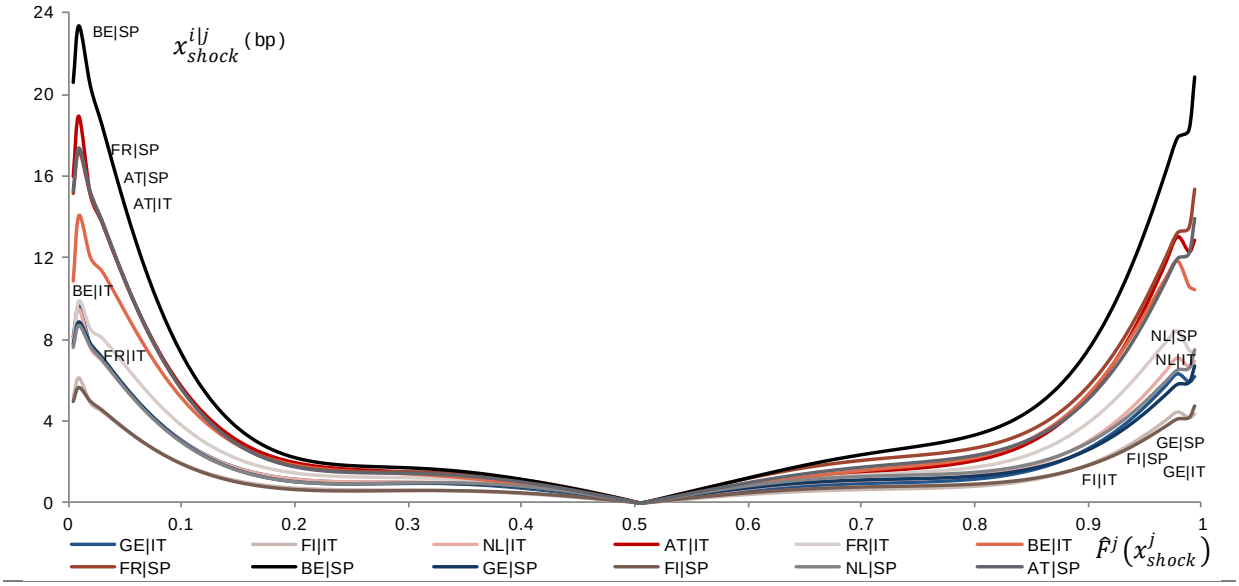

Graph 86 displays the market reaction $x^{i|j}_{shock}$ in soft-core and core countries as a response to a shock materialising in Spain and Italy. Overall, the general shape of the market reaction is very similar to Graph 85, with still a clear demarcation between the regime of mild contagion and the non-linear expansion in the tails, roughly at the same place of the distribution as before (ie. $\hat{F}^j(x^j_{shock}) = 0.2$ and $\hat{F}^j(x^j_{shock}) = 0.8$). A minor change however, is that the reversal at the very end of the distribution is now less pronounced than before.

We mentioned that France and Belgium are more exposed to Spain than to Italy. In comparison, Austria now looks to be equally exposed to both (see AT|SP and AT|IT in Graph 86). FR|IT is also much smaller than numbers relative to Austria and Belgium, though still above the bundle of curves relative to core countries. This suggests that French assets offer more protection against developments in Italy than Belgian and Austrian securities do.

In line with market observations, core countries are the most resilient sovereigns. Finland in particular shows the smallest reaction, at just $4-5bp$ in the tails. Then Germany and the Netherlands display very close results, with the market reaction remaining much contained in these countries too, at $6-8bp$.

Table 30. Market reaction in the upper tail at 2% level (bp)

$x^{i\|j}_{shock,2\%}$		EXPECTED REACTION ON THIS COUNTRY										
		UK	GE	FI	NL	AT	FR	BE	IT	SP	IR	PT
WHEN A SHOCK HAPPENS ON THIS COUNTRY	UK		3	2	4	7	8	11	18	17	49	36
	GE	4		3	4	10	12	12	32	38	20	46
	FI	4	5		6	11	13	11	35	41	46	64
	NL	4	4	4		10	13	14	33	39	21	60
	AT	4	5	4	6		14	16	37	43	32	67
	FR	3	4	3	5	9		12	15	30	18	47
	BE	4	4	2	5	9	11		19	37	22	57
	IT	4	6	4	7	13	8	12		32	42	48
	SP	3	6	4	7	12	13	18	25		31	38
	IR	8	3	4	3	8	8	10	32	30		64
	PT	4	5	4	7	13	14	19	26	26	46	`

The 2% level in the upper tail (ie. for $\hat{F}^j(x^j_{shock}) = 0.98$) is an interesting threshold as this is usually the point of maximum market reaction in the upper tail, when risk aversion is close to its climax. As a result we extract these values as to summarise the whole dynamics. We denote this indicator $x^{i|j}_{shock,2\%}$, in Table 30.

Table 30 is a straightforward illustration of x^j_{shock} that involves all the combinations of sovereigns (i, j). As we previously noted, peripheral countries are more subject to contagion than other credits. Portugal in particular sees a notable acceleration of the market reaction, with more than 50% bigger price variations than in Italy/Spain/Ireland. In other non-core countries, the average market reaction is at $27bp$ in Italy, and $33bp$ in both Spain and Ireland. This overall suggests that Italian securities are slightly more resilient to contagion risk.

Soft-core countries look much more stable, with just $10bp$, $11bp$ and $13bp$ average reaction in Austria, France and Belgium; while core countries confirm their pole position and prove remarkably less impacted by shocks in general.

Now looking at the origin of the shock, we note that France and Ireland are causing slightly less contagion than comparable credits do. More generally, we see little evidence of any pattern that would suggest that some sovereigns are systematically a bigger source of contagion than others.

Still we extract additional information from Table 30, that we display in Table 31 and Table 32: Table 31 shows the average market reaction from selected countries onto each asset category (core / soft-core / non-core). Then Table 32 exhibits the average market reaction stemming from each asset category onto selected countries.

Table 31. Average market reaction for selected countries in each category (bp)

		EXPECTED REACTION ON :		
		CORE	SOFT-CORE	NON-CORE
WHEN A SHOCK HAPPENS ON	AT	5		45
	FR	4		27
	BE	4		34
	IT	5	11	
	SP	5	14	
	IR	5	9	
	PT	5	15	

Table 32. Average value of the market reaction from soft-core and non-core countries (bp)

	EXPECTED CONTAGION ON THIS COUNTRY										
	UK	GE	FI	NL	AT	FR	BE	IT	SP	IR	PT
From a schock on:											
Non-Core	5	5	4	6	12	11	15	27	29	40	50
Soft-Core	4	4	3	5	9	12	14	24	37	24	57

Table 31 indicates how big the market reaction is supposed to be on each of the three main categories: core, soft-core and non-core countries. **Essentially, an upfront shock in Italy leads to greater market reaction in core countries (average response at $5.4bp$) than other shocks do**. However, the greater exposure to Italy is not replicated in soft-core countries which look more exposed to Portugal and Spain than Italy and Ireland.

Numbers also show that non-core countries would be hit by contagion harder when the initial shock is coming from Austria than from France or Belgium. The differentiation this time is sizeable as a shock from Austria leads to a reaction almost twice as big as when the upfront shock is materialising on French CDS.

Table 32 gives a bit more details by comparing soft-core and non-core countries as a source of contagion. Peripheral countries first, look almost equally exposed to each asset category, with an average reaction at $37bp$ (non-core) and $35bp$ (soft-core), while in a few cases a shock in soft-core countries lead to greater market reaction than a shock in non-core countries. This is true for Spain, Portugal, and France; all other countries are more impacted by peripheral countries. We also note that Ireland is significantly more exposed to non-core countries, with an average reaction at $40bp$ versus just $24bp$ when contagion is stemming from soft-core countries.

Aside from this general understanding of contagion, let us gauge to what extent contagion effectively materialised in the past. We mentioned earlier that Spain and Italy are meaningful sources of contagion as both countries display sizeable dependence with other sovereigns. As a result, and for better clarity we will focus on these two countries in the following analysis.

Contagion or idiosyncratic factors: which was prevailing during the crisis?

We now reintroduce the temporal aspect of time series x_t. While we assumed the realisation of an upfront shock in the latter version of $x_{shock}^{i|j}$, we now seek to quantify the theoretical contagion that should have arisen from the actual price variation x_t^j (drawn from the dataset). We therefore adjust the notation of the market reaction to $x_t^{i|j}$, and its formula as well:

$$x_t^{i|j} = \frac{abs(x_t^j)}{\hat{h}_t^j}\,\hat{h}_t^{i|j} \times \lambda_l\left(\hat{F}^j\left(x_t^j\right)\right) \text{ for } \hat{F}^j\left(x_t^j\right) < 0.5$$

$$x_t^{i|j} = \frac{abs\left(x_t^j\right)}{\hat{h}_t^j}\hat{h}_t^{i|j} \times \lambda_u\left(\hat{F}^j\left(x_t^j\right)\right) \text{ for } \hat{F}^j\left(x_t^j\right) > 0.5 \qquad (42)$$

$$\text{With: } \begin{cases} \hat{h}_t^j \sim {a_0}^j \times \hat{F}^j\left(x_t^j\right)^2 + {a_1}^j \times \hat{F}^j\left(x_t^j\right) + {a_2}^j \\ \hat{h}_t^{i|j} \sim {a_0}^i \times \hat{F}^j\left(x_t^j\right)^2 + {a_1}^i \times \hat{F}^j\left(x_t^j\right) + {a_2}^i \end{cases}$$

Since we replace the upfront shock x_{shock}^j by x_t^j, we remove the $shock$ denomination in all parameters. In the end, $x_t^{i|j}$ illustrates the expected market reaction on CDS^i that is supposed to arise from the price action x_t^j on CDS^j, at time t. $\hat{h}_t^j$ and $\hat{h}_t^{i|j}$ this time are also time-dependent. We calculate these indicators on Spain ($x_t^{i|SP}$ in Graph 87) and Italy ($x_t^{i|IT}$ in Graph 88).

Graph 87. Expected market reaction (bp) from x_t^{SP}

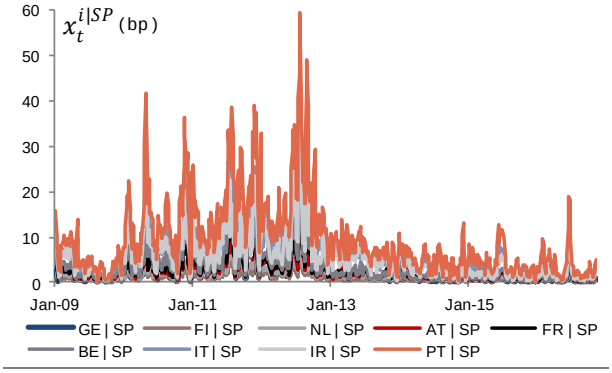

Graph 88. Expected market reaction (bp) from x_t^{IT}

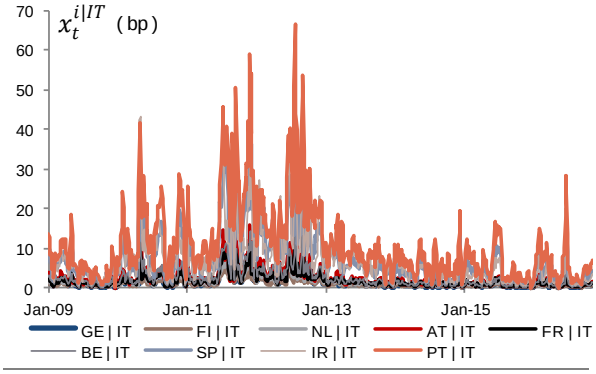

These two graphs are not very much convenient to use; we just note that contagion is more intense during periods of risk aversion, ie. when there was significant widening in SPGB/Bund and BTP/Bund spreads (e.g. 2010, 2011, 2012 in Graph 89).

Looking at France, the series $x_t^{FR|SP}$ and $x_t^{FR|IT}$ indicate by how much French CDS spreads are supposed to rise just 'by pure contagion' from the performance of Spanish (x_t^{SP}) and Italian CDS (x_t^{IT}). ➔ **It looks sensible to evaluate how big this contagion is, in comparison to the actual price action on French CDS.**

In Graph 90 and Graph 91 in particular, we compare $x_t^{FR|SP}$ and $x_t^{FR|IT}$ to the available data x_t^{FR}. In these two graphs we focus on the period from January 2010 to end-2012, as contagion into soft-core countries is less of a driver outside of this range. And while $x_t^{i|j} \geq 0$, x_t^{FR} in contrast can be negative. However, we only focus on $x_t^{FR} \geq 0$ which reflects an actual increase of the CDS price, and thus an increase in the underlying risk aversion.

We see several interesting periods in Graph 90. Between July 2010 and July 2011 first, the actual price variation $|x|_t^{FR}$ is smaller than its expected value $x_t^{FR|SP}$. This suggests that there was very little contagion operating from Spain during this period.

In contrast to this dynamics, x_t^{FR} is bigger than $x_t^{FR|SP}$ between July 2011 and April 2012. This suggests that contagion into French CDS spreads materialised in full. And since $x_t^{FR} > x_t^{FR|SP}$, there were presumably additional drivers behind the sharp volatility in French CDS spreads, including a few idiosyncratic factors given the generalised confidence crisis during this period.

Finally, x_t^{FR} looks relatively comparable to $x_t^{FR|SP}$ between April 2012 and until January 2013. This illustrates the fact that any price increase in French CDS was mostly driven by peripheral countries during this period (and this is generally true for the whole spread complex), with very little influence from idiosyncratic factors in general. **This period is coincident with the emergence of a stronger commitment from the ECB to stabilise financial markets; and this mostly justifies the disappearance of idiosyncratic factors as a main driver of French CDS spreads.**

Graph 89. Contagion is bigger in Graph 88 when 10Y SPGB/Bund and BTP/Bund spreads are on the rise

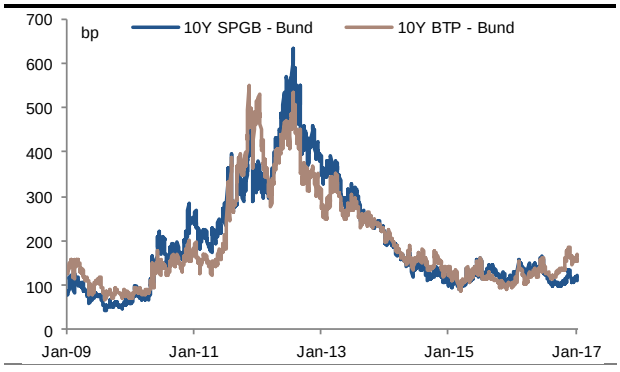

Graph 90. Contagion from Spain into France, in comparison to the actual price action – focus on the sovereign crisis

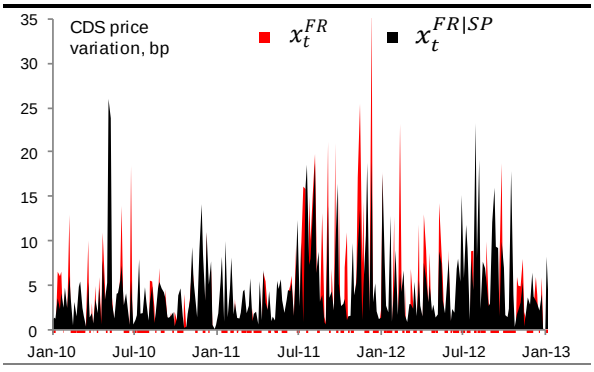

In line with our previous observations, Graph 91 indicates that contagion from Italian securities is smaller than from Spanish CDS. From that point of view, Graph 90 is a more relevant benchmark of the potential contagion into French CDS.

Looking at Germany in Graph 92, it is striking to see that $x_t^{GE|SP}$ is very close to x_t^{GE} during the full period, even at the fore of the sovereign crisis. From July 2011 to April 2012 in particular, the limited differentiation between x_t^{GE} and $x_t^{GE|SP}$ indicates that there was no particular erosion of confidence in Germany: the price action on German CDS was just reflecting risk aversion at the periphery and the ensuing risk propagation; nothing more. **This is in contrast to French CDS during the same period as the bigger price increase there, beyond the levels of contagion, reflects the emergence of a confidence crisis (reflecting sizeable idiosyncratic concerns).**

Graph 91. Contagion from Italy into France, in comparison to the actual price action – focus on the sovereign crisis

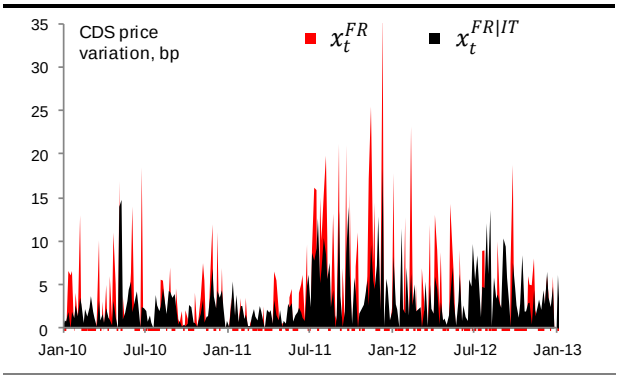

Graph 92. Contagion from Italy into Germany, in comparison to the actual price action – focus on the sovereign crisis

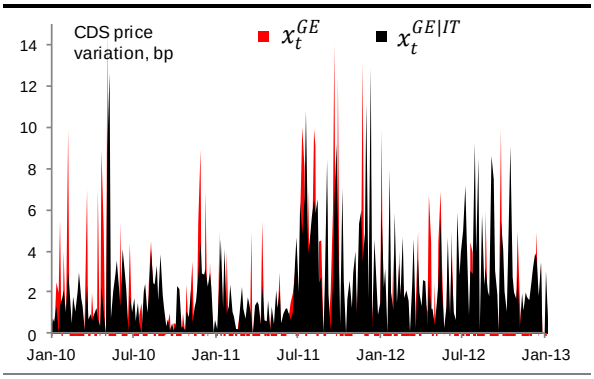

Another interesting point we think, is that in terms of volatility, the induced contagion is relatively similar to the realised volatility. Graph 90 in particular shows that $x_t^{FR|SP} \sim x_t^{FR}$ in terms of volatility. On that basis, it would probably be a non-sense to consider that the **actual contagion is the sum of all the potential contagion**. As an example, $x_t^{FR|SP} + x_t^{FR|IT} + x_t^{FR|PT}$ is more than twice as big as x_t^{FR} in absolute terms, so clearly this cannot be seen as 'the potential contagion stemming from non-core countries'. A more adequate approach would be just to take the mean value:

$$x_t^{FR|NON-CORE} \sim \frac{x_t^{FR|SP} + x_t^{FR|IT} + x_t^{FR|PT}}{3}$$

This is similarly to our calculation in Table 31, where we discriminate contagion by asset category.

Conclusion

In this first chapter, we have explored the calibration of a multivariate model that helps understand the strength of contagion within European CDS spreads. Generalised Hyperbolic distributions proved particularly adequate to capture fat tails, which are commonly attributable to periods of financial distress. The second major tool our exploration relies on, is the 'GAS method' that revealed itself as a particularly convenient approach to reproduce the erratic aspect of the historical volatilities, in particular when risk aversion is intense.

We also derived an un-temporal definition of the univariate distribution of the data via an adequate 'fair-value' estimator $\hat{h}$ of the underlying volatility. $\hat{h}$ is no longer conditional on immediate realisations in the past, and this is an interesting upgrade to the GAS estimator σ_t.

We then conducted a pair-wise analysis of the bivariate connections within the dataset and we calibrated the corresponding multivariate distribution functions using an adjusted formulation of the GAS method. While the resulting correlation coefficients proved time-invariant, the dependence coefficients associated to each distribution indicates that the propagation of risks is not constant: it reaches a peak at the 5% level in each tail.

Combining the dependence coefficients λ_u and λ_l with our un-temporal volatility estimator $\hat{h}$, we designed some novel estimators of the resulting market reaction to shocks. This helped understand the potential losses within portfolios when risk aversion tends to surge. We also compared the impact of contagion during the sovereign crisis, in comparison to the domestic deterioration that hit most of the countries. This illustrates the greater resilience in German CDS, in comparison to French CDS, with the difference reflecting a more palpable confidence crisis on French CDS.

Our model explores bivariate connections. While we got insightful information on the joint behaviour of CDS spreads, an obvious limitation all the same is that the approach does not allow for a propagation of contagion from multiple epicentres at the same time. In fact, we have briefly explored the calibration in dimension 3. Results are conclusive in the sense that the resulting calibrations are properly calibrated (based on ADC). Though this gives a more accurate correlation matrix, this is also at the cost of a substantially bigger calibration time; something that can prove a drag if the model has to be recalibrated frequently.

References

Abad, P., Chuliá, H., Gómez-Puig, M., (2010). EMU and European government bond market integration. Journal of Banking & Finance, Elsevier, vol. 34(12), pages 2851-2860, December.

Abbas, S M A, L Blattner, M De Broeck, A El-Ganainy, and M Hu (2014c), Sovereign Debt Composition in Advanced Economies: A Historical Perspective, IMF Working Paper 14/162.

Acharya V., S. Steffen (2013). The "greatest" carry trade ever? Understanding Eurozone bank risks, NBER Working Paper, No. 19039.

Ahnert, T., Bertsch, C., 2013. A Wake-up Call: Information Contagion and Strategic Uncertainty. Sveriges Riksbank Working Paper Series No. 282.

Allen W., Moessner R., (2012). The liquidity consequences of the euro area sovereign debt crisis. BIS Working aper 390, Bank for Internaitonal Settlements, Basel, Switzerland.

Amezcua, van Leeuwen, (2014). Gaussian anamorphosis in the analysis step of the EnKF: a joint state variable / observation approach Department of Meteorology, University of Reading.

Anderson, Darling, (1952). Asymptotic theory of certain 'goodness of fit' criteria based on stochastic processes. The Annals of Mathematical Statistics 23, 193–212.

Andrade, S. C., 2009, A Model of Asset Pricing under Country Risk, *Journal of International Money and Finance* 28(4), 671–695.

Angelini P, Grande G and Panetta F (2014). The negative feedback loop between banks and sovereigns. Occasional Paper No. 213

Angeloni, C., and G. Wolff, 2012, Are Banks Affected by Their Holdings of Government Debt?, Bruegel Working Paper 2012/07.

Apostolakisa, G., Papadopoulos, A. P., 2014. Financial stress spillovers in advanced economies. *Journal of International Financial Markets, Institutions and Money* 32, 128-149

Arellano, C., 2008, Default Risk and Income Fluctuations in Emerging Economies, *American Economic Review* 98(3), 690–712.

Arghyrou and Kontonikas (2011) .The EMU sovereign-debt crisis: Fundamentals, expectations and contagion.European Economy - Economic Papers 436, Directorate General Economic and Monetary Affairs, European Commission.

Arghyrou and Tsoukalas (2011) .The Greek Debt Crisis: Likely Causes, Mechanics and Outcomes. *The World Economy* 34, pp. 173-191

Armstrong Margaret and Galli Alain, Copulas, Presented at the SPE ATW Risk Analysis Applied to Field Development Under Uncertainty, Rio de Janeiro, Brazil, 29-30 August 2002.

Arslanpa, Tsuda, (2012). Tracking Global Demand for Advanced Economy Sovereign Debt. IMF Working Paper No. 12/284.

Aßmann and Boysen-Hogrefe (2011) .Determinants of government bond spreads in the euro area: in good times as in bad. *Empirica* (3 June 2011), pp. 1-16

Attinasi, Checherita and Nickel (2009) .What explains the surge in euro area sovereign spreads during the .nancial crisis of 2007-09?.ECB Working Paper 1131

Awartania, B., Maghyerehb, A.I., Al Shiabc, M., 2013. Directional spillovers from the U.S. and the Saudi market to equities in the Gulf Cooperation Council countries. *Journal of International Financial Markets, Institutions and Money* 27, 224-242.

Barbosa and Costa (2010) .Determinants of sovereign bond yield spreads in the euro area in the context of the economic and financial crisis. Banco de Portugal WP 22.

Barndorff-Nielsen (1977). Exponentially Decreasing Distributions for the Logarithm of Particle Size. Proc. Roy. Soc. London, A(353):401-419.

Barndorff-Nielsen, Shephard, (2001). Non-Gaussian Ornstein-Uhlenbeck-Based Models and some of their Uses in Financial Econometrics (with discussion). *Journal of the Royal Statistical Society* B, 63:167-241.

Barrios, Iversen, Lewandowska and Setzer (2009) .Determinants of intra-euro area government bond spreads during the financial crisis. European Commission, Economic Papers 388

Basel Committee on Banking Supervision. The Liquidity Coverage Ratio and liquidity risk monitoring tools. Bank for International Settlements (2013).

Battistini N., M. Pagano, S. Simonelli (2013), Systemic risk and home bias in the euro area, European Commission, European Economy, Economic Papers, No. 494.

Bekaert, G., M. Ehrmann, M. Fratzscher, and A. J. Mehl (2014). Global Crisis and Equity Market Contagion. *Journal of Finance.*

Bekaert, Hoerova and Lo Duca (2010) .Risk, Uncertainty and Monetary Policy. NBER Working Papers 16397

Bernardia M., Catania L., (2015). Switching-GAS Copula Models for Systemic Risk Assessment.

Bernoth and Erdogan (2012) .Sovereign bond yield spreads: A time-varying coefficient approach. *Journal of International Money and Finance* 31, pp. 639-656

Bernoth, von Hagen and Schuknecht (2012) .Sovereign risk premiums in the European government bond market. *Journal of International Money and Finance.*

Bettendorf, Timo: Spillover effects of credit default risk in the euro area and the effects on the euro Spillover effects of credit default risk in the euro area and the effects on the euro : a GVAR approach / Timo Bettendorf. - Frankfurt am Main : Deutsche Bundesbank, 2016. Discussion paper ; 2016,42)

Bibby, Sorensen, (1997). A Hyperbolic Diffusion Model for Stock Prices. *Finance and Stochastics*, 1:25-41.

Bibby, Sorensen, (2003). Hyperbolic processes in Finance, in: Handbook of Heavy Tailed Distributions in Finance, S. T. Rachev (Ed), 212–248, Elsevier Science B. V.

Bodie, Z., Gray, D. F. and R. C. Merton, 2007, Contingent Claims Approach to Measuring and Managing Sovereign Credit Risk, *Journal of Investment Management* 5(4), 5–28.

Borio C, McCauley R, McGuire P and Sushko V, Covered interest parity lost: understanding the cross-currency basis, *BIS Quarterly Review*, September 2016, pp 45–64.

Borio C, McCauley R, McGuire P and Sushko V, The failure of covered interest parity: FX hedging demand and costly balance sheets, *BIS Working Papers*, no 590, October 2016.

Breymann, Luthi (2013). Ghyp: a package on generalized hyperbolic distributions.

Brutti F., Sauré P. (2012). Transmission of Sovereign Risk in the Euro Crisis.

Bucalossi, A. et. al. Basel III and recourse to Eurosystem monetary policy operations. ECB Occasional Paper (2016).

Caceres, Guzzo and Segoviano (2010). Sovereign Spreads: Global Risk Aversion, Contagion or Fundamentals?.IMF Working Paper 120

Calomiris, Charles W. and Heider, Florian and Hoerova, Marie, A Theory of Bank Liquidity Requirements (April 15, 2015). Columbia Business School Research Paper No. 14-39. Available at SSRN: https://ssrn.com/abstract=2477101

Chau, F. and Deesomsak, R. (2014). Does linkage fuel the fire? The transmission of financial stress across the markets, *International Review of Financial Analysis*, 36, issue C, p. 57-70.

Creal, D. and Koopman, S. J. and Lucas, A. (2010). A Dynamic Multivariate Heavy-Tailed Model for Time-Varying Volatilities and Correlations (March 15, 2010). Tinbergen Institute Discussion Paper 10-032/2. Available at SSRN: https://ssrn.com/abstract=1573471 or http://dx.doi.org/10.2139/ssrn.1573471

Creal, D,. Koopman, S. J., Lucas, A. (2013). Generalized Autoregressive Score Models with Applications. *Journal of Applied Econometrics*, forthcoming.

Creal D., Koopman S. J., Lucas A. (2012). Univariate Generalized Autoregressive Score Volatility Models. Preliminary Draft.

Creal D., Koopman S. J., Lucas, A. (2011), A Dynamic Multivariate Heavy-Tailed Model for Time-varying Volatilities and Correlations, *Journal of Business & Economic Statistics*, Vol. 29, No. 4, pp. 552-563.

Creal D., Koopman S. J., Lucas A., Zamojski, M. (2016), Generalized Autoregressive Method of Moments. Tinbergen Institute, Discussion Paper.

Cronin, D., (2014). The interaction between money and asset markets: A spillover index approach. *Journal of Macroeconomics* 39, 185-202

Dalla Valle L., De Giuli M. E., Tarantola C., Manelli C., (2014). Default Probability Estimation via Pair Copula Constructions

Das U.S., Oliva A.O., and Tsuda T. (2012). Sovereign Risk: A Macro-Financial Perspective, Public Policy Review Vo. 8, No. 3 (Ministry of Finance, Japan).

Diebold, F. X., Yilmaz, K., (2012). Better to give than to receive: Predictive directional measurement of volatility spillovers. *International Journal of Forecasting* 28, 57-66.

Diebold, F. X., Yilmaz, K., (2014). On the network topology of variance decompositions: Measuring the connectedness of financial firms. Journal of Econometrics 182, 119–134.

Doshi, H., Ericsson, J., Jacobs, K., and S. M. Turnbull, (2011). On Pricing Credit Default Swaps With Observable Covariates, Working Paper, University of Houston.

Du W., Tepper A. and Verdelhan A. (2016). Deviations from covered interest rate parity, Available at SSRN: https://ssrn.com/abstract=2768207.

Du W., Schreger J. (2013). Local Currency Sovereign Risk. Board of Governors of the Federal Reserve System , International Finance Discussion Papers

Duffie, D., Pedersen, L. H. and K. J. Singleton, (2003). Modeling Sovereign Yield Spreads: A Case Study of Russian Debt, *Journal of Finance* 58(1), 119–159.

Duncan, A. S., Kabundi, A., (2013). Domestic and foreign sources of volatility spillover to South African asset classes. *Economic Modelling* 31, 566-573.

Eberlein, E. & Keller, U. (1995). Hyperbolic Distributions in Finance. *Bernoulli*, 1:281-299.

Eberlein, E.; Keller, U. & Prause, K. (1998). New Insights into Smile, Mispricing and Value at Risk: The Hyperbolic Model. *Journal of Business*, 71:371-406.

ECB (2013), Liquidity regulation and monetary policy implementation, Monthly Bulletin, April.

ECB Banking Supervision: SSM priorities 2016

Eichengreen, B., Ashoka M. (2000). What Explains Changing Spreads on Emerging-Market Debt?, in (Sebastian Edwards, ed.) *The Economics of International Capital Flows*, University of Chicago Press, Chicago, IL.

Elliott G. (1998) "Time Series Analysis, Nonstationary and Noninvertible Distribution Theory: by Katsuto Tanaka, John Wiley and Sons, 1996", Econometric Theory, 14(4), pp. 511–516.

Embrechts P., Lindskog F. and McNeil A. (2001). Modelling Dependence with Copulas and Applications to Risk Management, ETHZ, Department of Mathematics.

Eom, Y., Helwege, J., Huang, J. (2004). Structural Models of Corporate Bond Pricing: An Empirical Analysis. Review of Financial Studies 17 (2), 499-544.

Erce , A. (2015). Bank and Sovereign Risk Feedback Loops. European Stability Mechanism Working Paper Series No. 1.

ESRB (2015), ESRB report on the regulatory treatment of sovereign exposures, European Systemic Risk Board, Frankfurt /Main.

Eyigungor, B. (2006). Sovereign debt spreads in a Markov switching regime. Manuscript, UCLA.

Favero, C. and F. Giavazzi (2002). Is the international propagation of financial shocks non-linear? Evidence from the ERM. *Journal of International Economics* 57, 231–246.

Favero, Pagano and von Thadden (2010). How Does Liquidity Affect Government Bond Yields? *Journal of financial and quantitative analysis* 45, pp. 107-134

Fei F., Fuertesy A.-M., Kalotychou E. (2013). Modeling Dependence in CDS and Equity Markets: Dynamic Copula with Markov-Switching, Faculty of Finance, Cass Business School, City University London.

Fontana A. and Scheicher M. (2010). An analysis of euro area sovereign CDS and their relation with government bonds. ECB Working Paper 1271.

Forbes, K. J., Rigobon R. (2002). No contagion, only interdependence: measuring stock market comovements. *The Journal of Finance* 57(5), 2223–2261.

Foucault, T., Pagano, M. and Röell, A. (2013): Market Liquidity, Oxford University Press, New York.

Gapen, M., Gray, D., Hoon Lim, C., and Xiao, Y. (2008). Measuring and Analyzing Sovereign Risk with Contingent Claims IMF Staff Papers Vol. 55, No. 1.

Gerlach S., Schulz A., Wolff G. (2010) .Banking and sovereign risk in the euro area. CEPR Discussion Papers 7833.

Geyer, A., Kossmeier S., and Pichler S., (2004), Measuring Systematic Risk in EMU Government Yield Spreads, *Review of Financee* 8, 171-197.

Gibson, R. and S. Sundaresan, (2001). A Model of Sovereign Borrowing and Sovereign Yield Spreads. Working Paper, Columbia University.

Gómez-Puig, M. (2009) .Systemic and Idiosyncratic Risk in EU-15 Sovereign Yield Spreads after Seven Years of Monetary Union. European Financial Management 15, pp. 971-1000.

Gros D. (2013), Banking union with a sovereign virus – The self-serving regulatory treatment of sovereign debt in the euro area, CEPS Policy Brief, No. 289, 27 March 2013.

Harvey A. and Luati A. (2014). Filtering with heavy tails. Journal of the American Statistical Association, forthcoming.

Harvey A. C. (2013). Dynamic Models for Volatility and Heavy Tails: With Applications to Financial and Economic Time Series. Cambridge University Press, volume 52.

Haugh D., Ollivaud P. and Turner D. (2009) .What Drives Sovereign Risk Premiums?: An Analysis of Recent Evidence from the euro area., OECD Economics Department Working Papers 718.

Hayri, A. (2000). "Debt Relief," Journal of International Economics 52(1), 137–152.

Hilscher, J. and Y. Nosbusch, (2010) Determinants of Sovereign Risk: Macroeconomic fundamentals and the pricing of sovereign debt. *Review of Finance* 14(2), 235-262.

Hurst, (1997). On the Stochastic Dynamics of Stock Market Volatility. PhD thesis, Australian National University.

Janus, P., Koopman, S. J., and Lucas, A. (2014). Long memory dynamics for multivariate dependence under heavy tails. *Journal of Empirical Finance*, 29(0):187 - 206.

Javaheri A., Lautier D., Galli A. (2003). Filtering in finance, *Wilmott magazine*, vol 5, p 67-83.

Jiang, W. (2000). Some Simulation-based Models towards Mathematical Finance. PhD thesis, University of Aarhus.

Jones, E., Mason, S., Rosenfeld, E., (1984). Contingent Claims Analysis of Corporate Capital Structures. Journal of Finance 39 (3), 611-625.

Kallestrup, R., Lando, D., & Murgoci, A. (2012). Financial sector linkages and the dynamics of sovereign and bank credit spreads. Copenhagen Working Paper.

Kamin S., and K. von Kleist, (1999), The Evolution and Determinants of Emerging Market Credit Spreads in the 1990s, Working paper No. 68, Bank for International Settlements.

Keister T. and Morten Bech L. (2012). On the liquidity coverage ratio and monetary policy implementation. BIS Quarterly Review, December.

Kilponen J., Laakkonen H., Vilmunen J. (2012). Sovereign risk, European crisis resolution policies and bond yields, Bank of Finland Working Paper no 22.

Kilponen J., Laakkonen H, Vilmunen J. (2012) The effects of debt crisis-related policy decisions in European sovereign bond markets. Bank of Finland Bulletin, February 2012

King, M. R. (2013), The Basel III Net Stable Funding Ratio and bank net interest margins, *Journal of Banking & Finance*, 37(11): 4144–4156.

Kuchler, U., Neumann, K., Sorensen, M., Streller, A., (1999). Stock Returns and Hyperbolic Distributions. *Mathematical and Computer Modelling*, 29:1-15.

Lagi M. and Bar-Yam Y. (2012). The European debt crisis: Defaults and market equilibrium," Tech. Rep., NECSI, 2012. arXiv:1209.6369 [q-fin.GN]. http://necsi.edu/research/economics/bondprices/.

Lane, P. (2010). Some Lessons for Fiscal Policy from the Financial Crisis. *Nordic Economic Policy Review* 1(1): 13–34.

Lawrence H. Summers Homer Jones Memorial Lecture delivered at the Federal Reserve Bank of St. Louis, April 6, 2016. (JEL E52, E61, H50) Federal Reserve Bank of St. Louis Review, Second Quarter 2016, 98(2), pp. 93-110. http://dx.doi.org/10.20955/r.2016.93-110

Lee, H. C., Chang, S.L., (2013). Finance spillovers of currency carry trade returns, market risk sentiment, and U.S. market returns. *North American Journal of Economics and Finance* 26, 197-216.

Longstaff, F. A., Pan, J., Pedersen, L. H., and K. J. Singleton, (2011), How Sovereign Is Sovereign Credit Risk, *American Economic Journal: Macroeconomics* 3(2), 75–103.

Longstaff, F, Pan, J., Pedersen, L., and Singleton K. (2011). How sovereign is sovereign credit risk? *American Economic Journal: Macroeconomics* 3 (2), 75–103.

Lucas A., Schwaab B., Zhang X. (2012). Conditional probabilities for euro area sovereign default risk. ECB Financial research.

Lusinyan, L., Muir, D. (2012). Assessing the macroeconomic impact of structural reforms: the case of Italy. IMF Working Paper No. 13/22,

Malherbe, F. (2014). Self-Fulfilling Liquidity Dry-Ups. *The Journal of Finance* 69.2 (2014): 947–970.

Manganelli S. and Wolswijk G. (2009). What drives spreads in the euro area government bond market?.*Economic Policy* 24, pp. 191-240.

Narayan, P.K. Narayan, S., Prabheesh K.P., (2014). Stock returns, mutual fund flows and spillover shocks. *Pacific-Basin Finance Journal* 29, 146-162.

Oliveira L., Curto J. and Nunes J. (2012) .The determinants of sovereign credit spread changes in the Euro-zone. *Journal of International Financial Markets, Institutions and Money* 22, pp. 278-304

Pan, J. and K. Singleton, (2008), Default and Recovery Implicit in the Term Structure of Sovereign CDS Spreads, *Journal of Finance* 63(5), 2345–2384.

Pozzi, L., Wolswijk G. (2012). The Time-Varying Integration of Euro Area Government Bond Markets. *European Economic Review* 56 (1): 35–53.

Press W., Teukolsky S., Vetterling W., Flannery B., (1991). Numerical Recipes in Fortran: The Art of Scientific Computing, 2nd edition. Cambridge University Press, New York.

Rachev, S. T. (2003). Handbook of Heavy-Tailed Distributions in Finance, Elsevier/North Holland.

Ratovomirija G. (2015). Multivariate Stop loss Mixed Erlang Reinsurance risk: Aggregation, Capital allocation and Default risk. (arXiv:1501.07297v1 [q-fin.RM]).

Reiss E., Botelho M. (2013). Performance of Robust Estimators: Sampling, Variables and Dimensions. Proceedings of the 59th ISI World Statistics Congress, Hong Kong, Ciência-IUL.

Remolona, E., Scatigna, M., and E. Wu, (2008). The Dynamic Pricing of Sovereign Risk in Emerging Markets: Fundamentals and Risk Aversion, *Journal of Fixed Income* 17(4), 57–71.

Remolona, E., Scatigna M., and E. Wu, (2007). The Dynamic Pricing of Sovereign Risk in Emerging Markets: Fundamentals and Risk Aversion, Working paper, The Bank for International Settlements.

Rozada, M., and E. Yeyati, (2005). Global Factors and Emerging Market Spreads, Working paper, Universidad Torcuato Di Tella.

Rydberg, T. H. (1999). Generalized Hyperbolic Diusion Processes with Applications in Finance. *Mathematical Finance*, 9:183-201.

Santos, A. O. and D. Elliott (2012). Estimating the costs of financial regulation", IMF Staff Discussion Note, 11 September.

Savona R., Vezzoli, M. (2011). Fitting and Forecasting Sovereign Defaults Using Multiple Risk Signals. SSRN eLibrary.

Schmidt, T. (2006). Coping with Copulas in 'Copulas: From Theory to Applications in Finance. London: Risk Books.

Schwarz, K. (2010) .Mind the Gap: Disentangling Credit and Liquidity in Risk Spreads.at SSRN: http://ssrn.com/abstract=1486240

Sgherri, S., Zoli, E. (2009). Euro area Sovereign Risk During the Crisis. IMF Working Paper 222.

Shin H. S. (2016). The bank/capital markets nexus goes global, speech at the London School of Economics.

Simion, G., Rigoni, U., Cavezzali, E. and Veller A. (2016). Basel liquidity regulation and credit risk market perception: evidence from large European banks.

Sinyagini-Woodruff, Y. (2003). Russia, Sovereign Default, Reputation and Access to Capital Markets, *Europe-Asia Studies* 55, 521-551.

Summers, L. H. (2014a). Reflections on the New Secular Stagnation. In Secular Stagnation: Facts, Causes and Cures, edited by Coen Teulings and Richard Baldwin, 27–40. London: CEPR Press.

Summers, L. H. (2014b). US Economic Prospects: Secular Stagnation, Hysteresis, and the Zero Lower Bound. *Business Economics* 49, pp. 65–73.

Totouom Tangho, D., Armstrong M. (2007a). Dynamic Copulas and Forward Starting Credit Derivatives, Working Paper, February.

Totouom Tangho, D., Armstrong M. (2007b), Dynamic Copulas Processes: Comparison with Five 1-Factor Models for Pricing CDOs, Working Report, February .

Tsai, I.C., (2014). Spillover of fear: Evidence from the stock markets of five developed countries. International Review of Financial Analysis 33, 281-288.

Venter, G. (2002). Tails of Copulas, *Proceedings of the Casualty Actuarial Society* 89, 2002, pp. 68—113.

Westphalen, M. (2002). Valuation of Sovereign Debt with Strategic Defaulting and Rescheduling, Working Paper, University of Lausanne.

Xu, W., Hou, Y., Hung, Y. S., Zou, Y. (2010). Comparison of Spearman's rho and Kendall's tau in normal and contaminated normal models. ArXiv:cs/1011.2009.

Yilmaz, K., (2010). Return and volatility spillovers among the East Asian equity markets. *Journal of Asian Economics* 21, 304-313.

Yue, V. Z., (2010). Sovereign Default and Debt Renegotiation. *Journal of International Economics* 80(2), 176–187.

Zhang, B. Y., Zhou, H., Zhu, H., (2009). Explaining Credit Default Swap Spreads with Equity Volatility and Jump Risks of Individual Firms. *Review of Financial Studies* 22 (12), 5099_5131.

Zhang X., Creal D., Koopman S. J., Lucas A. (2012a). A new model for dynamic correlations under skewness and fat tails. VU University Amsterdam and Tinbergen Institute.

Zhang X., Creal D., Koopman S. J., Lucas A. (2012b). Modelling dynamic volatilities and correlations under skewness and fat tails. TI-DSF Discussion paper 11-078/DSF22

Zhang, X., Schwaab, B. and A. Lucas (2012). Conditional Probabilities and Contagion Measures for Euro Area Sovereign Default Risk, No 11-176/2/DSF29, Tinbergen Institute Discussion Papers, Tinbergen Institute.

Zhou, X., Zhang, W., Zhang, J., (2012). Volatility spillovers between the Chinese and world equity markets. *Pacific-Basin Finance Journal* 20, 247-270.

Zoli, E. (2012). Italian Sovereign Spreads: Their determinants and Pass-through to bank funding costs and lending conditions. IMF Working Paper No. 13/84, Washington: International Monetary Fund.

Chapter II.

Deriving contagion from stress tests

Résumé du Chapitre II

Le Chapitre II explore différentes manières d'exploiter notre modèle probabiliste. Afin d'identifier la dynamique de la contagion entre les obligations souveraines, nous proposons de quantifier la réaction de marché résultant de chocs financiers. Nous considérons une série de chocs, univariés et multivariés, avec un niveau de sévérité croissant, et nous définissons un indicateur de vulnérabilité qui illustre l'accélération de la réaction de marché attendue, à mesure que l'intensité du choc augmente. Le degré important de granularité dans les résultats nous permet d'identifier des lois empiriques supposées généraliser le comportement de la réaction de marché lorsque l'aversion au risque s'intensifie. En particulier, les résultats indiquent que la réaction de marché suit un comportement quadratique sur le plan univarié, et un comportement logarithmique sur le plan multivarié à mesure que l'intensité du choc augmente. Il apparaît aussi qu'il existe une relation linéaire qui relie l'intensité maximum du coefficient de vulnérabilité en fonction de la réaction de marché correspondante, et ce entre tous les pays. Cette relation est inattendue et suggère qu'il existe bien un dénominateur commun qui relie tous les pays entre eux lorsque l'on s'intéresse à la dynamique de la détérioration de la qualité du crédit en période d'aversion au risque.

Dans un second temps, nous explorons la validité de nos résultats dans un contexte de gestion obligataire. Nous incorporons nos estimateurs de volatilité et de réaction de marché à certaines approches reconnues d'optimisation de portefeuille, et nous notons une amélioration de la résistance des portefeuilles, dans cette nouvelle version. Finalement, nous développons une nouvelle méthodologie d'optimisation de portefeuille basée sur le principe de mean-reversion. Les portefeuilles que nous obtenons avec nos propres estimateurs sont plus robustes que ceux obtenus avec une définition empirique de la covariance entre les souverains. Comme la méthode GAS permet de calculer une prédiction de volatilité sur la période à venir, nous nous intéressons aussi à la robustesse de cet indicateur. Les résultats suggèrent que la composante prévisionnelle du modèle est intéressante pour la plupart des pays considérés.

"One of the most important functions of Stress-testing is to identify hidden vulnerabilities, often the result of hidden assumptions, and make clear to trading managers and senior management the consequences of being wrong in their assumptions." President of NY Fed commission bank.

Introduction.

The Global Financial Crisis has been a powerful incentive for regulatory authorities to consider developing and strengthening the framework surrounding the assessment of banks' robustness. Regulators, in this respect, have stressed the need for a better centralisation of the methodology amongst concerned institutions. They have also emphasized the benefit of combining both the micro-and macro-approach into their prudential approach.

Improving stress tests methodologies has been identified as a sensible strategy at the regulatory level, especially as these models help understand the detrimental consequences of targeted risk events. The appetite for developing stress tests favoured the publication of an abundant literature, and encouraged the emergence of new approaches in recent years.

By and large, the success of stress test models comes from an interesting combination of versatility, straightforwardness, and a wide range of utilisation. Versatility reflects the fact that different kind of scenarios can be implemented, with most of the time the ability to track the deterioration resulting from different levels of financial distress. Stress tests are particularly straightforward in the sense that the framework involves well chosen simplifying assumptions. The degree of simplification can be adjusted to the desired complexity of the model, with even basic approaches showing interesting conclusions (like the Eisenberg-Noe framework developed in the literature review). Finally, the range of utilisation is particularly wide, from purely academic thoughts, up to formalised macro-or micro-prudential recommendations at the level of bank management or politics.

First we explore popular approaches to stress testing in the literature review. Then, we design a specific methodology, adjusted for sovereign risk exploration. In particular, we differentiate univariate from multivariate implications from shocks. The univariate angle offers a view on the expected credit deterioration, while the multivariate analysis illustrates the pure contagion effect.

Our analysis gives extensive details on the dynamics of both the market reaction to shocks and the resulting contagion with regards to the degree of volatility; our calculations are based on the price dynamics of recent years including the GFC and the sovereign crises. We also explore a generalisation of these behaviours, with the resulting model providing meaningful flexibility and ease of use to explore synthetic case studies.

Finally, we consider these estimators and more generally the statistical model developed in Chapter 1 in the context of risk management. First we explore the robustness of the volatility forecast delivered by the GAS method, and we demonstrate the benefit of using this indicator instead of more conventional volatility estimator in risk management procedures. We also develop a novel asset allocation procedure based on our own contagion estimators. This approach outperforms more conventional methodologies.

Literature review

Introduction

Stress tests are specific quantitative models, used to understand the potential vulnerabilities caused by systemic risk, and to visualise implications of financial shocks on the banking system. This kind of simulation requires modelling a dedicated framework, based on a basket of relevant variables and involving adequate quantitative tools. As capturing and replicating financial linkages in a convenient manner is a meaningful purpose of the simulation, the quantitative approach is a key feature.

Stress tests have been used for a wide variety of purposes. The diversity of these applications has grown over the past decade, evolving from pure risk-management considerations towards regulatory-based decision taking. The rising enthusiasm from governing authorities (central bankers, regulators…) to consider stress tests as an engaging macro-prudential tool in recent years is an evidence of the ongoing interest in developing new methodologies or improving established approaches to systemic risk evaluation. This has encouraged the publication of an abundant literature on the subject, in the past decade.

Systemic risk characterises the possible collapse of a given financial entity in the event of a sudden and massive rise in financial distress. As banks are meaningful pillars of the financial system, most of the literature available on systemic risk focuses on modelling the resilience or exposure of the banking sector to particular scenarios. Regulatory capital ratios and interbank flows resulting from the funding requirements of financial institutions are examples of relevant variables that are carefully scrutinised in stress tests scenarios. One of the limitations though, of the bank-level focus is the numerous data that need to be integrated. Studies centred on the United States for instance need to absorb a massive amount of information because of the size of the banking sector there. Another common caveat is that the required information is not always publicly available, and this is amplified by the fact that regulatory constraints in terms of disclosures can differ from one jurisdiction to another. From that perspective, it is relatively challenging to conduct cross-country comparisons out of bank-level investigations of systemic risk. A possible way to overcome this issue is to consider market data exclusively. Models based on CDS spreads or bond valuations have gained considerable traction in recent years as the debt crisis in Europe has been an incentive to move the exploration of systemic risk to the level of sovereigns (and not just to banks), in particular by exploring implications of a confidence crisis on the sovereign credit robustness. The approach can take the form of probabilistic models that integrate a dataset of fundamental or market-based time series. And such analyses usually offer a broader understanding of systemic risk (ie. over a wider scope of geographical areas) than bank-related models. This greater flexibility however, may be at the cost of a certain loss of precision as market-based information sometimes does not reflect the complexity of intrinsic linkages between sovereign Treasuries and banks. Finally, another category of Stress test models seek to illustrate systemic risk, but from an investor point of view. This means estimating the potential market reaction to mounting financial distress, in order to apprehend the ensuing losses in portfolios: for portfolio managers, "*stress tests provide a useful check on VaR analysis by carefully working out the consequence of a particular, intuitively appealing scenario for the value of an asset portfolio*" (Hirtle, Lehnert (2014)). The goal of systemic risk exploration in this context is to take decisions on the optimal asset allocation as to minimise the exposure of the portfolio to shocks. This approach is largely depending on the nature of the assets: e.g. a credit

portfolio would prefer micro-based analyses of systemic risk, eventually helping to draw conclusions on the credit worthiness of a given firm, in a stressed environment. A macro portfolio in contrast, involving sovereign securities for instance, would take advice from more general macro-based models. As portfolios may be limited to very specific assets (like a particular sector in equities), it is tempting to use simplifying assumptions. Too stringent simplification though is a risk to ignore significant aspects of the global macroeconomic picture that could prove much influent on the price action when risk aversion is on the rise.

Conducting a stress test exercise also implies designing a model that understands the origin of risk aversion, and how risk propagation translates into price deterioration. The capability to interpret the shock is thus a key feature of stress tests models. First, this requires considering a set of relevant variables, supposed to reflect the dynamics of mounting risk aversion: these variables usually take extreme values in the stressed environment. The procedure to design the shock takes various forms in the literature. Bank-level approaches usually consider shocking cash flows on particular entities. A failure to repay its debt obligations, a significant rise in bank's liabilities or severe losses on mark-to-market valuations are examples among others of common scenarios implemented to simulate an unanticipated shock on individual banks. Other approaches can also involve data at the macroeconomic level: e.g. by simulating a sharp rise in unemployment, depleting growth or a largely disadvantageous current account, as all this would cause significant contagion into financial institutions. As investors' confidence erodes, this scenario naturally pushes interest rates to new highs. Funding, in turn, becomes abnormally expensive, and this feeds further depletion of the credit quality. Shock scenarios may also involve a specific assumption on the ex-post situation in financial markets. As an example, one can assume that a given CDS or sovereign spread may widen beyond pre-determined thresholds. In this case it would be interesting to estimate the resulting contagion on different asset classes. **The methodology behind the assumed scenario is a fundamental feature in stress tests modelling. We explore this feature more in depth in the following paragraphs, illustrating the available literature.** Another meaningful feature in the literature is how contagion is defined and quantified. For a given scenario, it is crucial to set up an appropriate framework that reflects how risk aversion translates into contagion and ultimately into a price variation on the securities affected by the shock. This component within stress test models is usually called a "satellite model"; and there is a large variety of satellite models in the literature. A widespread methodology is to build a synthetic banking network that is supposed to replicate the actual interbank linkages. The network may also allow for some counterparty risk while incorporating interesting models to derive future incomes, losses and capital ratios. Conclusions in this case depend largely on the network structure, ie. the concentration of nodes and bilateral links. More sophisticated approaches on the quantitative side may involve complex econometric tools; this is another way to derive the outcome of the shock. These statistical tools dedicated to systemic risk exploration usually rely on correlation measures and estimators of causal relationships. More intuitive methodologies can also be based on empirical observations of the spillover effect, for instance during periods marked by fire sales, or by an extremely low liquidity, or a notable loss of confidence in the past. These models are prompt to consider original indicators (e.g. 'bankruptcy costs'). **We explore satellite models further in a dedicated paragraph below.** Assessing contagion and taking decisions accordingly is the last stage of stress testing from a very general point of view. The resulting predictions that illustrate the resilience or exposure of a given entity actually need to be seen in light of the purpose of the exercise. A goal at the regulatory level is to provide a macro-

prudential feedback to member participants: banks seen as insolvent in a risk-averse environment are required to recapitalise themselves. Comparing the predicted capital ratios with the regulatory requirements (Basel, Solvency) helps identify the level of recapitalisation. Results can also lead to broader recommendations like structural reforms at the national level. For risk management purposes, stress tests results can reveal a difference between the observed robustness in the simulation and the corresponding ratings (from official agencies). Results may also highlight more important divergences, emphasizing unexpected resilience or exposure that is worth to highlight to investors. In some cases, stress tests can also reveal an ongoing depreciation or strengthening of the credit quality. This kind of conclusions is an invitation for investors to reallocate accordingly, allowing them to reduce the global exposure of portfolios in a risk-averse environment. From a more academic point of view, stress test models may be conducted to promote novel methodologies to quantify contagion, advertising thereby new features of financial inter-connectivity. This kind of approach has the significant advantage of being independent from any banking, governing or supervising authority. This confers greater autonomy in investigating the topic.

The general description of the framework around stress testing highlights the numerous approaches to address the question of systemic risk exploration. We conduct a literature review in the following pages, based on research papers that look relevant in the context of this analysis.

The framework

The heart of stress testing methodologies is the specific framework they rely upon. This framework has to understand the magnitude of risk-aversion, while reflecting the channels of risk propagation. This is a key feature to get a sensible picture of the shock implications in the distressed environment. The literature reflects mostly two main approaches as to define the framework. First of all, one has to pick-up some input variables that will be under pressure when the stress test scenario comes into force. These variables play a major role in the simulation. Another meaningful challenge is to provide a relevant structure that will properly integrate the propagation of financial stress. This structure can take various forms. First, a lot of papers focus on modelling a virtual network of financial entities, which is meant to replicate the actual linkages between the participants via adequate quantitative models. Eisenberg, Noe (2001) in particular is seen as the precursor of network-based models. The authors design a multi-firm network (each firm is a node) that takes revenues and payments from each entity as an input to the simulation. In the end, the model computes a “clearing payment vector” that illustrates bilateral liabilities. This vector provides a consistent way of valuing the nodes. It also gives a picture of the risks that each entity may not fulfil its future payment, highlighting thereby the relative soundness of the whole financial system. In this framework, each participant is described via three main variables, which look sufficient information to test the viability of the entity. As a variable of prime importance, the model looks at **nominal liabilities**. These flows illustrate promised payments due to other firms (ie. to other nodes). Since these obligations constitute a burden for the firm, excessive liabilities raise some risk of insolvency (De Groen, Gros (2015)). The second feature of interest is **nominal claims**, which reflect payments due by other nodes. Thirdly, the model also takes **exogenous operating cash flows** into account. These flows correspond to cash infusion to the node from sources outside the network; they prevent too much simplification of the actual inter-firm linkages. Then, nominal obligations and operating cash flows define what the authors call a “financial system”. Similar frameworks have explicitly taken inspiration from Eisenberg, Noe (2001) like Anand, Kartike et al. (2014), Acemoglu, Daron et al. (2014),

Glasserman, Paul and Young, Peyton (2013), Houy, Jouneau-Sion (2016), Visentin, Battiston, D'Errico (2016), Feinstein, Rudloff, (2015) – every time implementing their own variations. Acemoglu, Daron et al. (2014) for instance considers interbank lending and borrowing as the main sources of risk propagation too, but they also assume the presence of contingency covenants in every debt contract. This allows the lender to charge different interest rates depending on the risk-taking behaviour of their borrowers. Adding this variable helps ensure that the extent of counterparty risk is (at least partially) reflected in the interbank contracts: banks with higher risk of default face higher risk-premia. Overall, this is a relevant way to estimate how counterparty risk may drive financial distress and lead to contagion over the entire banking structure. In those models where risk propagation is largely dependent on the form of the banking network, the connections between participating entities are particularly straightforward to plot. By symbolizing participating banks by circles (or nodes), the bilateral connections usually appear as arrows. Each arrow is attached to two nodes, with the origin being the lending entity while the targeted circle is the borrowing bank (Graph 93, Graph 94).

Graph 93. The three-chain financial network

Source: Acemoglu, Daron et al. (2014)

Graph 94. The ring financial network

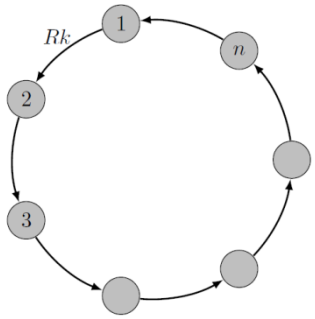

Source: Acemoglu, Daron et al. (2014)

This graphical approach offers a genuine interpretation of how financial stress propagates into the network. It also provides a singular flexibility to explore various structures by modifying the distribution of the arrows. Acemoglu, Daron et al. (2014) and Glasserman, Paul and Young, Peyton (2013) in particular investigate different kinds of connections, and evaluate how the distribution of the arrows impacts the behaviour of the banks. Graph 95 and Graph 96 are extracted from their analyses; these graphs highlight two different networks where the disposition allows for more or less complexity in bilateral connections. Anand, Kartike et al. (2014) offers another interesting network-based approach to systemic risk exploration. Like in previous examples, connections between the nodes (ie. participating banks) illustrate the total lending and borrowing amount observed on balance sheets; this interpretation is largely based on the Eisenberg-Noe framework (Eisenberg, Noe (2001)). The difference in this case is that Anand, Kartike et al. (2014) also involves empirical observations of the dynamic of bilateral connections. In particular, the authors acknowledge that interbank linkages are typically disassortative: "small banks seek to match their lending and borrowing needs through relationships with larger banks that are well placed to satisfy those needs". This behaviour is then interpreted as the main driver of risk propagation in their own model as it induces a higher concentration of borrowing requirements on safer banks during periods of stress from the more troubled institutions. The authors also explore a novel approach to designing the channel of risk propagation: they incorporate the probability that banks may fail to borrow/lend one to each other as an additional criterion. Arguably, quantifying empirical observations also presents some risks. In particular one needs to verify that the aforementioned assumption of disassortativity

remains valid, regardless of the level of financial distress. Interestingly, Glasserman, Paul and Young, Peyton (2013) also explores additional variables like node size, leverage, bankruptcy costs and the impact of the loss of confidence in financial entities. The node size is seen as the exposure at default (EAD), which measures the total claim on all other banks; while leverage is seen as the ratio of the net worth of the bank over the outstanding of its outside assets. Finally, bankruptcy costs are introduced via a dedicated factor (γ) that follows the theory of Elliott et al. (2013). The decline in confidence is evaluated by marked-to-market potential losses for a lender well before the point of default. Glasserman, Paul and Young, Peyton (2013) ultimately demonstrates that those additional factors favour a faster deterioration of the network.

Graph 95. The interlinked rings financial network

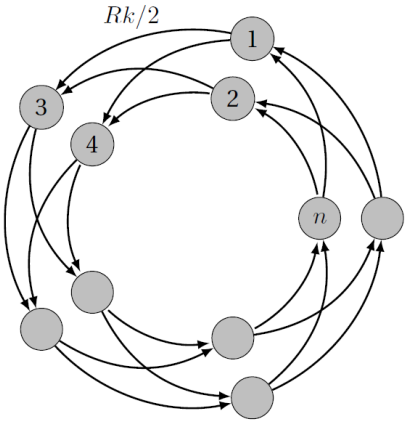

Source: Acemoglu, Daron et al. (2014)

Graph 96. Network example

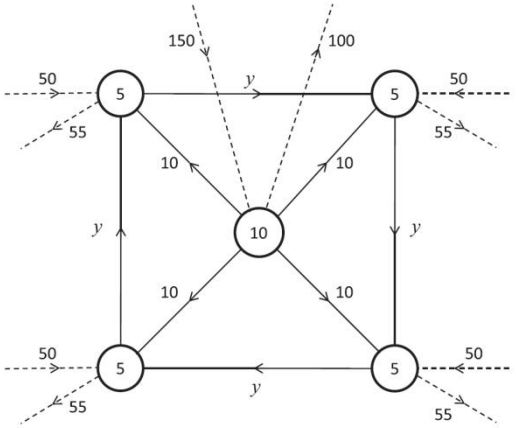

Source: Glasserman, Paul and Young, Peyton (2013)

In contrast to these approaches, other frameworks involve a minimal knowledge of the network topology. These models usually involve variables not taken at the balance sheet level, but consider instead more general information like financial market data or macroeconomic indicators as the main source of financial risk. Hirtle, Lehnert (2014), Kok (2013), ECB (2013), Angeloni (2015), Angeloni (2016), review the main approaches to stress tests from a regulatory perspective. These papers introduce 'macro' models and 'financial shock' models as alternative ways to the more traditional "funding shock" models that we describe above. Macro models in general consider market-based information as much appropriate information to quantify systemic risk. Hesse, Salman, Schmieder (2014) in particular implements a sophisticated framework where a combination of market data and macroeconomic variables are seen as relevant variables to design a shock. And since the model largely focuses on the Euro Area, peripheral sovereign yield spreads are part of the inputs. In addition, the model also incorporates macroeconomic variables at the national level like the GDP trajectory, inflation rates, current accounts and the level of public debt. These variables are then computed to determine the resilience/exposure of each country. Interestingly, Hesse, Salman, Schmieder (2014) explores multiple channels of risk transmission: aside from macro data and financial variables, the authors also take information at the micro level, namely incorporating cash flows and asset values as indicated by the balance sheets of the selected banks. As a consequence, the resulting framework is one of the most complex approaches that we have seen. Market-based information effectively adds some value to network-based frameworks. Glasserman, Paul and Young, Peyton (2013) for instance tends to model the impact of a loss of confidence, that would occur ahead of default. Losses in this context are evaluated via different shock scenarios on the price dynamics of debt and equities. Market-based information like in Glasserman, Paul and Young, Peyton

(2013) or Hesse, Salman, Schmieder (2014), is used as one of the main sources of contagion. In Hesse, Salman, Schmieder (2014) for instance, introducing market-based time series allows the authors to quantify how interest rates would react following a fire sale on peripheral sovereign bonds. In other approaches like in Darolles, Gagliardini, Gourieroux (2014), stress tests are even exclusively based on market prices: the authors consider the distribution of liquidation counts of hedge funds using the Lipper TASS database. This database offers a discrimination of the dynamics of the liquidations throughout 9 management styles: Long/Short Equity, Event driven, managed futures, equity market neutral, fixed income arbitrage, global macro, emerging markets, multi strategy and convertible arbitrage. Aside from the input itself, Darolles, Gagliardini, Gourieroux (2014) are also creative in the sense that they consider statistical estimators as relevant descriptors of risk propagation. In particular they involve two main criteria: 1) A "contagion matrix", which is a correlation-like estimator that highlights dependencies between financial entities. 2) A "common factor", seen as a proxy for the access to funding liquidity. Then stress tests are conducted as a shock on these two variables: on one side they reset the contagion matrix with much larger coefficients than in normal market conditions. By doing so, they track the consequences of financial stress on the joint dynamics: this scenario is a shock on exogenous factors. On the other side, a second type of scenarios tends to stress the "common factor". In this case the authors analyse how risk aversion tends to impact the access to funding and liquidity. This is seen as a shock on endogenous factors. Hirtle, Lehnert (2014) consider that this kind of approaches, largely based on historical correlations, offer insightful information on the expected decline in equity prices in the aftermath of shocks. This approach has notable benefits: transparent, straightforward to manipulate and it involves only publicly available data. And since market sentiment is largely incorporated, these models tend to capture investors' interpretation of underlying risks to a large extent. Market-based time series are also very convenient to implement thorough quantitative models (like Bayesian models) given the higher frequency of the available data in comparison to more fundamental indicators. Quite the opposite, the lack of uniformity between firms, possible variations in the frequency of the releases, and the fact that the required information is not always publically available make stress tests at the balance sheet levels rather inappropriate for a probabilistic exploration of systemic risk.

Stress scenarios

Designing the stress test scenario is another important feature of the simulation. The scenario plays a major role as it has to reflect both the rationale of the shock, and the risk (or the probability) attached to it. Consequently, it has to be a reliable illustration of how risk-aversion is supposed to emerge. Given the complexity of financial linkages, and the large amount of variables potentially affected by financial distress, designing stress scenarios is not a straightforward exercise. As Hirtle, Lehnert (2014) argues, scenarios are typically drawn, either out of particular episodes in the available history, or based on the ex-post situation, for instance a specific (and extreme) price variation on certain securities. The scenario may be defined by its probability to happen, which is relatively convenient when the model involves probabilistic tools. An interesting approach is also to consider not just one scenario, but a set of different shocks instead, with different levels of severity. Schmieder et al. (2012) for instance, explore four different scenarios that provide an interesting granularity in the results. Camara, Pessarossi, Philippon (2016), Board of Governors of the Fed (2016), De Groen (2016) also propose similar methodologies that explore a bunch of scenarios. We note above that Hesse, Salman, Schmieder (2014) explores a sophisticated network-based model, which involves a combination of macro-indicators assorted with information taken at the balance

sheet level. The diversity of the dataset enables the authors to consider a variety of different scenarios. In particular, the analysis differentiates shocks affecting liquidity conditions from those impacting solvency. Stress tests on liquidity, follow the methodology described in Schmieder et al. (2012). In this approach, four scenarios are designed; all of them focus on banks' liabilities and assets. Banks' liabilities are also broken down into customer deposits, short-term wholesale funding and contingent liabilities (mostly derivatives' funding and long term funding like senior debt and subordinated debt). **These variables are subject to a specific level of deterioration ex-ante, in each scenario.** On the asset side, the different scenarios assume a particular level of haircut on four variables: c**ash, government securities** (1% to 10% haircut), **trading assets** (3% to 100%), and **other securities** (10% to 100%). The ECB is promoting a similar approach to designing scenarios that are meant to test banks' liquidity, like in ECB (2013). The authors emphasize in particular that the duality between funding constraints and haircuts on the asset side has the advantage to allow for the impact of potential 'fire sale'-related losses and loan supply restrictions. Another interesting point in ECB (2013) is that the severity of each scenario is described as a ratio against a 'Lehman-type' benchmark. The 'Lehman-type' scenario corresponds to the situation encountered by large banks in OECD countries that were hit severely during the month after the Lehman collapse. As a consequence, the 'moderate scenario' is designed as being a quarter the intensity of the Lehman crisis conditions (ratio of 0.25), while the medium, severe and very severe scenarios respectively see a factor of $\times\ 0.5$, $\times\ 1$ and $\times\ 2$ the Lehman's crisis. Darolles, Gagliardini, Gourieroux (2014) also gives extensive details on funding liquidity risks. They differentiate three types of measures to analyse the funding liquidity risk and to model its evolution:

> **1) Refinancing costs**; a notion also used in Schmieder et al. (2012). The methodology is based on the frequent interpretation of the TED spread[9] in the literature like in Gupta, Subrahmaniam (2000), Boyson, Stahel, Stulz (2010) and Teo (2011).
>
> 2) **A direct measure of market liquidity** such as the size of the bid-ask spread. The chosen methodology is similar to Brunnermeir, Pederson (2009) and Goyenko, Subrahmaniam, Ukhov (2011).
>
> 3) **Thirdly, liquidity is regarded from its impact on asset prices.** In this respect, Vayanos (2004) models the liquidity premium by comparing the market response of different assets with similar characteristics but a different level of liquidity (for instance comparing on-the-run versus off-the-run bonds).

The second category of shocks in Hesse, Salman, Schmieder (2014) focuses on **solvency, ie. on projections of capital ratios with regards to liabilities imposed by the scenario**. From a general perspective, ECB (2013) defines this direct approach to banks' solvency as a supervisory tool to calculate the capital shortfall ensuing from shocks. In Hesse, Salman, Schmieder (2014), the methodology is based on the approach of Hardy, Schmieder (2013), where credit losses, pre-impairment income and the trajectories of risk-weighted assets (RWA) for a 2-year horizon are computed out of GDP trajectories, and assuming some contagion on peripheral sovereign spreads (from $100bp$ to $300bp$ spread widening). Five different scenarios with gradual levels of severity are implemented: **normal conditions, moderate stress, medium stress, severe stress, extreme stress**. Each scenario corresponds to a particular percentile of credit losses, extracted from the empirical distribution (80^{th} for moderate stress, 97.5^{th} for severe stress). The authors then derive the

[9] The Treasury-Eurodollar (TED) spread, equal to the difference between the 3-month Eurodollar LIBOR rate and the 3-month Treasury bill rate

expected values of pre-impairment income and RWA, using relevant assumptions. The shock in the end involves micro-variables only (at the balance-sheet level). This helps understand the implications of a shock emerging from within the banking sector itself. While such a parameterisation is highly relevant from a macro-prudential perspective, an obvious limitation is that this scenario does not take any macroeconomic development or any reversal in market sentiment into account. As a means to address this limitation, Glasserman, Nouri (2012) for instance, seeks to capture investors' perception of the surrounding risks by adding assumptions on the risk free rate. An essential feature common to these simulations is that stress tests do not assume the materialisation of a proper default: the variety of the dataset is an incentive to explore the implications of a gradual deterioration in fundamental variables, instead of the impact of a full-blown default. As a consequence, results are 'capital ratios-oriented', ie. they do not highlight at which point exactly a default is supposed to occur; in contrast they provide a picture of how capital requirements are expected to surge under extreme scenarios. Another benefit of exploring gradual levels of severity is the refined granularity of the results, which makes possible to track closely how systemic risk propagates into the whole financial system.

In contrast to this approach, scenarios built around the Eisenberg and Noe framework put a considerable emphasis on the default itself. In their original paper (Eisenberg, Noe (2001)), the scenario is composed of a set of more or less abundant defaults hitting selected firms at the same time. These firms under default are no longer able to satisfy their obligations, and this impairment has significant implications on the 'clearing vector'. As the authors explain, the iterative algorithm provides a (unique) clearing vector that resolves financial liabilities in the network every time the routine is called. If the clearing vector identifies additional defaulting firms, these entities are added to the initial set and the routine is compiled again. The procedure stops once equilibrium is found. The final clearing vector highlights the resulting firms that are supposed to default, conditional on the initial set of defaulting firms. This approach shows the notable benefit of involving straightforward calculations, and results are very understandable by the general public. But we also see some caveats: a particular weakness, according to Glasserman, Paul and Young, Peyton (2013), is that the Eisenberg-Noe framework does not model the dynamics by which financial institutions enter into obligations to one another. Papers like Glasserman, Paul and Young, Peyton (2013), Acemoglu, Daron et al. (2014) and Anand, Kartike et al. (2014) seek to improve the original methodology. Glasserman, Paul and Young, Peyton (2013) for instance implement two modifications to the initial framework: First they consider the probability distribution of the shock as an additional and relevant variable, and for this purpose they explore a variety of distribution functions like the beta, exponential, normal distributions. Secondly, they build two separate networks with and without interbank connections, computing every time the clearing vector on both frameworks separately. This comparison delivers valuable insight on the overreaction that comes from interbank relationships. Similarly, Acemoglu, Daron et al. (2014) implements an "Eisenberg-Noe"-type model that also takes control on the probability that the shock tends to materialise. A difference though, is that the shock in this paper is no longer defined as a set of defaulting firms, but it is designed as a shortfall imposed to banks on expected investment returns. This definition delivers comprehensive insight on how the shock propagates within the network. The authors in particular identify a threshold for the amplitude of the shock under which no contagion occurs. Still in an attempt to improve the Eisenberg-Noe framework, Anand, Kartike et al. (2014) investigates other adjustments. First, the authors observe that even if interbank bilateral positions can be obtained from regulatory

filings or credit registers, most of the banks do not report their bilateral exposures. In this context, the leading method is to consider the available information on each bank's total interbank lending (Upper 2011, Elsinger et al. 2013). This approach, known as *maximum entropy* (ME), assumes that banks diversify their exposure by spreading their lending and borrowing across all other active banks. But this can prove misleading as ME tends to maximise interbank connections, and this to some point can obscure the true structure of linkages in the original network. As a consequence, Anand, Kartike et al. (2014) explores an alternative benchmark - the *minimum density* (MD) method – which is based on the rationale that interbank linkages are costly to add and maintain. The procedure determines a pattern of linkages for allocating interbank positions that is efficient in the sense of minimizing these costs. The approach identifies the most probable links and loads them with the largest possible exposures consistent with the total lending and borrowing observed for each bank that could be obtained from the bank balance sheet. The trigger event is a combination of a single failure (ie. the default of an individual bank), and an across-the-board decline of regulatory capital of 2%. Banks go into default when their regulatory capital falls under a common regulatory requirement of 6%. Solving the clearing vector delivers 1) the number and identity of banks that default as a result of contagion and 2) the total assets and interbank liabilities of defaulting banks ex-post. Comparing the results obtained with MD and ME models, it appears that the traditional ME approach underestimates systemic risk substantially, while MD tends to slightly overestimate the true extent of contagion. **In the end, modifying the early version of the Eisenberg-Noe framework, and re-designing the shock helped obtain a more reliable picture of potential contagion.** We also note that other approaches like Jaeck, Lautier (2012) manage to implement an adaptive design of the topology of the nodes via the Minimum Spanning Trees (MST) approach. This helps identify the most relevant distribution of the financial interconnectedness within the network.

Stress test models based on market data exclusively, are usually based on a different understanding of the shock. As we noted above, the dataset itself makes a statistical exploration of systemic risk relatively convenient. This is for instance the case in Darolles, Gagliardini, Gourieroux (2014), where the shock is based on the probability distribution function of the stressed variables, seen as potential sources of financial distress. By and large, the most important variable is the **frailty coefficient**, which illustrates the deterioration ensuing from shocks. A first series of scenarios assumes that this parameter will surge up to its $95\% - 99\%$ percentile. The calibration of their probabilistic model is based on different filtering techniques. Ultimately, this helps understand the distribution of the frailty coefficient. The authors also consider other kind of shocks, like scenarios assuming a disruption of the dependence structure between the assets. These shocks take the form of a sharp increase in the **contagion matrix**: larger correlation coefficients are supposed to reflect greater multivariate linkages in risk averse market conditions. Another round of shocks is also implemented on the **frailty persistence parameter**. This stress scenario is seen as simulating heightened risks of hedge fund liquidations throughout an amplification of the contagion stemming from exogenous shocks. The shocks we design in this report are largely inspired from this methodology, developed in Darolles, Gagliardini, Gourieroux (2014). Finally, "reverse stress tests" constitute another interesting way to investigate stress testing. In this approach, one goal is to identify the least severe scenario that is going to cause a pre-determined outcome. This outcome can take various forms like the failure of a firm or a sudden surge in peripheral sovereign spreads (Grigat, Caccioli (2017), Grundke, Pliszka (2015)). In contrast to traditional stress tests where the shock is defined ex-ante, "reverse stress tests" simulations assume an ex-post definition of the shock.

Modelling contagion

Contagion is the intriguing force that stress tests are supposed to capture and illustrate. The notion of contagion refers to the generalised amplification of multivariate linkages that occurs under tough risk aversion. Contagion usually leads to massive price deteriorations within the financial system, and the cascade effect can be seen as a consequence of latent dependencies that take over in deteriorated market conditions. Crises in the past show that financial securities have a tendency to conjointly sell-off when the degree of risk aversion exceeds a particular threshold. This specific price action is in sharp contrast with established correlations in the normal course of financial markets. Against this backdrop, stress tests are regarded as an interesting procedure to identify how financial distress tends to spill-over. But drawing a reliable forecast of the market reaction to shocks – via appropriate satellite models - is a tough challenge: in most cases, conclusions are drawn from the experience of crises in the past, which (thankfully) are relatively infrequent. And while quantitative models offer a wide panel of different tools, risk propagation is much complex and requires making the right assumptions, at the risk of too much simplification. Another drawback is that every period has its own special features; thus it would be naive to expect the replication of past observations 'as is'. Contagion in essence, is depending on numerous parameters and it can take different shapes. Kok (2013) for instance identifies three potential types of contagion: the one **stemming from financial frictions** (e.g. in a macro shock), then the spillover-effect that results from **financial interconnectedness**, and thirdly contagion related to **financial imbalances**. Allowing for different kinds of contagion within a single model requires a sophisticated framework. In Glasserman, Nouri, (2012) for instance, the satellite model explores both the dynamics of capital requirements and credit yield spreads for banks, in light of several variables: the volatility of the firm's assets, the level of the available tranche of convertible debt (into equities) and the recovery rate in the event that the firm breaches its minimum capital requirement and is seized by regulators (Graph 97, Graph 98). Other – more original - approaches to contagion also explore the analogy between medical and financial contagion. Darolles, Gagliardini, Gourieroux (2014) in this sense found inspiration in the literature on epidemiology to quantify financial contagion, adjusting the "baseline intensity" model of Anderson, Britton (2000) to financial data.

Graph 97. Sensitivity of senior debt to volatility and minimum capital ratio when 10% of debt is replaced with convertible debt

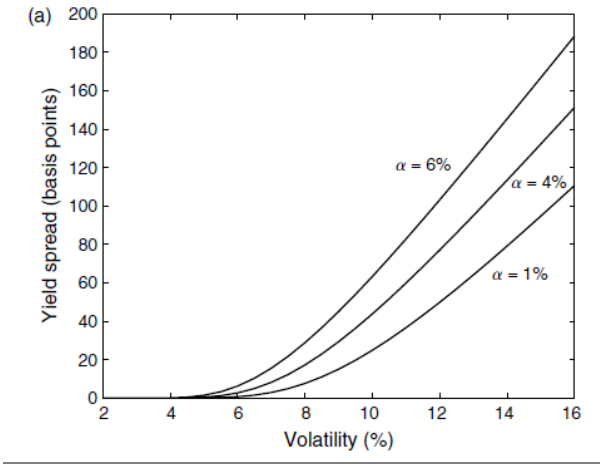

Source: Glasserman, Nouri, (2012)

Graph 98. Coupon rates for convertible debt

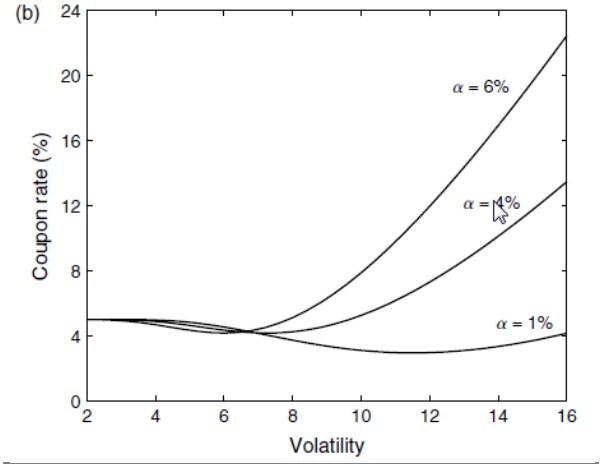

Source: Glasserman, Nouri, (2012)

The Eisenberg-Noe framework also provides a singular framework to understand contagion. In contrast to models that account for a multitude of stressed variables, Eisenberg, Noe (2001) only looks at the set of firms that are supposed to default in the early stage of the simulation. In this case, contagion emerges from the firm's incapacity to satisfy its obligations, causing therefore a chain reaction directed towards other firms. Assuming numerous connections in the framework, the upfront impairment is transmitted to other firms, and this ends up with a sequence of payment shortfalls along the chain. The set of additional firms in default at the end of the simulation indicates the amplitude of contagion. In this case, contagion is seen as the consequence of the shock as a whole. This stands in contrast to other interpretations: contagion for instance, can be also understood as the portion of the market reaction 'in excess' to what is expected in normal market conditions, like in Hesse, Salman, Schmieder (2014). We already mentioned that Eisenberg, Noe (2001) does not allow for any contagion stemming from market sentiment since the input is made of information taken at the balance-sheet level exclusively. And as result, Anand, Kartike et al. (2014) considers that the Eisenberg-Noe methodology is 'internally inconsistent': in determining the system's loss given default (LGD) endogenously, the Eisenberg-Noe framework assumes that all assets can be liquidated at book value to meet the liabilities of defaulting banks. The authors also note: "the more contagion, the less tenable this assumption becomes". This remark brings to light the fact that factors external to the Eisenberg-Noe framework can exacerbate the deterioration within the network and this dimension of contagion is disregarded in Eisenberg, Noe (2001). In order to address this issue, Anand, Kartike et al. (2014) include an additional criterion that reflects the missing shortfall imposed on asset valuations at default times. More sophisticated approaches, also based on the Eisenberg-Noe network, have explored other ways to address this limitation. Acemoglu, Daron et al. (2014) in particular proposes to revise the definition of the shock: they design it as a failure in investment returns, characterised by its probability to happen. This enables the authors to track the dynamics of the market reaction as the shock becomes more and more stringent. Contagion is then estimated as the gradual acceleration of the deterioration incurred by extreme scenarios. Essentially, the authors identify a threshold from which contagion is seen as emerging. This adds to the initial conclusions of Eisenberg, Noe (2001). From a more general point of view, Darolles, Gagliardini, Gourieroux (2014) identifies some requirements a stress test model has to fulfil in order to differentiate the effects of a common shock, from contagion itself: "(i) the model has to include lagged endogenous variables to represent the propagation mechanism of contagion, (ii) the specification has to allow for two different sets of factors, namely common factors (or systemic factors) representing un-diversifiable risk, and idiosyncratic factors representing diversifiable risks". Finally, Darolles, Gagliardini, Gourieroux (2014) note that when the observable variables are not exogenous at all, the estimated contagion matrix (that captures the dependencies) is biased. As a consequence it is necessary to estimate not just the market reaction to the shock but also the dynamics of 'the common factors' in order to predict future risks. **This has become a requirement in modern financial regulations as to capture uncertainties on the sources of risk correlation.**

As Acemoglu, Daron et al. (2014) argues, the satellite model has to indicate how financial distress translates into price deterioration; and this requires appropriate assumptions. The literature highlights various types of satellite models based on different interpretations of the channels of contagion. Assuming an Eisenberg-Noe type network for instance, Anand, Kartike et al. (2014) questions the relevance of the original 'maximum entropy' (ME) - developed in Eisenberg L., Noe T.

(2001) - for stress testing purposes. Some evidence in particular shows that the ME tends to underestimate contagion, and as a consequence the authors develop an alternative approach, the 'minimum density' (MD). MD relies upon the rationale that interbank linkages are costly to add and maintain. The procedure determines therefore a pattern of linkages which is efficient in the sense of minimizing the costs, hence differentiating itself from the 'maximum entropy' approach where the number of interbank connections are maximised. As it looks credible that banks will tend to reduce their costs in periods of stress, the 'minimum density' assumes a contraction of interbank linkages in the sense of a cost reduction. This helps apprehend the sudden change of behaviour that is supposed to operate in financial institutions on mounting risk aversion. Models dedicated to the exploration of contagion may also investigate the question of 'hidden' dependencies within the financial system. Statistical estimators are powerful tools in this context. Empirical estimators of linear correlations like the Panel approach in Hesse, Salman, Schmieder (2014) or measures of 'cross market correlations' in Darolles, Gagliardini, Gourieroux (2014) are meant to reflect the strength of interconnections between financial assets. Those estimators may offer interesting insight on how asset prices are 'theoretically' supposed to evolve when financial distress is on the rise, but one needs to keep in mind that the correlation structure is largely affected when contagion is fierce. Non-linear procedures are usually more adequate than empirical estimators to capture this modification of the correlation structure. Hesse, Salman, Schmieder (2014) for instance implements a DCC GARCH model which captures the heteroskedasticity in the data, and provides a time-varying correlation parameter. This model helps the authors identify country-specific co-movements. This is an interesting approach to identify how much contagion is supposed to emerge from each European country separately. In the same vein, Kok (2013) introduce DSGE, GVAR and CCA-GVAR models as particularly adequate methodologies to model contagion from a regulatory point of view. In particular the fact that correlations are calculated only during periods of financial distress helps distinguish the excess market reaction due to the pure contagion effect, from the expected reaction in normal times. The quantitative approach may also involve statistical tests, like the Chow test in Darolles, Gagliardini, Gourieroux (2014). This estimator gives a range for the expected contagion (upper and lower bounds), while it also offers a view on the statistical robustness of contagion estimators. We already mentioned that models based on the Eisenberg-Noe framework explore the propagation of risks until equilibrium is reached. From an algorithmic point of view, this requires implementing an iterative algorithm, which necessarily has to converge towards a unique solution. Eisenberg L., Noe T. (2001) in fact gives evidence of the existence and uniqueness of the solution, and this comforts the relevance of their 'fictitious default algorithm'. In statistical models involving an econometric exploration of systemic risk, results in contrast are obtained after just a one-off call of the routine. **In sum, the higher computational burden ensuing from the more quantitative approach does not necessarily imply longer calculation times.** From an empirical point of view, contagion can also be estimated as the overreaction of the market compared to a benchmark. In Hesse, Salman, Schmieder (2014) for instance, risk aversion is described by two variables: the level of high-yield credit spreads and the VIX index. Both indices are seen as a benchmark of credit risk and volatility that are supposed to illustrate ongoing financial distress. In the end, the gap between the observed market reaction and risk aversion benchmarks highlights contagion at work.

One can also stick to the basic definition of financial contagion, ie. an overreaction of the financial system due magnified financial linkages. Acemoglu, Daron et al. (2014) for instance, investigate two specific questions: ***"First, to what extent is the default of a given entity more likely when contagion is emanating from other nodes in the framework, in comparison to a direct shock on its own assets***

from sources outside of the financial system, like households and nonfinancial firms? And secondly, how much does the network increase the probability and magnitude of losses compared to a situation where there are no connections?" Considering interbank connections as the main source of contagion (like Eisenberg-Noe), Acemoglu, Daron et al. (2014) undertakes stress tests on two separate networks. First they compute the probability that a default at a given node (ex-ante) causes defaults at other nodes via risk propagation throughout the network (ex-post). Then they compare this with the probability that all these nodes default because of a direct shock on their 'outside' assets with no network transmission. The authors finally derive a general formula highlighting that contagion is weak when the latter probability is larger than the former. One will note that this approach to modelling contagion is quite different from the foundational work of Eisenberg, Noe (2001). And Acemoglu, Daron et al. (2014) dips further into the characteristics of the spillover effect, and differentiates two main regimes. First they argue that systemic risk can be decomposed into two components: (i) first the probability that a given set of nodes D effectively defaults, and (ii) the loss in value conditional on D - D being the default set. This decomposition emphasizes two main dimensions: **pure contagion and amplification**. **Pure contagion occurs when defaults at some nodes trigger defaults by other nodes through a domino effect. Amplification occurs when contagion stops but the losses among defaulting nodes keep escalating because of their indebtedness to one another**. The first effect is identified as a "widening" of the crisis, while the second fact refers to a "deepening" of the crisis. In Acemoglu, Daron et al. (2014), the original way to describe the dynamics of contagion is also improved by the addition of novel parameters like bankruptcy costs and the loss of confidence in financial market. This comprehensive understanding of contagion finally delivers new formulations for the probability that the spillover effect leads to the default of a given node. It also widens the scope of mathematical exploration of the contagion mechanism.

Stress test results

Stress tests models largely differ from one another when it comes to understanding the 'results'. First, a lot of models seek to identify and then distinguish local losses in a given entity, from broader implications on the whole financial system (ie. LGD). Those models are usually based on the Eisenberg-Noe framework, which is seen as a relatively convenient approach to reach these two goals. This is in particular because the specific network of Eisenberg-Noe makes it possible to track how missing payments from the set of defaulting firms translate into a loss on the balance sheet of other entities. The foundational approach in Eisenberg, Noe (2001) however remains very general on how to calculate losses at the balance sheet level. Interestingly, this flexibility has largely contributed to the success of their approach as it has encouraged a profusion of interesting variations to the initial model in the literature. From a regulatory perspective in comparison, ECB (2013) provides meaningful insight on the estimation of the LGD. The post-shock P&L at the balance-sheet level is broken down into four sub-components: **net income, loan losses and impairment, market risks and the final profit and loss calculation**. The net interest income module focuses on loans, deposits and wholesale funding as sources of income, out of which expenses are subtracted. Then the calculation of loan losses and impairment combines conditional projections of country-level credit risk with bank-specific balance sheet evolutions; while the market risk module seeks to assess any profit and loss impact from the investment portfolios of participating institutions. In practice, a specific haircut is applied on the valuation of securities held on the trading book. In the final module, net interest income, loan loss impairments and the market risk impact for each entity are merged with other income components. In a similar approach, Schmieder et al. (2012) gives extensive details on the

effective capital requirements resulting from each scenario. Assuming a 'substantial spillover stress regime', one sees for instance that a shock of $200bp$ (type 2b) on peripheral sovereign spreads will imply $\$4bn$ capital needs in the European banking system (Graph 99). This amount sharply increases on a scenario that simulates $300bp$ spread widening (type 2c) with capital requirements mounting to $\$21bn$. Considering similar levels of financial distress, liquidity stress tests indicate that 0.25% of the liquidity requirement amounts to 0.25% of the assets in the scenario 2b) while these requirements rise to 1% in a scenario-type 2c) (Graph 100). Considering both solvency and liquidity shocks, mild scenarios with lower intensity than in 2b) induce very limited losses. This, combined with the sharp increase in the deterioration between the scenarios 2b) and 2c), illustrate the non-linear aspect of contagion. Anand, Kartike et al. (2014) also provides practical results on the effect of contagion. Not surprisingly, larger LGD leads to a greater number of defaults, with also more harmful implications on the ex-post value of assets affected by the shock, and greater deadweight loss. Considering the German banking sector, results in Anand, Kartike et al. (2014) suggest that about just one bank would default (on average) as a result of the failure of an arbitrary single bank, and this rises to 2 to 3 banks in default when LGD exceed a few percent (Graph 101). In contrast to this 'still reasonable' situation, the worst case scenario engenders more than 1200 contagious defaults, in the end accounting for 70% of the whole banking sector. Interestingly, the number of banks failing because of pure contagion amounts to 500 banks on average for high LGDs. This time again, the authors try to gauge the cascade effect led by risk propagation, and they note that the severity of contagion jumps significantly when LGD exceeds 40%. This is in line with observations in Upper and Worm (2004). While these approaches to systemic risk, largely based on the Eisenberg-Noe framework, offer a thorough picture of the expected losses and capital requirements, they usually do not explore the trajectory of the deterioration at the balance sheet level when the shock becomes more and more intense. Other approaches – that we review below - provide a more granular understanding of contagion.

Graph 99. Outcome of solvency stress tests

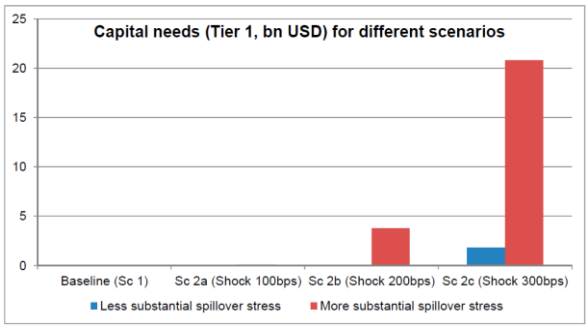

Source: Schmieder et al. (2012)

Graph 100. Outcome of liquidity tests in terms of assets

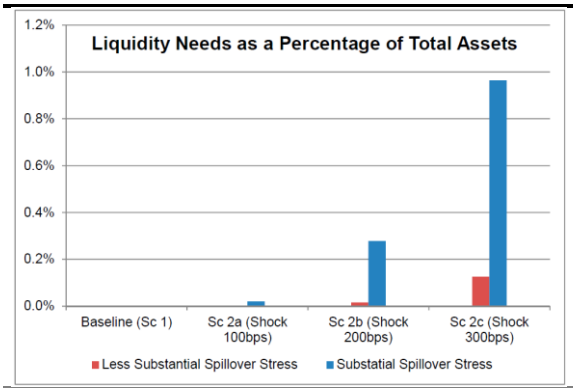

Source: Schmieder et al. (2012)

Graph 101. Results of the first stress test using the sequential default algorithm

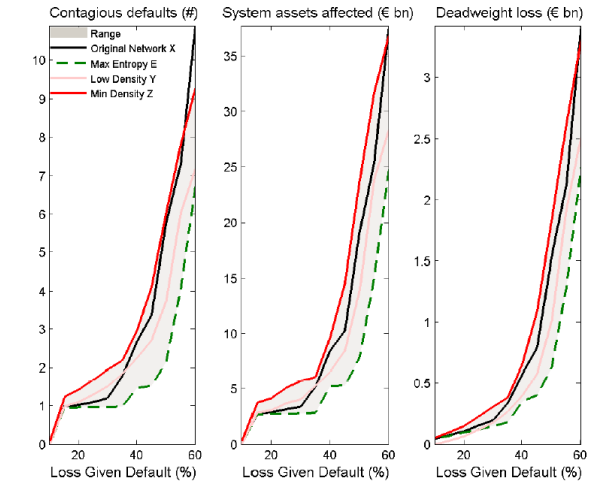

Source: Anand, Kartike et al. (2014)

Graph 102. Liability value as a function of asset level in the presence of bankruptcy costs and credit quality (Fig 3 p12)

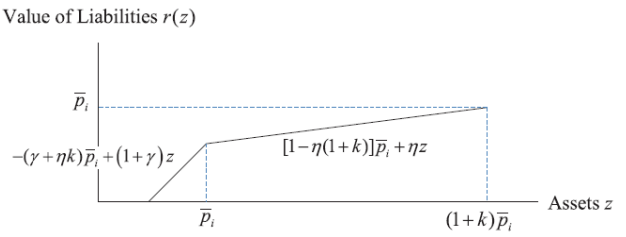

Source: Glasserman, Paul and Young, Peyton (2013)

Analyses like Hesse, Salman, Schmieder (2014), Acemoglu, Daron et al. (2014), Glasserman, Paul and Young, Peyton (2013) offer a higher-level of granularity in the observed contagion than models based on the Eisenberg-Noe framework. The refined understanding of contagion this time, makes the drawing of recommendations on how to strengthen the network against the spillover effect more convenient. Glasserman, Paul and Young, Peyton (2013) for instance explores the relevance of several factors seen as potential catalysts for higher contagion. First the authors reassess the well admitted role of fire sales and the drying up liquidity as influential drivers of contagion. They also evaluate the negative impact of **bankruptcy costs** and **losses of confidence** on the resilience of the network. Bankruptcy costs are seen as having two main implications: they increase both the total shortfall and the 'node depth', ie. the degree of risk amplification on each entity. Interestingly, the dynamics of the shortfall led by bankruptcy costs highlights that the amplitude of the losses is dependent on how quickly systemic risk dissipates in the network: bankruptcy tends to be more and more stringent as the quality of the financial system deteriorates. Finally, Glasserman, Paul and Young, Peyton (2013) demonstrate that 'losses of confidence' is a meaningful driver of contagion too, which is in practice ignored in models like Eisenberg,Noe (2001). While bankruptcy costs refer to the acceleration of contagion once a failure is detected, the 'losses of confidence' coefficient is a descriptor of the contagion operating before default is certified. This distinction is valuable because uncertainties in anticipation of a default may be more harmful than default itself once it is agreed and implemented. Hesse, Salman, Schmieder (2014) also shows that contagion is more or less pronounced depending on the features of the emanating sovereign. In particular the authors show that a 1% shock on Euro peripheral spreads translates into a 0.5 percentage point increase in the risk premium of the 35 countries in most cases; but not for Spain and Italy whereby a shock of this amplitude leads to one full percentage point increase in risk premiums. Looking at the drivers of contagion, it appears that global risk aversion at the time of the shock, the size of the peripheral country (ie. GDP), and the slope of the US yield curve, are meaningful descriptors of systemic risk in periods of crisis. From a statistical point of view, the DCC GARCH model in Hesse, Salman, Schmieder (2014) indicates that the correlation between peripheral countries and Austria, Belgium, France, or the Netherlands was as high as $0.7 - 0.8$ during periods of tough risk aversion. In contrast, the same correlation between non-core countries and Germany or the UK was much lower and oscillates

between 0 and 0.2. Eisenberg, Noe (2001) also takes a look at the empirical drivers of contagion, emphasizing for instance that a larger volatility favours a greater deterioration of the financial system in place. Our analysis largely focuses on volatility, and we explore how the acceleration of the risk propagation takes place in regimes of higher volatility. An interesting approach in Acemoglu, Daron et al. (2014) considers that the behaviour of banks is a notable driver of contagion. The authors in particular note that banks are prompt to 'overlend' in equilibrium, thus creating channels over which shocks on individual entities will systemically cause financial contagion over the entire network. Acemoglu, Daron et al. (2014) also emphasizes that some banks may not sufficiently diversify their lending among the set of potential borrowers, and this creates new channels for the emergence of systemic risk.

Focusing now on the more quantitative approaches, a recurring observation is the 'non-linear' aspect of contagion. And while this dimension is frequently mentioned, only a few papers seek to quantify the cascade effect in financial losses. Hesse, Salman, Schmieder (2014) for instance mentions the 'exponential' surge in capital and liquidity requirements as the severity of the scenario increases, but there is in effect no particular exploration of how this increase is meant to materialise, e.g. as a function of the amplitude of the shock. An analytical formulation of that kind would probably be useful to apprehend financial contagion more effectively, and to improve the forecasting capability of stress testing procedures. Eisenberg, Noe (2001) for instance demonstrates that the clearing payment vector is a multidimensional concave function of both operating cash flows and the level of nominal payments, while the value of equity is generally a convex expression of operating cash flows. This already offers some insight in terms of how the behaviour of contagion can be quantified. Other approaches offer more details on the relationship between the magnitude of the spillover effects and the value of the underlying parameters. In Glasserman, Paul and Young, Peyton (2013) for instance, every recognised driver of contagion in the paper is expressed via an adequate analytical formulation of the resulting losses. The impact of bankruptcy costs, as an example, is estimated as a continuous function of the 'size' of the assets (as per Graph 102). Glasserman, Nouri (2012) involves another statistical framework that delivers a detailed view of the expected reaction in the network in the aftermath of the shock. In particular, the model describes how, for a given firm, the yield spread on the senior tranche of the debt is supposed to evolve as a function of the volatility: as Graph 103 indicates, the dynamics of the spread widening is almost linear. In a similar fashion, the model explores the dynamics of the coupon rate of convertible debt under different conditions of volatility. The authors also examine the dynamics of the reaction function in the network as time goes by, and in particular the amount of expected contingent capital converted to equity on a 2-year horizon, and so for different values of capital ratios and asset volatility. Results show a consistent and logarithmic-like increase of contingent capital, which overall reflects the huge amount to convert during the first six months following the shock. Darolles, Gagliardini, Gourieroux (2014) also analyses the dynamics of the liquidation risk in the hedge fund industry. For each management style, the model delivers an estimated term structure of liquidations assuming a funding liquidity shock. Overall, results indicate that the effect of the shock is fading relatively quickly, and disappears after 12 months on average (Graph 104). An interesting observation is that Long-Short equity hedge funds are hit by shocks more immediately than other management style like Fixed Income funds, for which there is a temporal lag between the shock and the perceived implications. The analysis also explores the channels of contagion, and suggests that contagion operates along the following directions: **Multi Strategy → Equity Market Neutral → Event Driven → Fixed income Arbitrage → Emerging Markets** (Graph 105). Interestingly too, there is little evidence

that contagion could occur in the reverse direction. The Long-Short equity management style is the most represented management style in the dataset in terms of number of funds and total asset under management. But the lack of central role of Long-Short equity hedge funds in the contagion scheme confirms the idea that **systemic relevance is not necessarily associated with size.**

Graph 103. Sensitivity of senior debt to volatility and minimum capital ratio alpha in the absence of convertible debt

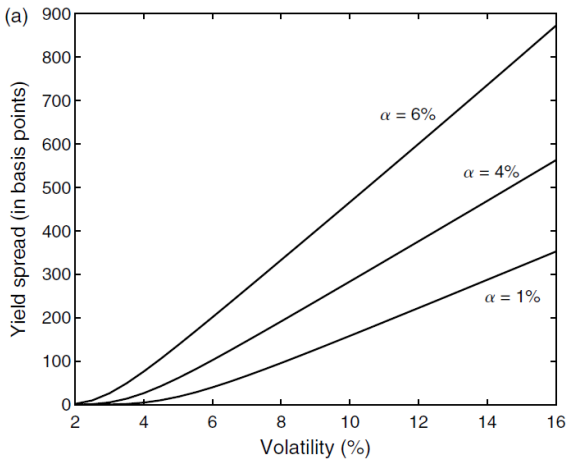

Source: Glasserman, Nouri (2012)

Graph 104. Term structure of expected liquidation counts when stressing the current factor value (Figure 12)

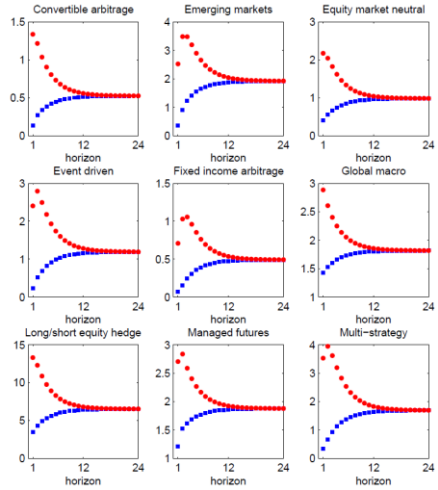

Source: Darolles, Gagliardini, Gourieroux (2014)

Let us now explore the purposes of stress tests. The available literature as a whole is obviously an attempt to develop stress testing tools further, in one way or another. On one side for instance, many papers seek to contribute to the methodological aspect of stress testing. These papers usually emphasize the relevance of novel procedures or new ways to quantify systemic risk and therefore they are explicitly 'research-oriented'. And while this approach proves very interesting from an academic point of view, in many cases it also ignores the prudential dimension naturally attached to stress tests. In this paragraph, we first focus on 'research-oriented' papers, then we review analyses that provide an insightful reflection on the macro-prudential vocation of stress testing. 'Research-oriented' papers usually put a bigger emphasis on showing the coherence of the approach, rather than specifying what a large-scale industrialisation of the proposed methodology would require in terms of resources. As a result, 'research-oriented' analyses can afford exploring stress tests from a more theoretical point of view. This usually leads to very general and relevant observations about the contagion mechanism and the magnitude of systemic risk under tough risk aversion. Hesse, Salman, Schmieder (2014) for instance explores capital requirements and asset liquidity shortfalls, by comparing the amplitude of financial losses in different kind of scenarios. A caveat though, is the very limited granularity of the results, with for instance little differentiation in terms of which financial entity might be the more exposed or resilient to financial distress. Instead, the authors focus on illustrating the highly non-linear aspect of contagion; something which is effectively very neat in the results. In a similar fashion, Anand, Kartik et al. (2014) seeks to demonstrate the relevance of the minimum density (MD) as a new way to model risk propagation. Arguably, MD helps address some limitations of the more common maximum entropy (ME); this is the major benefit of the methodology. Acemoglu, Daron et al. (2014) also shows some innovation, but at the level of the network itself and the interpretation of the drivers of systemic risk. Among other things, the analysis

introduces new descriptive variables to the initial Eisenberg-Noe framework, like the 'contingency covenant' which is supposed to replicate counterparty risk in liquidity funding. This variable makes possible to stress liquidity conditions as an isolated dimension of the network, with the results ultimately reflecting its propensity to generate contagion.

Graph 105. The contagion scheme for the model with contagion and frailty (Fig 8 p51)

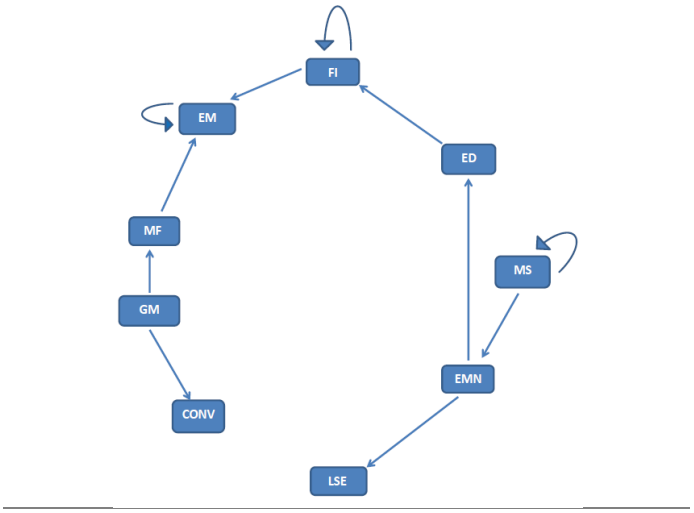

Source: Darolles, Gagliardini, Gourieroux (2014)

Acemoglu, Daron et al. (2014) also presents 'overlending' and 'the lack of diversification' in lending as meaningful drivers of contagion. This helps the authors differentiating themselves from the rest of the literature that usually does not explicitly distinguish these two dimensions of risk propagation. In a similar attempt to improve an already existing framework, Glasserman, Paul and Young, Peyton (2013) estimates the relative likelihood that a given node will cause other nodes to fail because of contagion. The calculation involves three variables: the net worth of the node, the outside leverage (ratio of a node's asset outside the network over net worth) and the financial connectivity (bilateral connections). Glasserman, Paul and Young, Peyton (2013) offers a relevant sophistication of the quantitative approach of Eisenberg, Noe (2001), and the authors compute a contagion index that illustrates the soundness of the financial system via a set of default probabilities. In contrast, the foundational approach in Eisenberg, Noe (2001) delivers only a bilateral outcome with 'default' or 'non-default'.

Aside from 'research-oriented' papers that concentrate innovation at the level of the methodology and the stress test theory, another category of analyses put a particular emphasis on the micro-or macro-prudential vocation of stress test models. Hirtle, Lehnert (2014) for instance highlights the role of stress tests in recent years as a supervisory tool, with an emphasis on how the methodology was chosen in light of the prudential dimension of the program. A coordinated supervisory stress test programme on large bank holding companies was first launched in the United States in February 2009, during a period of extreme stress in the US banking industry, following the collapse of Lehman Brothers. The Supervisory Capital Assessment Program (SCAP) involved stress tests of the 19 largest US-owned bank holding companies (Board of Governors of the Federal Reserve System (2009a)), representing about two thirds of the assets of the US banking system. The goal of the SCAP was to ensure that the largest US bank holding companies had sufficient capital to withstand a worse-than-

anticipated macroeconomic outcome and continue to lend. By requiring large bank holding companies to build a buffer of capital, presumably big enough to withstand potential stressed losses, the SCAP was intended to reduce uncertainty and promote confidence in individual banking companies and in the banking system (Board of Governors of the Federal Reserve System (2009b)). This proved very efficient for the SCAP to fulfil its prudential at both micro and macro levels (see Hirtle, Schuermann, Stiroh (2009)). By allowing for a macroeconomic understanding of the financial system, the procedure largely widens the universe of potential drivers of systemic risk. Regulatory stress tests, on that basis, have brought noticeable innovation in the way stress tests are conducted. On top of that, the high degree of granularity in the results this time offers a comprehensive illustration of the intrinsic exposure of each participating bank to systemic risks. We also note that the results of regulatory stress tests are generally made public, in contrast to micro-prudential assessments like the reports published by rating agencies (not available for free). Those two features give regulatory stress tests greater credibility, and this largely justifies the sizeable impact they have on the reputation of banks. Another benefit of the macro-prudential dimension, is that it helps avoid too stringent micro-prudential recommendations during periods that followed a crisis. In a context of muted growth and reasonably contained systemic risk, the macro-prudential supervision may want to bolster investment by increasing the amount of liquidity made available to banks (via e.g. TLTRO, QE or accommodative policies in general). In contrast, such a context may be too uncertain from a purely micro-prudential point of view, thus encouraging banks to tighten lending conditions (Angeloni (2015)). Assessing the soundness of the financial system via macro-prudential stress tests should thus help detect situations where too tight micro-prudential supervision can become a drag for the economy. Looking at the outcome of regulatory stress tests, the SCAP delivered an aggregate capital shortfall for the 19 participating companies of $\$185bn$. After taking into account asset sales and the restructuring of capital instruments, the net shortfall was $\$75bn$, largely concentrated on 10 entities out of the 19. Stress testing at the supervisory level has also become more authoritative in Europe as well: The European Banking Authority (EBA) conducted a series of stress tests[10] in 2008, 2009, 2010, 2011, 2014, 2016 (EBA (2014), EBA (2015), EBA (2016)). The relevance of this procedure to identify underlying weaknesses in the financial system is largely recognised and helps stress tests become increasingly integrated into the ongoing supervision of banks. For this purpose, the comprehensive capital analysis and review (CCAR) and the Dodd-Franck act stress testing (DFAST) were introduced in the US in 2011 and 2013. Hirtle, Lehnert (2014) gives extensive details on the purposes of each programme. CCAR is particularly innovative as the underlying quantitative model seeks to achieve a tilt from 'discretion' towards 'rules': institutions that see stressed capital ratios falling below the regulatory minimum levels face objection to their capital plans and specific constrains in their ability to distribute capital to shareholders. The public disclosure of the results reinforces the credibility of these 'rules'. The major benefits of implementing regulatory stress tests are largely developed in Hirtle, Lehnert (2014): they contribute to strengthen the credibility of the supervisory authority, and they support better transparency and market discipline. In a fair way, Hirtle, Lehnert (2014) also explores the potential risks attached to the exercise of macro-prudential stress tests. First, the authors identify a risk of 'model monoculture' that could encourage too much uniformity in the understanding of systemic risk. In this case, all the banks have a tendency to show the same interpretation of the risks attached to each asset class, and this interpretation might be biased from actual risks. Secondly, the ranking of the banks, as indicated by stress test results, may

[10] http://www.eba.europa.eu/risk-analysis-and-data/eu-wide-stress-testing

also be a source of heightened contagion as it induces a 'hierarchy' in the network. This may strengthen interbank dependencies, causing an amplification of contagion should one of the 'best' banks collapse. This mostly justifies the introduction of a tougher regulation for systemically important financial institutions via the Dodd-Frank act in the US (Wan (2016)). In the end, 'regulatory-based' analyses usually offer a discussion on the macro-prudential purpose of stress testing, while addressing interrogations surrounding the implementation and the manipulation of the chosen methodology. This focus on the practicality of the procedure is in sharp contrast with 'research-oriented' models.

Risk management-oriented stress test is another category of models largely represented in the available literature. By and large, a common approach is the exploration of the VaR (Value at Risk) as a meaningful indicator of the maximum loss on a particular time horizon and for specific levels of confidence (like in Hirtle, Lehnert (2014)). Although modern regulations like Basel accords provide rules to calculate market capital risk, internal risk managers may want to use their own approach (sometimes more sophisticated) to evaluate the risks attached to investments within the portfolio. For one thing, using its own stress test procedures allows them to simulate a broader range of co-movements in both ex-ante and ex-post volatilities. And for another, an in-house approach to the determination of VaR helps focus on more realistic assumptions about the joint distribution of the portfolio's risk factors (see Alexander (2001)). Since there is a clear evidence that correlations in financial markets are significantly altered by mounting risk aversion, estimating joint dependencies in distressed market conditions is a challenging exercise (Feria Dominguez, Oliver Alfonso (April 2004)). As Aragones and Blanco (2001) show, arbitrarily adjusting the correlation matrix in an attempt to replicate the dynamics under fierce contagion is vain as the resulting correlation matrix is usually no longer definite positive. Hence the need to develop, either models that are naturally able to understand and replicate the dynamics of financial linkages in distressed market conditions, or models that prove able to capture the behaviour of the dependencies 'as a whole', like methodologies involving heavy-tailed probability distribution functions. In the end, the resulting picture of potential losses emphasizes the resilience/exposure of each asset to shocks. Aside from presenting an update view on potential losses, stress tests also offer some guidelines on how to optimise risk-diversification during periods of risk-averse market conditions. In this case, portfolio managers will be prompt to underweight these securities that look excessively exposed to systemic risk, decreasing thereby the general exposure of the portfolio. Risk management-oriented stress tests can also unveil temporary or persistent discrepancy in market valuations, in particular on securities that are supposed to reflect the credit robustness of the underlying entity. This time again, an appropriate rebalancing of the portfolio should help take advantage of these market discrepancies either on the side of increased speculation (ie. being positioned as to benefit from a normalisation of these valuations) or on the side of prudence (ie. underweighting the concerned securities in order to avoid the larger volatility induced by a normalisation of the valuations). Koziol et al. (2015), Angeloni (2016) give additional insight on stress testing procedures from a risk management standpoint.

In conclusion, the literature review has unveiled numerous aspects of the usual approaches to stress testing. In this paper we explore a few angles that prove very relevant in the context of sovereign risk exploration. For this purpose, we set up a network composed of pair-wise connections between the involved sovereign entities. The network in particular assumes that there is a unique epicentre of

contagion, ie. only one recognised source of financial distress in each simulation. Our model involves market-based information exclusively, namely daily price variations of both sovereign CDS spreads and sovereign asset swap spreads (Aussenegg, Götz, Jelic (2012)). Stress tests, in this report, are designed according to the methodology of VaR calculations, that we consider in the context of the model calibrated in Chapter 1. Our shock scenario assumes the materialization of an extreme price variation, like a sudden rise in CDS prices or a sharp spread widening in asset swap spreads. The assumed price variation is characterized by two criteria: either by the amplitude of the variation in absolute value, ie. expressed in basis points; or by the probability that the shock materialises (e.g. $5\%, 2\%, 1\%$). Then we identify implications at both uni-and multivariate levels by exploring a gradual panel of severity, and varying degrees of volatility. We also define an estimator of the univariate frailty. In some aspects, our interpretation of the frailty is comparable to Darolles, Gagliardini, Gourieroux (2014). While univariate stress tests help us understand the dynamics of the frailty on each sovereign, the multivariate approach delivers a comprehensive view on how contagion is seen as propagating throughout the sample. In the end, we draw some recommendations on how to maximise risk diversification in sovereign investments. In the subsequent part of the report, we also explore some practical implementations of these recommendations in portfolio optimisation procedures. First we review the effectiveness of recognised approaches as to mitigate the portfolio's exposure to systemic risk (e.g. Minimum Variance, Equal Risk Contribution, Maximum Diversification portfolios). Then, we design a new methodology which delivers outstanding results as to restrain the portfolio exposure while not conceding too much on total returns.

Deriving the probability of default out of CDS prices

Fixed Income vanilla products - like bonds - usually involve some risk of default, because the bond issuer may become insolvent in a future date. In this case he will be unable to repay its debt, thus causing a credit event.

In effect, most of credit events are "partial defaults": there is a persistent portion of the debt that is still 'alive' after the restructuring. This is in opposition to "total defaults" where the full outstanding of the debt is erased. In partial defaults, the **risk neutral recovery rate** characterizes the portion of debt that is remaining. While advanced models explore the dynamics of time varying recovery rates (Jeanblanc et al. (2006), Altman, Resti, Sironi (2003)), **the recovery rate is usually regarded as a fixed parameter.** As Edwards (2015) shows, the average haircut on sovereign debt over the period 1978 to 2010 was around 37%. The recovery rate plays a minor role in our analysis, so we adopt a relatively simple approach and we consider $\rho = 40\%$ as an acceptable value. In this case, the default is effective on 60% of the total debt outstanding.

Bond holders, on a default, will obviously bear a significant loss on the face value of the bond. When this risk turns to be more palpable, investors may want to hedge themselves via appropriate protections, like Credit Derivatives Swaps (CDS). A CDS is a contract providing insurance against a credit event. These contracts bind the protection buyer and the protection seller to transfer the credit risk of an asset without the actual transfer of the asset.

CDS have a lot in common with regular insurance contracts: the buyer must make regular payments to the seller until the end of the contract period, at least until no default materializes. This premium, paid in exchange for protection, is expressed in terms of "spread": this is the CDS spread.

If a default occurs, the buyer not longer has to pay the CDS premium, though he has to pay the accrued premium effective at this time. Both parties then proceed to the settlement of the swap, either physically or in cash. If the contract requires a physical delivery, the CDS buyer delivers the bond to the seller in exchange for its par value. When a cash settlement is required, the mid market price P of the bond some specified days after the credit event is used as a reference. The seller eventually provides the buyer $(100 - P)\%$ of the notional principal.

As an insurance against a potential default, the value of the CDS spread has to reflect the default probability of the underlying entity, which means evaluating the risk that a credit event will materialize during the life T of the contract. Logic dictates that the risk of default rises along with the time horizon T; as a result the CDS spread is larger for contracts with a longer maturity T. This characterisation of the CDS spread as a function of the time horizon T defines the whole term structure of the CDS curve. The literature reports two main approaches to estimate the probability of default from a very general perspective (Delianedis, Geske (1999); Derbali, Hallara (2013); Schaefer (2012); Hull, Predescu, White (2005)): **structural models and intensity models**.

Structural models first (Derbali, Hallara (2013)), assume that default is always consecutive to a sharp deterioration of the fundamental picture. Default in this case is effective when the deterioration on a basket of relevant fundamental variables exceeds some predefined thresholds. In this approach, the likelihood of a default is computed out of fundamental indicators, like the debt outstanding, the equity ratio for corporate, or some macroeconomic variables (GDP growth, inflation, current account). When these indicators experience a notable decline and move excessively, beyond some

pre-specified limits, then the firm is seen as defaulting on its future debt repayment. The first generation of structural models was introduced by Merton Merton (1974) and then, developed by Leland (1994), Leland and Toft (1996), Anderson and Sundaresan (1996) and Jarrow (2011). These models mostly rely upon the "physical" meaning of the debt and the corresponding financial assets, and they usually assume that the firm value follows a geometric Brownian motion. The equity of the firm is then interpreted as a call option on the underlying value with a strike price equal to the face value of the firm's debt maturity. One of the limitations however, is that the framework is able to predict a default only at maturation of the debt. Black and Cox (1976) explore in some ways potential improvements to the methodology. Their updated version takes a time varying barrier into account, and the authors define the default as the first passage time across the barrier. Generally speaking, the probability of default is endogenous in structural models, ie. the likelihood of default is derivable from the price of a stock and balance sheet of a company. A more detailed review of structural models is available in Sundaresan (2013).

On the other hand, intensity based credit risk models characterize defaults as exogenous events (Guillermo (2010), Yi Lan (2011))**.** The model now does not try to capture the reasons that justify a default, but it focuses on the pattern with which a default occurs. In intensity based models, the local implied probability of default over a small time interval is modelled as proportional to the length of the time interval. This gives such models a great deal of analytic tractability. The proportionality factor is known as the hazard rate of default over the infinitesimal time increment. The risk of default in an intensity model is defined via a counting process $N(t)$ which increases by jumps of one unit:

$$\Delta N(s) = N(t+\Delta t) - N(t) \qquad \begin{cases} 1 & if\ one\ event\ arrives\ in\ [t, t+\Delta t] \\ 0 & if\ no\ event\ arrives\ in\ [t, t+\Delta t] \end{cases}$$

The default intensity $\lambda(t)$ over the time interval $[t, t+\Delta t]$ is then characterized as the frequency of credit events over this period. This parameter can be modelled through deterministic functions or stochastic terms. In practice, default is usually defined as the first jump of a Poisson process with intensity λ. The default time is therefore distributed according to an exponential law from which we deduce:

- The probability function of the default $f(\tau) = \lambda . \exp(-\lambda\tau)$ with τ: default time
- The default probability over the time interval $[0, t]$: $P(\tau < t) = 1 - \exp(-\lambda\tau)$
- The survival probability over the time interval $[0, t]$: $Q(\tau < t) = \exp(-\lambda\tau)$

Let us now look at the relationship between the CDS spread (of maturity T) and the intensity of default λ. A CDS spread is usually seen as the sum of a risk-free interest rate swap OIS (IRS), plus a risky component relative to the default of the underlying asset.

The duration of a risk free swap OIS with maturity T is:

$$Df^{rf}(t) = \sum_{\{T_i\}} (T_i - T_{i-1}) . Df^{rf}(T_i)$$

With T_i the fixed rate payment dates and Df^{rf} the risk-free discount factor relative to this IRS.

In a simplified model, we can assume a flat swap curve, described by an interest rate r with continuous payments. We therefore obtain:

$$Df^{rf}(t) = \exp(-rt)$$

As previously mentioned, the buyer of the protection has to provide a fixed payment s over the life time of the contract, equal to the CDS spread (Graph 106). This is the fixed leg of the contract, which corresponds to a gain from the point of view of the seller.

On the side of the seller, any payment is conditional to the realization of a default. This leg is known as the floating leg, which represents a loss from the seller's perspective.

Graph 106. Fixed rate payments by the buyer as time goes by

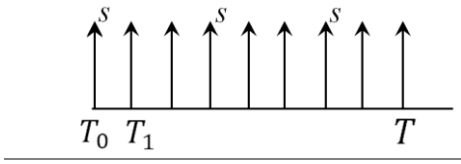

Graph 107. Payment by the seller in case of a default

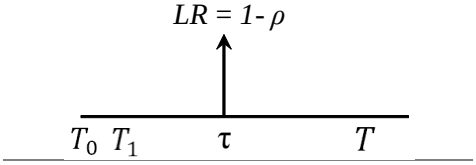

As the fixed payments are interrupted when the contract expires (at maturity or if a default occurs), we can define a "truncated duration" for the CDS spread:

$$D^{min}(t) = \sum_{\{T_i\}} (\min(t, T_i) - \min(t, T_{i-1})).Df^{rf}(\min(t, T_i))$$

Where $Df^{rf}(t)$ is the discount factor of a risk free zero coupon bond of maturity t.

In a no-arbitrage model, the Net Present Value (NPV) of the fixed and floating legs should be the same:

NPV of the fixed leg:

$$NPV_{FIXED} = E_\tau\left(\int_0^T s.Df^{rt}(u).1_{\tau>u}du\right)$$
$$= s.\int_0^T e^{-ru}.E_\tau(1_{\tau>u})du$$
$$= s.\int_0^T e^{-ru}.e^{-\lambda u}du$$
$$= \frac{s}{r+\lambda}\left(1 - e^{-(r+\lambda)T}\right)$$

NPV of the floating leg:

$$NPV_{FLOAT} = E_\tau(e^{-r\tau}.1_{\tau\leq T}.LR)$$
$$= (1-\rho)\int_0^T e^{-ru}\lambda.e^{-\lambda u}du$$
$$= (1-\rho)\frac{\lambda}{r+\lambda}\left(1 - e^{-(r+\lambda)T}\right)$$

In an arbitrage-free world, both legs are supposed to be equal, so we obtain: $s = (1-\rho)\lambda$ (43)

➔ **Eq. (43) shows that the CDS spread s linearly evolves with the default density λ.**

In our analysis, we consider annual default probabilities with constant default intensity λ. For a 5Y CDS spread we thus obtain:

$$P(\tau \leq 1\ year) = 1 - e^{-\lambda} = 1 - e^{-\frac{s}{1-\rho}} \quad (44)$$

Eq. (43) shows that the CDS spread is a linear function of the corresponding default probability. This kind of intensity model suggests that the probability of default is independent of the maturity T of

the contract. While this is a simplification of the actual situation, this approach is sufficiently accurate in the context of our analysis.

➔ **In the next paragraphs, we consider probabilities of default in sovereigns as a starting point for implementing stress tests.**

Considering 5Y and 10Y CDS spreads, we calculate the probabilities of default of European countries based on eq. (44). Graph 108 and Graph 109 show the results; we refer to these series in a later paragraph.

Graph 108. 5Y default probabilities

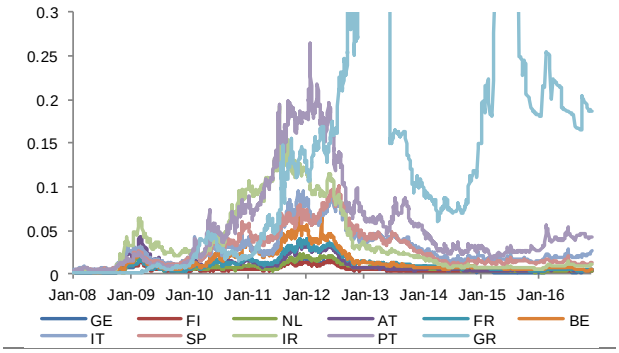

Graph 109. 10Y default probabilities

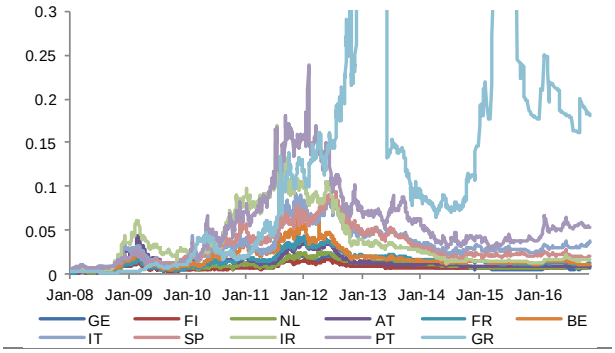

Table 33. Average probability of default over the period 2008-2016

	GE	FI	NL	AT	FR	BE	IT	SP	IR	PT	GR
5Y	0.007	0.006	0.008	0.012	0.013	0.017	0.032	0.033	0.046	0.062	0.117
10Y	0.010	0.008	0.011	0.015	0.016	0.020	0.035	0.035	0.044	0.058	0.107

Implementing stress tests on European asset swap spreads

In Chapter 1, we described the calibration of a probabilistic model that proved a successfully tool to illustrate the univariate and multivariate dynamics of European CDS spreads over the period from 2008 to end-2016. We also designed an un-temporal estimator of the intrinsic volatility $\hat{h}$, from what we established an un-conditional version of the distribution function p of the data. We also calculated some preliminary estimators of the volatility raised by contagion when market sentiment turns sharply risk averse.

As we note in the literature review, stress tests are powerful tools to evaluate the influence of multivariate linkages between financial securities, and to identify their impact during periods marked by tough risk aversion. Calculations in Chapter 2 are largely based on the multivariate model described in Chapter 1, and are mostly inspired by the methodology of stress tests, in particular tests based on the determination of VaR (Value at Risk).

In the following section, we explore the idiosyncratic and joint behaviour of sovereign securities further in-depth. First we look at the impact of a shock from a univariate point of view. We explore in particular the expected surge in intrinsic volatilities that would ensue from financial distress. Then, we investigate the multivariate implications, and we derive an estimate of the price variations that would result from the shocks. **In both cases, we derive an analytical description of the general market dynamics. This makes the manipulation and further extrapolation of these observations particularly straightforward.**

How to define a shock/scenario

We define a shock as a sudden and sharp increase in the CDS spread $s_{i,t}$ between two time increments. On that basis, we see two main approaches as to control the severity of the shock:

First we reason in terms of the effective price variation, in basis points. In this case a shock effectively happens when the price increase in the CDS spread exceeds a pre-defined level (in basis points). The scenario may consist, for instance, of a price variation of 10bp or more. For a given sovereign CDS referring to Country i, we thus define the shock via the magnitude of the price increase S_i:

$$s_{i,t} \geq s_{i,t-1} + S_i \text{ that we can rewrite as } x_{i,t} \geq S_i \text{ based on Chapter 1's notations} \quad (45)$$

In a second approach, stress test scenarios can be defined according to the probability that the shock effectively materialises. In this case the severity of the scenario is controlled by setting this probability to a desired level. We denote by R_i the probability of the shock. **Combining both definitions, R_i illustrates the probability (or the risk) that the price increase S_i exceeds a certain amplitude.**

Based on Chapter 1, R_i can be expressed as a function of S_i via the univariate probability density function p_y of x_i, that involves the un-temporal volatility estimator $\hat{h}\left(\hat{F}(y_i)\right)$:

$$R_i = P(x_i \geq S_i) = \int_{S_i}^{+\infty} p_y(x_i)dx_i = 1 - F_y(S_i)$$

Since the coefficient $\hat{h}$ will play a major role in the following analysis, and because $\hat{h}$ is calculated out of y_i, we rename $p_y(x_i)$ as $p(x_i, \hat{h})$ and $F_y(S_i)$ as $F(S_i, \hat{h})$. In this case we rewrite the expression of R_i as:

$$R_i = P(x_i \geq S_i) = \int_{S_i}^{+\infty} p(x_i, \hat{h}) dx_i = 1 - F(S_i, \hat{h}) \quad (46)$$

Graph 110 and Graph 111 illustrate the relationship between F_i, the probability R_i, and the market reaction S_i for $R_i = 5\%$. In this synthetic example, a shock with a probability of 5% to materialize corresponds to an increase of the CDS price of at least $1.3bp$. Graph 111 describes how R_i relates to the upper 5% tail: the event $S_i \geq 1.3bp$ corresponds to 5% of the distribution in the upper tail.

Because of the shape of the cumulative distribution, the probability R_i and the magnitude S_i move in opposite directions: when S_i increases, the shock is more severe and its probability to happen is therefore smaller. This is visible in Graph 111: $S_i = 2.5bp$ for $R_i = 1\%$, while $S_i = 1.3bp$ at the 5% level.

Based on the same reasoning, a larger probability R_i describes a shock that is more likely to materialize. This is therefore a more indulgent risk scenario, thus characterised by smaller amplitude S_i. In Graph 110 and Graph 111 for instance, a shock of $S_i = 0.7bp$ has a large probability $R_i = 20\%$ to happen.

In terms of volatility this time, assuming that R_i is fixed, a larger volatility $\hat{h}$ would cause an increase of the amplitude S_i. And in contrast, a more contained $\hat{h}$ leads to a contraction of S_i. **Overall, this corroborates the natural understanding that a shock, e.g. designed such that $R_i = 1\%$, will cause bigger variations in CDS prices on the more volatile countries.**

Graph 110. Shock with an amplitude S_i

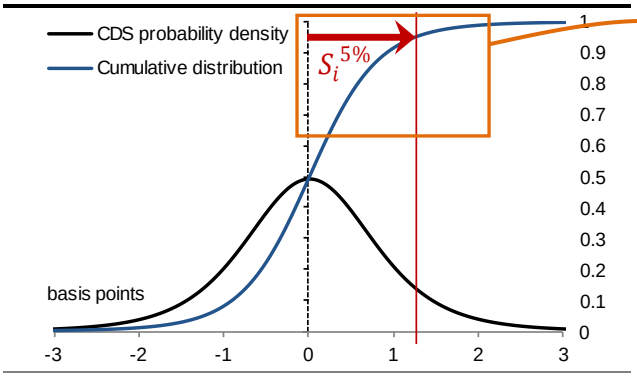

Graph 111. Relationship between S_i and $R_{i,}$

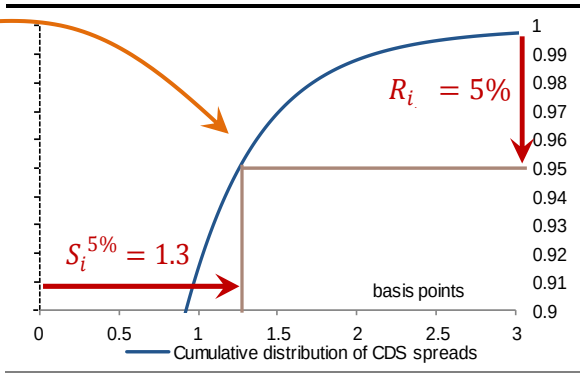

We also derive a temporal version of the shock. We incorporate the temporal and conditional probability distribution function $p(x_{i,t}|x_{i,t-1})$ calibrated in Chapter 1 into the denomination of the shock, as per eq. (47). This new version is a temporal definition, which takes the 'sample path' into account, and involves the GAS volatility estimator σ_t.

$$R_{i,t} = P(x_{i,t} \geq S_{i,t}) = \int_{S_{i,t}}^{+\infty} p(x_{i,t}|x_{i,t-1}) dx_{i,t} \quad (47)$$

As an example with $R_{i,t} = 1\%$, Graph 112 shows the resulting price variation $S_{i,t}$ calculated on the conditional probability distributions p calibrated in Chapter 1.

Graph 112. Amplitude of the 1% Shock on European CDS $S_{i,t}^{1\%}$

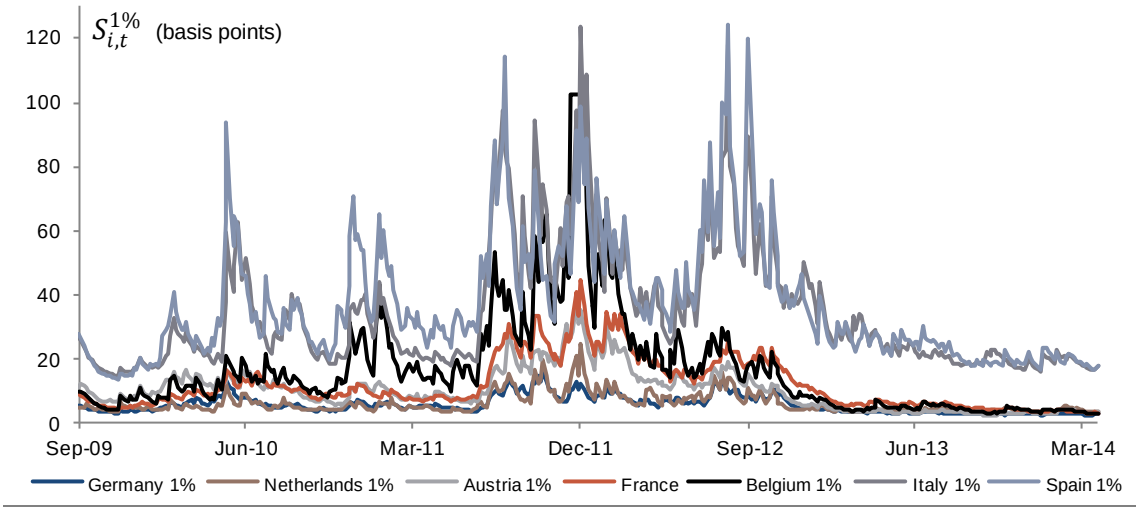

Lucas, Schwaab, Zhang (2012) seek derive the magnitude induced by default probabilities. And to do so, the authors implement VaR-based stress tests, by imposing that $R_{i,t} = P_{i,t}^{Default\ CDS}$.

In our opinion, it is not clear if such a stress test scenario can effectively be comparable to the advent of a proper default. However, we find this connection between the severity of the simulation and the market-implied probability of default very relevant to **approach a situation of a 'worst case scenario'.** In this case, even if the simulation does not lead to a proper default, results should highlight a situation where a credit event is already substantially more likely. ➔ **This approach looks interesting in the context of our analysis given that we seek to understand the dynamics of risk aversion, not only in the vicinity of the default, but also very much upstream, ie. when expectations of a default in the market start to heighten.**

While we are keen to consider the parameterisation of Lucas, Schwaab, Zhang (2012), we note that the proposed methodology (ie. $R_{i,t} = P_{i,t}^{Default\ CDS}$) looks incoherent in certain cases: for instance, if one considers a country with a probability of default set at $P_i^{Default\ CDS} = 0.5$. Then $R_i = 0.5$ leads to $S_i = 0$ if we assume that the distribution is centred (a fair assumption based on Chapter 1). However, $S_i = 0$ means that no variation to CDS prices is required to approach a situation where default is a likely outcome. In sum, country i is already in a state of default by the time we realise the shock. This is incoherent with $P_i^{Default\ CDS} = 0.5$ as we should have $P_i^{Default\ CDS} = 1$ instead. On the other hand, if we consider a country which is effectively in a situation of default by the start of the simulation, we can assume that $P_i^{Default\ CDS} = 1$ and so $R_i = 1$ according to the proposed parameterisation. This finally leads to a market reaction of $S_i = \pm\infty$. This is inconsistent as well given that a default is already priced in by the start of the simulation. As a consequence, $S_i = 0$ is the expected value, instead of $S_i = -\infty$.

In sum, these two examples highlight a contradiction in the formulation of Lucas, Schwaab, Zhang (2012):

- $\{R_i = 0.5 \rightarrow S_i > 0\}$ instead of $\{R_i = 0.5 \rightarrow S_i = 0\}$
- $\{R_i = 1 \rightarrow S_i = 0\}$ instead of $\{R_i = 1 \rightarrow S_i = -\infty\}$

Based on these observations, we propose to modify the initial formulation of the "credit event-like" shock into $R_{i,t} = P_{i,t}^{Default\ CDS}/2$; instead of $R_{i,t} = P_{i,t}^{Default\ CDS}$. This modification is justified by the fact that a deterioration of the credit quality necessarily implies **a rise of the CDS price**. Since a negative variation of the CDS price is not a possible outcome in the aftermath of the shock, the lower half of the distribution (which describes negative price variations) has to be ignored - in other words, $\boldsymbol{P_{i,t}^{Default\ CDS}}$ **has to be seen as conditional on a rise in CDS prices** (ie. conditional on $x_{i,t} \geq 0$). Since $(x_{i,t})$ is centred and symmetric (see Chapter 1), the non-conditional probability of default is therefore $P_{i,t}^{Default\ CDS}/2$.

We also note that the new parameterisation $R_{i,t} = P_{i,t}^{Default\ CDS}/2$ respects the boundary constraints $\{R_i = 1 \rightarrow S_i = 0\}$ and $\{R_i = 0.5 \rightarrow S_i > 0\}$.

While we consider this approach in the following analysis as providing interesting results, we also keep in mind the uncertainties that surround the interpretation of this definition of the shock. In particular, stress tests based on $\boldsymbol{R_{i,t} = P_{i,t}^{Default\ CDS}/2}$ are just partially involved in the whole analysis.

Graph 113. Amplitude of the Shock on European CDS when $R_{i,t} = P_{i,t}^{Default\ CDS}/2$

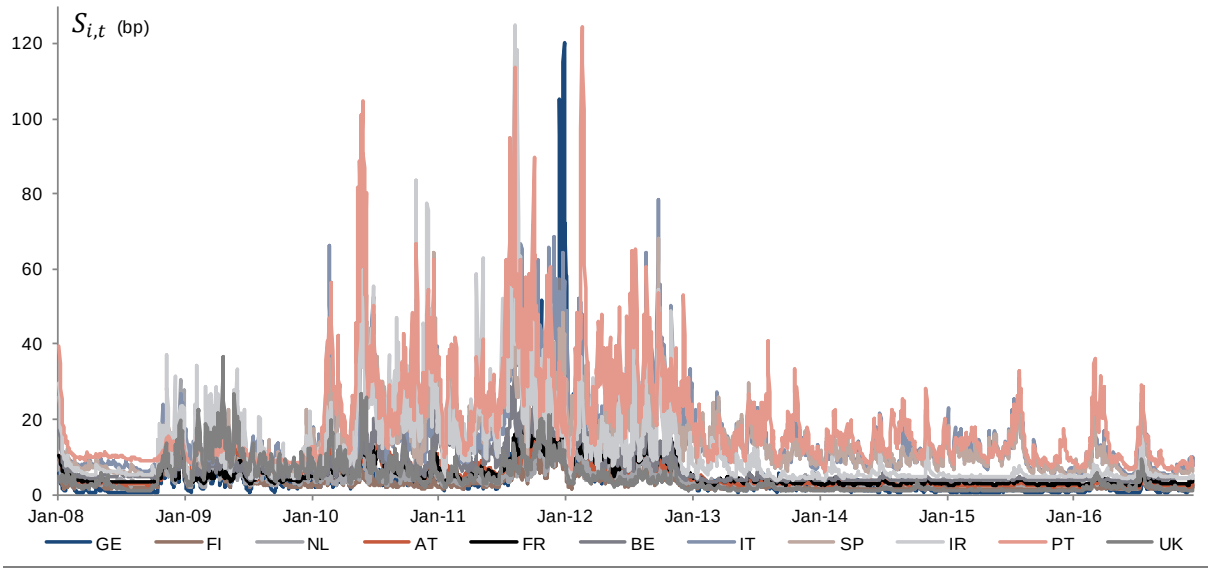

A non-temporal approach to financial contagion

In this section, we explore the market reaction to shocks. Our stress test methodology largely involves the probabilistic model described and calibrated in Chapter 1. We now take a different dataset to what we had in Chapter 1. As they are an interesting (and liquid) proxy for CDS spreads, we prefer exploring sovereign asset swap spreads (10Y maturity, see (Aussenegg, Götz, Jelic (2012))).

Sovereign 10Y asset swap spreads

Asset swap spreads (more conveniently 'ASW') qualifies the return of a position whereby an investor is holding a bond while paying an Interest Rate Swap (here the 'EUR' swap rate), both of the same maturity. An Interest Rate Swap ('IRS') is a contract in which two parties agree to exchange interest rate cash flows for a given period of time (the maturity of the contract), on a fixed-floating basis: the interest rate is fixed on one side of the contract (for instance, one of the participants is entitled to annual payments at a fixed rate of 4.5% like in Graph 114); while the rate remains floating on the other side of the contract (e.g. the other participant is entitled to semi annual payments at the 6-month Euribor rate). The amount effectively exchanged is calculated on the basis of the notional of the trade. In essence, IRS are used as a means to convert fixed payments into floating cash flows. In an environment of rising interest rates in particular, bonds experience a price depreciation ensuing from higher yields. While fast money investors (like Hedge Funds) will take advantage of this bearish environment (on rates) by shorting bonds, institutional investors like pension funds and insurance companies are forced to hold bonds as a means to hedge future liabilities, and therefore they do not have much flexibility. IRS in this context, offer a meaningful hedge against the upward trend in rates: investors paying the fixed-rate leg and receiving the floating-rate leg in particular will experience a gain when the floating interest rate is on the rise (Euribor), as it offers bigger returns compared to the fixed rate (unchanged during the whole life of the contract). In this case investors are said to be 'payers' of the IRS.

Graph 114. Breakdown of cash flows involved in an IRS

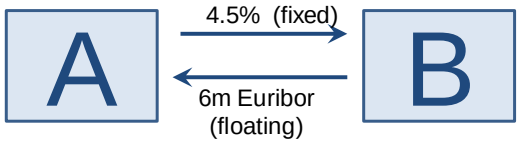

Back to sovereign bonds, an investor may want to pay the IRS as a means to hedge the fact that sovereign rates are expected to rise in the future. The resulting position is said to be an "asset swap" position. The corresponding yield of the position is then described as the asset swap spread (or ASW), which is relatively similar to the spread between the bond yield and the fixed rate of the IRS (Fabozzi (2003), Tuckman (2003), O'Kane (2001)):

$$ASW_i(t) = YTM(10, i, t) - EUR(10, t) \tag{48}$$

Where $YTM(10, i, t)$ is the yield to maturity of the 10Y sovereign bond for a given country i at time t, while $EUR(10, t)$ is the value of the 10Y Euro swap rate (fixed leg).

Since credit risk is a prominent driver of sovereign interest rates when the credit quality deteriorates, the appetite for asset swap positions is relatively correlated to the perception of the credit

worthiness of the entity. **To some extent, asset swap spreads can be seen as a proxy for CDS spreads** (Aussenegg, Götz, Jelic (2012))**.**

A concern however when manipulating ASW, lies in the fact that the sovereign bond under consideration does not have a constant maturity, since the remaining life of the bond decreases as time goes by. In contrast, the swap rate $EUR(10,t)$has constant parameter, of 10 years. This intrinsic difference may induce some inaccuracy in the results, especially for smaller debt issuers that do not replace their benchmarks very often. **In order to address this caveat, we replaced $\boldsymbol{YTM(10,i,t)}$ with the yield to maturity of a constant maturity synthetic 10-year bond.** The pricing of this synthetic bond is deduced from the Nelson-Siegel-Svensson (NSS) model, calibrated on the whole term structure.

The NSS model (eq. (49)) is highly regarded and largely employed in the industry. As eq. (49) shows, the model involves five unknowns: $\{\beta_1,\beta_2,\beta_3,\lambda_1,\lambda_2\}$, that we calibrate via the appropriate routine (Gilli, Grosse, Schumann (2010)). Then we compute $\widehat{YTM}(10,i,t)$ and we calculate $\widehat{ASW}_i$ as per eq. (50).

$$\widehat{YTM}(\tau,i,t) = \beta_1 + \beta_2\left[\frac{1-\exp(-\tau/\lambda)}{\tau/\lambda}\right] + \beta_3\left[\frac{1-\exp(-\tau/\lambda_1)}{\tau/\lambda_1} - \exp(-\tau/\lambda_1)\right] + \beta_4\left[\frac{1-\exp(-\tau/\lambda_2)}{\tau/\lambda_2} - \exp(-\tau/\lambda_2)\right] \quad (49)$$

$$\widehat{ASW}_i(t) = \widehat{YTM}(10,i,t) - EUR(10,t) \quad (50)$$

We consider daily variations of 10Y sovereign ASW for eleven countries (Germany, Finland, Netherlands, Austria, France, Belgium, Italy, Spain, Ireland, Portugal and Greece) from 1 January 2008 to 31 December 2016.

As Graph 116 shows, asset swap spreads show positive values in non-core countries, mostly because of the extra risk premium on these sovereign curves. In contrast, the data is negative in core and soft-core countries (Graph 115): the sovereign curve in these jurisdictions has been trading below the EUR swap curve in recent years. We follow the same methodology as in Chapter 1 considering the daily variations of $\widehat{ASW}_i$ (see eq. (51)) as the variable we will work on. In line with previous notations, we denote it x_i; Graph 115 and Graph 116 show the dynamics of the data.

$$x_i(t) = \widehat{ASW}_i(t) - \widehat{ASW}_i(t-1) \quad (51)$$

Graph 115. $\widehat{ASW}_i$ for core and soft-core countries

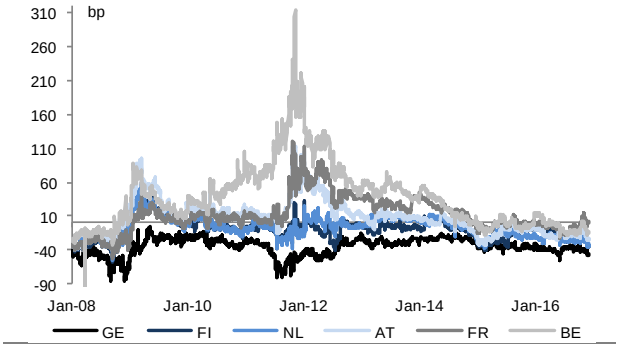

Graph 116. $\widehat{ASW}_i$ for non-core countries

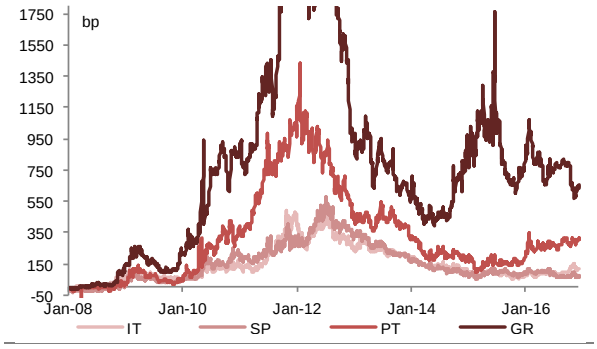

While there is more data available this time about Greece, there are still periods without any quotes. Around the debt restructuring that took place in Q1 2012 in particular, the 10Y sovereign bond (GGB) actually stopped being quoted for a couple of weeks in April. In order to maintain the same level of consistency for each country, we compensate this lack of data by collecting Greek ASW over a longer period, so that all time series are of the same size.

We calibrated the model described in Chapter 1 onto this new dataset. First we estimated the coefficients of the univariate conditional GHT distributions using the GAS method: Graph 117 shows the resulting CPIT for Spain and the ADC criteria for all countries. The ADC for Germany and Greece are slightly less compelling than for other countries, but they remain much satisfactory (see e.g. the CPIT for Greece in Graph 118). We also show the resulting GAS volatility for Portugal as an example in Graph 119 against its empirical benchmark.

Graph 117. CPIT for Spain and univariate ADC

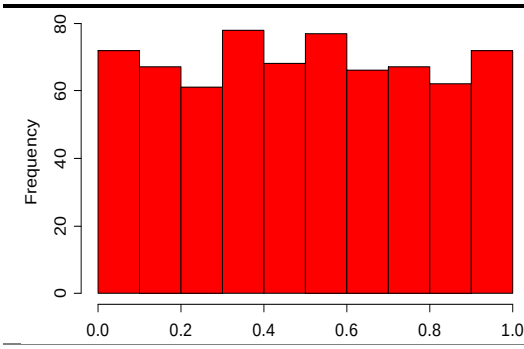

	ADC
GE	1.1
FI	0.6
NL	0.7
AT	0.7
FR	0.7
BE	0.8
IT	0.8
SP	0.5
IR	0.9
PO	0.7
GR	1.9

Graph 118. CPIT for Greece

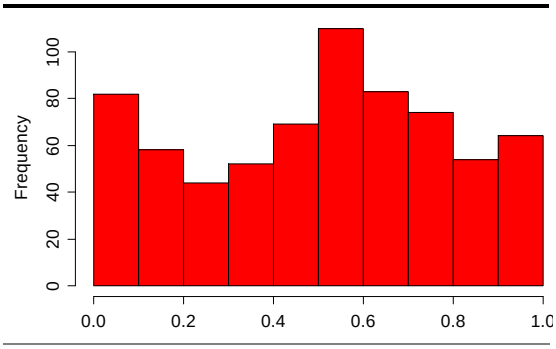

Graph 119. Portugal GAS volatility versus empirical benchmark

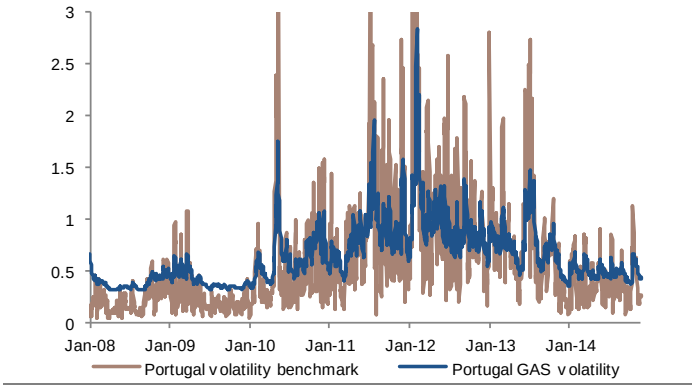

We then calculated the un-temporal GHT distributions, based on the volatility estimator $\hat{h}$. The resulting distributions p_y delivered much satisfactory ADC as well. Graph 120 shows the resulting un-temporal volatility $\hat{h}$: for most of the countries, values are very close to what we obtained in Chapter 1.

Graph 120. Volatility $\hat{h}$ in bp/day as a function of the empirical cumulative distribution

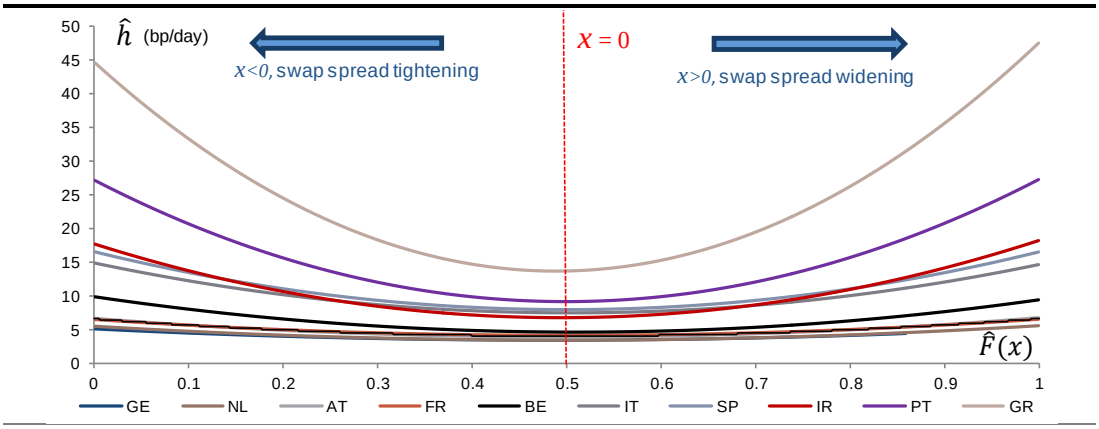

In our approach, the methodology of stress tests has a lot in common with the calculation of VaR. In the usual methodology, one has to fix in advance the level α of tolerated losses. Then with this information at hand, the Value at Risk can be calculated. In the context of this analysis now, the degree of risk that needs to needs be identified upstream has to reflect the **"worst case scenario"**, ie. the most extreme expected scenario. In the worst case scenario, the asset is seen as experiencing the largest **possible** price deterioration during the considered period (ie. one day). We denote this level of stress as $S_{i,max}$.

In a first instance, we seek to calculate this estimator. Intuitively, estimating the largest expected price deterioration $S_{i,max}$ could be achieved by exploring the expected market reaction to temporal stress tests, all over the history. Then we should be able to draw conclusions from the observed market reaction $S_{i,t}$. As mentioned above, temporal stress tests involve the GAS volatility σ_t which tends to capture the very short term momentums in the volatility (something we stress in Chapter 1). We also mentioned that $R_{i,t} = P_{i,t}^{Default\ CDS}/2$ looks an interesting parameterisation for temporal stress tests.

In this context, we computed time varying stress tests on the series, as defined in eq. (47), and on the basis that $R_{i,t} = P_{i,t}^{Default\ CDS}/2$ (as shown in Graph 109). We plotted some of the results in Graph 121, for the Netherlands, France and Italy as examples.

Graph 121 shows the expected market reaction in case of a shock of magnitude $P_{i,t}^{Default\ CDS}/2$ throughout the selected period. A possibility as to derive $S_{i,max}$ could be just to consider the maximum value of these series, and to take it as the expected reaction in a "worst case scenario". That said, we remain mindful that the volatility is sometimes spiking to an abnormally large level on the emergence of risk aversion, just because liquidity proves extremely scarce. This may favour the appearance of irrational market prices, and thus tends to make the dataset irrelevant at this date. **Capturing this 'noise' is a risk when we move towards the very end of the tails of the distribution.** As a result, and instead of taking the maximum value 'as is', we prefer defining our estimator of "maximum market reaction" $S_{i,max}$ to the Type I shock as the 99% percentile of the distribution of S_i. Table 34 shows the resulting values for each country. While these numbers look coherent, we

understand the 'arbitrary' dimension of the approach. For this reason, we will also consider the gross 'maximum value' in a second instance.

Graph 121. Market reaction $S_{i,t}$ to temporal shocks for selected ASW: Netherlands, France and Italy
There stress tests were conducted on the basis that $R_{i,t} = P_{i,t}^{Default\ CDS}/2$

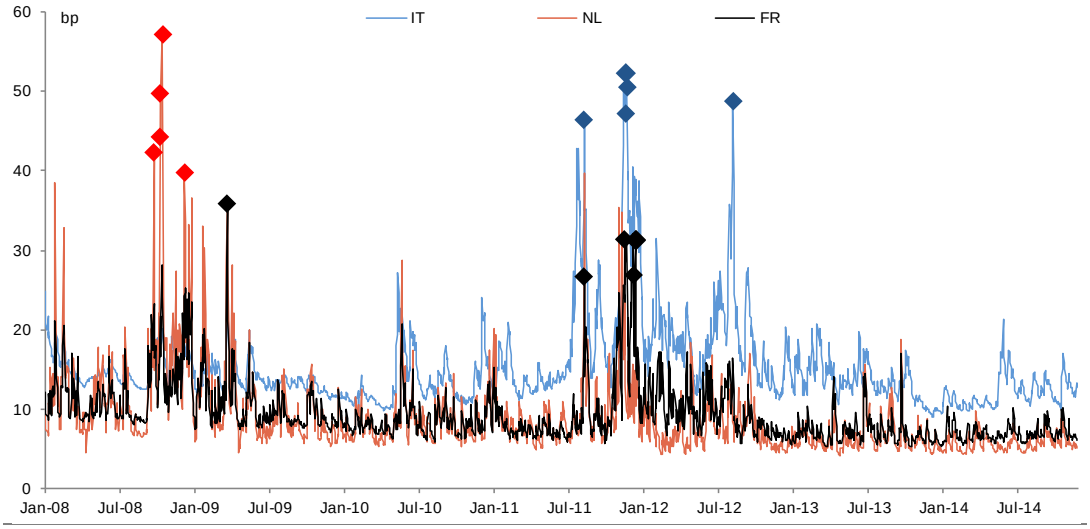

Table 34. $S_{i,max}$, the worst case scenario in basis points

Max market reaction	GE	FI	NL	AT	FR	BE	IT	SP	IR	PT	GR
	25	33	32	24	26	32	42	42	54	66	179

As a general observation in Table 34, the expected maximum market reaction to shocks is bigger for the more exposed countries in general. For Portugal and Greece for instance $S_{i,max}$ is peaking at $66bp$ and $179bp$, while the market reaction is much smaller for core and soft-core countries, at around $25 - 33bp$.

In Graph 121, we also highlight some of the most extreme values for each country with coloured diamonds. Overall the periods that see the largest market reaction to shocks tend to differ depending on the asset category (core, soft-core, non-core).

Italian ASW for instance (as an illustration for peripheral countries in general) **exhibit a larger market reaction at the climax of the sovereign crisis, ie. during the years 2011-2012** (blue diamonds in Graph 121). Though Graph 116 shows that Italian CDS spreads were trading at their highest levels by this time, $R_{i,t} = P_{i,t}^{Default\ CDS}/2$ also indicates that a higher CDS spread leads to a larger $R_{i,t}$ and therefore to a smaller $S_{i,t}$. ➔ **The larger $P_{i,t}^{Default\ CDS}$ cannot be seen as a tangible reason behind the surge in $S_{i,t}$ in 2011-2012.**

As Graph 122 shows, σ_t was also unusually large during the years 2011-2012, as it surged from roughly $10bp/day$ in normal market conditions to more than $30bp/day$ in e.g. November 2011. The larger GAS volatility σ_t, in contrast to the CDS level $s_{i,t}$, favours larger $S_{i,t}$ in eq. (47). ➔ **The GAS volatility σ_t is a prevalent factor in peripheral countries during the periods of very large $S_{i,t}$ in**

Graph 121. Even if not displayed in this graphs, other non-core countries follow the same dynamics.

Looking at core countries now, Dutch CDS in Graph 121 exhibit much smaller market reaction than soft-and non-core countries during the sovereign crisis (see red line). This is understandable as the large risk aversion in 2011-2012 fanned the demand for safer bonds. As a result, core interest rates were trading at much lower levels than soft-core and non-core rates during the crisis, and the GAS volatility σ_t remained much contained on more resilient credits in general. This overall justifies the relatively small $S_{i,t}$ during this period in core countries. **Based on Graph 121, the market reaction for Dutch CDS spreads (and for other core countries in general) in fact reaches a peak in October 2008**. 2008 is notorious for the global financial crisis (GFC), that hurt financial markets worldwide. In Europe, core CDS spreads were trading at a very low level just ahead of the crisis (Graph 123). Dutch CDS for instance were trading at just 12$ until end Q3 2008, close to French CDS (15$) but well below Italian CDS (50$). In this context, $P_{i,t}^{Default\ CDS}$ (in eq. (44)) was at extremely low levels in core sovereigns. And as we just mentioned, a lower probability of default tends to encouraged a larger market reaction $S_{i,t}$. In core countries specifically, this effect was largely offset by the volatility σ_t, which remained persistently small until end September 2008 (green area in Graph 124). But things changed when global risk aversion hit the market by the end of September 2008 as it pushed volatility in general to record highs (red area in Graph 124), even in core economies. This led to the combination of a very low $P_{i,t}^{Default\ CDS}$ and a very large volatility σ_t, both supporting a bigger market reaction $S_{i,t}$. This mostly justifies the large values in Graph 121 during the periods around H4 2008 for France and the Netherlands. ➔ **Overall, this shows that $P_{i,t}^{Default\ CDS}$, along with CDS prices by analogy, were much too low in core countries, just by the wake of the global financial crisis.** As a result, CDS prices in core countries experienced a remarkable correction in October-November 2008 (e.g. Dutch CDS in Graph 123), with prices soaring from 12$ to 90$, in just two months.

➔ **These observations highlight the contrarian influence of both the probability of default and the GAS volatility on the market reaction $S_{i,t}$.**

Graph 122. CDS peaking in 2011-2012

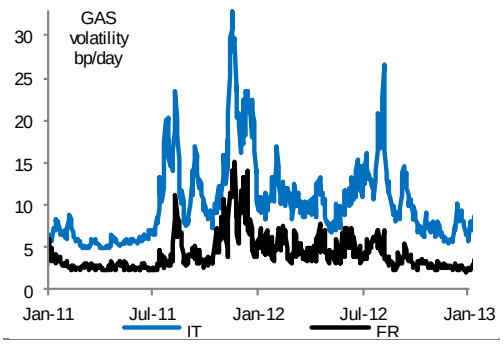

Graph 123. Core CDS at low levels in 2008

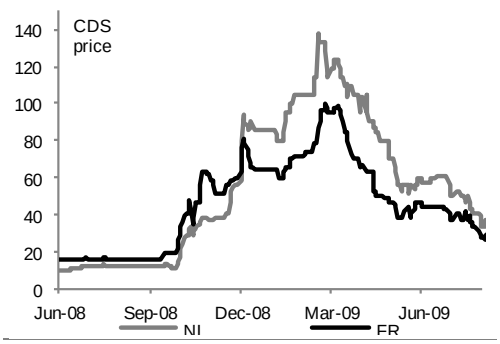

Graph 124. GAS Volatility regime in 2008

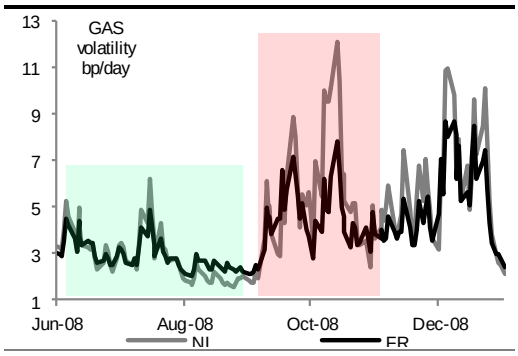

French assets in Graph 121, offer interesting information as well. Arguably, soft-core CDS spreads were trading above core CDS spreads in 2008. The higher probability of default, thus led to a more contained market reaction than in core: this is observable in Graph 121. On top of that, the volatility in soft-core credits is significantly smaller than in peripheral countries. This justifies the smaller market reaction during the years 2011-2012 for French ASW in comparison to Italy in Graph 121. In the end, black diamonds that show extreme market reactions on French ASW take place at different periods in the sample, with some of the points during the years 2008-2009, and others during the sovereign crises in 2011-2012.

➔ **These observations already reveal some information on the influence of σ_t and $P_{i,t}^{Default\ CDS}$.** The sample size also appears to be an important factor as a shorter history – e.g. excluding the 2008 crisis – would have led to much smaller estimations of the maximum market reaction $S_{i,max}$ for core countries. **This would have caused an underestimation of potential risks in core credits.**

Influence of the univariate volatility

In the literature, volatility is commonly seen as a major catalyst for contagion on financial markets (Darolles et al. (2013); Darolles et al. (2014); Glasserman, Nouri (2012)). In this section we explore this relationship between volatility and the market reaction to shocks. We achieve a series of shocks on each sovereign entity separately and under different volatility regimes, then we look at the resulting market reaction. **In sum, we seek to understand the implications of a rising volatile, on the intrinsic exposure/resilience to financial shocks.** In (Darolles et al. (2013) and Darolles et al. (2014)), the deterioration of the credit robustness to shocks, when the univariate volatility is mounting, is designated as a 'frailty' coefficient. **This is the parameter that we seek to explore and quantify.**

Graph 120 shows the un-temporal volatility $\hat{h}$. Looking at Italian ASW more specifically in Graph 125, we empirically segmented the plot into three main categories, all supposed to describe a particular volatility regime. First we identify a regime of **"equilibrium volatility",** which qualifies very stable market conditions (green area at the centre of the distribution, ie. for $\hat{F}(x)\sim 0.5$). The volatility here reaches its lowest values, and ASW variations are very small as well ($\hat{F}(x)\sim 0.5$). Then we acknowledge a **"mild volatility"** regime (yellow areas), with slightly higher volatility this time. ASW variations on the x-axis are also bigger ($0.15 < \hat{F}(x) < 0.35$ and $0.65 < \hat{F}(x) < 0.85$). Intuitively, one would think that a shock will probably have a bigger impact under this regime than under the equilibrium volatility. Finally we consider the volatility in the tails as the **"extreme volatility"** regime

(red areas). This time, volatility reaches its largest values. As it is located in the wings ($\hat{F}(x)\sim 0$ and $\hat{F}(x)\sim 1$), this regime corresponds to very large variations in ASW. A shock under these conditions will probably lead to the most harmful market reaction, surely bigger than in the two other regimes.

Graph 125. Volatility coefficient $\hat{h}$ in bp/day as a function of the empirical cumulative distribution

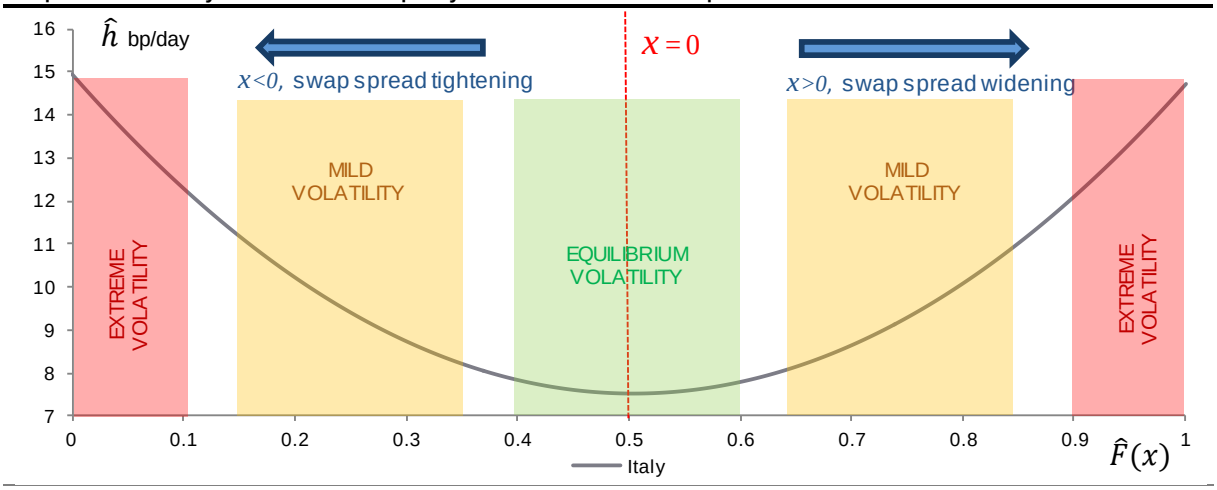

Let us now consider our un-temporal definition of stress tests, that involves both the un-temporal volatility estimator $\hat{h}$, and the univariate distribution function p_y:

$$R_i = P(x_i \geq S_i) = \int_{S_i}^{+\infty} p(x_i, \hat{h}) dx_i = 1 - F(S_i, \hat{h})$$

We seek to assess the consequences of stress tests under different volatility regimes separately. In Graph 125 we identified three different regimes only, but we generalise this approach and we consider each point on the curve as a particular volatility regime.

We conduct a series of shocks with a gradual intensity. We denote $R_{i,max}$ the probability of the most severe shock, and we compute it as the percentile on p that corresponds to the largest expected market reaction $S_{i,max}$. Since the maximum market reaction is supposed to be reached under the most extreme volatility regime, we calculate $R_{i,max}$ under the assumption that $\hat{h}_i = \hat{h}\left(\hat{F}(x_i) = 1\right) = \hat{h}_{i,max}$. Then we calculate $R_{i,max}$ such that:

$$R_{i,max} = \int_{S_{i,max}}^{+\infty} p(x_i, \hat{h}_{max}) dx_i = 1 - \hat{F}_i(S_{i,max}, \hat{h}_{max}) \qquad (52)$$

The resulting values are in Table 35:

Table 35. $R_{i,max}$, ie. the probability attached to the most severe shocks

Max risk level (percentile, %)	GE	FI	NL	AT	FR	BE	IT	SP	IR	PT	GR
	0.012	0.006	0.008	0.037	0.021	0.050	0.098	0.155	0.081	0.201	0.029

Since $S_{i,max}$ in Table 34 is assumed to be reached for $\hat{h} = \hat{h}_{max}$ specifically, we rename it as $S_{i,max}(\hat{h}_{max})$.

For each volatility regime $\hat{h}$, we consider a series of shocks with gradually decreasing intensities. The most severe scenario is defined by $R_i = R_{i,max}$. And for the shock of least intensity, $R_i = 50\%$ will cause no market reaction at all given that p is centred:

$$R_i^{II} = 50\% \quad \rightarrow \quad 0.5 = \int_{S_i}^{+\infty} p(x_i, \hat{h}) dx_i \quad \rightarrow \quad S_i = 0\ bp \ \text{, so no market reaction} \tag{53}$$

We also consider intermediate levels of risk. Those levels are set arbitrarily, they are meant to illustrate the behaviour of the market reaction with regards to shocks of mild severity, ie. between the maximum risk level $R_i = R_{i,max}$ and the "equilibrium risk level" reached for $R_i = 50\%$. Given the levels of $R_{i,max}$ in Table 35, we consider two different sets for $\{R_{i,j}\}$:

- First we note that $R_{i,max} < 0.2\%$ for every country except Portugal. As a consequence, we arbitrarily choose to explore the following 7 different levels of shocks (*j* indicates the risk level):

$$\{R_{i,j}\} = \{R_{i,max}, 0.2\%, 0.5\%, 1\%, 5\%, 15\%, 50\%\} \tag{54}$$

- Then for Portugal, we adjust it to:

$$\{R_{i,j}\} = \{R_{i,max}, 1\%, 2\%, 5\%, 10\%, 15\%, 50\%\} \tag{55}$$

As we will see later, this difference does not alter the quality of the final estimate of the frailty coefficient.

As eq. (46) indicates, the stress test procedure consists of calculating the magnitude of the market reaction S_i, which illustrates the variation in the asset swap spread that is supposed to result from the shock. For a given volatility regime $\hat{h}$ and a country i, eq. (56) indicates $S_i(\hat{h})$ is computed, assuming that we simulate a shock of amplitude $R_{i,j}$. This definition shows the relationship between the market reaction S_i (expressed in basis points) and the intensity $R_{i,j}$ of the shock. Comparing S_i for different values of $\hat{h}$ eventually offers a comprehensive picture of how the market reaction is supposed to increase when the volatility rises.

$$R_{i,j} = \int_{S_{i,j}}^{+\infty} p(x_i, \hat{h}) dx_i \tag{56}$$

The V-shape of $\hat{h}$ in Graph 125 makes any exploration of $S_{i,j}$ as a function of $\hat{h}$ relatively inconvenient. Instead, **we prefer looking at $S_{i,j}$ as a function of the empirical cumulative distribution function $\hat{F}$**. This is more straightforward given that $\hat{h}(x_i) = a_0 \times \hat{F}(x_i)^2 + a_1 \times \hat{u}(x_i) + a_2$ (see Chapter 1). **We will then consider S_i as a function of $\hat{h}$ in a second stage.**

Graph 126 and Graph 127 show the results for German and Italian ASW. For better clarity, we include just three different levels of intensity in these two graphs: 0.2%, 0.5%, $R_{i,max}^{II}$. **With no surprise the market reaction tends to worsen when the shock becomes more and more severe.** German ASW for instance, shows a market reaction of $25bp$ under $R_{GE,max}$ (Graph 126) - by definition this is equal to $S_{i,max}$. New information comes from the fact that the market reaction falls to respectively $12bp$ and $10bp$ for shocks with a risk level R_i of 0.2% and 0.5%. Italian ASW exhibit a similar dynamics overall, with the market reaction falling from $41bp$ for $R_{IT,max}$ to $35bp$ and $28bp$ for scenarios with a risk level of 0.2% and 0.5%.

Graph 126. Market reaction S_i vs. $\hat{F}$ and $\hat{h}$ (Germany)
$R_i = \{0.2\%, 0.5\%, R_{i,max}\}$

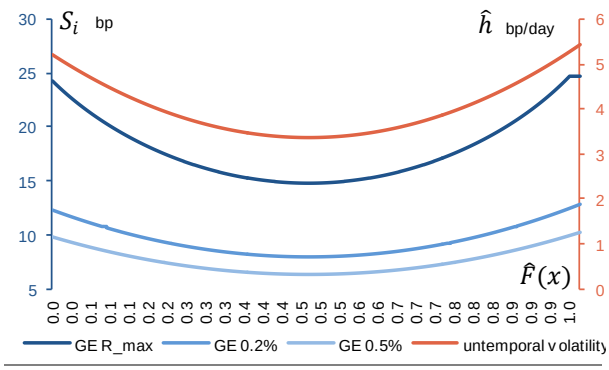

Graph 127. Market reaction S_i versus $\hat{F}$ and $\hat{h}$ (Italy)
$R_i = \{0.2\%, 0.5\%, R_{i,max}\}$

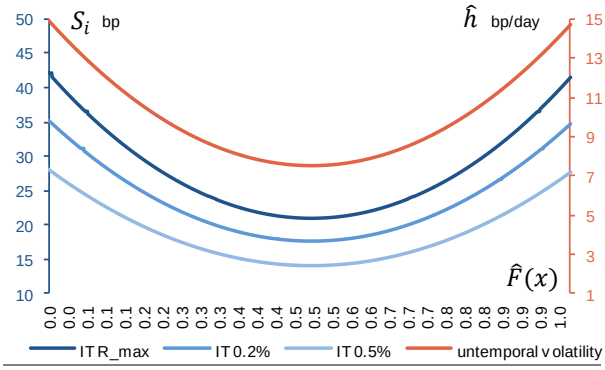

We also added the volatility coefficient $\hat{h}$ in orange (right-hand side) in Graph 126 and Graph 127. This helps understand the dynamics of the market reaction when volatility is mounting: in both cases, the rise in the market reaction S_i is coincident with a larger underlying volatility.

➔ **The bigger market reaction in volatile market conditions illustrates the 'frailty'. This specifically describes the market reaction 'in excess', compared to the reaction S_i at the belly of the distribution** (ie. under the equilibrium volatility regime)**. We explore the market reaction and frailty further, in the following paragraphs, and we propose a quantification of their respective behaviour.**

The series $\{S_i^{R_{i,max}}, S_i^{0.2\%}, S_i^{0.5\%}, S_i^{1\%}, S_i^{5\%}, S_i^{15\%}, S_i^{50\%}\}$ in eq. (54) or in eq. (55) can be seen as successive levels of the market reaction as the shock becomes increasingly more severe. On that basis, we adjusted the presentation of the results and we plotted the market reaction of all European ASW in Graph 128 to Graph 138. In these graphs, each band corresponds to a specific range for the expected market reaction as specified in the legend: the highest tranche for instance corresponds in general to $0.2\% \geq R_i \geq R_{i,max}$, except for Portuguese ASW where this is $1\% \geq R_i \geq R_{i,max}$. The reasoning is similar for other tranches, up to the lowest section that corresponds to $50\% \geq R_i \geq 15\%$.

Graph 139 also compares the market reaction in all countries for the most severe shock. This highlights the sharp differentiation in terms of credit robustness, between peripheral countries and other core/soft-core countries (especially in the tail regions), in the worst case scenario.

Graph 128. Market reaction S_i for various R (Germany)

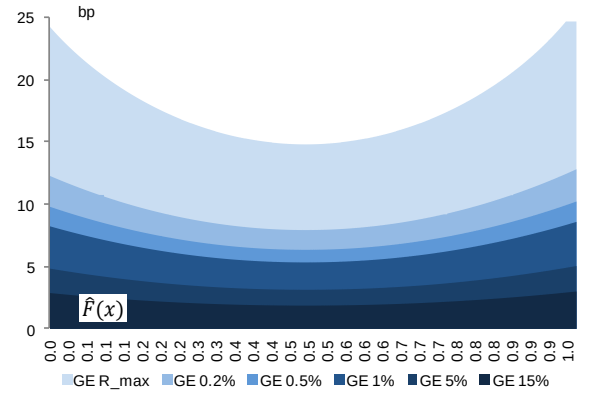

Graph 129. Market reaction S_i for various R(Finland)

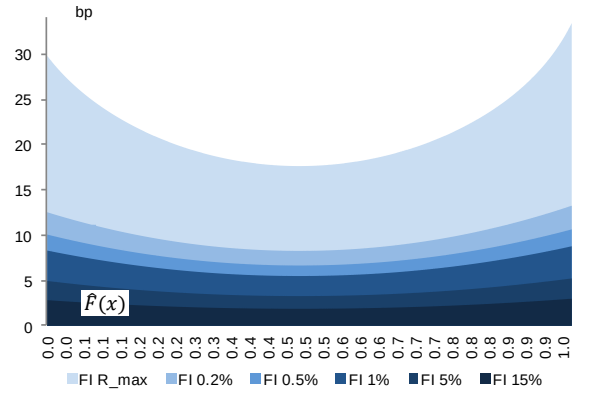

Graph 130. Market reaction S_i for various R (Nether)

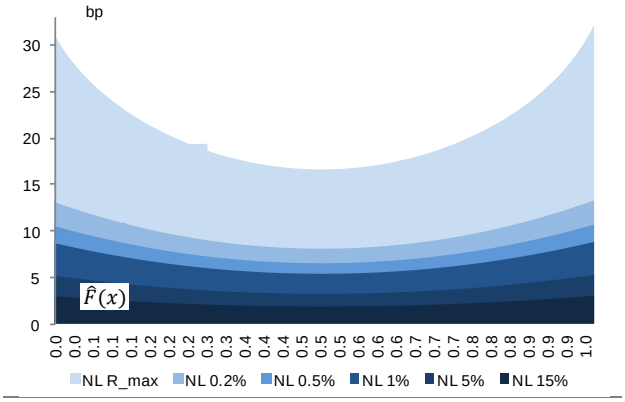

Graph 131. Market reaction S_i for various R (Austria)

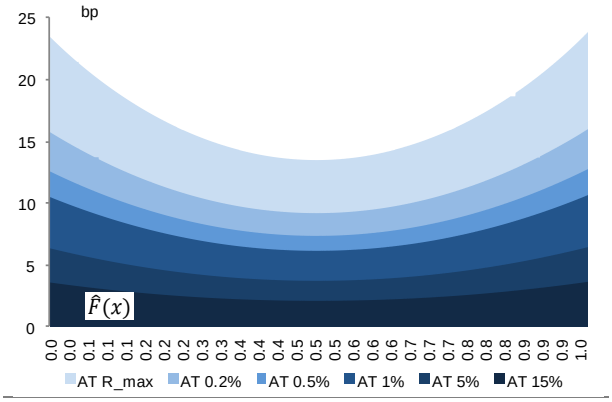

Graph 132. Market reaction S_i for various R (France)

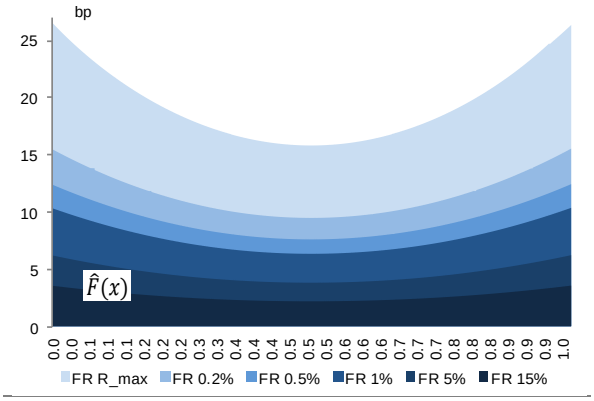

Graph 133. Market reaction S_i for various R (Belgium)

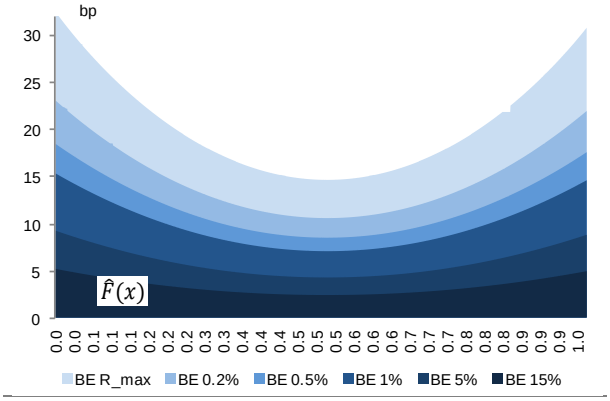

Graph 134. Market reaction S_i for various R (Italy)

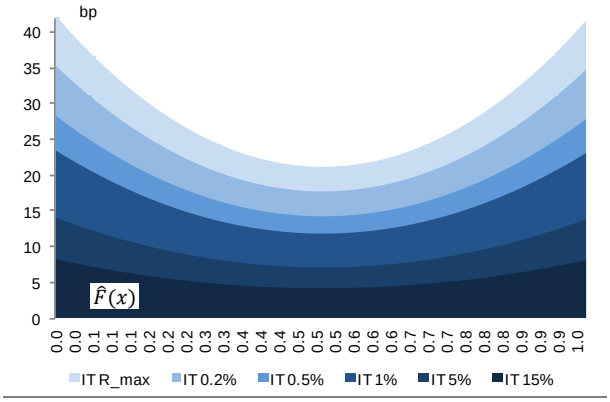

Graph 135. Market reaction S_i for various R (Spain)

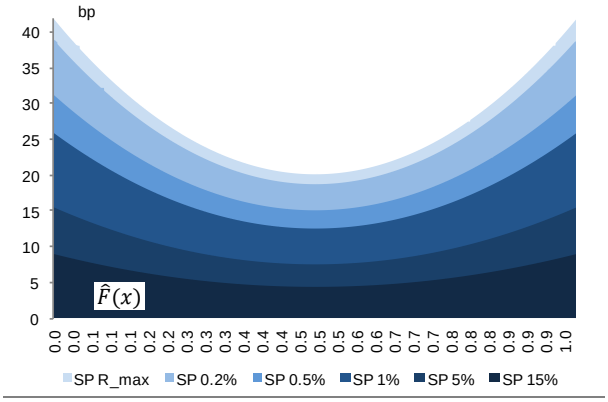

Graph 136. Market reaction S_i for various R (Ireland)

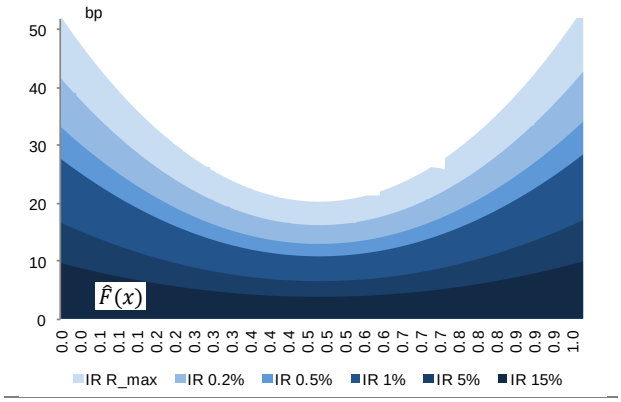

Graph 137. Market reaction S_i for various R (Portugal)

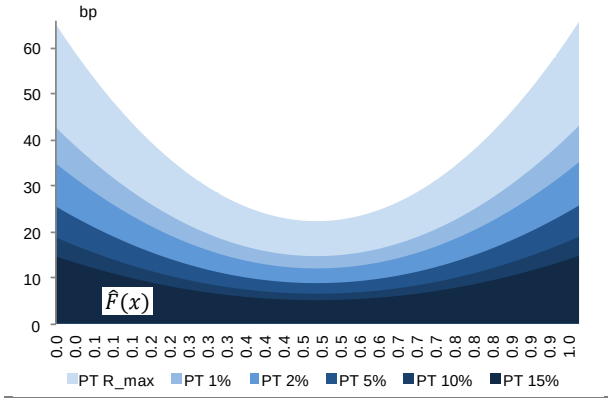

Graph 138. Market reaction S_i for various R (Greece)

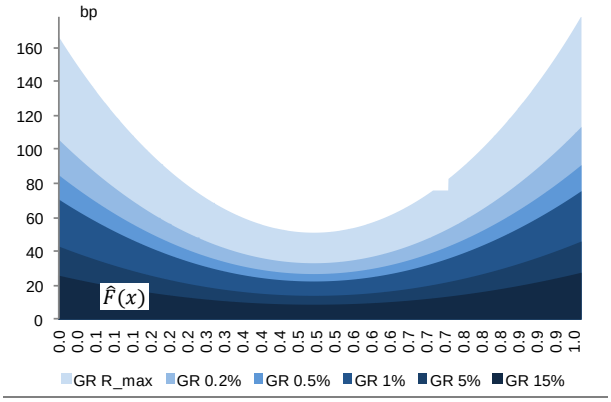

Graph 139. Market reaction S_i for $R = R_{i,max}$

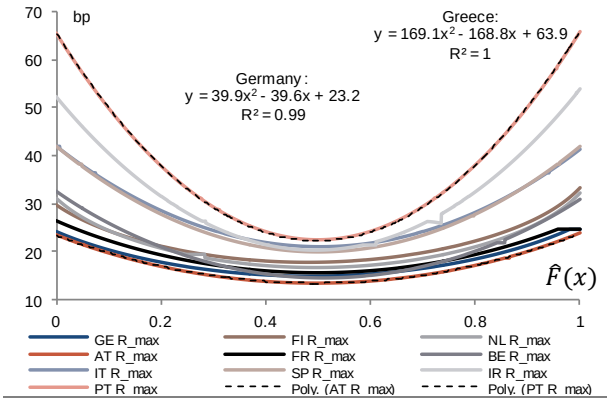

A general observation is that the market reaction always reaches extreme values for $\hat{F}(x) = 0$ and $\hat{F}(x) = 1$ while S_i is much smaller in the centre of the distribution ($\hat{F}(x) \sim 0.5$).

For a given level of stress, the market reaction looks like a parabola. This is an illustration of the non-linear acceleration of the price deterioration as we approach the tail regions. In other words, a shock will have much worst implications on the asset price when the underlying volatility is already large at the initial stage of the simulation. **The parabolic shape is worth to note, we will exploit it further in a subsequent paragraph.**

Based on the definition of Darolles et al. (2013) and Darolles et al. (2014), the acceleration in S_i is an illustration of the frailty phenomenon, which turns to be particularly damageable when the volatility rises. While our calculation of the frailty is different, our indicator is based on the same definition: for a given level R, we define the frailty coefficient $W_i^R\left(\hat{F}(x)\right)$ as the difference between the expected market reaction for a given level of volatility $\hat{h}$ and the expected market reaction when the volatility is in the equilibrium regime ie. for $\hat{h}\left(\hat{F}(x) = 0.5\right)$, as per eq. (57):

$$W_i^R\left(\hat{F}(x_i)\right) = S_i\left(\hat{F}(x_i)\right) - S_i(0.5) \tag{57}$$

Our definition implies that there is no frailty under the equilibrium volatility regime, which looks fair. In general terms, the frailty coefficient W_i^R reflects the portion of the market reaction S_i that is in excess to the market reaction obtained under the equilibrium regime (so for $S_i\left(\hat{F}(x) = 0.5\right)$).

Using this definition, we obtain a specific curve W_i^R for each level of stress $R_{i,j}$: Graph 140 to Graph 152 show the results. Each tranche this time illustrates the frailty coefficient in the range $\left[R_{i,j}^{II}, R_{i,j-1}^{II}\right]$. The legend denotes the lower and upper limits of the corresponding range. The upper tranche in the plots for instance corresponds to the expected frailty for shocks in the range $[0.2\%, R_{i,max}^{II}]$ (or $[1\%, R_{i,max}^{II}]$ for Portugal).

As to highlight the strength of the frailty, we collated the maximum frailty of each country in Table 35. Germany and Austria exhibit the smallest frailty, at just $10bp$. In core countries, Finland and the Netherlands experience slightly more frailty at $16bp$ and $15bp$. France exhibits a low maximum frailty of $11bp$, ie. very close to Germany, while Belgium yields a slightly higher frailty parameter, at $18bp$. Table 36 also shows that the maximum frailty is quite similar for Spanish and Italian ASW at $21bp$ each. **This means that out of $42bp$ and $41bp$ respectively in $S_{i,max}$ (see Table 34), $21bp$ is attributable to the 'frailty' effect.** As expected, the maximum frailty is bigger for other peripheral countries with namely $33bp$ frailty in Ireland, $42bp$ in Portugal and $125bp$ in Greece.

Table 36. Maximum frailty $W_{i,max}$, expressed in basis points and as a share of $S_{i,max}$

	GE	FI	NL	AT	FR	BE	IT	SP	IR	PT	GR
Maximum univariate frailty	10	16	16	10	11	18	21	22	34	44	128
share of Si_max	39%	41%	46%	42%	40%	55%	50%	52%	61%	66%	69%

We also added the ratio of $W_{i,max}$ over $S_{i,max}$ in Table 36. This illustrates the maximum frailty ($W_{i,max}$) as a share of the corresponding market reaction ($S_{i,max}$). Arguably, the portion corresponding to the pure frailty effect within $S_{i,max}$ is smaller for core and soft-core countries, with a ratio at around $40\% - 45\%$ of $S_{i,max}$. Then the ratio tends to rise for non-core countries, from 50% for Spain and Italy up to 69% for Greece. ➔ **Numbers highlight that the frailty plays a bigger role for countries with a less robust credit quality.**

Graph 140. Frailty W_i for various R (Germany)

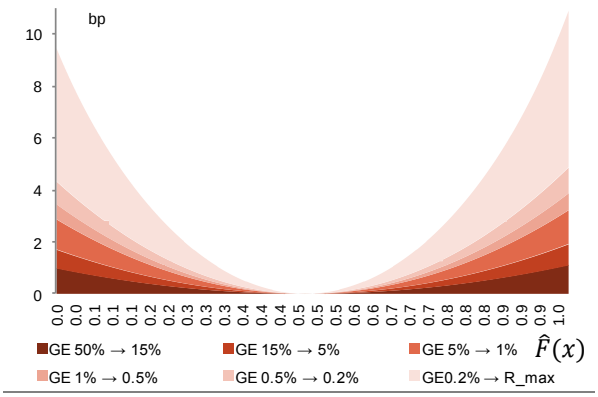

Graph 141. Frailty W_i for various R (Finland)

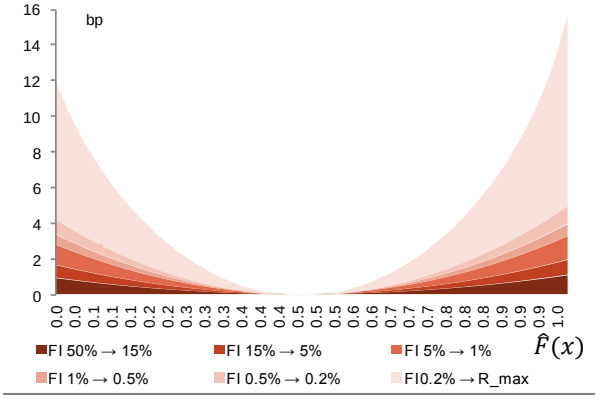

Graph 142. Frailty W_i for various R (Netherlands)

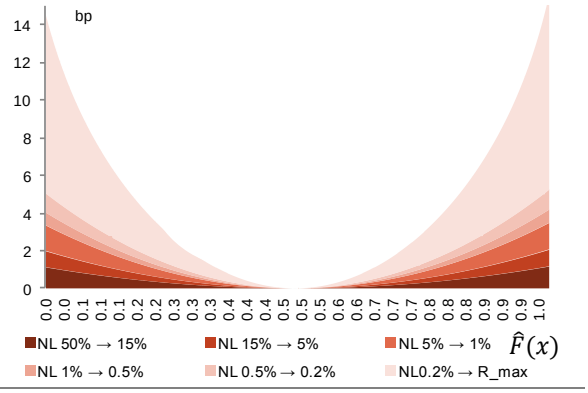

Graph 143. Frailty W_i for various R (Austria)

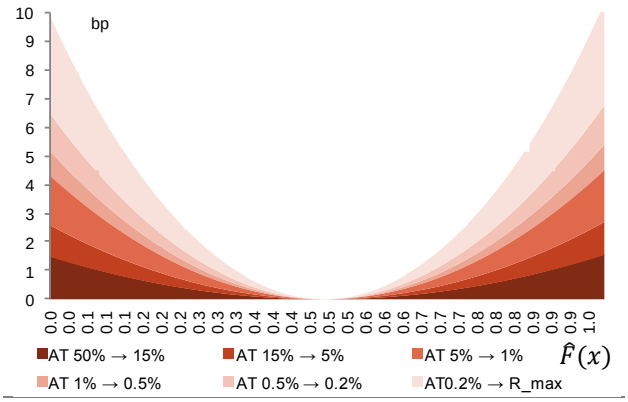

Graph 144. Frailty W_i for various R (France)

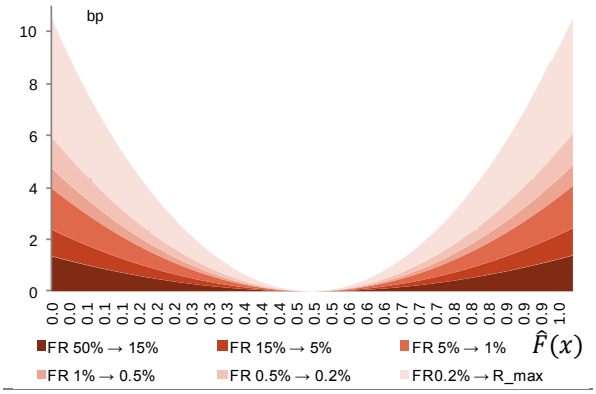

Graph 145. Frailty W_i for various R (Belgium)

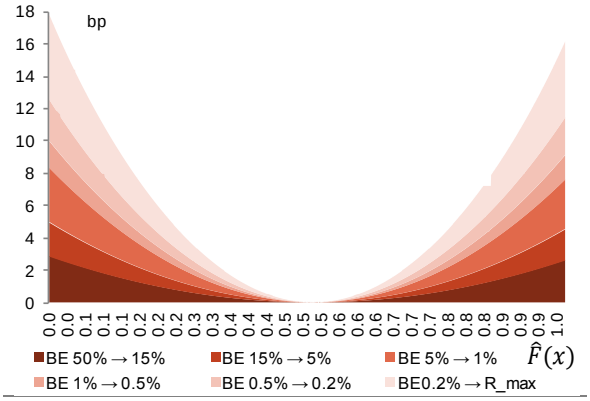

Graph 146. Frailty W_i for various R (Italy)

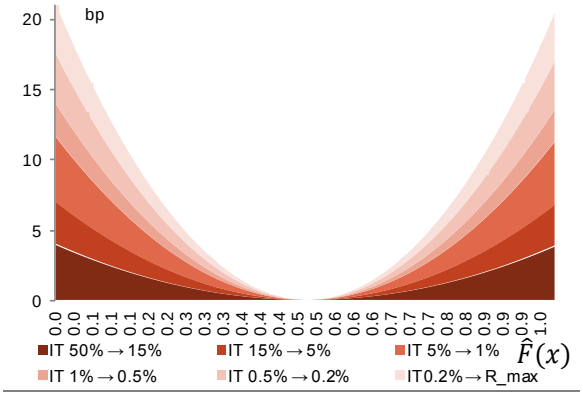

Graph 147. Frailty W_i for various R (Spain)

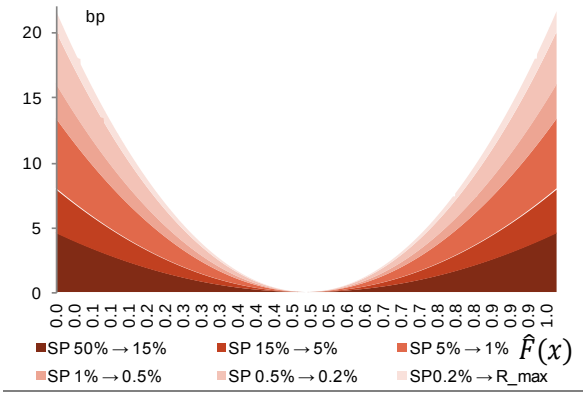

Graph 148. Frailty W_i for various R (Ireland)

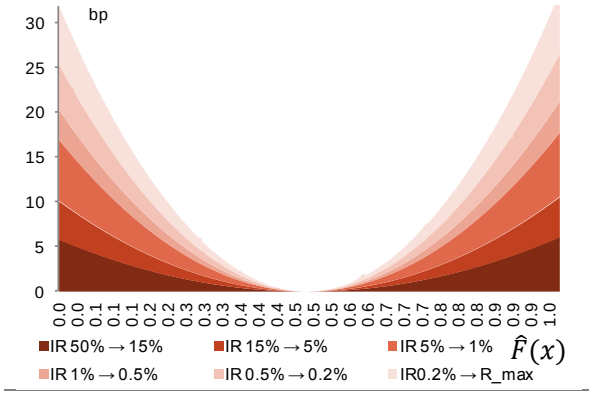

Graph 149. Frailty W_i for various R (Portugal)

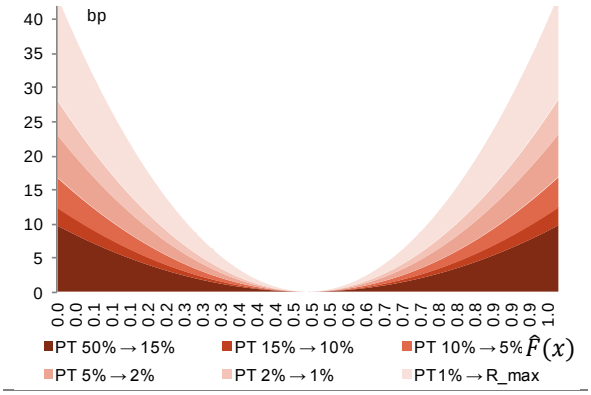

Graph 150. Frailty W_i for various R (Greece)

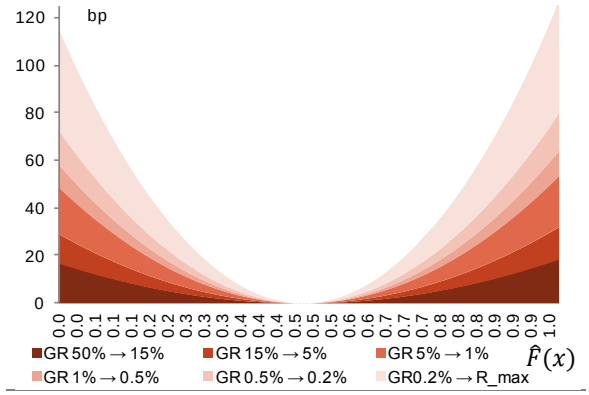

Graph 151. Maximum frailty for non-core

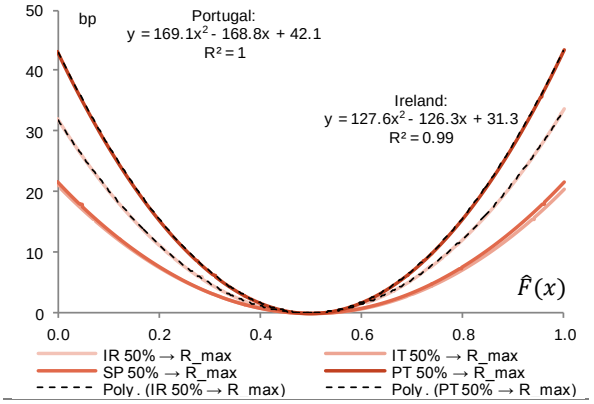

Graph 152. Maximum frailty for core/soft-core

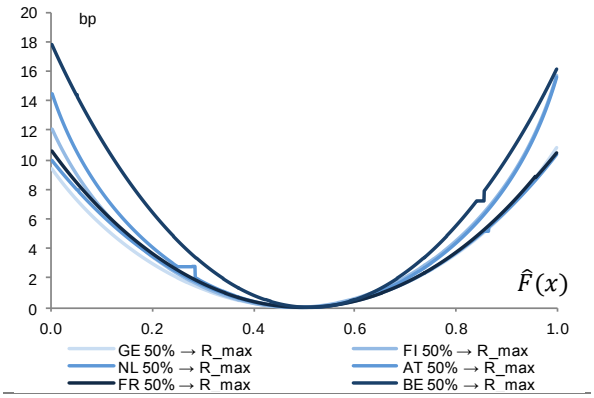

Table 37. Coefficients of the polynomial interpolation

	MARKET REACTION Si			FRAILTY Wi		
	a2	a1	a0	b2	b1	b0
GE	38.9	-37.8	23.9	39.2	-38.0	9.1
FI	51.2	-48.9	29.0	51.2	-48.9	11.3
NL	54.5	-53.9	29.6	54.5	-53.9	13.0
AT	40.1	-39.8	23.3	40.1	-39.8	9.8
FR	41.2	-41.3	26.1	42.0	-41.9	10.4
BE	67.2	-68.7	32.2	67.2	-68.7	17.5
IT	82.7	-83.4	42.1	82.7	-83.4	21.0
SP	86.5	-86.6	41.8	86.5	-86.6	21.6
IR	130.7	-129.2	52.1	130.3	-128.8	31.8
PT	173.1	-172.8	65.4	173.1	-172.8	43.1
GR	484.4	-473.7	166.7	483.9	-472.9	115.3

In line with its definition in eq. (57), the maximum frailty (reached for $R_{i,max}$) looks like a parabola in Graph 140 to Graph 152. The non-linear aspect of the frailty is particularly pronounced when we near the tail regions of the distribution. We also extracted the frailty coefficients obtained for the most severe shock ($R_{i,max}$) in Graph 151 and Graph 152, and this helps make some cross-country comparisons. Overall, we note that core and soft-core see somewhat similar frailty (Graph 151) while non-core countries are much more exposed to shocks (Graph 152).

An interesting aspect of S_i and W_i^R is the parabolic shape of the results. A second order polynomial equations effectively provides an outstanding fit to the resulting series, and so for both coefficients (see Graph 139 and Graph 152). ➔ **This quantification of the market reaction and the frailty phenomenon is valuable as it makes any out-of-sample exploration of these results particularly easy.**

For the sake of clarity we focus on one level of financial stress: the worst case scenario (ie. $R_i = R_{i,max}$. We define the second order polynomial interpolation according to the parameterisation in eq. (58) and eq. (59). We then estimate the coefficients of the interpolation using the usual least squares method. We put the resulting coefficients in Table 37.

$$\tilde{S}_i = a_2\hat{F}(x_i)^2 + a_1\hat{F}(x_i) + a_0 \quad (58)$$

$$\widetilde{W}_i = b_2\hat{F}(x_i)^2 + b_1\hat{F}(x_i) + b_0 \quad (59)$$

Considering this polynomial model makes the determination of the market reaction and the corresponding frailty coefficient particularly straightforward, in particular for out-of-sample explorations. As an example, let us assume a daily price variation of $x_i = 25bp$ on a given peripheral ASW. Based on the dataset at hand, we can first deduce the value of the cumulative $\hat{F}(x_i)$:

Table 38. Empirical cumulative distribution function $\hat{F}(x_i)$ associated to a rise in asset swap spreads of 25bp

	IT	SP	IR	PT	GR
$\hat{F}(x_i)$	0.989	0.989	0.980	0.969	0.917

Then, assuming the worst case scenario, we apply eq. (58) and eq. (59) using the calibrated coefficients in Table 37 and the data in Table 38. This reveals the expected market reaction and the frailty coefficient expected on the materialisation of a shock of amplitude $R_{i,max}$:

Table 39. Expected market reaction $\tilde{S}_i$ and contagion $\widetilde{W}_i$ in basis points

	IT	SP	IR	PT	GR
$\tilde{S}_i$	41	41	51	61	140
$\widetilde{W}_i$	19	21	31	38	88

Table 39 shows that a shock at the $R_{i,max}$ level - assuming that asset swap spreads have risen by some $25bp$ – will lead to a market reaction of $41bp$ in Spain and Italy, of which $19bp$ and $21bp$ respectively are due to the frailty effect. $\tilde{S}_i^1$ then rises to $51bp$ for Ireland and $61bp$ for Portugal, of which $31bp$ and $38bp$ relate to the frailty (ie. 61% and 62% of the reaction). With no surprise, Greece sees a more harmful reaction at $140bp$, with $88bp$ frailty (63% of the reaction).

These estimators of the market reaction/frailty provide useful insight in absolute terms for risk management purposes as it helps apprehend the potential shortfall if a shock comes up in sovereigns. The methodology also makes cross country comparisons of underlying risks, e.g. between peripheral countries, relatively convenient. **One for instance can get a clear idea of how much additional risk Portuguese assets adds to a given portfolio in comparison to Spanish or Italian assets.**

Let us now explore the relationship between the market reaction to shocks and the volatility. Graph 153 shows the market reaction S_i as a function of the volatility coefficient $\hat{h}$ for Germany. First it appears that the market reaction is a linear function of the volatility. The slope in particular tends to increase when the shock is more severe. We also see no particular differentiation between each side of the distribution (ie for $\hat{F}(x) \geq 0.5$ in comparison to $\hat{F}(x) < 0$).

We generalize this analysis to other countries in Graph 154 (core and soft-core countries) and Graph 155 (peripheral countries) considering the most severe shocks only ($R_{i,max}$). Overall, most of S_i curves exhibit a linear dynamics. But this is not the case for Finnish and Dutch ASW, for which the reaction tends to accelerate beyond a certain level when the volatility nears its highest values. This distinction may be due to the lower $R_{i,max}$ for Finland and the Netherlands in comparison to other countries (see Table 35). As a result, stress tests at the $R_{i,max}$ level for Finnish and Dutch ASW go much farther in the tail of the distribution ($R_{FI,max}$ and $R_{NL,max}$ are both below 0.01%). In these two cases, the relationship between S_i and $\hat{h}$ is quadratic.

Graph 153. Market reaction S_i vs $\hat{h}$ (Germany)

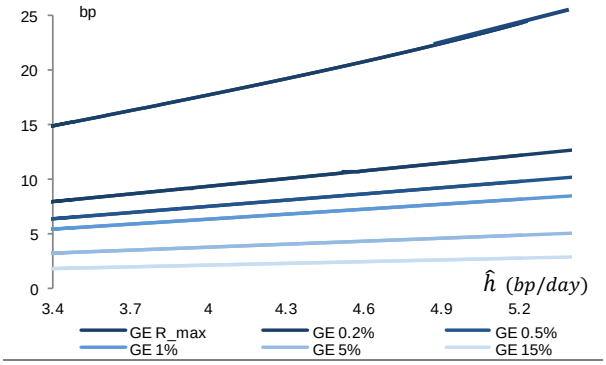

Graph 154. Market reaction S_i vs $\hat{h}$ (core, soft-core)

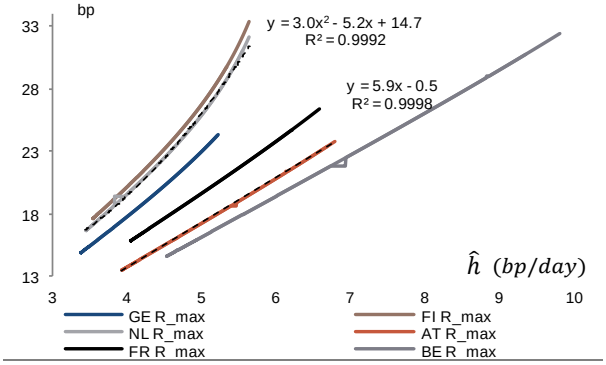

Graph 155. Market reaction S_i vs $\hat{h}$ (peripherals)

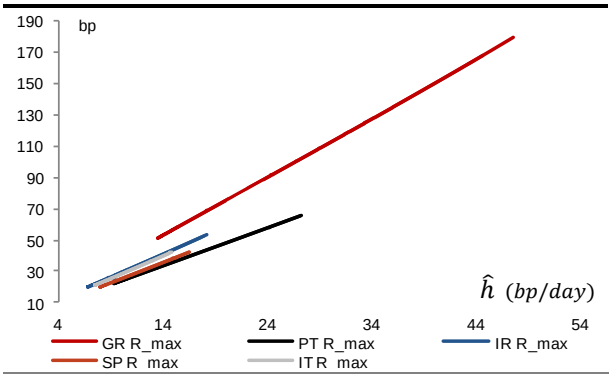

Table 40. Interpolation of $\tilde{S}_i$ versus $\hat{h}$

	MARKET REACTION *Si*		
	c2	c1	c0
GE		5.0	-2.2
FI	1.2	-4.1	17.1
NL	1.1	-3.1	14.7
AT		3.6	-0.5
FR		4.0	-0.5
BE		3.3	-0.4
IT		2.8	-0.2
SP		2.5	-0.1
IR		3.0	-0.2
PT		2.4	0.0
GR		3.7	0.3

Graph 154 and Graph 155 also show that the relationship between the market reaction and the volatility can be successfully described **by a second order polynomial function for Finland and the Netherlands and by a linear function for other countries**: eq. (60) formalizes the corresponding parameterization and Table 40 shows the corresponding coefficients; we denote $\tilde{S}_i$ the estimated

variable. ➔ **For a given volatility $\hat{h}$, we can now deduce the expected market reaction to a shock in the worst case scenario:**

$$\tilde{S}_i = c_1\hat{h} + c_0 \text{ for all countries except Finland and the Netherlands} \quad (60)$$

$$\tilde{S}_i = c_2\hat{h}^2 + c_1\hat{h} + c_0 \text{ for Finland and the Netherlands} \quad (61)$$

Let us now look at the relationship between the univariate frailty W_i^R and the volatility $\hat{h}$. Graph 63 shows the frailty coefficient obtained for German ASW as a function of the volatility. This time again the expected frailty looks like a linear function of the volatility, with the slope rising along with the severity of the shock. Then extending this observation to other countries in Graph 157, we obtain a general picture very similar to Graph 154: most of the countries admit a linear relationship between the frailty and the volatility, except for Finnish and Dutch ASW which display a quadratic relationship. This is not surprising given that W_i^R is a linear transformation of S_i in eq. (57).

Based on the same approach as before, we model the expected frailty coefficient $\widetilde{W}_i$ as a polynomial function of the volatility for Finnish and Dutch ASW and as a linear function for other countries (see eq. (62)). We calculate the corresponding unknowns and we put the results in Table 41.

$$\widetilde{W}_i = d_2\hat{h}^2 + d_1\hat{h} + d_0 \text{ for all countries except Finland and the Netherlands} \quad (62)$$

$$\widetilde{W}_i = d_2\hat{h}^2 + d_1\hat{h} + d_0 \text{ for Finland and the Netherlands} \quad (63)$$

Graph 156. Univariate frailty W_i vs $\hat{h}$ (Germany)

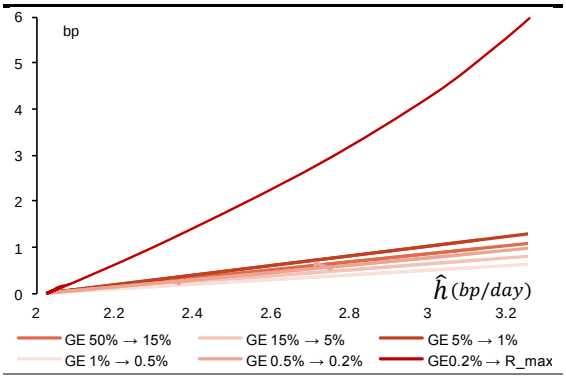

Graph 157. Univariate frailty W_i for core, soft-core

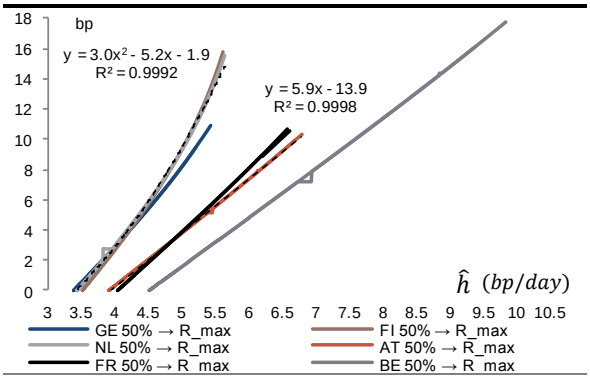

Graph 158. Univariate frailty W_i for peripherals

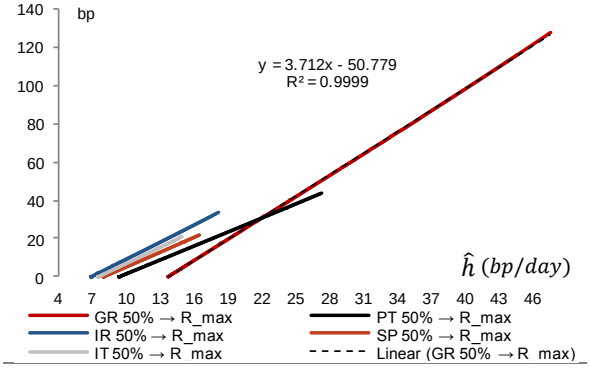

Table 41. Coefficients of the interpolation (W_i vs $\hat{h}$)

	FRAILTY *Wi*		
	c2	c1	c0
GE		5.0	-17.2
FI	1.2	-4.1	-0.5
NL	1.1	-3.1	-1.9
AT		3.6	-14.0
FR		4.1	-16.7
BE		3.3	-15.0
IT		2.8	-21.3
SP		2.5	-20.3
IR		2.9	-20.3
PT		2.4	-22.3
GR		3.7	-50.8

This model makes rather convenient the exploration of synthetic examples. If we assume for instance that peripheral countries see a volatility coefficient of $\hat{h} = 11bp/day$. Based on Graph 155

and Graph 158 this is a pretty large volatility regime. While this is outside of the range of the observed values for Spanish and Italian ASW, we can now derive the expected market reaction and frailty:

Table 42. Expected market reaction $\tilde{S}_i^2$ and contagion $\widetilde{W}_i^2$ in basis points

	IT	SP	IR	PT	GR
$\tilde{S}_i$	52	46	54	44	68
$\widetilde{W}_i$	31	26	34	22	17

Results in Table 42 indicate that the frailty is smaller for Portuguese ASW than for Spanish and Italian assets. This is because we do not take the probability of the event $\hat{h} = 11bp/day$ into account. We mentioned that $\hat{h} = 11bp/day$ is a rare event for Italian and Spanish ASW (thus justifying the huge market reaction of $52bp$ and $46bp$), but this is not the case for Portuguese ASW since $11bp/day$ is not that far from the "equilibrium regime" in Graph 120. This justifies the smaller reaction of $44bp$.

➔ **Our model in eq. (62) and eq. (63) offers insightful information on the behaviour of the market reaction/frailty, relative to the volatility. The relationship between these variables is mostly linear** (except for Finnish and Dutch ASW), which means that these three coefficients tend to rise "in proportion" one compared to each other.

We also take a look at the relationship between the market reaction S_i and the shock intensity $R_{i,j}$. In particular assuming a regime of maximum volatility for $\hat{h}$, Graph 159 shows that S_i is sharply rising when $R_i < 1\%$. In this case too, the acceleration of the market reaction is highly non-linear, though this time the acceleration takes (more or less) the shape of a logarithmic function.

Graph 159. Market reaction S_i as a function of the shock intensity R_i, and assuming a regime of extreme volatility for $\hat{h}$

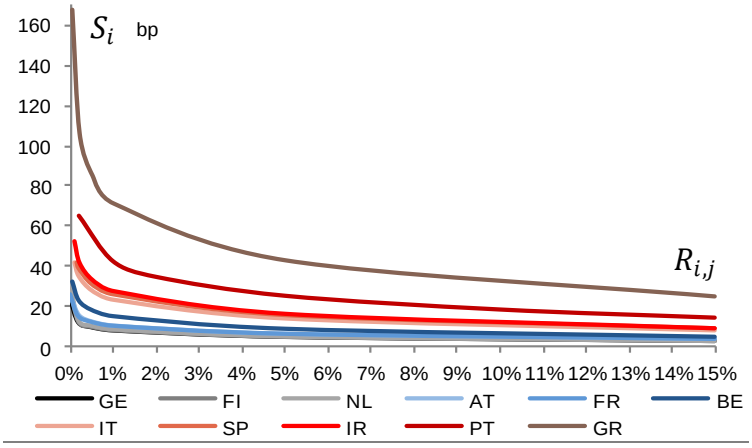

Let us now explore the dynamics of the market reaction and the frailty on a cross-country basis. **Considering the worst case scenario, we now compare the coefficients $S_{i,max}(\hat{h})$, $R_{i,max}(\hat{h})$, $W_{i,max}(\hat{h})$ under a scenario of extreme volatility, ie. when $\hat{h} = \hat{h}_{max}$** for the different countries (ie. when i varies).

In Graph 160 and Graph 161 first, we plot the maximum expected market reaction $S_{i,max}(\hat{h}_{max})$ and the maximum expected frailty $W_{i,max}(\hat{h}_{max})$, against the corresponding volatility $\hat{h}_{max}$. As the

proposed interpolation shows, the worst expected market reaction and the biggest frailty follow a quadratic dynamics when the underlying volatility $\hat{h}_{i,max}$ rises. R-squared are very high, suggesting that the relationship makes sense. **This time again, the polynomial dimension illustrates the non-linear acceleration in $S_{i,max}(\hat{h}_{max})$ and $W_{i,max}(\hat{h}_{max})$, which is particularly visible when the expected volatility $\hat{h}_{max}$ is larger than $12bp/day$. Irish, Portuguese and Greek ASW, on that basis, look particularly affected by this parabolic escalation of the risk propagation.**

In fact in practice, it appears that the polynomial interpolation also holds when the volatility is not at its climax. For any realisation $x_{i,t}$ in the data for instance, the following interpolation is acceptable:

$$\tilde{S}_{i,t} = b_{2,t} \times \hat{h}(x_{i,t})^2 + b_{1,t} \times \hat{h}(x_{i,t}) + b_{0,t} \quad (64)$$

Where i refers to the country.

Graph 162 for instance shows the interpolated line at the specific date of 1 December 2011. In this formulation, every day provides its own set of variables $\{b_{0,t}, b_{1,t}, b_{2,t}\}$.

For any point $x_{i,t}$ in the sample we are now left with two different formulations of the expected market reaction S_i:

$$\begin{cases} \tilde{S}_i^1 = \mathrm{a}_2 \hat{F}(x_{i,t})^2 + a_1 \hat{F}(x_{i,t}) + a_0 \\ \tilde{S}_{i,t}^2 = b_{2,t} \times \hat{h}(x_{i,t})^2 + b_{1,t} \times \hat{h}(x_{i,t}) + b_{0,t} \end{cases}$$ respectively taken from both eq. (58) and eq. (64)

In terms of rationale, $\tilde{S}_i^1$ is very different from $\tilde{S}_{i,t}^2$. On one side, $\tilde{S}_{i,t}^2$ is an estimate of the market reaction in light of the whole spread complex, which means that $\tilde{S}_{i,t}^2$ is based on the multivariate dynamics of the data, and this dynamics, illustrated by $\{b_{0,t}, b_{1,t}, b_{2,t}\}$, is only valid at time t. In contrast to $\tilde{S}_{i,t}^2$, $\tilde{S}_i^1$ is time-invariant (a_0, a_1, a_2 are unchanged as time goes by) and involves only idiosyncratic information about country i: every country has its own set of parameters $\{a_0, a_1, a_2\}$.

➔ **We can therefore think of $\tilde{S}_i^1$ as a long-term intrinsic estimate of the market reaction S_i. In contrast, $\tilde{S}_{i,t}^2$ is a short-term fair value of S_i, which largely depends on the market sentiment in place at time t.** Since contagion is a temporary factor that may take investors by surprise, we can suppose that $\tilde{S}_{i,t}^2$ is faster to react to contagion. This is also reinforced by the fact that contagion is supposed to be more stringent in peripheral countries, something that $\tilde{S}_{i,t}^2$ should capture as its calculation involves the cross market dynamics. **In the end, $\tilde{S}_{i,t}^2$ can be seen as a reference for detecting contagion. Persistent contagion in particular should encourage $\tilde{S}_i^1$ to move towards the more reactive $\tilde{S}_{i,t}^2$.**

Graph 160. Max reaction $S_{i,max}$ vs max volatility $\hat{h}_{max}$

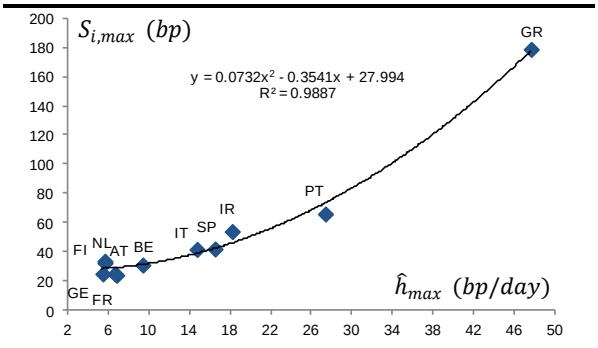

Graph 161. Max frailty $W_{i,max}$ vs max volatility $\hat{h}_{max}$

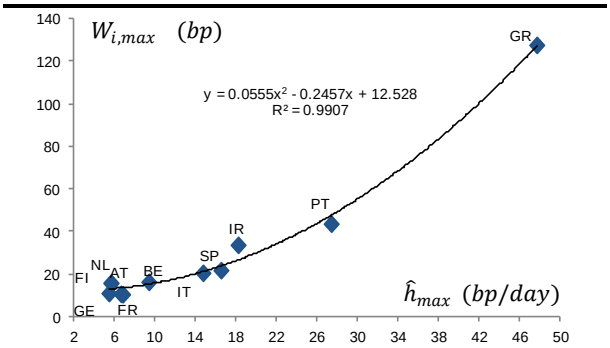

Graph 162. Quadratic relationship between S_i and h, at a specific date t (1 Dec 2011)

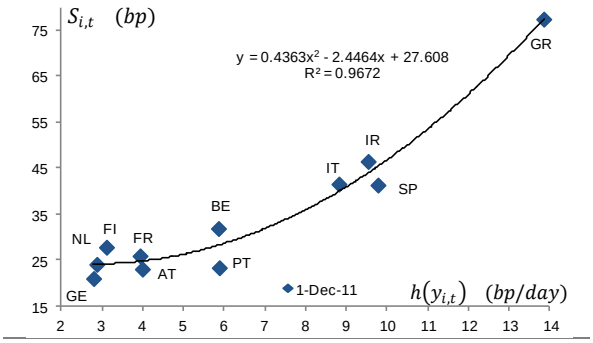

Graph 163. Max frailty $W_{i,max}$ vs max reaction $S_{i,max}$

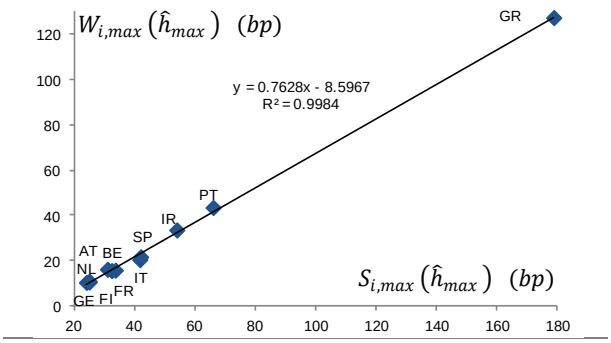

In Graph 163, we also plot the maximum frailty $W_{i,max}(\hat{h}_{max})$ against the maximum market reaction $S_{i,max}(\hat{h}_{max})$. As the interpolation shows, there is apparently a linear relationship between $S_{i,max}$ and $W_{i,max}$, that we formalize as:

$$S_{i,max}(\hat{h}_{max}) = A_{max} S_{i,max}(\hat{h}_{max}) + B_{max} \tag{65}$$

➔ **The relationship revealed in Graph 160, Graph 161, Graph 163 is a meaningful innovation. As we show in the next paragraph, there is no particular mathematical constraint in our methodology that could justify these observations. This suggests that the linear ordering reflects intrinsic features of sovereigns. The linear relationship between $W_{i,max}(\hat{h}_{max})$ and $S_{i,max}(\hat{h}_{max})$ is meaningful as it indicates that sovereigns altogether can be seen as following the same dynamics, when we look at the deterioration of the credit robustness implied by a shock in the worst case scenario.**

Considering a shock of maximal intensity ($R_{i,max}$), the frailty $W_{i,max}$ is a linear function of the market reaction $S_{i,max}$ (see eq. (57): $W_{i,max}(\hat{h}) = S_i(\hat{h}) - S_i(\hat{F}(x_i) = 0.5)$), with a slope coefficient equal to 1. For all the countries $\{GE, FI, \ldots, GR\}$, we therefore have the following relationship - in its general form on the left, and in the specific case of an extreme volatility $\hat{h} = \hat{h}_{max}$ on the right:

$$\begin{cases} W_{GE,max}(\hat{h}) = S_{GE}(\hat{h}) + B_{GE} \\ W_{FI,max}(\hat{h}) = S_{FI}(\hat{h}) + B_{FI} \\ \vdots \quad \vdots \quad \vdots \\ W_{GR,max}(\hat{h}) = S_{GR}(\hat{h}) + B_{GR} \end{cases} \rightarrow\rightarrow \begin{cases} W_{GE,max}(\hat{h}_{max}) = S_{GE,max}(\hat{h}_{max}) + B_{GE} \\ W_{FI,max}(\hat{h}_{max}) = S_{FI,max}(\hat{h}_{max}) + B_{FI} \\ \vdots \quad \vdots \quad \vdots \\ W_{GR,max}(\hat{h}_{max}) = S_{GE,max}(\hat{h}_{max}) + B_{GR} \end{cases} \tag{66}$$

Graph 163 also shows that there is a linear relationship that relates $W_{i,max}(\hat{h}_{max})$ to $S_{i,max}(\hat{h}_{max})$ for all countries i; with **a common intercept, equal to $-8.6bp$**. As a consequence we can write that:

$$W_{i,max}(\hat{h}_{max}) = S_{i,max}(\hat{h}_{max}) + B \quad \text{with } B = -8.6 \text{ for } i = \{GE, FI, NL, \dots, GR\}$$

We see two possible meanings behind this linear relationship:

- A) Either the linear behaviour between $W_{i,max}(\hat{h}_{max})$ and $S_{i,max}(\hat{h}_{max})$ comes from some "mathematical constraints" implied by the analytical formulation of the problem. **In this case the linear relationship is not a proper innovation, this is just a natural consequence of our assumptions.** And in this case we should have:

$$B_{GE} = B_{FI} = B_{NL} = B_{AT} = B_{FR} = B_{BE} = B_{IT} = B_{SP} = B_{IR} = B_{PT} = B_{GR} = B = -8.6 \qquad (67)$$

- B) Or the linear relationship is a fortuitous conclusion with no mathematical foundation. In this case the linear behaviour is worth to highlight as it suggests that all sovereigns adhere to the same dynamics when we look at the detrimental effect of financial shocks in the worst case scenario. In this case, the linear behaviour in Graph 163 reveals an intrinsic feature of sovereigns. **This would constitute a proper innovation for those who want to explore sovereign risk in general.**

In order to conclude on the relevance of the linear relationship between $W_{i,max}(\hat{h}_{max})$ and $S_{i,max}(\hat{h}_{max})$, we plot $W_{i,max}(\hat{h})$ against $S_{i,max}(\hat{h})$ in Graph 164 and Graph 165. We also add the points $\{W_{i,max}(\hat{h}_{max}); S_{i,max}(\hat{h}_{max})\}$ as blue diamonds, as well as the linear curve obtained in Graph 163 as a dark dashed line.

Graph 164. Frailty $W_{i,max}$ vs. the market reaction $S_{i,max}$

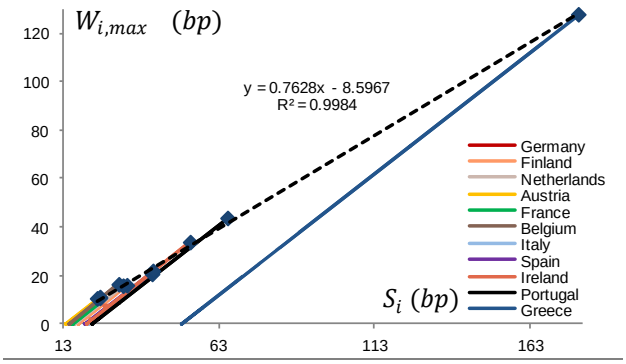

Graph 165. Frailty $W_{i,max}$ vs. the market reaction S_i

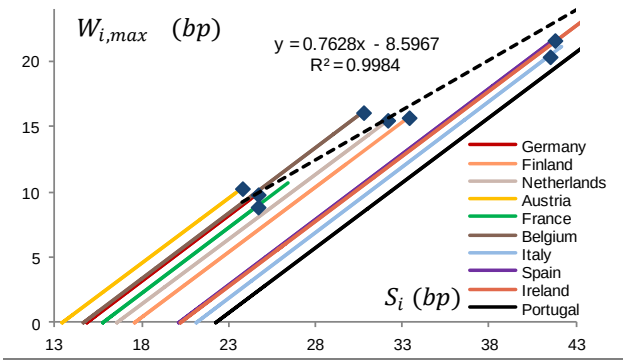

The first observation is that the linear relationship between $W_{i,max}(\hat{h})$ and $S_{i,max}(\hat{h})$ is very much explicit now, with the corresponding curves parallel to each other. **But they do not overlap, showing that the assumption in eq. (67) is not verified.**

Plus it is clear now that the linear relationship between $W_{i,max}(\hat{h}_{max})$ and $S_{i,max}(\hat{h}_{max})$ is different and independent from the linear relationship that binds $W_{i,max}(\hat{h})$ to $S_{i,max}(\hat{h})$. **As a result, the relationship between $W_{i,max}(\hat{h}_{max})$ and $S_{i,max}(\hat{h}_{max})$ is not due to a mathematical constraint.** This is coherent with the fact that $\{S_{i,max}(\hat{h}_{max})\}$ in Table 34 were arbitrarily calculated,

independently of one another. ➔ **The linear relationship between $W_{i,max}(\hat{h}_{max})$ and $S_{i,max}(\hat{h}_{max})$ appears therefore as a fortuitous fact.**

In conclusion, we showed that $\widetilde{W}_{i,max}(\hat{h}_{max}) = 0.763 \times S_{i,max}(\hat{h}_{max}) - 8.597$ is a generalised description of the univariate frailty in the worst case scenario that holds for all countries in the sample (equation in Graph 163). This formula is very convenient to use as the only required variable is the expected market reaction $S_{i,max}(\hat{h}_{max})$, ie. the response of the asset to the shock in the "worst case scenario". **Assuming that $S_{i,max}(\hat{h}_{max})$ is the largest tolerated loss in a given portfolio, one can now deduce the expected portion $\widetilde{W}_{i,max}(\hat{h}_{max})$ that is attributable to the frailty phenomenon. The relationship in Graph 160 also helps identify the intensity of the underlying volatility in these circumstances.**

Arguably, the deterioration $W_{i,max}(\hat{h}_{max})$ that occurs for peripheral countries in Graph 163 is a linear function of $S_{i,max}(\hat{h}_{max})$: Ireland, Portugal and Greece are almost perfectly aligned on the interpolation curve. ➔ **From a risk management perspective, the general behaviour of European sovereign ASW highlighted in Graph 160 to Graph 163 help understand the trajectory of the market response to stress tests $S_{i,max}(\hat{h}_{max})$ and the corresponding frailty when the intrinsic credit robustness is facing a sharp deterioration. This can prove much interesting as to apprehend a slide in ratings for instance.**

This generalisation of the dynamics of the frailty to all countries also sheds some light on the influence of $S_{i,max}(\hat{h}_{max})$. This variable was arbitrarily set as the 1% biggest market reaction in temporal stress tests. There is still an open question on the relevance of such a definition. **In particular, we would like to observe if our findings still hold under a slightly different parameterisation of $S_{i,max}(\hat{h}_{max})$.**

The linear relationship between $W_{i,max}(\hat{h}_{max})$ and $S_{i,max}(\hat{h}_{max})$ makes possible to forecast the corresponding frailty should we decide to change the definition of $S_{i,max}(\hat{h}_{max})$. As an example, let us redefine it simply as the maximum value of the market reaction to temporal stress tests (Graph 121). Table 43 shows the new values for $S_{i,max}(\hat{h}_{max})$. These are obviously higher than in the previous definition.

Table 43. New values for $S_{i,max}$ defined as the maximum reaction to temporal stress tests – basis points

	GE	FI	NL	AT	FR	BE	IT	SP	IR	PT	GR
Maximum market reaction to Type I shock	36	59	57	31	36	40	52	56	72	117	256

Then considering the linear relationships in Graph 164 and Graph 165 between $S_{i,max}(\hat{h})$ and $W_{i,max}(\hat{h})$ we can deduce the expected frailty $W_{i,max}(\hat{h}_{max})$:

Table 44. Corresponding maximum frailty $W_{i,max}$ in basis points

	GE	FI	NL	AT	FR	BE	IT	SP	IR	PT	GR
Corresponding max frailty	21	42	41	18	20	26	31	36	52	95	205

Then comparing $\{W_{GE,max}(\hat{h}_{max}), W_{FI,max}(\hat{h}_{max}), \dots, W_{GR,max}(\hat{h}_{max})\}$ in Graph 166, **it appears that the linear behaviour between all countries is still holding** (though the coefficients have slightly changed compared to Graph 163).

Graph 166. New profile between $W_{i,max}$ and $S_{i,max}$

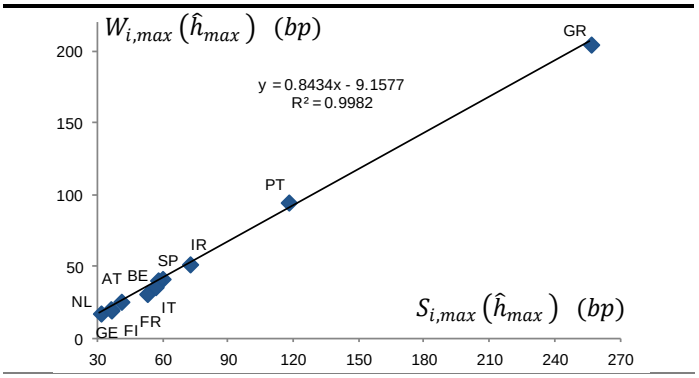

In conclusion to this section, we have rationalised the dynamics of the deterioration, in terms of credit quality, that arises from the emergence of shocks. Our approach involves two different definitions of the shock: one, temporal, is based on the market-implied probability of default; this formulation involves the GAS volatility estimator. A second definition investigates the relevance of time-invariant stress tests and finally delivers an estimator of the expected market reaction, from a more general standpoint than the temporal approach. We considered a series of many shocks with gradual intensity. The analysis offers a high degree of granularity in the results, and this proved particularly helpful to extrapolate empirical rules on the general behaviour of 1) the intrinsic volatility, 2) the market response to shocks, 3) the expected frailty hitting the credit quality.

On a cross country basis, our analysis also shows that there exists a linear trajectory amongst the different sovereigns (Graph 163), that relates the maximum market reaction to what we consider as a measure of the frailty induced by financial distress. This linear behaviour is insightful information, which was unexpected.

The multivariate contagion

Let us now take a look at contagion, from a multivariate point of view. As we note in the literature review, empirical observations show that risk aversion tends to magnify multivariate linkages between financial securities. As a result of stronger correlations, any sell-off is systematically replicated among all assets classes, even those that look normally safer or just disconnected from the fundamental source of risk aversion. This obviously can have dramatic implications in portfolios, hence the interest to explore, investigate and quantify the behaviour of multivariate cross-asset connections under intense risk aversion.

In this section we conduct a quantitative exploration of multivariate contagion between European sovereign ASW. Our approach largely involves the mulitvariate model we calibrated in Chapter 1.

We consider the same dataset as in the previous paragraphs, ie. 10Y European sovereign ASW over a history from January 2008 to end-December 2016. Let us now calibrate the corresponding bivariate distributions as described in Chapter 1. The procedure is composed of three stages: 1) **standardisation of the univariate data** using the GAS volatility, 2) calibration of the **multivariate GHT probability distribution functions**, 3) calculation of the **ADC** (Anderson-Darling criterion) and display of the **PIT** as estimators of the goodness of fit.

We conduct the calibration for each pair of ASW. As a result, ADC in Table 45 indicate that most of the calibrations are successful (ie. $ADC < 2.5$) - except for a few pairs involving Greece that prove more difficult to calibrate. The PIT also give additional insight on the quality of the calibration. For the pair "Greece-Spain" which displays a weak ADC of 2.7 for instance, the PIT in Graph 167 shows that the error essentially consists of a slight underestimate of the left wing, and an overestimate of the right wing, with just 5% of the points deviating from the expected uniform distribution. In a sense, this looks relatively acceptable. Graph 168 also shows the PIT relative to the combination "Greece-Finland" (ADC of 2.7 in Table 45). This time, the multivariate distribution is rather well calibrated, except in the upper tail which is a bit underestimated (4.5% of the points misplaced). Let us now take a look at the parameters of each distribution.

Table 45. Multivariate ADC prove outstanding, except for the pair "Greece-Ireland"

ADC		COUNTRY 1									
		FI	NL	AT	FR	BE	IT	SP	IR	PT	GR
COUNTRY 2	GE	1.7	0.9	1.4	1.8	2.4	1.6	1.8	1.9	1.6	1.8
	FI		0.9	0.9	1.1	1.9	1.8	1.8	2.8	1.2	2.7
	NL			0.8	1.7	1.6	0.9	1.3	1.4	1.4	2.6
	AT				1.0	1.0	1.1	1.8	1.6	1.1	1.0
	FR					1.3	0.9	1.0	1.2	1.2	2.3
	BE						1.1	1.2	1.8	1.3	1.2
	IT							1.1	0.4	1.1	1.2
	SP								0.9	1.2	2.7
	IR									1.7	1.6
	PT										1.7

As exposed in Chapter 1, the covariance matrix of the multivariate distributions is a correlation matrix. The corresponding coefficients, in Table 46, show that correlations are in the range $[0.53, 0.98]$.

Table 47 shows the mean vector $\mu = [\mu_1, \mu_2]$. The overall pattern is relatively similar to what we had in Chapter 1: μ is more negative for countries of a lesser credit worthiness while it remains closer to

0 for the more robust country. Pairs made of two countries with a comparable credit quality also show closer coefficients (μ_1, μ_2), like the pair $(Belgium;\ France)$ in Table 47.

Graph 167. PIT for the pair "GR-SP" (ADC=2.7)

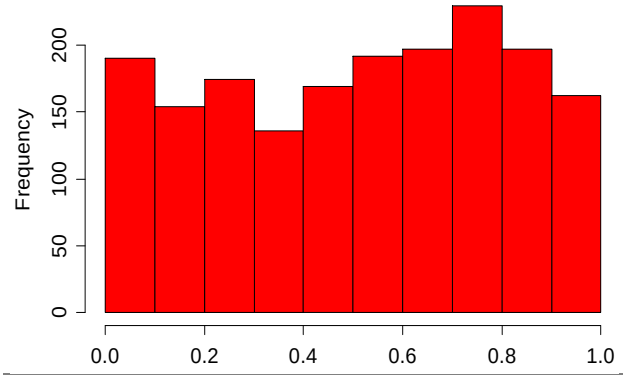

Graph 168. PIT for the pair "GR_FI" (ADC=2.1)

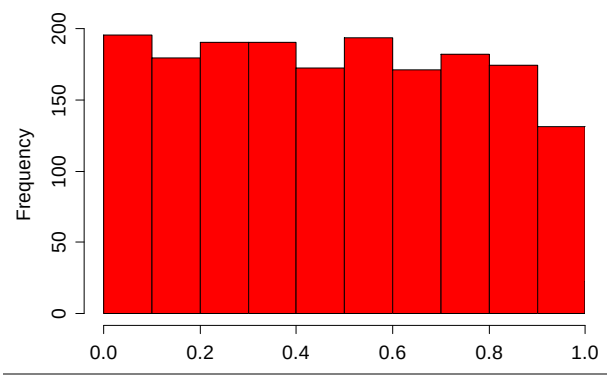

Table 46. Calibrated correlation coefficient

Σ	COUNTRY 1									
COUNTRY 2	FI	NL	AT	FR	BE	IT	SP	IR	PT	GR
GE	0.97	0.78	0.63	0.85	0.82	0.81	0.53	0.89	0.81	0.53
FI		0.91	0.77	0.63	0.72	0.87	0.90	0.77	0.98	0.90
NL			0.76	0.95	0.89	0.94	0.69	0.85	0.94	0.69
AT				0.80	0.90	0.89	0.96	0.96	0.89	0.96
FR					0.81	0.79	0.81	0.85	0.79	0.98
BE						0.81	0.81	0.86	0.83	0.82
IT							0.87	0.82	0.97	0.91
SP								0.83	0.77	0.86
IR									0.81	0.80
PT										0.81

Table 47. Mean coefficients $\mu = [\mu_1, \mu_2]$ for all pairs under study

	COUNTRY 1																			
	FI		NL		AT		FR		BE		IT		SP		IR		PT		GR	
COUNTRY 2	μ1	μ2	μ1	μ2	μ1	μ2	μ1	μ2	μ1	μ2	μ1	μ2	μ1	μ2	μ1	μ2	μ1	μ2	μ1	μ2
GE	-0.01	-0.96	-0.12	-0.67	-0.54	-0.34	-0.12	-0.55	-0.73	-0.29	-1.56	-0.07	-1.64	-0.13	-0.88	-0.32	-1.56	-0.07	-1.64	-0.13
FI			-0.16	-0.37	-0.17	-0.61	-0.49	-0.32	-0.61	-0.19	-0.94	-0.14	-0.76	-0.24	-0.49	-0.35	-1.8	-0.03	-0.76	-0.24
NL					-0.72	-0.14	-0.07	-0.69	-0.44	-0.28	-1.74	-0.06	-1.1	-0.14	-1.7	-0.1	-1.74	-0.06	-1.1	-0.14
AT							-0.96	-0.02	-0.5	-0.16	-1.1	-0.11	-1.66	-0.08	-0.48	-0.3	-1.1	-0.11	-1.66	-0.08
FR									-0.41	-0.23	-1.28	-0.08	-1.11	-0.1	-1.08	-0.1	-1.28	-0.08	-1.44	-0.14
BE											-1.11	-0.1	-1.11	-0.1	-0.16	-0.95	-1.52	-0.09	-1.34	-0.12
IT													-0.49	-0.23	-0.84	-0.05	-1.84	-0.05	-0.92	-0.11
SP															-0.71	-0.04	-0.84	-0.15	-0.46	-0.39
IR																	-0.14	-0.69	-0.96	-0.12
PT																			-1.11	-0.1

Results show that the multivariate calibration was successful for most of the pairs. Let us now explore the design and the implementation of bivariate stress tests. For better clarity, this is a short description of the different probability distribution functions involved in the calculations. These definitions are similar to Chapter 1:

- $p(x_{C1})$ and $p(x_{C2})$ are the univariate GHT distributions calibrated with the GAS method.
- $g(z_{C1})$ and $g(z_{C2})$ are the standardised versions of $p(x_{C1})$ and $p(x_{C2})$; G is the cumulative distribution.
- $q(\Sigma, \mu, z_{C1}, z_{C2})$ is the bivariate GHT distribution that we obtained using the multivariate GAS method. This distribution is no longer centred, as $\mu = [\mu_{C1}, \mu_{C2}] \neq [0,0]$. Q is the cumulative.

The multivariate analysis in Chapter 1 explores the behaviour of a standardised version of the data denoted $z = [z_{C1}, z_{C2}]$. While our approach to stress testing largely involves the corresponding multivariate distribution q, any conclusion drawn from z is dimensionless, and therefore absolutely not convenient to exploit. **As a result every result from stress tests, in the standardised frame, will be systematically converted in the (original) frame of x, ie. where the expected market reaction is expressed in basis points.** The conversion from a price variation z into a coefficient x in basis points is based on the fact that the cumulative distribution function between both variables is supposed to be conserved (ie. $F(x) = G(z)$):

$$x = z \times \hat{h}\left(\hat{F}(x)\right) = z \times \hat{h}\big(G(z)\big) \tag{68}$$

Where i relates to the country, and $\hat{h}$ is the un-temporal volatility coefficient of x.

As a first approach to multivariate stress tests, we seek to explore the market reaction on Country 2 assuming that an upfront shock has materialised on Country 1. Like in the univariate analysis, the input of the simulation is the intensity of the upfront shock, this time denoted $S1$, on $C1$. **This time again, we explore a set of shocks, with a gradual level of severity.** We adjust our definition of non-temporal stress tests in eq. (46) to the standardised dataset z_{C1}, and its corresponding distribution function g:

$$R_{C1} = \int_{S_{C1}}^{+\infty} g(z_{C1}) dz_{C1} = 1 - G(S_{C1}) \tag{69}$$

We consider the following levels of severity:

$$\{R_{C1,j}\} = \{2\%, 5\%, 10\%, 15\%, 20\%, 25\%, 30\%, 35\%, 40\%, 50\%\} \tag{70}$$

This is an arbitrary decision, and we will also consider shocks outside of this range at a later stage.

Contagion on Country 2, caused by the upfront shock $S1$ on Country 1, can actually be seen as the expected market reaction on Country 2, conditional on the realisation of $S1$. In other words, contagion can be seen as the **expectation of the random variable z_{C2}, conditional on the realisation of $S1$**. We denote this contagion coefficient as $\overline{C_d^{C2|C1}}(R_{C1})$, calculated such that:

$$\overline{C_d^{C2|C1}}(R_{C1}) = E[z_{C2}|S1] \tag{71}$$

So by definition, we have:

$$\mathbb{E}[z_{C2}|S1] = \int_{-\infty}^{+\infty} z_{C2} \times p(z_{C2}|S1)\, dz_{C2} = \overline{C_d^{C2|C1}}(R_{C1}) \tag{72}$$

On top of that we can develop $p(z_{C2}|S1)$ further:

$$P(z_{C2}|S1) = \frac{P(z_{C2} \cap S1)}{P(S1)} = \int_{S_{C1}}^{+\infty} \frac{q(\Sigma, \mu, z_{C1}, z_{C2})}{R_{C1}} dz_{C1}$$

In the end we need to calculate $\overline{C_d^{C2|C1}}$ such that:

$$\int_{-\infty}^{+\infty} z_{C2} \int_{S_{C1}}^{+\infty} \frac{q(\Sigma, \mu, z_{C1}, z_{C2})}{R_{C1}} dz_{C1}\, dz_{C2} = \mathbb{E}[z_{C2}|S1] \tag{73}$$

Graph 169. Illustration of how $\overline{C_d^{C2|C1}}$ is calculated, out of the bivariate distribution

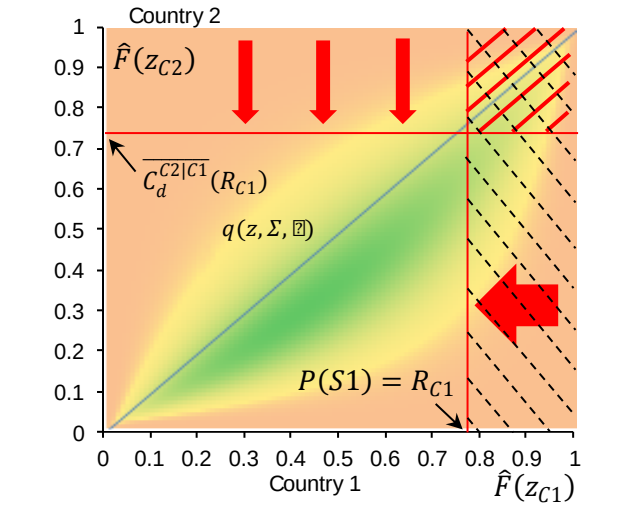

The threshold $\overline{C_d^{C2|C1}}(R_{C1})$ in Graph 169 is calculated such that the area delimited by the red lines be equal to $\overline{C_d^{C2|C1}}(R_{C1}) = E[z_{C2}|S1]$. This is a graphical interpretation of eq. (73).

As a general interpretation, we assume that contagion is emanating from the less robust countries (in terms of credit quality), and is oriented towards credits of an equivalent or a more robust credit quality. **We thus consider contagion stemming from peripheral countries towards soft-core and core countries, as well as contagion out of soft-core countries and into core countries.** On that basis, we calculate $\overline{C_d^{C2|C1}}$ for the relevant pairs. We run the simulation for the different levels of stress intensity as listed in eq. (70). In the end, and as indicated in eq. (73), $\overline{C_d^{C2|C1}}$ is a quantile of q, drawn from z_{C2} . $\overline{C_d^{C2|C1}}$, as a consequence, is a standardised measure of contagion, that we convert it into an estimator $\overline{C^{C2|C1}}$ in basis points using eq. (68).

Table 48 to Table 55 exhibit the results: each number is the expected contagion out of an upfront shock on a given sovereign ASW (Country 1), and directed towards another specific sovereign ASW (relative to Country 2). In this configuration, every column corresponds to a specific shock intensity for the upfront shock on Country 1, while lines in general show the "path" of contagion on Country 2 when the shock on Country 1 tends to intensify (when you read from right to left).

With no surprise, the global pattern of $\overline{C^{C2|C1}}$ confirms that non-core countries are exposed to larger contagion than soft-core and core countries. Portugal in particular sees the biggest reaction to any shock in general, while Ireland, Spain and Italy are clearly more resilient.

In terms of exposure/resilience, Spain, Italy and Ireland constitute an interesting pool. Spain and Italy for instance are usually perceived by market participants as credits of a relatively similar credit quality. **An observation however from our results, is that Italian ASW should see a larger market**

reaction than Spanish assets when contagion comes from Greece and Portugal. In contrast, Spanish ASW are more exposed than Italian assets to contagion from Ireland.

We mentioned earlier that Ireland shows a specific un-temporal volatility coefficient $\hat{h}$: lower and thus more stable than Italy and Spain at the centre of the distribution, but much bigger in the tails (Graph 120). Against this backdrop, Table 52 shows that Irish ASW are more robust than Spanish ASW to contagion emanating from Italy. And in the same vein, Irish ASW are more resilient than Italian assets to an upfront shock in Spain (Table 51). And when the upfront shock happens in Portugal or Greece Table 48 and Table 49 indicate that Irish ASW see a market response comparable to Spain and Italy.

In addition, Table 53 to Table 55 show contagion arising from soft-core countries and propagating into core.

Table 48. $\overline{C^{C2|C1}}$, expected contagion in basis points

R_{C1}	GREECE									
COUNTRY 2	2%	5%	10%	15%	20%	25%	30%	35%	40%	50%
GE	7	5	4	3	3	2	2	2	1	1
FI	8	6	5	4	3	3	2	2	2	1
NL	8	6	4	4	3	3	2	2	2	1
AT	14	12	11	10	9	9	8	8	7	7
FR	13	11	10	9	8	7	7	7	6	5
BE	11	8	6	5	4	3	3	2	2	2
IT	25	20	16	13	12	10	9	8	7	6
SP	21	16	12	10	8	7	6	5	4	3
IR	22	17	12	10	8	6	5	5	4	3
PT	34	26	19	15	13	11	9	8	6	5

Table 49. $\overline{C^{C2|C1}}$, expected contagion in basis points

R_{C1}	PORTUGAL									
COUNTRY 2	2%	5%	10%	15%	20%	25%	30%	35%	40%	50%
GE	7	5	4	3	3	2	2	2	1	1
FI	12	11	9	9	8	8	7	7	6	6
NL	12	10	9	8	8	7	7	6	6	6
AT	12	10	8	7	7	6	6	5	5	4
FR	12	10	9	8	7	7	6	6	5	5
BE	28	15	13	12	11	10	10	9	9	8
IT	32	27	24	22	20	19	18	17	16	15
SP	25	20	16	14	12	11	10	9	8	7
IR	31	25	20	17	15	13	12	11	10	8
GR	86	71	60	53	49	45	42	39	36	31

Table 50. $\overline{C^{C2|C1}}$, expected contagion in basis points

R_{C1}	IRELAND									
COUNTRY 2	2%	5%	10%	15%	20%	25%	30%	35%	40%	50%
GE	8	7	5	5	4	4	3	3	3	2
FI	7	5	4	3	3	2	2	2	2	1
NL	12	10	9	8	7	7	7	6	6	5
AT	11	8	7	5	5	4	3	3	3	2
FR	12	10	8	7	6	6	5	5	5	4
BE	11	8	6	4	4	3	2	2	2	1
IT	29	25	21	19	18	17	16	15	14	12
SP	37	31	28	25	24	22	21	20	19	17
PT	27	17	10	7	5	3	2	1	1	-1
GR	65	48	36	29	24	20	17	14	12	8

Table 51. $\overline{C^{C2|C1}}$, expected contagion in basis points

R_{C1}	SPAIN									
COUNTRY 2	2%	5%	10%	15%	20%	25%	30%	35%	40%	50%
GE	7	6	5	5	4	4	4	4	3	3
FI	10	8	6	5	5	4	4	3	3	3
NL	8	7	6	5	5	4	4	4	3	3
AT	14	12	10	9	9	8	8	7	7	6
FR	12	10	8	7	7	6	6	5	5	4
BE	16	13	11	10	9	8	8	7	6	6
IT	19	14	11	9	8	7	6	5	5	3
IR	17	12	9	7	5	4	4	3	2	2
PT	19	10	5	3	2	1	0	0	-1	-2
GR	65	49	37	30	25	22	19	15	14	10

Table 52. $\overline{C^{C2|C1}}$, expected contagion in basis points

R_{C1}	ITALY									
COUNTRY 2	2%	5%	10%	15%	20%	25%	30%	35%	40%	50%
GE	11	9	8	7	7	6	6	6	5	5
FI	9	8	6	6	5	5	4	4	4	3
NL	12	10	9	8	8	7	7	6	6	6
AT	12	10	8	7	7	6	6	5	5	4
FR	12	10	9	8	7	7	6	6	5	5
BE	16	13	11	10	9	8	8	7	6	6
SP	30	24	21	18	17	15	14	13	12	11
IR	27	21	17	15	13	12	10	9	8	7
PT	30	22	16	13	10	8	7	6	5	4
GR	51	34	22	15	11	8	6	4	3	1

Table 53. $\overline{C^{C2|C1}}$, expected contagion in basis points

R_{C1}	BELGIUM									
COUNTRY 2	2%	5%	10%	15%	20%	25%	30%	35%	40%	50%
GE	8	6	5	4	4	3	3	3	2	2
FI	7	6	5	4	3	3	3	2	2	2
NL	8	6	5	4	4	3	3	2	2	2
AT	11	8	7	6	5	4	4	3	3	2
FR	9	7	5	4	4	3	3	2	2	2

Table 54. $\overline{C^{C2|C1}}$, expected contagion in basis points

	R_{C1}	FRANCE 2%	5%	10%	15%	20%	25%	30%	35%	40%	50%
COUNTRY 2	GE	6	4	3	2	2	1	1	1	0	0
	FI	5	4	3	3	2	2	2	1	1	1
	NL	6	4	3	2	1	1	1	0	0	0
	AT	12	10	8	7	6	6	5	5	5	4
	BE	16	13	11	9	9	8	7	7	6	5

Table 55. $\overline{C^{C2|C1}}$, expected contagion in basis points

	R_{C1}	AUSTRIA 2%	5%	10%	15%	20%	25%	30%	35%	40%	50%
COUNTRY 2	GE	5	4	3	2	2	2	2	1	1	1
	FI	5	3	2	2	1	1	1	0	0	0
	NL	8	6	5	5	4	4	3	3	3	2
	FR	8	6	4	4	3	2	2	2	1	1
	BE	7	4	2	2	1	1	0	0	0	-1

While results look interesting overall, we also make a few odd observations. Table 48 for instance shows that an upfront shock in Greece will cause a market reaction on Portuguese ASW of $5bp$ when the severity of shock is set at $R_{C1} = 50\%$. But $R_{C1} = 50\%$ suggests that $z_{C1} = 0$ since (z_i) are standardised time series. In the same vein, contagion sometimes turned to be negative when we approach $R_{C1} = 50\%$ (like in Table 51), and this obviously looks strange. Reviewing the procedure, it appears that this is a consequence of the non-zero mean coefficients $[\mu_{C1}, \mu_{C2}]$ - which overall a pre-requisit to get satisfactory PIT and the ADC criteria in Chapter 1. In contrast, imposing $[\mu_{C1}, \mu_{C2}] = [0,0]$ makes the calibration irrelevant.

➔ **In sum we identify two consequences from having $[\mu_{C1}, \mu_{C2}] \neq [0,0]$:**

1) $[\mu_{C1}, \mu_{C2}] \neq [0,0]$ implies that $\overline{C^{C2|C1}} \neq 0$ in the equilibrium volatility regime (ie. for $R_{C1} = 50\%$). This value of contagion – reached in the equilibrium regime - can be seen as the lower bound of contagion, meant to materialise on stable market conditions.

2) Contagion may be negative as we near the equilibrium volatility regime. This is the case for instance, for Portugal in Table 50 and Table 52. This time again, this is due to the structure of the multivariate distribution. We also need to keep in mind that contagion is meant to occur on "extreme", and hence rare, events. **Contagion is thus at work in the tails of the distribution and not at the centre, so $R_{C1} = 50\%$ is not a sensible area to observe contagion anyway**. Statistical tests (ADC, PIT) indicate that the tails and the centre are both properly calibrated, which means that negative values make sense from a statistical point of view.

Looking now at the dynamics of contagion, results indicate that the market reaction $\overline{C_d^{C2|C1}}$ rises in a non-linear fashion when the severity of the shock on Country 1 increases. As an illustration, Graph 170 and Graph 171 focus on contagion emanating from Greece and Spain: contagion in these graphs follows a logarithmic dynamics. **The acceleration due to the logarithmic behaviour is particularly neat when we near the tail of the distribution** (ie. for $R_{C1} \to 0$); R-squared in the graph are compelling.

➔ **A deeper analysis shows that we can generalise this approach to the whole sample.** As a result, we formalise the algorithmic behaviour of contagion in eq. (74):

$$\overline{C_{est}^{C2|C1}(R_{C1})} = A_{C2|C1} \times \ln(R_{C1}) + B_{C2|C1} \tag{74}$$

Graph 170. Multivariate contagion from Greece

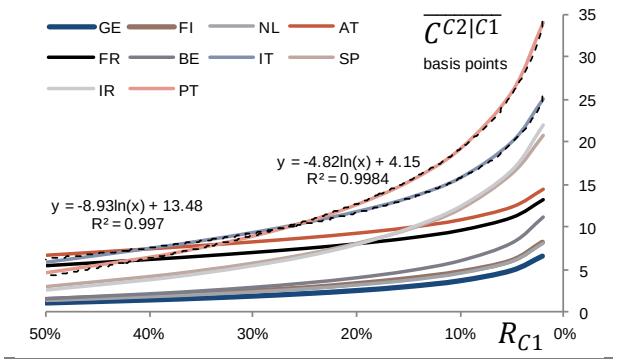

Graph 171. Multivariate contagion from Spain

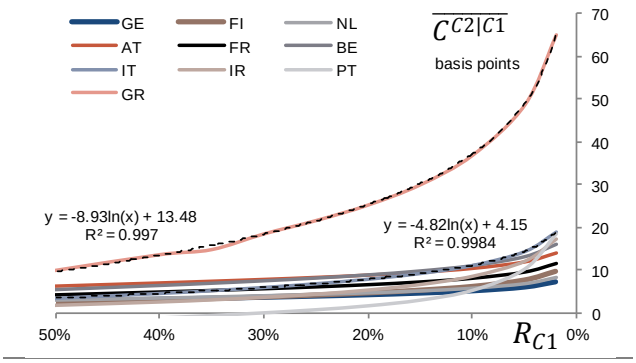

We calculate the coefficients $A_{C2|C1}$ and $B_{C2|C1}$ for each pair and we put the resulting values in Table 56 and Table 57:

Table 56. Estimated $A_{C2|C1}$ coefficients

COUNTRY 2 \ COUNTRY 1	GR	PT	IR	SP	IT	BE	FR	AT
GE	-1.7	-1.7	-1.9	-1.3	-1.9	-1.9	-1.7	-1.4
FI	-2.1	-2.0	-1.8	-2.2	-2.0	-1.7	-1.4	-1.6
NL	-2.1	-2.0	-2.0	-1.7	-2.0	-2.1	-1.8	-1.8
AT	-2.4	-2.4	-2.8	-2.4	-2.4	-2.6	-2.4	
FR	-2.3	-2.3	-2.3	-2.3	-2.3	-2.2		-2.3
BE	-3.0	-5.4	-3.1	-3.3	-3.3		-3.2	-2.4
IT	-5.9	-5.2	-5.2	-4.8				
SP	-5.6	-5.5	-5.8		-5.8			
IR	-6.1	-7.2		-4.9	-6.1			
PT	-9.3		-8.4	-6.2	-8.4			
GR		-16.6	-17.6	-17.1	-15.7			

Table 57. Estimated $B_{C2|C1}$ coefficients

COUNTRY 2 \ COUNTRY 1	GR	PT	IR	SP	IT	BE	FR	AT
GE	-0.2	-0.2	1.0	2.2	3.7	0.7	-1.2	-0.1
FI	0.0	4.7	-0.1	1.2	1.8	0.6	-0.2	-1.3
NL	-0.2	4.4	4.1	1.8	4.4	0.1	-1.5	1.1
AT	5.2	2.7	0.1	4.8	2.7	0.7	2.6	
FR	4.1	3.4	2.6	2.8	3.4	0.1		-0.8
BE	-0.7	2.8	-1.3	3.6	3.6		3.2	-2.7
IT	2.1	11.8	9.3	0.2				
SP	-0.9	3.3	14.1		7.2			
IR	-1.9	3.1		-2.3	3.0			
PT	-2.2		-8.0	-7.5	-2.9			
GR		21.2	-4.5	-2.1	-12.9			

Using eq. (74) we can now calculate the expected contagion $\overline{C^{C2|C1}}$ at any level of risk R_{C1}. This is particularly straightforward to derive an upper-bound of contagion, assuming for instance that the intensity of the upfront shock $S1$ is peaking (ie. $R_{C1} \to 0$). We already estimated the "maximum" risk intensity, denoted $R_{i,max}$ in Table 35. We adjust this notation as $R_{C1,max}$ in Table 58, and we now consider a shock $S1$ with this specific level of severity. We calculate the resulting contagion using eq. (75), that we denote $\overline{C^{C2|C1}_{est-max}}$ in Table 59

$$\overline{C^{C2|C1}_{est-max}} = A_{C2|C1} \times \ln(R_{C1,max}) + B_{C2|C1} \tag{75}$$

Table 58. $R_{C1,max}$ (same as Table 35)

	Max risk level (percentile, %)
GE	0.012
FI	0.006
NL	0.008
AT	0.037
FR	0.021
BE	0.050
IT	0.098
SP	0.155
IR	0.081
PT	0.201
GR	0.029

Table 59. Maximum contagion $\overline{C^{C2|C1}_{est-max}}$ derived from $R_{C1,max}$

COUNTRY 2 \ COUNTRY 1	GR	PT	IR	SP	IT	BE	FR	AT
GE	14	10	14	11	17	15	13	11
FI	17	17	13	15	15	14	12	11
NL	17	17	18	13	18	16	14	15
AT	25	17	20	20	19	21	23	
FR	23	18	19	18	19	17		17
BE	23	36	21	25	26		31	16
IT	50	44	46	31				
SP	45	38	56		47			
IR	48	48		29	45			
PT	73		52	33	55			
GR		124	121	108	96			

$\overline{C_{est-max}^{C2|C1}}$ **in Table 59 gives interesting insight on the asymptotic behaviour of contagion**. As a first observation, the differentiation between Greece, Portugal and the rest of peripheral countries is much more pronounced now. Contagion on Greek ASW for instance evolves in a range from $96bp$ to $124bp$. In comparison, contagion operating on Portuguese assets is significantly smaller as it evolves between $52bp$ and $73bp$. Then Italy, Spain and Ireland see relatively similar contagion, from $29bp$ to $56bp$.

Table 59 also highlights some idiosyncratic behaviours:

- A shock in Greece produces fewer contagion on Spanish than Italian ASW ($45bp$ versus $50bp$).
- Spanish ASW are more resilient to a shock in Portugal than Italian ASW are ($38bp$ versus $44bp$).
- Spanish ASW are more exposed to Irish ASW than Italian and Portuguese ASW are ($56bp$ vs. $46bp$ and $52bp$ respectively), and Irish ASW are surprisingly more resilient to contagion emanating from Spain (see the very low $29bp$) than from Italy or Portugal (as high as $48bp$ and $56bp$).
- Spain causes larger contagion on Portugal and Greece than Italy does, and Spain looks more exposed to Italy, than Italy is exposed to Spain ($47bp$ versus $31bp$).

These differences within peripheral countries largely emphasize the role of the two main parameters of the multivariate distribution. **The correlation coefficient Σ first, has great influence on the size of the tails.** Contagion out of Greece for instance is smaller into Germany than into Finland and the Netherlands. This largely reflects the lower correlation coefficient (in Table 46) for the pair "Greece-Germany".

The second parameter is the average coefficients $[\mu_{C1}, \mu_{C2}]$ which also have an influence on the shape of the tails. As Table 47 shows, a lot of combinations (especially those involving non-core countries) are quite unbalanced, with $\mu_{C1} \sim -1.50$ and $\mu_{C2} \sim 0$. This is especially the case for the pair "Portugal-Germany". In order to understand the effect of such a negative value for μ_{C1}, we made a synthetic case study on this specific pair, and we re-calculated contagion assuming that $\mu_{C1} = 0$. **As a result, contagion hitting German ASW from a shock in Portugal fell from $16bp$ to $10bp$.**

➔ **Variations in μ_{C1} in Table 47 have sizeable implications on the determination of contagion: a more pronounced gap between μ_{C1} and μ_{C2} tends to amplify the contagion phenomenon.** This relationship between the mean coefficient $[\mu_{C1}, \mu_{C2}]$ and the shape of the tails suggests that $[\mu_{C1}, \mu_{C2}] \neq [0,0]$ offers meaningful flexibility for the calibration of the tails (and not just as to identify the location of the mean).

Looking at core and soft-core countries, Table 59 shows that Germany, Finland and the Netherlands are significantly more resilient than Austria, France and Belgium. This distinction is an illustration of the structural difference between core and soft-core countries. We also make a few additional observations:

- Germany and Finland are the most resilient countries. That said, Finnish ASW look more exposed to a shock from Greece than Germany and the Netherlands are. In contrast, Finnish assets are more resilient to a shock from Ireland than German and Dutch ASW are ($13bp$ versus $14bp$ and $18bp$).

- Germany is more exposed to Italy and Portugal rather than to other non-core countries. This contrasts with Finland which is more exposed to Greece and Portugal rather than to Spain and Italy. The pattern is slightly different in the Netherlands as Dutch ASW will widen more on a shock in Ireland or Italy than on a shock in Portugal or Greece.
- In the soft-core space, Belgium is more exposed to peripheral countries than France and Austria are. Weakness is also illustrated by the large market reaction to a shock from France into Belgian ASW ($31bp$). In contrast, a shock in Belgium leads to only $17bp$ widening on French assets.
- Austrian ASW look very similar to France.

In order to understand the strength of the maximum multivariate contagion $\overline{C_{est-max}^{C2|C1}}$, in light of the equivalent univariate contagion $S_{C2,max}$, we also calculate the ratio of $\overline{C_{est-max}^{C2|C1}}$ over $S_{C2,max}$, that we name $r_{C2|C1}$ in the following equation. Table 60 shows the resulting values.

$$r_{C2|C1} = \frac{\overline{C_{est-max}^{C2|C1}}}{S_{C2,max}} \times 100$$

Table 60. Multivariate over univariate reaction ($r_{C2|C1}$, %)

COUNTRY 2 \ COUNTRY 1	GR	PT	IR	SP	IT	BE	FR	AT
GE	56	42	58	43	69	62	55	44
FI	51	51	38	45	46	41	36	34
NL	52	52	57	40	56	50	43	48
AT	103	73	83	85	80	86	95	
FR	87	67	73	67	73	64		66
BE	72	112	64	76	81		95	51
IT	119	105	110	74				
SP	107	90	133		113			
IR	90	88		54	84			
PT	112		79	50	84			
GR		70	68	61	54			

$r_{C2|C1}$ illustrates the amplitude of the multivariate contagion, in light of the underlying idiosyncratic risks. Table 60 in particular shows that a shock on Greek ASW will have more negative implications for Portugal, Italy, Spain and Austria than for other sovereigns. **For these more exposed countries, the ratio $r_{C2|C1}$ is higher than 100%: the multivariate contagion is larger than the market reaction resulting from a univariate shock of a similar intensity.**

$r_{C2|C1} > 100\%$ in essence is an illustration that contagion could have dramatic implications, sometimes even more harmful than a univariate shock. And as Table 60 shows, this is a major risk for peripheral countries.

➔ The analysis we just conducted delivered some insight on the consequences of a sudden and negative shock on Country 1's asset swap spreads, onto Country 2's. **In comparison, let us now explore the consequences of a positive shock. In particular would positive shocks incur as much (positive) contagion as a negative shock does?**

A positive shock is meant to reflect a surge in risk appetite, which naturally translates into an outperformance of the sovereign bond relative to the swap rate. **In other words, a positive shock is comparable to a sharp tightening of the asset swap spread** (ie. $x < 0$).

In the following section, we explore the implications on Country 2 of a sudden tightening of the ASW in Country 1, ie. we calculate the expected market reaction on Country 2 that would result from a positive shock on Country 1's ASW. Comparing "positive" against "negative" contagion may then deliver interesting insights.

We consider the same methodology as before. The only difference is that shocks take place in the lower tail of the multivariate distribution $q(\Sigma, \mu, z_{C1}, z_{C2})$ – ie. the $(0,0)$ corner in Graph 172. In contrast, negative shocks were located in the upper tail of q (ie. the $(1,1)$ corner in Graph 169).

We adjust the definition of R_{C1} such that:

$$R_{C1} = \int_{-\infty}^{S_{C1}} g(z_{C1}) dz_{C1} = G(S_{C1}) \tag{76}$$

As a result we have: $0 < R_{C1} < 0.5$.

We explore the same set of shocks $\{R_{C1,j}\}$ as before (eq. (70)), and we calculate the corresponding "positive contagion", denoted $\overline{C_{d-pos}^{C2|C1}}$, on a similar rationale as well:

$$\overline{C_{d-pos}^{C2|C1}}(R_{C1}) = E[P(S2|S1)] \tag{77}$$

By definition, we have:

$$\mathbb{E}[z_{C2}|S1] = \int_{-\infty}^{-\infty} z_{C2} \times P(z_{C2}|S1)\, dz_{C2} \tag{78}$$

We also adjust the expression of $p(z_{C2}|S1)$ as:

$$P(z_{C2}|S1) = \frac{P(z_{C2} \cap S1)}{P(S1)} = \int_{-\infty}^{S_{C1}} \frac{q(\Sigma, \mu, z_{C1}, z_{C2})}{R_{C1}} dz_{C1}$$

In the end, we calculate $\overline{C_{d-pos}^{C2|C1}}$ such that:

$$\int_{-\infty}^{+\infty} z_{C2} \int_{-\infty}^{S_{C1}} \frac{q(\Sigma, \mu, z_{C1}, z_{C2})}{R_{C1}} dz_{C1}\, dz_{C2} = \mathbb{E}[z_{C2}|S1] = \overline{C_{d-pos}^{C2|C1}} \tag{79}$$

Then we derive the final "positive" contagion denoted $\overline{C_{pos}^{C2|C1}}$ in basis points, using the same procedure as before.

Graph 172. Illustration of how $\overline{C_{d-pos}^{C2|C1}}$ is calculated from the bivariate distribution

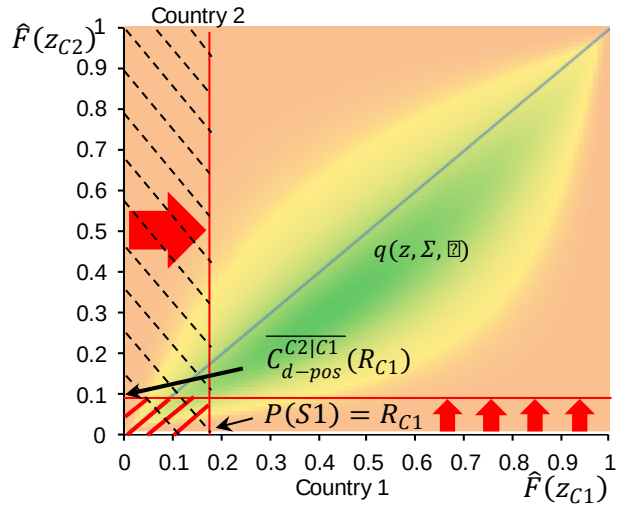

Graph 172 is a schematic interpretation of eq. (79):

The threshold $\overline{C_{d-pos}^{C2|C1}}(R_{C1})$ in Graph 172 is calculated such that the volume delimited by the red lines is equal to $\overline{C_{d-pos}^{C2|C1}}(R_{C1}) = E[z_{C2}|S1]$.

Table 61 to Table 68 show the resulting values for $\overline{C_{pos}^{C2|C1}}$ (in basis points).

Table 61. $\overline{C_{pos}^{C2|C1}}$, expected positive contagion in bp

COUNTRY 2 \ R_{C1}	2%	5%	10%	15%	20%	25%	30%	35%	40%	50%
GREECE										
GE	-3	-1	-1	-1	-1	0	0	0	0	0
FI	-2	-1	-1	0	0	0	0	0	0	0
NL	-2	-1	-1	-1	0	0	0	0	0	0
AT	-5	-3	-2	-1	-1	-1	-1	-1	-1	-1
FR	-5	-3	-2	-2	-1	-1	-1	-1	-1	-1
BE	-5	-3	-2	-1	-1	-1	-1	-1	-1	-1
IT	-17	-12	-8	-7	-5	-5	-4	-4	-3	-3
SP	-11	-7	-4	-3	-3	-2	-2	-2	-2	-1
IR	-19	-13	-9	-7	-5	-5	-4	-3	-3	-2
PT	-14	-7	-4	-3	-2	-2	-2	-1	-1	-1

Table 62. $\overline{C_{pos}^{C2|C1}}$, expected positive contagion in bp

COUNTRY 2 \ R_{C1}	2%	5%	10%	15%	20%	25%	30%	35%	40%	50%
PORTUGAL										
GE	-3	-1	-1	-1	-1	0	0	0	0	0
FI	-2	-1	-1	0	0	0	0	0	0	0
NL	-2	-1	-1	-1	0	0	0	0	0	0
AT	-5	-3	-2	-1	-1	-1	-1	-1	-1	-1
FR	-4	-2	-2	-1	-1	-1	-1	-1	-1	0
BE	-5	-3	-2	-1	-1	-1	-1	-1	-1	-1
IT	-5	-2	-1	-1	-1	-1	-1	-1	-1	0
SP	-11	-7	-4	-3	-3	-2	-2	-2	-2	-1
IR	-17	-12	-8	-6	-5	-4	-3	-3	-3	-2
GR	-21	-11	-6	-5	-4	-3	-2	-2	-2	-2

Table 63. $\overline{C_{pos}^{C2|C1}}$, expected positive contagion in bp

COUNTRY 2 \ R_{C1}	2%	5%	10%	15%	20%	25%	30%	35%	40%	50%
IRELAND										
GE	-5	-4	-3	-2	-2	-2	-1	-1	-1	-1
FI	-6	-5	-4	-3	-3	-2	-2	-2	-2	-2
NL	-11	-10	-8	-8	-7	-7	-6	-6	-6	-5
AT	-4	-2	-2	-1	-1	-1	-1	-1	-1	0
FR	-7	-4	-3	-2	-2	-2	-2	-1	-1	-1
BE	-13	-10	-8	-7	-6	-5	-5	-4	-4	-4
IT	-7	-4	-2	-2	-1	-1	-1	-1	-1	-1
SP	-5	-2	-1	-1	-1	-1	-1	-1	0	0
PT	-24	-16	-11	-8	-7	-5	-5	-4	-4	-3
GR	-54	-42	-32	-26	-22	-19	-16	-14	-13	-10

Table 64. $\overline{C_{pos}^{C2|C1}}$, expected positive contagion in bp

COUNTRY 2 \ R_{C1}	2%	5%	10%	15%	20%	25%	30%	35%	40%	50%
SPAIN										
GE	-2	-1	-1	-1	-1	0	0	0	0	0
FI	-6	-4	-3	-2	-2	-2	-2	-1	-1	-1
NL	-4	-2	-2	-1	-1	-1	-1	-1	-1	-1
AT	-3	-2	-1	-1	-1	-1	0	0	0	0
FR	-5	-3	-2	-1	-1	-1	-1	-1	-1	-1
BE	-7	-4	-3	-2	-2	-1	-1	-1	-1	-1
IT	-16	-11	-8	-7	-6	-5	-5	-4	-4	-3
IR	-13	-9	-7	-6	-5	-5	-4	-4	-4	-3
PT	-6	-3	-2	-1	-1	-1	-1	-1	-1	0
GR	-16	-9	-5	-4	-3	-3	-3	-3	-3	-2

Table 65. $\overline{C_{pos}^{C2|C1}}$, expected positive contagion in bp

R_{C1}	ITALY									
COUNTRY 2	2%	5%	10%	15%	20%	25%	30%	35%	40%	50%
GE	-3	-1	-1	-1	-1	0	0	0	0	0
FI	-4	-3	-2	-2	-1	-1	-1	-1	-1	-1
NL	-2	-1	-1	-1	0	0	0	0	0	0
AT	-5	-3	-2	-1	-1	-1	-1	-1	-1	-1
FR	-4	-2	-2	-1	-1	-1	-1	-1	-1	0
BE	-7	-4	-3	-2	-2	-1	-1	-1	-1	-1
SP	-10	-6	-4	-3	-2	-2	-1	-1	-1	-1
IR	-14	-9	-6	-5	-4	-3	-3	-2	-2	-2
PT	-17	-10	-6	-4	-3	-3	-2	-2	-2	-2
GR	-34	-33	-32	-31	-30	-29	-28	-27	-26	-25

Table 66. $\overline{C_{pos}^{C2|C1}}$, expected positive contagion in bp

R_{C1}	BELGIUM									
COUNTRY 2	2%	5%	10%	15%	20%	25%	30%	35%	40%	50%
GE	-5	-4	-3	-2	-2	-2	-2	-1	-1	-1
FI	-5	-4	-3	-2	-2	-2	-1	-1	-1	-1
NL	-7	-5	-4	-3	-3	-3	-2	-2	-2	-2
AT	-8	-6	-4	-3	-3	-2	-2	-2	-2	-1
FR	-8	-6	-4	-4	-3	-3	-2	-2	-2	-2

Table 67. $\overline{C_{pos}^{C2|C1}}$, expected positive contagion in bp

R_{C1}	FRANCE									
COUNTRY 2	2%	5%	10%	15%	20%	25%	30%	35%	40%	50%
GE	-8	-7	-5	-5	-4	-4	-4	-3	-3	-3
FI	-5	-4	-3	-2	-2	-2	-2	-2	-2	-1
NL	-7	-6	-4	-4	-3	-3	-2	-2	-2	-2
AT	-5	-3	-2	-1	-1	-1	-1	-1	-1	0
FR	-7	-4	-3	-2	-2	-1	-1	-1	-1	-1

Table 68. $\overline{C_{pos}^{C2|C1}}$, expected positive contagion in bp

R_{C1}	AUSTRIA									
COUNTRY 2	2%	5%	10%	15%	20%	25%	30%	35%	40%	50%
GE	-5	-4	-3	-2	-2	-2	-2	-2	-2	-1
FI	-8	-6	-5	-5	-4	-4	-4	-3	-3	-3
NL	-5	-3	-2	-2	-2	-1	-1	-1	-1	-1
FR	-10	-7	-6	-5	-4	-4	-4	-3	-3	-2
BE	-14	-12	-9	-8	-7	-7	-6	-6	-5	-4

This time again, we can describe the actual behaviour of contagion as a logarithmic function of R_{C1} (Graph 173 and Graph 174). We thus define a generalised estimator of positive contagion, that we denote $\overline{C_{est-pos}^{C2|C1}}$:

$$\overline{C_{est-pos}^{C2|C1}}(R_{C1}) = A_{C2|C1-pos} \times \ln(R_{C1}) + B_{C2|C1-pos} \quad (80)$$

We calculate the unknowns $A_{C2|C1-pos}$ and $B_{C2|C1-pos}$ in eq. (80), that we show in Table 69 and Table 70. Then we derive the maximum expected positive contagion as $\overline{C_{est-max-pos}^{C2|C1}} = \overline{C_{est-pos}^{C2|C1}}(R_{C1,max})$ using the same approach as in eq. (75), with $R_{C1,max}$ coming from Table 58.

Graph 173. Positive contagion from a shock in Greece

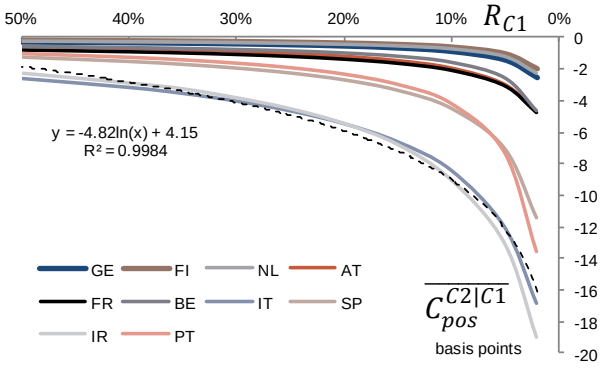

Graph 174. Positive contagion from a shock in Spain

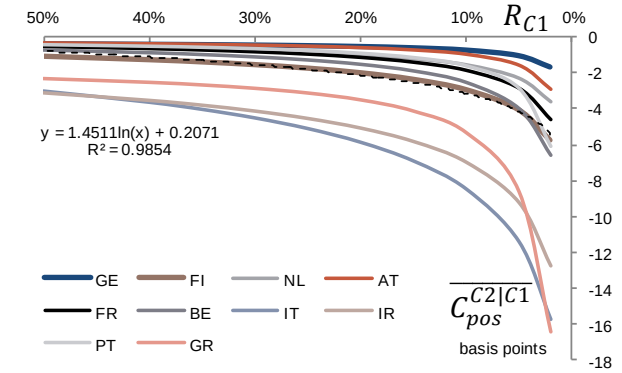

Table 69. Estimated $A_{C2|C1-pos}$ coefficients

COUNTRY 2 \ COUNTRY 1	AT	FR	BE	IT	SP	IR	PT	GR
GE	1.1	1.7	1.3	0.7	0.4	1.2	0.7	0.7
FI	1.6	1.1	1.2	1.1	1.5	1.4	0.5	0.5
NL	1.3	1.8	1.7	0.6	0.9	1.8	0.6	0.6
AT		1.3	2.0	1.3	0.7	1.1	1.3	1.3
FR	2.2		1.9	1.1	1.2	1.7	1.1	1.2
BE	3.0	1.9		1.8	1.8	3.0	1.2	1.2
IT					3.9	1.8	1.3	4.4
SP				2.8		1.2	3.1	3.1
IR				3.8	3.0		4.7	5.2
PT				4.6	1.6	6.4		3.7
GR				2.8	4.1	13.9	5.8	

Table 70. Estimated $B_{C2|C1-pos}$ coefficients

COUNTRY 2 \ COUNTRY 1	AT	FR	BE	IT	SP	IR	PT	GR
GE	-0.4	-1.5	0.0	0.4	0.0	-0.1	0.4	0.4
FI	-1.7	-0.4	0.1	0.4	0.2	-0.4	0.4	0.4
NL	0.3	-0.3	-0.3	0.4	0.3	-4.3	0.4	0.4
AT		0.8	0.4	0.6	0.5	0.6	0.6	0.6
FR	-0.9		-0.2	0.6	0.6	0.5	0.6	0.4
BE	-2.4	1.2		1.0	1.0	-1.3	0.8	0.8
IT					0.2	1.3	0.9	1.2
SP				2.1		0.9	1.8	1.8
IR				1.7	-0.6		2.3	2.3
PT				3.1	1.3	3.0		2.9
GR				-24.5	2.2	0.3	4.7	

Table 71 shows the expected maximum positive contagion $\overline{C^{C2|C1}_{est-max-pos}}$. First we recognise the same pattern as before, with a larger market reaction in peripheral countries (as Country 2), and a more contained reaction in core. We also note that the shock $S1$ has bigger implications when it occurs on a core or soft-core country rather than a peripheral country.

Table 71. $\overline{C^{C2|C1}_{est-max-pos}}$ - maximum positive contagion in basis points (red colour highlights the largest market reaction)

COUNTRY 2 \ COUNTRY 1	GR	PT	IR	SP	IT	BE	FR	AT
GE	-5	-4	-9	-3	-4	-10	-16	-9
FI	-4	-3	-10	-9	-8	-9	-10	-14
NL	-4	-3	-17	-6	-4	-13	-15	-10
AT	-10	-7	-7	-4	-8	-15	-11	
FR	-9	-6	-12	-7	-7	-14		-18
BE	-9	-7	-23	-10	-11		-15	-26
IT	-35	-7	-12	-25				
SP	-23	-17	-8		-18			
IR	-40	-27		-20	-24			
PT	-27		-43	-9	-29			
GR		-32	-99	-24	-44			

Table 72. $r_{P/N,max}$ - Positive over negative contagion in %

COUNTRY 2 \ COUNTRY 1	GR	PT	IR	SP	IT	BE	FR	AT
GE	36	35	59	24	25	66	118	83
FI	23	17	83	61	49	68	85	124
NL	26	19	92	43	20	81	112	63
AT	39	41	37	22	42	73	47	
FR	41	34	61	41	35	85		107
BE	39	19	109	42	43		49	159
IT	70	16	25	81				
SP	52	46	14		37			
IR	83	57		67	54			
PT	37		82	28	52			
GR		25	82	22	46			

In order to compare positive versus negative contagion, we also derive the ratio $r_{P/N,max} = \frac{\overline{C^{C2|C1}_{est-pos-max}}}{\overline{C^{C2|C1}_{est-max}}} * 100$. On that basis, positive contagion is lower than negative contagion when $r_{P/N,max} < 100$, and on the contrary, positive contagion is larger than negative contagion when $r_{P/N,max} > 100$. Interestingly too, a very small or a very large $r_{P/N,max}$ would illustrate significant asymmetry between positive and negative events. The colour code in Table 72 differentiates areas where positive contagion is prevailing (green cells) from domains where negative contagion is predominating (red cells).

Table 72 shows the ratio $r_{P/N,max}$. Essentially, we identify two main domains in Table 72. **Cells with a red edge first, exhibit a very low positive contagion in comparison to the negative contagion.** This dynamics for instance is prevailling for core and soft-core countries **when a "positive" shock $S1$ happens in Greece or Portugal.** In contrast to that, cells with blue edges highlight a pattern where positive contagion is larger than negative contagion. This domain still focuses on pairs involving a core and a soft-core country at the same time, especially when the shock is emanating from a soft-core country.

The difference between these two domains is an illustration of the risk aversion/risk appetite paradigm: in the red domain, the positive shock is emanating from Greece or Portugal. In this environment, investors are prompt to overweight peripheral securities as a means to take advantage of the positive momentum surrounding the positive shock. A natural consequence on financial markets is that non-core sovereign bonds tend to outperform core and soft-core securities in this environment. **Since we measure the amplitude of contagion as the performance of the asset in the post-shock environment, "positive contagion" is meant to be smaller in core than in non-core, in the event of a shock on a peripheral country. Hence the lower values in the red domain.**

In contrast to these observations, the ratio $r_{P/N,max}$ is larger in the green area (with blue edges). In this domain, a positive shock emanating from soft-core countries leads to a relatively high positive contagion compared to the equivalent contagion in the case of a negative shock. Part of that, in our opinion, reflects the greater resilience that characterises core and soft-core countries when risk aversion is mounting.

Multivariate stress tests have delivered an estimate of how much of a shock on Country 1 is supposed to propagate onto Country 2. A key feature so far is that the simulation explores the "average" implication of the shock. This is apparent in the conditional mean $\mathbb{E}[z_{C2}|S1]$ in eq. (71).

While results delivered interesting insight on the general exposure to shocks, these give little information on how the structural behaviour of the targeted country (ie. Country 2) is altered in the aftermath of the upfront shock $S1$.

In order to address this limitation, we now investigate how the robustness of a given sovereign entity is affected by the materialisation of a shock in another jurisdiction. In the univariate section, we demonstrate that the idiosyncratic volatility is a catalyst of risk aversion. This time, we seek to evaluate to what extent the materialisation of a shock in another jurisdiction make other sovereigns around more vulnerable to financial distress, and thus tends to cause a notable deterioration of the idiosyncratic robustness to shocks. **We update the simulation accordingly: we now explore the market reaction of Country 2's ASW to a series of idiosyncratic shocks $S2$, assuming that an upfront shock $S1$ already hit Country 1's ASW upstream. Tracking the market reaction on Country 2's ASW under various shock intensities for $S1$ and $S2$ should deliver insightful information on the deterioration of the credit robustness caused by contagion.**

The simulation now consists of exploring the consequence of a shock $S2$ on Country 2's ASW given that a shock $S1$ has previously materialised on a given Country 1's ASW.

First we need to define the shock $S1$ simulated on Country 1's ASW. As in the preceding paragraphs, we denote R_{C1} the intensity of this shock. **We previously considered shocks with a probability $\{R_{C1}\}$ to materialise from 0.2% to 50%.** Then we formalised the general dynamics of contagion using common interpolation methods. This finally helped derive an upper-bound on the maximum expected contagion. **We follow the same methodology this time again.**

We consider the same list of coefficients $\{R_{C1,j}\}$ as in eq. (70), and we define R_{C1} according to eq. (69):

$$R_{C1} = \int_{S_{C1}}^{+\infty} g(z_{C1}) dz_{C1} = 1 - G(S_{C1}) = P(S1)$$

Given the shock $S1$, we now simulate a shock $S2$ onto Country 2's ASW. We denote $R_{C2|C1}$ the intensity of this shock, and we consider the same set of intensities $\{R_{C2|C1,j}\}$ as for $\{R_{C1,j}\}$ (eq. (70)). **We also denote $S_{C2|C1}$ the corresponding market reaction that results from the shock $S2$: this is the variable we are after as it reflects the contagion surging from the event $S2|S1$.** By definition $R_{C2|C1}$ is the probability that $S2$ would materialize given that the shock $S1$ already happened. We can therefore formalise the calculation of $R_{C2|C1}$ as:

$$R_{C2|C1} = P(S2|S1) = \frac{P(S2 \cap S1)}{P(S1)} = \frac{P([z_{C2} > S_{C2|C1} \cap z_{C1} > S_{C1}])}{R_{C1}} = \frac{\iint_{S_{C1}}^{+\infty}\int_{S_{C2|C1}}^{+\infty} q(\Sigma, \mu, z_{C1}, z_{C2})dz}{R_{C1}} \quad (81)$$

With R_{C1} and $R_{C2|C1}$ fixed to some pre-defined levels. The only unknown to calculate in eq. (81) is $S_{C2|C1}$. In particular we calculate it using the following equality:

$$\iint_{S_{C1}}^{+\infty}\int_{S_{C2|C1}}^{+\infty} q(\Sigma, \mu, z_{C1}, z_{C2})dz = R^{II}_{C2|C1} \times R^{II}_{C1} \quad (82)$$

With $R^{II}_{C2|C1} \times R^{II}_{C1}$ illustrating the probability that the whole scenario effectively materialises.

We calculate $S_{C2|C1}$ for all the pairs in Table 72; we put the results in Table 73 to Table 137. The general dynamics in all the graphs indicates that the market reaction $S_{C2|C1}$ sharply accelerates along with the intensity of both shocks $S1$ and $S2$.

As one could expect, $S_{C2|C1}$ does not accelerate at the same pace for every pair. Considering a shock $S1$ at the 2% level on Portuguese ASW for instance, the market reaction seen on Irish ASW to a shock $S2$ increases from $31bp$ to $77bp$ (Table 91). In comparison, the corresponding market reaction on Italian ASW rises faster, from $32bp$ up to $97bp$ (Table 89).

Table 73. GE|GR – Multivariate contagion $S_{C2|C1}$ in bp

GERMANY	R_{C1} \ $R_{C2\|C1}$	GREECE 2%	5%	10%	15%	20%	25%	30%	35%	40%	50%
	2%	16	13	12	11	10	10	9	9	8	8
	5%	13	11	9	8	8	7	7	7	6	6
	10%	11	9	8	7	6	6	5	5	5	4
	15%	10	8	7	6	5	5	5	4	4	4
	20%	9	7	6	5	5	4	4	4	3	3
	25%	8	6	5	5	4	4	3	3	3	3
	30%	8	6	5	4	4	3	3	3	3	2
	35%	8	6	5	4	3	3	3	2	2	2
	40%	7	6	4	4	3	3	2	2	2	2
	50%	7	5	4	3	3	2	2	2	1	1

Table 74. FI|GR – Multivariate contagion $S_{C2|C1}$ in bp

FINLAND	R_{C1} \ $R_{C2\|C1}$	GREECE 2%	5%	10%	15%	20%	25%	30%	35%	40%	50%
	2%	17	14	12	11	11	10	10	9	9	8
	5%	14	12	10	9	9	8	8	7	7	6
	10%	12	10	9	8	7	6	6	6	5	5
	15%	11	9	8	7	6	5	5	5	4	4
	20%	10	8	7	6	5	5	4	4	4	3
	25%	10	8	6	5	5	4	4	4	3	3
	30%	9	7	6	5	4	4	4	3	3	2
	35%	9	7	6	5	4	4	3	3	3	2
	40%	9	7	5	4	4	3	3	3	2	2
	50%	8	6	5	4	3	3	2	2	2	1

Table 75. NL|GR – Multivariate contagion $S_{C2|C1}$ in bp

NETHERLANDS	R_{C1} \ $R_{C2\|C1}$	GREECE 2%	5%	10%	15%	20%	25%	30%	35%	40%	50%
	2%	16	14	12	11	10	10	9	9	9	8
	5%	14	12	10	9	8	8	7	7	7	6
	10%	12	10	8	7	7	6	6	5	5	5
	15%	11	9	7	6	6	5	5	5	4	4
	20%	10	8	7	6	5	5	4	4	4	3
	25%	9	8	6	5	5	4	4	3	3	3
	30%	9	7	6	5	4	4	3	3	3	2
	35%	9	7	5	4	4	3	3	3	2	2
	40%	8	6	5	4	4	3	3	2	2	2
	50%	8	6	4	4	3	3	2	2	2	1

Table 76. AT|GR – Multivariate contagion $S_{C2|C1}$ in bp

AUSTRIA	R_{C1} \ $R_{C2\|C1}$	GREECE 2%	5%	10%	15%	20%	25%	30%	35%	40%	50%
	2%	31	28	25	24	23	22	21	21	20	20
	5%	27	24	21	20	19	18	18	17	17	16
	10%	23	20	18	17	16	15	15	14	14	13
	15%	21	18	16	15	14	14	13	13	12	12
	20%	19	17	15	14	13	12	12	12	11	11
	25%	18	16	14	13	12	11	11	11	10	10
	30%	17	15	13	12	11	11	10	10	10	9
	35%	16	14	12	11	11	10	10	9	9	8
	40%	16	13	12	11	10	9	9	9	8	8
	50%	14	12	11	10	9	9	8	8	7	7

Table 77. FR|GR – Multivariate contagion $S_{C2|C1}$ in bp

$R_{C2\|C1}$ \ R_{C1}	GREECE 2%	5%	10%	15%	20%	25%	30%	35%	40%	50%
FRANCE 2%	32	28	24	22	21	20	19	18	17	16
5%	27	23	20	18	17	16	15	15	14	13
10%	23	19	17	15	14	14	13	12	12	11
15%	20	17	15	14	13	12	11	11	10	10
20%	19	16	14	12	12	11	10	10	9	9
25%	17	15	13	11	11	10	9	9	9	8
30%	16	14	12	11	10	9	9	8	8	7
35%	15	13	11	10	9	9	8	8	8	7
40%	15	12	11	9	9	8	8	7	7	6
50%	13	11	9	9	8	7	7	7	6	6

Table 78. BE|GR – Multivariate contagion $S_{C2|C1}$ in bp

$R_{C2\|C1}$ \ R_{C1}	GREECE 2%	5%	10%	15%	20%	25%	30%	35%	40%	50%
BELGIUM 2%	36	29	24	21	19	17	16	14	13	12
5%	29	23	19	16	14	13	12	11	10	9
10%	23	18	15	13	11	10	9	8	8	7
15%	20	15	12	11	9	8	8	7	6	5
20%	17	14	11	9	8	7	6	6	5	4
25%	15	12	9	8	7	6	5	5	4	4
30%	14	11	8	7	6	5	5	4	4	3
35%	13	10	8	6	5	5	4	4	3	3
40%	11	9	7	6	5	4	4	3	3	2
50%	11	8	6	5	4	3	3	2	2	2

Table 79. IT|GR – Multivariate contagion $S_{C2|C1}$ in bp

$R_{C2\|C1}$ \ R_{C1}	GREECE 2%	5%	10%	15%	20%	25%	30%	35%	40%	50%
ITALY 2%	65	54	45	40	36	33	31	29	27	25
5%	54	44	37	32	29	27	25	23	22	19
10%	46	37	30	27	24	22	20	19	17	15
15%	41	33	27	23	21	19	17	16	15	13
20%	37	30	24	21	19	17	15	14	13	11
25%	35	28	22	19	17	15	14	13	12	10
30%	32	26	21	18	16	14	13	11	10	9
35%	30	24	19	16	14	13	12	10	10	8
40%	29	23	18	15	13	12	11	10	9	7
50%	25	20	16	13	12	10	9	8	7	6

Table 80. SP|GR – Multivariate contagion $S_{C2|C1}$ in bp

$R_{C2\|C1}$ \ R_{C1}	GREECE 2%	5%	10%	15%	20%	25%	30%	35%	40%	50%
SPAIN 2%	47	40	35	32	30	28	26	25	24	23
5%	40	33	28	25	23	22	21	19	19	17
10%	34	28	23	21	19	17	16	15	14	13
15%	31	25	21	18	16	15	13	12	12	10
20%	29	23	19	16	14	13	12	11	10	8
25%	27	21	17	14	13	11	10	9	8	7
30%	26	20	16	13	11	10	9	8	7	6
35%	24	19	15	12	10	9	8	7	6	5
40%	23	18	14	11	10	8	7	6	5	4
50%	21	16	12	10	8	7	6	5	4	3

Table 81. IR|GR – Multivariate contagion $S_{C2|C1}$ in bp

$R_{C2\|C1}$ \ R_{C1}	GREECE 2%	5%	10%	15%	20%	25%	30%	35%	40%	50%
IRELAND 2%	49	42	36	33	31	29	28	26	25	24
5%	41	35	29	26	24	23	21	20	19	17
10%	35	29	24	21	19	18	16	15	14	13
15%	32	26	21	18	16	15	14	13	12	10
20%	30	23	19	16	14	13	12	11	10	8
25%	28	22	17	14	13	11	10	9	8	7
30%	26	20	16	13	11	10	9	8	7	5
35%	25	19	15	12	10	9	8	7	6	4
40%	24	18	14	11	9	8	7	6	5	4
50%	22	17	12	10	8	6	5	5	4	3

Table 82. PT|GR – Multivariate contagion $S_{C2|C1}$ in bp

$R_{C2\|C1}$ \ R_{C1}	GREECE 2%	5%	10%	15%	20%	25%	30%	35%	40%	50%
PORTUGAL 2%	76	65	56	51	48	45	43	42	40	37
5%	64	54	46	41	38	35	33	31	30	27
10%	55	45	38	33	30	28	26	24	23	20
15%	50	40	33	29	26	23	21	20	18	16
20%	46	37	30	26	23	20	18	17	15	13
25%	43	34	27	23	20	18	16	15	13	11
30%	41	32	25	21	18	16	14	13	11	9
35%	39	30	23	19	16	14	13	11	10	8
40%	37	28	22	18	15	13	11	10	9	7
50%	34	26	19	15	13	10	9	8	6	5

Table 73 to Table 82 show the results for $S_{C2|C1}$ assuming that a shock $S1$ happened in Greece. Results are in line with previous observations in Table 48: $S_{C2|C1}$ is larger for non-core countries. The only interesting deviation compared to what we had before is about Belgium, as the market reaction on Belgian ASW this time tends to increase faster than on French and Austrian assets ($36bp$ reaction in Belgium in the worst case scenario compared to $32bp$ and $31bp$ in French and Austrian ASW). In the worst case scenario, we also note that Spain and Ireland ($47bp$ and $49bp$) prove more resilient than Italy and Portugal ($65bp$ and $76bp$).

Table 83. GE|PT – Multivariate contagion $S_{C2|C1}$ in bp

$R_{C2\|C1}$ \ R_{C1}	PORTUGAL 2%	5%	10%	15%	20%	25%	30%	35%	40%	50%
GERMANY 2%	26	22	19	18	17	16	15	14	14	13
5%	22	18	16	15	14	13	12	12	11	11
10%	18	16	14	12	11	11	10	10	9	9
15%	16	14	12	11	10	10	9	9	8	8
20%	15	13	11	10	9	9	8	8	7	7
25%	14	12	10	9	8	8	8	7	7	6
30%	13	11	9	9	8	7	7	7	6	6
35%	12	10	9	8	7	7	7	6	6	5
40%	12	10	8	8	7	7	6	6	6	5
50%	11	9	8	7	6	6	6	5	5	4

Table 84. FI|PT – Multivariate contagion $S_{C2|C1}$ in bp

$R_{C2\|C1}$ \ R_{C1}	PORTUGAL 2%	5%	10%	15%	20%	25%	30%	35%	40%	50%
FINLAND 2%	30	26	23	21	20	19	18	17	17	16
5%	25	22	19	18	16	16	15	14	14	13
10%	21	18	16	15	14	13	13	12	12	11
15%	19	16	14	13	12	12	11	11	10	10
20%	18	15	13	12	11	11	10	10	9	9
25%	16	14	12	11	10	10	9	9	9	8
30%	15	13	11	10	10	9	9	8	8	8
35%	14	12	11	10	9	9	8	8	8	7
40%	14	12	10	9	9	8	8	8	7	7
50%	12	11	9	9	8	8	7	7	6	6

Table 85. NL|PT – Multivariate contagion $S_{C2|C1}$ in bp

$R_{C2\|C1}$ \ R_{C1}	PORTUGAL 2%	5%	10%	15%	20%	25%	30%	35%	40%	50%
NETHERLANDS 2%	35	31	27	25	23	22	21	20	19	18
5%	29	25	22	20	19	18	17	16	16	15
10%	24	20	18	16	15	14	14	13	13	12
15%	21	18	16	14	13	13	12	11	11	10
20%	19	16	14	13	12	11	11	10	10	9
25%	17	15	13	12	11	10	10	9	9	8
30%	16	14	12	11	10	9	9	9	8	8
35%	15	13	11	10	9	9	8	8	8	7
40%	14	12	10	9	9	8	8	7	7	6
50%	12	10	9	8	8	7	7	6	6	6

Table 86. AT|PT – Multivariate contagion $S_{C2|C1}$ in bp

$R_{C2\|C1}$ \ R_{C1}	PORTUGAL 2%	5%	10%	15%	20%	25%	30%	35%	40%	50%
AUSTRIA 2%	31	26	23	21	19	18	17	16	15	14
5%	26	22	19	17	15	14	14	13	12	11
10%	22	18	15	14	13	12	11	11	10	9
15%	19	16	14	12	11	10	10	9	9	8
20%	17	15	12	11	10	9	9	8	8	7
25%	16	13	11	10	9	9	8	8	7	6
30%	15	12	10	9	8	8	7	7	7	6
35%	14	12	10	9	8	7	7	6	6	5
40%	13	11	9	8	7	7	6	6	6	5
50%	12	10	8	7	7	6	6	5	5	4

Table 87. FR|PT – Multivariate contagion $S_{C2|C1}$ in bp

$R_{C2\|C1}$ \ R_{C1}	PORTUGAL 2%	5%	10%	15%	20%	25%	30%	35%	40%	50%
FRANCE 2%	33	28	24	22	20	19	18	17	16	15
5%	27	23	20	18	16	15	15	14	13	12
10%	23	19	16	15	14	13	12	11	11	10
15%	20	17	14	13	12	11	11	10	10	9
20%	18	15	13	12	11	10	9	9	9	8
25%	17	14	12	11	10	9	9	8	8	7
30%	16	13	11	10	9	9	8	8	7	7
35%	15	12	10	9	9	8	7	7	7	6
40%	14	12	10	9	8	7	7	7	6	6
50%	12	10	9	8	7	7	6	6	5	5

Table 88. BE|PT – Multivariate contagion $S_{C2|C1}$ in bp

$R_{C2\|C1}$ \ R_{C1}	PORTUGAL 2%	5%	10%	15%	20%	25%	30%	35%	40%	50%
BELGIUM 2%	38	36	34	33	32	31	31	30	30	29
5%	34	31	28	27	26	25	25	24	24	23
10%	31	27	24	23	22	21	20	19	19	18
15%	29	25	22	20	19	18	17	17	16	15
20%	28	24	21	19	17	16	15	15	14	13
25%	27	23	19	17	16	15	14	13	13	11
30%	26	22	18	16	15	14	13	12	11	10
35%	26	21	17	15	14	13	12	11	10	9
40%	25	20	17	14	13	12	11	10	9	8
50%	28	15	13	12	11	10	10	9	9	8

Table 89. IT|PT – Multivariate contagion $S_{C2|C1}$ in bp

$R_{C2\|C1}$ \ R_{C1}	PORTUGAL 2%	5%	10%	15%	20%	25%	30%	35%	40%	50%
ITLAY 2%	97	81	68	61	56	52	49	46	44	40
5%	79	66	56	50	46	43	40	38	36	33
10%	65	54	46	41	38	35	33	32	30	27
15%	57	47	40	36	34	31	30	28	27	24
20%	51	43	36	33	30	28	27	25	24	22
25%	46	39	33	30	28	26	25	23	22	21
30%	43	36	31	28	26	24	23	22	21	19
35%	39	33	29	26	24	23	21	20	20	18
40%	37	31	27	24	23	21	20	19	18	17
50%	32	27	24	22	20	19	18	17	16	15

Table 90. SP|PT – Multivariate contagion $S_{C2|C1}$ in bp

$R_{C2\|C1}$ \ R_{C1}	PORTUGAL 2%	5%	10%	15%	20%	25%	30%	35%	40%	50%
SPAIN 2%	65	55	48	44	41	38	36	35	33	31
5%	53	44	38	35	32	30	29	27	26	23
10%	45	38	32	29	26	25	23	22	21	18
15%	40	33	28	25	23	21	20	19	18	16
20%	36	30	25	23	21	19	18	17	16	14
25%	34	28	23	20	19	17	16	15	14	12
30%	31	26	21	19	17	16	15	14	13	11
35%	30	24	20	17	16	15	13	12	11	10
40%	28	23	18	16	15	13	12	11	10	9
50%	25	20	16	14	12	11	10	9	8	7

Table 91. IR|PT – Multivariate contagion $S_{C2|C1}$ in bp

IRELAND $R_{C2\|C1}$ \ PORTUGAL R_{C1}	2%	5%	10%	15%	20%	25%	30%	35%	40%	50%
2%	77	64	54	48	44	41	38	36	34	31
5%	64	53	44	39	36	33	31	29	27	24
10%	54	44	37	32	29	27	25	23	22	19
15%	49	40	33	29	26	23	22	20	19	16
20%	45	36	30	26	23	21	19	18	16	14
25%	42	33	27	24	21	19	17	16	15	13
30%	39	31	25	22	19	17	16	14	13	11
35%	37	29	24	20	18	16	15	13	12	10
40%	35	28	22	19	17	15	13	12	11	9
50%	31	25	20	17	15	13	12	10	9	8

Table 92. GR|PT – Multivariate contagion $S_{C2|C1}$ in bp

GREECE $R_{C2\|C1}$ \ PORTUGAL R_{C1}	2%	5%	10%	15%	20%	25%	30%	35%	40%	50%
2%	295	240	198	174	157	143	133	123	115	102
5%	235	192	159	139	126	115	106	99	93	82
10%	190	155	129	113	102	94	87	81	76	67
15%	164	134	111	98	88	81	75	70	66	58
20%	145	119	99	87	79	72	67	62	59	52
25%	131	107	89	79	71	65	61	57	53	47
30%	119	98	81	72	65	60	55	52	49	43
35%	109	89	75	66	60	55	51	48	45	40
40%	100	82	69	61	55	51	47	44	41	37
50%	86	71	60	53	49	45	42	39	36	31

Table 83 to Table 92 show the dynamics of the exposure to a shock in Portugal. This time again, we can recognise roughly the same pattern as in Table 49, in terms of resilience/exposure to risk aversion. A few variations are of interest: while Table 49 suggests that contagion is more intense on Belgian ASW than in Spain, the market reaction this time rises much faster on Spanish ASW when $R_{C1} \to 2\%$ and $R_{C2|C1} \to 2\%$ (Table 90). The market reaction on French ASW is also quite similar to Belgian assets in the worst case scenario ($33bp$ versus $38bp$). This was not the case in Table 49.

Table 93. GE|IR – Multivariate contagion $S_{C2|C1}$ in bp

GERMANY $R_{C2\|C1}$ \ IRELAND R_{C1}	2%	5%	10%	15%	20%	25%	30%	35%	40%	50%
2%	21	18	16	14	13	13	12	11	11	10
5%	17	14	13	11	11	10	9	9	8	8
10%	15	12	10	9	9	8	8	7	7	6
15%	13	11	9	8	8	7	6	6	6	5
20%	12	10	8	7	7	6	6	5	5	4
25%	11	9	8	7	6	6	5	5	4	4
30%	10	8	7	6	6	5	5	4	4	3
35%	10	8	7	6	5	5	4	4	4	3
40%	9	7	6	5	5	4	4	4	3	3
50%	8	7	5	5	4	4	3	3	3	2

Table 94. FI|IR – Multivariate contagion $S_{C2|C1}$ in bp

FINLAND $R_{C2\|C1}$ \ IRELAND R_{C1}	2%	5%	10%	15%	20%	25%	30%	35%	40%	50%
2%	29	16	14	13	12	11	10	10	9	9
5%	22	13	11	10	9	8	8	7	7	6
10%	17	11	9	8	7	7	6	6	5	5
15%	14	9	8	7	6	6	5	5	4	4
20%	11	8	7	6	5	5	4	4	4	3
25%	10	8	6	5	5	4	4	4	3	3
30%	8	7	6	5	4	4	3	3	3	2
35%	7	7	5	4	4	3	3	3	2	2
40%	6	6	5	4	4	3	3	2	2	2
50%	7	5	4	3	3	2	2	2	2	1

Table 95. NL|IR – Multivariate contagion $S_{C2|C1}$ in bp

NETHERLANDS $R_{C2\|C1}$ \ IRELAND R_{C1}	2%	5%	10%	15%	20%	25%	30%	35%	40%	50%
2%	31	27	24	22	21	20	19	19	18	17
5%	25	22	20	18	17	16	16	15	15	14
10%	21	18	16	15	14	13	13	12	12	11
15%	19	16	14	13	12	12	11	11	10	10
20%	17	15	13	12	11	10	10	10	9	9
25%	16	14	12	11	10	10	9	9	8	8
30%	15	13	11	10	9	9	8	8	8	7
35%	14	12	10	9	9	8	8	7	7	7
40%	13	11	10	9	8	8	7	7	7	6
50%	12	10	9	8	7	7	7	6	6	5

Table 96. AT|IR – Multivariate contagion $S_{C2|C1}$ in bp

AUSTRIA $R_{C2\|C1}$ \ IRELAND R_{C1}	2%	5%	10%	15%	20%	25%	30%	35%	40%	50%
2%	21	18	16	15	14	13	12	12	11	10
5%	18	16	13	12	11	10	10	9	9	8
10%	16	13	11	10	9	8	8	7	7	6
15%	15	12	10	9	8	7	7	6	6	5
20%	14	11	9	8	7	6	6	5	5	4
25%	13	11	9	7	6	6	5	5	4	4
30%	13	10	8	7	6	5	5	4	4	3
35%	12	10	8	6	6	5	4	4	3	3
40%	12	9	7	6	5	4	4	3	3	2
50%	11	8	7	5	5	4	3	3	2	2

Table 97. FR|IR – Multivariate contagion $S_{C2|C1}$ in bp

$R_{C2\|C1}$ \ R_{C1}	IRELAND									
	2%	5%	10%	15%	20%	25%	30%	35%	40%	50%
FRANCE 2%	29	25	22	19	18	17	17	16	15	14
5%	24	21	18	16	15	14	13	13	12	11
10%	21	17	15	13	12	12	11	10	10	9
15%	18	15	13	12	11	10	10	9	9	8
20%	17	14	12	11	10	9	9	8	8	7
25%	16	13	11	10	9	8	8	7	7	6
30%	15	12	10	9	8	8	7	7	6	6
35%	14	11	10	9	8	7	7	6	6	5
40%	13	11	9	8	7	7	6	6	6	5
50%	12	10	8	7	6	6	5	5	5	4

Table 98. BE|IR – Multivariate contagion $S_{C2|C1}$ in bp

$R_{C2\|C1}$ \ R_{C1}	IRELAND									
	2%	5%	10%	15%	20%	25%	30%	35%	40%	50%
BELGIUM 2%	30	28	28	28	17	16	15	14	14	12
5%	27	28	16	14	13	12	11	11	10	9
10%	22	16	13	11	10	9	8	8	7	6
15%	19	14	11	10	9	8	7	6	6	5
20%	17	13	10	8	7	7	6	5	5	4
25%	15	12	9	7	6	6	5	4	4	3
30%	14	11	8	7	6	5	4	4	3	2
35%	13	10	7	6	5	4	4	3	3	2
40%	12	9	7	5	5	4	3	3	2	2
50%	11	8	6	4	4	3	2	2	2	1

Table 99. IT|IR – Multivariate contagion $S_{C2|C1}$ in bp

$R_{C2\|C1}$ \ R_{C1}	IRELAND									
	2%	5%	10%	15%	20%	25%	30%	35%	40%	50%
ITALY 2%	82	69	59	53	49	46	44	42	40	37
5%	67	56	48	44	40	38	36	34	32	30
10%	56	47	40	36	34	31	30	28	27	25
15%	49	41	35	32	30	28	26	25	24	22
20%	44	37	32	29	27	25	24	22	21	20
25%	41	34	29	27	24	23	22	21	20	18
30%	38	32	27	25	23	21	20	19	18	17
35%	35	30	25	23	21	20	19	18	17	16
40%	33	28	24	22	20	19	17	17	16	15
50%	29	25	21	19	18	17	16	15	14	12

Table 100. SP|IR – Multivariate contagion $S_{C2|C1}$ in bp

$R_{C2\|C1}$ \ R_{C1}	IRELAND									
	2%	5%	10%	15%	20%	25%	30%	35%	40%	50%
SPAIN 2%	90	78	69	64	60	57	55	53	51	48
5%	75	65	57	53	50	47	45	44	42	40
10%	63	55	48	44	42	40	38	37	35	33
15%	57	49	43	40	37	35	34	32	31	29
20%	52	45	39	36	34	32	31	30	28	27
25%	48	41	36	33	31	30	28	27	26	25
30%	45	39	34	31	29	28	26	25	24	23
35%	43	37	32	29	27	26	25	24	23	21
40%	40	35	30	28	26	25	23	22	22	20
50%	37	31	28	25	24	22	21	20	19	17

Table 101. PT|IR – Multivariate contagion $S_{C2|C1}$ in bp

$R_{C2\|C1}$ \ R_{C1}	IRELAND									
	2%	5%	10%	15%	20%	25%	30%	35%	40%	50%
PORTUGAL 2%	73	62	51	45	41	38	35	33	31	28
5%	59	47	38	33	29	27	24	22	21	18
10%	49	38	29	25	21	19	17	15	13	11
15%	42	33	24	20	17	14	12	11	9	7
20%	38	29	21	17	14	11	9	8	7	5
25%	34	26	18	14	11	9	7	6	5	3
30%	32	23	16	12	9	7	6	5	4	2
35%	29	21	15	11	8	6	5	3	3	1
40%	27	19	13	9	7	5	4	3	2	1
50%	27	17	10	7	5	3	2	1	1	-1

Table 102. GR|IR – Multivariate contagion $S_{C2|C1}$ in bp

$R_{C2\|C1}$ \ R_{C1}	IRELAND									
	2%	5%	10%	15%	20%	25%	30%	35%	40%	50%
GREECE 2%	149	125	106	96	88	84	79	75	71	65
5%	125	103	86	76	69	64	59	55	52	47
10%	107	86	71	62	54	51	45	42	39	34
15%	96	77	62	53	46	42	39	35	32	27
20%	89	70	56	47	42	37	33	30	27	22
25%	83	65	51	43	37	33	29	26	23	18
30%	78	60	47	39	33	29	26	23	20	16
35%	74	57	43	36	30	26	23	20	17	13
40%	70	53	41	33	28	23	21	18	15	11
50%	65	48	36	29	24	20	17	14	12	8

Table 103. GE|SP – Multivariate contagion $S_{C2|C1}$ in bp

$R_{C2\|C1}$ \ R_{C1}	SPAIN									
	2%	5%	10%	15%	20%	25%	30%	35%	40%	50%
GERMANY 2%	23	21	19	17	17	16	15	15	14	13
5%	19	17	15	14	13	13	12	12	11	10
10%	16	14	12	11	11	10	10	9	9	8
15%	14	12	11	10	9	9	8	8	8	7
20%	13	11	10	9	8	8	7	7	7	6
25%	11	10	9	8	7	7	7	6	6	5
30%	10	9	8	7	7	6	6	6	5	5
35%	10	8	7	6	6	6	5	5	5	4
40%	9	7	6	6	5	5	5	5	4	4
50%	7	6	5	5	4	4	4	4	3	3

Table 104. FI|SP – Multivariate contagion $S_{C2|C1}$ in bp

$R_{C2\|C1}$ \ R_{C1}	SPAIN									
	2%	5%	10%	15%	20%	25%	30%	35%	40%	50%
FINLAND 2%	25	21	17	15	14	13	12	12	11	10
5%	21	17	14	13	11	11	10	9	9	8
10%	17	14	12	10	9	9	8	7	7	6
15%	15	13	10	9	8	7	7	6	6	5
20%	14	11	9	8	7	7	6	6	5	5
25%	13	10	9	7	7	6	6	5	5	4
30%	12	10	8	7	6	6	5	5	4	4
35%	11	9	7	6	6	5	5	4	4	3
40%	11	9	7	6	5	5	4	4	4	3
50%	10	8	6	5	5	4	4	3	3	3

Table 105. NL|SP – Multivariate contagion $S_{C2|C1}$ in bp

$R_{C2\|C1}$ \ R_{C1}	SPAIN 2%	5%	10%	15%	20%	25%	30%	35%	40%	50%
NETHERLANDS 2%	38	21	20	19	19	18	18	13	13	12
5%	36	19	18	13	12	11	11	10	10	9
10%	19	13	12	11	10	9	9	8	8	7
15%	17	12	10	9	9	8	8	7	7	6
20%	13	11	9	8	8	7	7	6	6	5
25%	13	10	9	8	7	7	6	6	6	5
30%	11	9	8	7	7	6	6	5	5	4
35%	10	9	7	7	6	6	5	5	5	4
40%	9	8	7	6	6	5	5	4	4	4
50%	8	7	6	5	5	4	4	4	3	3

Table 106. AT|SP – Multivariate contagion $S_{C2|C1}$ in bp

$R_{C2\|C1}$ \ R_{C1}	SPAIN 2%	5%	10%	15%	20%	25%	30%	35%	40%	50%
AUSTRIA 2%	36	31	27	25	23	22	21	20	19	18
5%	30	26	22	20	19	18	17	16	16	15
10%	25	22	19	17	16	15	14	14	13	12
15%	22	19	17	15	14	13	13	12	12	11
20%	20	17	15	14	13	12	11	11	10	10
25%	19	16	14	13	12	11	11	10	10	9
30%	18	15	13	12	11	10	10	9	9	8
35%	17	14	12	11	10	10	9	9	8	8
40%	16	13	11	10	10	9	9	8	8	7
50%	14	12	10	9	9	8	8	7	7	6

Table 107. FR|SP – Multivariate contagion $S_{C2|C1}$ in bp

$R_{C2\|C1}$ \ R_{C1}	SPAIN 2%	5%	10%	15%	20%	25%	30%	35%	40%	50%
FRANCE 2%	29	25	21	20	18	18	17	16	15	14
5%	24	21	18	16	15	14	13	13	12	11
10%	20	17	15	13	12	12	11	11	10	9
15%	18	15	13	12	11	10	10	9	9	8
20%	17	14	12	11	10	9	9	8	8	7
25%	16	13	11	10	9	9	8	7	7	6
30%	15	12	10	9	8	8	7	7	7	6
35%	14	11	10	9	8	7	7	6	6	5
40%	13	11	9	8	7	7	6	6	6	5
50%	12	10	8	7	7	6	6	5	5	4

Table 108. BE|SP – Multivariate contagion $S_{C2|C1}$ in bp

$R_{C2\|C1}$ \ R_{C1}	SPAIN 2%	5%	10%	15%	20%	25%	30%	35%	40%	50%
BELGIUM 2%	36	33	30	29	29	28	28	28	28	28
5%	31	28	25	24	23	22	22	21	17	15
10%	27	23	21	20	17	18	15	17	14	12
15%	24	21	18	17	15	15	13	14	12	11
20%	23	19	17	15	14	13	12	12	11	10
25%	21	18	15	14	13	12	11	10	10	9
30%	20	17	14	13	11	11	10	9	9	8
35%	19	16	13	12	10	10	9	8	8	7
40%	18	15	12	11	10	9	8	7	7	7
50%	16	13	11	10	9	8	8	7	6	6

Table 109. IT|SP – Multivariate contagion $S_{C2|C1}$ in bp

$R_{C2\|C1}$ \ R_{C1}	SPAIN 2%	5%	10%	15%	20%	25%	30%	35%	40%	50%
ITALY 2%	89	43	37	33	31	29	28	26	25	23
5%	67	51	29	26	24	22	21	20	19	17
10%	51	28	24	21	19	18	17	15	15	13
15%	41	32	21	18	17	15	14	13	12	11
20%	34	23	19	16	15	13	12	11	10	9
25%	29	23	17	15	13	12	11	10	9	8
30%	25	20	16	13	12	11	10	9	8	6
35%	23	17	14	12	11	10	9	8	7	6
40%	18	14	13	11	10	9	8	7	6	5
50%	19	14	11	9	8	7	6	5	5	3

Table 110. IR|SP – Multivariate contagion $S_{C2|C1}$ in bp

$R_{C2\|C1}$ \ R_{C1}	SPAIN 2%	5%	10%	15%	20%	25%	30%	35%	40%	50%
IRELAND 2%	58	43	37	33	31	29	27	26	25	23
5%	43	34	28	25	23	21	20	19	18	17
10%	35	28	22	20	18	16	15	14	13	12
15%	31	24	19	16	15	13	12	11	10	9
20%	27	21	17	14	12	11	10	9	8	7
25%	25	19	15	12	11	10	9	8	7	6
30%	24	18	13	11	9	8	7	6	6	5
35%	22	16	12	10	8	7	6	5	5	4
40%	20	15	11	9	7	6	5	4	4	3
50%	17	12	9	7	5	4	4	3	2	2

Table 111. PT|SP – Multivariate contagion $S_{C2|C1}$ in bp

$R_{C2\|C1}$ \ R_{C1}	SPAIN 2%	5%	10%	15%	20%	25%	30%	35%	40%	50%
PORTUGAL 2%	74	59	48	43	39	36	33	31	29	26
5%	58	44	35	30	27	24	22	20	18	16
10%	46	34	26	22	18	16	14	12	11	9
15%	40	29	21	17	14	11	10	8	7	5
20%	35	25	17	13	10	8	7	6	5	3
25%	31	21	14	11	8	6	5	4	3	2
30%	28	19	12	8	6	5	4	3	2	1
35%	26	16	10	7	5	3	2	2	1	0
40%	23	14	8	5	4	2	2	1	0	-1
50%	19	10	5	3	2	1	0	0	-1	-2

Table 112. GR|SP – Multivariate contagion $S_{C2|C1}$ in bp

$R_{C2\|C1}$ \ R_{C1}	SPAIN 2%	5%	10%	15%	20%	25%	30%	35%	40%	50%
GREECE 2%	136	116	101	92	86	81	79	75	72	67
5%	116	97	83	75	69	63	60	56	54	49
10%	100	83	69	61	56	51	48	44	41	37
15%	91	74	61	53	48	44	39	37	34	30
20%	85	68	55	48	42	38	35	32	29	25
25%	80	63	51	43	38	34	31	28	26	22
30%	76	60	47	40	35	31	28	25	22	18
35%	72	56	44	37	32	28	25	22	20	16
40%	69	53	41	34	29	25	22	20	18	14
50%	65	49	37	30	25	22	19	15	14	10

Table 113. GE|IT – Multivariate contagion $S_{C2|C1}$ in bp

GERMANY $R_{C2\|C1}$ \ ITALY R_{C1}	2%	5%	10%	15%	20%	25%	30%	35%	40%	50%
2%	30	25	22	20	18	17	16	16	15	14
5%	25	21	18	16	15	14	13	13	12	11
10%	21	17	15	14	13	12	11	11	10	9
15%	18	15	13	12	11	10	10	9	9	8
20%	17	14	12	11	10	9	9	9	8	8
25%	15	13	11	10	9	9	8	8	7	7
30%	14	12	10	9	9	8	8	7	7	6
35%	13	11	10	9	8	8	7	7	6	6
40%	13	11	9	8	8	7	7	6	6	6
50%	11	9	8	7	7	6	6	6	5	5

Table 114. FI|IT – Multivariate contagion $S_{C2|C1}$ in bp

FINLAND $R_{C2\|C1}$ \ ITALY R_{C1}	2%	5%	10%	15%	20%	25%	30%	35%	40%	50%
2%	23	20	17	16	15	14	13	13	12	11
5%	19	16	14	13	12	11	11	10	10	9
10%	16	14	12	11	10	9	9	8	8	7
15%	15	12	10	9	9	8	8	7	7	6
20%	13	11	9	8	8	7	7	6	6	5
25%	12	10	9	8	7	6	6	6	5	5
30%	12	10	8	7	6	6	6	5	5	4
35%	11	9	8	7	6	6	5	5	5	4
40%	10	9	7	6	6	5	5	5	4	4
50%	9	8	6	6	5	5	4	4	4	3

Table 115. NL|IT – Multivariate contagion $S_{C2|C1}$ in bp

NETHERLANDS $R_{C2\|C1}$ \ ITALY R_{C1}	2%	5%	10%	15%	20%	25%	30%	35%	40%	50%
2%	35	31	27	25	23	22	20	20	19	19
5%	29	25	22	20	19	18	17	18	16	15
10%	24	20	18	16	15	14	14	13	13	10
15%	21	18	16	14	13	13	12	11	11	10
20%	19	16	14	13	12	11	11	10	10	8
25%	17	15	13	12	11	10	10	9	9	8
30%	16	14	12	11	10	9	9	9	8	8
35%	15	13	11	10	9	9	8	8	8	7
40%	14	12	10	9	9	8	8	7	7	6
50%	12	10	9	8	8	7	7	6	6	6

Table 116. AT|IT – Multivariate contagion $S_{C2|C1}$ in bp

AUSTRIA $R_{C2\|C1}$ \ ITALY R_{C1}	2%	5%	10%	15%	20%	25%	30%	35%	40%	50%
2%	31	26	23	21	19	18	17	16	16	14
5%	26	22	19	17	15	14	14	13	12	11
10%	22	18	15	14	13	12	11	11	10	9
15%	19	16	14	12	11	10	10	9	9	8
20%	17	15	12	11	10	9	9	8	8	7
25%	16	13	11	10	9	9	8	8	7	6
30%	15	12	10	9	8	8	7	7	7	6
35%	14	12	10	9	8	7	7	6	6	5
40%	13	11	9	8	7	7	6	6	6	5
50%	12	10	8	7	7	6	6	5	5	4

Table 117. FR|IT – Multivariate contagion $S_{C2|C1}$ in bp

FRANCE $R_{C2\|C1}$ \ ITALY R_{C1}	2%	5%	10%	15%	20%	25%	30%	35%	40%	50%
2%	33	28	24	22	20	19	18	17	16	15
5%	27	23	20	18	16	15	15	14	13	12
10%	23	19	16	15	14	13	12	11	11	10
15%	20	17	14	13	12	11	11	10	10	9
20%	18	15	13	12	11	10	10	9	9	8
25%	17	14	12	11	10	9	9	8	8	7
30%	16	13	11	10	9	9	8	8	7	7
35%	15	12	10	9	9	8	8	7	7	6
40%	14	12	10	9	8	7	7	7	6	6
50%	12	10	9	8	7	7	6	6	5	5

Table 118. BE|IT – Multivariate contagion $S_{C2|C1}$ in bp

BELGIUM $R_{C2\|C1}$ \ ITALY R_{C1}	2%	5%	10%	15%	20%	25%	30%	35%	40%	50%
2%	36	33	30	29	29	28	28	28	28	28
5%	31	28	25	24	23	22	28	28	17	15
10%	27	23	21	20	17	18	15	17	14	12
15%	24	21	18	17	15	15	13	14	12	11
20%	23	19	17	15	14	13	12	12	11	10
25%	21	18	15	14	13	12	11	10	10	9
30%	20	17	14	13	11	11	10	9	9	8
35%	19	16	13	12	10	10	9	8	8	7
40%	18	15	12	11	10	9	8	7	7	7
50%	16	13	11	10	9	8	8	7	6	6

Table 119. SP|IT – Multivariate contagion $S_{C2|C1}$ in bp

SPAIN $R_{C2\|C1}$ \ ITALY R_{C1}	2%	5%	10%	15%	20%	25%	30%	35%	40%	50%
2%	75	64	55	50	47	44	42	40	39	36
5%	62	53	45	41	38	35	34	32	31	28
10%	53	44	38	34	32	30	28	27	25	23
15%	47	39	34	30	28	26	24	23	22	20
20%	43	36	30	27	25	23	22	21	20	18
25%	40	33	28	25	23	21	20	19	18	16
30%	37	31	26	23	21	20	19	17	17	15
35%	35	29	24	22	20	18	17	16	15	14
40%	33	27	23	20	19	17	16	15	14	13
50%	30	24	21	18	17	15	14	13	12	11

Table 120. IR|IT – Multivariate contagion $S_{C2|C1}$ in bp

IRELAND $R_{C2\|C1}$ \ ITALY R_{C1}	2%	5%	10%	15%	20%	25%	30%	35%	40%	50%
2%	69	58	51	46	43	41	39	37	35	33
5%	57	48	41	37	34	32	30	29	27	25
10%	48	40	34	31	28	26	24	23	22	19
15%	43	35	30	27	24	23	21	20	19	16
20%	39	32	27	24	22	20	19	17	16	14
25%	36	30	25	22	20	18	17	16	14	12
30%	34	27	23	20	18	17	15	14	13	11
35%	32	26	21	18	17	15	14	13	12	10
40%	30	24	20	17	15	14	13	12	11	9
50%	27	21	17	15	13	12	10	9	8	7

Table 121. PT|IT – Multivariate contagion $S_{C2|C1}$ in bp

	R_{C1} / $R_{C2\|C1}$	ITALY 2%	5%	10%	15%	20%	25%	30%	35%	40%	50%
PORTUGAL	2%	76	65	57	51	48	45	43	41	39	37
	5%	63	53	44	40	36	34	32	30	29	27
	10%	53	43	36	32	29	26	25	23	22	19
	15%	47	38	31	27	24	22	20	19	17	15
	20%	43	34	28	24	21	19	17	16	14	12
	25%	40	32	25	21	18	16	15	13	12	10
	30%	37	29	23	19	16	14	13	11	10	8
	35%	35	27	21	17	15	13	11	10	9	7
	40%	33	25	19	16	13	11	10	8	7	6
	50%	30	22	16	13	10	8	7	6	5	4

Table 122. GR|IT – Multivariate contagion $S_{C2|C1}$ in bp

	R_{C1} / $R_{C2\|C1}$	ITALY 2%	5%	10%	15%	20%	25%	30%	35%	40%	50%
GREECE	2%	131	107	92	81	74	68	64	60	57	51
	5%	107	86	70	60	53	48	44	41	38	33
	10%	89	70	56	45	39	35	31	28	25	21
	15%	78	60	47	37	32	27	24	21	19	14
	20%	71	54	41	32	26	22	19	16	14	10
	25%	65	49	36	28	23	19	15	13	11	7
	30%	60	44	32	24	19	16	13	10	8	5
	35%	56	41	29	22	17	13	10	8	6	4
	40%	53	38	26	19	15	11	9	6	5	2
	50%	51	34	22	15	11	8	6	4	3	1

Table 93 to Table 122 show the dynamics of $S_{C2|C1}$, assuming that a shock happened in Ireland, Spain and Italy. The big picture is relatively similar to Table 50, Table 51 and Table 52. Greek ASW in particular see the largest market reaction, with $S_{C2|C1}$ rising from 65bp to $136bp$ in Graph 160, when the upfront shock is hitting Spanish assets. In comparison, the same shock on Portuguese assets leads to a smaller reaction, between $19bp$ to $74bp$ (Graph 158). The worst case scenario on Greek assets (ie. $R_{C2|C1} = 2\%$) also leads to a relatively similar market reaction when financial stress is stemming from Ireland ($149bp$ in Table 102), Spain ($136bp$ in Table 112) or Italy ($131bp$ inTable 122). This illustrates some consistency in the global methodology as Spain and Italy are somewhat comparable in terms of credit quality, while Ireland was very much exposed to credit risk during the sovereign crisis.

Considering a shock on Spanish ASW, results show that Italian, Irish and Portuguese ASW exhibit a similar market reaction $S_{C2|C1}$ on a mild shock (ie. $R_{C2|C1} = 50\%$) at $16bp$, $19bp$, and $17bp$ respectively (see Table 109, Table 110, Table 111). However, the materialisation of a shock $S2$ (ie. for $R_{C2|C1} < 50\%$) then leads to a sharp differentiation of the market reaction: contagion rises up to $74bp$ on Portuguese ASW (Table 111), $58bp$ on Irish assets (Table 110), and $89bp$ on Italian ASW (Table 109). The market reaction to the shock is therefore more severe on Italian ASW.

The pair Spain/Italy is interesting too. Italy and Spain do not exhibit the same dynamics. We already mentioned that the expected contagion on Spanish ASW, emanating from a shock on Italian ASW, is larger than the equivalent contagion onto Italian ASW in the aftermath of a shock in Spain (e.g. $30bp$ versus $19bp$ in Table 52 and Table 51 for $R_{C1} = 2\%$). In fact, this behaviour tends to reverse when the shock $S2$ comes in force: in the worst case scenario in particular, $S_{C2|C1}$ resulting from a shock $S2$ on Spanish ASW in the aftermath of a shock $S1$ on Italian assets rises to (just) $75bp$ (Table 119). In comparison, a shock $S2$ on Italian ASW in the aftermath of a shock $S1$ on Spanish assets produces a greater market reaction of 89bp (Table 109). **On that basis, the contagion induced by Spain turns to be particularly harmful to Italian ASW, when idiosyncratic market conditions tend to deteriorate in Italy.**

In core countries, $S_{C2|C1}$ tends to rise faster on Dutch ASW than on Austrian or French securities. This is especially true when the shock $S1$ occurs in Spain (Table 105): the market reaction on Dutch ASW in this case is peaking at $38bp$, while in comparison Austrian or French ASW show a smaller $36bp$ and $29bp$. We identify the same dynamics when the shock $S1$ occurs on Italian ASW: Dutch

assets are set to endure a large $35bp$ market reaction in the worst case scenario, which compares with only $31bp$ and $33bp$ for Austrian and French ASW.

With no surprise German and Finnish ASW are the most resilient assets to any shock in the Euro area. Germany for instance sees just $30bp$ reaction in the worst case scenario, on the back of a shock $S1$ on Italian ASW (Table 113).

Table 123. GE|BE – Multivariate contagion $C^{C2|C1}$ in bp

	R_{C1}	BELGIUM									
	$R_{C2\|C1}$	2%	5%	10%	15%	20%	25%	30%	35%	40%	50%
GERMANY	2%	21	17	15	14	13	12	11	11	10	9
	5%	17	14	12	11	10	9	9	8	8	7
	10%	14	12	10	9	8	8	7	7	6	6
	15%	13	11	9	8	7	7	6	6	5	5
	20%	12	10	8	7	6	6	5	5	5	4
	25%	11	9	7	6	6	5	5	4	4	4
	30%	10	8	7	6	5	5	4	4	4	3
	35%	10	8	6	5	5	4	4	4	3	3
	40%	9	7	6	5	5	4	4	3	3	2
	50%	8	6	5	4	4	3	3	3	2	2

Table 124. FI|BE – Multivariate contagion $C^{C2|C1}$ in bp

	R_{C1}	BELGIUM									
	$R_{C2\|C1}$	2%	5%	10%	15%	20%	25%	30%	35%	40%	50%
FINLAND	2%	30	17	15	14	13	12	11	11	10	10
	5%	16	14	12	11	10	9	9	8	8	7
	10%	14	11	10	9	8	7	7	7	6	6
	15%	12	10	8	8	7	6	6	6	5	5
	20%	12	9	8	7	6	6	5	5	5	4
	25%	10	8	7	6	6	5	5	4	4	3
	30%	9	8	6	6	5	5	4	4	4	3
	35%	9	7	6	5	5	4	4	3	3	3
	40%	7	7	5	5	4	4	3	3	3	2
	50%	7	6	5	4	3	3	3	2	2	2

Table 125. NL|BE – Multivariate contagion $C^{C2|C1}$ in bp

	R_{C1}	BELGIUM									
	$R_{C2\|C1}$	2%	5%	10%	15%	20%	25%	30%	35%	40%	50%
NETHERLANDS	2%	20	16	14	13	12	11	10	10	9	9
	5%	16	14	11	10	9	9	8	8	7	6
	10%	14	11	9	8	8	7	6	6	6	5
	15%	12	10	8	7	6	6	5	5	5	4
	20%	11	9	8	6	6	5	5	4	4	3
	25%	11	9	7	6	5	5	4	4	4	3
	30%	10	8	6	5	5	4	4	4	3	3
	35%	10	7	6	5	4	4	4	3	3	2
	40%	9	7	6	5	4	4	3	3	3	2
	50%	8	6	5	4	4	3	3	2	2	2

Table 126. AT|BE – Multivariate contagion $C^{C2|C1}$ in bp

	R_{C1}	BELGIUM									
	$R_{C2\|C1}$	2%	5%	10%	15%	20%	25%	30%	35%	40%	50%
AUSTRIA	2%	24	21	18	16	15	14	13	13	12	11
	5%	21	17	15	13	12	11	10	10	9	8
	10%	18	15	12	11	10	9	8	8	7	7
	15%	16	13	11	9	9	8	7	7	6	6
	20%	15	12	10	9	8	7	6	6	6	5
	25%	14	11	9	8	7	6	6	5	5	4
	30%	13	10	8	7	6	6	5	5	4	4
	35%	12	10	8	7	6	5	5	4	4	3
	40%	12	9	7	6	6	5	4	4	4	3
	50%	11	8	7	6	5	4	4	3	3	2

Table 127. FR|BE – Multivariate contagion $C^{C2|C1}$ in bp

	R_{C1}	BELGIUM									
	$R_{C2\|C1}$	2%	5%	10%	15%	20%	25%	30%	35%	40%	50%
FRANCE	2%	22	19	16	15	14	13	12	12	11	10
	5%	18	15	13	12	11	10	9	9	8	8
	10%	16	13	11	9	9	8	7	7	6	6
	15%	14	11	9	8	7	7	6	6	5	5
	20%	13	10	8	7	7	6	5	5	5	4
	25%	12	9	8	7	6	5	5	4	4	3
	30%	11	9	7	6	5	5	4	4	4	3
	35%	10	8	6	6	5	4	4	3	3	3
	40%	10	8	6	5	4	4	3	3	3	2
	50%	9	7	5	4	4	3	3	2	2	2

Table 128. GE|FR – Multivariate contagion $C^{C2|C1}$ in bp

	R_{C1}	FRANCE									
	$R_{C2\|C1}$	2%	5%	10%	15%	20%	25%	30%	35%	40%	50%
GERMANY	2%	15	13	11	10	9	8	8	8	7	7
	5%	13	10	8	7	7	6	6	5	5	5
	10%	11	8	7	6	5	5	4	4	4	3
	15%	9	7	6	5	4	4	3	3	3	2
	20%	8	6	5	4	4	3	3	2	2	2
	25%	8	6	4	4	3	3	2	2	2	1
	30%	7	5	4	3	3	2	2	2	1	1
	35%	7	5	4	3	2	2	2	1	1	1
	40%	6	5	3	3	2	2	1	1	1	1
	50%	6	4	3	2	2	1	1	1	0	0

Table 129. FI|FR – Multivariate contagion $C^{C2|C1}$ in bp

$R_{C2\|C1}$ \ R_{C1}	FRANCE 2%	5%	10%	15%	20%	25%	30%	35%	40%	50%
FINLAND 2%	19	16	14	12	11	11	10	10	9	9
5%	15	12	10	9	9	8	8	7	7	6
10%	12	10	8	7	7	6	6	5	5	5
15%	11	9	7	6	6	5	5	4	4	4
20%	10	8	6	5	5	4	4	4	3	3
25%	9	7	6	5	4	4	4	3	3	2
30%	8	6	5	4	4	3	3	3	2	2
35%	7	6	4	4	3	3	3	2	2	2
40%	7	5	4	3	3	3	2	2	2	1
50%	5	4	3	3	2	2	2	1	1	1

Table 130. NL|FR – Multivariate contagion $C^{C2|C1}$ in bp

$R_{C2\|C1}$ \ R_{C1}	FRANCE 2%	5%	10%	15%	20%	25%	30%	35%	40%	50%
NETHERLANDS 2%	15	12	11	10	9	8	8	7	7	6
5%	12	10	8	7	6	6	5	5	5	4
10%	10	8	6	5	5	4	4	3	3	3
15%	9	7	5	4	4	3	3	3	2	2
20%	8	6	5	4	3	3	2	2	2	1
25%	7	6	4	3	3	2	2	2	1	1
30%	7	5	4	3	2	2	2	1	1	1
35%	6	5	3	3	2	2	1	1	1	0
40%	6	4	3	2	2	1	1	1	1	0
50%	5	4	3	2	1	1	1	0	0	0

Table 131. AT|FR – Multivariate contagion $C^{C2|C1}$ in bp

$R_{C2\|C1}$ \ R_{C1}	FRANCE 2%	5%	10%	15%	20%	25%	30%	35%	40%	50%
AUSTRIA 2%	29	25	22	20	18	17	16	16	15	14
5%	24	21	18	16	15	14	13	12	12	11
10%	21	17	15	13	12	11	11	10	10	9
15%	18	15	13	12	11	10	9	9	9	8
20%	17	14	12	11	10	9	9	8	8	7
25%	16	13	11	10	9	8	8	7	7	6
30%	15	12	10	9	8	8	7	7	6	6
35%	14	11	10	8	8	7	7	6	6	5
40%	13	11	9	8	7	7	6	6	5	5
50%	12	10	8	7	6	6	5	5	5	4

Table 132. BE|FR – Multivariate contagion $C^{C2|C1}$ in bp

$R_{C2\|C1}$ \ R_{C1}	FRANCE 2%	5%	10%	15%	20%	25%	30%	35%	40%	50%
BELGIUM 2%	35	32	29	29	27	28	28	28	28	28
5%	30	27	24	23	22	21	20	17	16	15
10%	26	23	20	19	16	15	16	16	13	12
15%	24	20	18	16	15	14	14	13	11	10
20%	22	18	16	14	13	13	12	11	10	9
25%	21	17	15	13	12	11	11	10	9	8
30%	20	16	14	12	11	10	9	9	9	7
35%	19	15	13	11	10	9	8	8	8	7
40%	18	14	12	10	9	9	8	7	7	6
50%	16	13	11	9	9	8	7	7	6	5

Table 133. GE|AT – Multivariate contagion $C^{C2|C1}$ in bp

$R_{C2\|C1}$ \ R_{C1}	AUSTRIA 2%	5%	10%	15%	20%	25%	30%	35%	40%	50%
GERMANY 2%	18	15	13	12	11	11	10	9	9	8
5%	15	12	10	9	9	8	8	7	7	6
10%	12	10	8	7	7	6	6	5	5	5
15%	11	8	7	6	6	5	5	4	4	4
20%	9	8	6	5	5	4	4	4	3	3
25%	9	7	5	5	4	4	3	3	3	2
30%	8	6	5	4	4	3	3	3	2	2
35%	7	6	4	4	3	3	3	2	2	2
40%	7	5	4	3	3	2	2	2	2	1
50%	5	4	3	2	2	2	2	1	1	1

Table 134. FI|AT – Multivariate contagion $C^{C2|C1}$ in bp

$R_{C2\|C1}$ \ R_{C1}	AUSTRIA 2%	5%	10%	15%	20%	25%	30%	35%	40%	50%
FINLAND 2%	17	14	11	10	9	9	8	8	7	7
5%	13	11	9	8	7	6	6	5	5	5
10%	11	8	7	6	5	5	4	4	4	3
15%	10	7	6	5	4	4	3	3	3	2
20%	9	6	5	4	3	3	3	2	2	2
25%	8	6	4	3	3	2	2	2	2	1
30%	7	5	4	3	2	2	2	1	1	1
35%	7	5	3	3	2	2	1	1	1	1
40%	6	4	3	2	2	1	1	1	1	0
50%	5	3	2	2	1	1	1	0	0	0

Table 135. NL|AT – Multivariate contagion $C^{C2|C1}$ in bp

$R_{C2\|C1}$ \ R_{C1}	AUSTRIA 2%	5%	10%	15%	20%	25%	30%	35%	40%	50%
NETHERLANDS 2%	33	20	19	18	13	13	12	12	11	10
5%	26	20	13	11	11	10	9	9	9	8
10%	20	12	10	9	9	8	8	7	7	6
15%	16	13	9	8	8	7	7	6	6	5
20%	14	10	8	7	7	6	6	5	5	5
25%	12	10	8	7	6	6	5	5	5	4
30%	11	9	7	6	6	5	5	4	4	4
35%	10	8	7	6	5	5	4	4	4	3
40%	8	7	6	5	5	4	4	4	3	3
50%	8	6	5	5	4	4	3	3	3	2

Table 136. FR|AT – Multivariate contagion $C^{C2|C1}$ in bp

$R_{C2\|C1}$ \ R_{C1}	AUSTRIA 2%	5%	10%	15%	20%	25%	30%	35%	40%	50%
FRANCE 2%	19	16	14	13	12	11	11	10	10	9
5%	16	13	11	10	9	8	8	8	7	6
10%	14	11	9	8	7	7	6	6	5	5
15%	12	10	8	7	6	6	5	5	4	4
20%	11	9	7	6	5	5	4	4	4	3
25%	11	8	7	5	5	4	4	3	3	2
30%	10	8	6	5	4	4	3	3	3	2
35%	9	7	6	5	4	3	3	3	2	2
40%	9	7	5	4	3	3	3	2	2	1
50%	8	6	4	4	3	2	2	2	1	1

Table 137. BE|AT – Multivariate contagion $C^{C2|C1}$ in bp

$R_{C2\|C1}$ \ R_{C1}		AUSTRIA									
		2%	5%	10%	15%	20%	25%	30%	35%	40%	50%
BELGIUM	2%	29	28	17	15	14	13	12	11	11	10
	5%	28	16	13	11	10	9	8	7	7	6
	10%	16	12	9	8	7	6	5	5	4	4
	15%	14	10	8	6	5	4	4	3	3	2
	20%	13	9	6	5	4	3	3	2	2	2
	25%	11	8	6	4	3	3	2	2	1	1
	30%	10	7	5	4	3	2	2	1	1	1
	35%	10	6	4	3	2	2	1	1	1	0
	40%	9	6	3	2	2	1	1	1	0	0
	50%	7	4	2	2	1	1	0	0	0	-1

Table 126 to Table 137 show the market reaction to a shock $S1$ materialising in soft-core countries. The dynamics of the market reaction is in line with the general understanding in financial markets: a shock $S1$ in Belgium leads to a greater market reaction than a shock $S1$ in Austria or France would. The market reaction induced by a shock $S1$ on Belgium also tends to rise faster on Finnish ASW (from $7bp$ to $30bp$ in Table 124) than in another jurisdiction (e.g. just $21bp$ on German ASW and $20bp$ on Dutch assets, see Table 123 and Table 125). In the same vein, Dutch assets look more exposed to a shock $S1$ in Austria (the market reaction rises from $8bp$ to $33bp$ in Table 135) than in France or Belgium ($8bp$ to $20bp$ in Table 137).

Let us now formalize the general dynamics of $S_{C2|C1}$. Empirical observations show that $S_{C2|C1}$ still admits a logarithmic acceleration when the shocks $S1$ and $S2$ intensify. As a result, we consider the following formulation:

$$S^{est}_{C2|C1}(R_{C1}, R_{C2|C1}) = a_{C2|C1}.ln(R_{C2|C1}).ln(R_{C1}) + b_{C2|C1}.ln(R_{C1}) + c_{C2|C1}.ln(R_{C2|C1}) + d_{C2|C1} \quad (83)$$

This model involves four unknowns: $\{a_{C2|C1}, b_{C2|C1}, c_{C2|C1}, d_{C2|C1}\}$ that we calibrate. We put the results in Table 138 to Table 141.

R-squared in Table 142 also indicates that the chosen interpolation model provides an outstanding fit. Then Graph 176 to Graph 179 offer a view on the true value of $S_{C2|C1}$ (in red) against its estimated version $S^{est}_{C2|C1}$ (in green) that comes from the model.

Graph 175. $S_{C2|C1}$ as a function of $R_{C2|C1}$

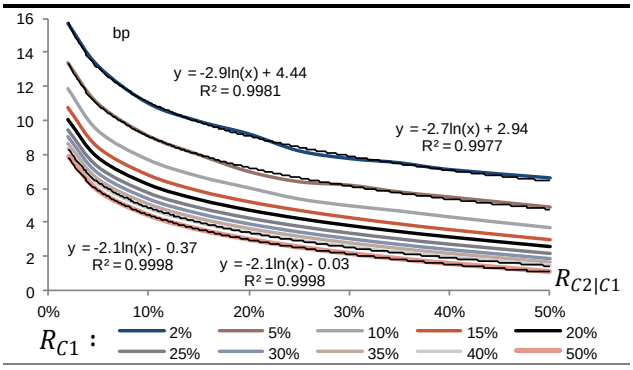

Table 138. Estimated $a_{C2|C1}$ coefficients

$a_{C2\|C1}$ \ COUNTRY 1		GR	PT	IR	SP	IT	BE	FR	AT
COUNTRY 2	GE	0.2	0.6	0.5	0.5	1.0	0.5	0.3	0.5
	FI	0.2	0.8	2.0	0.8	0.5	1.6	0.5	0.4
	NL	0.1	1.0	0.6	1.9	1.0	0.4	0.3	2.1
	AT	0.4	0.9	0.1	1.0	0.9	0.5	0.7	
	FR	0.8	1.1	0.7	0.7	1.1	0.5		0.3
	BE	1.6	-0.8	1.2	-0.2	-0.2		-0.1	1.4
	IT	2.0	4.0	2.7	6.5				
	SP	0.5	1.5	0.7		2.0			
	IR	0.6	2.0		1.5	1.6			
	PT	0.8		1.9	-0.1	1.3			
	GR		13.4	2.6	1.4	3.0			

Table 139. Estimated $b_{C2|C1}$ coefficients

$b_{C2\|C1}$	COUNTRY 1							
COUNTRY 2	GR	PT	IR	SP	IT	BE	FR	AT
GE	-1.5	-1.5	-1.6	-1.1	-1.3	-1.6	-1.5	-1.2
FI	-1.9	-1.4	0.7	-1.7	-1.6	0.2	-1.2	-1.4
NL	-1.9	-1.4	-1.7	0.2	-1.4	-1.8	-1.6	0.3
AT	-2.1	-1.8	-2.8	-1.7	-1.8	-2.3	-1.9	
FR	-1.7	-1.6	-1.8	-1.9	-1.6	-1.9		-2.1
BE	-1.5	-6.0	-2.1	-4.1	-4.1		-3.9	-1.4
IT	-4.9	-2.5	-3.3	2.2				
SP	-5.5	-4.5	-5.4		-4.5			
IR	-5.7	-6.2		-3.9	-5.1			
PT	-8.8		-7.2	-10.3	-7.5			
GR		-7.4	-16.2	-16.1	-13.9			

Table 140. Estimated $c_{C2|C1}$ coefficients

$c_{C2\|C1}$	COUNTRY 1							
COUNTRY 2	GR	PT	IR	SP	IT	BE	FR	AT
GE	-1.9	-2.2	-2.1	-2.9	-2.1	-2.0	-1.8	-2.0
FI	-2.0	-2.5	0.1	-1.7	-2.1	-0.5	-2.0	-1.8
NL	-2.0	-3.3	-3.3	-1.0	-3.3	-1.9	-1.8	-0.1
AT	-3.7	-2.5	-2.6	-2.8	-2.5	-2.3	-2.5	
FR	-2.7	-2.4	-2.5	-2.6	-2.4	-2.3		-2.3
BE	-2.2	-7.6	-2.8	-6.8	-6.8		-6.3	-1.9
IT	-4.4	-4.7	-5.5	2.0				
SP	-5.9	-6.2	-9.3		-6.2			
IR	-6.3	-5.9		-5.5	-6.8			
PT	-9.7		-8.1	-16.8	-9.4			
GR		-12.3	-16.0	-16.6	-14.4			

Table 141. Estimated $d_{C2|C1}$ coefficients

$d_{C2\|C1}$	COUNTRY 1							
GR	PT	IR	SP	IT	BE	FR	AT	
GE	-1.4	1.6	-0.5	0.3	2.2	-0.6	-2.6	-1.5
FI	-1.4	3.0	1.5	-0.2	0.3	1.4	-1.6	-2.7
NL	-1.6	1.8	1.5	1.7	1.8	-1.3	-3.0	1.9
AT	2.7	0.9	-2.0	2.9	0.9	-1.0	0.8	
FR	2.3	1.7	0.9	0.9	1.7	-1.5		-2.4
BE	-1.9	-2.4	-3.4	-2.9	-2.9		-2.8	-4.3
IT	-1.5	8.5	5.5	5.0				
SP	-5.4	-0.8	8.6		2.8			
IR	-6.6	-1.7		-6.2	-1.6			
PT	-9.3		-14.9	4.2	-9.5			
GR		12.2	-17.0	-14.0	-25.2			

Table 142. Corresponding R-squared

R^2	COUNTRY 1							
COUNTRY 2	GR	PT	IR	SP	IT	BE	FR	AT
GE	1.000	0.999	0.999	0.998	0.999	0.999	0.999	0.999
FI	0.999	0.999	0.841	0.999	0.999	0.866	0.999	0.999
NL	0.999	0.980	0.975	0.932	0.980	0.999	0.997	0.919
AT	0.999	0.999	0.998	0.998	0.999	0.999	0.999	
FR	0.999	0.999	0.999	0.999	0.999	1.000		0.999
BE	0.946	0.917	0.958	0.939	0.939		0.957	0.975
IT	0.998	0.999	0.999	0.822				
SP	0.999	0.999	0.999		0.999			
IR	0.999	0.999		0.996	0.999			
PT	0.999		0.995	0.978	1.000			
GR		0.990	0.998	0.876	0.994			

Graph 176. FR|PT – Multivariate contagion as a function of both R_{C1} and $R_{C2|C1}$

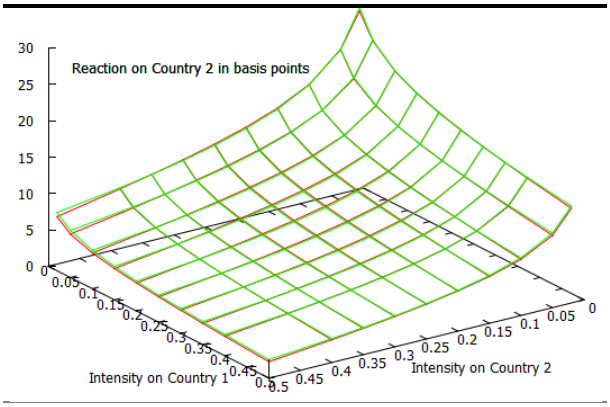

Graph 177. GE|FR– Multivariate contagion as a function of both R_{C1} and $R_{C2|C1}$

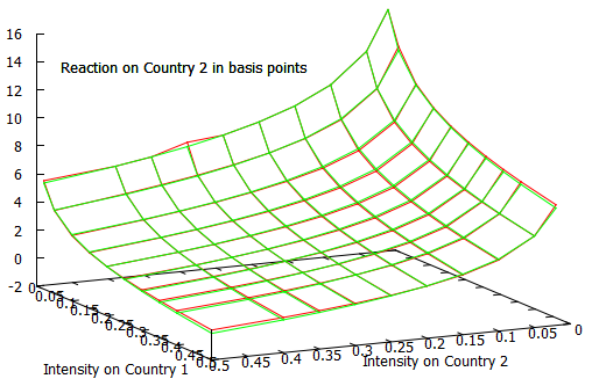

Graph 178. IR|SP– Multivariate contagion as a function of both R_{C1} and $R_{C2|C1}$

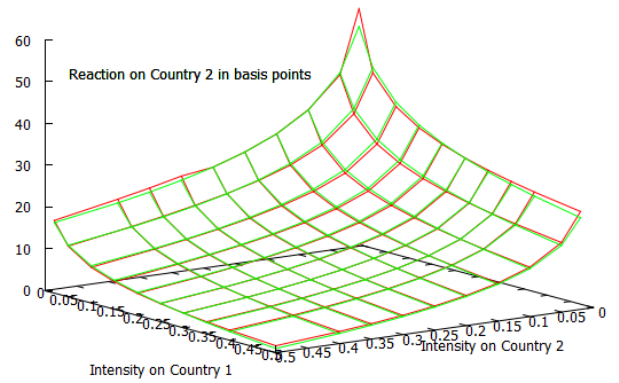

Graph 179. FI|IT– Multivariate contagion as a function of both R_{C1} and $R_{C2|C1}$

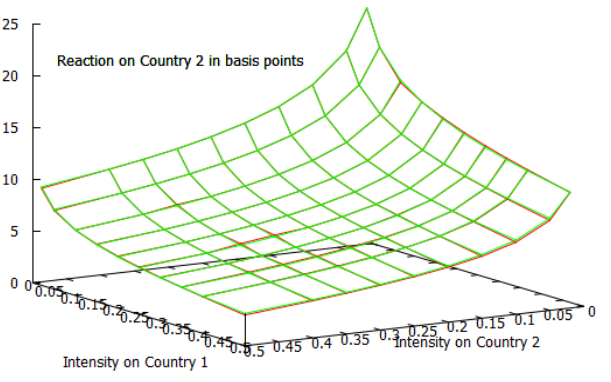

The generalisation of $S_{C2|C1}$ in eq. (83) makes the exploration of out-of-sample cases very straightforward. The worst case scenario so far was arbitrary chosen as $(R_{C1} = 2\%, R_{C2|C1} = 2\%)$, as drawn from the list in eq. (70). In practice though, the maximum level of financial distress is different and was estimated as $R_{i,max}$ in Table 35. **Let us consider these values as an upper-bound for the intensity of the upfront shock $S1$, that we denote $R_{C1,max}$.**

We now need to calculate $R_{C2|C1,max}$. First we focus on the equivalent percentile $S_{C2,max}$ that we calculate as the 99% percentile of the empirical conditional distribution $P(x_{C2}|x_{C1} = S_{C1,max})$; with $S_{C1,max}$ taken out of Table 34.

Once we have $S_{C2,max}$, we then deduce $R_{C2|C1,max}$ using the same approach as in eq. (81):

$$R_{C2|C1,max} = \frac{\iint_{S_{C1,max}}^{+\infty} {}_{S_{C2,max}}^{+\infty} q(\Sigma, \mu, z_{C1}, z_{C2}) dz}{R_{C1,max}} \tag{84}$$

Table 143 and Table 144 show the resulting values.

Table 143. $S_{C2,max}$, the maximum amplitude of the conditional shock (basis points)

$S_{C2\|C1,max}$		COUNTRY 1							
		GR	PT	IR	SP	IT	BE	FR	AT
COUNTRY 2	GE	9.2	9.0	9.9	10.4	9.6	9.1	8.7	11.4
	FI	6.7	9.7	10.4	10.9	9.4	6.7	6.8	11.4
	NL	6.8	10.3	10.5	11.2	11.1	6.8	6.8	14.1
	AT	8.9	9.4	10.2	10.3	9.4	8.7	8.7	
	FR	8.6	10.1	10.4	10.6	10.4	8.5		11.5
	BE	8.9	11.1	11.6	11.5	11.4		9.2	12.2
	IT	12.6	16.1	17.2	16.0				
	SP	12.4	16.5	17.2		15.9			
	IR	12.4	15.5		15.2	14.6			
	PT	11.9		19.5	17.2	15.6			
	GR		39.2	40.8	38.8	41.7			

Table 144. $R_{C2|C1,max}$, the maximum risk level of the conditional shock $S2|S1$

$R_{C2\|C1,max}$		COUNTRY 1							
		GR	PT	IR	SP	IT	BE	FR	AT
COUNTRY 2	GE	0.2	0.3	0.3	0.3	0.3	0.2	0.3	0.3
	FI	0.4	0.5	0.5	0.4	0.4	0.4	0.4	0.4
	NL	0.3	0.5	0.5	0.5	0.5	0.3	0.3	0.4
	AT	0.6	0.6	0.6	0.6	0.6	0.6	0.5	
	FR	0.2	0.3	0.2	0.3	0.2	0.2		0.2
	BE	0.2	0.3	0.3	0.3	0.3		0.2	0.3
	IT	0.6	0.5	0.5	0.5				
	SP	0.5	0.5	0.4		0.4			
	IR	0.9	0.8		0.9	0.7			
	PT	0.8		0.7	0.7	0.7			
	GR		0.3	0.2	0.2	0.1			

We then calculate $S^{est}_{C2|C1}(R_{C1,max}, R_{C2|C1,max}) = S^{est-max}_{C2|C1}$ in Table 145: this is the maximum expected market reaction $S_{C2|C1}$. **From a practical point of view, $S^{est-max}_{C2|C1}$ can be interpreted as an upper bound for $S_{C2|C1}$.**

Table 145. Upper bound $S^{est-max}_{C2|C1}$ in basis points

		COUNTRY 1							
		GR	PT	IR	SP	IT	BE	FR	AT
COUNTRY 2	GE	35	47	42	44	62	46	37	42
	FI	34	51	72	48	44	71	43	37
	NL	33	61	55	71	66	42	36	92
	AT	55	53	37	62	57	47	63	
	FR	75	63	63	54	73	49		44
	BE	102	49	78	55	56		63	80
	IT	144	179	161	204				
	SP	92	111	168		145			
	IR	92	126		91	121			
	PT	142		142	151	133			
	GR		614	313	252	312			

$S_{C2|C1}$, by nature, is the market reaction to a shock $S2$ on Country 2's ASW, assuming that an upfront shock $S1$ materialised upstream, in another jurisdiction. **As a result, part of $S_{C2|C1}$ is attributable to**

idiosyncratic factors, while another part is imputable to the multivariate contagion arising from $S1$. And as generally understood, the multivariate contagion is supposed to amplify the idiosyncratic exposure, to the shock $S2$ here.

As a means to illustrate this phenomenon, we consider the market reaction S_{C2} to a shock $S2$ in the univariate framework, ie. when $S1$ is no longer supposed to happen. We already calculated this estimator, that we plotted in Graph 159. Then we compare $S_{C2|C1}\left(R_{C1,max}, R_{C2|C1,j}\right)$ against $S_{C2}\left(R_{C2,j}\right)$ in Graph 180 to Graph 187: **the difference between the red and blue lines in these graphs is an illustration of the multivariate contagion at work in the multivariate framework.** These plots indicate that the multivariate contagion is effectively massive, and leads to a substantial deterioration of the idiosyncratic robustness to shocks. From an analytical point of view, eq. (83) suggests that the multivariate contagion operates at two levels, via the terms $a_{C2|C1}.\ln(R_{C1})$ and $b_{C2|C1}.\ln(R_{C1})$.

Graph 180. Multi-versus Uni-variate market reaction, Greece x-axis: $R_{C2,j}$ (univariate case); $R_{C2|C1,j}$ (multivariate)

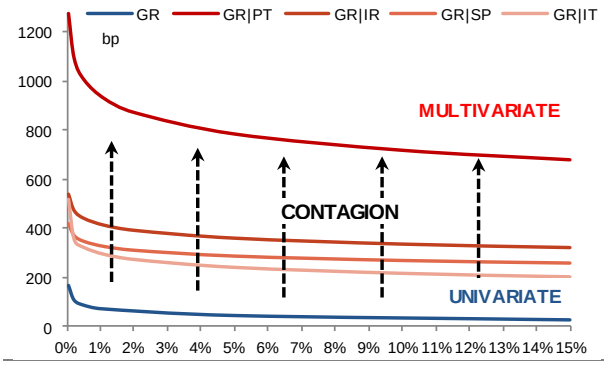

Graph 181. Multi-versus Uni-variate market reaction, Portugal x-axis: $R_{C2,j}$ (univariate case); $R_{C2|C1,j}$ (multivariate)

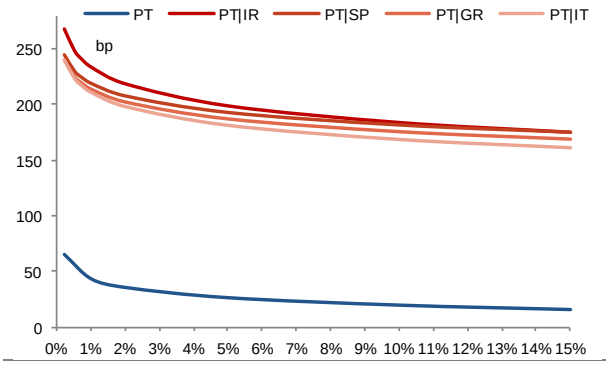

Graph 182. Multi-versus Uni-variate market reaction, Ireland x-axis: $R_{C2,j}$ (univariate case); $R_{C2|C1,j}$ (multivariate)

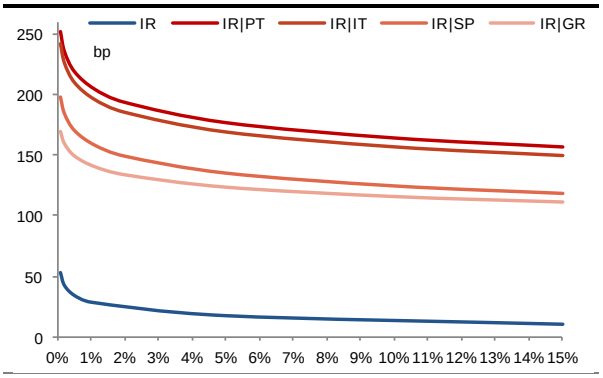

Graph 183. Multi-versus Uni-variate market reaction, Spain x-axis: $R_{C2,j}$ (univariate case); $R_{C2|C1,j}$ (multivariate)

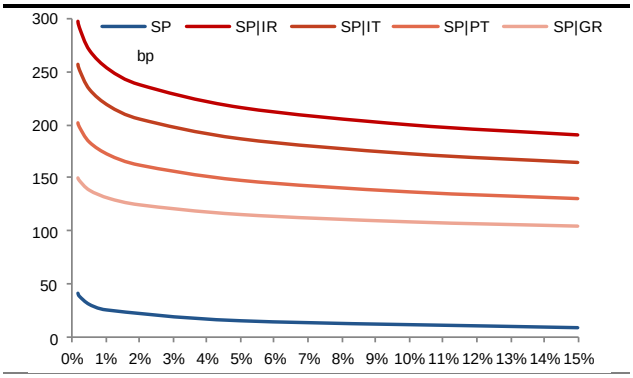

Graph 184. Multi-versus Uni-variate market reaction, Italy x-axis: $R_{C2,j}$ (univariate case); $R_{C2|C1,j}$ (multivariate)

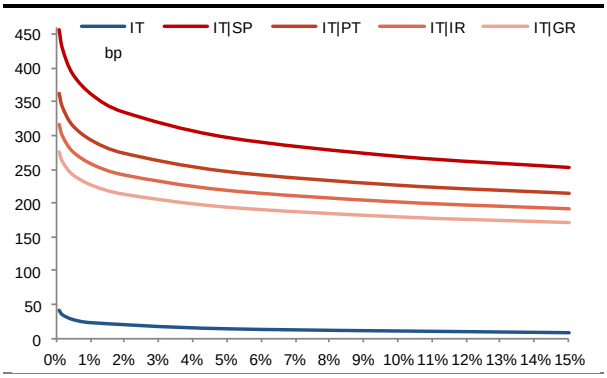

Graph 185. Multi-versus Uni-variate market reaction, Belgium x-axis: $R_{C2,j}$ (univariate case); $R_{C2|C1,j}$ (multivariate)

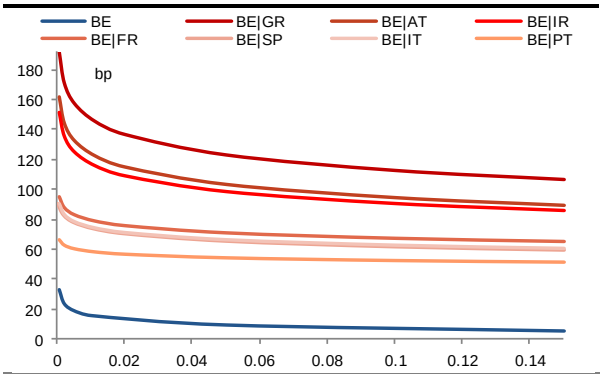

Graph 186. Multi-versus Uni-variate market reaction, France x-axis: $R_{C2,j}$ (univariate case); $R_{C2|C1,j}$ (multivariate)

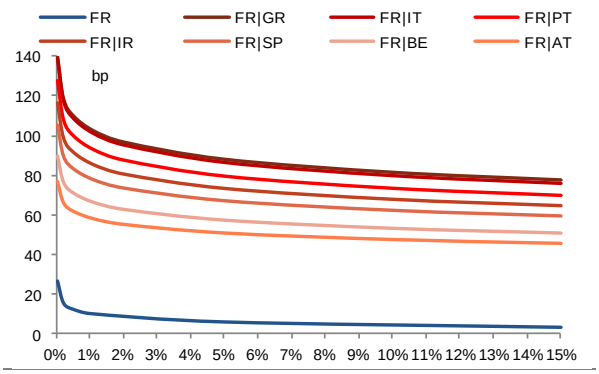

Graph 187. Multi-versus Uni-variate market reaction, Austria x-axis: $R_{C2,j}$ (univariate case); $R_{C2|C1,j}$ (multivariate)

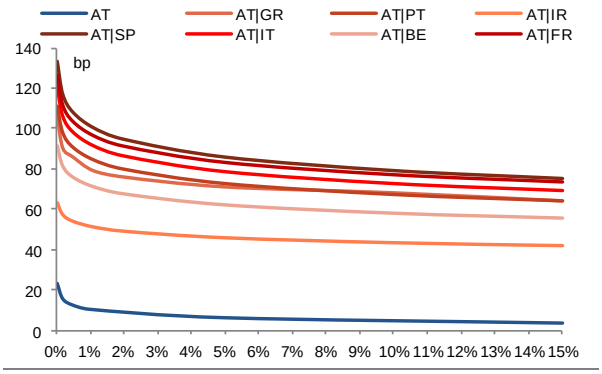

In conclusion to this section, we have explored the dynamics of the market reaction to shocks, from a multivariate perspective. Our analysis shows that the general acceleration of the market reaction admits a logarithmic behaviour, when expressed as a function of the shock intensity. Our multivariate framework also delivered interesting insight on how the idiosyncratic robustness is supposed to be affected by financial distress.

Practical applications of the model

We now explore a few applications of our multivariate model. These involve both the calibrated parameters and some of the variables we previously obtained on frailty and contagion. Portfolio optimisation is a popular approach in risk management, which delivers recommendations in terms of asset allocations based on specific constrains. One of the main goals in particular, is to mitigate the portfolio's exposure to systemic risk. The procedure is based on the minimization of an error function which ultimately delivers the optimal weight on each security. Then the portfolio is rebalanced according to the proposed 'optimal' weighting, and the weights are maintained unchanged for the whole investment period.

In financial investments, risk minimisation and return maximisation are conflicting forces: the higher-yielding products are usually facing substantially larger risks as well. An aggressive asset allocation for instance, based on an unconstrained return maximisation, will systematically favour securities with a larger intrinsic volatility. But this eventually could be at the cost of massive losses, especially when risk aversion is coming up. In contrast, a prudent asset allocation will seek to overweight the safest securities. But safe-haven offer meagre yields and tiny returns; so this is at the risk to miss the objective return at the end of the period. ➔ **Quantitative approaches to asset allocation, like portfolio optimisation, are supposed to offer an interesting trade-off between return maximisation and risk minimisation.**

An abundant literature has been dedicated to risk management procedures in the aftermath of the global financial crisis in 2008, leading to a profusion of new approaches. And while prudence in investment has turned to be a major goal following years of crises, interest rates in developed markets have also reached remarkably low levels of late, thereby narrowing the yield offered by Fixed Income securities dramatically (Gründl (2015), Bernardino (2016)). ➔ **Intense risk aversion during the years of crisis, and then now the ultra-low rates environment, both have contributed to make any deviation from the optimal risk-allocation particularly costly for portfolio managers.**

In this context, exploring new risk management-oriented procedures is a relevant exercise, with the purpose of designing more flexible tools able to offer both enhanced protection during periods of crisis, and compelling returns when risk appetite is prevailing. ➔ **Being able to detect swings in market sentiment is a key feature.**

Portfolio optimisation relies upon minimizing a dedicated risk measure (or risk metric). The optimal weighting is then deduced out of the minimised metric. In the following analysis, we explore the relevance of both the chosen risk metric and the optimisation procedure itself, separately – we consider several versions of each. Historical volatilities and rolling empirical correlations are already a basic example of risk metrics, that could potentially deliver relevant insight on underlying risks. But as we demonstrate below, this formulation is in fact relatively poor, partly because of the lack of any predicting power attached to these estimators. In practice, more sophisticated formulations of the risk measure are a better option, in particular as they offer a deeper understanding of the volatility risk (see Bronshtein, Fabozzi, Rachev et al. (2008)).

Overall, the ideal risk measure is seen as being able to detect and hedge the appearance of 'tail events' like shocks, while forecasting any swing in underlying volatility regimes that would require an

adjustment in the allocation strategy. The forecasting capability for instance can prove very helpful to switch into a more cautious allocation in due time, ahead of the materialisation of the risks.

From a general point of view, we see two main approaches in portfolio optimisation. **On the one hand, 'tactical allocation' seeks to detect short term arbitrage opportunities: the resulting positioning assumes that market discrepancies are going to fade.** In this approach, the risk-measure has to be reactive. The signal is seen as more or less robust depending on whether it is able to differentiate short term deviations, from long term momentums. Then the weighting is derived from the identified market discrepancies, on the basis that they are supposed to narrow in the future. As a consequence of the relatively small investment horizon, it is preferable to calculate the weights on a shorter version of the dataset, e.g. up to one year in the past. This helps focus on the most recent market trends at work. By contrast, taking too much history into consideration is a risk to hurt the performance because of a possible disconnection between the more distant history and the prevailing market dynamics at this moment. As a means to improve the responsiveness of the resulting allocation, asset managers may also be prompt to incorporate indicators based on the intraday volatility (Liu (2009), Ziegelmann, Borges (2015)).

On the other hand, another challenge in optimisation-based risk management is to consider a consistent risk measure, effective in the sense that it has to reflect underlying risks in a proper manner. The potential implications of shocks for instance, and how the price deterioration is supposed to spill-over throughout the network are important features: any misguiding on the contagion mechanism can lead to dramatic losses in portfolios. In order to maximise the consistency of the risk measure, it is recommended to involve a sufficiently large amount of data, and preferably to incorporate episodes of crises in the past. The optimisation procedure can then deduce the expected dynamics of risk aversion out of these past events. **And because shocks are rare in essence, the risk measure will be more effective when the available history is longer.**

In the end, asset managers need to find the appropriate compromise between consistency and responsiveness. In this analysis, we consider market prices since January 2008. This enables us to capture both the global financial crisis in H2 2008 and the more recent sovereign crisis of 2011-2012 in Europe. Having these two episodes in the dataset should help improve the consistency of the risk measure. We also explore the relevance of other estimators, specific to our statistical framework. The GAS method developed in Chapter 1 fort instance is able to provide a volatility forecast for the $t+1$ period. We take a look at this feature, and we investigate the benefit of involving the resulting volatility forecast instead of regular estimators of historical volatilities.

Global Minimum Variance, Risk Budgeting, and Most Diversified Portfolios.

In this analysis, we consider the volatility (σ_t) and correlation (Σ) estimators derived from the GAS model in Chapter 1, along with the frailty and contagion estimators we obtained in the preceding section, as material information. And we investigate the potential benefit of using these indicators in the context of portfolio optimisation, instead of more common estimators.

In the general theory of portfolio optimisation, the vector of the desired (or potential) returns denoted μ^P here, is an important component of the procedure as well. μ^P in particular is worth to be added when investors have to achieve a specific performance during the full investment period (like in Markovitz or Mean-Variance portfolios for instance, as described in Varga-Haszonits, Caccioli,

Kondor (2016), and Davis (2013)). Achieving a particular return necessarily implies being exposed to higher-yielding securities. This is obviously at the risk of larger losses as well, given the more aggressive risk-reward on these assets. As a result, imposing a target return μ^P as an objective constraint generally leads to more volatile portfolios, ex-post. In comparison, optimisation procedures free of any target return are more inclined to encourage a prudent positioning, with the flexibility of overweighting safer assets in time of crises, and so regardless of the incurred shortfall in terms of returns. ➔ **On that basis, optimisation procedures that rely on minimising a risk metric without involving any target return $\boldsymbol{\mu^P}$ look more appropriate to understand the pure risk management component.** And since the purpose of this analysis is to design novel approaches to risk management, we prefer discarding the return objectives component μ^P. Instead, we focus on methodologies that do not involve any constraints on the expected portfolio performance. Kempf, Memmel (2003) also shows that the risk-measure is usually a more accurate predictor of the performance than estimators of potential returns - this is another reason for not considering any constraint on the expected performance.

In the following paragraphs we explore three popular approaches to portfolio optimisation: the 'Global Minimum Variance' (GMV), the 'Equal Risk Contribution' (ERC) which is a subset of risk budgeting portfolios (RB), and the 'Most diversified portfolios' (MDP). **The three methodologies are volatility-based approaches, ie. the risk metric is deduced from the covariance matrix of the considered securities.**

Let us consider a portfolio of n securities. We define w_i as the weight attached to the i^{th} asset (or the exposure to it) and $R(w_1, \dots, w_n)$ as the risk measure of the portfolio $w = (w_1, \dots, w_n)$. If the risk measure is coherent and convex (see Artzner et al., 1999), it verifies the following Euler decomposition:

$$R(w_1, \dots, w_n) = \sum_{i=1}^{n} w_i \frac{\partial R(w_1, \dots, w_n)}{\partial w_i} \tag{85}$$

The risk measure is then the sum of the product of the exposure by its marginal risk. In this case, it is natural to define the risk contribution RC_i of the i^{th} asset as:

$$RC_i(w_1, \dots, w_n) = w_i \frac{\partial R(w_1, \dots, w_n)}{\partial w_i} \tag{86}$$

Since we focus on volatility risk-measures exclusively, we define R as:

$$R(w) = \sigma(w) = \sqrt{w^T \Sigma w} \tag{87}$$

The GMV portfolio is the portfolio which delivers the lowest ex-ante return variance for a given covariance matrix Σ. As a consequence, the GMV portfolio is the solution of the following minimization problem:

$$w_{GMV} = arg \min_{w=(w_1,\dots,w_n)^T} \sigma(w)^2 = \min_{w=(w_1,\dots,w_n)^T} w^T \Sigma w \quad \text{s.t.} \quad w^T . \underline{1} = 1 \quad \text{and } w_i \geq 0 \tag{88}$$

Where $\underline{1}$ is a column vector of the appropriate dimension whose entries are ones and because we also prefer having a long-only portfolio, all the weights have to be positive. The weights of the GMV portfolio are then deduced by solving the problem in eq. (88).

The return of the portfolio μ_{GMV} and the portfolio variance σ_{MV} are then calculated as:

$$\mu_{GMV} = \mu^T w_{GMV} = \mu^T \frac{\Sigma^{-1}\underline{1}}{\underline{1}^T \Sigma^{-1}\underline{1}} \tag{89}$$

where μ is a vector composed of the (ex-post) returns of each security during the investment period.

$$\sigma_{GMV} = \sqrt{w_{GMV}^T \, \Sigma \, w_{GMV}} = \frac{\underline{1}}{\sqrt{\underline{1}^{\mathrm{T}} \Sigma^{-1} \underline{1}}} \tag{90}$$

We also calculate the marginal risk and the risk contribution of the i^{th} security as:

$$\frac{\partial R(w_{GMV})}{\partial w_i} = \frac{(\Sigma w)_i}{\sqrt{w^T \Sigma \, w}}$$

$$RC_i\left(w_{GMV,1}, \dots, w_{GMV,n}\right) = \sigma_{i,GMV} = w_{i,GMV}^T \frac{(\Sigma w)_i}{\sqrt{w^T \Sigma \, w}} \tag{91}$$

We check that the volatility verifies the Euler decomposition:

$$\sum_{i=1}^{n} RC_i(w_1, \dots, w_N) = \sum_{i=1}^{n} w_i \frac{(\Sigma w)_i}{\sqrt{w^T \Sigma \, w}}$$

$$= w_{GMV}^T \frac{\Sigma w}{\sqrt{w^T \Sigma \, w}} = \sqrt{w_{GMV}^T \, \Sigma \, w_{GMV}} = \sigma_{GMV} = R_{GMV} \tag{92}$$

Different definitions of the covariance matrix Σ will obviously lead to different weights, and thus different returns ex-post. **There is therefore a need to identify the optimal definition for the covariance matrix Σ.** In the following paragraphs we explore different formulations of the covariance matrix, and we assess the relevance of each candidate. These definitions are largely based on parameters obtained with the GAS method.

GMV portfolios face some notable limitations. First, the final weights may exhibit little risk diversification, with a too high concentration on the safer securities. True, the ex-ante portfolio volatility is reduced as much as possible in this approach, but excessively small weights on the more volatile (and thus higher yielding) securities may also cause a massive deterioration of the portfolio return ex-post. The second caveat comes from the sensitivity of the GMV algorithm to the correlation matrix, in particular to the degenerated values (see Senneret, Malevergne et al. (2016)). As a consequence, the weights may be irrationally instable. This makes rebalancing particularly challenging as the excessive turnover translates into prohibitive transaction costs, and a lack of coherence in the allocation strategy. On top of that, Roncalli (2012) also notes that slight differences in the input can lead to dramatic changes in the resulting allocation and thus leads to portfolios heavily invested in very few assets.

In a risk budgeting (RB) approach, the investor has to set up the desired risk repartition between each security within the portfolio, and so regardless of consideration of returns. This helps address the risk of a too high concentration/sensitivity that we just mentioned in the GMV methodology. Risk contributions are defined as 'risk budgets', and help control the contribution of each asset to the portfolio variance (Roncalli, Bruder (2012)). 'Equal Risk Contribution' (ERC) portfolios is a popular subclass of risk budgeting portfolios, whereby the risk contribution from each asset is made equal. In

this case, Maillard, Roncalli, Teiletche (2010) shows that the ex-post volatility in ERC portfolios is located between the GMV and equally-weighted portfolios.

From a general perspective, we consider a set of given risk budgets $b = (b_1, \dots, b_n)$. The risk budgeting portfolio is then defined by the following conditions:

$$\begin{cases} RC_1(w_{RB,1}, \dots, w_{RB,n}) = b_1 \\ \vdots \\ RC_i(w_{RB,1}, \dots, w_{RB,n}) = b_i \\ \vdots \\ RC_N(w_{RB,1}, \dots, w_{RB,n}) = b_n \end{cases} \quad (93)$$

Risk contributions also have to be positive, otherwise the resulting portfolio will be highly concentrated on assets with positive risk contributions, which is not acceptable since the ERC approach is supposed to improve risk diversification. We thus consider the following constraint: $b^T . \underline{1} = 1$ and $b_i > 0$. In the end, the general formulation of RB portfolios is the following:

$$\begin{cases} w_i(\Sigma w)_i = b_i(w^T \Sigma w) \\ b_i > 0 \\ w_i \geq 0 \\ \sum_{i=1}^{n} b_i = 1 \\ \sum_{i=1}^{n} w_i = 1 \end{cases} \quad (94)$$

In ERC portfolios, all the involved securities are contributing to a similar extent to the portfolio variance. In this case, we define the budgets as $b_i = 1/n$, and we update the formulation in eq. (94) accordingly:

$$\begin{cases} w_i(\Sigma w)_i = b_i(w^T \Sigma w) \\ b_i = \frac{1}{n} \\ w_i \geq 0 \\ \sum_{i=1}^{n} b_i = 1 \\ \sum_{i=1}^{n} w_i = 1 \end{cases} \quad (95)$$

Finally we derive the formulation of the ERC optimisation problem:

$$w_{ERC} = \left\{ w \in [0,1]^n : \sum_{i=1}^{n} w_i = 1 \, , b_i = \frac{1}{n}, w_i(\Sigma w)_i = b_i(w^T \Sigma w) \right\} \quad (96)$$

Interestingly, Roncalli, Bruder (2012) demonstrates that there always exists a unique portfolio that satisfies eq. (96).

Finally, the "Most Diversified Portfolio" (MDP) tends to maximise risk diversification. Choueifaty, Froidure, Reynier (2011) introduces the concept of maximum diversification based on a formal definition of portfolio diversification via the diversification ratio (DR) formalised in eq. (97):

$$DR(w) = \frac{\sum_{i=1}^{n} w_i \sigma_i}{\sqrt{w^T \Sigma w}} \tag{97}$$

DR is the ratio of the portfolio's weighted average asset volatility over the total portfolio variance. Since different asset classes are not perfectly correlated to each other, this ratio is generally higher than 1 and a well diversified portfolio will exhibit a larger ratio.

Diversification is a fundamental aspect of risk management. As Choueifaty, Froidure, Reynier (2013) argues, it is intuitive that "concentrated" weights and/or highly correlated holdings are poorly diversified. And as a consequence, too little diversification translates into an unexpectedly large exposure to idiosyncratic risks. **Enhancing diversification means that a larger weight is given to non-correlated assets.** This helps abate the portfolio exposure to unsystematic risk, and thus improves the resilience of the portfolio against idiosyncratic developments. We also understand that there are other recognized estimators of portfolio diversification like measures of entropy (see Carmichael, Koumou, Moran (2015)) that look sensible as well.

As additional descriptors of the portfolio's behaviour, Choueifaty, Froidure, Reynier (2013) also considers the volatility-weighted concentration ratio CR (eq. (98)), and the volatility-weighted average correlation ρ_c (eq. (99)):

$$CR(w) = \frac{\sum_{i=1}^{n} (w_i \sigma_i)^2}{\left(\sum_{i=1}^{N} w_i \sigma_i\right)^2} \tag{98}$$

and:

$$\rho_c(w) = \frac{\sum_{i \neq j} (w_i \sigma_i w_j \sigma_j) \rho_{i,j}}{\sum_{i \neq j} (w_i \sigma_i w_j \sigma_j)} \tag{99}$$

The concentration of the weights is effectively a meaningful characteristic of the portfolio. Too much concentration on risk-free assets for instance will cause a shortfall in returns, ex-post. Based on eq. (98), a lower ratio is preferable.

In the end, the three estimators DR, CR and ρ_c are bound together such that:

$$DR(w) = \frac{1}{\sqrt{\rho_c(w)(1 - CR(w)) + CR(w)}} \tag{100}$$

The MDP is defined as the portfolio which maximizes $DR(w)$. We denote w_{MDP} as the solution of the MDP problem, which is defined as:

$$w_{MDP} = arg\ \max_{w \in [0,1]^n} DR(w) \quad \text{s.t.} \quad w^T . \underline{1} = 1 \quad \text{and } w_i \geq 0 \tag{101}$$

Choueifaty, Froidure, Reynier (2013) also demonstrates that the long-only MDP always exists and is unique when the covariance matrix Σ is definite.

Choueifaty, Froidure, Reynier (2013) have made a comparative exploration of recognised approaches to portfolio optimisation. The authors investigate basic properties that an unbiased, agnostic portfolio construction process should respect. They consider in particular some invariance properties based on the ground that an unbiased optimisation procedure is supposed to produce exactly the same portfolio when considering a universe equivalent to the original one.

The authors consider three different invariance properties:

- **Duplication invariance:** consider a universe where an asset has been replicated. An unbiased optimisation procedure should produce the same portfolio, regardless of whether the asset was duplicated.
- **Leverage invariance:** imagine that a company chooses to deleverage/leverage. All else being equal, the weights allocated by the portfolio to the company's underlying business(es) should not change, as its cash exposure is dealt with separately.
- **Polico invariance:** the addition of a positive linear combination of assets already belonging to the universe (e.g. the creation of a long-only leveraged exchange-traded fund on a subset of the universe) should not affect the portfolio's weights to the original assets, as they were already available in the original universe. In this case, "positive linear combination" is abbreviated as "polico".

The authors then demonstrate that the more compliant risk measure is the MDP, while the GMV portfolio is duplication invariant only, while the ERC is leverage invariant only. Table 146 summarises the results.

Table 146. Invariance properties

Portfolio	Duplication	Leverage	Polico
GMV	Yes	No	No
ERC	Non	Yes	No
MDP	Yes	Yes	Yes

The data. We consider a portfolio of daily $10\mathrm{Y}$ European sovereign asset swap spreads for $n = 11$ countries in the euro area from January 2008 to December 2016. We understand that every rebalancing induces a cost that turn to be more expensive on a frequent rebalancing. But we also seek to illustrate the relevance of risk-metrics derived from our previous analysis with the GAS method. Since the GAS approach has been calibrated on daily price variations, it looks appropriate to consider daily-based risk indicators. But since a daily rebalancing of the portfolio is not realistic, we explore two different scenarios: first the rebalancing of the weights is assumed to happen on a daily basis. This delivers very short term recommendations. Then we assume a monthly rebalancing of the portfolio. Amongst other things, this helps differentiate which risk measure is the most appropriate in each scenario.

Finally, we explore an in-house definition of the risk metric that delivers interesting results, especially in periods of crisis.

The theory of risk management indicates how to calculate the return $r_{i,t}$ of an asset swap spread position held for L sessions from $t - L$ to t (Fabozzi, Davis, Choudry (2006)):

$$r_{i,t} = \frac{ASW_{i,t-L} \times \frac{\mathrm{L}}{365} + \Delta ASW_{i,t} \times Dur_{i,t}}{10000} \tag{102}$$

Where L is the investment period for which the weights are kept unchanged; $ASW_{i,t-L}$ is the asset swap spread of country i at time $t-L$, and $\Delta ASW_{i,t}$ is the asset swap variation over the period L, ie. $\Delta ASW_{i,t} = ASW_{i,t} - ASW_{i,t-L}$. Note that $r_{i,t}$ needs to be multiplied by 100 to be expressed in %.

$Dur_{i,t}$ is also the modified duration of the sovereign bond: this is a measure of the change in price for a small change in the yield :

$$Dur_{i,t} = -\frac{\mathrm{dP}}{\mathrm{d}} \times \frac{1}{\mathrm{P}}$$

Where P is the price of the bond (see Fabozzi (2003)).

We approximate the modified duration using its exponential form, as described in Livingston, Zhou (2005), and Tchuindjo (2007). The calculation is then based on the maturity and the yield to maturity of the bond:

$$Dur_{i,t} \cong \frac{1 - \exp\left(-\frac{YTM_{i,t} * \mathrm{Mat}}{100}\right)}{1 - \exp\left(-\frac{YTM_{i,t}}{100}\right)} \tag{103}$$

Where $YTM_{i,t}$ is the yield to maturity of the 10Y benchmark government bond of country i at time t (expressed in %) and $\mathrm{Mat} = 10\ years$.

The portfolio value P_t that is calculated as the weighted sum of the performance of each asset:

$$P_t = \sum_{i=1}^{n} w_i . P_{i,t} \tag{104}$$

$P_{i,t}$ is the performance of the i^{th} security within the portfolio. We calculate $P_{i,t}$ out of $r_{i,t}$ for the period $[t-L, t[$:

$$P_{i,t} = P_{i,t-L} \times \exp\left(r_{i,t}\right) \tag{105}$$

With the convention that $P_{i,0} = 100$.

Forecasting volatility using the GAS method

As mentioned in Chapter 1, the GAS volatility σ_t is calculated via a score f_t, such that $\sigma_t = \sqrt{\exp\left(f_t\right)}$. The calculation of f_t depends on the chosen formulation of the GAS method. In our case, f_t is an autoregressive expression of parameters that refer to market realisations at $t-1$:

$$f_{t-1} = \omega + A\,.\,s_{t-2} + B.f_{t-2} \tag{106}$$

Where $\{\omega, A, B\}$ are three unknowns, that need to be calibrated.

The autoregressive relationship in eq. (106) makes the determination of a forecast for the one-step ahead period relatively straightforward: at a given time $T-1$, the score forecast $\hat{f}_T$ is calculated as:

$$\hat{f}_T = \omega + A\,.\,s_{T-1} + B.\ f_{T-1} \tag{107}$$

Where $\{\omega, A, B\}$ are calibrated on the time interval $[0, T-1[$. This interval is of prime importance because the calculation of the true value $f_T = \omega + A \,.\, s_T + B.f_T$ involves three different coefficients $\{\omega, A, B\}$ calibrated on the interval $[0, T[$.

As a result, and for better clarity we update the notation of $\{\omega, A, B\}$ as $\{\omega^T, A^T, B^T\}$. This helps understand on which interval these three unknowns have been calibrated. We also stick to the initial notation of $\{\omega, A, B\}$ when the three unknowns are calibrated on the full sample.

We then update the formulation of our score forecast $\hat{f}_T$ as:

$$\hat{f}_T = \omega^{T-1} + A^{T-1} \,.\, s_{T-1} + B^{T-1}.f_{T-1} \tag{108}$$

Then we compute the volatility forecast $\hat{\sigma}_T$ out of the score forecast:

$$\hat{\sigma}_T = \sqrt{\exp\left(\hat{f}_T\right)} \tag{109}$$

We seek to evaluate the quality of the volatility forecast $\hat{\sigma}_T$. **To do so, we consider that T is varying from January 2010 up to end-2016.** We arbitrarily choose to start the simulation with $T = 522$ points, which is long enough to ensure coherence and stability. Some observations indicate that the calibration on smaller samples is more challenging.

Then we calculate $\widehat{\sigma}_T$. In line with the preceding sections, we consider the ADC criterion as a relevant estimator of the quality of the calibrations (when T is moving). We plot the results relative to Germany and Italy in Graph 188 and Graph 189: there is a large concentration of the points below the 2.5 threshold, which indicates that the calibration is successful in most cases. There are a few outliers though, with values closer to 3.0 - but this is in a relatively marginal proportion.

Graph 188. ADC relative to Germany

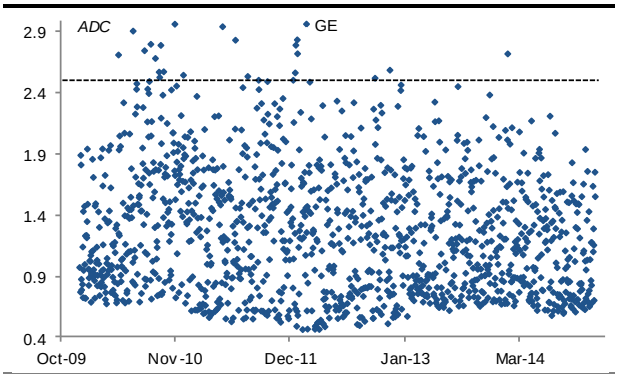

Graph 189. ADC relative to Italy

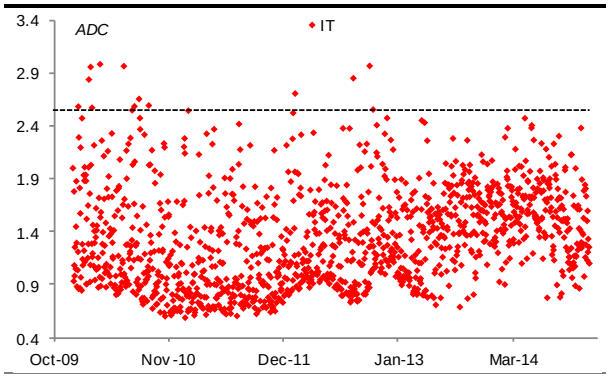

We calculate the 10% and 90% percentiles of the ADCs for all countries, that we show in Table 147. The numbers confirm that calibrations are compelling in most of the countries, although a bit more difficult for Greece and Portugal.

Table 147. Summary of all ADC, with 10% and 90% percentiles

ADC	GE	FI	NL	AT	FR	BE	IT	SP	IR	PT	GR
Mean	1.3	1.5	1.3	1.1	0.9	0.9	1.3	1.6	1.7	2.1	2.1
10% percentile	0.7	0.8	0.6	0.6	0.5	0.5	0.8	1.0	1.1	1.4	1.6
90% percentile	2.0	2.3	2.0	1.7	1.5	1.6	1.9	2.2	2.3	2.7	2.7

Looking at the prediction, we compare the forecast $\hat{\sigma}_T$ to the true volatility σ_T: Graph 190 and Graph 191 shows that the forecast is fairly close to the actual value, and replicates the general trend relatively well.

Let us now consider the average error (AE):

$$AE = \frac{1}{n}\sum_T (\hat{\sigma}_T - \sigma_T)$$

As Table 148 shows, the average error is relatively contained, which is a sign that there is not too much divergence between the forecast and the true values.

Table 148. Average error against the prediction and its true value

	GE	FI	NL	AT	FR	BE	IT	SP	IR	PT	GR
Average Error (bp/day)	-0.20	-0.13	-0.08	-0.27	-0.36	-0.62	-0.61	-0.82	-0.14	-0.03	0.69

Graph 190. Prediction versus true volatility, Germany

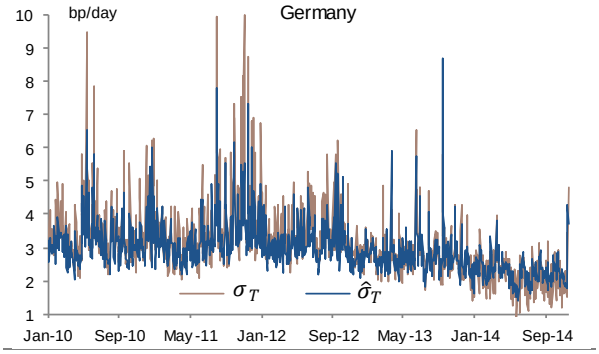

Graph 191. Prediction versus true volatility, Italy

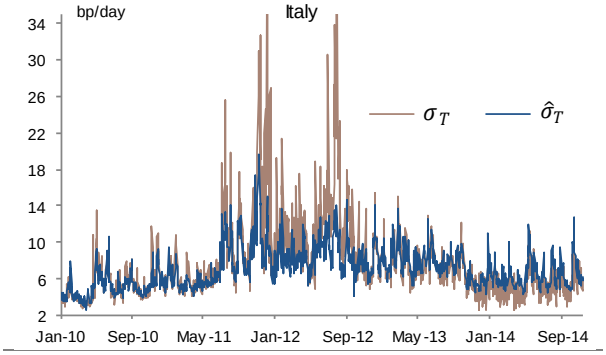

And as a measure of the error in absolute terms we also calculate the root mean square deviation (RMSE):

$$RMSE = \frac{1}{n}\sum_T \sqrt{(\hat{\sigma}_T - \sigma_T)^2}$$

Table 149. RMSE between the prediction and the true value

	GE	FI	NL	AT	FR	BE	IT	SP	IR	PT	GR
RMSE (bp/day)	0.41	0.38	0.36	0.67	0.81	1.30	1.61	1.95	2.35	3.35	10.14

This time we note a sharp deterioration for Ireland, Portugal, Greece. That said, and in contrast to these numbers, Graph 192 and Graph 193 also suggest that the deviation between the forecast and the true volatility may be not so huge for Portugal and Greece. In this case effectively, the larger $RMSE$ could just reflect the fact that the intrinsic volatility – in absolute terms - is larger at the periphery.

Graph 192. Forecast versus true value for Portugal

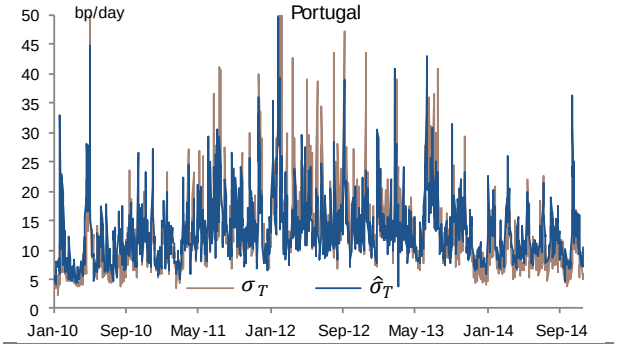

Graph 193. Forecast versus true value for Greece

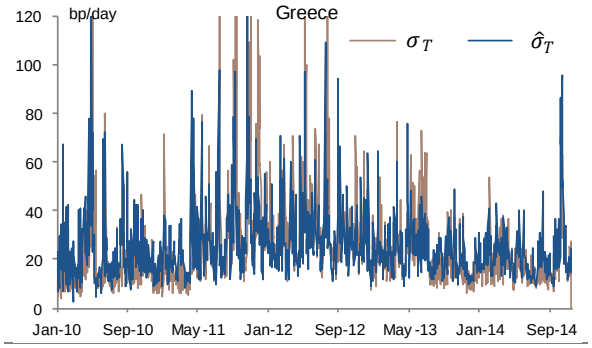

As a consequence, we explore an adjusted version of the RMSE, which this time illustrates the error as a share of the true volatility:

$$RMSE_{adj} = \frac{1}{n}\sum_{T}\frac{\sqrt{(\hat{\sigma}_T - \sigma_T)^2}}{\sigma_T}$$

Table 150. Adjusted RMSE (%)

	GE	FI	NL	AT	FR	BE	IT	SP	IR	PT	GR
adj. RMSE (%)	13	12	11	18	21	25	21	23	26	26	41

Finally, results in Table 150 indicate that the error in Ireland and Portugal is just slightly more important than in France, Belgium and Italy. For Greece in contrast, we still have a massive deviation. As Graph 194 shows, the forecast error in the case of Greece, is largely driven by the presence of spikes (see red arrows), which are much difficult to forecast.

It is also worth to note that the forecast error is very small, at $11-13\%$ of the average volatility for core countries (Table 150), and a bit larger ($18-26\%$) for soft-and non-core countries (excluding Greece).

Graph 194. For Greece, the error is largely driven by spikes

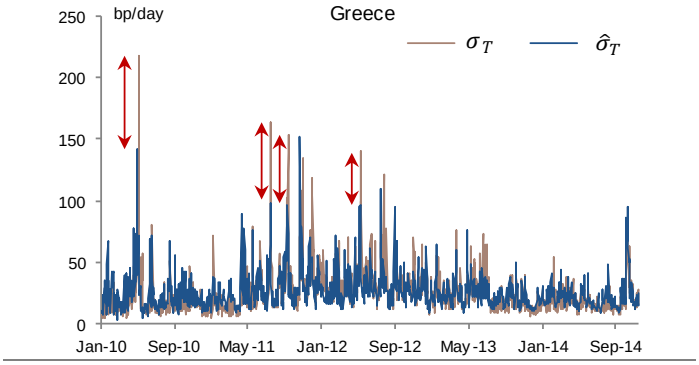

Let us now consider the consistency of the forecast on a larger time-step. For portfolio optimisation purposes in particular, having a next-day volatility forecast may prove useless given that the weights of the portfolio are usually kept unchanged for longer periods. We therefore adjust the methodology

and explore another scenario where rebalancing occurs every two weeks. **Let us see if the GAS method is still prompt to provide decent forecasts in these circumstances.**

We consider the same portfolio as before, though with bimonthly market variations this time. In order to improve the consistency of the calibration we consider a bigger sample, and we consider market valuations from January 2000 (instead of 2008).

We calculate the forecast on the new dataset following the same procedure as before; we denote the forecast as $\hat{\sigma}_{bm,T}$. We also take a look at the ADC criteria for all the calibrated distributions - Table 151 shows the results. ADCs on average are relatively similar to what we had in Table 147, with compelling results for almost all countries, except for Greece and Portugal, which are much beyond the 2.5 limit. This deterioration is largely attributable to the sharp variations in market sentiment during the considered period.

Table 151. ADC in the case of bimonthly data

ADC	GE	FI	NL	AT	FR	BE	IT	SP	IR	PT	GR
Mean	0.8	0.7	0.8	1.0	1.2	1.0	1.9	1.6	1.4	2.9	3.4
10% percentile	0.6	0.5	0.6	0.7	0.8	0.6	1.3	1.1	0.8	2.2	2.1
90% percentile	1.2	1.1	1.1	1.3	1.8	1.6	2.6	2.4	2.3	3.6	4.7

We also calculate the corresponding RMSE and the adjusted RMSE. Table 152 shows that the deviation between the forecast and the true value is much bigger this time. For Portugal and Greece in particular, the forecast error is abnormally large, so definitely the forecasting aptitude of the model is very limited for these two countries.

Table 152. RMSE and adjusted RMSE assuming a bimonthly rebalancing of the portfolio

	GE	FI	NL	AT	FR	BE	IT	SP	IR	PT	GR
RMSE (bp/day)	1	1	1	2	2	3	8	14	32	90	129
adj. RMSE (%)	22	18	23	26	25	37	58	85	85	107	156

We also plotted the forecast $\hat{\sigma}_{bm,T}$ against the true value $\sigma_{bm,T}$ in Graph 195 and Graph 196 for the Netherlands and France as examples. In both cases, there is limited deviation between both variables. We consider these volatility forecasts in the context of portfolio optimisation in the next section. **This will provide additional insightful on the forecasting capability of the GAS model.**

Graph 195. Forecast versus true value for the Netherlands

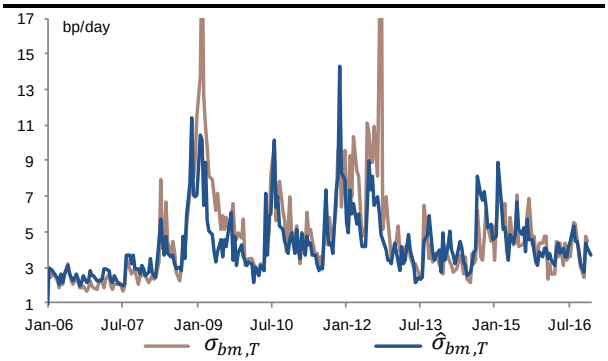

Graph 196. Forecast versus true value for France

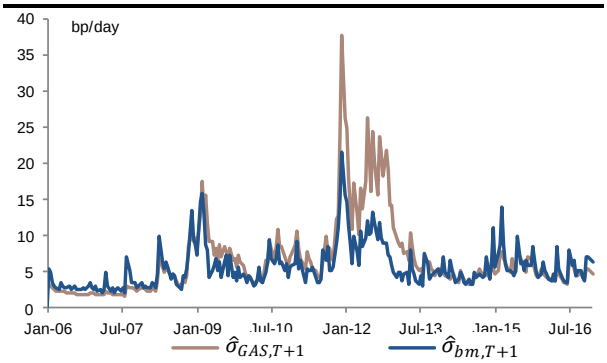

A view on optimal portfolio rebalancing

We now take a look at popular portfolio optimisation procedures, and we implement different versions of each model, every time based on a specific definition of the (volatility-based) risk metric.

'Global Minimum Variance' (**GMV**), 'Equal Risk Contribution' portfolio (**ERC**), and 'Most diversified portfolios' (**MDP**) are three popular approaches in risk management. These three models rely on risk minimization exclusively, without any performance objectives. As a consequence, the covariance matrix of the data is the only information needed to calculate the weights of the portfolio (see eq. (88), (96)).

➔ **We look at the performance of portfolios obtained with different definitions of the covariance matrix. All these versions involve some volatility estimators calculated in the preceding sections.** This will help identify the most effective risk management procedure and the optimal definition of the risk metric.

So far we have manipulated four different indicators of the univariate volatility:

- The empirical volatility, calculated as the rolling standard deviation, that we denote $\boldsymbol{\sigma_{emp,t}}$.
- The GHT volatility obtained with the GAS method, which is denoted $\boldsymbol{\sigma_t}$.
- The un-temporal volatility coefficient $\widehat{\boldsymbol{h}}(\boldsymbol{y_t})$ (see methodology in Chapter 1).
- The volatility forecast $\widehat{\boldsymbol{\sigma}}_{\boldsymbol{t}}$ that we just calculated.

In terms of correlations, we consider the matrix ρ composed of all the correlation coefficients obtained with the GAS method:

$$\rho = \begin{bmatrix} 1 & 0.97 & 0.78 & 0.63 & 0.85 & 0.82 & 0.81 & 0.53 & 0.89 & 0.81 & 0.53 \\ 0.97 & 1 & 0.91 & 0.77 & 0.63 & 0.72 & 0.87 & 0.90 & 0.77 & 0.98 & 0.90 \\ 0.78 & 0.91 & 1 & 0.76 & 0.95 & 0.89 & 0.94 & 0.69 & 0.85 & 0.94 & 0.69 \\ 0.63 & 0.77 & 0.76 & 1 & 0.80 & 0.90 & 0.89 & 0.96 & 0.96 & 0.89 & 0.96 \\ 0.85 & 0.63 & 0.95 & 0.80 & 1 & 0.81 & 0.79 & 0.81 & 0.85 & 0.79 & 0.98 \\ 0.82 & 0.72 & 0.89 & 0.90 & 0.81 & 1 & 0.81 & 0.81 & 0.86 & 0.83 & 0.82 \\ 0.81 & 0.87 & 0.94 & 0.89 & 0.79 & 0.81 & 1 & 0.87 & 0.82 & 0.97 & 0.91 \\ 0.53 & 0.90 & 0.69 & 0.96 & 0.81 & 0.81 & 0.87 & 1 & 0.83 & 0.77 & 0.86 \\ 0.89 & 0.77 & 0.85 & 0.96 & 0.85 & 0.86 & 0.82 & 0.83 & 1 & 0.81 & 0.80 \\ 0.81 & 0.98 & 0.94 & 0.89 & 0.79 & 0.83 & 0.97 & 0.77 & 0.81 & 1 & 0.81 \\ 0.53 & 0.90 & 0.69 & 0.96 & 0.98 & 0.82 & 0.91 & 0.80 & 0.80 & 0.81 & 1 \end{bmatrix} \quad (110)$$

Since ρ is not a proper correlation matrix but an aggregate of correlation coefficients (derived from bivariate distributions), ρ is not necessarily a definite positive matrix. When this condition is not verified, we consider the adjustment algorithm of Higham (2002) which determines the closest definite positive matrix. We use it every time when required, including with other definitions of the covariance matrix that may need it.

Portfolio optimisation based on the empirical volatility. In this paragraph we explore the optimisation of the GMV, ERC and MDP portfolios based on the empirical estimator $\sigma_{emp,t}$. In this case, the covariance matrix Σ is calculated as the following product:

$$\Sigma = diag(\sigma_{emp,t}) * \rho * diag(\sigma_{emp,t}) \quad (111)$$

Where $diag(\sigma_{emp,t})$ is a $n \times n$ matrix with the diagonal holding the n values of $\sigma_{emp,t}$.

We first consider daily variations of sovereign asset swap spreads as the dataset. We assume a daily rebalancing of the weights and long-only positions. We do not take any transaction fee into account. We understand that a daily rebalancing is not realistic per se, given that portfolio managers generally rebalance far less frequently. However, the higher frequency induced by daily data could reveal interesting information on the effectiveness of each version of the risk metric as to detect short-term opportunities in the market. **This could prove especially useful for tactical asset managers** (like fast money investors).

We measure the quality of the portfolios on the basis of several metrics. The **portfolio return and portfolio values** indicate how productive investments have been over the period, while the **portfolio variance** σ illustrates at what cost these returns have been achieved. The purpose of portfolio optimisation is obviously to find a relevant trade-off between reduced variance and increased returns.

The **marginal risk contribution** RC_i is another estimator worth to look at as it highlights the contribution of each asset to the portfolio variance. This helps identify a potentially too high concentration of the risks on certain securities. For ERC portfolios obviously we must find $RC_i = b_i$ where b_i are the risk budgets.

We also consider the **diversification** and the **concentration ratios** DR and CR (as expressed in eq. (97) and eq. (98)), along with the **portfolio turnover** (TR) which highlights the volume of trades required to achieve the rebalancing. We consider the definition of turnover described in De Miguel, Garlappi, Nogales (2009), and as indicated in eq. (112). A lower turnover is preferable as it leads to smaller rebalancing costs.

$$TR(t) = \sum_{i=1}^{n} \left| w_{i,t+1} - w_{i,t+1} \right| \tag{112}$$

Finally we also calculate the commonly used **Sharpe ratio** (eq. (113)), which illustrates the performance of the portfolio in light of the risks, ie. adjusted by both the performance of a risk-free portfolio (r_f) and the underlying volatility (σ).

$$SR = \frac{\mu - r_f}{\sigma} \tag{113}$$

Where r_f is the return of a risk-free portfolio over the period. In this analysis, the risk-free portfolio is made of a long position of a 10Y German asset swap spread. This 'Long Bund Only' portfolio (denoted LBO) is understood as a benchmark measure of the risk-free performance.

The performance of the LBO is shown in Graph 197. The portfolio shows a performance of 5pp (percentage point) during the sovereign crisis (2010 to mid-2012), which is coincident with a large spread widening in Spain (grey line). ➔ **This outlines the risk-free dimension of the LBO portfolio.**

The value of the LBO portfolio is also on a decline during the period that followed the sovereign crisis. The years 2013 to 2016 were essentially driven by risk-appetite in sovereign spreads. This positive momentum favoured an underperformance of risk-free securities in general compared to higher-yielding products. On top of that, 10Y German asset swap spreads have been trading at negative levels during this period, which means that the position induced a negative carry (something visible in eq. (102)) – hence the deteriorated performance of the LBO after the peak of the crisis.

Graph 197. Performance of the risk-free portfolio 'LBO'

More generally, the dynamics of the dataset in Graph 198 and Graph 199 suggests that asset swaps spreads have been consistently on the rise from Jan-2008 to Feb-2012. During this period, sovereign bonds have been underperforming the swap rate, hence the persistent widening. By large this was a consequence of the GFC in 2008 amplified by mounting uncertainties on Greece in the following years.

➔ **The period from 2008 to 2012 was marked by fierce risk aversion in Euro sovereigns. The risk-off price action in particular reached a peak between January and May 2012, before receding in line with global risks in the years that followed.**

In contrast to this period where risk aversion was dominating, asset swap spreads have consistently tightened from mid-2012 until end-2014. This reflects a substantial change in market sentiment, as sovereign bonds were outperforming swaps during this second phase in the sample. And as the general momentum was turning much more supportive for risky assets, a very accommodative ECB also helped bolster risk appetite while refraining any contagion from persisting concerns (like in Greece or Italy). ➔ **Risk appetite has been prevailing in the second part of the sample, from mid-2012 onwards.**

This subdivision of the price action in the sample (Graph 198 and Graph 199) **makes the identification of the most appropriate portfolios under each regime** (risk aversion or risk appetite) **much convenient**.

Graph 198. Two prevailing momentums in the sample: risk aversion, followed by risk appetite (focus on peripheral countries)

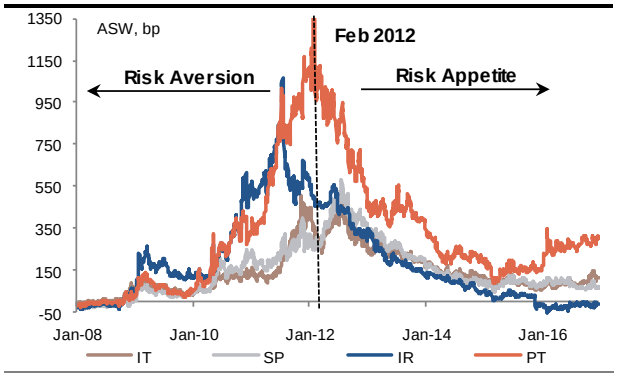

Graph 199. Two prevailing momentums in the sample: risk aversion, followed by risk appetite (core, soft-core)

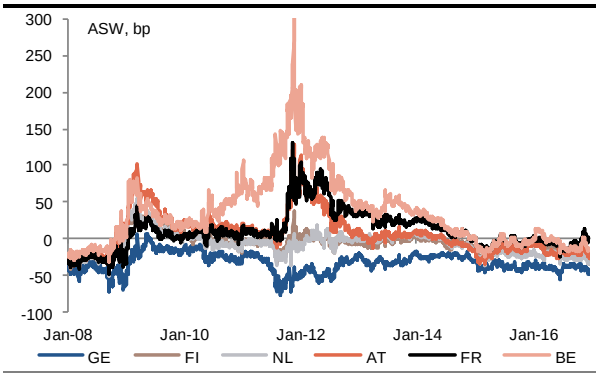

We build GMV, ERC, MDP and LBO portfolios using the empirical volatility estimator $\sigma_{emp,t}$ as defined in eq. (111). Graph 200 to Graph 205 displays the performance of the resulting portfolios.

Graph 200. GMV, ERC, MDP portfolios, empirical version

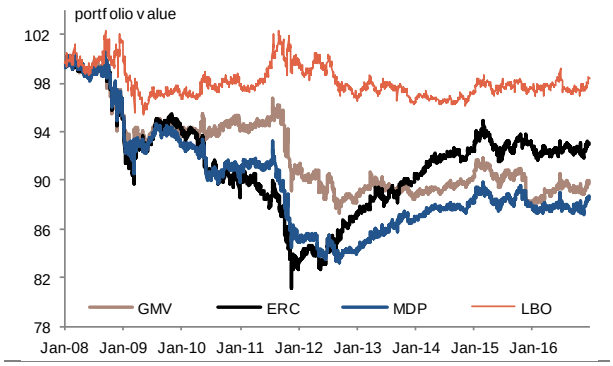

Graph 201. Portfolio volatility (standard deviation)

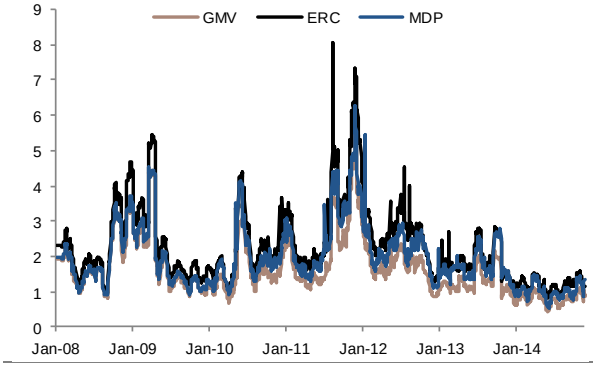

Graph 200 first, indicates that the LBO benchmark outperforms the three other approaches. ➔ **This illustrates the fact that empirical estimators of the volatility offer very limited protection against risk aversion. Hence the need to consider more sophisticated definitions.**

We also note that the ERC portfolio outperforms other approaches over the full period, though losses are more important as well at the fore of the peak of the sovereign crisis. While the performance of the GMV portfolio is much disappointing, the variance of the portfolio is the smallest in Graph 201. As a consequence the loss around end-2011 is more contained than in MDP and ERC portfolios.

We look at the weights w in Graph 202, Graph 203 and Graph 204, and we also plot average weights in Table 153 for better clarity. First we note that Germany is consistently overweighted in the three approaches. This preference for Germany is more pronounced for the MDP, which allocates 50% of the weights on German securities on average. This compares with just 32% in the GMV portfolio, and 15% in the ERC.

Interestingly, the ERC is the least conservative approach as in this framework every asset is meant to contribute equally to the portfolio volatility. As a result, the allocation involves a decent portion of all securities (Graph 203), and this helps avoiding too much concentration (Table 154). In contrast to the ERC, the MDP involves only six securities in the sample, including Germany, France, Spain and Greece. As expected, the diversification ratio is higher for the MDP in Graph 205, which is a sign of coherence. The higher diversification is achieved via higher weights allotted to these securities that look the most de-correlated to each other (see eq. (110)).

As Graph 202 shows, turnover is also incredibly high for the GMV portfolio, and more contained for the ERC and MDP.

Graph 202. GMV weights w^{GMV}

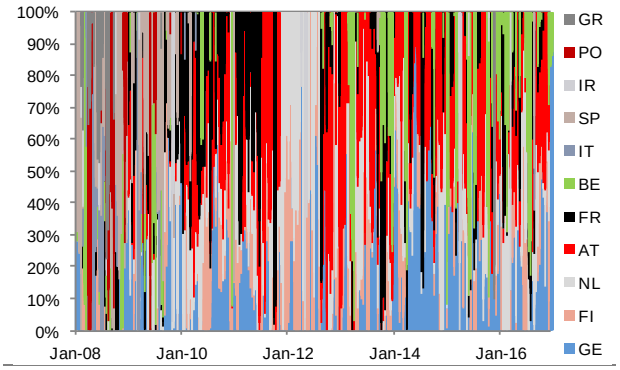

Graph 203. ERC weights w^{ERC}

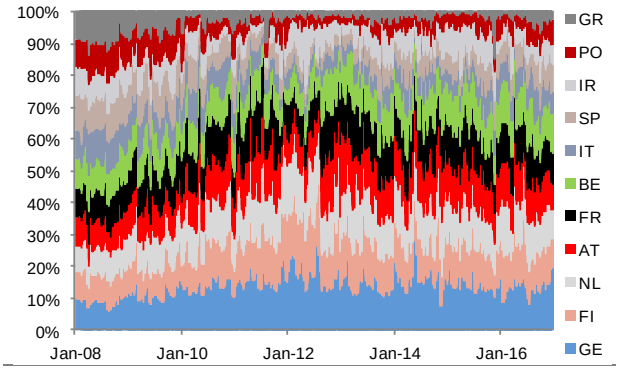

Graph 204. MDP weights w^{MDP}

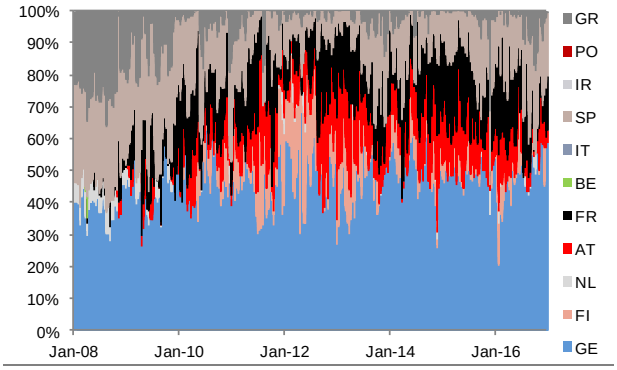

Graph 205. Diversification ratio

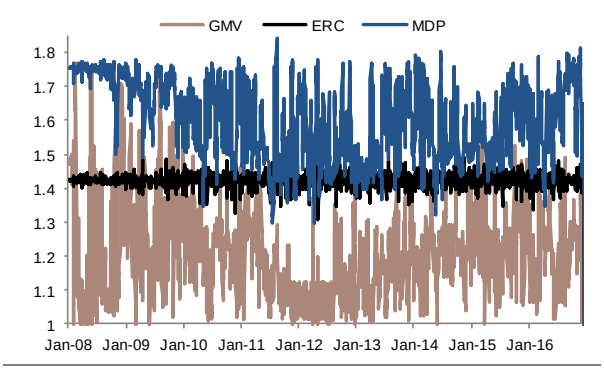

Table 153. Summary of the GMV, ERC, MDP portfolios with empirical covariance

GMV	GE	FI	NL	AT	FR	BE	IT	SP	IR	PO	GR
Average Weights (%)	32	13	15	17	9	6	2	4	1	1	1
Contrib to total vol (%)	26	15	16	16	8	5	3	7	1	2	1
ERC											
Average Weights	15	13	14	11	11	10	6	6	6	4	3
Contrib to total vol (%)	2	9	8	10	12	11	11	11	10	10	6
MDP											
Average Weights	50	6	1	9	14	0	0	15	0	0	5
Contrib to total vol (%)	36	6	1	8	14	0	0	25	0	0	9

The marginal risk contribution to the portfolio volatility gives additional information on how the weights translate into a more or less risky position within the portfolio. The definition of the risk contribution in eq. (91) is applicable here:

$$RC_i(w_1, \dots, w_n) = w_i^T \frac{(\Sigma w)_i}{\sqrt{w^T \Sigma w}} = \sigma_i$$

σ_i highlights how much risk is attached to each asset, in light of the total portfolio variance. Volatile assets for instance may contribute to a larger extent to the total volatility than expected, even if they are given a smaller weight than other securities.

Graph 206 shows that for the GMV portfolio, the marginal risk (or volatility) contributions are relatively similar to the weights, which is consistent with the analytical definition of the optimisation. In this configuration, the portfolio volatility is optimally reduced. But as Graph 206 shows, this is at

the expense of a greater turnover (the graph is too volatile), and a notable loss in returns as the weights have a tendency to focus on the securities that offer the smaller return.

In the ERC approach in contrast, every asset contributes equally to the portfolio variance (Graph 207). The variations of the weights in Graph 203 are therefore decided so that the risk contribution of each security remains unchanged as time goes by. And because the desired risk contribution is independent of the credit quality, there is a sizeable exposure to the more volatile securities in general. This largely explains the bigger losses during the sovereign crisis in Graph 200, and the faster recovery rate when market sentiment improved.

In the MDP finally, a good chunk of the portfolio variance is attributable to Germany (Graph 208). Spain and Greece are also largely involved, though in a sensible way as we see a notable underweight on these two countries during the crisis. Austria and France instead are preferred during this period. While this selection looks relatively coherent, the performance is much disappointing during the risk aversion period in Graph 200. ➔ **Clearly the defensive re-allocation of the portfolio happens too late.**

Graph 206. GMV volatility contribution, Germany contributes more

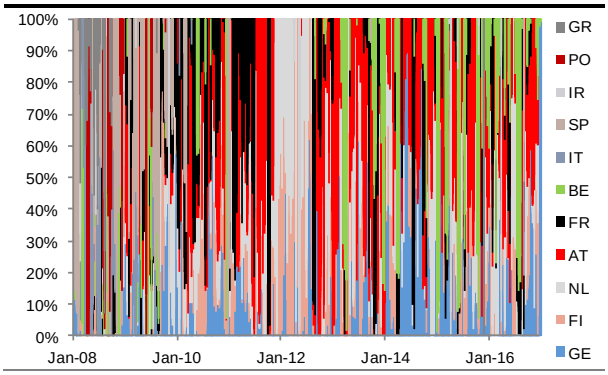

Graph 207. ERC volatility contribution, equally distributed

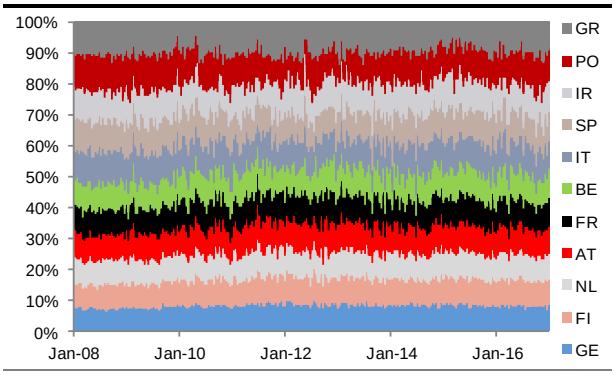

➔ **In the end, portfolios based on empirical estimators largely underperform the benchmark LBO during the whole period. This reflects the limitation of empirical estimators in risk management.**

We previously emphasized that the deterioration induced by risk aversion is non-linear. We consider now other formulations of the risk measure that could potentially reflect this phenomenon in a more effective manner.

Graph 208. Volatility contribution to the MDP portfolio

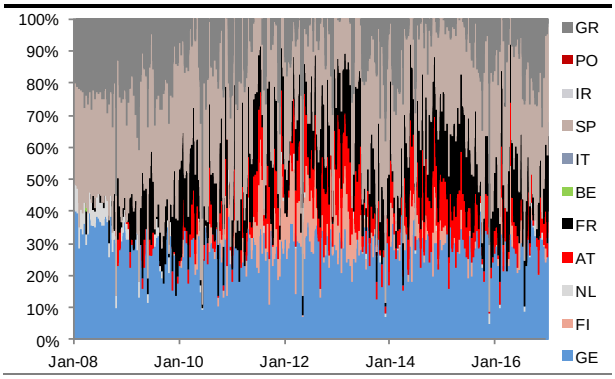

Table 154. Criterions of the portfolios with empirical covariance

	Empirical covariance			
	Diversification	Concentration	Turnover	Portfolio Variance
GMV	1.76	0.43	0.09	4.1
ERC	1.65	0.11	0.04	4.1
MDP	1.96	0.40	0.02	4.2

Let us now consider three additional versions of the portfolio:

- First a version that involves the GAS volatility σ_t instead of the empirical estimator $\sigma_{emp,t}$. Inthis case the covariance matrix is denoted Σ_{GAS}:

$$\Sigma_{GAS} = diag(\sigma_t) * \rho * diag(\sigma_t) \tag{114}$$

- Then another version based on the un-temporal volatility coefficient $\hat{h}(y_t)$. In this case we denote the covariance matrix Σ_h:

$$\Sigma_h = diag\left(\hat{h}(y_t)\right) * \rho * diag\left(\hat{h}(y_t)\right) \tag{115}$$

- Finally we calculate a version based on the volatility forecast $\hat{\sigma}_{t+1}$. In this case we denote the covariance matrix Σ_{fcst}:

$$\Sigma_{fcst} = diag(\hat{\sigma}_{t+1}) * \rho * diag(\hat{\sigma}_{t+1}) \tag{116}$$

Graph 209. Performance of GMV portfolios

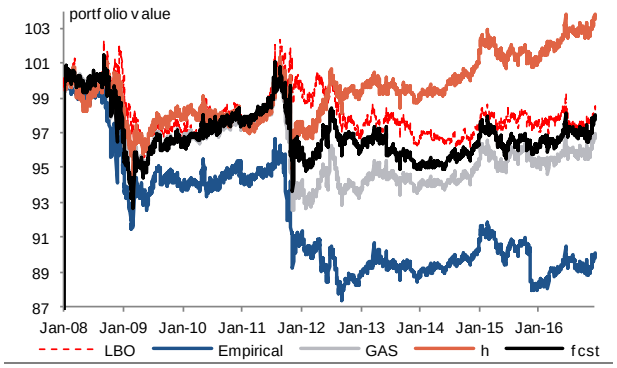

Graph 210. Performance of ERC portfolios

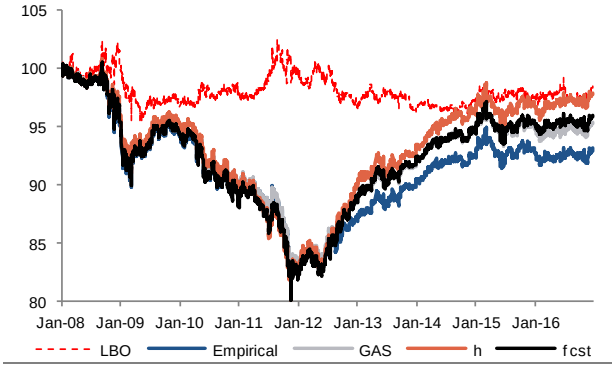

Graph 209, Graph 210 and Graph 211 show the performance of these different portfolios. First we note that in each category, the empirical portfolio is the worst performer. This outlines that the GAS volatility σ_t, the un-temporal estimator $\hat{h}$ and the volatility forecast $\hat{\sigma}_t$ are more adequate descriptors of the volatility risk than the basic standard deviation.

Another observation if that the 'GMV $\hat{h}$' portfolio outperforms all other portfolios (Graph 209). Although this version does not provide as much protection as the LBO benchmark during the risk aversion period, losses around the end of 2011 (ie. on tough risk aversion) are relatively small compared to other portfolios. Then the recovery of the 'GMV $\hat{h}$' portfolio during the risk appetite period is outstanding, and offers a consistent return from 2012 to end-2016. In comparison the LBO fails to provide such a reward.

The ERC and MDP portfolios are much disappointing in comparison to the 'GMV $\hat{h}$' definition: losses from 2010 to 2012 are substantial in Graph 210 and Graph 211, and the recovery rate is not sufficiently robust to compensate this deterioration. In this configuration, we also note that there is little upside in using the forecast $\hat{\sigma}_{t+1}$ instead of the volatility estimator σ_t.

Graph 211. Performance of MDP portfolios

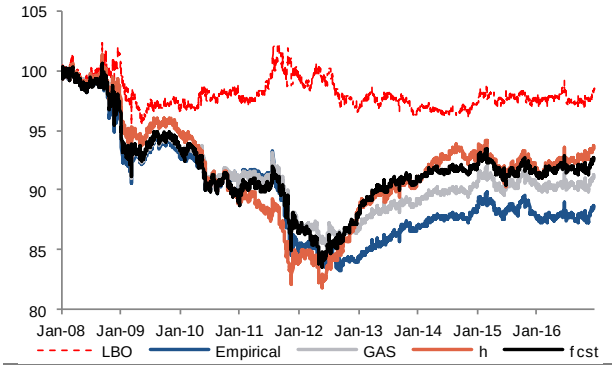

Graph 212. Contribution to the portfolio volatility (GMV $\hat{h}$)

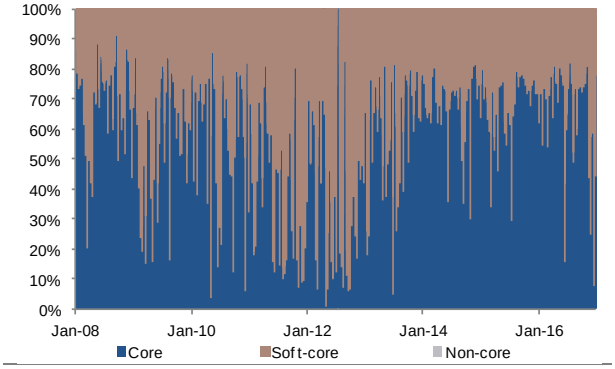

Looking at the 'GMV $\hat{h}$' portfolio, Graph 212 shows the contribution of each asset to the portfolio variance, with a breakdown by asset category. Arguably, non-core securities are excluded from the portfolio, which is coherent with the fact that the GMV methodology focuses on the least volatile securities. And because the coefficient $\hat{h}$ is an illustration of the 'intrinsic' volatility, this estimator is a fair representation of the underlying risks - hence the outperformance of the '$\hat{h}$' version compared to the GAS portfolio in Graph 209. In contrast to these observations, other portfolios always involve peripheral securities to some extent: this is in effect largely responsible for the massive loss observed during the risk aversion period. ➔ **The un-temporal GHT volatility $\hat{h}$ delivers interesting results when applied to the GMV methodology. And while protection is not as high as in the risk-free benchmark, the performance of the 'GMV $\hat{h}$' portfolio over the risk appetite period is much more appealing than in the LBO, with gains largely offsetting the depreciation accumulated in the years 2008 to 2011.**

Less engaging, Table 155 shows that the turnover of the 'GMV $\hat{h}$' portfolio is high and larger than in other portfolios. Rebalancing looks thus particularly costly here. Risk diversification also is a bit small, but this is a natural consequence of the fact that peripheral assets are excluded from within the portfolio.

Table 155. Diversification, Concentration and Turnover ratios

	Empirical	GAS	$\hat{h}$	forecast
GMV				
Diversification	1.21	1.20	**1.17**	1.20
Concentration	0.45	0.45	**0.37**	0.43
Turnover	0.35	0.44	**0.77**	0.74
ERC				
Diversification	1.42	1.42	1.42	1.41
Concentration	0.09	0.10	0.11	0.10
Turnover	0.06	0.07	0.13	0.10
MDP				
Diversification	1.60	1.60	1.60	1.61
Concentration	0.28	0.29	0.32	0.29
Turnover	0.10	0.11	0.28	0.19

Table 156, Table 157 and Table 158 offer additional insight on the features of each portfolio.

Table 156. Statistics summary of GMV portfolios (all versions)

	GE	FI	NL	AT	FR	BE	IT	SP	IR	PO	GR
Average Weights											
Empirical	0.3	0.1	0.2	0.2	0.1	0.1	0.0	0.0	0.0	0.0	0.0
GAS	0.4	0.1	0.2	0.2	0.1	0.0	0.0	0.0	0.0	0.0	0.0
$\hat{h}$	0.4	0.2	0.2	0.1	0.0	0.0	0.0	0.0	0.0	0.0	0.0
Forecast	0.3	0.1	0.2	0.1	0.1	0.0	0.0	0.0	0.0	0.0	0.0
Contrib to total vol (%)											
Empirical	26	15	16	16	8	5	3	7	1	2	1
GAS	31	14	25	20	12	2	1	2	0	0	0
$\hat{h}$	37	29	30	15	4	1	0	0	0	0	0
Forecast	27	16	30	17	16	2	1	2	0	0	0
Risk contribution (%)											
Empirical	30	14	14	15	9	5	3	7	1	2	1
GAS	33	13	21	19	9	2	0	2	0	0	0
$\hat{h}$	35	22	24	14	4	1	0	0	0	0	0
Forecast	29	14	23	15	13	2	0	2	0	0	0

Table 157. Statistics of ERC portfolios (all versions)

	GE	FI	NL	AT	FR	BE	IT	SP	IR	PO	GR
Average Weights											
Empirical	0.2	0.1	0.1	0.1	0.1	0.1	0.1	0.1	0.1	0.0	0.0
GAS	0.2	0.1	0.1	0.1	0.1	0.1	0.1	0.1	0.1	0.0	0.0
$\hat{h}$	0.2	0.1	0.1	0.1	0.1	0.1	0.1	0.1	0.1	0.0	0.0
Forecast	0.2	0.1	0.1	0.1	0.1	0.1	0.1	0.1	0.1	0.0	0.0
Contrib to total vol (%)											
Empirical	2	9	8	10	12	11	11	11	10	10	6
GAS	2	8	8	10	12	11	10	10	10	11	6
$\hat{h}$	2	8	8	9	11	10	10	11	10	11	10
Forecast	1	7	7	9	12	11	11	12	10	11	8
Risk contribution (%)											
Empirical	9.1	9.1	9.1	9.1	9.1	9.1	9.1	9.1	9.1	9.1	9.2
GAS	9.0	9.0	9.1	9.0	9.1	9.1	9.0	9.2	9.0	9.1	9.3
$\hat{h}$	8.9	8.9	8.9	8.9	8.9	9.0	9.0	9.1	9.3	9.5	9.6
Forecast	9.0	9.0	9.0	9.0	9.0	9.0	9.0	9.1	9.1	9.2	9.6

Table 158. Statistics of MDP portfolios (all versions)

	GE	FI	NL	AT	FR	BE	IT	SP	IR	PO	GR
Average Weights											
Empirical	0.5	0.1	0.0	0.1	0.1	0.0	0.0	0.1	0.0	0.0	0.0
GAS	0.5	0.1	0.0	0.1	0.1	0.0	0.0	0.1	0.0	0.0	0.0
$\hat{h}$	0.6	0.0	0.0	0.1	0.1	0.0	0.0	0.2	0.0	0.0	0.0
GHT forecast	0.5	0.0	0.0	0.1	0.2	0.0	0.0	0.2	0.0	0.0	0.0
Contrib to total vol (%)											
Empirical	36	6	1	8	14	0	0	25	0	0	9
GAS	40	5	1	8	16	0	0	24	0	0	6
$\hat{h}$	34	2	0	4	11	0	0	27	0	0	21
GHT forecast	29	2	1	5	15	0	0	34	0	0	14
Risk contribution (%)											
GHT correl	41	6	1	7	12	0	0	23	0	0	10
GAS	41	4	1	7	13	0	0	24	0	0	10
$\hat{h}$	41	2	0	5	10	0	0	26	0	0	17
GHT forecast	41	2	1	6	13	0	0	25	0	0	13

Let us now consider a monthly rebalancing of the weights. We consider the same estimators as before, and we take the bimonthly volatility forecast previously calculated (ie. $\hat{\sigma}_{bm,t+1}$) as the forecast involved in Σ_{fcst} :

$$\Sigma_{fcst} = diag\left(\hat{\sigma}_{bm,t+1}\right) * \rho * diag\left(\hat{\sigma}_{bm,t+1}\right) \tag{117}$$

All other versions remain unchanged. **Graph 213 to Graph 218 and Table 159 show the performance of the resulting portfolios.**

Results are much different this time: for the three methodologies (GMV, ERC, MDP), the 'forecast' version (based on Σ_{fcst}) distinctly outperforms other definitions of the portfolio. The ERC and MDP 'forecast' portfolios even show a gain (of 4pp and 3.5pp) at the end of the period. The GMV version in contrast is much less volatile than the two others, and this tends to harm returns.

In comparison to the 'forecast' portfolios, the empirical portfolio is still the worst methodology, while the GAS (involving σ_t) and un-temporal (involving $\hat{h}$) versions show a relatively similar performance, and consistently underperform the 'forecast' version.

Graph 213. GMV portfolio, monthly rebalancing

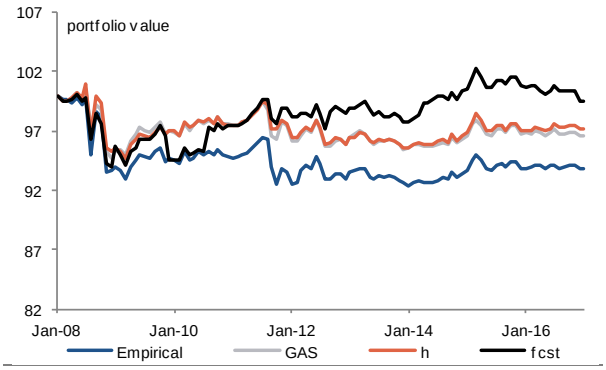

Graph 214. ERC portfolio, monthly rebalancing

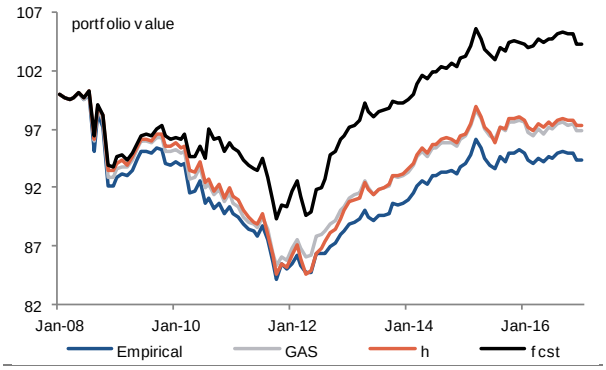

The protection offered by considering the forecast estimator $\hat{\sigma}_{bm,t+1}$ is particularly obvious now: in all cases, losses around end-2011 are more than 5pp smaller in 'forecast' portfolios compared to the worst versions. The recovery during the period of risk appetite is also much faster in 'forecast' portfolios, which means that the forecast risk measure helps achieve a more efficient switch in the asset allocation when risk aversion is abating.

Graph 215. MDP portfolio, monthly rebalancing

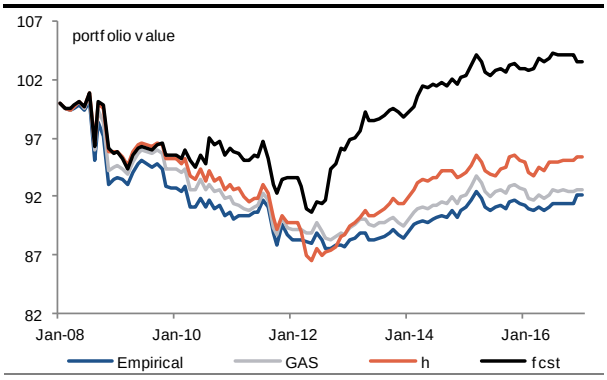

Graph 216. Volatility contribution in the 'GMV forecast' portfolio

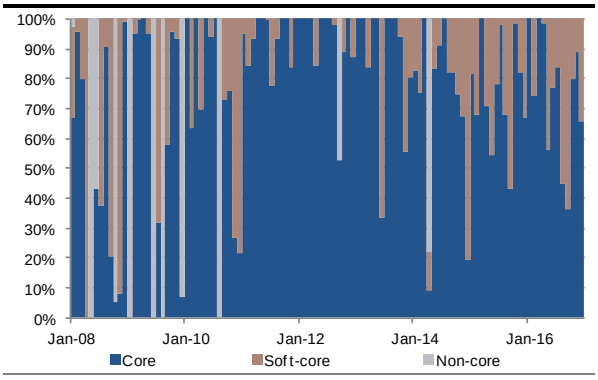

Looking at the risk contribution, Graph 216 shows that the GMV 'forecast' portfolio is prompt to overweight core securities when risk aversion is mounting. This largely explains the remarkable resilience of this portfolio in Graph 213. This version however is very slow to re-adjust the risk exposure of the portfolio when risk appetite is back, and this explains the very modest performance between 2012 and end-2013.

Graph 217 and Graph 218 shows the risk contribution in the **ERC and MDP 'forecast' portfolios**. In these two approaches, the exposure to peripheral countries does not noticeably shrink during the

crisis. These two portfolios however outperform their peers during the risk aversion period in Graph 214 and Graph 215, so the proposed risk contribution offers interesting protection.

Graph 217. Volatility contribution in the 'ERC forecast' portfolio

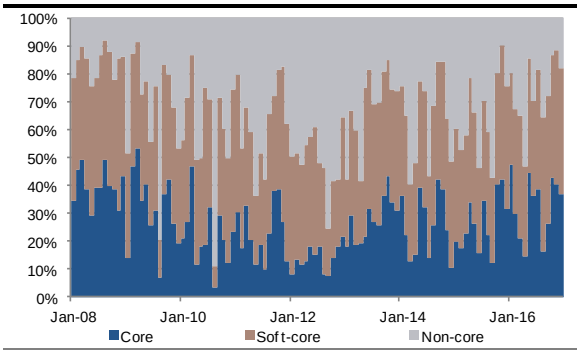

Graph 218. Volatility contribution in the 'MDP forecast' portfolio

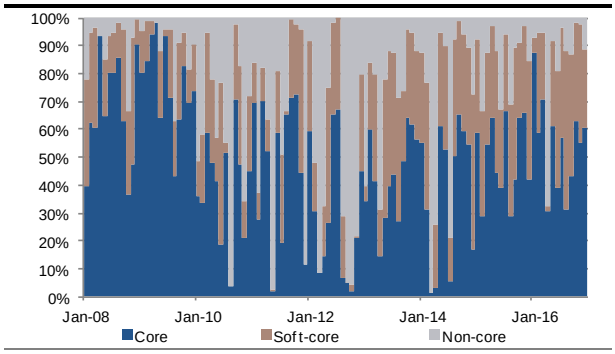

An interesting point in Table 159 is that the ERC and MDP 'forecast' portfolios display a very small turnover, and a much decent diversification ratio. This suggests that a proper implementation of these two portfolios could be less of an issue than when we assumed a daily rebalancing.

Table 159. Diversification, Concentration and Turnover ratios

	Empirical	GAS	$\hat{h}$	forecast
GMV				
Diversification	1.22	1.20	1.16	1.14
Concentration	0.40	0.42	0.29	0.54
Turnover	0.87	0.77	0.32	1.11
ERC				
Diversification	1.41	1.41	**1.41**	1.39
Concentration	0.10	0.10	**0.10**	0.12
Turnover	0.15	0.13	**0.05**	0.27
MDP				
Diversification	1.57	1.58	**1.63**	1.50
Concentration	0.28	0.28	**0.31**	0.32
Turnover	0.22	0.21	**0.13**	0.43

➔ **The monthly rebalancing of the portfolio underscores the relevance of considering the forecast value $\hat{\sigma}_{t+1}$ instead of the present estimators σ_t or $\hat{h}$, for portfolio optimisation purposes. On that basis, we conclude that the forecasting capability of the GAS model is robust and could be used to enhance risk manage procedures.**

A novel optimisation procedure based on mean reversion

Aside from these recognised portfolio optimisation procedures, we now describe an in-house empirical procedure to calculate the weights of the portfolio. We still consider a long-only portfolio, with normalized weights (ie. $w_i \geq 0$ and $\sum w_i = 1$), and we seek to design a relevant and simple risk measure, ideally able to provide a sensible trade-off between protection and return.

Let us denote this metric as $R_{i,t}$ for a given country i at time t. **As a common practice, we consider mean-reversion as a sensible rationale to take decision on the weights.** Mean reversion assumes that the greater the deviation of a random variable from its mean, the greater the probability that the next measures will converge towards the mean. We assume that $R_{i,t}$ will mean-revert as time goes by. In this case, periods of very large deviations from the mean value will be perceived as a signal to overweight or underweight certain securities, on the basis that the position will take advantage of a convergence towards the mean value.

In the previous chapter we defined two different formulations of the market reaction to a shock S_i:

$$\begin{cases} \tilde{S}_i^1 = \mathrm{a}_2 \hat{F}(x_{i,t})^2 + a_1 \hat{F}\left(x_{i,t}\right) + a_0 \\ \tilde{S}_{i,t}^2 = b_{2,t} \times \hat{h}(x_{i,t})^2 + b_{1,t} \times \hat{h}(x_{i,t}) + b_{0,t} \end{cases}$$ respectively taken from both eq. (58) and eq. (64)

Since $\tilde{S}_i^1$ and $\tilde{S}_{i,t}^2$ are supposed to describe the same entity, we can assume that both variables are mean reverting one against each other. If this assumption is true, the differential $\Delta S_{i,t} = \tilde{S}_i^1 - \tilde{S}_{i,t}^2$ must be stationary. And effectively, this is confirmed by unit-root tests. The mean reverting dimension is also visible in Graph 219 for Germany, France and Spain (as examples). ➔ **Since $\Delta S_{i,t}$ is mean reverting, we consider this variable as a starting point to design the risk measure.**

A meaningful caveat with mean reversion however, is that this assumption may not hold in periods of severe risk aversion because correlations are largely distorted in deteriorated market conditions. In Graph 219 for instance, $\Delta S_{i,t}$ is temporarily peaking in 2011-2012. In this configuration, the deviation from the mean goes much beyond the usual range, and this can lead to a misguiding signal in times of crisis.

➔ **Mean reverting behaviours in "normal" market conditions are usually broken in periods of crisis as risk aversion tends to stretch market valuations. Our risk-metric somehow has to reflect this change of regime, when risk aversion becomes a dominant factor.**

Graph 219. $\Delta S_{i,t} = \tilde{S}_i^1 - \tilde{S}_{i,t}^2$ for selected countries

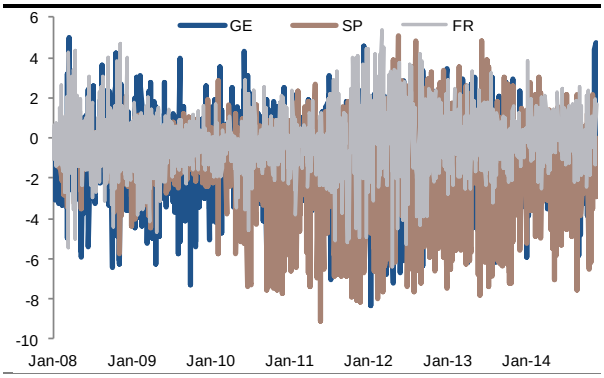

Graph 220. 10Y Sovereign interest rate (%)

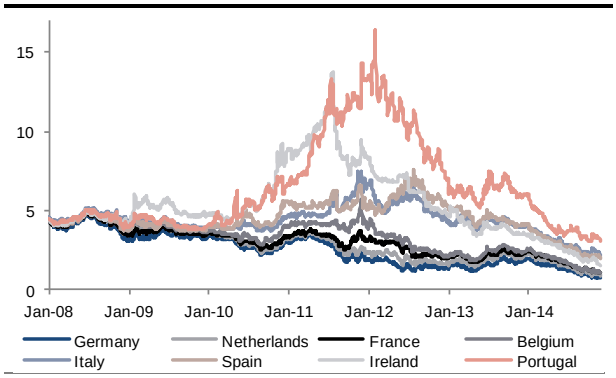

As a means to address this issue, we introduce 10-year sovereign interest rates in absolute terms as a relevant additional variable. Graph 220 in particular shows that sovereign interest rates were abnormally high during the period of intense risk aversion in Q4 2011/Q1 2012. This is an illustration of larger risk-premia and therefore increased risks of contagion by then.

We already mentioned that contagion influences interest rates, sometimes heavily, and push them to higher levels. ➔ **This connection between sovereign interest rates and the risk of contagion can be used to gauge the underlying uncertainties in market sentiment**. We therefore decide to adjust the differential $\Delta S_{i,t}$ by the corresponding 10Y sovereign interest rate $r_{i,t}$ in order to capture the risk of any distortion in mean reversion when risk aversion is mounting. $\Delta S_{i,t}$ is thus re-defined as:

$$\Delta S_{i,t} = \frac{\tilde{S}_i^1 - \tilde{S}_{i,t}^2}{r_{i,t}}$$

$\Delta S_{i,t}$ is now much more contained during periods of financial distress. Graph 221 for instance shows the difference between the two definitions, with the adjusted (blue line) and the non-adjusted (grey line) versions of $\Delta S_{i,t}$ for Ireland. Graph 222 shows the same series for Italy. In these two graphs, the adjusted version in blue is smaller during the sovereign crisis than during periods of risk appetite. **From a mean reverting standpoint, the smaller variations in $\Delta S_{i,t}$ in 2011-2012 (ie. under tough risk aversion) reflect very little market opportunities during this period. ➔ This is coherent with the fact that portfolio managers have limited room for rebalancing portfolios when risk aversion is fierce.** Unit root tests also indicate that the new version of $\Delta S_{i,t}$ is still stationary.

We consider this 'interest rate'-adjusted version of $\Delta S_{i,t}$ as a relevant risk-indicator. We now focus on designing an optimisation procedure that will help compute the weights out of $\Delta S_{i,t}$.

Graph 221. The interest rate adjustment leads to more contained $S_{i,t}$ indicators during periods of financial distress (Ireland)

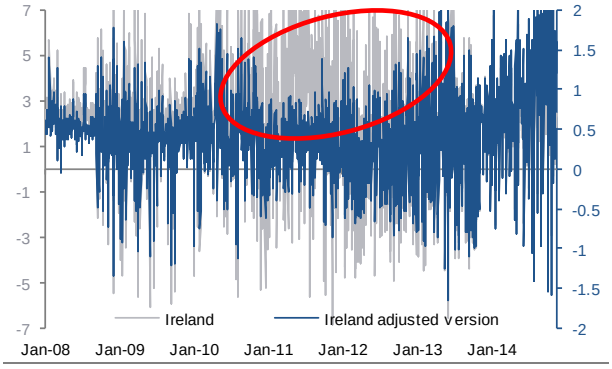

Graph 222. The interest rate adjustment leads to more contained $S_{i,t}$ indicators during periods of financial distress (Spain)

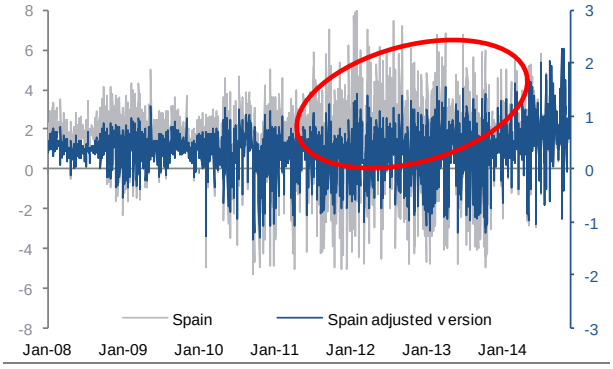

Under the assumption of mean-reversion, **a given variable delivers meaningful information only if it sits sufficiently far from the mean.** In this case, the expected reversion towards the mean is seen as a market opportunity.

We already mentioned that **$\tilde{S}_{i,t}^2$ is more reactive than $\tilde{S}_i^1$. And as a result, $\tilde{S}_{i,t}^2$ can be seen as a reference for detecting contagion.** A very high and positive coefficient $\Delta S_{i,t}$ for instance, indicates that $\tilde{S}_i^1 \gg \tilde{S}_{i,t}^2$. In this case, the intrinsic measure $\tilde{S}_i^1$ is much higher than it should be - compared to the multivariate measure $\tilde{S}_{i,t}^2$ (which takes the whole spread complex into account) and in light of

the underlying idiosyncratic risks illustrated by $r_{i,t}$. Invoking mean reversion when $\Delta S_{i,t}$ is very large essentially means that $\tilde{S}_i^1$ has risen too much compared to $\tilde{S}_{i,t}^2$. Based on eq. (58), this implies that $\hat{F}(x_{i,t})$ and consequently $x_{i,t}$ are too large as well, and should correct downwards in the future. The downward correction in $x_{i,t}$ means that the sovereign bond in country i is seen as outperforming the interest rate swap. In this case, you can make a profit if you open a long position on the asset swap spread in country i (ie. you buy the bond and you pay the IRS). But this makes sense only if $\Delta S_{i,t}$ is large enough, **ie. only if $\boldsymbol{\Delta S_{i,t}}$ has exceeded a certain threshold that we denote $\boldsymbol{S_{th,i}}$.** Below this threshold, the mean reverting rationale is null and void.

By analogy, a very negative $\Delta S_{i,t}$ means that it could be profitable to short the asset swap spread. However, we consider a long only portfolio, so this recommendation is not applicable. We restrain therefore our analysis to $\Delta S_{i,t} \geq 0$.

In order to quantify any deviation in $\Delta S_{i,t}$ from its mean, we consider the z-score estimator as defined in Abdi (2010):

$$Z_{s,i}(t) = \frac{\Delta S_{i,t} - \mathbb{E}[\Delta S_{i,t}]}{\sigma(\Delta S_{i,t})} \tag{118}$$

Where $\mathbb{E}[\Delta S_{i,t}]$ and $\sigma(\Delta S_{i,t})$ are the empirical mean and standard deviation of $\Delta S_{i,t}$. Because we seek to observe the out-of-sample performance of the portfolio we calculate $\mathbb{E}[\Delta S_{i,t}]$ and $\sigma(\Delta S_{i,t})$ over the sub-period from January 2008 to December 2010.

The z-score $Z_{s,i}$is an illustration of the deviation of $\Delta S_{i,t}$ against its mean value $\mathbb{E}[\Delta S_{i,t}]$ as a share of its standard deviation $\sigma(\Delta S_{i,t})$. This will prove a convenient estimator to define a threshold $S_{th,i}$.

Before calculating $S_{th,i}$ we would like to add a differentiation criterion that will help discriminate countries in the sample according to their credit quality. We distinguish three main categories: core, soft-core (or semi-core) and non-core countries (or peripheral) countries. This qualitative categorisation in Table 160 is based on the general understanding of each country by market participants. We note in particular that peripheral countries are more numerous in the sample (5 peripheral countries versus 3 soft-core and 3 core countries).

We believe it is worth discriminating countries in order to avoid an inconvenient concentration of the weights on the more volatile countries. As a result we give each country a score k_i that will be used as a "guide" to ensure a more conservative selection of the assets. We define the score k_i on the basis of two arbitrary conditions:

- First, so that the score in soft-core countries be twice as big as for non-core countries; and so that the score for core countries be once and half as big as for soft-core countries, ie:
$$\{k_{soft-core} = 2 \times k_{non-core};\ k_{core} = 1.5 \times\ k_{soft-core}\}$$
- Secondly, the scores is normalised: $\sum k_i = 1$

In the end these are sufficient to get a unique score for each group, as displayed in Table 160. In this configuration, we get a total score of 45% for core countries, 30% for soft-core countries, and 25% for peripheral countries.

Table 160. Breakdown between core/soft-core and peripheral countries and corresponding scores k_i

	GE	FI	NL	AT	FR	BE	IT	SP	IR	PT	GR
Category	Core	Core	Core	Soft-core	Soft-core	Soft-core	Non-core	Non-core	Non-core	Non-core	Non-core
Score k	0.15	0.15	0.15	0.10	0.10	0.10	0.05	0.05	0.05	0.05	0.05

The role of the score k_i is comparable to the optimised criterion in the GMV, ERC and MDP frameworks, namely the portfolio volatility (GMV), the univariate risk contribution (ERC), and the portfolio diversification criterion (MDP).

The proposed definition of the score k_i is an arbitrary choice, other definitions could provide interesting results as well. A more sophisticated definition e.g. involving the average volatility could be an alternative too. In the present analysis however, we want the score to have little influence so that we can focus on the role of $\Delta S_{i,t}$. So we prefer a simple definition of k_i.

As we mention before, we have to estimate a threshold $S_{th,i}$ which makes the mean reversion reasoning applicable when $\Delta S_{i,t} > S_{th,i}$. By definition, $Z_{s,i}$ are standardized time series, ie. with normalised variance and a centred mean. Higher moments tend to differ from one country to another, and as a result the absolute z-scores $|Z|_{s,i}$ exhibit different mean values.

A key consideration is that we seek to build a conservative portfolio that is supposed to enhance prudence in investments during periods of risk aversion. Since German ASW is the safest security in the sample, the corresponding z-scores $Z_{s,GE}$ exhibit small tails. And since $\mathbb{E}\big[|Z|_{s,GE}\big]$ is an illustration of the average absolute magnitude of $Z_{s,GE}$, We assume that $Z_{s,GE}$ is mean-reverting when $Z_{s,GE}(t) \geq \mathbb{E}\big[|Z|_{s,GE}\big]$. But this only makes sense for Germany, which is particularly stable and resilient to financial distress.

The score k_i is supposed to restrain the proportion of soft-core and peripheral securities within the portfolio. In order to make the selection for mean reverting strategies less frequent in soft-and non-core countries, we need to get a more stringent threshold $S_{th,i}$ on these countries. In particular, we consider the ratio $\frac{k_{GE}}{k_i}$ as a 'penalty' coefficient, that we apply to $\mathbb{E}\big[|Z|_{s,GE}\big]$.

On that basis, we consider that mean reversion on country i makes sense only if:

$$Z_{s,i}(t) \geq \mathbb{E}\big[|Z|_{s,GE}\big] \times \frac{k_{GE}}{k_i}$$

This tends to make the asset selection more severe. Then considering the point where the equality holds, we obtain the following equation:

$$\mathbb{E}\big[|Z|_{s,GE}\big] \times \frac{k_{GE}}{k_i} = \frac{S_{th,i} - \mathbb{E}[\Delta S_{i,t}]}{\sigma(\Delta S_{i,t})}$$

This gives the value of the threshold $S_{th,i}$:

$$S_{th,i} = \mathbb{E}\big[|Z|_{s,GE}\big] \frac{k_{GE}}{k_i} \sigma\big(\Delta S_{i,t}\big) + \mathbb{E}[\Delta S_{i,t}] \tag{119}$$

Table 161 shows the resulting $S_{th,i}$, along with the corresponding percentile taken on the empirical distribution of $\Delta S_{i,t}$ from the upper tail. This percentile indicates which portion of $\Delta S_{i,t}$ is above the threshold $S_{th,i}$ and thus will lead to a trade in the portfolio. Table 161 indicates that this portion

consistently declines for countries of a lesser credit quality: around $25-40\%$ of the distribution for core countries, then $8-20\%$ for soft-core credits, and finally just $4-9\%$ in peripheral markets. **➔ The reduced portion in peripheral markets illustrates the more severe selection procedure for volatile countries.**

Table 161. thresholds above which mean reverting is seen as applicable, and corresponding percentiles

	GE	FI	NL	AT	FR	BE	IT	SP	IR	PO	GR
$S_{th,i}$	0.1	0.9	0.7	-0.2	0.2	0.3	1.0	0.5	1.9	0.4	0.6
Percentile from upper tail	24%	43%	40%	8%	20%	13%	9%	4%	9%	6%	6%

We have now defined a selection procedure for all countries: a given security is selected in the portfolio if $\Delta S_{i,t}$ is larger than $S_{th,i}$.

We now have to determine the weight attached to each asset. A large z-score means that there is a high probability that mean reversion will effectively materializes. It looks therefore coherent to consider z-scores themselves as a an estimate of the weights, that we then normalise so that $\sum w_i = 1$.

In the end we formalise the weight estimation procedure as per the following equations:

$$\begin{cases} t_{i,t} = \delta_{i,t} \times Z_{s,i}(t) \\ w_{i,t} = \dfrac{t_{i,t}}{\sum_{j=1}^{11} t_{j,t}} \end{cases} \qquad (120)$$

Where $\begin{cases} \delta_{i,t} = 1 & \text{if } \Delta S_{i,t} \geq S_{th,i} \\ \delta_{i,t} = 0 & \text{otherwise} \end{cases}$ and because we consider 11 different securities.

Unlike the GMV, ERC and MDP approaches, it is important to note that there is no constraint in terms of portfolio volatility, risk contribution or diversification. Instead of seeking to reduce one of these parameters, the risk metric has been designed to detect market discrepancies and to take advantage of a possible reversion to the mean.

We denote the resulting portfolio as a 'z-score portfolio', and we compare it to the GMV $\hat{h}$ version that delivered an interesting performance (Graph 209). As Graph 223 shows, the z-score portfolio largely outperforms the GMV $\hat{h}$ version in terms of return, with a stunning 40% gain over the full period.

Graph 223. The z-score portfolio outperforms other optimization procedure (daily rebalancing)

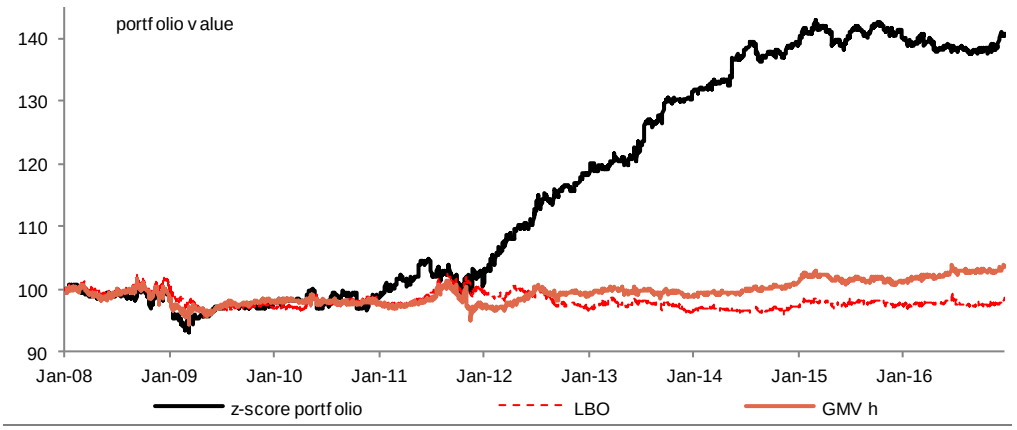

Looking at the dynamics, we note all the same that the z-score portfolio is very similar to the LBO and the GMV $\hat{h}$ versions until end-2010, ie. during the period we consider to calculate $E[\Delta S_{i,t}]$, $\sigma(\Delta S_{i,t})$, and $E\left[|Z|_{s,GE}\right]$. Then there is a notable differentiation, with a sharp rebound emerging in January 2011, which is albeit partly offset by some losses in H2 when contagion is intense. By end-2011, the z-score portfolio is at an equivalent level to the risk-free LBO portfolio, **suggesting that our asset selection offers sensible protection during the risk aversion period.** The portfolio value then consistently rises from 2012 to 2015 and shows an outstanding performance during the whole risk appetite period.

Looking at the weights within the portfolio, Graph 224 indicates that core securities are in a big portion, around 60% on average, while there is just 25% invested in soft-core assets and 15% in peripherals.

The risk contribution however is much different in Graph 225. First we note that core countries account for a smaller portion of the portfolio variance than the weights suggest. There is also a clear preference for soft-core securities between 2010 and 2012, while the exposure to non-core assets is declining meanwhile. **This partly explains some robustness compared to other methodologies during this period.** Finally, the portfolio slides towards a greater exposure to peripheral countries from 2013 onwards**. Thus largely boosted the performance of the portfolio during these years, marked by risk appetite and tighter asset swap spreads in general.**

Graph 226**,** Graph 227**,** Graph 228 give more clarity on the contribution of each country separately. Table 162 is a summary.

Graph 224. Weights in the z-score portfolio

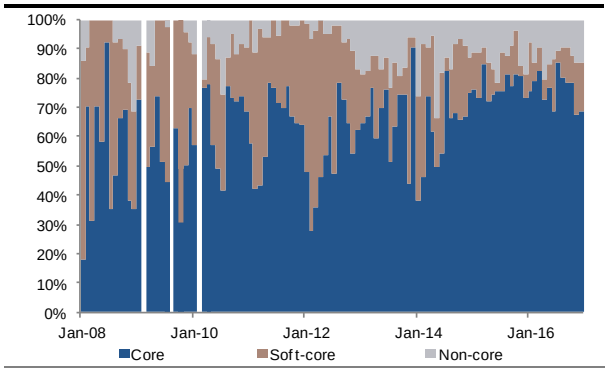

Graph 225. Contribution to portfolio volatility, z-score portfolio

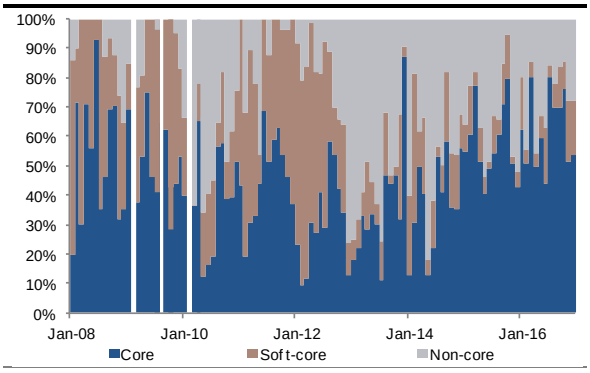

Graph 226. Contribution from core countries to the portfolio volatility, expressed as a share of the total contribution by these three countries

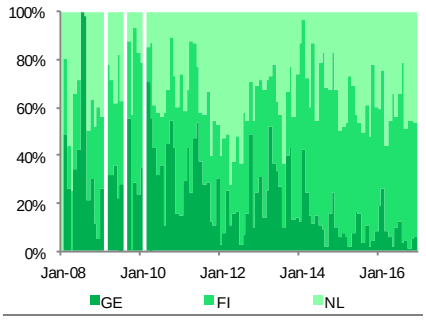

Graph 227. Contribution from soft-core countries to the portfolio volatility, expressed as a share of the total contribution by these three countries

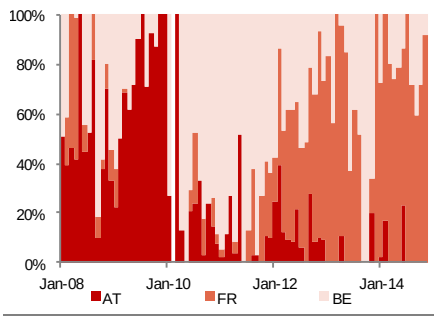

Graph 228. Contribution from non-core countries to the portfolio volatility, expressed as a share of the total contribution by these five countries

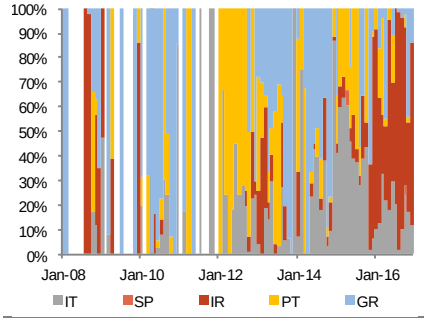

Table 162. Summary of the z-score portfolio

Average Values	GE	FI	NL	AT	FR	BE	IT	SP	IR	PO	GR
Weights (%)	15	26	23	5	12	8	3	0	3	2	3
Contribution to total volatility (%)	10	17	16	5	11	12	5	0	5	7	13

This time, the greater ability to adjust the exposure to core/soft-core/non-core bonds when market conditions turn sharply risk-averse offers meaningful protection. This also helps enhance returns in periods of risk-appetite by overweighting the higher yielding securities. In the end our assumption of mean reversion in $\Delta S_{i,t}$ proves coherent and efficient to detect market opportunities.

Like in the preceding analysis, we also consider a monthly rebalancing of the weights. We follow the same methodology and some empirical tests indicate that the following formulation of the threshold $S_{th,i}$ offers interesting results:

$$S_{th,i} = 0.055 \frac{k_{GE}}{k_i} \sigma\left(s_{i,t}\right) + \mathbb{E}[\Delta S_{i,t}] \tag{121}$$

Compared to the initial formulation in eq. (119), we replaced $\mathbb{E}\left[|Z|_{s,GE}\right]$ by 0.055, which looks more adequate for monthly rebalancing.

Graph 229 shows the resulting portfolio. This time again, the z-score portfolio outperforms the GHT and MDP forecast versions that we previously identified as interesting. Graph 230 shows the contribution of each asset category to the portfolio variance. First we note that only a few trades happened between 2008 and 2011, which means that there was no particular mean reverting opportunities detected during this period. Then from mid-2011 onwards, core countries have a dominating influence in the portfolio. Non-core securities in comparison are largely involved in 2012, but their contribution is less important during the following years. Soft-core countries in the end are selectively involved.

Graph 229. Performance of the z-score portfolio, monthly rebalancing

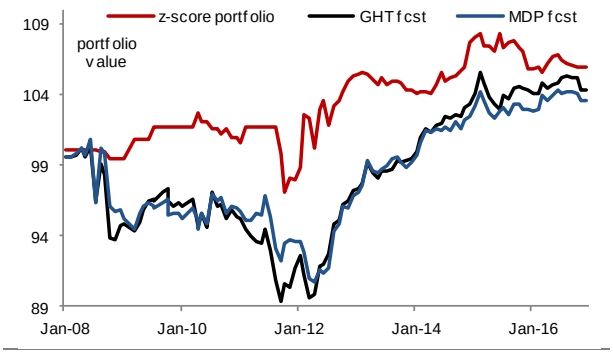

Graph 230. Contribution to the portfolio volatility

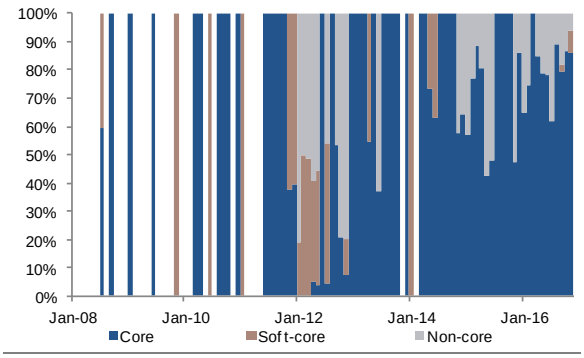

Conclusion

In conclusion, we showed in this Chapter that our statistical approach is able to deliver insightful conclusions on how risk-propagation is supposed to operate, from both univarite and multivariate perspectives.

First, we have rationalised the dynamics of the deterioration, in terms of credit quality, that arises from the emergence of shocks. Our approach involves two different definitions of the shock: one, temporal, is based on the market-implied probability of default; this formulation involves the GAS volatility estimator obtained in Chapter 1. A second definition investigates the relevance of time-invariant stress tests and finally delivers an estimator of the expected market reaction from a more general point of view than the temporal approach. We considered a series of many shocks with gradual intensity. The analysis offers a high-degree of granularity in the results, and this proved particularly helpful to extrapolate empirical rules on the general behaviour of 1) the intrinsic volatility, 2) the market response to shocks, 3) the expected frailty ensuing from the shock.

On a cross country basis, our analysis also shows that there exists a linear trajectory amongst the different sovereigns (Graph 163), that relates the maximum market reaction to what we consider as a measure of the frailty induced by financial distress. This linear behaviour is insightful information, which was unexpected.

Then, in a second part, we focused on multivariate dependencies and how these are affected by shocks. Our analysis shows that the general acceleration of the joint market reaction to shocks admits a logarithmic behaviour, when expressed as a function of the shock intensity. Results also suggest that a purely univariate exploration of sovereign risk tends to underestimate the market reaction to shocks, hence there is a visible benefit in considering a multivariate framework.

Finally, we explored an application of the model in the context of portfolio optimisation. First we explored the relevance of incorporating our own volatility or market reaction to shocks into popular portfolio optimisation procedures (GMV, ERC, MDP). Results indicate that the modified version, involving our in-house risk-estimators, consistently outperform the more standard formulations found in the literature. Involving our measure of intrinsic volatility $\hat{h}$ or the volatility forecast $\hat{\sigma}_{t+1}$ in particular, greatly enhance the robustness of returns. Portfolios based on $\hat{\sigma}_{t+1}$ also show an interesting performance when rebalancing happens on a monthly basis. This reaffirms the forecasting capability of the GAS model, which is a valuable dimension of the methodology.

In the last part of the chapter, we designed an in-house methodology for optimal portfolio rebalancing, based on mean reversion. This approach offers outstanding results, overall demonstrating that the allocation strategy is able to fit many different market environments. In particular, a back-test over the full period shows that reallocation out of risk-seeking strategies and into more prudent positioning takes place as soon as there are palpable signs of mounting risk aversion. This is a sign of robustness. While mean-reverting approaches offer simplicity, they usually prove more hazardous when financial markets are very directional. We address this issue via sensible adjustments; overall results suggest that mean reversion can effectively be used for risk management purposes.

References

A macro stress testing *framework* for assessing systemic risks in the banking sector. ECB, Oct 2013

Abdi H, (2010). Normalizing Data, in Neil Salkind (Ed.), *Encyclopedia of Research Design*. Thousand Oaks, CA: Sage. 2010.

Alexander, C. (2001). Market models: A guide to financial data analysis. Chichester, UK: Wiley. Chapter 9.1, *Scenario analysis and stress testing*.

Altman E., Resti A. and Sironi A. (2003). Default Recovery Rates in Credit Risk Modeling: A Review of the Literature and Empirical Evidence. *Economic Notes* 33:183-208

Anand, K., Ben R. Craig, G. von Peter, (2014). Filling in the Blanks: Network Structure and Interbank Contagion, Federal Reserve Bank of Cleveland, Working Paper no. 14-16.

Andersson, H. and Britton, T. (2000). Stochastic epidemic models and their statistical analysis. Springer Lecture Notes in Statistics, 151. Springer-Verlag, New York.

Anderson R. W., Sundaresan S. (1996). Design and Valuation of Debt Contracts. *The Review of Financial Studies* 9 (1): 37-68.

Angeloni I. (2016). Macroprudential policies to contain systemic risks. 32nd SUERF Colloquium and Deutsche Bundesbank/Foundation Geld und Währung Conference; Commerzbank and SUERF.

Angeloni I., (2015). Towards a macro-prudential framework for the single supervisory area. Belgium Financial Forum, Brussels.

Aragonés J. , Blanco, C., Dowd, K. (2001). Incorporating Stress Tests into Market Risk Modelling, *Derivatives Quarterly*, Institutional Investor, primavera.

Artzner, P., Delbaen, F., Eber, M., and Heath, D. (1999). Coherent measures of risk. *Mathematical Finance*, 9:203–228.

Aussenegg W., Götz L., Jelic R. (2012). European Asset Swap Spreads and the Credit Crisis.

Bernardino G. (2016). Low level of interest rates and their implications for insurers and pension funds. European Systemic Risk Board Annual Conference, Frankfurt.

Black F, Cox J.C. (1976). Valuing corporate securities: some effects of bond indenture provisions. *Journal of Finance* 31:351–67

Board of Governors of the Federal Reserve System (2009a). The Supervisory Capital Assessment Program: Design and Implementation.

Board of Governors of the Federal Reserve System (2009b). Guidelines on liquidity buffers and survival periods, London.

Board of Governors of the Federal Reserve System (2016). 2016 Supervisory Scenarios for Annual Stress Tests Required under the Dodd-Frank Act Stress Testing Rules and the Capital Plan Rule (Washington, DC: Board of Governors, January 28)

Boyson, N., Stahel, C., and R., Stulz (2010). Hedge Fund Contagion and Liquidity Shocks, *Journal of Finance*, 65, 1789-1816.

Bronshtein, E. M., Fabozzi F. J., Rachev S. T., Sereda E. N., Stoyanov S. and W. Sun (2008). Distortion Risk Measures in Portfolio Optimization, Working Paper.

Brunnermeier, M., and L. H. Pedersen (2009). Market Liquidity and Funding Liquidity, *Review of Financial Studies*, 22, 2201-2238.

Camara B., Pessarossi P., and Philippon T. (2016). Back-testing bank stress tests. Stern University.

Carmichael B., Koumou G., Moran K. (2015). Unifying Portfolio Diversification Measures Using Rao's Quadratic Entropy. CIRPEE Working Paper 15-08.

Choueifaty Y., Froidure T., Reynier J. (2013). Properties of the Most Diversified Portfolio. *Journal of Investment Strategies*, Vol.2(2), Spring 2013, pp.49-70.

Daron A., Ozdaglar A., and Tahbaz-Salehi A. (2014). Systemic Risk in Endogenous Financial Networks. Columbia Business School, November 2014.

Darolles S., Gagliardini P., Gourieroux C. (2013). Survival of Hedge Funds: Frailty versus Contagion. Working Paper, CREST, Paris.

Darolles S., Gagliardini P., Gourieroux C. (2014). Contagion and systemic risk: an application to the survival of hedge funds. Working Paper, CREST.

Davis, M. (2013). Consistency of Risk Measure Estimates, October. Available at SSRN: https://ssrn.com/abstract=2342279 or http://dx.doi.org/10.2139/ssrn.2342279

De Groen W. P. (2016). The EBA EU-wide Stress Test 2016: Deciphering the black box. CEPS Policy Brief, No. 346, August 2016.

De Groen, W.P. and D. Gros (2015), Estimating the bridge financing needs of the Single Resolution Fund: How expensive is it to resolve a bank?, In-Depth Analysis, European Parliament.

Delianedis G., Geske R. (1999), Credit risk and risk neutral probabilities: information about rating migrations and defaults, WP UCLA, May.

DeMiguel, V., Garlappi, L., Uppal, R., (2009). Optimal Versus Naive Diversification: How Inefficient is the 1/N Portfolio Strategy? *The Review of Financial Studies*, Vol. 22, Issue 5, pp. 1915-1953.

Derbali A., Hallara S. (2013). How the Default Probability is Defined by the Credit Portfolio Models: A Comparative Analysis between the Theoretical Structural Models? (August 1, 2013). *Global Journal of Management and Business Research*, Volume 13, Issue 1. Available at SSRN: https://ssrn.com/abstract=2540839 or http://dx.doi.org/10.2139/ssrn.2540839

Edwards S. (2015). Sovereign default, debt restructuring and recovery rates: Was the Argentianean haircut excessive?, NBER Working Paper 20964.

Eisenberg L., Noe T. (2001). Systemic Risk in Financial Systems *Management Science*, 47, (2), 236-249.

Elsinger, H., Lehar A., and M. Summer (2013). Network models and systemic risk assessment. In J.-P. Fouque and J. Langsam (Eds.), Handbook on Systemic Risk, pp. 287–305. Cambridge University Press.

European Banking Authority, (July 2016) 2016 EU-wide stress tests results.

European Banking Authority, Consultation Paper (2018). Draft Guidelines on stress testing and supervisory stress testing, December 18.

European Banking Authority, (2014) Guidelines on common procedures and methodologies for the supervisory review and evaluation process (SREP), December 19.

European Central Bank (2013). A macro stress-testing framework for bank solvency analysis. ECB Monthly Bulletin, pp.93-109, August.

Fabozzi, F. (2003). The Handbook of Fixed Income Securities". Wiley.

Fabozzi, F. J., Davis H. A. and Choudry M. (2006). Introduction to Structured Finance, Hoboken, New Jersey: John Wiley & Sons, Inc.

Feinstein, Z., Rudloff, B. (2015). Measures of Systemic Risk. Leibniz Universität Hannover.

Feria Dominguez J. M., Oliver Alfonso M. D. (2004). Applying Stress-Testing On Value at Risk (VaR) Methodologies, Investment Management and Financial Innovations.

Gilli M., Große S. and Schumann E. (2010). Calibrating the Nelson–Siegel–Svensson model.

Glasserman P., Nouri B., (2012). Contingent Capital with a Capital-Ratio Trigger. *Management Science* 58:10, 1816-1833.

Glasserman, P. and Young, P., (2013), How Likely is Contagion in Financial Networks?, No 13-06, Working Papers, Office of Financial Research, US Department of the Treasury.

Goyenko, R. (2012). Treasury Liquidity and Funding Liquidity: Evidence from Mutual Fund Returns, DP McGill University.

Grigat D., Caccioli F. (2017). Reverse stress testing interbank networks. University College London, Department of Computer Science, Systemic Risk Centre, London School of Economics and Political Sciences,.

Grundke P. and Pliszka K. (2015). A macroeconomic reverse stress test. Bundesbank Discussion Paper No. 30.

Guillermo, P. J. (2010). Modeling Credit Risk through Intensity Models. Uppsala universitet / Matematiska institutionen.

Gupta, A., and M., Subrahmaniam (2000). An Empirical Investigation of the Convexity Bias in the Pricing of Interest Rate Swaps, *Journal of Financial Economics*, 55, 239-279.

Hardy, D. C. and C. Schmieder (2013). Rules of Thumb for Bank Solvency Stress Testing, IMF Working Paper, WP/13/232.

Hesse H., Salman F., Schmieder C. (2014). How to Capture Macro-Financial Spillover Effects in Stress Tests?, IMF Working Paper No.14/103.

Hirtle B, Lehnert A. (2014). Supervisory Stress Tests Federal Reserve Bank of New York Staff Reports, no. 696. JEL classification: G21, G01.

Hirtle B., Schuermann T., Stiroh K. J. (2009). Macroprudential Supervision of Financial Institutions: Lessons from the SCAP. FRB of New York Staff Report No. 409. Available at SSRN: or http://dx.doi.org/10.2139/ssrn.1515800

Houy N., Jouneau-Sion F. (2016). Defaulting Firms and Systemic Risks in Financial Networks.

Hull J., Predescu M., White A. (2005). Bond prices, Default Probabilities, and Risk Premiums. *Journal of Credit Risk* 1, no. 2 (Spring 2005): 53-60.

Jarrow, R. A. (2011). The Economics of Credit Default Swaps, Annual Review of Financial Economics. Vol. 3:235-257. DOI: 10.1146/annurev-financial-102710-144918

Kempf A., Memmel C. "On the Estimation of the Global Minimum Variance Portfolio" (February 28, 2003).

Kok C. "Tools for macro stress testing and macro prudential policy assessment: The ECB perspective". Oct 2013.

Koziol, Philipp and Schell, Carmen and Eckhardt, Meik, Credit Risk Stress Testing and Copulas: Is the Gaussian Copula Better than its Reputation? (2015). Bundesbank Discussion Paper No. 46/2015. Available at SSRN:

Lautier D., Raynaud F. (2012). Systemic Risk in Energy Derivative Markets, A Graph-Theory Analysis, *The Energy Journal*, 33(3), 217-242, 2012.

Leland, H. E. (1994). Corporate Debt Value, Bond Covenants, and Optimal Capital Sturcture, J. Finance 49, 1213–1252.

Leland, H., and K. B. Toft (1996). Optimal Capital Structure, Endogenous Bankruptcy, and the Term Structure of Credit Spreads, J. Finance 51, 987–1019.

Liu, Q. (2009). On Portfolio Optimization: How Do We Benefit from High Frequency Data. *Journal of Applied Econometrics*, 24(4), 560-582.

Livingston M., Zhou, L. (2005). Exponential Duration: a more accurate estimation of interest rate risk. *Journal of Financial Research*, 28: 343–361. doi:10.1111/j.1475-6803.2005.00128.x

Lucas A., Schwaab B., Zhang X. (2012). Conditional probabilities for euro area sovereign default risk. ECB Financial research.

Maillard S., Roncalli T., Teiletche J. (2010). The properties of equally-weighted risk contributions portfolios. *The Journal of Portfolio Management*. Summer 2010, Vol. 36, No. 4: pp. 60-70. DOI: 10.3905/jpm.2010.36.4.060

Merton, R. (1974). On the pricing of corporate debts: the risk structure of interest rates. *Journal of Finance*, (29):449–470.

O'Kane, D. (2001). Credit Derivatives Explained. Lehman Brothers Structured Credit Research.

Roncalli T. (2012) Portfolio Optimization versus Risk-Budgeting Allocation. WG RISK ESSEC.

Roncalli T., Bruder B. (2012). Managing Risk Exposures using the Risk Budgeting Approach. Séminaire de Mathématiques Appliquées, Laboratoire de Mathématiques Jean Leray, Atelier Finance & Risque, Laboratoire LEMNA, Université de Nantes, March 29, 2012.

Schaefer, S. M. (2012). The Default Intensity Model and the Copula Approach, Credit Risk Elective.

Schmieder, C., Hesse, H., Neudorfer, B., Puhr C., and Schmitz S. W. (2012), Next Generation System-Wide Liquidity Stress Testing, IMF Working Paper 12/3 (Washington: International Monetary Fund).

Senneret M., Malevergne Y., Abry P., Perrin G., Jaffres L. (2016). Covariance versus Precision Matrix Estimation for Efficient Asset Allocation. IEEE Journal on Selected Topics in Signal Processing, September 2016, 10(6):982-993.

Sundaresan S. (2013). A Review of Merton's Model of the Firm's Capital Structure with Its Wide Applications. *Annual Review of Financial Economics* Vol. 5:21-41. DOI: 10.1146/annurev-financial-110112-120923

Tchuindjo L. (2007) An Accurate Formula for Bond-Portfolio Stress Testing. *The Journal of Risk Finance*, Vol. 9, No. 3, 2008, pp. 262-277.

Teo, M. (2011). The Liquidity Risk of Liquid Hedge Funds, *Journal of Financial Economics*, 100, 24-44.

Tuckman, B. (2003). Measures of Asset Swap Spread and their Corresponding Trades. Lehman Brothers Fixed Income Research, January 2003.

Upper, C. (2011). Simulation methods to assess the danger of contagion in interbank markets. *Journal of Financial Stability* 7(3), 111–125.

Upper, C. and A. Worm (2004). Estimating bilateral exposures in the german interbank market: Is there a danger of contagion? *European Economic Review* 48, 827–849.

Varga-Haszonits I., Caccioli F., Kondor I. (2016). Replica approach to mean-variance portfolio optimization. *Journal of Statistical Mechanics*: Theory and Experiment, 2016(12):123404, 2016.

Vayanos, D. (2004). Flight to Quality, Flight to Liquidity, and the Pricing of Risk. NBER WP 10327

Visentin G., Battiston S., D'Errico M., (2016) Rethinking Financial Contagion.

Wan, Joshua S., (2016). Systemically Important Asset Managers: Perspectives on Dodd-Frank's Systemic Designation Mechanism. *Columbia Law Review* 805.

Yi Lan (2011). Survival Probability and Intensity Derived from Credit Default Swaps. MSc Thesis, Worcester Polytechnic Institute, Financial Mathematics.

Ziegelmann F. A., Borges B. (2015). Selection of Minimum Variance Portfolio Using Intraday Data: An Empirical Comparison Among Different Realized Measures for BM&FBovespa Data. *Brazilian Review of Econometrics*, 35(1).

Chapter III.

Price discovery in bond options

Résumé du Chapitre III

Le Chapitre III est dédié au pricing de produits dérivés de taux. Nous considérons maintenant que l'aversion au risque cause l'émergence de discontinuités dans les prix de marché, que nous simulons par le biais de processus stochastiques à sauts. Notre modèle se concentre sur les processus de Hawkes qui ont l'avantage de capturer la présence d'auto-excitation dans la volatilité. Le manque de données sur les volatilités implicites traitées sur le marché rend la calibration du modèle particulièrement difficile.

Dans un premier temps nous considérons le modèle proposé par Ait-Sahalia (2010). L'auteur cherche à distinguer la dynamique discontinue des prix de marchés, visible en période d'aversion au risque, de la dynamique purement continue, qui domine en période de sentiment de marché plus stable. Au final, le modèle proposé implique un nombre considérable d'inconnues à calibrer. Nous notons aussi un risque de redondance entre les coefficients continus et discontinus qui rend la calibration relativement instable. Les calibrations que nous avons menées n'ont pas donné de résultats tangibles et nous avons été contraints de considérer une approche alternative.

Le second modèle que nous explorons se base sur l'approche de Hainaut (2016). Notre formulation du problème est relativement similaire à l'approche initiale, cependant nos hypothèses sont très différentes car nous supposons que les sauts ne sont pas observables et font donc parties des données latentes du problème. Ceci implique des changements majeurs quant à la calibration du modèle et nous développons une procédure de calibration qui se distingue des méthodologies habituellement trouvées dans la littérature. Les résultats de volatilité implicite sont cohérents avec la volatilité réalisée, et suggèrent que les coefficients de prime de risque ont été estimés avec succès.

Introduction

Chapter 1 and Chapter 2 stress that the transformation induced by risk aversion is fairly described by heavy-tailed probability distribution functions. While the heavy-tailed component is an illustration of the non-linear aspect of the market reaction when flight-to-quality is intense, we also note that the probabilistic nature of the framework is equivalent to assuming a **continuous** transition in market prices. This is visible for instance when we move from the centre-region of the distribution and towards the tails, in a context of fierce risk aversion. To some extent, this assumption on the continuous nature of any risk-off-induced market reaction, may be seen as narrowing the scope of the analysis. **We thus revisit it in the third chapter of this dissertation.**

As an alternative approach to sovereign risk exploration, we now consider that risk aversion favours the emergence of **noticeable discontinuities in market prices**, that we model as stochastic jumps. We also focus on the observed hysteresis in the dynamics of the price action: empirical observations suggest that periods of recurrent jumps are likely to be followed by periods of even more frequent and bigger jumps (in terms of their amplitude). **This supports the existence of a self-feeding component, that tends to affect the jump dynamics in a meaningful way during periods of intense risk aversion.** In this context, we consider Hawkes processes as a relevant descriptor of the jump dynamics. This category of models is based on stochastic jumps, and introduces self-excited jump intensities. Self-excitation is a key component that we explore in depth. First we replicate the model of Ait-Sahalia (2010), but results are disappointing and the calibration is not successful. As a substitute, we consider a modified version of the model explored in Hainaut (2016). We also investigate a multivariate formulation of the model, which helps identify **the contagion effect** within a basket of different securities.

Stochastic models are popular for pricing financial derivatives. Their diffusive capability, in particular, makes the exploration of synthetic scenarios on the future trajectory of market prices especially convenient. **We explore this feature as well, and we draw guidelines on the expected implied volatility, for sovereign bond options.**

Bond options is (still) a very modest market in terms of size and this makes the case for a pronounced lack of information on traded products. In particular, we were not given the chance to involve a reliable set of quoted implied volatilities. This naturally added to the general complexity of the model, encouraging us to design a novel methodology for the calibration. **In the end, our methodology differentiates itself in many ways from more traditional approaches commonly seen in the literature.**

Literature review and context

In the previous chapters, we showed that fat-tailed probability distribution functions are a relevant choice to explore the dynamics of the volatility arising from risk-averse market conditions. The heavy-tailed component looks especially appropriate to model the acceleration in price variations when flight to quality is fierce. And aside from the tails, the general shape of Generalized Hyperbolic distributions also helped identify how the switch from moderate volatility into a more extreme regime of widespread price deteriorations operates. The continuous dimension of probability distribution functions has been a meaningful feature as well. First this made the calculation of VaR-based stress tests relatively straightforward. Plus, the continuous approach allowed us to explore a series of numerous stress scenarios, with varying intensity. The assumption of a continuous transition in price variations when moving into risk averse market conditions also offered some computational tractability, and we largely took advantage of it in Chapter 2. While results look consistent with the actual price dynamics, we understand that the deployed methodology has also built-in limitations. First, we note that every financial crisis results from a unique set of different circumstances. Since each episode has its own particularities, risk aversion may be impacted by the very specific nature of each crisis. As a result, the price action may be impacted in a peculiar manner every time, depending on the nature of growing concerns in the background. For instance, liquidity-based or credit crunch-based crises will probably hit main asset classes differently during the early stages of the market rout. Then, as time goes by, further escalation in risk aversion may favour more convergence in terms of how market prices is impacted in both cases – at least episodes of generalised market debacle in the past have proven somewhat similar beyond a certain degree of risk aversion. Given that the dynamics of risk aversion may vary from one crisis to another (depending on nature of the underlying shocks), the relevance of 'summarising' the price action during financial crises into just one and unique probability distribution function may be questionable. **While any model has to deal with this issue of robustness, our assumption that risk propagation occurs in a continuous manner, as we did in Chapter 1, may prove particularly restrictive in this respect.** Stochastic models to some extent, may offer greater flexibility on this specific issue. Another drawback relates to the fact that shocks in financial markets, at least in developed markets, are (thankfully) infrequent. As a result, the portion of data supposed to describe a proper financial crisis in the sample, is relatively small compared to the data illustrating the normal course of financial markets. **This scarcity of information could negatively weigh on the robustness of tail-related observations and on the ensuing conclusions.** Finally, a third limitation comes from the continuous dimension itself, which looks empirically questionable as to explore periods marked by major discontinuities in the market volatility.

As an alternative approach to sovereign risk exploration, we now consider that risk aversion is prompt to generate noticeable discontinuities in market valuations. These discontinuities, admittedly, stand in contrast with the continuous dynamics prevailing when volatility is more contained. Since the seminal paper of Merton (1976), stochastic models with jumps have been gaining importance, especially for option pricing and risk management purposes. A basic assumption is that jumps are independent one from each other. This occasioned the emergence of many models involving compounded Poisson jumps (see Embrechts et al. (1997), Katz (2002), Scalas (2006), Basawa and Brockwell (1982), Buchmann (2009), Chen et al. (2010), Comte and Genon-Catalot (2009, 2010, 2011), Figueroa-Lopez and Houdré (2006), Figueroa-Lopez (2009), Gugushvili (2009, 2012),

Jongbloed et al. (2005), Kim (1999), Neumann and Reiss (2009), Ueltzhofer and Kluppelberg (2011), Zhao and Wu (2009)). These models are usually based on Levy processes, where increments are independent and stationary. More recently, the exploration of high-frequency data has encouraged broader investigations on the dynamics of jumps, with a focus on justifying the emergence of such market discontinuities (see Barndorff-Nielsen and Shephard (2006), Ait-Sahalia and Jacod (2009a, 2009b, 2011, 2012), Ait-Sahalia, Jacod, and Li (2012), Jing, Kong, Liu, and Mykland (2012), Bollerslev and Todorov (2011)). For this purpose, the assumption of pure temporal independence between jumps looked less relevant, and had to be revised. This was comforted by the basic empirical observation that the presence of jumps in financial markets is usually coincident with typical situations of growing risk aversion. As it was observed that a persistence of this momentum (in the background) tends to encourage more frequent and bigger jumps as time goes by, there exists a logical connection between the volatility itself, and the jump intensity. While investigating the impact of exogenous factors on the jump dynamics is a sound way to get a deeper understanding of shocks (like in Goutte (2012)), other studies also explored an adjustment of the intrinsic definition of the shock dynamics. Christoffersen, Jacobs, and Ornthanalai (2012) for instance propose a discrete time model, whereby the jump intensity is a function of itself. Another interesting approach in Ait-Sahalia, Cacho-Diaz, and Laeven (2010) seeks to reconcile the observed persistence of the volatility during financial crisis and the notable hysteresis in jumps during these periods. In many cases for instance, it was shown that durable risk aversion tends to amplify weakness in market prices, hence making jumps more frequent and bigger in terms of amplitude. As a means to capture this feature, Ait-Sahalia, Cacho-Diaz, and Laeven (2010) consider that there exists a self-exciting dimension attached to jumps, which they incorporate into a specific redenomination of the jump intensity, involving Hawkes processes. A valuable feature of Hawkes processes is that the occurrence of a jump increases temporarily the probability of subsequent jumps in the future. As shown in Errais et al. (2010), this approach is a notable innovation when it comes to illustrating how risk aversion nurtures the deterioration of credit quality on a prolonged period of flight to quality. Ait-Sahalia, Laeven, Plizzon (2014) also offers an interesting exploration of Hawkes processes: the authors show that Hawkes processes are sufficiently versatile to model the dynamics of CDS spreads during financial crisis in general, with a focus on the European sovereign crisis. This approach can be extended to more sophisticated frameworks. In the case of a multivariate analysis for instance, Hawkes processes make possible the existence of some cross-excitation: a jump on a given security increases not only the probability of future jumps on this specific market, but on other surrounding markets as well. This can illustrate the propagation of financial distress via contagion. **We seek to identify and quantify this phenomenon in the following analysis.** Aside from credit risk, Hawkes processes have also found much wider applications like the modelling of limit order books in high frequency trading (see e.g. Alfonsi and Blanc (2016), and Abergel and Jedidi (2015)), or the design of rules for optimal decision making on the duration of trades (Bauwens and Hautsch (2009)). Buy and sell orders can also be seen as admitting a Hawkes dynamics (Bacry et al. (2013)). While Hawkes processes offer some value when it comes to pricing financial derivatives, the literature dedicated to stochastic jumps in the context of option pricing, is still relatively scarce. One of the first approaches was the Merton Jump model (Burger, Kliaras (2013)). The main incentive for designing a variation to the Black-Scholes formulation was to capture the negative skewness and excess kurtosis of the log stock price density by the addition of a compound Poisson jump process. Results suggest that option prices are more accurately estimated under this framework than the usual Black-Scholes model. As Burger, Kliaras (2013) indicates, the Kou model is another interesting variation, as it does not assume a

normal distribution of the stock returns. This approach is based on a double exponential jump diffusion model, which offers a higher peak and two heavier tails than a Gaussian distribution. Other approaches like in Fulop, Li, Yu (2014), Todorov (2009) and Chen and Poon (2013) also show the relevance of involving Hawkes processes as a means to model volatility risk premiums.

For Fixed Income derivatives, term structure models, like in Duffie and Kan (1996), Dai and Singleton (2000), have gained popularity for pricing swaptions and coupon-bond options. The affine approach in particular accommodates mean-reverting, correlated factors, and offers the possibility to consider stochastic volatility. Plus the estimation procedure is made straightforward by the fact that the conditional characteristic function of an affine process is known in closed-form (Duffie, Pan, and Singleton (2000),Bakshi and Madan (2000)). Then the price of a zero-coupon bond option is easily computed using Fourier inversion (Chen and Scott (1995), Chen (1996), Chacko and Das (1998), Nunes, Clewlow, and Hodges (1999), Duffie, Pan, and Singleton (2000), and Bakshi and Madan (2000)). In this context, there is little surprise that the affine class of term structure models (as characterized by Duffie and Kan (1996)) has effectively become the dominant class of models, and so mostly because of its analytical tractability: by restricting the spot rate, the risk neutral drift, and the instantaneous covariance matrix of the state vector to be linear in the state vector, bond prices inherit a simple exponential affine structure. As a result, coupon bond options or swaptions can be priced accurately and efficiently, and analytical solutions exist for the optimal bond portfolio choice problem. These models became the focus of a series of papers including Carverhill (1994), Ritchken and Sankarasubramanian (1995), Bhar and Chiarella (1997), Inui and Kijima(1998) and Jong and Santa-Clara (1999). Chiarella and Kwon (2001b) brings to light an interesting generalisation of the affine approach, in which the components of the forward rate volatility process satisfy ordinary differential equations in the maturity variable. As a result, and this is the main innovation, the forward rate curve can be expressed as an affine function of the state variables while conversely these state variables can be expressed as a function of each other. The introduced state variables however, do not have clear links to market observed quantities, and this can be seen as a limitation. The closed-form solution provided by the class of affine models has been a major reason for its success (see e.g. Duffie, Pan, and Singleton (2000)). This category of models has also been exploited to develop efficient approximation methods for pricing swaptions (Collin-Dufresne and Goldstein (2002b), Singleton and Umantsev (2002)), and closed-form moment conditions for empirical analysis (Singleton (2000), Pan (2002)). As such, it has generated much attention both theoretically and empirically.

Back to our concern of exploring market discontinuities, we note that Cont, Tankov, Voltchkova (2007) investigate the implications of adding jumps onto an affine pricing framework. They stress in particular, that discontinuities in X tend to create some market incompleteness. This leads to some hedging error when considering the Black-Scholes model, an error that the authors seek to estimate. Tankov (2010) and Tankov, Kohatsu-Higa (2010) give extensive details on how to improve hedging procedures, in light of this market incompleteness. This question of maximising the effectiveness of the hedging procedure when dealing with jump models is also investigated in Cont, Tankov, Voltchkova (2007). In this paper, the authors explore an optimal hedging strategy involving the underlying asset as well as a set of different options. This offers greater tractability than more common quadratic hedges (see e.g. Arai (2005)). Considering jump models applied to Fixed Income derivatives specifically, we see two main approaches. In equilibrium-based models on one side, the

dynamics of the term structure is deduced from short term interest rates, via a set of factors (jointly Markov). The process for these factors under the real measure P is supposed to be given. Then one has to specify a market price of risk for each of these factors, as to move under the so-called risk-neutral measure Q, under which all discounted-asset-price processes are martingales (Harrison and Kreps (1979)). The market price of risk may either be arbitrarily defined (Vasicek (1977)) or derived from fundamental observations and appropriate restrictions (Cox, Ingersoll and Ross (1985)). Aside from equilibrium-based models, a second part of literature seeks to avoid specifying the complexity of an evolving term structure. This approach, initiated by Ho and Lee (1986) and generalized by Heath Jarrow Morton (1992) (HJM), takes the initial term structure as given and, using the no-arbitrage condition, derives some restrictions on the drift term of the process of the forward rates, under the risk-neutral probability measure Q. While this approach offers some advantages compared to equilibrium-based models, HJM models also face notable limitations. First and perhaps the most important, HJM models are non-Markovian in general, which means that consequently the theory of PDEs no longer apply. Secondly, the HJM framework introduces some path dependency to pricing problems, and this tends to increase computational times significantly. Another limitation is that there are generally no simple methods for pricing commonly-traded derivatives such as caps/floors and swaptions. Finally, if we model forward rates as log-normal processes then the HJM model may become instable (Sandmann, Sondermann (1997)). This last theoretical problem can be addressed by describing LIBOR and swap rates as log-normal rather than instantaneous forward rates.

In this report, we add to the existing literature in different ways. First we explore the model of Ait-Sahalia, Cacho-Diaz, and Laeven (2010). The model relies on a sophisticated framework that seeks to differentiate the continuous part of market prices from the discontinuous dimension induced by jumps. This necessarily leads to a fairly high sophistication of the model, with many unknowns involved. We show that the calibration, under these conditions, is very instable. Even when adding additional constraints, the model seems to involve too many latent variables. In our view, a proper calibration of the model is extremely difficult to achieve. As we explore two different versions of this model, we also show that the computational burden is even higher for models involving stochastic volatility (as a means to capture the continuous dynamics of prices). Results suggest that the combination of stochastic volatility and a Hawkes process is a bit irrelevant as it tends to induce some unnecessary redundancy within the variables. In this set-up in particular, it is not clear whether jumps come from the Hawkes intensity itself, or from the presumed stochastic nature of volatility. As an alternative to capture the continuous dynamics, we show that models relying on constant volatility (instead of stochastic volatility) are more efficiently calibrated, although it is still challenging to find a global optimum for every unknown variable. In a second part of this report, we consider the approach described in Hainaut (2016). This model can be seen as a simplified version of Ait-Sahalia, Cacho-Diaz, and Laeven (2010). The proposed framework this time focuses exclusively on jumps, with no particular reference to the continuous part of the market dynamics. While the author considers that every market realisation is a jump, we do not make this assumption. We agree that a series of jumps can logically occur during any trading session. But we prefer assuming that they are not observable (in our own sample at least), given that we only get market-close prices, with no particular insight on the daily intraday volatility. One could possibly identify jumps via empirical methods by involving high-frequency intraday data; but this was not possible for us. This difference with the approach provided in Hainaut (2016) led to sizeable modifications in the calibration procedure, that we highlight in the following sections.

Separating the (continuous) wheat from the (jumpy) chaff

Stochastic jumps have become a popular approach in the recent literature to describe the behaviour of shocks in financial markets. The non-continuous dimension of jumps makes them especially relevant to illustrate erratic variations observed in market prices during periods of distressed market conditions.

In the last chapters, shocks and financial crises were understood as 'tail-events'. As a result, we explored the tail regions of appropriately chosen/calibrated distributions, and this helped draw conclusions on the dynamics of financial markets under heavy risk aversion. In this chapter now, we consider that risk aversion favours more frequent and larger jumps than in more balanced market conditions. Hawkes processes offer a versatile formulation that enables capturing this phenomenon, via the introduction of mutually-excited jump intensities. This category of stochastic processes was introduced by the foundational work of Hawkes (1971), Hawkes and Oakes (1974), and Oakes (1975).

The self-exciting loop within Hawkes processes, has proven to be particularly helpful to illustrate the self-feeding dimension of financial crises. In practice, this phenomenon is visible in the fact that shocks are increasingly more frequent, and bigger, when financial distress is mounting. Ait-Sahalia, Cacho-Diaz, and Laeven (2010) has made an extensive exploration of Hawkes processes in the context of modelling financial contagion. In this approach, the asset price is modelled as the combination of a diffusion part (σdW) and a jump component (ZdN).

Hawkes processes are largely inspired from the more commonly used Poisson processes. Both are defined by the intensity process of the jump, that we denote $\lambda_{i,t}$. This describes the $\mathcal{F}_t$-conditional mean jump rate per unit of time for a given security i, **ie. the temporal frequency of shocks**. We also denote $N_{i,t}$ the point-process that counts the shocks from the beginning of the simulation, and we assume that there are n measures available ($t = 1..n$) in the sample, referring to m different countries. In the end we obtain the following dynamics:

$$\begin{cases} P\left[N_{i,t+\Delta} - N_{i,t} = 0 \middle| \mathcal{F}_t\right] = 1 - \lambda_{i,t}\Delta + o(\Delta) \\ P\left[N_{i,t+\Delta} - N_{i,t} = 1 \middle| \mathcal{F}_t\right] = \lambda_{i,t}\Delta + o(\Delta) \\ P\left[N_{i,t+\Delta} - N_{i,t} > 1 \middle| \mathcal{F}_t\right] = o(\Delta) \end{cases} \tag{122}$$

Ait-Sahalia, Cacho-Diaz, and Laeven (2010) define the intensity $\lambda_{i,t}$ as a Markov process:

$$\lambda_{i,t} = \lambda_{i,\infty} + \sum_{j=1}^{m} \int_{-\infty}^{t} g_{ij}(t-s) dN_{j,s} \tag{123}$$

As a result, (N, λ) is a Markov process too, and the adjusted process $N_{i,t} - \int_{-\infty}^{t} \lambda_{i,s} ds$ is a local martingale.

The intensity of the shock is a positive dimension by nature. As a result, Ait-Sahalia, Cacho-Diaz, and Laeven (2010) assumes that the constant $\lambda_{i,\infty} \geq 0$ for all $i = 1, \ldots, m$ and the function $g_{i,j}(u) \geq 0$ for all $u \geq 0$ and for all $i, j = 1, .., m$.

In the end, eq. (123) can be re-written as:

$$\lambda_{i,t} = \lambda_{i,\infty} + \sum_{j=1}^{m} \int_{-\infty}^{t} \lambda_j g_{ij}(t-s) ds = \lambda_{i,\infty} + \sum_{j=1}^{m} \left(\int_{0}^{+\infty} g_{i,j}(u) du \right) \lambda_j \tag{124}$$

Where Λ_∞ denotes the $m \times 1$ vector with components $\lambda_{i,\infty}$ and $\Gamma = \int_0^\infty G_u du$ the $m \times m$ matrix where G_u is the matrix with elements $g_{i,j}(u)$. Eq. (124) also comes from the fact $E[dN_{i,s}] = \lambda_i ds$.

Eq. (124) can also be expressed in the form of a vector: $\Lambda = \Lambda_\infty + \Gamma \cdot \Lambda$. Assuming that all elements of Λ are positive and finite, we can deduce that $\Lambda = (\mathrm{I} - \Gamma)^{-1}\Lambda_\infty$, where I is the identity matrix of the corresponding dimension.

Mutually Exciting Jump Diffusion

We consider a dataset of 10Y sovereign asset swap spreads (this is the same sample as in Chapter 2). As per Ait-Sahalia, Cacho-Diaz, and Laeven (2010), we also assume that daily price variations admit the following semi-martingale dynamics:

$$dX_{i,t} = \mu_i dt + \sigma_i dW_{i,t} + Z_{i,t} dN_{i,t} \qquad i = 1, \dots, m \tag{125}$$

This formulation consists of a drift term $\mu_i dt$, a volatility term $\sigma_i dW_{i,t}$, and mutually exciting jumps $Z_{i,t} dN_{i,t}$.

$W_t = [W_{1,t}, \dots, W_{m,t}]'$ is an $m-$dimensional vector of standard Brownian motions with constant correlation coefficients $\rho_{i,j}$, $i, j = 1, \dots, m$. Aside from the temporal intensity of the shock $\lambda_{i,t}$ and the corresponding criterion $dN_{i,t}$, we think that it is also important to model the amplitude of the jump as an independent variable. We therefore define $Z_{i,t}$ as the jump size, which we suppose are independently distributed, both serially and on a cross-country basis. We also assume that the amplitude $Z_{i,t}$ is distributed according to the probability distribution function f_{Z_i}. We denote the corresponding cumulative distribution function as F_{Z_i}. f_{Z_i} is a key feature of the model as it dictates the behaviour of the jump amplitude.

Finally, $\boldsymbol{N_t = [N_{1,t}, \dots, N_{m,t}]}$ is the vector of Hawkes processes. As indicated in eq. (125), the quantities μ_i and σ_i are constant parameters. The different vectors W, Z and N are supposed to be mutually independent.

We also want to explore the potential benefit of considering volatility as a stochastic variable. We consider therefore a second version of the model, which is also investigated in Ait-Sahalia, Cacho-Diaz, and Laeven (2010):

$$dX_{i,t} = \mu_i dt + \sqrt{V_{i,t}} dW_{i,t}^X + Z_{i,t} dN_{i,t} \tag{126}$$

Where the instantaneous variance $V_{i,t}$ admits the dynamics of Heston (1993):

$$dV_{i,t} = \kappa_i(\theta_i - V_{i,t})dt + \eta_i \sqrt{V_{i,t}} dW_{i,t}^V \tag{127}$$

κ_i, θ_i, η_i are constant parameters, and $V_{i,t}$ illustrates the stochastic volatility.

$V_{i,t}$ follows the square root process of Feller (1951) and is necessarily a positive (and non-zero) coefficient. The lower bound of zero cannot be achieved as long as Feller's condition is satisfied: $2\kappa_i\theta_i \geq {\eta_i}^2$. In this approach, the volatility is no longer observable.

This second model also incorporates a correlation coefficient between individual Brownian motions $W_{i,t}^X$ and $W_{i,t}^V$, which is denoted ρ_i^{XV}. This variable could reflect a change in correlation regimes, e.g. when financial distress is on the rise.

Mean Reversion-based Jump Intensities

The parameterization of the intensity processes $\lambda_{i,t}$ has meaningful implications on how contagion is effectively captured. In this respect, Ait-Sahalia, Cacho-Diaz, and Laeven (2010) assumes that the intensity is decaying 'exponentially' as time goes by:

$$g_{ij}(t-s) = \beta_{i,j} e^{-\alpha_i (t-s)}, \quad s < t, \quad i,j = 1,\dots,m \tag{128}$$
$$\text{with } \alpha_i > 0, \beta_{i,j} \geq 0 \text{ for all } i,j = 1,\dots,m.$$

This definition tends to fit empirical observations that panic in financial markets usually causes the emergence of knee-jerk market reactions. Then, as time goes by, the volatility is seen as converging towards sn equilibrium, more or less quickly.

The corresponding Γ matrix is then given by:

$$\Gamma = \begin{pmatrix} \frac{\beta_{11}}{\alpha_1} & \cdots & \frac{\beta_{1m}}{\alpha_1} \\ \vdots & \ddots & \vdots \\ \frac{\beta_{m1}}{\alpha_m} & \cdots & \frac{\beta_{mm}}{\alpha_m} \end{pmatrix} \tag{129}$$

The exponential decay in eq. (128) means that the jump intensity admits the dynamics of an Ornstein-Uhlenbeck process. This process is mean-reverting, with α_i illustrating the speed of reversion:

$$d\lambda_{i,t} = \alpha_i(\lambda_{i,\infty} - \lambda_{i,t})dt + \sum_{j=1}^{m} \beta_{i,j}\, dN_{j,t} \tag{130}$$

This definition looks consistent with our desire to capture financial contagion: on one side, $d\lambda_{i,t}$ takes past realisations to estimate the strength of mean reversion (via $\alpha_i(\lambda_{i,\infty} - \lambda_{i,t})$), this is jump clustering. On the other side, $\beta_{i,j}$ is supposed to reflect financial contagion, across the different securities.

The dynamics induced by the exponential decay also suggests that a long period with no shock materialising can be seen as a time of consolidation. On that basis, $\beta_{i,j}$ and α_i are key variables to understand the velocity of any market convalescence.

The model proposed in Ait-Sahalia, Cacho-Diaz, and Laeven (2010) belongs to the category of generalized affine jump-diffusion processes. To see this, consider the general form of affine jump-diffusion A in a state space $D \subset \mathbb{R}^{3\times m}$, defined as a strong solution to the stochastic differential equation:

$$dA_t = \mu^A(A_t)dt + \sigma^A(A_t)dW_t^A + \sum_{j=1}^{m} dJ_{j,t} \tag{131}$$

where $\mu^A : D \to \mathbb{R}^{3\times m}$, $\sigma^A : D \to \mathbb{R}^{(3\times m)\times(3\times m)}$, W^A is a Brownian motion in $\mathbb{R}^{3\times m}$, and J_j, $i = 1,\dots,m$, are jump processes with jump intensities $\lambda_{i,t}^A = \lambda_{i,t}^A(A_t)$, for some $\lambda_i^A : D \to [0,\infty)$, and with fixed jump size distributions on $\mathbb{R}^{3\times m}$.

It is possible to restrict a process A of the form (131) to be affine, by considering the special case where μ^A, $\sigma^A\sigma^{A^T}$ and λ_t^A are affine on D. Then the model with exponential decay can be restricted

to be affine by setting $A_t = [X_t, \sigma\sigma^T, \lambda_t]$ or $A_t = [X_t, V_t, \lambda_t]$ (depending on whether volatility is fixed or stochastic, ie. eq. (125) or (126)) with the corresponding μ^A, $\sigma^A{\sigma^A}^T$ and λ_t^A being affine.

Distribution of the jump amplitude

The amplitude of the shock is described by the random variable $Z_{i,t}$, distributed according to the probability distribution function $f_{Z_i}(x)$. Ait-Sahalia, Cacho-Diaz, and Laeven (2010) considers that the jump amplitude follows an exponential distribution function of the form:

$$f_{Z_i}^1(x) = \begin{cases} p_i \gamma_{i,1} e^{-\gamma_{i,1}(-x)} , & -\infty < x \leq 0; \\ (1-p_i)\gamma_{i,2} e^{-\gamma_{i,2}x} , & 0 < x < +\infty \end{cases} \quad (132)$$

with the corresponding cumulative distribution function:

$$F_{Z_i}^1(x) = \begin{cases} p_i e^{-\gamma_{i,1}(-x)} , & -\infty < x \leq 0; \\ p_i + (1-p_i)(1-e^{-\gamma_{i,2}x}) , & 0 < x < +\infty \end{cases} \quad (133)$$

The moments of the distribution are rather straightforward:

$$E\left[Z_i^k\right] = (-1)^k \frac{k!\, p_i}{{\gamma_{i,1}}^k} + \frac{k!\,(1-p_i)}{{\gamma_{i,2}}^k} \qquad k = 1,2,\ldots \quad (134)$$

This distribution is also used by Kou (2002), in a context of pricing financial derivatives.

As a possible alternative, we also consider that the jump amplitude Z admits a Variance Gamma (VG) distribution. In particular, the VG distribution shows bigger tails than the exponential distribution, and this feature can prove useful to understand the dynamics of jumps. In this case, f_{Z_i} is defined as:

$$f_{Z_i}^2(x) = c\left(c_i, \sigma_{VG,i}, \theta_i, \nu\right) \times e^{\left[\theta_i (x-c_i)/{\sigma_{VG,i}}^2\right]} |x-c_i|^{\left(\frac{1}{\nu}-\frac{1}{2}\right)} K_{\left(\frac{1}{\nu}-\frac{1}{2}\right)}\left(\frac{|x-c_i|\sqrt{2{\sigma_{GV,i}}^2/\nu + {\theta_i}^2}}{{\sigma_{VG,i}}^2}\right) \quad (135)$$

Where $K_\nu()$ is the modified Bessel function of the third kind, of order ν, and:

$$c\left(c_i, \sigma_{VG,i}, \theta_i, \nu\right) = \frac{2}{\sigma_{VG,i}\sqrt{2\pi}\nu^{1/\nu}\Gamma(1/\nu)} \left(\frac{1}{\sqrt{2{\sigma_{VG,i}}^2/\nu + {\theta_{VG,i}}^2}}\right)^{1/\nu - 1/2} \quad (136)$$

c_i is the location parameter, so we assume that $c_i = 0$ (we showed in Chapter 2 that the dataset is centred). We take the same degree of freedom ν as in Chapter 1, so $\nu = 5$. In the end, we see only two unknown parameters: $\sigma_{VG,i}$ and $\theta_{VG,i}$.

As we previously explained in Chapter 2, a positive shock translate into tighter asset swap spreads (the bond outperforms the IRS)**, which is a negative jump for $x_{i,t}$ ($x_{i,t} < 0$). In contrast, a negative shock leads to wider asset swap spreads** (the bond underperforms the IRS)**, and this is a positive jump, ie. $x_{i,t} > 0$.**

Our analysis in the previous chapters brought to light that positive and negative shocks do not propagate the same way throughout sovereign securities. As a consequence, jumps may exhibit some skewness.

In the case of $f_{Z_i}^1$, we note that $F_{Z_i}^1(0) = p_i$, and more generally we have: $\begin{cases} P(x \leq 0) = p_i \\ P(x > 0) = 1 - p_i \end{cases}$ As a result, p_i is driving the skewness of the distribution. In the case of $f_{Z_i}^1$, $\theta_{VG,i}$ describes the skewness of the distribution

Let us now undertake a few synthetic examples: Graph 231 to Graph 233 illustrate the shape of $f_{Z_i}^1$ and $f_{Z_i}^2$ for a selection of different parameters, described in Table 29. The first observation is that f^2 exhibits a significantly bigger kurtosis than f^1. As a result, the VG distribution (via f^2), is potentially a better choice to capture heavy tails.

Having said that, we note that f^1 is remarkably versatile, and probably more versatile than f^2 given the greater number of unknowns involved in the double exponential distribution (3 unknowns versus just 1 in the VG distribution).

Table 163. Parameters of the distributions in Graph 231 to Graph 233

	p_i	$\gamma_{i,1}$	$\gamma_{i,2}$
f1_1	0.5	1	1
f1_2	0.5	0.5	0.5
f1_3	0.2	0.4	0.4
f1_4	0.2		

	$\sigma_{VG,i}$	θ_i
f2_1	50	0
f2_2	20	0
f2_3	10	-100
f2_4	1000	-20

Graph 231. Synthetic examples

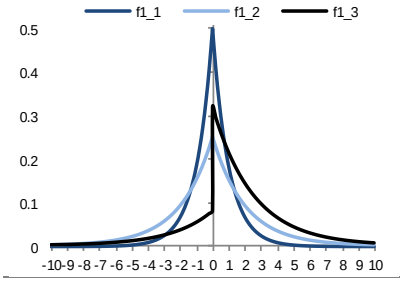

Graph 232. Synthetic examples

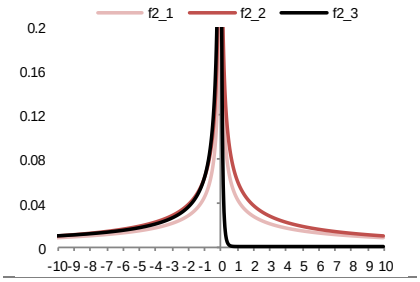

Graph 233. Synthetic examples

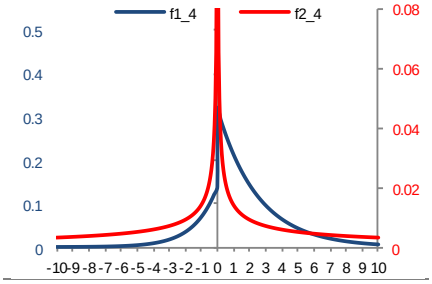

Calibration Procedure

The point processes $N_{i,t}$ and the intensity $\lambda_{i,t}$ are latent variables, ie. they are not observable. In the case of the version involving stochastic volatility, $V_{i,t}$ is an additional unobservable variable. We consider the Generalised Method of Moments (GMM) as a recognised approach to calibrate stochastic models involving unobservable variables. The estimation procedure involves the moments of the distribution of X_t.

In particular we consider the following moments:

$$\begin{cases} \mathbb{E}[\Delta X_{i,t}] \\ \mathbb{E}\left[\left(\Delta X_{i,t} - E[\Delta X_{i,t}]\right)^r\right], \quad r = 2,..,4 \\ \mathbb{E}\left[\Delta X_{i,t}\Delta X_{j,t} - E[\Delta X_{i,t}]E[\Delta X_{j,t}]\right], \quad i \neq j \\ \mathbb{E}\left[\Delta X_{i,t+\tau}\Delta X_{j,t} - E[\Delta X_{i,t}]E[\Delta X_{j,t}]\right], \quad \tau > 0 \end{cases} \tag{137}$$

These are the "natural" moments: variance, kurtosis, skewness and autocovariances. The formulation of these moments is given in Ait-Sahalia, Cacho-Diaz, and Laeven (2010).

The univariate calibration

In this section we explore the calibration of the model, from a univariate perspective. As mentioned above, we explore different versions: fixed or stochastic volatility, double exponential jumps ($f_{Z_i}^1$ in eq. (132)) or variance gamma distributed jumps ($f_{Z_i}^2$ in eq. (135)). We are thus left with four different models. Assuming a fixed variance (eq. (125)), we see either 7 or 8 unknowns to calibrate:

Exponentially distributed jumps: $\{\mu_i, \sigma_i, \alpha_i, \beta_i, \lambda_{i,\infty}, p_i, \gamma_{i,1}, \gamma_{i,2}\}$ 8 unknowns

Variance gamma jumps: $\{\mu_i, \sigma_i, \alpha_i, \beta_i, \lambda_{i,\infty}, \sigma_{VG,i}\}$ 6 unknowns

Now assuming stochastic volatility, we get either 9 or 11 unknowns to calibrate:

Exponentially distributed jumps: $\{\mu_i, \theta_i, \rho_i^{XV}, \eta_i, \kappa_i, \alpha_i, \beta_i, \lambda_{i,\infty}, p_i, \gamma_{i,1}, \gamma_{i,2}\}$ 11 unknowns

Variance gamma jumps: $\{\mu_i, \theta_i, \rho_i^{XV}, \eta_i, \kappa_i, \alpha_i, \beta_i, \lambda_{i,\infty}, \sigma_{VG,i}\}$ 9 unknowns

The univariate dimension means that there is just one term β involved in the dynamics of the shock intensity, namely $\beta_{i,i}$, that we simply rewrite as β_i (see eq. (130)):

$$d\lambda_{i,t} = \alpha_i(\lambda_{i,\infty} - \lambda_{i,t})dt + \beta_i dN_{i,t} \tag{138}$$

Ait-Sahalia, Cacho-Diaz, and Laeven (2010) considers a two stage calibration procedure. First the authors take a truncated version of the sample, where there is supposedly no jump. This allows them to ignore the discontinuous part of the model. Instead, they focus on the variables that relate to the continuous part. In the end, the first step of the calibration delivers as estimate for $\{\mu_i, \theta_i, \rho_i^{XV}, \eta_i, \kappa_i, \alpha_i\}$. Then in a second step, the authors take the full sample into account and they run the calibration on the remaining set of variables (ie. these supposed to illustrate the dynamics of the jumps).

First we considered a similar approach to the calibration issue; but results were not convincing. For instance, it was not possible to replicate the empirical distribution of the data via Monte Carlo diffusion with the set of parameters we obtained.

As another illustration, p_i, as a skewness coefficient, was very far from the empirical skewness calculated on the dataset. We explain the methodology used to calculate the empirical skewness in the next paragraph.

A measure of the empirical skewness

Since $N_{i,t}$ is a latent variable, none of $dN_{i,t}$ and $Z_{i,t}$ is observable. For convenience, we draw empirical rules to identify the distribution of shocks. In Ait-Sahalia, Cacho-Diaz, and Laeven (2010) for instance, the authors define two positive thresholds x_i^{z+} and x_i^{z-}: they assume that a positive jump happens when $\{0 < x_i^{z+} < x_i\}$, while a negative jump is detected when $\{x_i < x_i^{z-} < 0\}$. They also argue that any variations beyond the average value of $f_{Z_i}^1$ is a shock. As a result, they obtain:

$$x_i^{z+} = -1/\gamma_{i,1} \text{ and } x_i^{z-} = 1/\gamma_{i,2}$$

And thus: $F^1_{Z_i}(x_i^{z+}) = p_i e^{-1}$ and $F^1_{Z_i}(x_i^{z-}) = 1 + e^{-1}(p_i - 1)$ (139)

Let us now denote positive jumps as $Z^+_{i,t}$, and similarly negative jumps as $Z^-_{i,t}$. We then define our empirical skewness estimator $\hat{p}_i$ as the ratio:

$$\hat{p}_i = \frac{N_{\hat{Z}^-_{i,t}}}{N_{\hat{Z}^-_{i,t}} + N_{\hat{Z}^+_{i,t}}} \quad (140)$$

Where $N_{\hat{Z}^+_{i,t}}$ and $N_{\hat{Z}^-_{i,t}}$ is the quantity of positive and negative shocks 'empirically detected' in the sample. We calculate $\hat{p}_i$ for all possible values of (x_i^{z+}, x_i^{z-}) available. In the end, we obtain the following map for $\hat{p}_i$, which looks like a function of x_i^{z+} and x_i^{z-}.

We plot the results for Germany and Italy in Graph 234 and Graph 235. We identify three different regimes:

- "no skewness": in this case, both positive and negative jumps have the same probability to materialise, and thus $\hat{p}_i \sim 0.5$. This is described in **yellow** in the graphs.
- "positive skewness": from a statistical point of view, positive skewness means that the mass of the distribution function is concentrated on the lower part of the figure, ie. for $x_i < 0$. This describes a situation where negative jumps are more frequent than positive jumps. This is achieved for $\hat{p}_i \to 1$, which appears in **red** in the graphs.
- "negative skewness": negative skewness means that the mass of the distribution is concentrated on the upper part of the figure, ie. for $x_i > 0$. This describes a situation where positive jumps are much more frequent than negative jumps. This is achieved for $\hat{p}_i \to 0$, which appears in **green** in the graphs.

Graph 234. $\hat{p}_{GE}$, the empirical skewness for Germany
Yellow: $\hat{p}_i \sim 0.5$ green: $\hat{p}_i < 0.5$ red: $\hat{p}_i > 0.5$

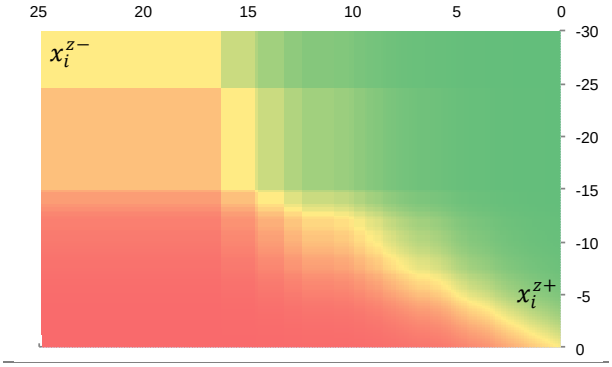

Graph 235. $\hat{p}_{IT}$, the empirical skewness for Italy
Yellow: $\hat{p}_i \sim 0.5$ green: $\hat{p}_i < 0.5$ red: $\hat{p}_i > 0.5$

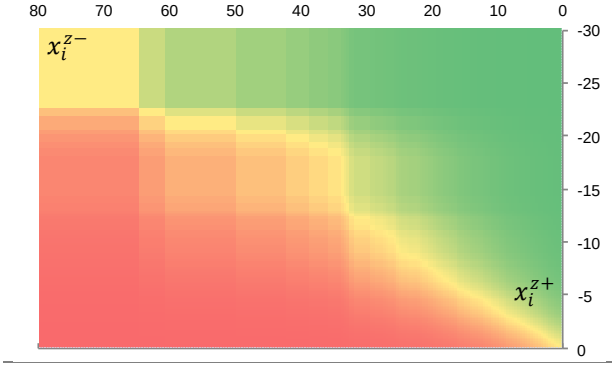

Overall, the shape of $\hat{p}_i$ looks coherent with our interpretation of the skewness. We make therefore the assumption that $\hat{p}_i$ is a reliable estimator of p_i ($p_i \sim \hat{p}_i$). We show later that this assumption is reasonable and helps simplify the calibration of the model. This way to estimate p_i differs from the methodology developed in Ait-Sahalia, Cacho-Diaz, and Laeven (2010), as instead the author assumes that $p_i = 1$. On our side, we prefer calculating $\tilde{p}_i$ out of x_i^{z+}, x_i^{z-} using a linear extrapolation on the surface shown in Graph 234 and Graph 235 (we get this kind of surface for each country).

In the case of variance gamma distributed jumps, an initial attempt to calibrate f^2 showed that the coefficient $\theta_{VG,i}$ is very instable, too instable in our view. And it is not clear either whether shocks

exhibit significant skewness or not. In Chapter 1 for instance, the un-temporal volatility was fairly symmetric although our approach allowed replicating the skewness. Generalized skewed distributions also did not outperform the corresponding unskewed versions.

➔ Overall, we think that the unstable $\theta_{VG,i}$ reflects the burden of having too many unknowns to calibrate. On top of that, the benefit of Variance Gamma distributions remains in the bigger tails, compared to exponential distributions. **In the end, we prefer considering a non-skewed version of the Variance Gamma and thus we force $\boldsymbol{\theta_{VG,i} = 0}$. This leaves us with just one variable to calibrate when considering the Variance Gamma distribution, ie. $\boldsymbol{\sigma_{VG,i}}$.**

Calibrating the remaining unknowns

Since p_i is now a function of $\gamma_{i,1}$ and $\gamma_{i,2}$, we are left with 10 unknowns to calibrate, when considering exponentially distributed jumps (f^1); this is still too many. In order to facilitate the calibration, we now seek to restrain the range of possible values for each variable.

μ_i is a drift coefficient. We already noted that ACF and PACF showed no particular evidence of any non-stationarity in the dataset. As a result, μ_i should be relatively small. We thus restrain initial values to the range $[0,0.01]$.

In order to respect the positivity of $\lambda_{i,t}$, we also constraint η_i such that $0 < \eta_i < \sqrt{2\kappa_i\theta_i}$ (this comes from $2\kappa_i\theta_i \geq {\eta_i}^2$). We also note that: $\lambda_i = \mathbb{E}(\lambda_{i,t}) = \frac{\alpha_i\lambda_{i,\infty}}{\alpha_i - \beta_i}$ with $\alpha_i > 0$, $\beta_i > 0$, and $\lambda_{i,\infty} > 0$.

Since $\mathbb{E}(\lambda_{i,t}) \geq 0$, we force β_i to remain in the range $0 < \beta_i < \alpha_i$.

It looks coherent to cap the average jump intensity at $1\ jump/day$. We thus restrain initial values on $\lambda_{i,\infty}$ so that $\mathbb{E}(\lambda_{i,t})\delta \leq 1$: $\lambda_{i,\infty} \leq (\alpha_i - \beta_i)/(\delta\alpha_i)$.

Based on empirical tests we also implement the following restrictions:

- $0 < \theta_i < 80$ and $0 < \alpha_i < 10$ look reasonable for all countries.
- κ_i is apparently largely dependent on the magnitude of the volatility. We identify three main regimes for the upper-bound of κ_i:

Table 164. Upper bound of κ_i is larger for peripheral countries

	GE	FI	NL	AT	FR	BE	IT	SP	IR	PT	GR
$\kappa_{i,max}$	45	45	45	45	110	110	110	110	250	250	250

- Finally, we also take initial values for $\gamma_{i,j}$ from within the range $[0,0.5]$.

If we denote the moment of the amplitude Z by $M[Z,k] = \mathbb{E}[Z^k]$, and $\lambda_i = \mathbb{E}[\lambda_{i,t}]$, Ait-Sahalia, Cacho-Diaz, and Laeven (2010) gives the corresponding expressions:

- **<u>Stochastic volatility:</u>**

$$\mathbb{E}[\Delta X_{i,t}] = (\mu_i + \lambda_i M[Z,1])\Delta + o(\Delta^2)$$

$$\mathbb{E}\left[\left(\Delta X_{i,t} - E[\Delta X_{i,t}]\right)^2\right] = (\theta_i + \lambda_i M[Z,2])\Delta + \frac{\beta_i\lambda_i(2\alpha_i - \beta_i)}{2(\alpha_i - \beta_i)} M[Z,1]^2\Delta^2 + o(\Delta^2)$$

$$\mathbb{E}\left[\left(\Delta X_{i,t} - E\left[\Delta X_{i,t}\right]\right)^3\right] = \lambda_i M[Z,3]\Delta + \frac{3}{2}\left(\eta_i\theta_i\rho_i^{XV} + \frac{(2\alpha_i - \beta_i)\beta_i\lambda_i M[Z,1]M[Z,2]}{(\alpha_i - \beta_i)}\right)\Delta^2 + o(\Delta^2)$$

$$\begin{aligned}\mathbb{E}\left[\left(\Delta X_{i,t} - E\left[\Delta X_{i,t}\right]\right)^4\right] &= \lambda_i M[Z,4]\Delta \\ &+ \left(\frac{3\theta_i\eta_i^2}{2\kappa_i} + 3\theta_i^2 + 6\theta_i\lambda_i M[Z,2] + 3\lambda_i\left(\lambda_i + \frac{(2\alpha_i - \beta_i)\beta_i}{2(\alpha_i - \beta_i)}\right)M[Z,2]^2\right. \\ &+ \left.\frac{2(2\alpha_i - \beta_i)\beta_i\lambda_i M[Z,1]M[Z,3]}{(\alpha_i - \beta_i)}\right)\Delta^2 + o(\Delta^2)\end{aligned}$$

Then the autocorrelation function of the process is given by:

$$\mathbb{E}\left[\left(\Delta X_{i,t} - E\left[\Delta X_{i,t}\right]\right)\left(\Delta X_{i,t+\tau} - E\left[\Delta X_{t+\tau}\right]\right)\right] = \frac{\beta_i\lambda_i(2\alpha_i - \beta_i)}{2(\alpha_i - \beta_i)}e^{-(\alpha_i - \beta_i)\tau}M[Z,1]^2\Delta^2 + o(\Delta^2) \qquad (141)$$

For all $\tau > 0$.

- **Fixed volatility:**

$$\mathbb{E}\left[\Delta X_{i,t}\right] = (\mu_i + \lambda_i M[Z,1])\Delta + o(\Delta^2)$$

$$\mathbb{E}\left[\left(\Delta X_{i,t} - E\left[\Delta X_{i,t}\right]\right)^2\right] = \left(\sigma_i^2 + \lambda_i M[Z,2]\right)\Delta + \frac{\beta_i\lambda_i(2\alpha_i - \beta_i)}{2(\alpha_i - \beta_i)}M[Z,1]^2\Delta^2 + o(\Delta^2)$$

$$\mathbb{E}\left[\left(\Delta X_{i,t} - E\left[\Delta X_{i,t}\right]\right)^3\right] = \lambda_i M[Z,3]\Delta + \frac{3}{2}\left(\frac{(2\alpha_i - \beta_i)\beta_i\lambda_i M[Z,1]M[Z,2]}{(\alpha_i - \beta_i)}\right)\Delta^2 + o(\Delta^2)$$

$$\begin{aligned}\mathbb{E}\left[\left(\Delta X_{i,t} - E\left[\Delta X_{i,t}\right]\right)^4\right] &= \lambda_i M[Z,4]\Delta \\ &+ \left(3\sigma_i^4 + 6\sigma_i^2\lambda_i M[Z,2] + 3\lambda_i\left(\lambda_i + \frac{(2\alpha_i - \beta_i)\beta_i}{2(\alpha_i - \beta_i)}\right)M[Z,2]^2 + \frac{2(2\alpha_i - \beta_i)\beta_i\lambda_i M[Z,1]M[Z,3]}{(\alpha_i - \beta_i)}\right)\Delta^2 + o(\Delta^2)\end{aligned}$$

Then the autocorrelation function of the process is given by:

$$\mathbb{E}\left[\left(\Delta X_{i,t} - E\left[\Delta X_{i,t}\right]\right)\left(\Delta X_{i,t+\tau} - E\left[\Delta X_{t+\tau}\right]\right)\right] = \frac{\beta_i\lambda_i(2\alpha_i - \beta_i)}{2(\alpha_i - \beta_i)}e^{-(\alpha_i - \beta_i)\tau}M[Z,1]^2\Delta^2 + o(\Delta^2) \qquad (142)$$

Results

We calibrate each model in a one-stage procedure, by imposing the aforementioned restrictions on initial values/admissible ranges and we ran the calibration 50 times. We then had to select the best combination. Looking at the calibration error first, Graph 237 shows that the error is relatively stable for the 35th-40th best combinations; then, the error tends to surge. As a result, we kept the 40 best combinations as potentially candidates for the best set of parameters.

Graph 236. $\lambda_\infty = 60$, $\alpha = 10$, $\beta = 3$

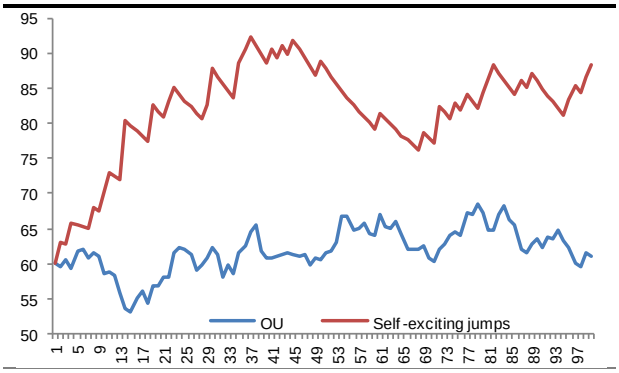

Graph 237. Calibration error surging beyond the 40th calibration

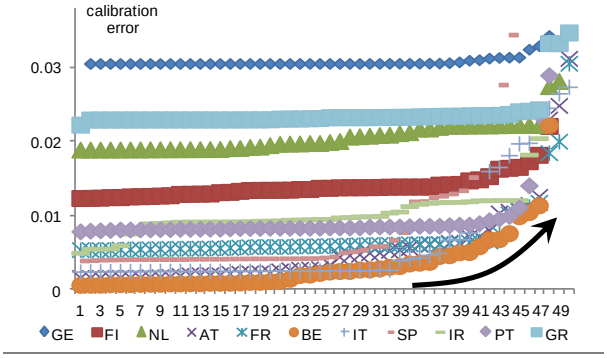

Results from the calibration are ordered on the x-axis on the basis that a higher index reflects a bigger calibration error

Table 165 shows the smallest error, out of the 50 runs. The error looks much bigger for models involving the Variance Gamma distribution ($f_{Z_i}^2$) rather than the double exponential approach. This is a sign that the calibration is probably less efficient with the variance gamma distribution.

Table 165. Value of the likelihood function at the end of the calibration (ie. resulting error)

	$f(Z)$	GE	FI	NL	AT	FR	BE	IT	SP	IR	PT	GR
Vol sto	$f_{Z_i}^1$	0.031	0.012	0.022	0.002	0.006	0.001	0.003	0.004	0.008	0.005	0.008
	$f_{Z_i}^2$	1.079	0.034	0.044	2.131	1.431	11.336	5.549	1632	15108	107766	1E+07
Vol fixed	$f_{Z_i}^1$	0.022	0.012	0.019	0.002	0.005	0.001	0.002	0.004	0.005	0.008	0.022
	$f_{Z_i}^2$	0.878	0.051	0.057	2.367	2.122	12.008	3.984	1232	10938	163608	2E+07

Then we calculate $dN_{i,t}$ and $\lambda_{i,t}$ for the 40 best combinations of parameters. Graph 238 and Graph 239 show the resulting series, for the calibrations providing the 5 smallest errors (e.g. in Graph 237), assuming a fixed volatility (eq. (125)) and exponentially distributed jumps (ie. f_Z^1).

Graph 238. Probability that a jump materializes in Italy

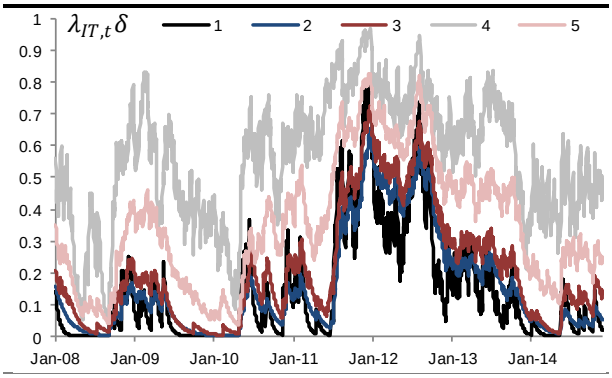

Graph 239. Probability that a jump materializes in Spain

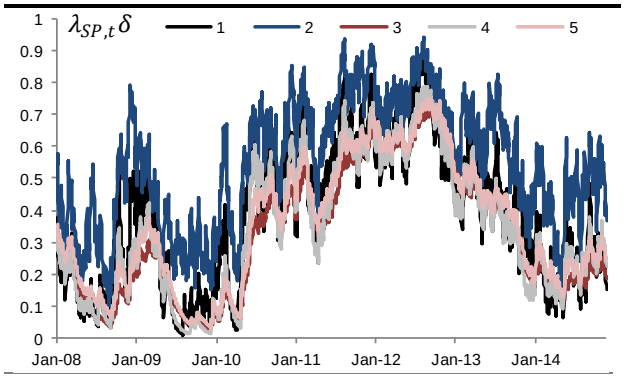

Monte Carlo simulations

The capability to replicate the empirical distribution of the data is a key determinant to identify the best set of parameters (out of the 40 selected best combinations). In order to understand if the model is able to replicate the empirical distribution of the data, we conduct Monte Carlo (MC) simulations, and we calculate the ADC criterion and Kolmogorov-Smirnov (KS) p-value that illustrate

the quality of fit between the generated and the empirical distributions. **These statistical tests are meant to highlight the best set of parameters.**

For coherence, we takes the profile of jumps $dN_{i,t}$ and intensities $\lambda_{i,t}$ that corresponds to the empirical probability distribution of the data (denoted $\hat{p}(x_{i,t})$). **This is an unchanged feature in all our MC simulations.** We generated 1000 time series $x_{i,t}$ for each country, via the diffusion of $Z_{i,t}$, and $dW_{i,t}$, (respectively $\left(dW_{i,t}^{X}, dW_{i,t}^{V}\right)$ in the case of the stochastic volatility model). Graph 240 shows a few paths generated for Italy, as an example.

We then calculate the corresponding ADC criterion and KS p-values. Both estimators are supposed to highlight the degree of similarity between both, generated and empirical distributions. Finally, we keep the best parameters based on the ADC (as in previous chapters). We check for coherence that the corresponding KS p-value is satisfactory as well. (ADC focuses on the quality of the distribution in the tails, while KS gives extra credentials to the centre of the distribution).

Graph 240. Jump intensity out of different models (jumps/years)

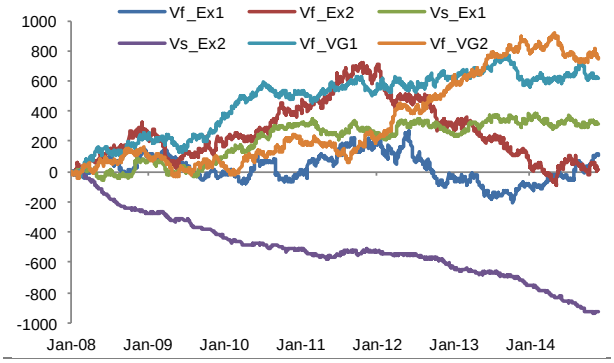

Graph 241. Jump intensity for different countries

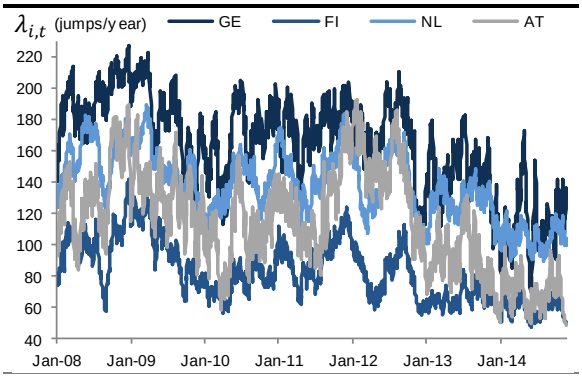

Table 166 shows the best ADC and KS p-value. **Overall, the model with exponential jumps and fixed volatility delivers better results than the three other versions.** This model also proves sensible, regardless of the credit quality it seems (core/soft-core or peripheral countries).

The calibration of the stochastic volatility model (third line in Table 166) delivers compelling results too, but only for six countries: Germany, Finland, the Netherlands, France, Italy, Spain. The calibration is not successful for Italy, Spain, Ireland, Portugal, Greece. **This is obviously a limitation.** Good results for both core and non-core countries suggest that the Variance Gamma offers some versatility, and therefore cannot be discarded as such.

Table 166. Minimum ADC and maximum KS p-values out of the 40 "best" combinations

		GE	FI	NL	AT	FR	BE	IT	SP	IR	PT	GR
Vol fixed, exp	*ADC*	1.5	1.3	1.8	1.3	1.2	1.7	1.6	1.4	1.6	1.5	2.2
	KS	36	49	36	47	56	18	52	54	27	47	1
Vol fixed, GV	*ADC*	1.4	1.7	1.1	3.0	2.0	3.7	1.7	2.2	5.1	2.9	4.0
	KS	28	41	65	2	9	1	28	13	0	6	0
Vol sto, exp	*ADC*	1.0	1.8	1.9	3.6	3.6	1.6	6.9	5.0	5.3	7.4	6.9
	KS	80	40	13	1	1	39	0	0	0	0	0
Vol sto, VG	*ADC*	4.0	2.4	3.3	3.6	6.9	11.0	7.7	3.7	4.6	3.3	6.0
	KS	0	14	2	1	0	0	0	0	0	8	0

Table 167. ADC (left) and KS p-values (right)

GE	FI	NL	AT	FR	BE	IT	SP	IR	PT	GR
4.3	2.9	2.8	6.7	5.8	4.4	18.5	5.8	2.0	4.4	23.1
3.0	2.2	3.1	12.6	3.0	6.4	5.5	6.1	6.5	4.5	4.9
2.9	2.2	4.0	4.9	1.5	7.3	20.9	4.8	5.3	4.2	23.7
3.0	4.1	1.8	17.1	1.2	5.3	19.2	4.4	5.3	4.4	23.6
3.0	4.1	4.9	3.1	6.9	1.7	6.1	3.9	3.8	5.5	23.7
3.0	3.0	1.9	6.7	7.1	6.1	3.6	3.3	5.6	5.6	23.7
2.9	12.2	10.8	2.2	10.4	5.9	12.8	3.7	5.4	5.2	15.4
2.9	12.2	2.1	4.7	8.1	4.1	14.5	6.7	5.4	3.6	13.3
3.0	9.1	2.2	5.2	7.3	7.7	11.1	5.7	5.3	4.8	7.0
3.0	4.8	2.5	5.9	5.8	7.4	7.1	2.5	5.1	4.2	6.9
3.0	8.9	10.8	2.3	6.2	5.2	19.5	3.2	5.1	3.2	6.7
3.0	8.2	11.6	3.7	5.5	4.2	13.8	5.1	5.0	4.9	6.1
3.0	1.5	10.9	2.0	1.8	5.5	25.5	3.9	5.1	4.9	5.2
3.0	3.1	3.5	3.8	5.7	8.7	22.1	4.1	5.0	5.2	4.8
3.0	9.3	1.9	2.9	8.2	4.6	13.6	7.9	5.0	4.8	4.8
3.0	8.3	1.9	6.2	5.6	5.8	28.3	2.0	5.1	2.3	11.2
3.0	8.4	5.0	1.3	6.7	2.8	10.2	6.5	5.0	4.8	4.9
3.0	7.0	2.9	2.4	3.4	5.2	17.2	6.2	5.1	5.0	4.6
3.0	7.8	3.4	5.0	5.7	8.7	21.9	1.4	5.1	5.2	5.6
3.0	4.0	9.2	2.7	5.4	6.1	21.6	6.2	5.0	4.6	8.4
3.0	2.9	9.1	4.3	3.9	4.0	22.2	6.9	5.0	4.7	6.1
3.0	1.4	1.9	4.0	5.4	4.6	7.4	5.6	5.1	4.9	6.9
2.9	2.2	2.5	4.4	4.0	4.8	1.9	10.0	5.1	7.3	8.0
2.9	2.4	8.9	7.4	5.1	6.6	1.6	3.5	5.1	4.6	16.0
3.0	9.3	9.1	2.8	4.0	6.1	1.7	3.1	5.1	4.5	7.1
3.0	5.1	8.8	3.4	4.9	4.6	4.4	14.3	5.3	3.7	7.6
2.9	5.2	8.7	3.8	5.2	4.4	5.4	2.9	5.3	4.4	5.2
2.7	5.1	8.6	3.6	4.6	4.3	9.6	3.0	3.6	4.0	6.2
2.1	5.3	10.8	2.7	4.5	5.4	6.8	6.9	4.0	1.5	2.3
2.4	5.2	2.1	4.9	4.6	5.4	6.7	2.9	1.6	3.6	2.2
2.0	3.1	2.1	8.4	5.1	5.4	6.3	6.9	3.0	4.0	4.6
2.4	6.3	4.0	3.9	4.2	4.5	4.7	9.6	15.7	4.3	2.5
1.8	4.6	5.5	2.9	5.1	4.5	7.2	3.2	4.4	2.2	2.7
1.5	1.3	1.8	4.7	5.6	5.3	7.6	3.3	15.7	7.2	4.3
1.5	1.5	2.1	2.5	5.6	4.7	7.2	6.9	5.4	3.7	3.0
2.2	5.8	6.9	2.7	5.1	5.2	3.8	7.0	2.1	7.4	3.2
1.6	2.3	3.0	4.1	4.5	5.3	6.6	6.8	4.3	3.5	3.0
2.0	3.4	10.6	3.9	4.2	4.5	8.0	6.0	3.9	3.7	2.9
2.9	3.3	1.8	4.1	3.7	4.6	6.5	6.0	4.8	2.9	3.3
3.2	3.3	2.3	4.0	4.2	5.1	7.0	5.5	4.7	4.1	4.1

GE	FI	NL	AT	FR	BE	IT	SP	IR	PT	GR
0	2	3	0	0	1	0	0	13	0	0
9	9	1	0	8	0	0	0	0	0	1
9	12	1	0	27	0	0	0	0	0	0
8	0	27	0	56	0	0	0	0	0	0
9	0	0	3	0	18	0	1	2	0	0
9	2	19	0	0	0	2	5	0	0	0
10	0	0	20	0	0	0	2	0	0	0
9	0	12	0	0	1	0	0	0	1	0
9	0	29	0	0	0	0	0	0	0	0
8	0	6	0	0	0	0	12	0	0	0
8	0	0	16	0	0	0	6	0	1	0
8	0	0	0	0	0	0	0	0	0	0
8	42	0	31	23	0	0	0	0	0	0
8	2	1	0	0	0	0	1	0	0	0
9	0	22	8	0	0	0	0	0	0	0
8	0	20	0	0	0	0	14	0	5	0
8	0	0	47	0	2	0	0	0	0	0
9	0	2	9	3	0	0	0	0	0	0
9	0	1	0	0	0	0	54	0	0	0
9	1	0	7	0	0	0	0	0	0	0
9	3	0	0	0	0	0	0	0	0	0
9	49	21	1	0	0	0	0	0	0	0
9	12	6	0	0	0	42	0	0	0	0
9	6	0	0	0	0	45	3	0	0	0
9	0	0	4	0	0	52	2	0	0	0
9	0	0	1	0	0	0	0	0	1	0
9	0	0	0	0	0	0	8	0	0	0
12	0	0	0	0	0	0	4	0	0	0
14	0	0	3	0	0	0	0	0	47	13
9	0	13	0	0	0	0	6	27	0	15
14	2	13	0	0	0	0	0	6	0	0
5	0	0	0	0	0	0	0	0	0	11
20	0	0	1	0	0	0	1	0	18	9
36	48	36	0	0	0	0	1	0	0	1
32	39	21	21	0	0	0	0	0	0	1
16	0	0	2	0	0	1	0	16	0	1
27	11	4	0	0	0	0	0	0	1	1
24	1	0	0	0	0	0	0	1	0	0
8	1	29	0	0	0	0	0	0	2	0
0	2	8	0	0	0	0	0	0	1	0

Results with stochastic volatility (in Table 166) look disappointing. ADCs in the last two rows of the table indicate that the calibration is just occasionally successful. Too many unknowns is probably one of the reasons for lacklustre results, as it makes the calibration more hazardous. We also think that there is a conflict in using stochastic volatility and jumps in the same time, as both were introduced for the same reasons, namely to simulate 'rare' events. There is therefore a logical redundancy between jumps and stochastic volatility, which may be responsible for some hazard during the calibration.

More positively, core countries and Belgium look properly calibrated when assuming exponential jumps, but even here, the quality of the calibration noticeably shrinks in the VG version (fourth row).

➔ **The model with fixed volatility and exponential jumps outperforms other approaches.**

Table 167 shows the ADC and KS p-values for all combinations. Results look remarkably instable: for every country, only a few calibrations shows 'acceptable' ADC/KS.➔ **Overall, this suggests little robustness, with some degree of complexity to find a global optimum during the calibration.**

Table 168. Calibrated parameters, vol fixed, Exponential distribution

vol fixed, Exponential distribution										
	μ_i	σ_i	$\lambda_{i,\infty}$	α_i	β_i	p_i	$\gamma_{i,1}$	$\gamma_{i,2}$	β_i/α_i	$E(\lambda_{i,t})$
GE	0.3	17.2	26.5	14.8	12.4	0.48	0.62	0.65	0.84	163
FI	16.8	30.5	43.5	13.8	6.4	0.58	0.53	0.41	0.47	81
NL	0.0	25.5	54.3	11.1	6.7	0.62	1.00	0.53	0.61	138
AT	34.9	29.3	42.5	21.2	13.3	0.58	0.43	0.34	0.63	114
FR	17.4	28.4	38.6	18.4	13.2	0.53	0.46	0.42	0.72	137
BE	0.0	41.2	62.0	23.7	4.5	0.53	0.24	0.22	0.19	76
IT	1.0	64.4	43.3	86.8	22.5	0.49	0.11	0.10	0.26	58
SP	63.0	65.2	18.7	0.5	0.4	0.51	0.12	0.11	0.81	97
IR	0.0	64.1	16.8	8.3	6.8	0.56	0.14	0.11	0.81	90
PT	0.0	73.2	12.5	88.6	79.8	0.46	0.12	0.13	0.90	126
GR	2.5	115.7	1.3	5.4	5.3	0.46	0.03	0.03	0.99	104

Table 169. Calibrated parameters, vol fixed, Variance Gamma distribution

vol fixed, Variance Gamma distribution								
	μ_i	σ_i	$\lambda_{i,\infty}$	α_i	β_i	$\sigma_{VG,i}$	β_i/α_i	$E(\lambda_{i,t})$
GE	0.2	26.2	134.6	1.3	0.6	2.54	0.31	241
FI	4.1	33.0	32.4	16.8	13.4	2.88	0.44	160
NL	3.0	30.5	63.3	16.4	11.1	2.63	0.40	197
FR	0.0	36.2	31.7	22.0	19.0	3.23	0.46	233
IT	18.7	75.1	26.2	21.8	18.9	8.21	0.46	195
SP	0.0	88.5	9.1	6.3	6.0	7.95	0.49	195

Table 170. Calibrated parameters, vol stochastic, Exponential distribution

vol stochastic, Exponential distribution													
	μ_i	θ_i	ρ_i^{XV}	η_i	κ_i	α_i	β_i	$\lambda_{i,\infty}$	$\gamma_{i,1}$	$\gamma_{i,2}$	p_i	β_i/α_i	$E(\lambda_{i,t})$
GE	0.3	56.7	0.6	41.3	19.2	17.0	16.2	5.0	0.7	0.7	0.49	0.95	104
FI	0.0	47.2	0.2	31.5	31.3	7.4	7.4	0.1	0.7	0.6	0.50	1.00	78
NL	0.0	7.6	0.6	3.4	41.0	2.2	2.2	0.1	0.8	0.7	0.52	1.00	196
BE	31.7	25.7	0.4	5.7	1.8	8.2	0.3	85.2	0.4	0.3	0.57	0.03	88

Table 168, Table 169 and Table 170 show the optimal parameters for each model. First we note that the parameter p_i is very close to 0.5, thus indicating that the jumps exhibit little skewness (This validates our assumption that $\theta_{VG,i}{\sim}0$). Another observation is that σ_i gradually rises for the more volatile countries, from 17bp/year for Germany up to 116bp/year for Greece. Though we were expecting μ_i to be closer to zero, it appears that there is a non-negligible trend. **Another observation if that β_i is large in general, and usually relatively close to α_i.** This means that the self-exciting loop is greatly instrumental on the dynamics of the jump intensity. From a general point of view, coefficients between France/Belgium and Italy/Spain are greatly dissimilar – we see no obvious reasons for that.

$\mathbb{E}(\lambda_{i,t})$ reveals interesting information as it describes the average numbers of jumps expected per year (we supposed 252 working days per year). Surprisingly, Germany, the Netherlands, Austria and France exhibit a bigger number of jumps than countries of lesser credit quality (e.g. 163 jumps/year for Germany, which compares with just 97 for Spain). **This is counterintuitive since jumps are supposed to reflect the materialisation of financial shocks,** and these are more likely to happen in peripheral countries. Market valuations in countries like Germany are in contrast more stable, and should thus exhibit less frequent jumps.

➔ **The larger $\mathbb{E}(\lambda_{i,t})$ in core countries suggests that the identification of jumps in the more robust countries is not successful. This highlights noticeable redundancy between continuous (σdW) and jump components (ZdN) inside the model.**

Results from the stochastic volatility model in Table 170 are a bit confusing: $\lambda_{i,\infty}$ is very small in Finland and the Netherlands, and this looks a bit discordant compared with the larger values we obtain for Germany and Belgium.

Graph 241, Graph 242 and Graph 243 show the jump intensity $\lambda_{i,t}$ for different countries. This time again, we see large variations in the dynamics of jumps from one country to another. **This suggests little consistency in the calibrated values.**

➔ The calibration of the model is not particularly conclusive. On one side, some indicators like ADC and KS p-values, suggest that the model is able to replicate the empirical distribution of the data. But playing against that, many calibrated values prove abnormally instable from one country to another, and this suggests little consistency in general. We are also surprised that only a tiny portion of the 50 calibrations (per country) provides acceptable results.

The rationale behind a common utilisation of Brownians and jumps, as exposed in Ait-Sahalia (2010) looks sensible. However, the observed lack of robustness may come from using too many unknowns. We explore an interesting alternative in the following section.

Graph 242. Jump intensities in core and soft-core countries

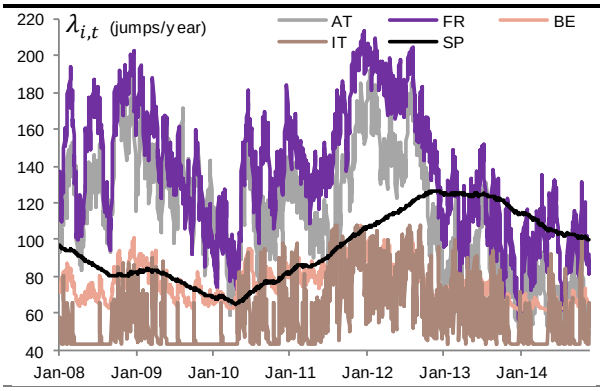

Graph 243. Jump intensities at the periphery

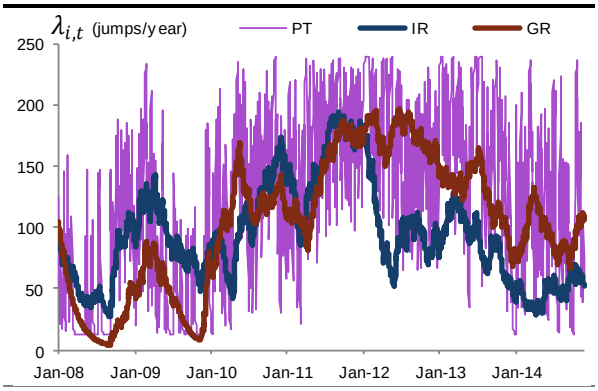

A model exclusively based on jumps

Hainaut (2016) explores bivariate Hawkes processes in the context of interest rates modelling. The proposed framework focuses on jumps, exclusively, with no particular reference to the continuous dimension of market prices. **As such, this may be an interesting alternative to Ait-Sahalia (2010)**, where the desire to separate the continuous part from the jumps led to a substantial increase of the computational burden.

In Hainaut (2016), the author assumes that every price realisation is a jump, driven either by the demand for, or the supply of, the underlying security. This approach looks particularly relevant when you can explore the dynamics of high-frequency market valuations as in this case, jumps may be observable. Getting intraday data was not possible for us, so it was clear from the beginning that jumps are not observable in our dataset (we explore close-to-close price variations). **In our model, jumps are therefore a latent (non-observable) variable.** And as we show below, this incurs major changes to the calibration procedure compared to Hainaut (2016).

An interesting feature in Hainaut (2016), is that supply and demand are illustrated by two different jump processes. This gives the model a 'bivariate' dimension, which is reinforced by the fact that both intensities are interconnected via a mutually-exciting loop (Hawkes process). In the end, the model offers an interesting framework to price zero-coupon bond options, with some simplifications compared to Ait-Sahalia (2010). In this report, we also explore a new version of the model, where we extend the dimension of the problem: **we assume that jumps intensities are also excited by contagion, emanating from exogenous time series.**

Formalisation of the problem, univariate case

Hainaut (2016) explores the dynamics of Fixed Income instruments, and the author assumes that the interest rate r_t is a combination of a function of time $\varphi(t)$ and a process X_t:

$$r_t = \varphi\, t + X_t \tag{143}$$

X_t is supposed to reflect the difference between supply of and demand for the underlying security, at the very front-end of the interest rate curve. As a general practice with interest rates models based on the short-term dynamics (e.g. Vasicek, LIBOR models…), X_t is seen as the **instantaneous interest rate**. We adopt the same approach here, and we will see later that *1-month* interest rates are a reasonable proxy for X_t.

Hainaut (2016) assumes that any price variation in the sample is a proper jump L, either positive or negative. Positive jumps on one side, lead to an increase of the yield to maturity of the bond, and thus a decline of the price. This category of jumps thus reflects the **'supply'** effect. They are denoted L_t^1. In contrast, negative jumps lead to a lower yield to maturity, and thus an increase of the price. Negative jumps therefore illustrate the **'demand'** effect; these jumps are denoted L_t^2. In both cases (positive and negative), the corresponding jump intensities λ_t^1 and λ_t^2 are described by Hawkes processes (see Bacry et al. (2013)).

From a very general perspective, the author defines the infinitesimal behaviour of X as:

$$dX_t = \alpha_1 L_t^1 - \alpha_2 L_t^2 \tag{144}$$

on a complete probability space $(\Omega, \mathcal{F}, P)$, with a right-continuous information filtration $F = (\mathcal{F}_t)_{t>0}$, and where P denotes the real probability measure.

In this framework, Hainaut (2016) assumes that the amplitude of the jumps is a random variable too, which is denoted O^1 and O^2. Both are drawn from two different probability distribution functions, $\nu_1(z)$ and $\nu_2(z)$. The first and second moments of these distributions are $\mu_1 = \mathbb{E}(O^1)$, $\mu_2 = \mathbb{E}(O^2)$, $\eta_1 = \mathbb{E}((O^1)^2)$, $\eta_2 = \mathbb{E}((O^2)^2)$. We also denote by N_t^1 and N_t^2 counting processes that reflect the number of jumps that happened from the beginning of the simulation. Finally we can express X_t as:

$$dX_t = \alpha_1 L_t^1 - \alpha_2 L_t^2 = \alpha_1 O^1 dN_t^1 - \alpha_2 O^2 dN_t^2 \tag{145}$$

The 'self-exciting' loop in Hawkes' processes is a key component of the model, and as such Hainaut (2016) assumes that intensities of jump arrivals are random processes governed by the following equation:

$$d\lambda_t^i = \kappa_i\left(c_i - \lambda_t^i\right)dt + \delta_{i,1} dL_t^1 + \delta_{i,2} dL_t^2 \qquad i = 1,2 \tag{146}$$

Where κ_i and c_i are part of a mean-reverting Ornstein Uhlenbeck process (like in Ait-Sahalia (1996)). $\delta_{1,1}$ and $\delta_{2,2}$ set the level of self-excitation, while $\delta_{1,2}$ and $\delta_{2,1}$ illustrate the cross impact of supply and demand.

Hainaut (2016) shows that if ψ_1, ψ_2 denote the moment generating functions of O^1, O^2:

$$\psi_i(\omega) = \mathbb{E}\left(e^{\omega O^i}\right) \qquad \text{for } i = 1,2 \tag{147}$$

Then the moment generating function of $\omega_0 X_T - \omega_1 \int_t^T X_s ds + \begin{pmatrix}\omega_1\\ \omega_2\end{pmatrix}^T \begin{pmatrix}\lambda_T^1\\ \lambda_T^2\end{pmatrix}$ is an affine function of X_t and of the jump intensities:

$$\mathbb{E}\left(e^{\omega_0 X_T - \omega_1 \int_t^T X_s ds + \begin{pmatrix}\omega_1\\ \omega_2\end{pmatrix}^T \begin{pmatrix}\lambda_T^1\\ \lambda_T^2\end{pmatrix}} | \mathcal{F}_t\right) = \exp\left(\left(\omega_0 - \omega_1(T-t)\right)X_t + A(t,T) + \begin{pmatrix}B_1(t,T)\\ B_2(t,T)\end{pmatrix}^T \begin{pmatrix}\lambda_T^1\\ \lambda_T^2\end{pmatrix}\right) \tag{148}$$

Where A, B_1, B_2 are solutions of a system of ODEs:

$$\begin{cases} \dfrac{\partial}{\partial t} B_1(t,T) = \kappa_1 B_1(t,T) - \left[\psi_1\left(B_1(t,T)\delta_{1,1} + \omega_0\alpha_1 - \omega_1\alpha_1(T-t) + B_2(t,T)\delta_{2,1}\right) - 1\right] \\ \dfrac{\partial}{\partial t} B_2(t,T) = \kappa_2 B_2(t,T) - \left[\psi_2\left(B_1(t,T)\delta_{1,2} - \omega_0\alpha_1 + \omega_1\alpha_1(T-t) + B_2(t,T)\delta_{2,2}\right) - 1\right] \\ \dfrac{\partial}{\partial t} A(t,T) = -\kappa_1 c_1 B_1(t,T) - \kappa_2 c_2 B_2(t,T) \end{cases} \tag{149}$$

With the terminal conditions $A(T,T) = 0$, $B_1(T,T) = \omega_2$, $B_2(T,T) = \omega_3$.

The moment generating function of $X_t$is an affine function of $\left(\lambda_t^1, L_t^1, \lambda_t^2, L_t^2\right)$, and therefore Hainaut (2016) consider an exponential affine change of measure of the form:

$$M_t(\theta_1,\theta_2) = \exp\left(\begin{pmatrix}a_1(\theta_1,\theta_2)\\ a_2(\theta_1,\theta_2)\end{pmatrix}^T \begin{pmatrix}\lambda_t^1\\ \lambda_t^2\end{pmatrix} + (\theta_1,\theta_2)\begin{pmatrix}L_t^1\\ L_t^2\end{pmatrix} - \varphi(\theta_1,\theta_2)t\right) \tag{150}$$

Where $\theta_1, \theta_2 \in \mathbb{R}$ are assimilated to risk premia. The author shows that the dynamics of interest rates is preserved under this new measure. Zhang et al. (2009) describes a similar change of measure, though for jumps with constant amplitude. In this set up, and as detailed in Hainaut (2016), M_t is a local martingale if it fulfils the following condition:

If for any given couple of parameters (θ_1, θ_2), there exist suitable solutions $a_1(\theta_1, \theta_2)$, $a_2(\theta_1, \theta_2)$, $a_3(\theta_1, \theta_2)$, $a_4(\theta_1, \theta_2)$ for the system of equations:

$$\begin{cases} a_1(\theta_1, \theta_2)\kappa_1 - \left(\psi_1\left(a_1(\theta_1, \theta_2)\delta_{1,1} + a_2(\theta_1, \theta_2)\delta_{2,1} + \theta_1\right) - 1\right) = 0 \\ a_2(\theta_1, \theta_2)\kappa_2 - \left(\psi_2\left(a_1(\theta_1, \theta_2)\delta_{2,1} + a_2(\theta_1, \theta_2)\delta_{2,2} + \theta_2\right) - 1\right) = 0 \end{cases} \quad (151)$$

Where $\psi_i(\omega) = \mathbb{E}\left(e^{\omega O^i}\right)$ for $i = 1,2$ and if $\varphi(\theta_1, \theta_2)$ is a linear combination of these solutions:

$$\varphi(\theta_1, \theta_2) = a_1\kappa_1 c_1 + a_2\kappa_2 c_2 \quad (152)$$

Then $M_t(\theta_1, \theta_2)$ is a local martingale. Assuming the existence of suitable solutions, an equivalent measure Q^{θ_1,θ_2} is defined by:

$$\frac{\partial Q^{\theta_1,\theta_2}}{\partial P} = \frac{M_t(\theta_1, \theta_2)}{M_0(\theta_1, \theta_2)} \quad (153)$$

This new measure Q^{θ_1,θ_2} may be used as a risk neutral measure by investors. In this case, the dynamics of intensities and aggregate supply or demand is modified but is still a Hawkes process (see Hainaut (2016)). Let $N_t^{1,Q}$, $N_t^{2,Q}$ be counting processes with respective intensities under the equivalent measure Q^{θ_1,θ_2}:

$$\begin{cases} \lambda_t^{1,Q} = \mathbb{E}\left(e^{\left(a_1\delta_{1,1} + a_2\delta_{2,1} + \theta_1\right)}\right)\lambda_t^1 \\ \lambda_t^{2,Q} = \mathbb{E}\left(e^{\left(a_1\delta_{2,1} + a_2\delta_{2,2} + \theta_2\right)}\right)\lambda_t^2 \end{cases} \quad (154)$$

On the other hand, if $O^{1,Q}$, $O^{2,Q}$ denote the random variables defined by the following moment generating function:

$$\begin{cases} \psi_1^Q(z) = \mathbb{E}\left(e^{zO^{1,Q}}\right) = \dfrac{\psi_1\left(z + \left(a_1\delta_{1,1} + a_2\delta_{2,1} + \theta_1\right)\right)}{\psi_1\left(a_1\delta_{1,1} + a_2\delta_{2,1} + \theta_1\right)} \\ \psi_2^Q(z) = \mathbb{E}\left(e^{zO^{2,Q}}\right) = \dfrac{\psi_2\left(z + \left(a_1\delta_{2,1} + a_2\delta_{2,2} + \theta_2\right)\right)}{\psi_2\left(a_1\delta_{2,1} + a_2\delta_{2,2} + \theta_2\right)} \end{cases} \quad (155)$$

And if the jump processes $L_t^{1,Q}$, $L_t^{2,Q}$ are defined such that:

$$L_t^{i,Q} = \sum_{k=1}^{N_t^{i,Q}} O_k^{i,Q} \quad i = 1,2,P1,P2 \quad (156)$$

Then intensities λ_t^i are driven by the following EDS under Q^{θ_1,θ_2}:

$$\begin{cases} d\lambda_t^{Q,1} = \kappa_1\left(c_1^Q - \lambda_t^{Q,1}\right)dt + \delta_{1,1}^Q dL_t^1 + \delta_{1,2}^Q dL_t^2 \\ d\lambda_t^{Q,2} = \kappa_2\left(c_2^Q - \lambda_t^{Q,2}\right)dt + \delta_{2,1}^Q dL_t^1 + \delta_{2,2}^Q dL_t^2 \end{cases} \quad (157)$$

Hainaut (2016) also considers that the amplitude O^i of jumps, under P, is exponentially distributed. The probability distribution functions of the jump amplitude are thus defined as:

$$\begin{cases} \nu_1(z) = \rho_1 e^{-\rho_1 z} 1_{\{z \geq 0\}} \\ \nu_2(z) = \rho_2 e^{\rho_2 z} 1_{\{z \leq 0\}} \end{cases} \text{ With } \rho_1, \rho_2 \in \mathbb{R}^+ \quad (158)$$

In this case, the first and second moments of O^1, O^2 are respectively equal to $\mu_1 = \frac{1}{\rho_1}$, $\mu_2 = \frac{1}{\rho_2}$, and to $\eta_i = \frac{2}{(\rho_i)^2}$. The moment generating functions are given by:

$$\psi_1(z) = \frac{\rho_1}{\rho_1 - z} \text{ for } z < \rho_1, \quad \psi_2(z) = \frac{\rho_2}{\rho_2 + z} \text{ for } z > -\rho_2$$

Then Hainaut (2016) shows that the distribution of the jump amplitude is exponential under Q as well, and the corresponding densities, denoted $\nu_i^Q(z)$, are defined such that:

$$\begin{cases} \rho_1^Q = \rho_1 - \left(\delta_{1,1}a_1 + \delta_{2,1}a_2 + \theta_1\right) \\ \rho_2^Q = \rho_2 - \left(\delta_{1,2}a_1 + \delta_{2,2}a_2 + \theta_2\right) \end{cases} \tag{159}$$

On top of that, Hainaut (2016) notes that the dynamics of the jump intensity is preserved under Q^{θ_1,θ_2}: the intensities of the counting processes $N_t^{1,Q}$, $N_t^{2,Q}$, $N_t^{P1,Q}$, $N_t^{P2,Q}$ are Hawkes processes with the same structure under Q as under the real measure P:

$$\begin{cases} d\lambda_t^{1,Q} = \kappa_1\left(c_1^Q - \lambda_t^{1,Q}\right)dt + \delta_{1,1}^Q dL_t^1 + \delta_{1,2}^Q dL_t^2 \\ d\lambda_t^{2,Q} = \kappa_2\left(c_2^Q - \lambda_t^{2,Q}\right)dt + \delta_{2,1}^Q dL_t^1 + \delta_{2,2}^Q dL_t^2 \end{cases} \tag{160}$$

with:

$$\begin{cases} c_1^Q = c_1\psi_1\left(\delta_{1,1}a_1 + \delta_{2,1}a_2 + \theta_1\right) \\ c_2^Q = c_2\psi_2\left(\delta_{1,2}a_1 + \delta_{2,2}a_2 + \theta_2\right) \\ \delta_{1,j}^Q = \delta_{1,j}\psi_1\left(\delta_{1,1}a_1 + \delta_{2,1}a_2 + \theta_1\right) \quad j = 1,2 \\ \delta_{2,j}^Q = \delta_{2,j}\psi_2\left(\delta_{1,1}a_1 + \delta_{2,1}a_2 + \theta_1\right) \quad j = 1,2 \end{cases} \tag{161}$$

If market participants adopt an exponential affine measure for the risk neutral one, equivalent to the real measure, then the price of a zero coupon bond is equal to the expected discount factor, under this risk neutral measure. The price of the zero coupon bond is thus denoted as:

$$\begin{aligned} P\left(t,T,\lambda_t^1,J_t^1,\lambda_t^2,J_t^2,\lambda_t^{P1},J_t^{P1},\lambda_t^{P2},J_t^{P2}\right) &= \mathbb{E}^Q\left(e^{-\int_t^T r_s ds}|\mathcal{F}_t\right) \\ &= e^{-\int_t^T \varphi(s)ds}\mathbb{E}^Q\left(e^{-\int_t^T X_s ds}|\mathcal{F}_t\right) \end{aligned} \tag{162}$$

And then we have:

$$\mathbb{E}^Q\left(e^{-\int_t^T X_s ds}|\mathcal{F}_t\right) = \exp\left(-X_t(T-t) + A(t,T) + \begin{pmatrix} B_1(t,T) \\ B_2(t,T) \end{pmatrix}^T \begin{pmatrix} \lambda_t^{1,Q} \\ \lambda_t^{2,Q} \end{pmatrix}\right) \tag{163}$$

Where $A(t,T)$, $B_1(t,T)$, $B_2(t,T)$ are solutions of the following system of ODEs:

$$\begin{cases} \dfrac{\partial}{\partial t}B_1 = \kappa_1 B_1(t,T) - \left[\psi_1^Q\left(B_1\delta_{1,1}^Q + B_2\delta_{2,1}^Q - \alpha_1(T-t)\right) - 1\right] \\ \dfrac{\partial}{\partial t}B_2 = \kappa_2 B_2(t,T) - \left[\psi_2^Q\left(B_1\delta_{1,2}^Q + B_2\delta_{2,2}^Q + \alpha_2(T-t)\right) - 1\right] \\ \dfrac{\partial}{\partial t}A = -\kappa_1 c_1^Q B_1 - \kappa_2 c_2^Q B_2 \end{cases} \tag{164}$$

With the terminal condition: $A(T,T) = 0$, $B_1(T,T) = B_2(T,T) = 0$.

The dynamics of bond prices depends on the random measures of jump processes, noted $L_t^{1,Q}(dt,dz)$, $L_t^{2,Q}(dt,dz)$ and such that:

$$L_t^{k,Q} = \int_0^{+\infty} \int_{-\infty}^{+\infty} L^{k,Q}(dt,dz) \qquad k = 1,2,P1,P2 \tag{165}$$

Furthermore the expectation of these measures is equal to $\mathbb{E}^Q\left(L^{k,Q}(dt,dz)|\mathcal{F}_t\right) = \lambda_t^{k,Q} v_k(z)dzdt$. As Hainaut (2016) shows, the bond prices $P\left(t,T,\lambda_t^{1,Q},J_t^{1,Q},\lambda_t^{2,Q},J_t^{2,Q}\right)$ are ruled by the following SDE:

$$\begin{aligned} dP = Pr_t dt &- \lambda_t^{1,Q} P\left[\psi_1^Q\left(B_1(t,T)\delta_{1,1}^Q + B_2(t,T)\delta_{2,1}^Q - \alpha_1(T-t)\right) - 1\right]dt \\ &- \lambda_t^{2,Q} P\left[\psi_2^Q\left(B_1(t,T)\delta_{1,2}^Q + B_2(t,T)\delta_{2,2}^Q - \alpha_2(T-t)\right) - 1\right]dt \\ &+ P\int_{-\infty}^{+\infty}\left(\exp\left(B_1(t,T)\delta_{1,1}^Q + B_2(t,T)\delta_{2,1}^Q - \alpha_1(T-t)\right) - 1\right)L^{1,Q}(dt,dz) \\ &+ P\int_{-\infty}^{+\infty}\left(\exp\left(B_1(t,T)\delta_{1,2}^Q + B_2(t,T)\delta_{2,2}^Q - \alpha_2(T-t)\right) - 1\right)L^{2,Q}(dt,dz) \end{aligned} \tag{166}$$

where $L_t^{1,Q}(dt,dz)$, $L_t^{2,Q}(dt,dz)$ are random measures of jump processes (see Hainaut (2016) for all the corresponding demonstrations).

Table 171. Descriptive Statistics

		1m	3m	6m	1Y	2Y	3Y	4Y	5Y	6Y	7Y	8Y	9Y	10Y
GERMANY	Mean of absolute values	0.00015	0.00016	0.00013	0.00018	0.00026	0.00028	0.00031	0.00032	0.00032	0.00032	0.00032	0.00032	0.00032
	standard deviation	0.00028	0.00032	0.00024	0.00029	0.00029	0.00042	0.00043	0.00044	0.00044	0.00044	0.00043	0.00044	0.00043
FINLAND	Mean of absolute values	0.00019	0.00019	0.00019	0.00025	0.00026	0.00026	0.00029	0.00031	0.00032	0.00031	0.00031	0.00032	0.00031
	standard deviation	0.00032	0.00035	0.00034	0.00039	0.0004	0.00039	0.00041	0.00043	0.00045	0.00044	0.00043	0.00043	0.00042
NETHER	Mean of absolute values	0.00015	0.00015	0.00015	0.00022	0.00024	0.00027	0.00029	0.00031	0.00032	0.00032	0.00031	0.00031	0.00031
	standard deviation	0.00026	0.00028	0.00027	0.00035	0.00038	0.00041	0.00042	0.00044	0.00044	0.00044	0.00042	0.00042	0.00042
AUSTRIA	Mean of absolute values	0.00011	0.00012	0.00018	0.00023	0.00025	0.00027	0.00029	0.00029	0.0003	0.00029	0.00031	0.00031	0.00031
	standard deviation	0.00036	0.00038	0.00038	0.00039	0.00041	0.00044	0.00045	0.00046	0.00045	0.00043	0.00042	0.00050	0.00043
FRANCE	Mean of absolute values	0.00015	0.00016	0.00014	0.00019	0.00028	0.00029	0.00030	0.00032	0.00032	0.00032	0.00032	0.00032	0.00032
	standard deviation	0.00042	0.00044	0.00038	0.00031	0.00036	0.00046	0.00043	0.00045	0.00045	0.00043	0.00043	0.00043	0.00043
BELGIUM	Mean of absolute values	0.00020	0.00021	0.00021	0.00021	0.00027	0.0003	0.00032	0.00033	0.00034	0.00033	0.00033	0.00033	0.00033
	standard deviation	0.00036	0.00037	0.00037	0.00037	0.00043	0.00046	0.00049	0.0005	0.00049	0.00049	0.00048	0.00048	0.00048
ITALY	Mean of absolute values	0.00031	0.00031	0.00027	0.00034	0.00038	0.00039	0.0004	0.0004	0.0004	0.00039	0.00038	0.00038	0.00038
	standard deviation	0.00062	0.00064	0.00064	0.00071	0.00067	0.00067	0.00064	0.00062	0.00059	0.00058	0.00059	0.00058	0.00058
SPAIN	Mean of absolute values	0.00025	0.00025	0.00025	0.00032	0.00039	0.00041	0.00042	0.00042	0.00042	0.00041	0.00041	0.00040	0.00040
	standard deviation	0.00067	0.00068	0.00066	0.00062	0.00070	0.00069	0.00069	0.00065	0.00066	0.00065	0.00062	0.00061	0.00062
IRELAND	Mean of absolute values	0.00040	0.0004	0.00041	0.00048	0.00046	0.00042	0.00048	0.00042	0.00039	0.00036	0.00037	0.00040	0.00039
	standard deviation	0.00082	0.00085	0.00086	0.0009	0.00089	0.00082	0.00086	0.00078	0.00077	0.00068	0.00066	0.00068	0.00066
PORTUGAL	Mean of absolute values	0.00035	0.00037	0.00035	0.00037	0.00050	0.00055	0.00057	0.00061	0.00058	0.00054	0.00053	0.00051	0.00051
	standard deviation	0.00086	0.00089	0.00086	0.00100	0.00105	0.00102	0.00108	0.00101	0.00093	0.00091	0.00091	0.00089	0.00085

Dataset and calibration of the univariate model

Our dataset is made of European sovereign zero coupon bond curves, taken from January 2000 up to end-December 2016. We get zero coupon curves from Bloomberg, and when needed, we calculate missing valuations by using the popular bootstrap approach. We consider the following set of maturities T:

$$\{T\} = \{1m, 3m, 6m, 1y, 2y, 3y, 4y, 5y, 6y, 7y, 8y, 9y, 10y\}$$

As an illustration, Graph 244 shows the dynamics of 5Y zero coupon bonds over the full period.

Graph 244. 5Y zero coupon bond, over the full period

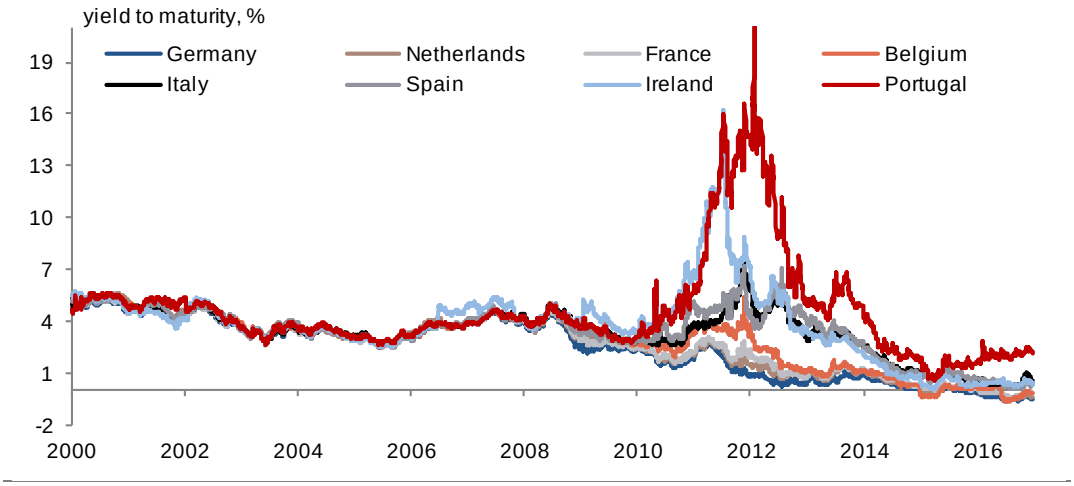

Then Graph 245 to Graph 248 show the shape of the zero coupon curves, for Germany, France, Italy and Spain. The curve is upward slopping in all cases, and the slope is almost flat at the very front-end of the curve. This suggests that the true instantaneous interest rate X_t must be relatively close to the 1-month interest rate (ie. the first point in the chart, starting from the left). We will thus consider the approximation that $X_t \sim 1\ month\ ZC\ rate$. As we show below, this assumption is helpful to refine the range of initial values during the calibration.

Graph 245. German zero coupon bonds at selected dates

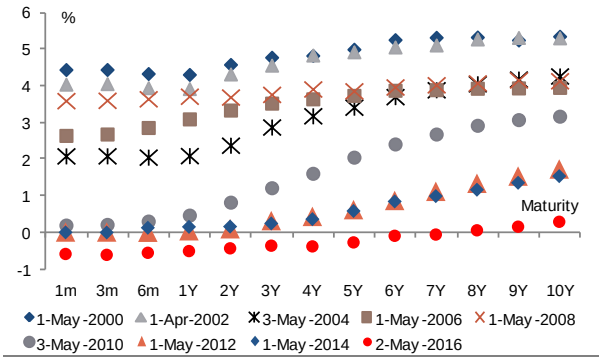

Graph 246. French zero coupon bonds at selected dates

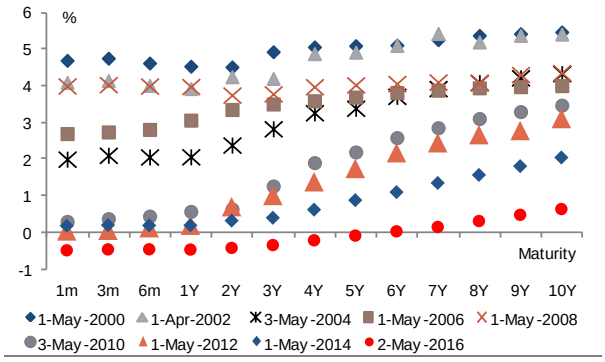

Graph 247. Italian zero coupon bonds at selected dates

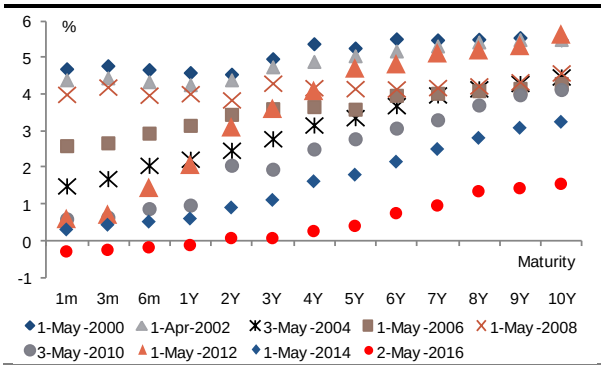

Graph 248. Spanish zero coupon bonds at selected dates

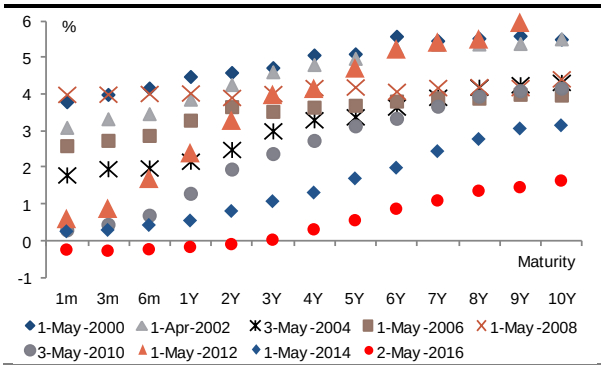

The amplitude of the jumps, in Hainaut (2016), is assumed to be exponentially distributed, and based on the distributions ν_1 and ν_2. Although this is a generalised approach in the literature (e.g. see Cremers, Driessen, Maenhout (2008), Kita (2012)), **there is little insight in Hainaut (2016) on the relevance of exponential distributions as to model jumps.**

We understand that the major benefit of considering exponential distributions is the very few number of unknown variables involved. In Hainaut (2016) for instance, the knowledge of ρ_1 and ρ_2 is sufficient to determine the distributions ν_1 and ν_2 as a whole. **A limitation however, is that the exponential distribution is not recognized as a "heavy-tailed" distribution.**

As we seek to understand whether exponential distributions are an appropriate choice for ν_1 and ν_2, we explore the goodness of fit offered by these distributions, when ρ_1 and ρ_2 are calibrated against the empirical distribution of the data. We calculate the corresponding ADC criterion, obtained under these circumstances, as a measure of similarity between both, the exponential distributions, and the empirical distribution of the dataset. Overall, results are relatively poor ($ADC > 2.5$ in many cases, see Table 172). ➔ On that basis, exponential distributions seem not to be a reliable descriptor of the dynamics of the dataset, **at least when we consider the full period (2000 to end-2016).**

Now focusing on reduced version of the sample, **that takes only financial crises into account** (ie. from 2008 up to end-2012), the ADC criterion improves significantly: in this case, and as Table 173 shows, the condition $ADC \leq 2.5$ is almost always verified.

➔ In the end, exponential distributions can be seen as a reliable descriptor of the market dynamics during periods of financial distress**. By extrapolation, it looks fair to assume that intraday jumps could be similarly distributed. This observation tends to validate the general assumption of exponentially distributed jumps.**

Table 172. ADC criterion calculated for the full period (2000-2016)

	3M	6M	1Y	2Y	3Y	4Y	5Y	6Y	7Y	8Y	9Y	10Y
GE	8.1	6.5	3.6	2.4	1.3	0.9	1.5	1.5	1.9	2.1	2.0	2.4
	5.9	4.9	2.8	1.2	0.9	1.9	2.4	2.7	3.3	3.5	3.7	3.4
FI	6.2	5.3	4.5	2.4	1.3	1.1	1.0	1.3	1.4	2.2	2.3	1.9
	6.7	5.2	2.3	1.0	1.0	1.5	2.4	2.2	2.3	3.6	3.8	4.1
NL	5.9	5.5	5.1	2.8	1.5	1.2	0.9	1.8	1.8	2.0	2.5	2.2
	4.0	4.0	2.6	1.8	1.5	1.4	2.3	2.4	3.5	3.8	3.9	3.9
AT	4.7	4.8	2.9	2.3	2.2	1.4	1.5	1.9	2.0	1.7	2.0	2.4
	3.8	3.7	2.2	1.4	1.2	0.8	1.5	2.5	2.9	3.5	1.9	3.2
FR	11.1	9.3	3.5	3.1	1.7	1.3	1.1	1.9	2.0	2.0	2.2	2.3
	7.1	6.6	3.2	3.2	1.8	1.7	2.5	2.5	3.4	3.6	4.0	3.9
BE	3.9	4.0	4.1	2.9	2.1	1.3	1.1	1.2	1.4	1.4	1.7	1.7
	4.1	4.0	3.9	1.8	1.0	1.0	1.5	3.1	2.6	3.5	3.9	3.9
IT	9.4	8.8	7.3	6.0	4.7	3.4	2.9	2.3	2.0	1.9	1.8	1.7
	8.1	6.7	4.9	4.4	2.6	2.3	1.9	1.8	2.1	1.9	2.4	2.4
SP	11.8	9.8	6.7	4.5	4.1	3.0	2.1	1.9	1.6	1.5	1.4	1.6
	10.7	9.3	5.6	5.2	3.3	2.9	2.0	2.3	2.1	1.9	1.9	2.0
IR	11.5	11.8	11.2	10.7	10.9	6.5	4.5	4.8	3.5	3.3	2.4	2.7
	9.7	9.5	9.3	9.3	9.1	5.1	3.2	3.2	2.6	1.7	2.0	2.1
PT	12.3	12.8	10.8	8.4	7.2	6.3	6.6	5.0	5.2	5.1	3.9	3.8
	11.0	11.4	12.1	9.5	8.2	5.9	6.1	5.4	5.3	4.5	3.8	4.1

Table 173. ADC criterion calculated for the sub-period 2008-2012

	3M	6M	1Y	2Y	3Y	4Y	5Y	6Y	7Y	8Y	9Y	10Y
GE	1.4	1.2	1.3	1.1	1.1	1.1	1.4	1.7	1.6	1.7	1.6	1.5
	1.7	1.6	1.4	0.9	1.0	2.0	1.8	2.1	2.2	2.2	1.9	1.9
FI	0.5	0.5	1.4	0.7	0.5	0.8	1.0	1.3	1.0	1.2	1.3	1.4
	0.8	0.8	0.9	0.7	0.8	1.1	1.6	1.5	2.0	1.9	1.8	1.6
NL	2.8	1.3	1.4	1.3	0.5	1.1	1.0	1.2	1.3	1.2	1.3	1.2
	1.6	1.8	1.4	1.1	0.7	1.1	1.3	1.4	1.7	1.6	1.7	1.6
AT	1.2	1.2	1.3	1.0	1.0	1.0	1.3	1.3	1.0	0.4	0.5	0.6
	1.0	1.2	0.9	0.6	0.7	0.7	0.8	1.1	1.4	0.8	1.1	1.1
FR	1.9	1.8	1.2	0.8	0.5	0.5	0.6	0.7	0.9	0.9	0.7	0.7
	1.5	1.5	1.0	0.8	0.7	1.0	1.0	1.0	1.2	1.1	1.4	1.6
BE	1.9	1.9	1.9	0.7	0.8	1.2	1.2	1.1	1.0	1.2	0.8	0.8
	0.6	0.6	0.6	0.4	0.5	0.8	1.6	1.0	0.9	0.7	0.9	1.0
IT	2.0	1.5	1.4	0.8	0.5	0.5	0.6	0.5	0.8	0.9	1.1	1.1
	1.2	1.3	0.8	0.6	0.5	0.8	0.6	0.6	1.0	0.5	0.7	0.8
SP	1.2	0.7	1.1	0.9	0.6	0.5	0.4	0.9	0.8	1.0	0.9	0.9
	0.8	0.7	1.0	0.6	0.8	0.5	0.8	0.4	0.6	0.6	1.0	0.8
IR	1.7	2.2	0.6	1.2	1.2	2.2	2.3	2.5	1.9	1.3	1.7	1.8
	3.3	3.3	0.8	0.8	1.3	1.0	1.0	1.4	1.2	1.3	1.7	1.6
PT	3.3	3.6	2.7	0.6	0.6	0.6	0.9	0.6	1.2	0.7	0.7	1.1
	3.2	3.3	3.0	0.9	0.7	1.0	0.7	1.6	1.8	1.6	0.6	1.1

Eq. (163) describes the behaviour of zero coupon bonds under the risk-neutral measure, in terms of price. Since we look at valuations in terms of yield to maturity, we consider Y as the main variable, and we write it as:

$$Y\left(t,T,\lambda_t^1,J_t^1,\lambda_t^2,J_t^2\right) = -\frac{1}{T-t}\log\left(\mathbb{E}^Q\left(e^{-\int_t^T r_s ds}|\mathcal{F}_t\right)\right)$$
$$= -\frac{1}{T-t}\log\left(\ e^{-\int_t^T \varphi(s)ds}\mathbb{E}^Q\left(e^{-\int_t^T X_s ds}|\mathcal{F}_t\right)\right)$$

For simplicity we denote Y as $Y(t,T)$, and we derive its behaviour from eq. (163) as:

$$Y(t,T) = \frac{1}{T-t}\int_t^T \varphi(s)ds - \frac{1}{T-t}\left(-X_t(T-t) + A(t,T) + \begin{pmatrix}B_1(t,T)\\B_2(t,T)\end{pmatrix}^T\begin{pmatrix}\lambda_t^{1,Q}\\\lambda_t^{2,Q}\end{pmatrix}\right)$$

Then under the historical measure, we obtain:

$$Y(t,T) = \frac{1}{T-t}\int_t^T \varphi(s)ds - \frac{1}{T-t}\left(-X_t(T-t) + A(t,T) + \begin{pmatrix} B_1(t,T) \\ B_2(t,T) \end{pmatrix}^T \begin{pmatrix} \lambda_t^1 \\ \lambda_t^2 \end{pmatrix}\right)$$

The volatility, both under the historical and the risk neutral measures, is not properly observable. However, we consider that empirical volatilities tend to approach the expected value of the volatility under the historical measure, ie. $\mathbb{E}^P\left(Var^P\left(Y(t,T)|\mathcal{F}_{t_0}\right)|\mathcal{F}_{t_0}\right)$, with:

$$Var^P\left(Y(t,T)|\mathcal{F}_{t_0}\right) = \frac{1}{(T-t)^2} Var\left(-X_t(T-t) + \begin{pmatrix} B_1(t,T) \\ B_2(t,T) \end{pmatrix}^T \begin{pmatrix} \lambda_t^1 \\ \lambda_t^2 \end{pmatrix} |\mathcal{F}_{t_0}\right)$$

However, the expectation $\mathbb{E}^P\left(Var^P\left(Y(t,T)|\mathcal{F}_{t_0}\right)|\mathcal{F}_{t_0}\right)$ also involves the autocovariance of $X_i X_j$, for which we do not have a dedicated expression. We prefer avoiding this additional complexity, although we reckon there might be a way to quantify the autocovariance. As an alternative to $\mathbb{E}^P\left(Var^P\left(Y(t,T)|\mathcal{F}_{t_0}\right)|\mathcal{F}_{t_0}\right)$, we prefer focusing on $\mathbb{E}^P\left(Y^2(t,T)|\mathcal{F}_{t_0}\right)$, which does not involve the autocovariance.

In the end, we calibrate the model by reducing the distance between the empirical estimator $Z(t-t_0) = \frac{1}{t-t_0+1}\sum_{k=0}^{t-t_0} Y^2(t_0+k,T)$ and the corresponding analytical expression $\mathbb{E}^P\left(Y^2(t,T)|\mathcal{F}_{t_0}\right)$ on a rolling time-window $[t_0 : t_N]$. We thus obtain the following optimisation problem:

$$Min_\theta\left(\sum_{t=t_0}^{t_N}\left(Z(t-t_0) - \frac{1}{t-t_0+1}\sum_{j=t_0}^{t} E^P\left(Y^2(j,T)|\mathcal{F}_{t_0}\right)\right)^2\right) \tag{167}$$

With:

$$\begin{aligned}
\mathbb{E}^P\left(Y^2(t,T)|\mathcal{F}_{t_0}\right) = &\left(\frac{1}{T-t}\int_t^T \varphi(s)ds\right)^2 \\
&- 2\left(\frac{1}{(T-t)^2}\int_t^T \varphi(s)ds\right)\left(-\mathbb{E}^P\left[X_t|\mathcal{F}_{t_0}\right](T-t) + A(t,T) + \begin{pmatrix} B_1(t,T) \\ B_2(t,T) \end{pmatrix}^T \begin{pmatrix} \mathbb{E}^P\left[\lambda_t^1|\mathcal{F}_{t_0}\right] \\ \mathbb{E}^P\left[\lambda_t^2|\mathcal{F}_{t_0}\right] \end{pmatrix}\right) \\
&+ \frac{1}{(T-t)^2}\left(\mathbb{E}^P\left[{X_t}^2|\mathcal{F}_{t_0}\right](T-t)^2 + A^2(t,T) + \begin{pmatrix} {B_1}^2(t,T) \\ {B_2}^2(t,T) \end{pmatrix}^T \begin{pmatrix} \mathbb{E}^P\left[{\lambda_t^1}^2|\mathcal{F}_{t_0}\right] \\ \mathbb{E}^P\left[{\lambda_t^2}^2|\mathcal{F}_{t_0}\right] \end{pmatrix}\right. \\
&- 2\mathbb{E}^P\left[X_t|\mathcal{F}_{t_0}\right](T-t)A(t,T) + 2A(t,T)\begin{pmatrix} B_1(t,T) \\ B_2(t,T) \end{pmatrix}^T \begin{pmatrix} \mathbb{E}^P\left[\lambda_t^1|\mathcal{F}_{t_0}\right] \\ \mathbb{E}^P\left[\lambda_t^2|\mathcal{F}_{t_0}\right] \end{pmatrix} \\
&\left.- 2(T-t)\begin{pmatrix} B_1(t,T) \\ B_2(t,T) \end{pmatrix}^T \begin{pmatrix} \mathbb{E}^P\left[X_t\lambda_t^1|\mathcal{F}_{t_0}\right] \\ \mathbb{E}^P\left[X_t\lambda_t^2|\mathcal{F}_{t_0}\right] \end{pmatrix} + 2B_1(t,T)B_2(t,T)\mathbb{E}^P\left[\lambda_t^1\lambda_t^2|\mathcal{F}_{t_0}\right]\right)
\end{aligned}$$

$\mathbb{E}^P\left[{\lambda_t^1}^2|\mathcal{F}_{t_0}\right]$, $\mathbb{E}^P\left[{\lambda_t^2}^2|\mathcal{F}_{t_0}\right]$, $\mathbb{E}^P\left[\lambda_t^1\lambda_t^2|\mathcal{F}_{t_0}\right]$ are already given in Hainaut (2016) so only $\mathbb{E}^P\left[{X_t}^2|\mathcal{F}_{t_0}\right]$, $\mathbb{E}^P\left[X_t\lambda_t^1|\mathcal{F}_{t_0}\right]$, $\mathbb{E}^P\left[X_t\lambda_t^2|\mathcal{F}_{t_0}\right]$ have to be calculated. Like in Hainaut (2016), we use the infinitesimal generator to calculate these expectations; and in particular we use the following properties of the infinitesimal generator:

As shown in Errais et al. (2010), if $J_t^i = \left(L_t^i, N_t^i\right)$ the process $K_t = \left(\lambda_t^1, J_t^1, \lambda_t^2, J_t^2\right)$ is a Markov process in the state space $D = (\mathbb{R}^+ \times \mathbb{R}^+ \times \mathbb{N})^2$ and its infinitesimal generator for any function $g: D \to \mathbb{R}$ with partial derivatives $g_{\lambda_1}, g_{\lambda_2}$, is such that:

$$\begin{aligned}\mathcal{A}.g(K) = {} & \kappa_1(c_1 - \lambda_t^1)g_{\lambda_1} + \kappa_2(c_2 - \lambda_t^2)g_{\lambda_2} \\ & + \lambda_t^1 \int_{-\infty}^{+\infty} \left[g\left(\lambda_t^1 + \delta_{1,1}z, J_t^1 + (Z,1)^T, \lambda_t^2 + \delta_{2,1}z, J_t^2\right) - g(K)\right] d\nu_1(z) \\ & + \lambda_t^2 \int_{-\infty}^{+\infty} \left[g\left(\lambda_t^1 + \delta_{1,2}z, J_t^1, \lambda_t^2 + \delta_{2,2}z, J_t^2 + (Z,1)^T\right) - g(K)\right] d\nu_2(z)\end{aligned} \tag{168}$$

Based on Errais et al. (2010), we consider the following property where the expectation of g is equal to the integral of the expected infinitesimal generator:

$$\mathbb{E}\left(g(K_t)|\mathcal{F}_{t_0}\right) = g(K) + \int_{t_0}^{t} \mathbb{E}(\mathcal{A}.g(K_t)|\mathcal{F}_s)ds \tag{169}$$

Another interesting property is the following: the derivative of $\mathbb{E}\left(g(K_t)|\mathcal{F}_{t_0}\right)$ with respect to time is also equal to its expected infinitesimal generator:

$$\frac{\partial}{\partial t}\mathbb{E}\left(g(K_t)|\mathcal{F}_{t_0}\right) = \mathbb{E}\left(\mathcal{A}.g(K_t)|\mathcal{F}_{t_0}\right) \tag{170}$$

First we calculate $\mathbb{E}^P\left[X_t\lambda_t^i|\mathcal{F}_{t_0}\right]$. Let us consider $g = X_t\lambda_t^1$. Using the infinitesimal generator we obtain the following relationship:

$$\begin{aligned}\mathbb{E}\left(\mathcal{A}.g|\mathcal{F}_{t_0}\right) = {} & \kappa_1\left(c_1\mathbb{E}\left(X_t|\mathcal{F}_{t_0}\right) - \mathbb{E}\left(X_t\lambda_t^1|\mathcal{F}_{t_0}\right)\right) + \delta_{1,1}\mathbb{E}\left(X_t\lambda_t^1|\mathcal{F}_{t_0}\right)\mu_1 + \alpha_1\mu_1\mathbb{E}\left(\lambda_t^{1^2}|\mathcal{F}_{t_0}\right) \\ & + \mathbb{E}\left(\lambda_t^1|\mathcal{F}_{t_0}\right)\alpha_1\eta_1\delta_{1,1} + \delta_{1,2}\mathbb{E}\left(X_t\lambda_t^2|\mathcal{F}_{t_0}\right)\mu_2 + \alpha_2\mu_2\mathbb{E}\left(\lambda_t^{2^2}|\mathcal{F}_{t_0}\right) \\ & + \mathbb{E}\left(\lambda_t^2|\mathcal{F}_{t_0}\right)\alpha_2\eta_2\delta_{1,2}\end{aligned}$$

Similarly with $g = X_t\lambda_t^2$, we obtain:

$$\begin{aligned}\mathbb{E}\left(\mathcal{A}.g|\mathcal{F}_{t_0}\right) = {} & \kappa_2\left(c_2\mathbb{E}\left(X_t|\mathcal{F}_{t_0}\right) - \mathbb{E}\left(X_t\lambda_t^2|\mathcal{F}_{t_0}\right)\right) + \delta_{2,1}\mathbb{E}\left(X_t\lambda_t^1|\mathcal{F}_{t_0}\right)\mu_1 + \alpha_1\mu_1\mathbb{E}\left(\lambda_t^{1^2}|\mathcal{F}_{t_0}\right) \\ & + \mathbb{E}\left(\lambda_t^1|\mathcal{F}_{t_0}\right)\alpha_1\eta_1\delta_{2,1} + \delta_{2,2}\mathbb{E}\left(X_t\lambda_t^2|\mathcal{F}_{t_0}\right)\mu_2 + \alpha_2\mu_2\mathbb{E}\left(\lambda_t^{2^2}|\mathcal{F}_{t_0}\right) + \mathbb{E}\left(\lambda_t^2|\mathcal{F}_{t_0}\right)\alpha_2\eta_2\delta_{2,2}\end{aligned}$$

Then using eq. (170) we obtain the following ODE:

$$\begin{pmatrix} \dfrac{d\mathbb{E}^P\left[X_t\lambda_t^1|\mathcal{F}_{t_0}\right]}{dt} \\ \dfrac{d\mathbb{E}^P\left[X_t\lambda_t^2|\mathcal{F}_{t_0}\right]}{dt} \end{pmatrix} = \begin{pmatrix} C_1(t) \\ C_2(t) \end{pmatrix} + \begin{pmatrix} \left(\delta_{1,1}\mu_1 - \kappa_1\right) & \delta_{1,2}\mu_2 \\ \delta_{2,1}\mu_1 & \left(\delta_{2,2}\mu_2 - \kappa_2\right) \end{pmatrix} \begin{pmatrix} \mathbb{E}^P\left[X_t\lambda_t^1|\mathcal{F}_{t_0}\right] \\ \mathbb{E}^P\left[X_t\lambda_t^2|\mathcal{F}_{t_0}\right] \end{pmatrix} \tag{171}$$

With:

$$\begin{pmatrix} C_1(t) \\ C_2(t) \end{pmatrix} = \begin{pmatrix} \kappa_1 c_1\mathbb{E}^P\left(X_t|\mathcal{F}_{t_0}\right) + \alpha_1\mu_1\mathbb{E}\left(\lambda_t^{1^2}|\mathcal{F}_{t_0}\right) + \mathbb{E}\left(\lambda_t^1|\mathcal{F}_{t_0}\right)\alpha_1\eta_1\delta_{1,1} + \alpha_2\mu_2\mathbb{E}\left(\lambda_t^2\lambda_t^1|\mathcal{F}_{t_0}\right) + \mathbb{E}\left(\lambda_t^2|\mathcal{F}_{t_0}\right)\alpha_2\eta_2\delta_{1,2} \\ \kappa_2 c_2\mathbb{E}^P\left(X_t|\mathcal{F}_{t_0}\right) + \alpha_1\mu_1\mathbb{E}\left(\lambda_t^1\lambda_t^2|\mathcal{F}_{t_0}\right) + \mathbb{E}\left(\lambda_t^1|\mathcal{F}_{t_0}\right)\alpha_1\eta_1\delta_{2,1} + \alpha_2\mu_2\mathbb{E}\left(\lambda_t^{2^2}|\mathcal{F}_{t_0}\right) + \mathbb{E}\left(\lambda_t^2|\mathcal{F}_{t_0}\right)\alpha_2\eta_2\delta_{2,2} \end{pmatrix}$$

Then we can solve this system of ordinary equations over the interval $[t_0; t]$. We obtain:

$$\begin{pmatrix}\mathbb{E}^P\left[X_t\lambda_t^1|\mathcal{F}_{t_0}\right]\\ \mathbb{E}^P\left[X_t\lambda_t^2|\mathcal{F}_{t_0}\right]\end{pmatrix} = V\begin{pmatrix}e^{\gamma_1(t-t_0)} & 0\\ 0 & e^{\gamma_2(t-t_0)}\end{pmatrix}\int_{t_0}^{t}\begin{pmatrix}e^{-\gamma_1(s-t_0)} & 0\\ 0 & e^{-\gamma_2(s-t_0)}\end{pmatrix}V^{-1}\begin{pmatrix}C_1(s)\\ C_2(s)\end{pmatrix}ds + V\begin{pmatrix}e^{\gamma_1(t-t_0)} & 0\\ 0 & e^{\gamma_2(t-t_0)}\end{pmatrix}V^{-1}\begin{pmatrix}X_{t_0}\lambda_{t_0}^1\\ X_{t_0}\lambda_{t_0}^2\end{pmatrix} \quad (172)$$

Where $\gamma_{1,2}$ are constant:

$$\gamma_{1,2} = \frac{1}{2}\left(\left(\delta_{1,1}\mu_1 - \kappa_1\right) + \left(\delta_{2,2}\mu_2 - \kappa_2\right)\right) \pm \frac{1}{2}\sqrt{\left(\left(\delta_{1,1}\mu_1 - \kappa_1\right) - \left(\left(\delta_{2,2}\mu_2 - \kappa_2\right)\right)\right)^2 + 4\delta_{1,2}\delta_{2,1}\mu_1\mu_2}$$

V, V^{-1} are given by:

$$V = \begin{pmatrix}-\delta_{1,2}\mu_2 & -\delta_{1,2}\mu_2\\ \left(\delta_{1,1}\mu_1 - \kappa_1\right) - \gamma_1 & \left(\delta_{1,1}\mu_1 - \kappa_1\right) - \gamma_2\end{pmatrix}$$

$$V^{-1} = \frac{1}{\Gamma}\begin{pmatrix}\left(\delta_{1,1}\mu_1 - \kappa_1\right) - \gamma_2 & \delta_{1,2}\mu_2\\ \gamma_1 - \left(\delta_{1,1}\mu_1 - \kappa_1\right) & -\delta_{1,2}\mu_2\end{pmatrix}$$

And Γ is the determinant of V defined as:

$$\Gamma = -\delta_{1,2}\mu_2\sqrt{\left(\left(\delta_{1,1}\mu_1 - \kappa_1\right) - \left(\left(\delta_{2,2}\mu_2 - \kappa_2\right)\right)\right)^2 + 4\delta_{1,2}\delta_{2,1}\mu_1\mu_2}$$

This approach is relatively similar to the calculation of $\mathbb{E}^P\left[\lambda_t^i|\mathcal{F}_{t_0}\right]$, shown in Hainaut (2016):

$$\begin{pmatrix}\mathbb{E}^P\left[\lambda_t^1|\mathcal{F}_{t_0}\right]\\ \mathbb{E}^P\left[\lambda_t^2|\mathcal{F}_{t_0}\right]\end{pmatrix} = V\begin{pmatrix}1/\gamma_1\left(e^{\gamma_1(t-t_0)} - 1\right) & 0\\ 0 & 1/\gamma_2\left(e^{\gamma_2(t-t_0)} - 1\right)\end{pmatrix}V^{-1}\begin{pmatrix}\kappa_1 c_1\\ \kappa_2 c_2\end{pmatrix} + V\begin{pmatrix}e^{\gamma_1(t-t_0)} & 0\\ 0 & e^{\gamma_2(t-t_0)}\end{pmatrix}V^{-1}\begin{pmatrix}\lambda_{t0}^1\\ \lambda_{t0}^2\end{pmatrix} \quad (173)$$

In both eq. (172) and eq. (173) convergence as time goes by is ensured only if $\gamma_1 < 0$ and $\gamma_2 < 0$. We thus add this condition to the calibration.

Then we have to identify $\mathbb{E}^P\left[{X_t}^2|\mathcal{F}_{t_0}\right]$. This time we consider $g = {X_t}^2$. Then using the infinitesimal generator, we obtain the following relationship:

$$\mathbb{E}\left(\mathcal{A}.g|\mathcal{F}_{t_0}\right) = \alpha_1\eta_1\mathbb{E}\left(\lambda_t^1|\mathcal{F}_{t_0}\right) + 2\mathbb{E}\left(X_t\lambda_t^1|\mathcal{F}_{t_0}\right)\alpha_1\mu_1 + \alpha_2\eta_2\mathbb{E}\left(\lambda_t^2|\mathcal{F}_{t_0}\right) + 2\mathbb{E}\left(X_t\lambda_t^2|\mathcal{F}_{t_0}\right)\alpha_2\mu_2$$

Then using eq. (169) we obtain:

$$\mathbb{E}\left[{X_t}^2|\mathcal{F}_{t_0}\right] = {X_{t_0}}^2 + \int_{t_0}^{t}\left[\alpha_1\eta_1\mathbb{E}\left(\lambda_u^1|\mathcal{F}_{t_0}\right) + 2\mathbb{E}\left(X_u\lambda_u^1|\mathcal{F}_{t_0}\right)\alpha_1\mu_1 + \alpha_2\eta_2\mathbb{E}\left(\lambda_u^2|\mathcal{F}_{t_0}\right) - 2\mathbb{E}\left(X_u\lambda_u^2|\mathcal{F}_{t_0}\right)\alpha_2\mu_2\right]du$$

In particular we consider a discrete version of the integral:

$$\mathbb{E}\left[{X_t}^2|\mathcal{F}_{t_0}\right] = {X_{t_0}}^2 + \Delta t\sum_{u=t_0}^{t}\left(\alpha_1\eta_1\mathbb{E}\left(\lambda_u^1|\mathcal{F}_{t_0}\right) + 2\mathbb{E}\left(X_u\lambda_u^1|\mathcal{F}_{t_0}\right)\alpha_1\mu_1 + \alpha_2\eta_2\mathbb{E}\left(\lambda_u^2|\mathcal{F}_{t_0}\right) + 2\mathbb{E}\left(X_u\lambda_u^2|\mathcal{F}_{t_0}\right)\alpha_2\mu_2\right)$$

Some empirical tests suggest that the exponential in eq. (173) tends to converge towards equilibrium for $200 < t < 300$. As a result, we arbitrarily decide to consider rolling time windows of 100 points (ie. conditional expectations are calculated on the interval $[t_0; t]$=$[t_0; t_0 + 100]$). Empirical observations suggest that results of the calibration wouldn't be that much affected by the length of the time-window anyway.

In the end, and for a given country, we see 10 'behavioural' unknown variables $\{\kappa_1, c_1, \delta_{1,1}, \delta_{1,2}, \kappa_2, c_2, \delta_{2,1}, \delta_{2,2}, \rho_1, \rho_2\}$, plus two risk-premium parameters $\{a_1, a_2\}$.

$\{\theta_1, \theta_2\}$ are also unknown; we calculate them out of $\{a_1, a_2\}$, using the martingale condition in eq. (151).

We also note that yields do not follow a unique and consistent trend over the full sample, as we see different periods of consistent rise or decline in valuations. As a result, we assume that positive and negative jumps have a similar speed of reversion, ie. $\kappa_1 = \kappa_2$ and $c_1 = c_2$. In the end, we are left with the following vector of unknowns: $\{\kappa, c, \delta_{1,1}, \delta_{1,2}, \delta_{2,1}, \delta_{2,2}, \rho_1, \rho_2\}$. It is also worth noting that because $\psi_1(\delta_{1,1}a_1 + \delta_{2,1}a_2 + \theta_1)$ is likely to differ from $\psi_2(\delta_{1,2}a_1 + \delta_{2,2}a_2 + \theta_2)$, we will probably have $c_1^Q \neq c_2^Q$. ➔ **There is still a certain degree of flexibility left under the risk-neutral measure.**

Jumps are not observable in our own framework. As a result λ_t^i is a latent variable that we do not calculate per se. **This is a meaningful change compared to the proposed methodology in Hainaut (2016)**. All the same, and as indicated above, the calculation of $\mathbb{E}^P[\lambda_t^i|\mathcal{F}_{t_0}]$ and $\mathbb{E}^P[X_t\lambda_t^i|\mathcal{F}_{t_0}]$ involves the vector $(\lambda_{t_0}^1, \lambda_{t_0}^2)$, which therefore has to be estimated.

We calculate an estimate of $(\lambda_{t_0}^1, \lambda_{t_0}^2)$ by reducing the distance between $\mathbb{E}^P[X_t|\mathcal{F}_{t_0}]$ against its empirical value (via an ordinary OLS method). In particular, we consider the system of equations obtained with $\{t = t_0 + 50; t = t_0 + 100\}$ that we calibrate against the empirical value of $\mathbb{E}[X_{t_0+50}|\mathcal{F}_{t_0}]$ and $\mathbb{E}[X_{t_0+100}|\mathcal{F}_{t_0}]$. For a matter of timing, we restrict the analysis to Germany, France, Italy and Spain.

We conduct a two-step calibration. In both steps, we reduce the distance between $E^P(Y^2(t,T)|\mathcal{F}_{t_0})$ (ie. under the historical measure, and with $t = t_0 + 100$), versus the equivalent 1-month empirical estimator, calculated on the interval $[t_0, t]$. t_0 is the rolling variable, and takes any time value in the sample.

In the first step, we focus on a simpler version of the problem, that takes the instantaneous interest rate X_t as the only available data:

$$Y(t, t+1) \sim X_t$$

This simplifies the problem, and helps identify relevant intervals for the generation of initial values in the second part of the calibration.

In the second step of the calibration, we take the full interest rate curve.

Table 174 shows the calibrated variables, under the historical measures. Then Table 175 highlights the risk-premium coefficients. Finally, Table 176 shows the coefficients obtained under the risk-neutral measure. **For each parameter, there is a visible stability from one country to another.** This is a sign of coherence.

Table 174. Behavioral coefficients under the historical measure

	κ	c	$\delta_{1,1}$	$\delta_{1,2}$	$\delta_{2,1}$	$\delta_{2,2}$	ρ_1	ρ_2
Germany	0.10	0.0012	0.500	-0.250	-0.083	0.531	30.0	15.3
France	0.10	0.0243	0.541	-0.355	-0.215	0.153	31.4	16.5
Italy	0.55	0.0176	0.877	-0.098	-0.155	1.558	20.2	7.5
Spain	0.50	0.0192	1.238	-0.257	-0.066	1.347	22.0	6.3

Table 175. Risk-premium coefficients

	a_1	a_2	θ_1	θ_2	$\psi_1(\delta_{1,1}a_1+\delta_{2,1}a_2+\theta_1)$	$\psi_2(\delta_{1,2}a_1+\delta_{2,2}a_2+\theta_2)$
Germany	1.33	0.97	2.8	-1.5	1.127	1.093
France	1.03	1.04	2.5	-1.3	1.099	1.100
Italy	1.45	0.88	6.0	-3.1	1.543	1.329
Spain	1.62	1.74	3.8	-3.7	1.352	1.379

Table 176. Coefficients under the risk premium measure

	ρ_1^Q	ρ_2^Q	c_1^Q	c_2^Q	$\delta_{1,1}^Q$	$\delta_{1,2}^Q$	$\delta_{2,1}^Q$	$\delta_{2,2}^Q$
Germany	26.6	14.0	0.001	0.001	0.564	-0.093	-0.090	0.581
France	28.6	15.0	0.027	0.027	0.594	-0.237	-0.237	0.168
Italy	13.1	5.6	0.027	0.023	1.354	-0.238	-0.205	2.070
Spain	16.2	4.6	0.012	0.026	1.674	-0.090	-0.091	1.857

The difference between $\mathbb{E}^P\left(Y^2(t,T)|\mathcal{F}_{t_0}\right)$ and its empirical equivalent is an illustration of the calibration error, which gives indications on the quality of the calibration. As shown in Graph 249 to Graph 252, we see periods of tight convergence between both indicators, as well as periods where the gap is more substantial. **But overall, the prevailing picture suggests that the calibration was effective for the majority of the period considered.** The error could surely be minimised further on a shorter sample (16 years means about 4450 points under study). The fit is also very much influenced by the shape of X_t, and how it differentiates itself from $Y(t,T)$. On that basis too, a shorter sample would probably improve the calibration.

Graph 249. Calculated $\mathbb{E}^P\left(Y^2(t,T)|\mathcal{F}_{t_0}\right)$ versus its empirical estimator, Germany (5Y maturity)

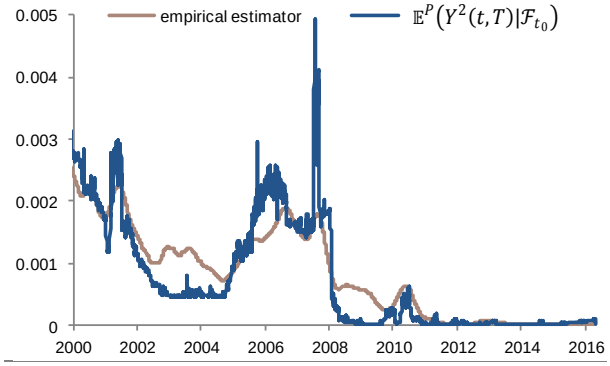

Graph 250. Calculated $\mathbb{E}^P\left(Y^2(t,T)|\mathcal{F}_{t_0}\right)$ versus its empirical estimator, France (5Y maturity)

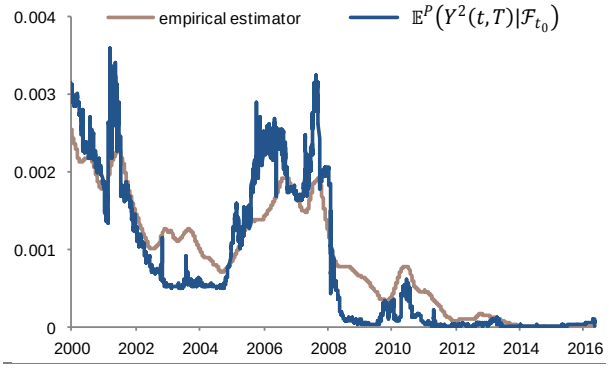

Graph 251. Calculated $\mathbb{E}^P\left(Y^2(t,T)|\mathcal{F}_{t_0}\right)$ versus its empirical estimator, Italy (5Y maturity)

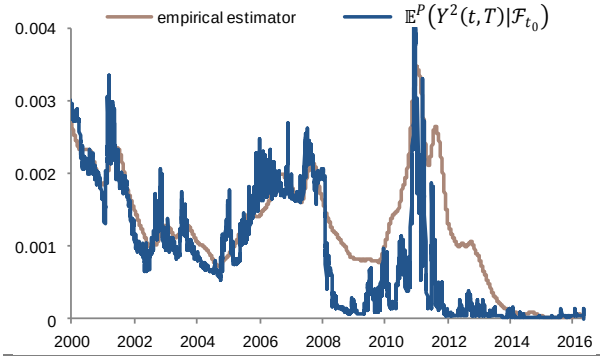

Graph 252. Calculated $\mathbb{E}^P\left(Y^2(t,T)|\mathcal{F}_{t_0}\right)$ versus its empirical estimator, Spain (5Y maturity)

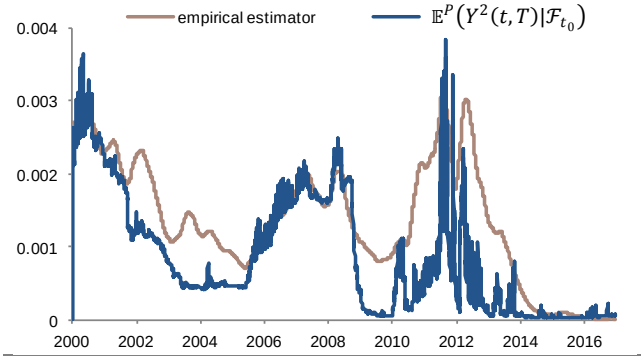

In order to understand the 'strength' of positive and negative jumps under the risk-neutral measure, let us consider a steady-state version of the jump amplitude, that we denote $\lambda_\infty^{1,Q}$ and $\lambda_\infty^{2,Q}$:

$$\begin{cases} 0 = \kappa\left(c_1^Q - \lambda_\infty^{1,Q}\right) + \delta_{1,1}^Q \mu_1^Q \lambda_\infty^{1,Q} + \delta_{1,2}^Q \mu_2^Q \lambda_\infty^{2,Q} \\ 0 = \kappa\left(c_2^Q - \lambda_\infty^{2,Q}\right) + \delta_{2,1}^Q \mu_1^Q \lambda_\infty^{2,Q} + \delta_{2,2}^Q \mu_2^Q \lambda_\infty^{2,Q} \end{cases}$$

This gives:

$$\begin{cases} \lambda_\infty^{1,Q} = \dfrac{1}{\left(\kappa - \delta_{1,1}^Q \mu_1^Q\right)}\left(\kappa c_1^Q - \dfrac{\delta_{1,2}^Q \mu_2^Q \kappa\left(c_2^Q \kappa - \delta_{1,1}^Q \mu_1^Q c_2^Q + \delta_{2,1}^Q \mu_1^Q c_1^Q\right)}{\left(\delta_{2,2}^Q \mu_2^Q - \kappa\right)\left(\kappa - \delta_{1,1}^Q \mu_1^Q\right) + \delta_{2,1}^Q \mu_1^Q \delta_{1,2}^Q \mu_2^Q}\right) \\ \lambda_\infty^{2,Q} = \dfrac{-\kappa\left(c_2^Q \kappa - \delta_{1,1}^Q \mu_1^Q c_2^Q + \delta_{2,1}^Q \mu_1^Q c_1^Q\right)}{\left(\delta_{2,2}^Q \mu_2^Q - \kappa\right)\left(\kappa - \delta_{1,1}^Q \mu_1^Q\right) + \delta_{2,1}^Q \mu_1^Q \delta_{1,2}^Q \mu_2^Q} \end{cases} \tag{174}$$

Finally we consider the coefficients $\Delta_{1,1}^Q = \delta_{1,1}^Q \mu_1^Q \lambda_\infty^{1,Q}$, $\Delta_{1,2}^Q = \delta_{1,2}^Q \mu_2^Q \lambda_\infty^{2,Q}$, $\Delta_{2,1}^Q = \delta_{2,1}^Q \mu_1^Q \lambda_\infty^{1,Q}$, $\Delta_{2,2}^Q = \delta_{2,2}^Q \mu_2^Q \lambda_\infty^{2,Q}$ as a reflection of the contribution of each, positive and negative jumps, onto the jump intensity $\lambda_t^{1,Q}$ and $\lambda_t^{2,Q}$. Table 177 shows the resulting values. **Overall, the colour code indicates that the self-exciting dimension is bigger for Italy and Spain than Germany and France.**

Table 177. $\Delta_{i,j}^Q$ highlight the strength of the self-exciting loop

	$\lambda_\infty^{1,Q}$	$\lambda_\infty^{2,Q}$	$\Delta_{1,1}^Q$	$\Delta_{1,2}^Q$	$\Delta_{2,1}^Q$	$\Delta_{2,2}^Q$
Germany	0.00	0.00	3.4E-05	-1.5E-05	-5.4E-06	9.5E-05
France	0.03	0.03	5.9E-04	-4.3E-04	-2.3E-04	3.1E-04
Italy	0.03	0.07	2.8E-03	-2.9E-03	-4.2E-04	2.5E-02
Spain	0.01	0.14	9.1E-04	-2.7E-03	-5.0E-05	5.5E-02

As already mentioned before, jump intensities are not observable. Instead, we calculate its conditional expectation (ie. $\mathbb{E}^P\left[\lambda_t^i | \mathcal{F}_{t_0}\right]$). Graph 253 to Graph 260 show this indicator, either under the historical measure (on the left), or under the risk-neutral measure (on the right).

Graph 253. Conditional expectation of jump intensities, under the historical measure

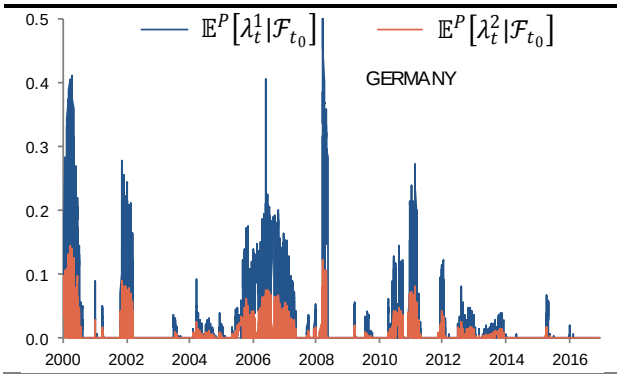

Graph 254. Conditional expectation of jump intensities, under the risk-neutral measure

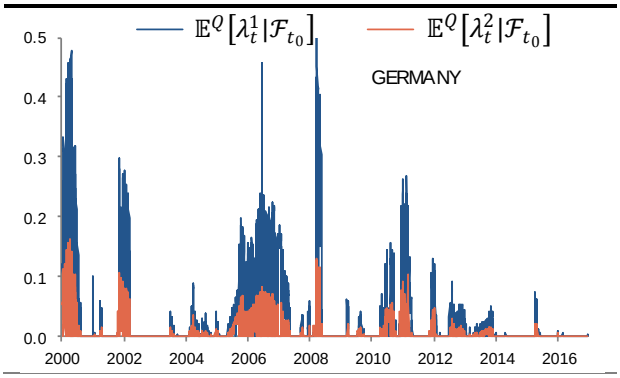

Graph 255. Conditional expectation of jump intensities, under the historical measure

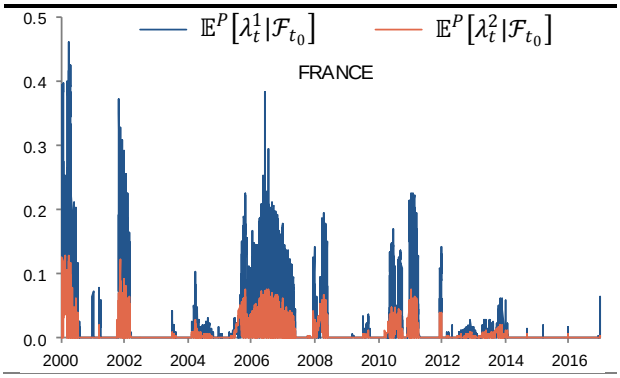

Graph 256. Conditional expectation of jump intensities, under the risk-neutral measure

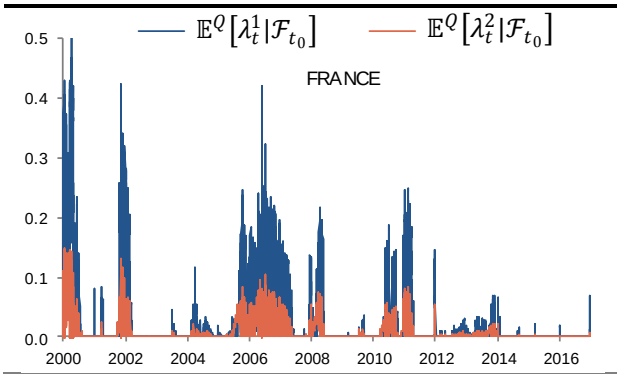

Graph 257. Conditional expectation of jump intensities, under the historical measure

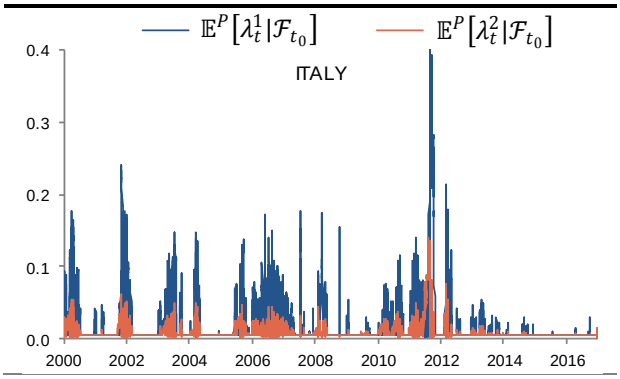

Graph 258. Conditional expectation of jump intensities, under the risk-neutral measure

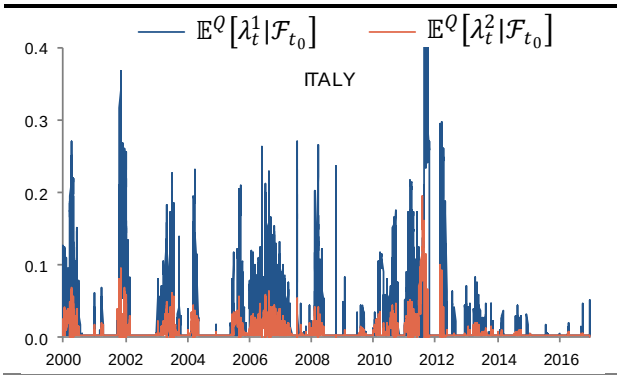

Graph 259. Conditional expectation of jump intensities, under the historical measure

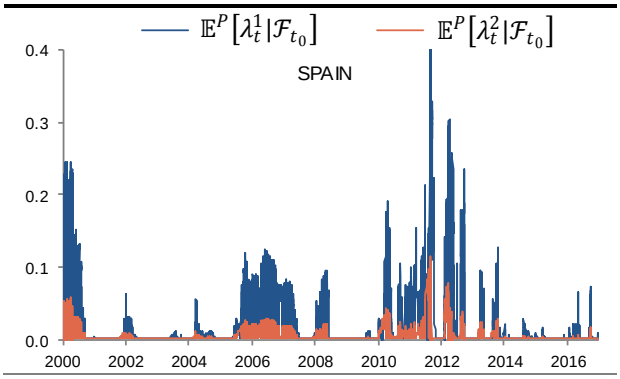

Graph 260. Conditional expectation of jump intensities, under the risk-neutral measure

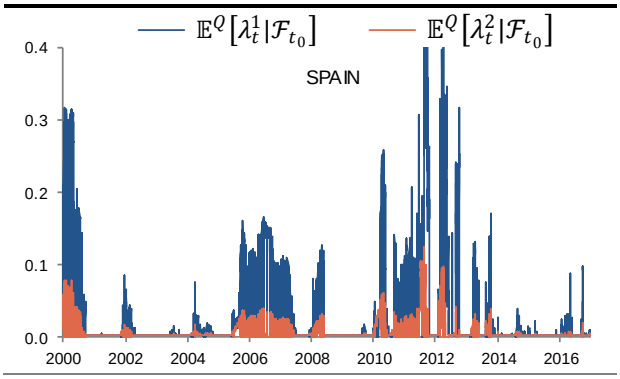

The multivariate version of the model

The model in Hainaut (2016) does not allow for any transmission of financial distress across securities. We therefore explore an extension of the model in this section, which seeks to address this limitation.

We consider a framework where financial contagion is supposed to emanate from a dedicated risk index $r_{P,t}$ recognised as a contagious time series. $r_{P,t}$ can be a real or a synthetic zero coupon bond.

We still denote by r_t the zero coupon bond under study, ie. the security targeted by contagion.

The problem is now formulated as:

$$\begin{cases} r_{P,t} = \varphi_P t + X_{P,t} \\ r_t = \varphi\, t + X_t \end{cases} \tag{175}$$

With:

$$\begin{cases} dX_{P,t} = \alpha_{P,1} L_t^{P,1} - \alpha_{P,2} L_t^{P,2} \\ dX_t = \alpha_1 L_t^1 - \alpha_2 L_t^2 \end{cases} \tag{176}$$

This formulation involves four different jumps L_t^1, L_t^2, $L_t^{P,1}$ and $L_t^{P,2}$. The amplitude of the jumps $L_t^{P,1}$ and $L_t^{P,2}$ is denoted by O^{P1} and O^{P2} with $\mu_{P1} = \mathbb{E}(O^{P1})$, $\mu_{P2} = \mathbb{E}(O^{P2})$, $\eta_{P1} = \mathbb{E}((O^{P1})^2)$, $\eta_{P2} = \mathbb{E}((O^{P2})^2)$ and we have:

$$dL_t^{P1} = O^{P1} dN_t^{P1} \quad \text{and} \quad dL_t^{P2} = O^{P2} dN_t^{P2} \tag{177}$$

$X_{P,t}$ is assumed to be driven by the dynamics highlighted in the univariate part, developed above, as this series is not subject to any exogenous contagion. We thus define the corresponding jump intensities as λ_t^{P1} and λ_t^{P2} as:

$$\begin{cases} d\lambda_t^{P1} = \kappa_{P1}(c_{P1} - \lambda_t^{P1})dt + \delta_{P1,1} dL_t^{P1} + \delta_{P1,2} dL_t^{P2} \\ d\lambda_t^{P2} = \kappa_{P2}(c_{P2} - \lambda_t^{P2})dt + \delta_{P2,1} dL_t^{P1} + \delta_{P2,2} dL_t^{P2} \end{cases} \tag{178}$$

We adjust the definition of the intensity λ_t^1 and λ_t^2 according to our assumption that X_t is exposed to contagion stemming from $r_{P,t}$. And in particular we consider the additional cross-market parameters $\delta_{1P,1}$, $\delta_{1P,2}$, $\delta_{2P,1}$, $\delta_{2P,2}$: these coefficients are supposed to illustrate the strength of the risk propagation stemming from the jumps L_t^{P1} and L_t^{P2}:

$$\begin{cases} d\lambda_t^1 = \kappa_1(c_1 - \lambda_t^1)dt + \delta_{1,1} dL_t^1 + \delta_{1,2} dL_t^2 + \delta_{1P,1} dL_t^{P1} + \delta_{1P,2} dL_t^{P2} \\ d\lambda_t^2 = \kappa_2(c_2 - \lambda_t^2)dt + \delta_{2,1} dL_t^1 + \delta_{2,2} dL_t^2 + \delta_{2P,1} dL_t^{P1} + \delta_{2P,2} dL_t^{P2} \end{cases} \tag{179}$$

In the end, $\delta_{1P,1}$, $\delta_{1P,2}$, $\delta_{2P,1}$, $\delta_{2P,2}$ describe the contagion effect.

We also define the first moment of the intensities as $m_1 = \mathbb{E}\left(\lambda_t^1 | \mathcal{F}_{t_0}\right)$, $m_2 = \mathbb{E}\left(\lambda_t^2 | \mathcal{F}_{t_0}\right)$, $m_{P1} = \mathbb{E}\left(\lambda_t^{P1} | \mathcal{F}_{t_0}\right)$, $m_{P2} = \mathbb{E}\left(\lambda_t^{P2} | \mathcal{F}_{t_0}\right)$.

We design our own risk index $r_{P,t}$ in the following section. Before that, we explore the implications ensuing from the addition of $r_{P,t}$ (as the engine of contagion) on to the methodology.

As shown in Errais et al. (2010), if $J_t^i = \left(L_t^i, N_t^i\right)$ the process $K_t = \left(\lambda_t^1, J_t^1, \lambda_t^2, J_t^2, \lambda_t^{P1}, J_t^{P1}, \lambda_t^{P2}, J_t^{P2}\right)$ is a Markov process in the state space $D = (\mathbb{R}^+ \times \mathbb{R}^+ \times \mathbb{N})^4$ and its infinitesimal generator for any function $g: D \to \mathbb{R}$ with partial derivatives $g_{\lambda_1}, g_{\lambda_2}, g_{\lambda_{P_1}}, g_{\lambda_{P2}}$, is such that:

$$\begin{aligned}
\mathcal{A}.\, g(K_t) = {} & \kappa_1(c_1 - \lambda_t^1) g_{\lambda_1} + \kappa_2(c_2 - \lambda_t^2) g_{\lambda_2} + \kappa_{P1}(c_{P1} - \lambda_t^{P1}) g_{\lambda_{P1}} \\
& + \kappa_{P2}(c_{P2} - \lambda_t^{P2}) g_{\lambda_{P2}} \\
& + \lambda_t^1 \int_{-\infty}^{+\infty} \left[g\left(\lambda_t^1 + \delta_{1,1} z, J_t^1 + (Z,1)^T, \lambda_t^2 + \delta_{2,1} z, J_t^2, \lambda_t^{P1}, J_t^{P1}, \lambda_t^{P2}, J_t^{P2}\right) \right. \\
& \left. - \; g(K_t) \right] d\nu_1(z) \\
& + \lambda_t^2 \int_{-\infty}^{+\infty} \left[g\left(\lambda_t^1 + \delta_{1,2} z, J_t^1, \lambda_t^2 + \delta_{2,2} z, J_t^2 + (Z,1)^T, \lambda_t^{P1}, J_t^{P1}, \lambda_t^{P2}, J_t^{P2}\right) \right. \\
& \left. - \; g(K_t) \right] d\nu_2(z) \\
& + \lambda_t^{P1} \int_{-\infty}^{+\infty} \left[g\left(\lambda_t^1 + \delta_{1P,1} z, J_t^1, \lambda_t^2 + \delta_{2P,1} z, J_t^2, \lambda_t^{P1} + \delta_{P1,1} z, J_t^{P1} \right. \right. \\
& \left. \left. + (Z,1)^T, \lambda_t^{P2} + + \delta_{P2,1} z, J_t^{P2}\right) - \; g(K_t) \right] d\nu_{P1}(z) \\
& + \lambda_t^{P2} \int_{-\infty}^{+\infty} \left[g\left(\lambda_t^1 + \delta_{1P,2} z, J_t^1, \lambda_t^2 + \delta_{2P,2} z, J_t^2, \lambda_t^{P1} + \delta_{P1,2} z, J_t^{P1}, \lambda_t^{P2} \right. \right. \\
& \left. \left. + \delta_{P2,2} z, J_t^{P2} + (Z,1)^T\right) - \; g(K_t) \right] d\nu_{P2}(z)
\end{aligned} \tag{180}$$

Proposition 1. (Moments of λ_t^i) The expected intensity $m_i(t) = \mathbb{E}\left(\lambda_t^i | \mathcal{F}_{t_0}\right)$ for $i = \{1,2,P1,P2\}$, is calculated as the solutions of the following system of differential equations:

$$\frac{\partial}{\partial t}\begin{pmatrix} \mathbb{E}\left(\lambda_t^1|\mathcal{F}_{t_0}\right) \\ \mathbb{E}\left(\lambda_t^2|\mathcal{F}_{t_0}\right) \\ \mathbb{E}\left(\lambda_t^{P1}|\mathcal{F}_{t_0}\right) \\ \mathbb{E}\left(\lambda_t^{P2}|\mathcal{F}_{t_0}\right) \end{pmatrix} = \begin{pmatrix} \kappa_1 c_1 \\ \kappa_2 c_2 \\ \kappa_{P1} c_{P1} \\ \kappa_{P2} c_{P2} \end{pmatrix} + \begin{pmatrix} (\delta_{1,1}\mu_1 - \kappa_1) & \delta_{1,2}\mu_2 & \delta_{1P,1}\mu_{P1} & \delta_{1P,2}\mu_{P2} \\ \delta_{2,1}\mu_1 & (\delta_{2,2}\mu_2 - \kappa_2) & \delta_{2P,1}\mu_{P1} & \delta_{2P,2}\mu_{P2} \\ 0 & 0 & (\delta_{P1,1}\mu_{P1} - \kappa_{P1}) & \delta_{P1,2}\mu_{P2} \\ 0 & 0 & \delta_{P2,1}\mu_{P1} & (\delta_{P2,2}\mu_{P2} - \kappa_{P2}) \end{pmatrix} \begin{pmatrix} \mathbb{E}\left(\lambda_t^1|\mathcal{F}_{t_0}\right) \\ \mathbb{E}\left(\lambda_t^2|\mathcal{F}_{t_0}\right) \\ \mathbb{E}\left(\lambda_t^{P1}|\mathcal{F}_{t_0}\right) \\ \mathbb{E}\left(\lambda_t^{P2}|\mathcal{F}_{t_0}\right) \end{pmatrix}$$

Which gives the solution:

$$\begin{aligned}
\begin{pmatrix} \mathbb{E}\left[X_t \lambda_t^1|\mathcal{F}_{t_0}\right] \\ \mathbb{E}\left[X_t \lambda_t^2|\mathcal{F}_{t_0}\right] \\ \mathbb{E}\left[X_t \lambda_t^{P1}|\mathcal{F}_{t_0}\right] \\ \mathbb{E}\left[X_t \lambda_t^{P2}|\mathcal{F}_{t_0}\right] \end{pmatrix} = {} & V \begin{pmatrix} 1/\gamma_1\left(e^{\gamma_1(t-t_0)} - 1\right) & 0 & 0 & 0 \\ 0 & 1/\gamma_2\left(e^{\gamma_2(t-t_0)} - 1\right) & 0 & 0 \\ 0 & 0 & 1/\gamma_{P1}\left(e^{\gamma_{P1}(t-t_0)} - 1\right) & 0 \\ 0 & 0 & 0 & 1/\gamma_{P2}\left(e^{\gamma_{P2}(t-t_0)} - 1\right) \end{pmatrix} V^{-1} \begin{pmatrix} \kappa_1 c_1 \\ \kappa_2 c_2 \\ \kappa_{P1} c_{P1} \\ \kappa_{P2} c_{P2} \end{pmatrix} \\
& + V \begin{pmatrix} e^{\gamma_1(t-t_0)} & 0 & 0 & 0 \\ 0 & e^{\gamma_2(t-t_0)} & 0 & 0 \\ 0 & 0 & e^{\gamma_{P1}(t-t_0)} & 0 \\ 0 & 0 & 0 & e^{\gamma_{P2}(t-t_0)} \end{pmatrix} V^{-1} \begin{pmatrix} \lambda_{t_0}^1 \\ \lambda_{t_0}^2 \\ \lambda_{t_0}^{P1} \\ \lambda_{t_0}^{P2} \end{pmatrix}
\end{aligned} \tag{181}$$

Where $\gamma_1, \gamma_2, \gamma_{P1}, \gamma_{P2}$ are the eigenvalues of:

$$\begin{pmatrix} (\delta_{1,1}\mu_1 - \kappa_1) & \delta_{1,2}\mu_2 & \delta_{1,P1}\mu_{P1} & \delta_{1,P2}\mu_{P2} \\ \delta_{2,1}\mu_1 & (\delta_{2,2}\mu_2 - \kappa_2) & \delta_{2,P1}\mu_{P1} & \delta_{2,P2}\mu_{P2} \\ 0 & 0 & (\delta_{P1,1}\mu_{P1} - \kappa_{P1}) & \delta_{P1,2}\mu_{P2} \\ 0 & 0 & \delta_{P2,1}\mu_{P1} & (\delta_{P2,2}\mu_{P2} - \kappa_{P2}) \end{pmatrix}$$

Which means that:

$$\begin{cases} \gamma_1 = \frac{1}{2}\Big((\delta_{1,1}\mu_1 - \kappa_1) + (\delta_{2,2}\mu_2 - \kappa_2)\Big) - \frac{1}{2}\sqrt{\Big((\delta_{1,1}\mu_1 - \kappa_1) - \big((\delta_{2,2}\mu_2 - \kappa_2)\big)\Big)^2 + 4\delta_{1,2}\delta_{2,1}\mu_1\mu_2} \\ \gamma_2 = \frac{1}{2}\Big((\delta_{1,1}\mu_1 - \kappa_1) + (\delta_{2,2}\mu_2 - \kappa_2)\Big) + \frac{1}{2}\sqrt{\Big((\delta_{1,1}\mu_1 - \kappa_1) - \big((\delta_{2,2}\mu_2 - \kappa_2)\big)\Big)^2 + 4\delta_{1,2}\delta_{2,1}\mu_1\mu_2} \\ \gamma_{P1} = \frac{1}{2}\Big((\delta_{P1,1}\mu_{P1} - \kappa_{P1}) + (\delta_{P2,2}\mu_{P2} - \kappa_{P2})\Big) - \frac{1}{2}\sqrt{\Big((\delta_{P1,1}\mu_{P1} - \kappa_{P1}) - \big((\delta_{P2,2}\mu_2 - \kappa_{P2})\big)\Big)^2 + 4\delta_{P1,2}\delta_{P2,1}\mu_{P1}\mu_{P2}} \\ \gamma_{P2} = \frac{1}{2}\Big((\delta_{P1,1}\mu_{P1} - \kappa_{P1}) + (\delta_{P2,2}\mu_{P2} - \kappa_{P2})\Big) + \frac{1}{2}\sqrt{\Big((\delta_{P1,1}\mu_{P1} - \kappa_{P1}) - \big((\delta_{P2,2}\mu_2 - \kappa_{P2})\big)\Big)^2 + 4\delta_{P1,2}\delta_{P2,1}\mu_{P1}\mu_{P2}} \end{cases}$$

The stationarity of the $\mathbb{E}\big(\lambda_t^i|\mathcal{F}_{t_0}\big)$ is ensured only if the eigenvalues γ_i are all negative. This is something we verify during the calibration.

Finally, V is the matrix of the eigenvectors, corresponding to $\gamma_1, \gamma_2, \gamma_{P1}, \gamma_{P2}$.

Then based on Hainaut (2016), the expectation of X_t is equal to:

$$\begin{cases} \mathbb{E}\big(X_{P,t}|\mathcal{F}_0\big) = X_{P,0} + \alpha_{P1}\mu_{P1}\int_0^t m_{P1}(s)ds - \alpha_{P2}\mu_{P2}\int_0^t m_{P2}(s)ds \\ \mathbb{E}(X_t|\mathcal{F}_0) = X_0 + \alpha_1\mu_1\int_0^t m_1(s)ds - \alpha_2\mu_2\int_0^t m_2(s)ds \end{cases} \tag{182}$$

Proposition 2. Let $\psi_1, \psi_2, \psi_{P1}, \psi_{P2}$ denote the moment generating functions of O^1, O^2, O^{P1}, O^{P2} in the multivariate franework:

$$\psi_i(\omega) = \mathbb{E}\left(e^{\omega O^i}\right) \qquad \text{for } i = 1,2,P1,P2 \tag{183}$$

The moment generating function of $\omega_0 X_T - \omega_1\int_t^T X_s ds + \begin{pmatrix}\omega_2\\ \omega_3\\ \omega_4\\ \omega_5\end{pmatrix}^T \begin{pmatrix}\lambda_T^1\\ \lambda_T^2\\ \lambda_T^{P1}\\ \lambda_T^{P2}\end{pmatrix}$ is an affine function of X_t

and of intensities:

$$\mathbb{E}\left(e^{\omega_0 X_T - \omega_1\int_t^T X_s ds + \begin{pmatrix}\omega_2\\ \omega_3\\ \omega_4\\ \omega_5\end{pmatrix}^T \begin{pmatrix}\lambda_T^1\\ \lambda_T^2\\ \lambda_T^{P1}\\ \lambda_T^{P2}\end{pmatrix}}|\mathcal{F}_t\right) = \exp\left(\big(\omega_0 - \omega_1(T-t)\big)X_t + A(t,T) + \begin{pmatrix}B_1(t,T)\\ B_2(t,T)\\ B_3(t,T)\\ B_4(t,T)\end{pmatrix}^T \begin{pmatrix}\lambda_T^1\\ \lambda_T^2\\ \lambda_T^{P1}\\ \lambda_T^{P2}\end{pmatrix}\right) \tag{184}$$

Where $A, B_1, B_2, B_{P1}, B_{P2}$ are solutions of a system of ODEs:

$$\begin{cases} \frac{\partial}{\partial t}B_1(t,T) = \kappa_1 B_1(t,T) - \big[\psi_1\big(B_1(t,T)\delta_{1,1} + \omega_0\alpha_1 - \omega_1\alpha_1(T-t) + B_2(t,T)\delta_{2,1}\big) - 1\big] \\ \frac{\partial}{\partial t}B_2(t,T) = \kappa_2 B_2(t,T) - \big[\psi_2\big(B_1(t,T)\delta_{1,2} - \omega_0\alpha_1 + \omega_1\alpha_1(T-t) + B_2(t,T)\delta_{2,2}\big) - 1\big] \\ \frac{\partial}{\partial t}B_{P1}(t,T) = \kappa_{P1} B_{P1}(t,T) - \big[\psi_{P1}\big(B_1(t,T)\delta_{1P,1} + B_2(t,T)\delta_{2P,1} + B_3(t,T)\delta_{P1,1} + B_4(t,T)\delta_{P2,1}\big) - 1\big] \\ \frac{\partial}{\partial t}B_{P2}(t,T) = \kappa_{P2} B_{P2}(t,T) - \big[\psi_{P2}\big(B_1(t,T)\delta_{1P,2} + B_2(t,T)\delta_{2P,2} + B_3(t,T)\delta_{P1,2} + B_4(t,T)\delta_{P2,2}\big) - 1\big] \\ \frac{\partial}{\partial t}A(t,T) = -\kappa_1 c_1 B_1(t,T) - \kappa_2 c_2 B_2(t,T) - \kappa_{P1} c_{P1} B_3(t,T) - \kappa_{P2} c_{P2} B_4(t,T) \end{cases} \tag{185}$$

With the terminal conditions $A(T,T)=0$, $B_1(T,T)=\omega_2$, $B_2(T,T)=\omega_3$, $B_3(T,T)=\omega_4$, $B_4(T,T)=\omega_5$.

Equivalent exponential affine measure and bond pricing:

Similarly to the univariate approach, and because the moment generating function of $X_t$is an affine function of $\left(\lambda_t^1, L_t^1, \lambda_t^2, L_t^2, \lambda_t^{P1}, L_t^{P1}, \lambda_t^{P2}, L_t^{P2}\right)$, we consider an exponential affine change of measure. The dynamics of interest rates the new measure is introduced by an exponential martingale of the form:

$$M_t(\theta_1,\theta_2,\theta_3,\theta_4) = \exp\left(\begin{pmatrix} a_1(\theta_1,\theta_2,\theta_3,\theta_4) \\ a_2(\theta_1,\theta_2,\theta_3,\theta_4) \\ a_3(\theta_1,\theta_2,\theta_3,\theta_4) \\ a_4(\theta_1,\theta_2,\theta_3,\theta_4) \end{pmatrix}^T \begin{pmatrix} \lambda_t^1 \\ \lambda_t^2 \\ \lambda_t^{P1} \\ \lambda_t^{P2} \end{pmatrix} + (\theta_1,\theta_2,\theta_3,\theta_4) \begin{pmatrix} L_t^1 \\ L_t^2 \\ L_t^{P1} \\ L_t^{P2} \end{pmatrix} - \varphi(\theta_1,\theta_2,\theta_3,\theta_4)t \right) \quad (186)$$

Where $\theta_1,\theta_2,\theta_3,\theta_4 \in \mathbb{R}$ and are assimilated later to risk premiums. The next proposition specifies the condition that $\theta_1,\theta_2,\theta_3,\theta_4$ have to fulfil so that M_t is a local martingale.

Proposition 3. If for any given couple of parameters $(\theta_1,\theta_2,\theta_3,\theta_4)$, there exists suitable solutions $a_1(\theta_1,\theta_2,\theta_3,\theta_4)$, $a_2(\theta_1,\theta_2,\theta_3,\theta_4)$, $a_3(\theta_1,\theta_2,\theta_3,\theta_4)$, $a_4(\theta_1,\theta_2,\theta_3,\theta_4)$ for the system of equations:

$$\begin{cases} a_1\kappa_1 - \left(\psi_1\left(a_1\delta_{1,1} + a_2\delta_{2,1} + \theta_1\right) - 1\right) = 0 \\ a_2\kappa_2 - \left(\psi_2\left(a_1\delta_{2,1} + a_2\delta_{2,2} + \theta_2\right) - 1\right) = 0 \\ a_3\kappa_{P1} - \left(\psi_{P1}\left(a_1\delta_{1P,1} + a_2\delta_{2P,1} + a_3\delta_{P1,1} + a_4\delta_{P2,1} + \theta_3\right) - 1\right) = 0 \\ a_4\kappa_{P2} - \left(\psi_{P2}\left(a_1\delta_{1P,2} + a_2\delta_{2P,2} + a_3\delta_{P1,2} + a_4\delta_{P2,2} + \theta_4\right) - 1\right) = 0 \end{cases} \quad (187)$$

Where $\psi_i(\omega) = \mathbb{E}\left(e^{\omega O^i}\right)$ for $i = 1,2,P1,P2$ and if $\varphi(\theta_1,\theta_2,\theta_3,\theta_4)$ is a linear combination of these solutions:

$$\varphi(\theta_1,\theta_2,\theta_3,\theta_4) = a_1\kappa_1 c_1 + a_2\kappa_2 c_2 + a_3\kappa_{P1} c_{P1} + a_4\kappa_{P2} c_{P2} \quad (188)$$

Then $M_t(\theta_1,\theta_2,\theta_3,\theta_4)$ is a local martingale.

Assuming the existence of suitable solutions for the system in eq. (187), an equivalent measure $Q^{\theta_1,\theta_2,\theta_3,\theta_4}$ is defined by:

$$\frac{\partial Q^{\theta_1,\theta_2,\theta_3,\theta_4}}{\partial P} = \frac{M_t(\theta_1,\theta_2,\theta_3,\theta_4)}{M_0(\theta_1,\theta_2,\theta_3,\theta_4)} \quad (189)$$

This may be used as risk neutral measure by investors. In this case, the dynamics of intensities and aggregate supply or demand is modified but is still a bivariate Hawkes process.

Proposition 4. Let $N_t^{1,Q}$, $N_t^{2,Q}$, $N_t^{P1,Q}$, $N_t^{P2,Q}$ be counting processes with respective intensities:

$$\begin{cases} \lambda_t^{1,Q} = \mathbb{E}\left(e^{\left(a_1\delta_{1,1} + a_2\delta_{2,1} + \theta_1\right)}\right)\lambda_t^1 \\ \lambda_t^{2,Q} = \mathbb{E}\left(e^{\left(a_1\delta_{2,1} + a_2\delta_{2,2} + \theta_2\right)}\right)\lambda_t^2 \\ \lambda_t^{P1,Q} = \mathbb{E}\left(e^{\left(a_1\delta_{1P,1} + a_2\delta_{2P,1} + a_3\delta_{P1,1} + a_4\delta_{P2,1} + \theta_3\right)}\right)\lambda_t^{P1} \\ \lambda_t^{P2,Q} = \mathbb{E}\left(e^{\left(a_1\delta_{1P,2} + a_2\delta_{2P,2} + a_3\delta_{P1,2} + a_4\delta_{P2,2} + \theta_4\right)}\right)\lambda_t^{P2} \end{cases} \quad (190)$$

under the equivalent measure $Q^{\theta_1,\theta_2,\theta_3,\theta_4}$. On the other hand, if $O^{1,Q}$, $O^{2,Q}$, $O^{P1,Q}$, $O^{P2,Q}$ denote the random variables defined by the following moment generating function:

$$\begin{cases} \psi_1^Q(z) = \mathbb{E}\left(e^{zO^{1,Q}}\right) = \dfrac{\psi_1\left(z + \left(a_1\delta_{1,1} + a_2\delta_{2,1} + \theta_1\right)\right)}{\psi_1\left(a_1\delta_{1,1} + a_2\delta_{2,1} + \theta_1\right)} \\ \psi_2^Q(z) = \mathbb{E}\left(e^{zO^{2,Q}}\right) = \dfrac{\psi_2\left(z + \left(a_1\delta_{2,1} + a_2\delta_{2,2} + \theta_2\right)\right)}{\psi_2\left(a_1\delta_{2,1} + a_2\delta_{2,2} + \theta_2\right)} \\ \psi_{P1}^Q(z) = \mathbb{E}\left(e^{zO^{P1,Q}}\right) = \dfrac{\psi_{P1}\left(z + \left(a_1\delta_{1P,1} + a_2\delta_{2P,1} + a_3\delta_{P1,1} + a_4\delta_{P2,1} + \theta_3\right)\right)}{\psi_{P1}\left(a_1\delta_{1P,1} + a_2\delta_{2P,1} + a_3\delta_{P1,1} + a_4\delta_{P2,1} + \theta_3\right)} \\ \psi_{P2}^Q(z) = \mathbb{E}\left(e^{zO^{P2,Q}}\right) = \dfrac{\psi_{P2}\left(z + \left(a_1\delta_{1P,2} + a_2\delta_{2P,2} + a_3\delta_{P1,2} + a_4\delta_{P2,2} + \theta_4\right)\right)}{\psi_{P2}\left(a_1\delta_{1P,2} + a_2\delta_{2P,2} + a_3\delta_{P1,2} + a_4\delta_{P2,2} + \theta_4\right)} \end{cases} \tag{191}$$

And if $L_t^{1,Q}$, $L_t^{2,Q}$, $L_t^{P1,Q}$, $L_t^{P2,Q}$ are defined by the jump processes:

$$L_t^{i,Q} = \sum_{k=1}^{N_t^{i,Q}} O_k^{i,Q} \quad i = 1,2,P1,P2 \tag{192}$$

Then intensities λ_t^i are driven by the following EDS under $Q^{\theta_1,\theta_2,\theta_3,\theta_4}$:

$$\begin{cases} d\lambda_t^{Q,P1} = \kappa_{P1}\left(c_{P1}^Q - \lambda_t^{Q,P1}\right)dt + \delta_{P1,1}^Q dL_t^{P1} + \delta_{P1,2}^Q dL_t^{P2} \\ d\lambda_t^{Q,P2} = \kappa_{P2}\left(c_{P2}^Q - \lambda_t^{Q,P2}\right)dt + \delta_{P2,1}^Q dL_t^{P1} + \delta_{P2,2}^Q dL_t^{P2} \\ d\lambda_t^{Q,1} = \kappa_1\left(c_1^Q - \lambda_t^{Q,1}\right)dt + \delta_{1,1}^Q dL_t^1 + \delta_{1,2}^Q dL_t^2 + \delta_{1P,1}^Q dL_t^{P1} + \delta_{1P,2}^Q dL_t^{P2} \\ d\lambda_t^{Q,2} = \kappa_2\left(c_2^Q - \lambda_t^{Q,2}\right)dt + \delta_{2,1}^Q dL_t^1 + \delta_{2,2}^Q dL_t^2 + \delta_{2P,1}^Q dL_t^{P1} + \delta_{2P,2}^Q dL_t^{P2} \end{cases} \tag{193}$$

This time again we assume an exponential distribution of the jumps:

$$\begin{cases} \nu_1(z) = \rho_1 e^{-\rho_1 z} 1_{\{z\geq 0\}} & \nu_2(z) = \rho_1 e^{\rho_2 z} 1_{\{z\leq 0\}} \\ \nu_{P1}(z) = \rho_{P1} e^{-\rho_{P1} z} 1_{\{z\geq 0\}} & \nu_{P2}(z) = \rho_{P2} e^{\rho_{P2} z} 1_{\{z\leq 0\}} \end{cases} \text{ with } \rho_1,\rho_2,\rho_{P1},\rho_{P2} \in \mathbb{R}^+ \tag{194}$$

In this case, the first and second moments of O^1, O^2, O^{P1}, O^{P2} are respectively equal to $\mu_1 = \frac{1}{\rho_1}$, $\mu_2 = \frac{1}{\rho_2}$, $\mu_{P1} = \frac{1}{\rho_{P1}}$, $\mu_{P2} = \frac{1}{\rho_{P2}}$ and to $\eta_i = \frac{2}{(\rho_i)^2}$. The moment generating functions are given by:

$$\psi_1(z) = \frac{\rho_1}{\rho_1 - z} \text{ for } z < \rho_1, \quad \psi_2(z) = \frac{\rho_2}{\rho_2 + z} \text{ for } z > -\rho_2$$

$$\psi_{P1}(z) = \frac{\rho_{P1}}{\rho_{P1} - z} \text{ for } z < \rho_{P1}, \quad \psi_{P2}(z) = \frac{\rho_{P2}}{\rho_{P2} + z} \text{ for } z > -\rho_{P2}$$

Then we have the following interesting corollary:

Corollary 1. The distribution of jump amplitudes are exponential under P and Q and the densities, noted $\nu_i^Q(z)$ under Q, are defined by parameters:

$$\begin{cases} \rho_1^Q = \rho_1 - \left(\delta_{1,1}a_1 + \delta_{2,1}a_2 + \theta_1\right) ; & \rho_{P1}^Q = \rho_{P1} - \left(\delta_{1P,1}a_1 + \delta_{2P,1}a_2 + \delta_{P1,1}a_3 + \delta_{P2,1}a_4 + \theta_{P1}\right) \\ \rho_2^Q = \rho_2 - \left(\delta_{1,2}a_1 + \delta_{2,2}a_2 + \theta_2\right) ; & \rho_{P1}^Q = \rho_{P2} - \left(\delta_{1P,2}a_1 + \delta_{2P,2}a_2 + \delta_{P1,2}a_3 + \delta_{P2,2}a_4 + \theta_{P2}\right) \end{cases} \tag{195}$$

Under $Q^{\theta_1,\theta_2,\theta_3,\theta_4}$, the dynamics of intensities are preserved (for similar reasons as in the univariate analysis): the intensities of counting processes $N_t^{1,Q}$, $N_t^{2,Q}$, $N_t^{P1,Q}$, $N_t^{P2,Q}$ are Hawkes processes having the same structure under Q, as these under the real measure P:

$$\begin{cases} d\lambda_t^{1,Q} = \kappa_1\left(c_1^Q - \lambda_t^{1,Q}\right)dt + \delta_{1,1}^Q dL_t^1 + \delta_{1,2}^Q dL_t^2 + \delta_{1P,1}^Q dL_t^{P1} + \delta_{1P,2}^Q dL_t^{P2} \\ d\lambda_t^{2,Q} = \kappa_2\left(c_2^Q - \lambda_t^{2,Q}\right)dt + \delta_{2,1}^Q dL_t^1 + \delta_{2,2}^Q dL_t^2 + \delta_{2P,1}^Q dL_t^{P1} + \delta_{2P,2}^Q dL_t^{P2} \\ d\lambda_t^{P1,Q} = \kappa_{P1}\left(c_{P1}^Q - \lambda_t^{P1,Q}\right)dt + \delta_{P1,1}^Q dL_t^{P1} + \delta_{P1,2}^Q dL_t^{P2} \\ d\lambda_t^{P2,Q} = \kappa_{P2}\left(c_{P2}^Q - \lambda_t^{P2,Q}\right)dt + \delta_{P2,1}^Q dL_t^{P1} + \delta_{P2,2}^Q dL_t^{P2} \end{cases} \quad (196)$$

Where the parameters under Q are:

$$\begin{cases} c_1^Q = c_1\psi_1\left(\delta_{1,1}a_1 + \delta_{2,1}a_2 + \theta_1\right) \\ c_2^Q = c_2\psi_2\left(\delta_{1,2}a_1 + \delta_{2,2}a_2 + \theta_2\right) \\ \delta_{1,j}^Q = \delta_{1,j}\psi_1\left(\delta_{1,1}a_1 + \delta_{2,1}a_2 + \theta_1\right) \quad j = 1,2 \\ \delta_{2,j}^Q = \delta_{2,j}\psi_2\left(\delta_{1,1}a_1 + \delta_{2,1}a_2 + \theta_1\right) \quad j = 1,2 \\ \delta_{1P,j}^Q = \delta_{1P,j}\psi_1\left(\delta_{1,1}a_1 + \delta_{2,1}a_2 + \theta_1\right) \quad j = 1,2 \\ \delta_{2P,j}^Q = \delta_{2P,j}\psi_2\left(\delta_{1,1}a_1 + \delta_{2,1}a_2 + \theta_1\right) \quad j = 1,2 \end{cases} \quad (197)$$

$$\begin{cases} c_{P1}^Q = c_{P1}\psi_{P1}\left(\delta_{1P,1}a_1 + \delta_{2P,1}a_2 + \delta_{P1,1}a_3 + \delta_{P2,1}a_4 + \theta_3\right) \\ c_{P2}^Q = c_{P2}\psi_{P2}\left(\delta_{1P,2}a_1 + \delta_{2P,2}a_2 + \delta_{P1,2}a_3 + \delta_{P2,2}a_4 + \theta_4\right) \\ \delta_{P1,j}^Q = \delta_{P1,j}\psi_{P1}\left(\delta_{1P,1}a_1 + \delta_{2P,1}a_2 + \delta_{P1,1}a_3 + \delta_{P2,1}a_4 + \theta_3\right) \quad j = 1,2 \\ \delta_{P2,j}^Q = \delta_{P2,j}\psi_{P2}\left(\delta_{1P,2}a_1 + \delta_{2P,2}a_2 + \delta_{P1,2}a_3 + \delta_{P2,2}a_4 + \theta_4\right) \quad j = 1,2 \end{cases}$$

We already mentioned that the price of a zero coupon bond is equal to the expected discount factor, under this risk neutral measure:

$$\begin{aligned} P\left(t,T,\lambda_t^1,J_t^1,\lambda_t^2,J_t^2,\lambda_t^{P1},J_t^{P1},\lambda_t^{P2},J_t^{P2}\right) &= \mathbb{E}^Q\left(e^{-\int_t^T r_s ds}|\mathcal{F}_t\right) \\ &= e^{-\int_t^T \varphi(s)ds}\mathbb{E}^Q\left(e^{-\int_t^T X_s ds}|\mathcal{F}_t\right) \end{aligned} \quad (198)$$

And in particular, adjusting the univariate formulation we obtain:

$$\mathbb{E}^Q\left(e^{-\int_t^T X_s ds}|\mathcal{F}_t\right) = \exp\left(-X_t(T-t) + A(t,T) + \begin{pmatrix} B_1(t,T) \\ B_2(t,T) \\ B_3(t,T) \\ B_4(,T) \end{pmatrix}^T \begin{pmatrix} \lambda_t^{1,Q} \\ \lambda_t^{2,Q} \\ \lambda_t^{P1,Q} \\ \lambda_t^{P2,Q} \end{pmatrix}\right) \quad (199)$$

Where $A(t,T)$, $B_1(t,T)$, $B_2(t,T)$, $B_3(t,T)$, $B_4(t,T)$ are solutions of the following system of ODEs:

$$\begin{cases} \frac{\partial}{\partial t}B_1 = \kappa_1 B_1(t,T) - \left[\psi_1^Q\left(B_1\delta_{1,1}^Q + B_2\delta_{2,1}^Q - \alpha_1(T-t)\right) - 1\right] \\ \frac{\partial}{\partial t}B_2 = \kappa_2 B_2(t,T) - \left[\psi_2^Q\left(B_1\delta_{1,2}^Q + B_2\delta_{2,2}^Q + \alpha_2(T-t)\right) - 1\right] \\ \frac{\partial}{\partial t}B_3 = \kappa_{P1}B_3(t,T) - \left[\psi_{P1}^Q\left(B_1\delta_{1P,1}^Q + B_2\delta_{2P,1}^Q + B_3\delta_{P1,1}^Q + B_2\delta_{P2,1}^Q\right) - 1\right] \\ \frac{\partial}{\partial t}B_4 = \kappa_{P2}B_4(t,T) - \left[\psi_{P2}^Q\left(B_1\delta_{1P,2}^Q + B_2\delta_{2P,2}^Q + B_3\delta_{P1,2}^Q + B_2\delta_{P2,2}^Q\right) - 1\right] \\ \frac{\partial}{\partial t}A = -\kappa_1 c_1^Q B_1 - \kappa_2 c_2^Q B_2 - \kappa_{P1}c_{P1}^Q B_3 - \kappa_{P2}c_{P2}^Q B_4 \end{cases} \quad (200)$$

With the terminal condition: $A(T,T) = 0$, $B_1(T,T) = B_2(T,T) = B_3(T,T) = B_4(T,T) = 0$

The dynamics of bond prices depends on the random measures of the jumps, noted $L_t^{1,Q}(dt,dz)$, $L_t^{2,Q}(dt,dz)$, $L_t^{P1,Q}(dt,dz)$, $L_t^{P2,Q}(dt,dz)$ and such that:

$$L_t^{k,Q} = \int_0^{+\infty} \int_{-\infty}^{+\infty} L^{k,Q}(dt,dz) \qquad k = 1,2,P1,P2 \tag{201}$$

The expectation of these measures is equal to $\mathbb{E}^Q\left(L^{kQ}(dt,dz)|\mathcal{F}_t\right) = \lambda_t^{k,Q}\nu_k(z)dzdt$.

Construction of the risk index

Our multivariate framework assumes that the risk index $r_{P,t}$ is the engine of financial contagion. While w could have considered Italian or Spanish zero coupon bonds as a possible time series for $r_{P,t}$, we prefer designing a specific risk index, calculated from a basket of those securities seen as potential candidates for financial contagion.

We calculate $r_{P,t}$ as a synthetic zero coupon bond, derived from the most 'contagious' time series in the sample, ie. those referring to peripheral countries (ie. Italy 'IT', Spain 'SP', Ireland 'IR' and Portugal 'PT').

At time t, and for a given time series of price variations Z_t, we measure the strength $\hat{R}_{i,t}$ of the price variation via its empirical cumulative distribution function $\hat{P}$ and such that:

$$\hat{R}_{i,t} = \begin{cases} \hat{P}\left(X_{i,t}\right) & \text{if } X_{i,t} \geq 0 \\ 1 - \hat{P}\left(X_{i,t}\right) & \text{if } X_{i,t} < 0 \end{cases}$$

Based on the available data on peripheral countries, and for every t in the sample, we identify the 'toughest' price variation as:

$$\hat{R}_{k,t} = \max\left(\hat{R}_{IT,t}, \hat{R}_{SP,t}, \hat{R}_{IR,t}, \hat{R}_{PT,t}\right)$$

Then we convert $\hat{R}_{k,t}$ as a synthetic data $X_{P,t}$ by calculating the quantile that corresponds to $\hat{R}_{k,t}$, drawn from a synthetic distribution function that we denote ν_P. In line with previous considerations, we assume that ν_P is an exponential distribution that involves both coefficients $\rho_{P,1}$ and $\rho_{P,2}$, calculated as the average value of respectively $\left(\rho_{IT,1}, \rho_{SP,1}, \rho_{IR,1}, \rho_{PT,1}\right)$ and $\left(\rho_{IT,2}, \rho_{SP,2}, \rho_{IR,2}, \rho_{PT,2}\right)$, with:

$$\rho_{C,1} = \frac{1}{E[\Delta X_t \geq 0]} \qquad \rho_{C,2} = -\frac{1}{E[\Delta X_t < 0]} \qquad \text{for } C = \{IT, SP, IR, PT\}$$

In the end, ν_P is defined as:

$$\begin{cases} \nu_P(z) = \rho_{P,1} e^{-\rho_{P,1} z} 1_{\{z \geq 0\}} \\ \nu_P(z) = \rho_{P,2} e^{\rho_{P,2} z} 1_{\{z \leq 0\}} \end{cases} \tag{202}$$

This looks rather consistent with the general methodology. We also assume that $\varphi_P(t)$ is the average value of $\left(\varphi_{IT}(t), \varphi_{SP}(t), \varphi_{IR}(t), \varphi_{PT}(t)\right)$.

We extend the procedure to all maturities in the range $\{1m, 3m, 6m, 1y, 2y, 3y, 4y, 5y, 6y, 7y, 8y, 9y, 10y\}$. Graph 261 shows the resulting time series.

Graph 261. The risk index $r_{P,t}$ in %, selection of different maturities

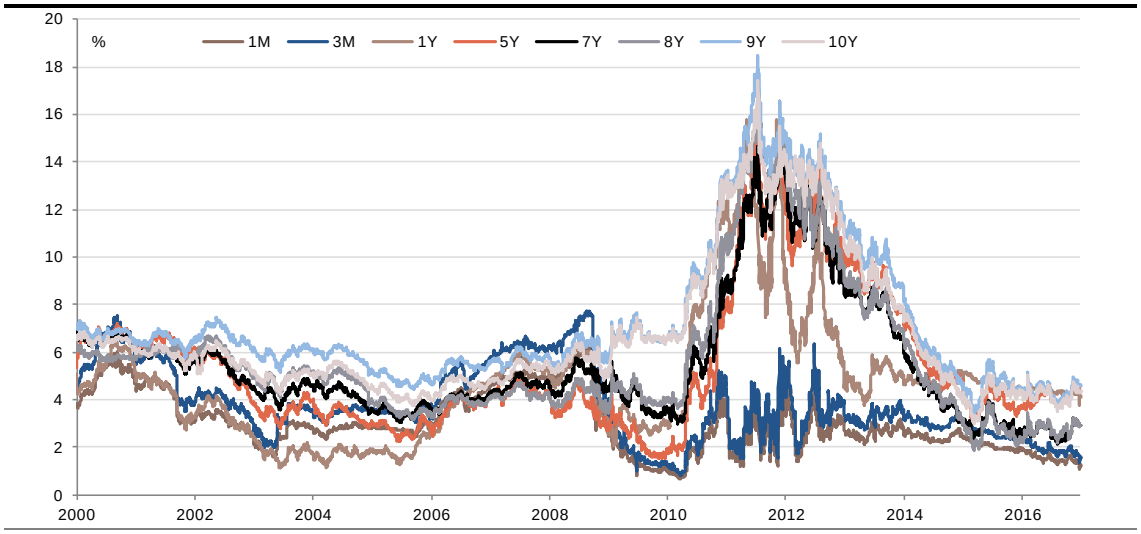

We also compare the resulting risk index with the values in the dataset for each peripheral country. As Graph 262 shows, our risk-index is very similar to Ireland and Portugal. The risk-index even takes slightly higher values than other countries during periods of intense risk aversion. **The commonality with peripheral countries looks consistent with the meaning of the risk index.**

Graph 262. 10Y risk-index compared to 10Y Zero coupon bonds in Italy, Spain, Ireland and Portugal

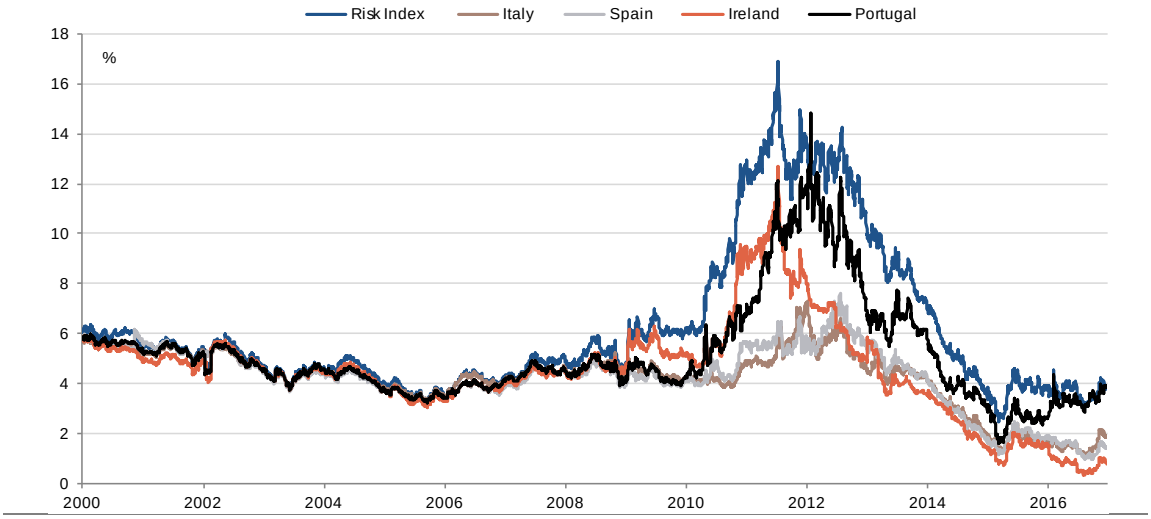

We conduct the calibration of the risk-index, based on the univariate model developed above. We assumed the following dynamics:

$$\begin{cases} d\lambda_t^{P1} = \kappa_P(c_P - \lambda_t^{P1})dt + \delta_{P1,1}dL_t^{P1} + \delta_{P1,2}dL_t^{P2} \\ d\lambda_t^{P2} = \kappa_P(c_P - \lambda_t^{P2})dt + \delta_{P2,1}dL_t^{P1} + \delta_{P2,2}dL_t^{P2} \end{cases} \quad (203)$$

And we obtain the following calibrated coefficients:

Table 178. Behavioral coefficients under the historical measure

	κ_P	c_P	$\delta_{P1,1}$	$\delta_{P1,2}$	$\delta_{P2,1}$	$\delta_{P2,2}$	ρ_{P1}	ρ_{P2}
Risk index	0.39	0.0044	1.498	-0.343	-0.118	1.514	10.9	4.5

Table 179. Risk-premium coefficients

	a_{P1}	a_{P2}	θ_{P1}	θ_{P2}	$\psi_{P1}(\delta_{P1,1}a_{P1}+\delta_{P2,1}a_{P2}+\theta_{P1})$	$\psi_{P2}(\delta_{P1,2}a_{P1}+\delta_{P2,2}a_{P2}+\theta_{P2})$
Risk Index	1.51	1.97	2.0	-4.4	1.592	1.769

Table 180. Risk-premium coefficients

	ρ^Q_{P1}	ρ^Q_{P2}	c^Q_{P1}	c^Q_{P2}	$\delta^Q_{P1,1}$	$\delta^Q_{P1,2}$	$\delta^Q_{P2,1}$	$\delta^Q_{P2,2}$
Risk index	7	3	0.007	0.01	2.38	-0.19	-0.21	2.68

We take a look at the error between the calculated $\mathbb{E}^P\left(Y^2(t,T)|\mathcal{F}_{t_0}\right)$ and the corresponding empirical estimator: results in Graph 263 show that the error is more or less important depending on the period; but overall the fit is better during periods marked by intense risk aversion. We also plot the conditional expectation of the jump intensities, under the historical measure in Graph 264, and under the risk-neutral measure in Graph 265.

Graph 263. Calculated variance versus empirical variance

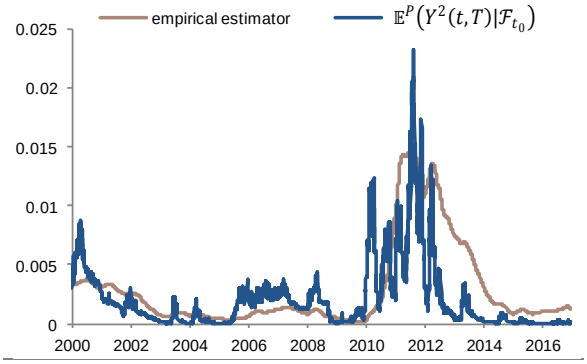

Graph 264. Conditional expectation of jump intensities, under the historical measure

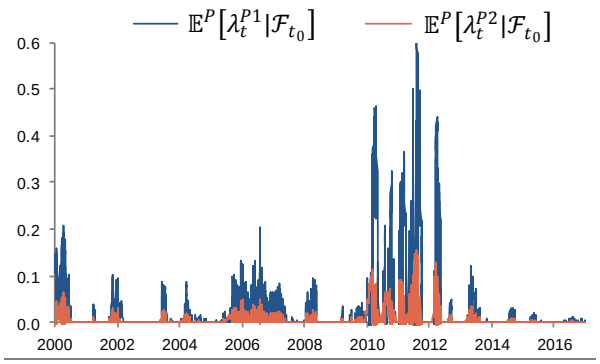

Graph 265. Conditional expectation of jump intensities, under the risk-neutral measure

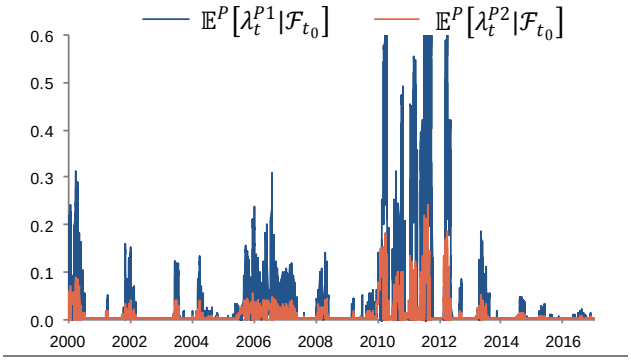

Calibration of the multivariate model

In the multivariate framework, the dynamics of the zero coupon bond under the risk neutral measure is the following:

$$Y(t,T,\lambda_t^1,J_t^1,\lambda_t^2,J_t^2,\lambda_t^{P1},J_t^{P1},\lambda_t^{P2},J_t^{P2}) = -\frac{1}{T-t}\log\left(\mathbb{E}^Q\left(e^{-\int_t^T r_s ds}|\mathcal{F}_t\right)\right)$$
$$= -\frac{1}{T-t}\log\left(\ e^{-\int_t^T \varphi(s)ds}\mathbb{E}^Q\left(e^{-\int_t^T X_s ds}|\mathcal{F}_t\right)\right)$$

Which is equivalent to:

$$Y(t,T) = \frac{1}{T-t}\int_t^T \varphi(s)ds - \frac{1}{T-t}\left(-X_t(T-t) + A(t,T) + \begin{pmatrix}B_1(t,T)\\B_2(t,T)\\B_3(t,T)\\B_4(t,T)\end{pmatrix}^T\begin{pmatrix}\lambda_t^{1,Q}\\\lambda_t^{2,Q}\\\lambda_t^{P1,Q}\\\lambda_t^{P2,Q}\end{pmatrix}\right)$$

Then under the historical measure we obtain:

$$Y(t,T) = \frac{1}{T-t}\int_t^T \varphi(s)ds - \frac{1}{T-t}\left(-X_t(T-t) + A(t,T) + \begin{pmatrix}B_1(t,T)\\B_2(t,T)\\B_3(t,T)\\B_4(t,T)\end{pmatrix}^T\begin{pmatrix}\lambda_t^{1}\\\lambda_t^{2}\\\lambda_t^{P1}\\\lambda_t^{P2}\end{pmatrix}\right)$$

Like in the univariate analysis, we calibrate the model by minimizing the distance between $\mathbb{E}^P\left(Y^2(t,T)|\mathcal{F}_{t_0}\right)$, and the corresponding rolling empirical estimator. This time, $\mathbb{E}^P\left(Y^2(t,T)|\mathcal{F}_{t_0}\right)$ is equal to:

$$\mathbb{E}^P\left(Y^2(t,T)|\mathcal{F}_{t_0}\right) = \left(\frac{1}{T-t}\int_t^T \varphi(s)ds\right)^2$$
$$-2\left(\frac{1}{(T-t)^2}\int_t^T \varphi(s)ds\right)\left(-\mathbb{E}^P\left[X_t|\mathcal{F}_{t_0}\right](T-t) + A(t,T) + \begin{pmatrix}B_1(t,T)\\B_2(t,T)\\B_3(t,T)\\B_4(t,T)\end{pmatrix}^T\begin{pmatrix}\mathbb{E}^P\left[\lambda_t^1|\mathcal{F}_{t_0}\right]\\\mathbb{E}^P\left[\lambda_t^2|\mathcal{F}_{t_0}\right]\\\mathbb{E}^P\left[\lambda_t^{P1}|\mathcal{F}_{t_0}\right]\\\mathbb{E}^P\left[\lambda_t^{P2}|\mathcal{F}_{t_0}\right]\end{pmatrix}\right)$$
$$+\frac{1}{(T-t)^2}\left(\mathbb{E}^P\left[{X_t}^2|\mathcal{F}_{t_0}\right](T-t)^2 + A^2(t,T) + \begin{pmatrix}{B_1}^2(t,T)\\{B_2}^2(t,T)\\{B_3}^2(t,T)\\{B_4}^2(t,T)\end{pmatrix}^T\begin{pmatrix}\mathbb{E}^P\left[{\lambda_t^1}^2|\mathcal{F}_{t_0}\right]\\\mathbb{E}^P\left[{\lambda_t^2}^2|\mathcal{F}_{t_0}\right]\\\mathbb{E}^P\left[{\lambda_t^{P1}}^2|\mathcal{F}_{t_0}\right]\\\mathbb{E}^P\left[{\lambda_t^{P2}}^2|\mathcal{F}_{t_0}\right]\end{pmatrix}\right.$$
$$-2\mathbb{E}^P\left[X_t|\mathcal{F}_{t_0}\right](T-t)A(t,T) + 2A(t,T)\begin{pmatrix}B_1(t,T)\\B_2(t,T)\\B_3(t,T)\\B_4(t,T)\end{pmatrix}^T\begin{pmatrix}\mathbb{E}^P\left[\lambda_t^1|\mathcal{F}_{t_0}\right]\\\mathbb{E}^P\left[\lambda_t^2|\mathcal{F}_{t_0}\right]\\\mathbb{E}^P\left[\lambda_t^{P1}|\mathcal{F}_{t_0}\right]\\\mathbb{E}^P\left[\lambda_t^{P2}|\mathcal{F}_{t_0}\right]\end{pmatrix}$$
$$-2(T-t)\begin{pmatrix}B_1(t,T)\\B_2(t,T)\\B_3(t,T)\\B_4(t,T)\end{pmatrix}^T\begin{pmatrix}\mathbb{E}^P\left[X_t\lambda_t^1|\mathcal{F}_{t_0}\right]\\\mathbb{E}^P\left[X_t\lambda_t^2|\mathcal{F}_{t_0}\right]\\\mathbb{E}^P\left[X_t\lambda_t^{P1}|\mathcal{F}_{t_0}\right]\\\mathbb{E}^P\left[X_t\lambda_t^{P2}|\mathcal{F}_{t_0}\right]\end{pmatrix} + 2B_1(t,T)B_2(t,T)\mathbb{E}^P\left[\lambda_t^1\lambda_t^2|\mathcal{F}_{t_0}\right]$$
$$+2B_1(t,T)B_{P1}(t,T)\mathbb{E}^P\left[\lambda_t^1\lambda_t^{P1}|\mathcal{F}_{t_0}\right] + 2B_1(t,T)B_{P2}(t,T)\mathbb{E}^P\left[\lambda_t^1\lambda_t^{P2}|\mathcal{F}_{t_0}\right] + 2B_2(t,T)B_{P1}(t,T)\mathbb{E}^P\left[\lambda_t^2\lambda_t^{P1}|\mathcal{F}_{t_0}\right]$$
$$\left.+2B_2(t,T)B_{P2}(t,T)\mathbb{E}^P\left[\lambda_t^2\lambda_t^{P2}|\mathcal{F}_{t_0}\right] + 2B_{P1}(t,T)B_{P2}(t,T)\mathbb{E}^P\left[\lambda_t^{P1}\lambda_t^{P2}|\mathcal{F}_{t_0}\right]\right)$$

We thus have to calculate: $\mathbb{E}^P\left[{X_t}^2|\mathcal{F}_{t_0}\right]$, $\mathbb{E}^P\left[{\lambda_t^i}^2|\mathcal{F}_{t_0}\right]$, $\mathbb{E}^P\left[\lambda_t^i\lambda_t^j|\mathcal{F}_{t_0}\right]$ for $\{i = 1,2,P1,P2\}$ and $\{j = 1,2,P1,P2\}$. Using the infinitesimal generator and following the same approach as in the univariate analysis, we obtain the following relationships:

$$\begin{aligned}\frac{\partial}{\partial t}\mathbb{E}^P\left[{\lambda_t^1}^2|\mathcal{F}_{t_0}\right] &= 2\mathbb{E}^P\left[\lambda_t^1|\mathcal{F}_{t_0}\right]\kappa_1 c_1 - 2\mathbb{E}^P\left[{\lambda_t^1}^2|\mathcal{F}_{t_0}\right]\kappa_1 + \left(2\mathbb{E}^P\left[{\lambda_t^1}^2|\mathcal{F}_{t_0}\right]\delta_{1,1}\mu_1 + \mathbb{E}^P\left[\lambda_t^1|\mathcal{F}_{t_0}\right]{\delta_{1,1}}^2\eta_1\right)\\ &+ \left(2\mathbb{E}^P\left[\lambda_t^1\lambda_t^2|\mathcal{F}_{t_0}\right]\delta_{1,2}\mu_2 + \mathbb{E}^P\left[\lambda_t^2|\mathcal{F}_{t_0}\right]{\delta_{1,2}}^2\eta_2\right)\\ &+ \left(2\mathbb{E}^P\left[\lambda_t^{P1}\lambda_t^1|\mathcal{F}_{t_0}\right]\delta_{1,P1}\mu_{P1} + \mathbb{E}^P\left[\lambda_t^{P1}|\mathcal{F}_{t_0}\right]{\delta_{1,P1}}^2\eta_{P1}\right)\\ &+ \left(2\mathbb{E}^P\left[\lambda_t^{P2}\lambda_t^1|\mathcal{F}_{t_0}\right]\delta_{1,P2}\mu_{P2} + \mathbb{E}^P\left[\lambda_t^{P2}|\mathcal{F}_{t_0}\right]{\delta_{1,P2}}^2\eta_{P2}\right)\end{aligned}$$

$$\begin{aligned}\frac{\partial}{\partial t}\mathbb{E}^P\left[{\lambda_t^2}^2|\mathcal{F}_{t_0}\right] &= 2\mathbb{E}^P\left[\lambda_t^2|\mathcal{F}_{t_0}\right]\kappa_2 c_2 - 2\mathbb{E}^P\left[{\lambda_t^2}^2|\mathcal{F}_{t_0}\right]\kappa_2 + \left(2\mathbb{E}^P\left[\lambda_t^1\lambda_t^2|\mathcal{F}_{t_0}\right]\delta_{2,1}\mu_1 + \mathbb{E}^P\left[\lambda_t^1|\mathcal{F}_{t_0}\right]{\delta_{2,1}}^2\eta_1\right)\\ &+ \left(2\mathbb{E}^P\left[{\lambda_t^2}^2|\mathcal{F}_{t_0}\right]\delta_{2,2}\mu_2 + \mathbb{E}^P\left[\lambda_t^2|\mathcal{F}_{t_0}\right]{\delta_{2,2}}^2\eta_2\right)\\ &+ \left(2\mathbb{E}^P\left[\lambda_t^{P1}\lambda_t^2|\mathcal{F}_{t_0}\right]\delta_{2,P1}\mu_{P1} + \mathbb{E}^P\left[\lambda_t^{P1}|\mathcal{F}_{t_0}\right]{\delta_{2,P1}}^2\eta_{P1}\right)\\ &+ \left(2\mathbb{E}^P\left[\lambda_t^{P2}\lambda_t^2|\mathcal{F}_{t_0}\right]\delta_{2,P2}\mu_{P2} + \mathbb{E}^P\left[\lambda_t^{P2}|\mathcal{F}_{t_0}\right]{\delta_{2,P2}}^2\eta_{P2}\right)\end{aligned}$$

$$\begin{aligned}&\frac{\partial}{\partial t}\mathbb{E}^P\left[{\lambda_t^{P1}}^2|\mathcal{F}_{t_0}\right]\\ &= 2\mathbb{E}^P\left[\lambda_t^{P1}|\mathcal{F}_{t_0}\right]\kappa_{P1}c_{P1} - 2\mathbb{E}^P\left[{\lambda_t^{P1}}^2|\mathcal{F}_{t_0}\right]\kappa_{P1} + \left(2\mathbb{E}^P\left[{\lambda_t^{P1}}^2|\mathcal{F}_{t_0}\right]\delta_{P1,1}\mu_{P1} + \mathbb{E}^P\left[\lambda_t^{P1}|\mathcal{F}_{t_0}\right]{\delta_{P1,1}}^2\eta_{P1}\right)\\ &+ \left(2\mathbb{E}^P\left[\lambda_t^{P2}\lambda_t^{P1}|\mathcal{F}_{t_0}\right]\delta_{P1,2}\mu_{P2} + \mathbb{E}^P\left[\lambda_t^{P2}|\mathcal{F}_{t_0}\right]{\delta_{P1,2}}^2\eta_{P2}\right)\end{aligned}$$

$$\begin{aligned}&\frac{\partial}{\partial t}\mathbb{E}^P\left[{\lambda_t^{P2}}^2|\mathcal{F}_{t_0}\right]\\ &= 2\mathbb{E}^P\left[\lambda_t^{P2}|\mathcal{F}_{t_0}\right]\kappa_{P2}c_{P2} - 2\mathbb{E}^P\left[{\lambda_t^{P2}}^2|\mathcal{F}_{t_0}\right]\kappa_{P2} + \left(2\mathbb{E}^P\left[\lambda_t^{P1}\lambda_t^{P2}|\mathcal{F}_{t_0}\right]\delta_{P2,1}\mu_{P1} + \mathbb{E}^P\left[\lambda_t^{P1}|\mathcal{F}_{t_0}\right]{\delta_{P2,1}}^2\eta_{P1}\right)\\ &+ \left(2\mathbb{E}^P\left[{\lambda_t^{P2}}^2|\mathcal{F}_{t_0}\right]\delta_{P2,2}\mu_{P2} + \mathbb{E}^P\left[\lambda_t^{P2}|\mathcal{F}_{t_0}\right]{\delta_{P2,2}}^2\eta_{P2}\right)\end{aligned}$$

$$\begin{aligned}\frac{\partial}{\partial t}\mathbb{E}^P\left[\lambda_t^1\lambda_t^2|\mathcal{F}_{t_0}\right] &= \mathbb{E}^P\left[\lambda_t^2|\mathcal{F}_{t_0}\right]\kappa_1 c_1 - \mathbb{E}^P\left[\lambda_t^1\lambda_t^2|\mathcal{F}_{t_0}\right]\kappa_1 + \mathbb{E}^P\left[\lambda_t^1|\mathcal{F}_{t_0}\right]\kappa_2 c_2 - \mathbb{E}^P\left[\lambda_t^1\lambda_t^2|\mathcal{F}_{t_0}\right]\kappa_2 + \mathbb{E}^P\left[{\lambda_t^1}^2|\mathcal{F}_{t_0}\right]\delta_{2,1}\mu_1\\ &+ \mathbb{E}^P\left[\lambda_t^1\lambda_t^2|\mathcal{F}_{t_0}\right]\delta_{1,1}\mu_1 + \mathbb{E}^P\left[\lambda_t^1|\mathcal{F}_{t_0}\right]\delta_{1,1}\delta_{2,1}\eta_1 + \mathbb{E}^P\left[{\lambda_t^2}^2|\mathcal{F}_{t_0}\right]\delta_{1,2}\mu_2 + \mathbb{E}^P\left[\lambda_t^1\lambda_t^2|\mathcal{F}_{t_0}\right]\delta_{2,2}\mu_2\\ &+ \mathbb{E}^P\left[\lambda_t^2|\mathcal{F}_{t_0}\right]\delta_{2,2}\delta_{1,2}\eta_2 + \mathbb{E}^P\left[\lambda_t^{P1}\lambda_t^1|\mathcal{F}_{t_0}\right]\delta_{2,P1}\mu_{P1} + \mathbb{E}^P\left[\lambda_t^{P1}\lambda_t^2|\mathcal{F}_{t_0}\right]\delta_{1,P1}\mu_{P1}\\ &+ \mathbb{E}^P\left[\lambda_t^{P1}|\mathcal{F}_{t_0}\right]\delta_{1,P1}\delta_{2,P1}\eta_{P1} + \mathbb{E}^P\left[\lambda_t^{P2}\lambda_t^1|\mathcal{F}_{t_0}\right]\delta_{2,P2}\mu_{P2} + \mathbb{E}^P\left[\lambda_t^{P2}\lambda_t^2|\mathcal{F}_{t_0}\right]\delta_{1,P2}\mu_{P2}\\ &+ \mathbb{E}^P\left[\lambda_t^{P2}|\mathcal{F}_{t_0}\right]\delta_{1,P2}\delta_{2,P2}\eta_{P2}\end{aligned}$$

$$\begin{aligned}&\frac{\partial}{\partial t}\mathbb{E}^P[\lambda_t^1\lambda_t^{P1}|\mathcal{F}_t]\\ &= \mathbb{E}^P\left[\lambda_t^{P1}|\mathcal{F}_{t_0}\right]\left(\kappa_1 c_1 + \delta_{1,P1}\delta_{P1,1}\eta_{P1}\right) - \mathbb{E}^P\left[\lambda_t^{P1}\lambda_t^1|\mathcal{F}_{t_0}\right]\left(\kappa_1 + \kappa_{P1} - \delta_{1,1}\mu_1 - \delta_{P1,1}\mu_{P1}\right)\\ &+ \mathbb{E}^P\left[\lambda_t^1|\mathcal{F}_{t_0}\right]\kappa_{P1}c_{P1} + \mathbb{E}^P\left[\lambda_t^{P1}\lambda_t^2|\mathcal{F}_{t_0}\right]\delta_{1,2}\mu_2 + \mathbb{E}^P\left[{\lambda_t^{P1}}^2|\mathcal{F}_{t_0}\right]\delta_{1,P1}\mu_{P1} + \mathbb{E}^P\left[\lambda_t^{P2}\lambda_t^1|\mathcal{F}_{t_0}\right]\delta_{P1,2}\mu_{P2}\\ &+ \mathbb{E}^P\left[\lambda_t^{P1}\lambda_t^{P2}|\mathcal{F}_{t_0}\right]\delta_{1,P2}\mu_{P2} + \mathbb{E}^P\left[\lambda_t^{P2}|\mathcal{F}_{t_0}\right]\delta_{1,P2}\delta_{P1,2}\eta_{P2}\end{aligned}$$

$$\begin{aligned}&\frac{\partial}{\partial t}\mathbb{E}^P\left[\lambda_t^1\lambda_t^{P2}|\mathcal{F}_{t_0}\right]\\ &= \mathbb{E}^P\left[\lambda_t^{P2}|\mathcal{F}_{t_0}\right]\left(\kappa_1 c_1 + \delta_{1,P2}\delta_{P2,2}\eta_{P2}\right) - \mathbb{E}^P\left[\lambda_t^1\lambda_t^{P2}|\mathcal{F}_{t_0}\right]\left(\kappa_1 + \kappa_{P2} - \delta_{1,1}\mu_1 - \delta_{P2,2}\mu_{P2}\right)\\ &+ \mathbb{E}^P\left[\lambda_t^1|\mathcal{F}_{t_0}\right]\kappa_{P2}c_{P2} + \mathbb{E}^P\left[\lambda_t^2\lambda_t^{P2}|\mathcal{F}_{t_0}\right]\delta_{1,2}\mu_2 + \mathbb{E}^P\left[\lambda_t^{P1}\lambda_t^1|\mathcal{F}_{t_0}\right]\delta_{P2,1}\mu_{P1} + \mathbb{E}^P\left[\lambda_t^{P1}\lambda_t^{P2}|\mathcal{F}_{t_0}\right]\delta_{1,P1}\mu_{P1}\\ &+ \mathbb{E}^P\left[\lambda_t^{P1}|\mathcal{F}_{t_0}\right]\delta_{1,P1}\delta_{P2,1}\eta_{P1} + \mathbb{E}^P\left[{\lambda_t^{P2}}^2|\mathcal{F}_{t_0}\right]\delta_{1,P2}\mu_{P2}\end{aligned}$$

$$\frac{\partial}{\partial t}\mathbb{E}^P\left[\lambda_t^2\lambda_t^{P1}|\mathcal{F}_{t_0}\right]$$
$$= \mathbb{E}^P\left[\lambda_t^{P1}|\mathcal{F}_{t_0}\right]\left(\kappa_2 c_2 + \delta_{2,P1}\delta_{P1,1}\eta_{P1}\right) - \mathbb{E}^P\left[\lambda_t^2\lambda_t^{P1}|\mathcal{F}_{t_0}\right]\left(\kappa_2 + \kappa_{P1} - \delta_{2,2}\mu_1 - \delta_{P1,1}\mu_{P1}\right)$$
$$+ \mathbb{E}^P\left[\lambda_t^2|\mathcal{F}_{t_0}\right]\kappa_{P1}c_{P1} + \mathbb{E}^P\left[\lambda_t^1\lambda_t^{P1}|\mathcal{F}_{t_0}\right]\delta_{2,1}\mu_1 + \mathbb{E}^P\left[\lambda_t^{P1^2}|\mathcal{F}_{t_0}\right]\delta_{2,P1}\mu_{P1} + \mathbb{E}^P\left[\lambda_t^{P2}\lambda_t^2|\mathcal{F}_{t_0}\right]\delta_{P1,2}\mu_{P2}$$
$$+ \mathbb{E}^P\left[\lambda_t^{P2}\lambda_t^{P1}|\mathcal{F}_{t_0}\right]\delta_{2,P2}\mu_{P2} + \mathbb{E}^P\left[\lambda_t^{P2}|\mathcal{F}_{t_0}\right]\delta_{2,P2}\delta_{P1,2}\eta_{P2}$$

$$\frac{\partial}{\partial t}\mathbb{E}^P\left[\lambda_t^2\lambda_t^{P2}|\mathcal{F}_{t_0}\right]$$
$$= \mathbb{E}^P\left[\lambda_t^{P2}|\mathcal{F}_{t_0}\right]\left(\kappa_2 c_2 + \delta_{2,P2}\delta_{P2,2}\eta_{P2}\right) - \mathbb{E}^P\left[\lambda_t^2\lambda_t^{P2}|\mathcal{F}_{t_0}\right]\left(\kappa_2 + \kappa_{P2} - \delta_{2,2}\mu_2 - \delta_{P2,1}\mu_{P1}\right)$$
$$+ \mathbb{E}^P\left[\lambda_t^2|\mathcal{F}_{t_0}\right]\kappa_{P2}c_{P2} + \mathbb{E}^P\left[\lambda_t^1\lambda_t^{P2}|\mathcal{F}_{t_0}\right]\delta_{2,1}\mu_1 + \mathbb{E}^P\left[\lambda_t^{P1}\lambda_t^{P2}|\mathcal{F}_{t_0}\right]\delta_{2,P1}\mu_{P1} + \mathbb{E}^P\left[\lambda_t^{P1}|\mathcal{F}_{t_0}\right]\delta_{2,P1}\delta_{P2,1}\eta_{P1}$$
$$+ \mathbb{E}^P\left[\lambda_t^{P2}\lambda_t^2|\mathcal{F}_{t_0}\right]\delta_{P2,2}\mu_{P2} + \mathbb{E}^P\left[\lambda_t^{P2^2}|\mathcal{F}_{t_0}\right]\delta_{2,P2}\mu_{P2}$$

$$\frac{\partial}{\partial t}\mathbb{E}^P\left[\lambda_t^{P1}\lambda_t^{P2}|\mathcal{F}_{t_0}\right]$$
$$= \mathbb{E}^P\left[\lambda_t^{P2}|\mathcal{F}_{t_0}\right]\left(\kappa_{P1}c_{P1} + \delta_{P1,2}\delta_{P2,2}\eta_{P2}\right) - \mathbb{E}^P\left[\lambda_t^{P1}\lambda_t^{P2}|\mathcal{F}_{t_0}\right]\left(\kappa_{P1} + \kappa_{P2} - \delta_{P1,1}\mu_{P1} - \delta_{P2,2}\mu_{P2}\right)$$
$$+ \mathbb{E}^P\left[\lambda_t^{P1}|\mathcal{F}_{t_0}\right]\kappa_{P2}c_{P2} + \mathbb{E}^P\left[\lambda_t^{P1^2}|\mathcal{F}_{t_0}\right]\delta_{P2,1}\mu_{P1} + \mathbb{E}^P\left[\lambda_t^{P1}|\mathcal{F}_{t_0}\right]\delta_{P1,1}\delta_{P2,1}\eta_{P1}$$
$$+ \mathbb{E}^P\left[\lambda_t^{P2^2}|\mathcal{F}_{t_0}\right]\delta_{P1,2}\mu_{P2}$$

Let us now calculate $\mathbb{E}^P\left[X_t\lambda_t^i|\mathcal{F}_{t_0}\right]$. We consider the same approach as in the univariate case:

$$\begin{pmatrix} \frac{d\mathbb{E}^P\left[X_t\lambda_t^1|\mathcal{F}_{t_0}\right]}{dt} \\ \frac{d\mathbb{E}^P\left[X_t\lambda_t^2|\mathcal{F}_{t_0}\right]}{dt} \\ \frac{d\mathbb{E}^P\left[X_t\lambda_t^{P1}|\mathcal{F}_{t_0}\right]}{dt} \\ \frac{d\mathbb{E}^P\left[X_t\lambda_t^{P2}|\mathcal{F}_{t_0}\right]}{dt} \end{pmatrix} = \begin{pmatrix} C_1(t) \\ C_2(t) \\ C_3(t) \\ C_4(t) \end{pmatrix} + \begin{pmatrix} \left(\delta_{1,1}\mu_1 - \kappa_1\right) & \delta_{1,2}\mu_2 & \delta_{1,P1}\mu_{P1} & \delta_{1,P2}\mu_{P2} \\ \delta_{2,1}\mu_1 & \left(\delta_{2,2}\mu_2 - \kappa_2\right) & \delta_{2,P1}\mu_{P1} & \delta_{2,P2}\mu_{P2} \\ 0 & 0 & \left(\delta_{P1,1}\mu_{P1} - \kappa_{P1}\right) & \delta_{P1,2}\mu_{P2} \\ 0 & 0 & \delta_{P2,1}\mu_{P1} & \left(\delta_{P2,2}\mu_{P2} - \kappa_{P2}\right) \end{pmatrix} \begin{pmatrix} \mathbb{E}^P\left[X_t\lambda_t^1|\mathcal{F}_{t_0}\right] \\ \mathbb{E}^P\left[X_t\lambda_t^2|\mathcal{F}_{t_0}\right] \\ \mathbb{E}^P\left[X_t\lambda_t^{P1}|\mathcal{F}_{t_0}\right] \\ \mathbb{E}^P\left[X_t\lambda_t^{P2}|\mathcal{F}_{t_0}\right] \end{pmatrix}$$

With:

$$\begin{pmatrix} C_1(t) \\ C_2(t) \\ C_3(t) \\ C_4(t) \end{pmatrix} = \begin{pmatrix} \kappa_1 c_1\mathbb{E}^P\left(X_t|\mathcal{F}_{t_0}\right) + \alpha_1\mu_1\mathbb{E}\left(\lambda_t^{1^2}|\mathcal{F}_{t_0}\right) + \mathbb{E}\left(\lambda_t^1|\mathcal{F}_{t_0}\right)\alpha_1\eta_1\delta_{1,1} + \alpha_2\mu_2\mathbb{E}\left(\lambda_t^2\lambda_t^1|\mathcal{F}_{t_0}\right) + \mathbb{E}\left(\lambda_t^2|\mathcal{F}_{t_0}\right)\alpha_2\eta_2\delta_{1,2} \\ \kappa_2 c_2\mathbb{E}^P\left(X_t|\mathcal{F}_{t_0}\right) + \alpha_1\mu_1\mathbb{E}\left(\lambda_t^1\lambda_t^2|\mathcal{F}_{t_0}\right) + \mathbb{E}\left(\lambda_t^1|\mathcal{F}_{t_0}\right)\alpha_1\eta_1\delta_{2,1} + \alpha_2\mu_2\mathbb{E}\left(\lambda_t^{2^2}|\mathcal{F}_{t_0}\right) + \mathbb{E}\left(\lambda_t^2|\mathcal{F}_{t_0}\right)\alpha_2\eta_2\delta_{2,2} \\ 0 \\ 0 \end{pmatrix}$$
$$+ \begin{pmatrix} \alpha_{P1}\mu_{P1}\mathbb{E}\left(\lambda_t^1\lambda_t^{P1}|\mathcal{F}_{t_0}\right) + \mathbb{E}\left(\lambda_t^{P1}|\mathcal{F}_{t_0}\right)\alpha_{P1}\eta_{P1}\delta_{1,P1} + \alpha_{P2}\mu_{P2}\mathbb{E}\left(\lambda_t^1\lambda_t^{P2}|\mathcal{F}_{t_0}\right) + \mathbb{E}\left(\lambda_t^{P2}|\mathcal{F}_{t_0}\right)\alpha_{P2}\eta_{P2}\delta_{1,P2} \\ \alpha_{P1}\mu_{P1}\mathbb{E}\left(\lambda_t^2\lambda_t^{P1}|\mathcal{F}_{t_0}\right) + \mathbb{E}\left(\lambda_t^{P1}|\mathcal{F}_{t_0}\right)\alpha_{P1}\eta_{P1}\delta_{2,P1} + \alpha_{P2}\mu_{P2}\mathbb{E}\left(\lambda_t^2\lambda_t^{P2}|\mathcal{F}_{t_0}\right) + \mathbb{E}\left(\lambda_t^{P2}|\mathcal{F}_{t_0}\right)\alpha_{P2}\eta_{P2}\delta_{2,P2} \\ \alpha_{P1}\mu_{P1}\mathbb{E}\left(\lambda_t^{P1^2}|\mathcal{F}_{t_0}\right) + \mathbb{E}\left(\lambda_t^{P1}|\mathcal{F}_{t_0}\right)\alpha_{P1}\eta_{P1}\delta_{P1,1} + \alpha_{P2}\mu_{P2}\mathbb{E}\left(\lambda_t^{P1}\lambda_t^{P2}|\mathcal{F}_{t_0}\right) + \mathbb{E}\left(\lambda_t^{P2}|\mathcal{F}_{t_0}\right)\alpha_{P2}\eta_{P2}\delta_{P1,2} \\ \alpha_{P1}\mu_{P1}\mathbb{E}\left(\lambda_t^{P1}\lambda_t^{P2}|\mathcal{F}_{t_0}\right) + \mathbb{E}\left(\lambda_t^{P1}|\mathcal{F}_{t_0}\right)\alpha_{P1}\eta_{P1}\delta_{P2,1} + \alpha_{P2}\mu_{P2}\mathbb{E}\left(\lambda_t^{P2^2}|\mathcal{F}_{t_0}\right) + \mathbb{E}\left(\lambda_t^{P2}|\mathcal{F}_{t_0}\right)\alpha_{P2}\eta_{P2}\delta_{P2,2} \end{pmatrix}$$

That we solve over the time interval $[t_0; t]$ as:

$$\begin{pmatrix} \mathbb{E}\left[X_t\lambda_t^1|\mathcal{F}_{t_0}\right] \\ \mathbb{E}\left[X_t\lambda_t^2|\mathcal{F}_{t_0}\right] \\ \mathbb{E}\left[X_t\lambda_t^{P1}|\mathcal{F}_{t_0}\right] \\ \mathbb{E}\left[X_t\lambda_t^{P2}|\mathcal{F}_{t_0}\right] \end{pmatrix} = V\begin{pmatrix} e^{\gamma_1(t-t_0)} & 0 & 0 & 0 \\ 0 & e^{\gamma_2(t-t_0)} & 0 & 0 \\ 0 & 0 & e^{\gamma_{P1}(t-t_0)} & 0 \\ 0 & 0 & 0 & e^{\gamma_{P2}(t-t_0)} \end{pmatrix}\int_{t_0}^{t}\begin{pmatrix} e^{-\gamma_1(s-t_0)} & 0 & 0 & 0 \\ 0 & e^{-\gamma_2(s-t_0)} & 0 & 0 \\ 0 & 0 & e^{-\gamma_{P1}(s-t_0)} & 0 \\ 0 & 0 & 0 & e^{-\gamma_{P2}(s-t_0)} \end{pmatrix}V^{-1}\begin{pmatrix} C_1(s) \\ C_2(s) \\ C_3(s) \\ C_4(s) \end{pmatrix}ds \quad (204)$$
$$+ V\begin{pmatrix} e^{\gamma_1(t-t_0)} & 0 & 0 & 0 \\ 0 & e^{\gamma_2(t-t_0)} & 0 & 0 \\ 0 & 0 & e^{\gamma_{P1}(t-t_0)} & 0 \\ 0 & 0 & 0 & e^{\gamma_{P2}(t-t_0)} \end{pmatrix}V^{-1}\begin{pmatrix} X_{t_0}\lambda_{t_0}^1 \\ X_{t_0}\lambda_{t_0}^2 \\ X_{t_0}\lambda_{t_0}^{P1} \\ X_{t_0}\lambda_{t_0}^{P2} \end{pmatrix}$$

Where $\gamma_1, \gamma_2, \gamma_{P1}, \gamma_{P2}$ are similar to eq. (181). Finally, V is the matrix of the eigenvectors, corresponding to $\gamma_1, \gamma_2, \gamma_{P1}, \gamma_{P2}$.

For a given country i, we are now left with 12 'behavioural' unknown variables $\{\kappa, c, \delta_{1,1}, \delta_{1,2}, \delta_{2,1}, \delta_{2,2}, \delta_{1,P1}, \delta_{1,P2}, \delta_{2,P1}, \delta_{2,P2}, \rho_1, \rho_2\}$, plus four risk-premium parameters $\{a_1, a_2, a_3, a_4\}$. $\{\theta_1, \theta_2, \theta_3, \theta_4\}$ are also unknown; we calculate them out of $\{a_1, a_2, a_3, a_4\}$, using the condition in eq. (187). We consider that the variables $\{\kappa_P, c_P, \delta_{P1,1}, \delta_{P1,2}, \delta_{P2,1}, \delta_{P2,2}, \rho_{P1}, \rho_{P2}\}$ are given in Table 178.

Since $\{a_3, a_4\}$ are intrinsic descriptors of $X_{P,t}$, we also involve $\mathbb{E}^P\left({Y_P}^2(t,T)|\mathcal{F}_{t_0}\right)$ into the calibration. Based on what we saw in the univariate analysis, we obtain the following equation:

$$\begin{aligned}
\mathbb{E}^P\left({Y_P}^2(t,T)|\mathcal{F}_{t_0}\right) = &\left(\frac{1}{T-t}\int_t^T \varphi_P(s)ds\right)^2 \\
&- 2\left(\frac{1}{(T-t)^2}\int_t^T \varphi_P(s)ds\right)\left(-\mathbb{E}^P\left[X_{P,t}|\mathcal{F}_{t_0}\right](T-t) + A(t,T) + \begin{pmatrix}B_1(t,T)\\B_2(t,T)\end{pmatrix}^T \begin{pmatrix}\mathbb{E}^P\left[\lambda_t^{P1}|\mathcal{F}_{t_0}\right]\\\mathbb{E}^P\left[\lambda_t^{P2}|\mathcal{F}_{t_0}\right]\end{pmatrix}\right) \\
&+ \frac{1}{(T-t)^2}\left(\mathbb{E}^P\left[{X_{P,t}}^2|\mathcal{F}_{t_0}\right](T-t)^2 + A^2(t,T) + \begin{pmatrix}{B_1}^2(t,T)\\{B_2}^2(t,T)\end{pmatrix}^T \begin{pmatrix}\mathbb{E}^P\left[{\lambda_t^{P1}}^2|\mathcal{F}_{t_0}\right]\\\mathbb{E}^P\left[{\lambda_t^{P2}}^2|\mathcal{F}_{t_0}\right]\end{pmatrix}\right. \\
&- 2\mathbb{E}^P\left[X_{P,t}|\mathcal{F}_{t_0}\right](T-t)A(t,T) + 2A(t,T)\begin{pmatrix}B_1(t,T)\\B_2(t,T)\end{pmatrix}^T \begin{pmatrix}\mathbb{E}^P\left[\lambda_t^{P1}|\mathcal{F}_{t_0}\right]\\\mathbb{E}^P\left[\lambda_t^{P2}|\mathcal{F}_{t_0}\right]\end{pmatrix} \\
&\left.- 2(T-t)\begin{pmatrix}B_1(t,T)\\B_2(t,T)\end{pmatrix}^T \begin{pmatrix}\mathbb{E}^P\left[X_t\lambda_t^{P1}|\mathcal{F}_{t_0}\right]\\\mathbb{E}^P\left[X_t\lambda_t^{P2}|\mathcal{F}_{t_0}\right]\end{pmatrix} + 2B_1(t,T)B_2(t,T)\mathbb{E}^P\left[\lambda_t^{P1}\lambda_t^{P2}|\mathcal{F}_{t_0}\right]\right)
\end{aligned}$$

Like in the univariate analysis, we conduct a two-step calibration. In both steps, we reduce the distance between between $\mathbb{E}^P\left(Y^2(t,T)|\mathcal{F}_{t_0}\right)$ and $\mathbb{E}^P\left({Y_P}^2(t,T)|\mathcal{F}_{t_0}\right)$ versus their respective empirical estimators. In the first part of the calibration, we focus on a simple version of the problem where:

$$Y(t,t+1) \sim X_t \text{ and } Y_P(t,t+1) \sim X_{P,t}$$

Then in a second part, we take the full curves into account. The interval of initial values is chosen based on the calibrated values obtained in the first step.

Table 181 shows the calibrated variables, under the historical measures. Then Table 182 highlights the risk-premium coefficients. Finally, Table 183 shows the coefficients obtained under the risk-neutral measure. **For each parameter, there is a visible stability from one country to another.**

Table 181. Behavioral coefficients under the historical measure

	κ	c	$\delta_{1,1}$	$\delta_{1,2}$	$\delta_{2,1}$	$\delta_{2,2}$	$\delta_{1P,1}$	$\delta_{1P,2}$	$\delta_{2P,1}$	$\delta_{2P,2}$	ρ_1	ρ_2
Germany	0.003	1.13	0.379	-0.06	-0.06	0.25	0.14	-0.01	0.00	0.02	356.1	183.4
France	0.021	0.19	0.933	-0.30	-0.23	0.45	0.44	0.00	-0.02	0.03	161.0	87.9
Italy	0.009	0.84	0.548	-0.15	-0.48	0.55	0.37	-0.01	-0.01	0.06	235.7	72.9
Spain	0.026	0.14	1.046	-0.32	-0.10	0.94	0.05	0.00	0.00	0.02	124.9	61.9

Table 182. Risk-premium coefficients

	a_1	a_2	a_{P1}	a_{P2}	θ_1	θ_2	θ_{P1}	θ_{P2}	$\psi_1(\delta_{1,1}a_1 + \delta_{2,1}a_2 + \theta_1)$	$\psi_2(\delta_{1,2}a_1 + \delta_{2,2}a_2 + \theta_2)$
Germany	1.27	1.10	1.57	2.10	1.08	-0.86	1.87	-4.36	1.004	1.004
France	0.43	1.35	1.57	2.36	1.37	-2.96	1.91	-4.78	1.009	1.029
Italy	1.82	1.21	1.56	1.15	3.49	-0.61	1.28	-2.96	1.003	1.003
Spain	1.06	0.40	1.55	0.93	2.32	-0.90	1.85	-2.58	1.014	1.014

	$\psi_{P1}(\delta_{1P,1}a_1 + \delta_{2P,1}a_2 + \delta_{P1,1}a_3 + \delta_{P2,1}a_4 + \theta_3)$	$\psi_{P2}(\delta_{1P,2}a_1 + \delta_{2P,2}a_2 + \delta_{P1,2}a_3 + \delta_{P2,2}a_4 + \theta_4)$
Germany	1.613	1.613
France	1.612	1.613
Italy	1.609	1.609
Spain	1.608	1.608

Table 183. Coefficients under the risk premium measure

	ρ_1^Q	ρ_2^Q	c_1^Q	c_2^Q	$\delta_{1,1}^Q$	$\delta_{1,2}^Q$	$\delta_{2,1}^Q$	$\delta_{2,2}^Q$	$\delta_{1P,1}^Q$	$\delta_{1P,2}^Q$	$\delta_{2P,1}^Q$	$\delta_{2P,2}^Q$
Germany	354.6	182.7	1.13	1.13	0.38	-0.06	-0.06	0.25	0.14	-0.01	0.00	0.02
France	159.5	85.5	0.20	0.20	0.94	-0.30	-0.24	0.46	0.45	0.00	-0.02	0.03
Italy	231.8	72.7	0.85	0.84	0.56	-0.15	-0.48	0.55	0.37	-0.01	-0.01	0.06
Spain	121.5	61.1	0.15	0.14	1.08	-0.33	-0.11	0.96	0.05	0.00	0.00	0.02

	ρ_{P1}^Q	ρ_{P2}^Q	c_{P1}^Q	c_{P2}^Q	$\delta_{P1,1}^Q$	$\delta_{P1,2}^Q$	$\delta_{P2,1}^Q$	$\delta_{P2,2}^Q$
Germany	6.8	2.8	0.007	0.007	2.42	-0.55	-0.19	2.44
France	6.8	2.8	0.007	0.007	2.42	-0.55	-0.19	2.44
Italy	6.8	2.8	0.007	0.007	2.41	-0.55	-0.19	2.44
Spain	6.8	2.8	0.007	0.007	2.41	-0.55	-0.19	2.43

The calibration error is shown in the following charts, where we compare $\mathbb{E}^P\left(Y^2(t,T)|\mathcal{F}_{t_0}\right)$ against its empirical value. This time again, the fit is not outstanding as we see periods of reduced error, and other periods with a sizeable gap between both series (Graph 249 to Graph 252). We also note that the resulting intensity is a bit more jumpy/instable than in the univariate simulation. Another observation is that Italy for instance shows a decent fit during the period until end-2012. Then, the algorithm is not able to fit the period (of ultra low rates) starting from early 2013. For Spain in contrast, the gap is larger during the period 2009-2014, then the period of ultra low rates is well fitted. In the end, and even if there are periods of significant gap between both series, the end-point of the model is to estimate implied volatilities, which has more to do with the variance of $Y(t,T)$, rather than the absolute estimate of it. **We will determine later in the report if there is a true benefit in considering a multivariate definition of the problem.**

Graph 266. Calculated variance versus empirical variance, Germany (both are averaged on all maturities)

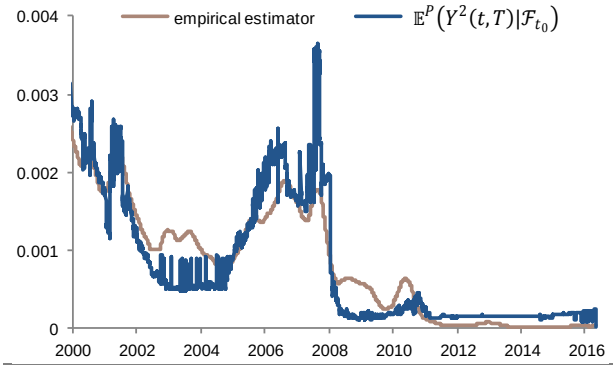

Graph 267. Calculated variance versus empirical variance, France (both are averaged on all maturities)

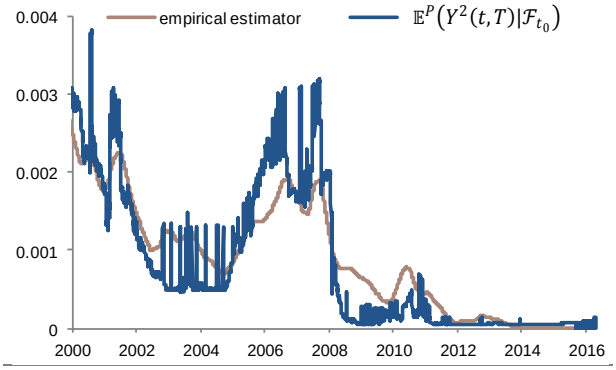

Graph 268. Calculated variance versus empirical variance, Italy (both are averaged on all maturities)

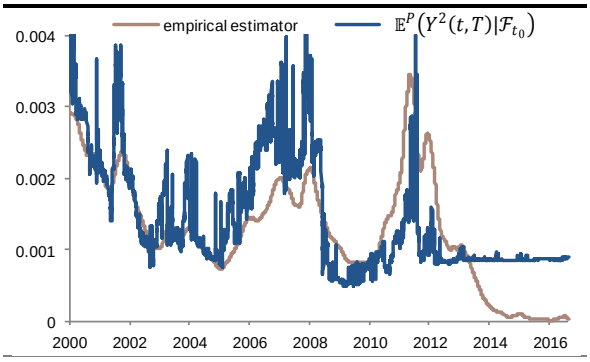

Graph 269. Calculated variance versus empirical variance, Spain (both are averaged on all maturities)

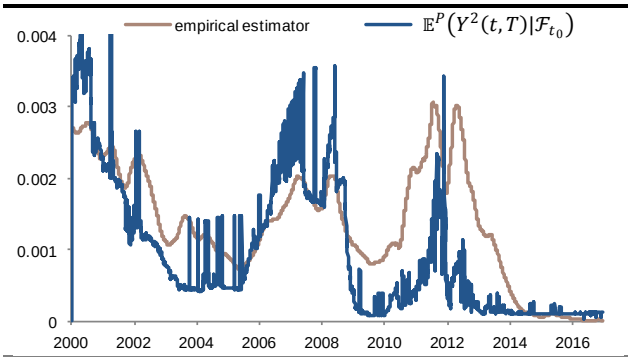

In order to understand the 'strength' of positive and negative jumps under the risk-neutral measure, we consider a steady-state version of the jump amplitude, that we denote $\lambda_\infty^{1,Q}$, $\lambda_\infty^{2,Q}$, $\lambda_\infty^{P1,Q}$, $\lambda_\infty^{P2,Q}$:

$$\begin{cases} 0 = \kappa\left(c_1^Q - \lambda_\infty^{1,Q}\right) + \delta_{1,1}^Q \mu_1^Q \lambda_\infty^{1,Q} + \delta_{1,2}^Q \mu_2^Q \lambda_\infty^{2,Q} + \delta_{1P,1}^Q \mu_{P1}^Q \lambda_\infty^{P1,Q} + \delta_{1P,2}^Q \mu_{P2}^Q \lambda_\infty^{P2,Q} \\ 0 = \kappa\left(c_2^Q - \lambda_\infty^{2,Q}\right) + \delta_{2,1}^Q \mu_1^Q \lambda_\infty^{1,Q} + \delta_{2,2}^Q \mu_2^Q \lambda_\infty^{2,Q} + \delta_{2P,1}^Q \mu_{P1}^Q \lambda_\infty^{P1,Q} + \delta_{2P,2}^Q \mu_{P2}^Q \lambda_\infty^{P2,Q} \\ 0 = \kappa_P\left(c_{P1}^Q - \lambda_\infty^{P1,Q}\right) + \delta_{P1,1}^Q \mu_{P1}^Q \lambda_\infty^{P1,Q} + \delta_{P1,2}^Q \mu_{P2}^Q \lambda_\infty^{P2,Q} \\ 0 = \kappa_P\left(c_{P2}^Q - \lambda_\infty^{P2,Q}\right) + \delta_{P2,1}^Q \mu_{P1}^Q \lambda_\infty^{P2,Q} + \delta_{P2,2}^Q \mu_{P2}^Q \lambda_\infty^{P2,Q} \end{cases}$$

Using the univariate approach, we get that:

$$\begin{cases} \lambda_\infty^{P1,Q} = \dfrac{1}{\left(\kappa_P - \delta_{P1,1}^Q \mu_{P1}^Q\right)}\left(\kappa_P c_{P1}^Q - \dfrac{\delta_{P1,2}^Q \mu_{P2}^Q \kappa_P \left(c_{P2}^Q \kappa_P - \delta_{P1,1}^Q \mu_{P1}^Q c_{P2}^Q + \delta_{P2,1}^Q \mu_{P1}^Q c_{P1}^Q\right)}{\left(\delta_{P2,2}^Q \mu_{P2}^Q - \kappa_P\right)\left(\kappa_P - \delta_{p1,1}^Q \mu_{P1}^Q\right) + \delta_{P2,1}^Q \mu_{P1}^Q \delta_{P1,2}^Q \mu_{P2}^Q}\right) \\ \lambda_\infty^{P2,Q} = \dfrac{-\kappa_P \left(c_{P2}^Q \kappa_P - \delta_{P1,1}^Q \mu_{P1}^Q c_{P2}^Q + \delta_{P2,1}^Q \mu_{P1}^Q c_{P1}^Q\right)}{\left(\delta_{P2,2}^Q \mu_{P2}^Q - \kappa_P\right)\left(\kappa_P - \delta_{P1,1}^Q \mu_{P1}^Q\right) + \delta_{P2,1}^Q \mu_{P1}^Q \delta_{P1,2}^Q \mu_{P2}^Q} \end{cases} \quad (205)$$

Then we also deduce that:

$$\begin{cases} \lambda_\infty^{1,Q} = \dfrac{\kappa c_1^Q + \delta_{1,2}^Q \mu_2^Q \lambda_\infty^{2,Q} + \delta_{1P,1}^Q \mu_{P1}^Q \lambda_\infty^{P1,Q} + \delta_{1P,2}^Q \mu_{P2}^Q \lambda_\infty^{P2,Q}}{\kappa - \delta_{1,1}^Q \mu_1^Q} \\ \lambda_\infty^{2,Q} = \dfrac{\dfrac{\delta_{2,1}^Q \mu_1^Q}{\kappa - \delta_{1,1}^Q \mu_1^Q}\left(\kappa c_1^Q + \delta_{1P,1}^Q \mu_{P1}^Q \lambda_\infty^{P1,Q} + \delta_{1P,2}^Q \mu_{P2}^Q \lambda_\infty^{P2,Q}\right) + \kappa c_2^Q + \delta_{2P,1}^Q \mu_{P1}^Q \lambda_\infty^{P1,Q} + \delta_{2P,2}^Q \mu_{P2}^Q \lambda_\infty^{P2,Q}}{\kappa - \dfrac{\delta_{2,1}^Q \mu_1^Q \delta_{1,2}^Q \mu_2^Q}{\kappa - \delta_{1,1}^Q \mu_1^Q} - \delta_{2,2}^Q \mu_2^Q} \end{cases} \quad (206)$$

Finally, we consider the coefficients $\Delta_{1,1}^Q = \delta_{1,1}^Q \mu_1^Q \lambda_\infty^{1,Q}$, $\Delta_{1,2}^Q = \delta_{1,2}^Q \mu_2^Q \lambda_\infty^{2,Q}$, $\Delta_{2,1}^Q = \delta_{2,1}^Q \mu_1^Q \lambda_\infty^{1,Q}$, $\Delta_{2,2}^Q = \delta_{2,2}^Q \mu_2^Q \lambda_\infty^{2,Q}$ as well as $\Delta_{P1,1}^Q = \delta_{P1,1}^Q \mu_{P1}^Q \lambda_\infty^{P1,Q}$, $\Delta_{P1,2}^Q = \delta_{P1,2}^Q \mu_{P2}^Q \lambda_\infty^{P2,Q}$, $\Delta_{P2,1}^Q = \delta_{P2,1}^Q \mu_{P1}^Q \lambda_\infty^{P1,Q}$, $\Delta_{P2,2}^Q = \delta_{P2,2}^Q \mu_{P2}^Q \lambda_\infty^{P2,Q}$, as a reflection of the contribution of each, positive and negative jumps, onto the jump intensity $\lambda_t^{1,Q}$, $\lambda_t^{2,Q}$.

Table 184 shows the resulting values. First we note that on average, $\Delta_{P1,1}^Q$, and $\Delta_{P2,1}^Q$ are bigger than $\Delta_{1,1}^Q$, $\Delta_{2,1}^Q$: this is a sign that a positive jump (ie. risk aversion) will cause sizeable contagion between

the risk-index and the different sovereigns. The other way round, and as $\Delta^{Q}_{P1,2}$, and $\Delta^{Q}_{P2,2}$ looks very small compared to $\Delta^{Q}_{1,2}$, and $\Delta^{Q}_{2,2}$, it seems that negative jumps (ie. risk appetite) will provoke limited risk propagation into sovereigns.

Table 184. Ratios illustrating the strength of risk propagation through jumps

	$\lambda^{1,Q}_{\infty}$	$\lambda^{2,Q}_{\infty}$	$\lambda^{P1,Q}_{\infty}$	$\lambda^{P2,Q}_{\infty}$
Germany	2.240	1.711	0.087	0.001
France	0.598	0.197	0.086	0.001
Italy	0.706	0.913	0.084	0.001
Spain	0.154	0.343	0.082	0.001

	$\Delta^{Q}_{1,1}$	$\Delta^{Q}_{1,2}$	$\Delta^{Q}_{2,1}$	$\Delta^{Q}_{2,2}$	$\Delta^{Q}_{P1,1}$	$\Delta^{Q}_{P1,2}$	$\Delta^{Q}_{P2,1}$	$\Delta^{Q}_{P2,2}$
Germany	2.4E-03	-5.4E-04	-3.9E-04	2.3E-03	3.1E-02	-1.5E-04	-2.4E-03	6.5E-04
France	3.5E-03	-6.9E-04	-8.8E-04	1.1E-03	3.1E-02	-1.5E-04	-2.4E-03	6.8E-04
Italy	1.7E-03	-7.6E-03	-1.5E-03	2.8E-02	3.0E-02	-1.9E-04	-2.3E-03	8.2E-04
Spain	1.4E-03	-1.8E-03	-1.3E-04	5.4E-03	2.9E-02	-2.0E-04	-2.3E-03	9.0E-04
Average	2.2E-03	-2.7E-03	-7.2E-04	9.2E-03	3.0E-02	-1.7E-04	-2.4E-03	7.6E-04

Finally, Graph 270 to Graph 285 show the resulting jump intensities, under the historical and risk-neutral measures.

Graph 270. Conditional expectation of the jump intensities λ^1_t and λ^2_t, under the historical measure

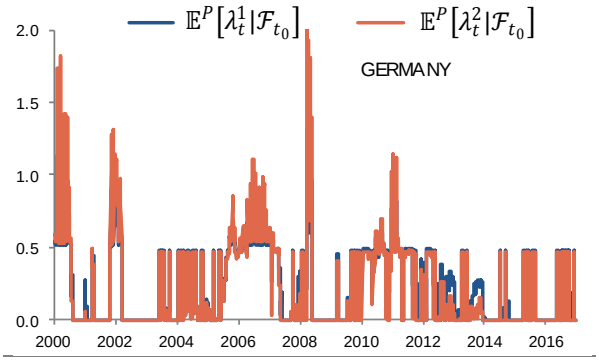

Graph 271. Conditional expectation of the jump intensities λ^1_t and λ^2_t, under the risk-neutral measure

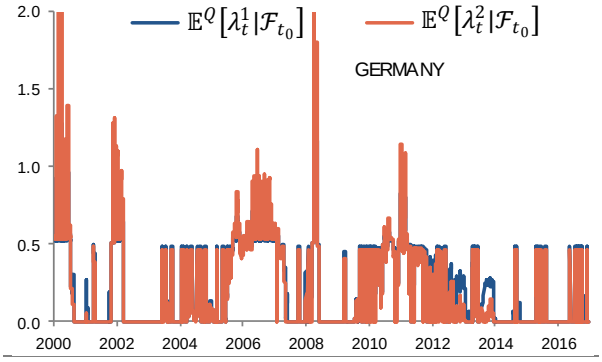

Graph 272. Conditional expectation of the jump intensities λ^{P1}_t and λ^{P2}_t, under the historical measure

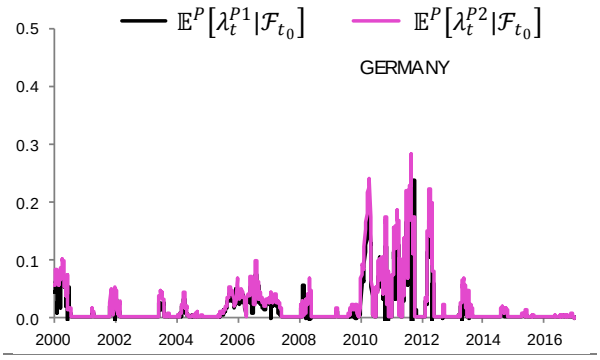

Graph 273. Conditional expectation of the jump intensities λ^{P1}_t and λ^{P2}_t, under the risk-neutral measure

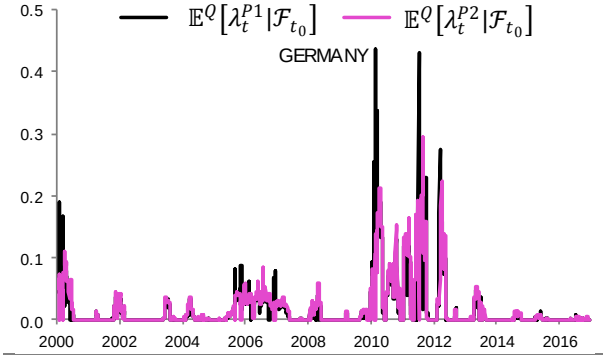

Graph 274. Conditional expectation of the jump intensities λ_t^1 and λ_t^2, under the historical measure

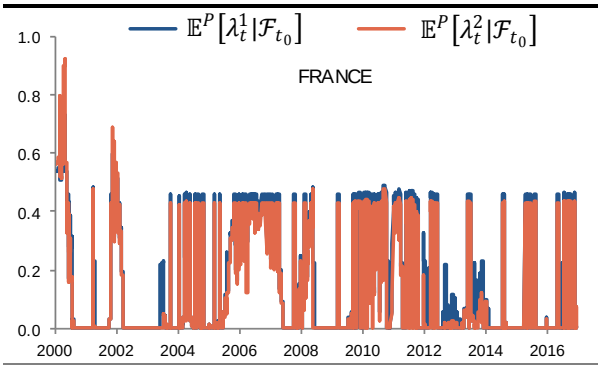

Graph 275. Conditional expectation of the jump intensities λ_t^1 and λ_t^2, under the risk-neutral measure

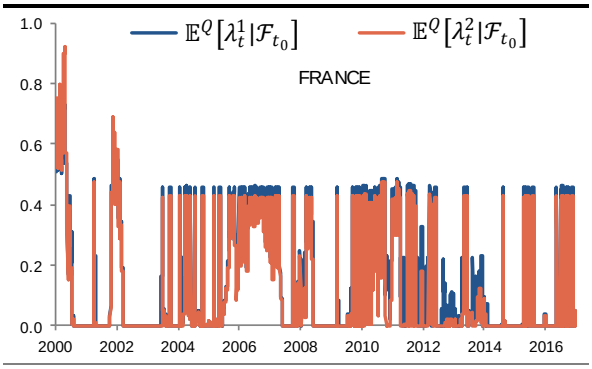

Graph 276. Conditional expectation of the jump intensities λ_t^{P1} and λ_t^{P2}, under the historical measure

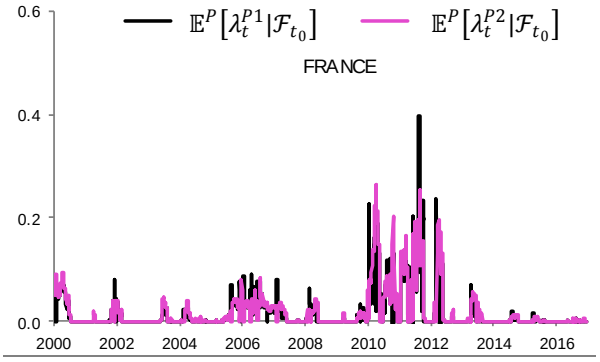

Graph 277. Conditional expectation of the jump intensities λ_t^{P1} and λ_t^{P2}, under the risk-neutral measure

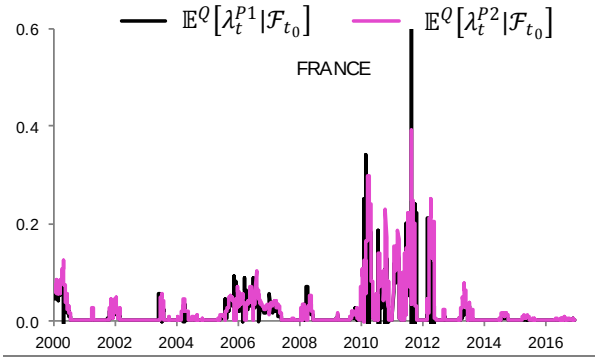

Graph 278. Conditional expectation of the jump intensities λ_t^1 and λ_t^2, under the historical measure

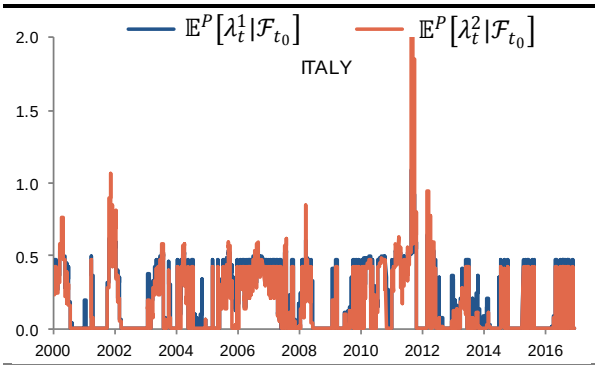

Graph 279. Conditional expectation of the jump intensities λ_t^1 and λ_t^2, under the risk-neutral measure

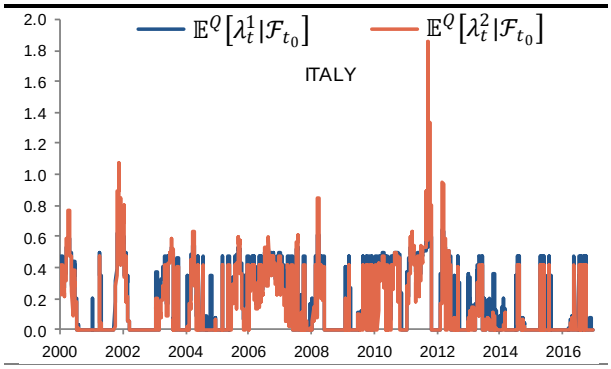

Graph 280. Conditional expectation of the jump intensities λ_t^{P1} and λ_t^{P2}, under the historical measure

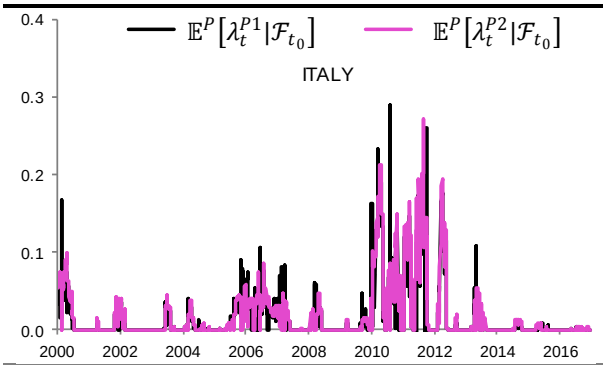

Graph 281. Conditional expectation of the jump intensities λ_t^{P1} and λ_t^{P2}, under the risk-neutral measure

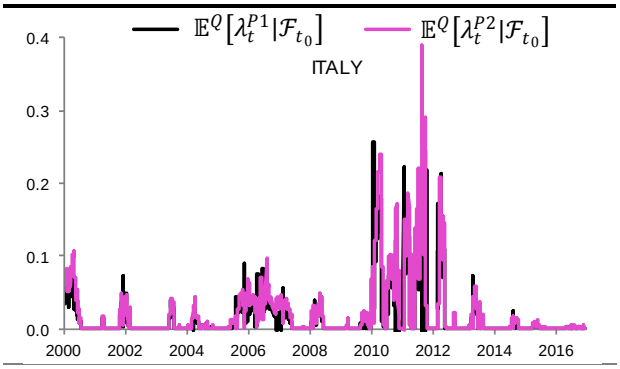

Graph 282. Conditional expectation of the jump intensities λ_t^1 and λ_t^2, under the historical measure

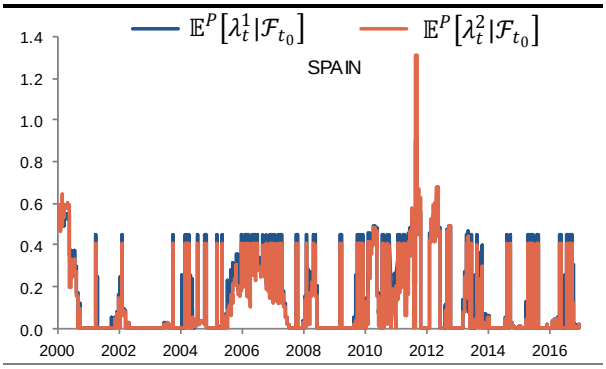

Graph 283. Conditional expectation of the jump intensities λ_t^1 and λ_t^2, under the risk-neutral measure

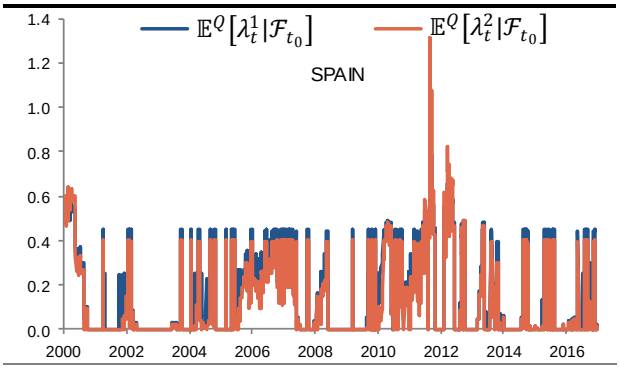

Graph 284. Conditional expectation of the jump intensities λ_t^{P1} and λ_t^{P2}, under the historical measure

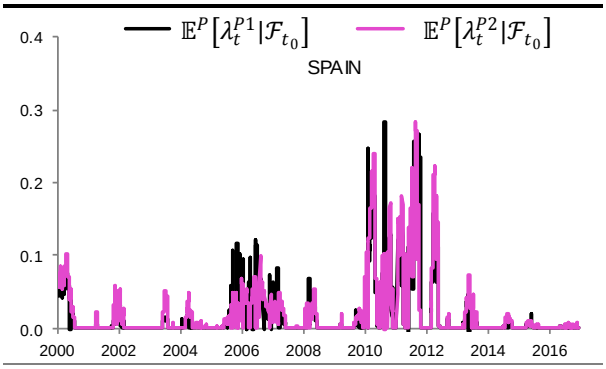

Graph 285. Conditional expectation of the jump intensities λ_t^{P1} and λ_t^{P2}, under the risk-neutral measure

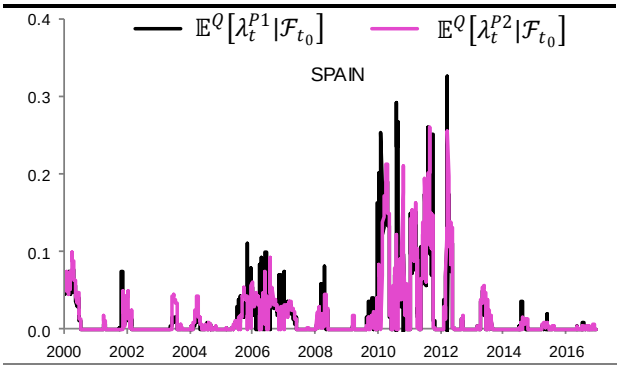

Pricing zero coupon bond options

Our jump model can be used for pricing options on zero coupon bonds, and we explore this special feature and the corresponding methodology in this section.

We define a forward interest rate on a given zero coupon bond curve, via its tenor S, (ie. the maturity of the corresponding zero coupon bond), and the forward date T. In practice, T is the expiration date of the considered option, ie. at a given time t_0 we get: $T = t_0 +$ expiry and $S = t_0 +$ maturity of the underlying). We denote the yield to maturity of a forward zero coupon bond as $Y(T,S)$, and the corresponding forward discount factor as $P(T,S)$.

$Y(T,S)$ is defined as:

$$Y(T,S) = -\frac{1}{S-T}\log P(T,S) = X_T + \frac{1}{S-T}\left(\int_T^S \varphi(s)ds - A(T,S)\right) - \frac{1}{S-T}\begin{pmatrix} B_1(T,S) \\ B_2(T,S) \\ B_3(T,S) \\ B_4(T,S) \end{pmatrix}^T \begin{pmatrix} \lambda_T^1 \\ \lambda_T^2 \\ \lambda_T^{P1} \\ \lambda_T^{P2} \end{pmatrix} \qquad (207)$$

We also denote by $V(Y(T,S))$ the payoff, paid at time $S \geq T$ relative to a European option written on the forward zero coupon bond $Y(T,S)$. As explained in Hainaut (2016), the payoff depends on the type of the option:

- For caplets: $V(Y(T,S)) = N(S-T)[Y(T,S) - K]_+$
- For floorlets: $V(Y(T,S)) = N(S-T)[K - Y(T,S)]_+$
- For a call option based on the discount factor of a zero coupon bond: $V(Y(T,S)) = N[\exp(-Y(T,S)(S-T)) - K]_+$

  N and K are respectively the principal and the strike of the option.

Then the option price is calculated as the conditional expectation of the corresponding discounted payoff, under the risk neutral measure:

$$\mathbb{E}^Q\left(e^{-\int_{t_0}^S r_s ds} V\big(Y(T,S)\big)|\mathcal{F}_{t_0}\right) = P(t_0,S)\mathbb{E}^S\big(V\big(Y(T,S)\big)|\mathcal{F}_{t_0}\big)$$
$$= P(t_0,S)\int_0^{+\infty} V(y) f_{Y(t,T)}^{t_0}(y)dy$$

where $f_{Y(T,S)}(y)$ is the density of $Y(T,S)$ under the forward measure. If $B(t)$ designates the market value of a cash account, ie. $B_t = e^{\int_0^t r_s ds}$, the Radon Nykodym derivative defining the S-forward measure, is equal to:

$$\frac{\partial F^S}{\partial Q} = \frac{1}{B_S}\frac{B_0}{P(0,S)} = \left(e^{\int_0^S r_s ds}\mathbb{E}^Q\left(e^{-\int_0^S r_s ds}|\mathcal{F}_0\right)\right)^{-1}$$

To calculate the expected payoff under F^S, a convenient approach consists of calculating the probability density function of $Y(T,S)$, denoted $f_{Y(t,T)}^{t_0}$, that we obtain by inverting the characteristic function $\varphi^{t_0,S}(i\omega)$, of $Y(T,S)$. Based on this formulation, $\varphi^{t_0,S}(\omega)$ is necessarily the moment generating function of $Y(T,S)$.

First, we focus on calculating the moment generating function $\varphi^{t_0,S}(\omega)$. In particular, we denote by $\varphi^{U,t_0,S}$ the version obtained in the univariate framework, and by $\varphi^{M,t_0,S}$ the corresponding moment generating function obtained in the multivariate framework. $\varphi^{U,t_0,S}(i\omega)$ and $\varphi^{M,t_0,S}(i\omega)$ are the characteristic functions of $Y(T,S)$.

As shown in Hainaut (2016), the univariate moment generating function $\varphi^{U,t_0,S}$, under the risk-neutral measure, is calculated as:

$$\varphi^{U,t_0,Q}(\omega) = \mathbb{E}^Q\big(e^{\omega Y(T,S)}|\mathcal{F}_{t_0}\big)$$
$$= \exp\left(\left(\frac{\omega}{S-T}\right)\int_T^S \varphi(s)ds + \omega X_{t_0}\right)$$
$$\times \exp\left(A^T(t_0,T) - A^S(t_0,S) + \begin{pmatrix} B_1^T(t_0,T) - B_1^S(t_0,S) \\ B_2^T(t_0,T) - B_2^S(t_0,S) \end{pmatrix}^T \begin{pmatrix} \lambda_T^{1,Q} \\ \lambda_T^{2,Q} \end{pmatrix}\right)$$

Where $A^S(t_0,S)$, $B_1^S(t_0,S)$, $B_2^S(t_0,S)$, $B_3^S(t_0,S)$, $B_4^S(t_0,S)$ are solutions of the system of ODEs in eq. (164) with a maturity S, and where $A^T(t_0,T)$, $B_1^T(t_0,T)$, $B_2^T(t_0,T)$ are solutions of the following system of ODEs:

$$\begin{cases} \frac{\partial}{\partial t}B_1^T(t,T) = \kappa_1 B_1^T(t,T) - \left[\psi_1\left(B_1^T(t,T)\delta_{1,1}^Q + B_2^T(t,T)\delta_{2,1}^Q + \left(\omega-(S-t)\right)\alpha_1\right) - 1\right] \\ \frac{\partial}{\partial t}B_2^T(t,T) = \kappa_2 B_2^T(t,T) - \left[\psi_2\left(B_1^T(t,T)\delta_{1,2}^Q + B_2^T(t,T)\delta_{2,2}^Q - \left(\omega-(S-t)\right)\alpha_2\right) - 1\right] \\ \frac{\partial}{\partial t}A^T(t,T) = -\kappa_1 c_1^Q B_1^T(t,T) - \kappa_2 c_2^Q B_2^T(t,T) \end{cases} \quad (208)$$

With the terminal conditions $A^T(T,T) = \left(1-\frac{\omega}{S-T}\right)A^S(T,S)$, $B_1^T(T,T) = \left(1-\frac{\omega}{S-T}\right)B_1^S(T,S)$, $B_2^T(T,T) = \left(1-\frac{\omega}{S-T}\right)B_2^S(T,S)$.

In the multivariate framework, we then obtain the following expression:

Corollary 2. The moment generating function of $Y(T,S)$ at time $t_0 \le T$ under the risk-neutral measure F^Q, denoted by $\varphi^{M,t_0,Q}(\omega)$, is given by:

$$\begin{aligned} \varphi^{M,t_0,Q}(\omega) &= \mathbb{E}^Q\left(e^{\omega Y(T,S)}|\mathcal{F}_{t_0}\right) \\ &= \exp\left(\left(\frac{\omega}{S-T}\right)\int_T^S \varphi(s)ds + \omega X_{t_0}\right) \\ &\times \exp\left(A^T(t_0,T) - A^S(t_0,S) + \begin{pmatrix} B_1^T(t_0,T) - B_1^S(t_0,S) \\ B_2^T(t_0,T) - B_2^S(t_0,S) \\ B_3^T(t_0,T) - B_3^S(t_0,S) \\ B_4^T(t_0,T) - B_4^S(t_0,S) \end{pmatrix}^T \begin{pmatrix} \lambda_T^{1,Q} \\ \lambda_T^{2,Q} \\ \lambda_T^{P1,Q} \\ \lambda_T^{P2,Q} \end{pmatrix}\right) \end{aligned}$$

Where $A^S(t_0,S)$, $B_1^S(t_0,S)$, $B_2^S(t_0,S)$, $B_3^S(t_0,S)$, $B_4^S(t_0,S)$ are solutions of the system of ODEs in eq. (200), with a maturity S, and where $A^T(t_0,T)$, $B_1^T(t_0,T)$, $B_2^T(t_0,T)$, $B_3^T(t_0,T)$, $B_4^T(t_0,T)$ are solutions of the following system of ODEs:

$$\begin{cases} \frac{\partial}{\partial t}B_1^T(t,T) = \kappa_1 B_1^T(t,T) - \left[\psi_1\left(B_1^T(t,T)\delta_{1,1}^Q + B_2^T(t,T)\delta_{2,1}^Q + \left(\omega-(S-t)\right)\alpha_1\right) - 1\right] \\ \frac{\partial}{\partial t}B_2^T(t,T) = \kappa_2 B_2^T(t,T) - \left[\psi_2\left(B_1^T(t,T)\delta_{1,2}^Q + B_2^T(t,T)\delta_{2,2}^Q - \left(\omega-(S-t)\right)\alpha_2\right) - 1\right] \\ \frac{\partial}{\partial t}B_3^T(t,T) = \kappa_{P1} B_3^T(t,T) - \left[\psi_{P1}\left(B_1^T(t,T)\delta_{1P,1}^Q + B_2^T(t,T)\delta_{2P,1}^Q + B_3^T(t,T)\delta_{P1,1}^Q + B_4^T(t,T)\delta_{P2,1}^Q\right) - 1\right] \\ \frac{\partial}{\partial t}B_4^T(t,T) = \kappa_{P2} B_4^T(t,T) - \left[\psi_{P2}\left(B_1^T(t,T)\delta_{1P,2}^Q + B_2^T(t,T)\delta_{2P,2}^Q + B_3^T(t,T)\delta_{P1,2}^Q + B_4^T(t,T)\delta_{P2,2}^Q\right) - 1\right] \\ \frac{\partial}{\partial t}A^T(t,T) = -\kappa_1 c_1^Q B_1^T(t,T) - \kappa_2 c_2^Q B_2^T(t,T) - \kappa_{P1} c_{P1}^Q B_3^T(t,T) - \kappa_{P2} c_{P2}^Q B_4^T(t,T) \end{cases} \quad (209)$$

With the terminal conditions $A^T(T,T) = \left(1-\frac{\omega}{S-T}\right)A^S(T,S)$, $B_1^T(T,T) = \left(1-\frac{\omega}{S-T}\right)B_1^S(T,S)$, $B_2^T(T,T) = \left(1-\frac{\omega}{S-T}\right)B_2^S(T,S)$, $B_3^T(T,T) = \left(1-\frac{\omega}{S-T}\right)B_3^S(T,S)$, $B_4^T(T,T) = \left(1-\frac{\omega}{S-T}\right)B_4^S(T,S)$.

At a given time t_0, the vectors $\left(\lambda_T^{1,Q}, \lambda_T^{2,Q}\right)$ and $\left(\lambda_T^{1,Q}, \lambda_T^{2,Q}, \lambda_T^{P1,Q}, \lambda_T^{P2,Q}\right)$ are obviously unknown (since $t_0 < T$). As a replacement, we take the vectors $\left(\mathbb{E}^Q\left(\lambda_T^{1,Q}|\mathcal{F}_{t_0}\right), \mathbb{E}^Q\left(\lambda_T^{2,Q}|\mathcal{F}_{t_0}\right)\right)$ and $\left(\mathbb{E}^Q\left(\lambda_T^{1,Q}|\mathcal{F}_{t_0}\right), \mathbb{E}^Q\left(\lambda_T^{2,Q}|\mathcal{F}_{t_0}\right), \mathbb{E}^Q\left(\lambda_T^{P1,Q}|\mathcal{F}_{t_0}\right), \mathbb{E}^Q\left(\lambda_T^{P2,Q}|\mathcal{F}_{t_0}\right)\right)$, which are the expected value of the jumps intensities, conditional on $t = t_0$. These conditional expectations are calculated with the calibrated coefficients obtained above.

Then we derive the corresponding probability distribution function by inverting the characteristic functions $\varphi^{U,t_0,S}(i\omega)$ and $\varphi^{M,t_0,S}(i\omega)$. We denote by $f_{Y(T,S)}^{U,t_0}$ and $f_{Y(T,S)}^{M,t_0}$ the resulting probability distribution functions obtained respectively in the univariate and multivariate frameworks:

$$\begin{cases} f_{Y(T,S)}^{U,t_0}(y) = \dfrac{1}{2\pi}\displaystyle\int_{-\infty}^{+\infty} \exp(-i\omega y)\varphi^{U,t_0,S}(i\omega)d\omega \\ f_{Y(T,S)}^{M,t_0}(y) = \dfrac{1}{2\pi}\displaystyle\int_{-\infty}^{+\infty} \exp(-i\omega y)\varphi^{M,t_0,S}(i\omega)d\omega \end{cases}$$

These integrals are resolved via a discrete (inverse) Fourier Transform. Hainaut (2016) gives extensive details on these calculations; we consider the same approach.

Deriving implied volatility from characteristic functions

Let us consider a floorlet, on a 5Y zero coupon bond, with an expiry of 3 months (ie. $T = t_0 + 66$ working days, $S = t_0 + 5$ years). Assuming that $f_{Y(T,S)}^{U,t_0}$ and $f_{Y(T,S)}^{M,t_0}$ are known, we seek to extract the corresponding implied volatility.

The price of the option p (or premium) is indicated by the payoff. Because we consider a floorlet, the premium is equal to $p = V(Y(T,S)) = N(S-T)[K - Y(T,S)]_+$.

Once we get the option price p, we then calculate the corresponding implied volatility using the pricing model of Bachelier (see Bachelier (1900), Bachelier (1912), Black (1976)), where volatility is assumed to be a Gaussian variable:

$$dY(T,S) = \sigma dW \tag{210}$$

Where W is a Brownian motion and $Y(T,S)$ is the forward interest rate. Then the price of put and call options of strike K and expiry $T - t_0$ are:

$$C(t_0) = e^{-rT}\left((Y(T,S) - K)n\left(\frac{Y(T,S)-K}{\sigma\sqrt{(T-t_0)}}\right) + \sigma\sqrt{(T-t_0)}\, n\left(\frac{Y(T,S)-K}{\sigma\sqrt{(T-t_0)}}\right)\right) \tag{211}$$

$$P(t_0) = e^{-rT}\left((K - Y(T,S))n\left(-\frac{Y(T,S)-K}{\sigma\sqrt{(T-t_0)}}\right) + \sigma\sqrt{(T-t_0)}\, n\left(\frac{Y(T,S)-K}{\sigma\sqrt{(T-t_0)}}\right)\right) \tag{212}$$

Where r is the risk-free interest rate, $n()$ is the standard Normal cumulative distribution function, and $n()$ is the standard Normal probability distribution function. Floorlets behave like a call option on the price of the zero coupon bond, so the option premium p is homogeneous to $C(t_0)$ in eq. (211). ➔ **We calculate the implied volatility out of eq. (211).**

A lack of data

Options on sovereign bonds have always been a relatively small market, and volumes have remained at a very low level in recent years compared to the pre-crisis environment. As there is only very few market participants, options on sovereign bonds see a pronounced illiquidity, which overall stands in sharp contrast with the more popular – and liquid – market of swaptions. As a result, there is a persistent concern in banks about how to price sovereign bond options. A common solution, is to price implied volatility on a sovereign security as a 'shift', which is added to the implied volatility of the equivalent swaption (in terms of maturity and strikes). **The shift, is supposed to reflect the fact that a sovereign bond yield can be seen as an IRS adjusted by a premium, mostly representing credit risk, liquidity conditions and a specific interpretation of the term premium component.** On that basis, drawing an estimate of the sovereign implied volatility by 'shifting' the swaption volatility may look consistent for at-the-money options, at least if the shift is correctly appreciated by traders.

In practice however, the value of the shift is usually calculated as an empirical transformation of the realised volatility of the underlying sovereign bond. **As a result, the calculation of the shift is generally disconnected from the different components of the considered option, ie. independent of its strike and its expiry**. And as a logical consequence, there no way to get a proper smile. ➔ **These are clear limitations of the 'shift' approach.**

In this challenging environment, we were not given the possibility to get a reliable set of implied volatilities on sovereign bond options. First, these are not tracked at SocGen, mostly as the methodology employed by traders to establish the shift is too empirical, and not necessarily robust from a mathematical standpoint. The few numbers we saw suggest that the mid-price, quoted at SocGen for these options, is extremely close to the historical volatility of the underlying, with remarkably wide bid-ask spreads depending on the nature of the bond (this is especially true for Italian and Spanish bonds as it is somewhat difficult to get a proper hedge on peripheral bonds).

It is worth noting that on one side our analysis is based on **zero coupon bond options**, while on the other side traders are mostly requested to price **coupon bond options**. Jamshidian (1989) introduced a simple and interesting approach to make a bridge between zero coupon bond and coupon bond options. In particular, the author shows that a coupon bond option can be seen as a portfolio of zero coupon options.

Results

We focus on at-the-money options (ie. $K = Y(t,T)$). We calculate the univariate distribution function $f_{Y(T,S)}^{U,t_0}$ over the full sample, for 3-month at-the-money options and we derive the corresponding implied volatility. We then compare the resulting implied volatility against the rolling 3-month standard deviation that we take as an estimator of the realised volatility.

Graph 286 to Graph 289 show the implied volatility obtained in the univariate framework. First we note that implied volatilities are somewhat jumpy. This surely reflects jumps at work. On average however, implied volatilities are very close to the series of realised volatility. **This is a sign of coherence.**

While there are periods where the implied volatility seems to be lagging a bit below the realised volatility, this is mostly during periods of stable financial markets. When we focus on periods of more volatile markets (like 2007-2010 and 2011-2013), the implied volatility is usually exceeding the realised volatility (though not for Spain). This is particularly visible with options on Italian bonds in Graph 288, during the sovereign crisis. From a general point of view, a sudden increase in the realised volatility is followed by a concomitant jump in the implied volatility: in fact jumps look particularly large in the early stage of risk aversion (arrows in the graphs illustrate some of these periods).

➔ **For us, this is a sign that the risk-premium coefficients were successfully calibrated.** This pattern of larger jumps when the underlying situation starts deteriorating could be used by market participants to take action before the crisis materialises in full.

While the implied volatility for options on Italian bonds tends to be significantly larger than the realised volatility during the years 2011 and 2012, this is not the case for options on Spanish bonds: the implied volatility is persistently underestimating the true volatility during this period in Graph 289. **The univariate approach looks a bit less relevant here.**

Graph 286. 3m5Y option on Germany bonds, implied versus realised volatility (univariate model)

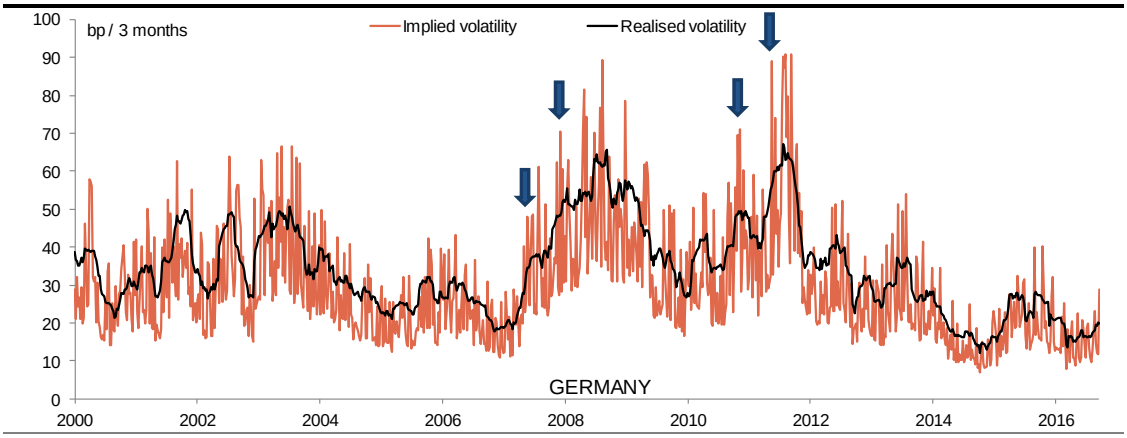

Graph 287. 3m5Y option on French bonds, implied versus realised volatility (univariate model)

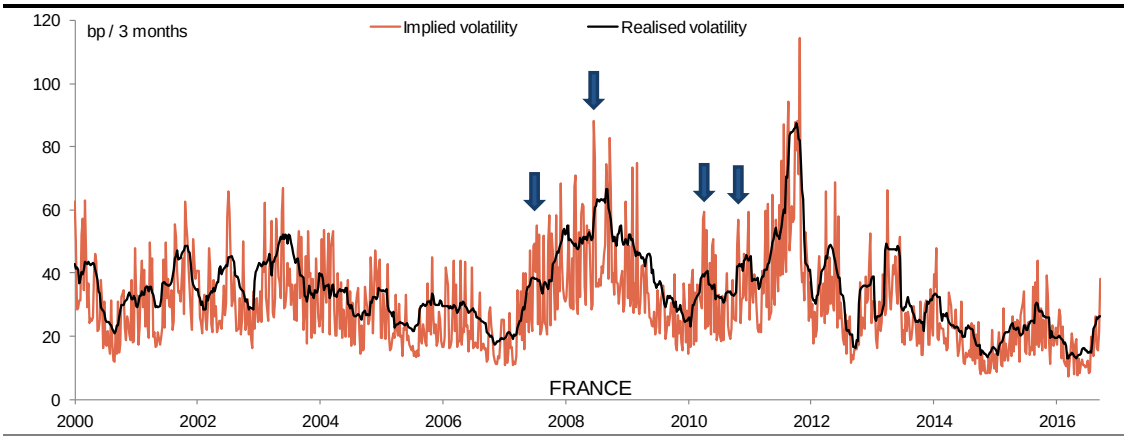

Graph 288. 3m5Y option on Italian bonds, implied versus realised volatility (univariate model)

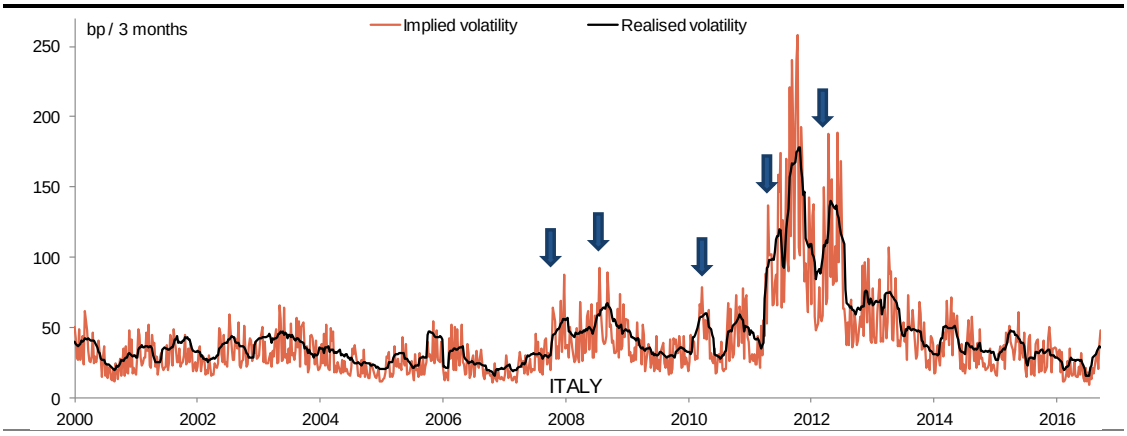

Graph 289. 3m5Y option on Spanish bonds, implied versus realised volatility (univariate model)

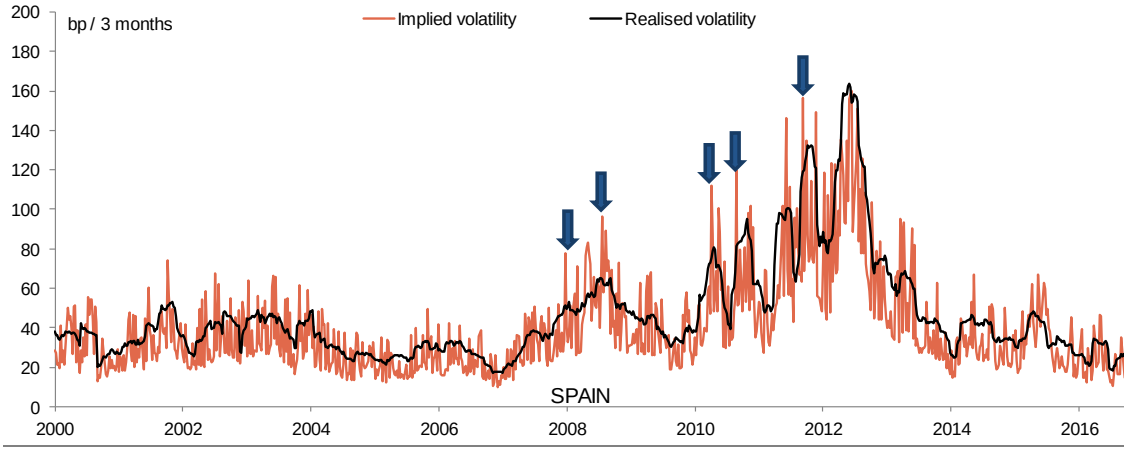

When we consider the general picture, the implied volatility obtained in the multivariate framework is very close to what we got from the univariate model (Graph 290 to Graph 293). Focusing on years of crisis (like 2011-2012) however, we note that for options on Italian bonds (Graph 292), the implied volatility is not jumping as much as in the univariate version (Graph 288).

For options on Spanish bonds in contrast (Graph 293), the multivariate model gives a better fit during the same period, than the univariate one in Graph 289.

Finally, Graph 294 to Graph 297 show an overlap of both implied volatilities with a focus on the 2008-2012 period. For Germany (Graph 294), the two volatilities are somewhat equivalent, with very little deviation one from each other. For France and Italy in contrast, the fit seems to be better with univariate calculations, especially during the period of intense contagion from July to December 2011 (Graph 295, Graph 296). For Spain finally, and as mentioned above, the multivariate approach slightly outperforms the univariate model (Graph 297).

➔ **It is not clear whether the multivariate approach improves the quality of the resulting implied volatilities. If it does, this is most probably just at the margin. In any way, the high degree of similarity between these two estimators is a sign that calculations are coherent.**

Graph 290. 3m5Y option on Germany bonds, implied versus realised volatility (multivariate model)

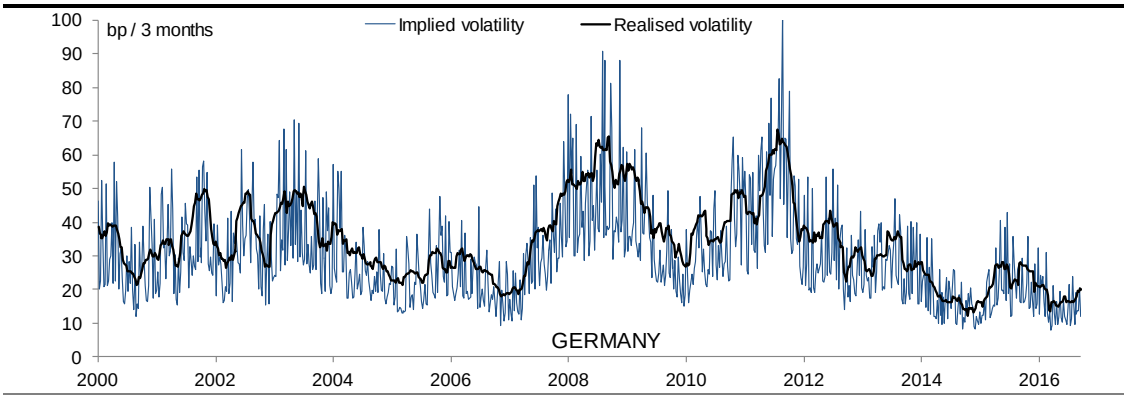

Graph 291. 3m5Y option on French bonds, implied versus realised volatility (multivariate model)

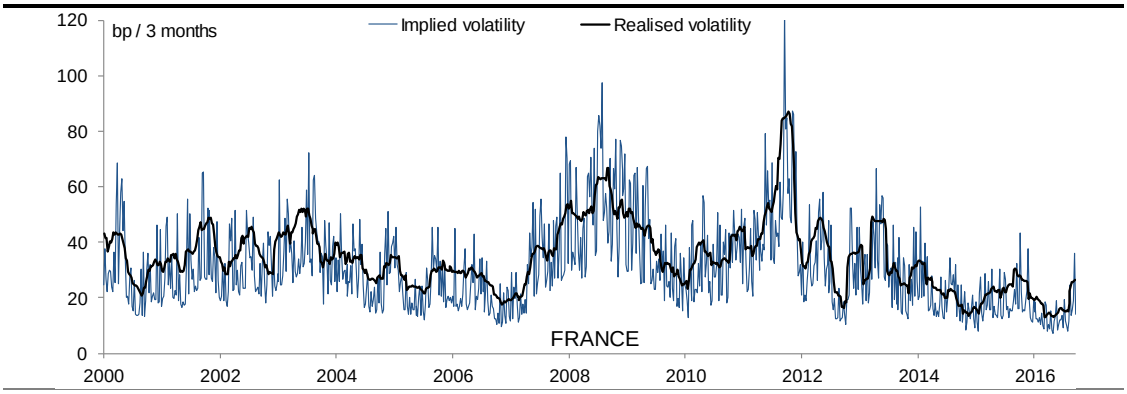

Graph 292. 3m5Y option on Italian bonds, implied versus realised volatility (multivariate model)

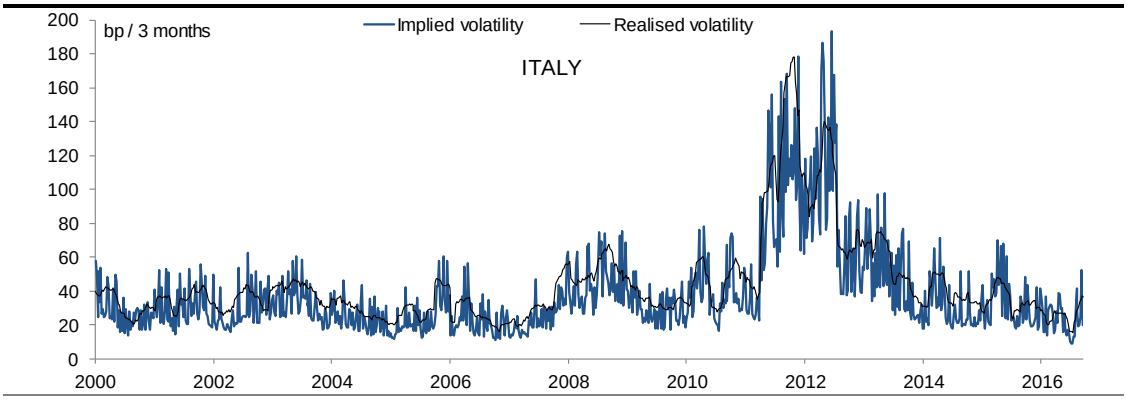

Graph 293. 3m5Y option on Spanish bonds, implied versus realised volatility (univariate model)

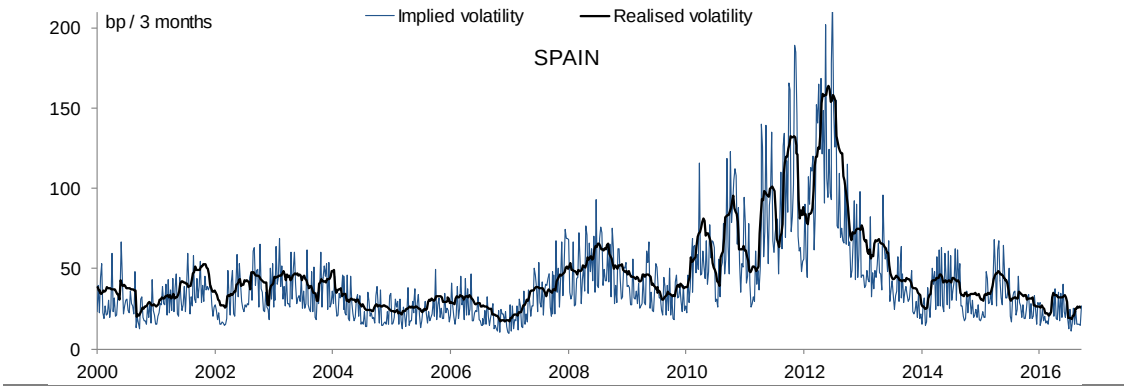

Graph 294. 3m5Y option on German bonds, implied volatility – univariate versus multivariate model

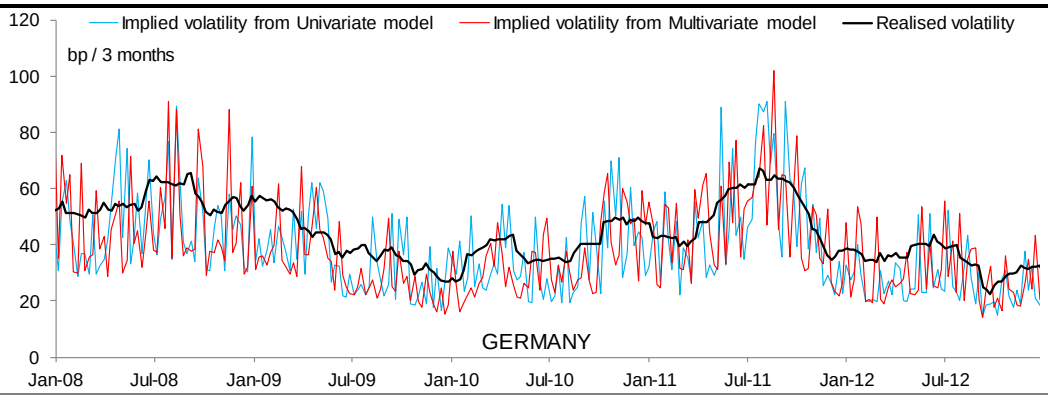

Graph 295. 3m5Y option on French bonds, implied volatility – univariate versus multivariate model

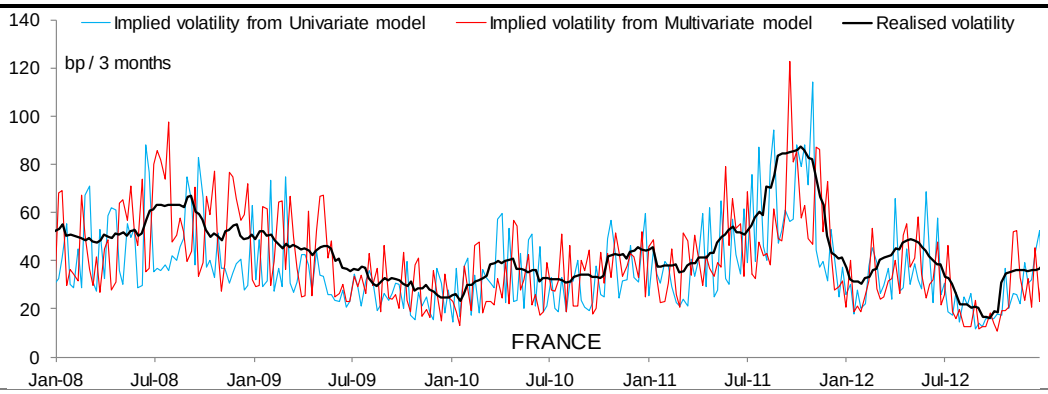

Graph 296. 3m5Y option on Italian bonds, implied volatility – univariate versus multivariate model

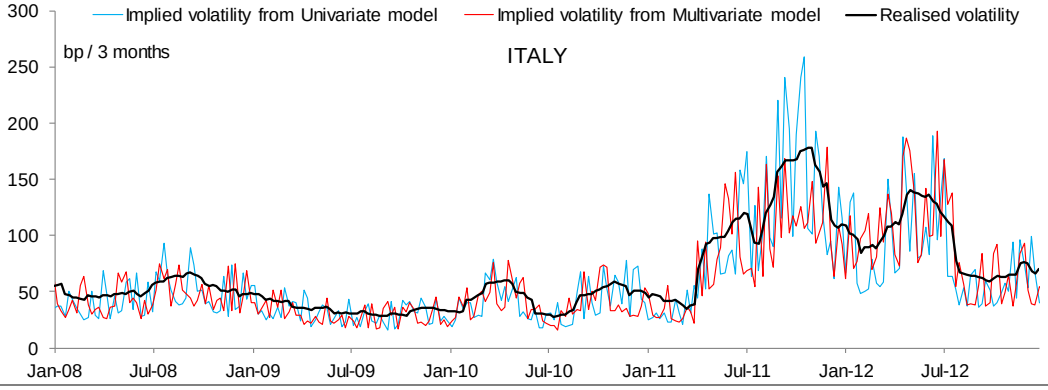

Graph 297. 3m5Y option on Spanish bonds, implied volatility – univariate versus multivariate model

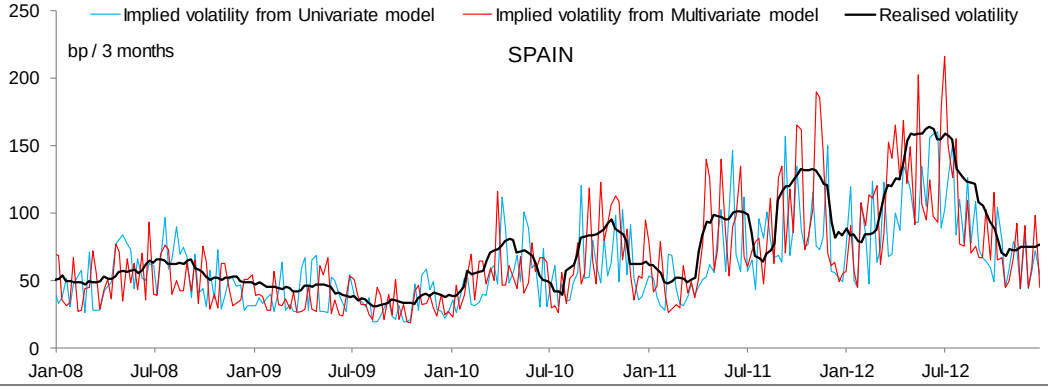

The shape of the distribution

A quick look at the shape of $f_{Y(T,S)}^{U,M,t_0}$ shows that the distribution is very close to a normal distribution, and this is irrespective of the dimension of the problem: assuming similar implied volatilities, the shape of $f_{Y(T,S)}^{M,t_0}$ is almost identical to $f_{Y(T,S)}^{U,t_0}$. **Overall, this corroborates comments made in Hainaut (2016) and Errais et al. (2010).**

Graph 298. The obtained distributions look Gaussian

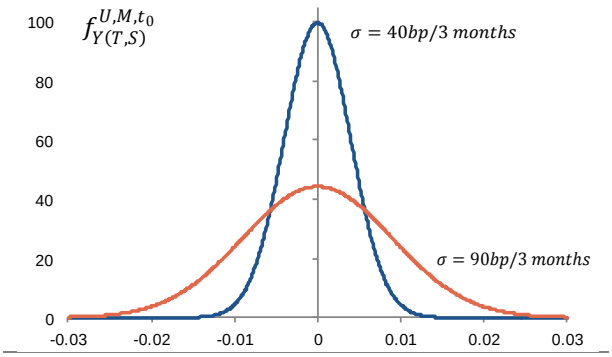

Graph 299. There is almost no skewness

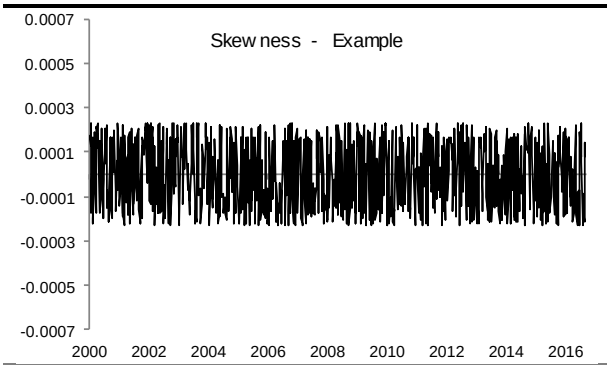

Exploring the statistical features of $f_{Y(T,S)}^{U,M,t_0}$, we note that the skewness of the distributions is erratic and close to zero, with values alternatively positive or negative (Graph 299). Digging a bit further about whether $f_{Y(T,S)}^{U,M,t_0}$ enables to generate some skewness, we conduct a few synthetic simulations. On one side we assume a symmetric distribution of the behavioural coefficients, as per Table 185. And since any asymmetry would come from very pronounced distortions between $\lambda_t^{1,Q}$ and $\lambda_t^{2,Q}$, we explore three different scenarios based different degrees of dissimilarity between $\lambda_t^{1,Q}$ and $\lambda_t^{2,Q}$ (Table 186).

Table 185. A symmetrical problem involving synthetic coefficients

κ	c_1^Q	c_2^Q	$\delta_{1,1}^Q$	$\delta_{1,2}^Q$	$\delta_{2,1}^Q$	$\delta_{2,2}^Q$	ρ_1^Q	ρ_2^Q
0.40	0.004	0.004	1.500	-0.500	-0.500	1.500	5	5

Table 186. Three different scenarios

	$\lambda_t^{1,Q}$	$\lambda_t^{2,Q}$	$\lambda_t^{P1,Q}$	$\lambda_t^{P2,Q}$
scenario 1	0.5	0.5	0.05	0.05
scenario 2	1.5	0.25	0.05	0.05
scenario 3	0.25	1.5	0.05	0.05

We calculate $f_{Y(T,S)}^{M}$ for the three different scenarios (multivariate coefficients not specified in Table 185 are taken from Table 180). As Graph 300 shows, the distribution is mostly symmetrical when $\lambda_t^{1,Q} = \lambda_t^{2,Q}$ (scenario 1, red line). The two other scenarios in comparison, involving very disparate values of $\lambda_t^{1,Q}$ and $\lambda_t^{2,Q}$, effectively see the emergence of some modest skewness inside the distribution (see Graph 300). In scenario 2 for instance, a larger $\lambda_t^{1,Q}$ makes the right-part of the distribution slightly bigger, while in scenario 3 the larger$\lambda_t^{2,Q}$ tends to increase the left-part of the distribution. This looks consistent with the natural interpretation that a higher $\lambda_t^{1,Q}$ reflects more

frequent positive jumps, and similarly a higher $\lambda_t^{2,Q}$ reflects more frequent negative jumps. ➔ The shape of the distribution function tends to adjust itself coherently to any deviation in the jump intensity. That said, the appearance of sizeable skewness requires substantial decoupling between $\lambda_t^{1,Q}$ and $\lambda_t^{2,Q}$. **This is not the case in our analysis where $\mathbb{E}^{Q}\left[\lambda_t^1|\mathcal{F}_{t_0}\right]$ and $\mathbb{E}^{Q}\left[\lambda_t^2|\mathcal{F}_{t_0}\right]$ are relatively close one to each other.**

Graph 300. Probability distribution functions under the forward measure, in each scenario

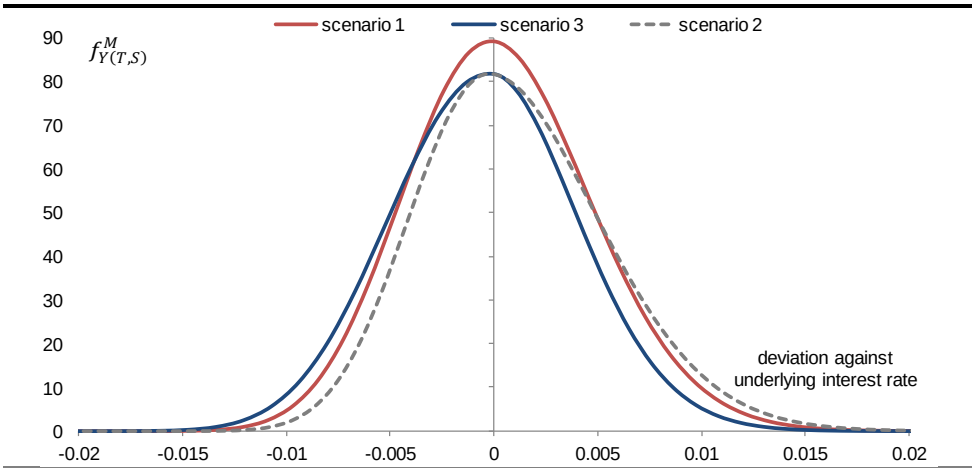

Conclusion

In Chapter III, we have explored different ways to quantify the behaviour of sovereign securities, with a particular emphasis on how sovereign risk tends to affect the price of financial derivatives in a risk-off environment. As a backbone of the analysis, we assumed that risk aversion and the ensuing volatility favour the emergence of sizeable discontinuities in market prices, that we model with stochastic jumps. **This is in contrast with the framework explored in the first two chapters**, where there is an implicit constraint that risk aversion induces a continuous transformation of the price dynamics.

The different approaches we investigate, extensively rely on Hawkes processes. These processes seek to estimate the durable impact of risk aversion onto the dynamics of jumps, via the introduction of dedicated self-exciting loops. Empirical observations already suggest that jumps are more frequent when market sentiment markedly deteriorates. And effectively, our model corroborates this assertion in full, with calibration indicating that a repeated occurrence of jumps at a given time literally increases the likelihood and the amplitude of jumps, in the future. As the strength of self-excitation is described by at least four different variables (ie. $\delta_{1,1}$, $\delta_{1,2}$, $\delta_{2,1}$, $\delta_{2,2}$, and up to eight coefficients in more complex versions), the model also quantifies the strength of any latent cross-excitation (via $\delta_{1,2}$, and $\delta_{2,1}$). Our approach, on that basis, looks particularly versatile. **Results overall, suggest that there is sizeable risk transmission through all these different channels. In the multivariate framework as well, contagion from the risk-index is significant.**

Calibrating the model has been a real challenge, for different reasons. First, there is a notable complexity rising from the fact that none of the jump intensity and the jump amplitude is observable in our framework. Plus, we did not have any reliable data on implied volatility. This made common approaches available in the literature inapplicable, as methodologies exploring the pricing of financial derivatives most frequently involve a reference dataset of implied volatilities, which greatly simplifies the calibration. **We therefore developed an original approach to the calibration, different from conventional procedures found in the literature.**

Results from the calibration look consistent from one country to another, and our implied volatility remains in the vicinity of the empirical realised volatility. Jumps seem to play an active role in the shape of the resulting time series. While this translates into a somewhat jumpy implied volatility, there is evidence that the model is able to jump as soon as from the early stages of a volatile period. **This is a sign of robustness, suggesting that risk premium coefficients were successfully estimated.**

A visible limitation with jump-based stochastic processes, is the relatively large number of unknowns involved into the calibration. Our unsuccessful attempt to replicate the sophisticated model of Ait-Sahalia (2010) is an illustration that too many latent variables is a risk to make the calibration remarkably instable. Even in the alternative approach inspired by Hainaut (2016), we were left with as much as twelve unknowns in the univariate case, and sixteen in the multivariate analysis. **This is significant, but thankfully convergence during the calibration was achievable.**

Finally, while our model delivered an interesting estimate of the implied volatility, it is not able to replicate the natural skewness visible in volatility smiles. Skewness is a key component when pricing financial derivatives; **further investigation and any improvement on that front could make this jump model very useful for market participants.**

General Conclusion

Periods of deep risk aversion are usually marked by sizeable distortions in market prices, and substantial losses in portfolios. As observed during every financial crisis, a generalized debacle in financial markets is a very negative shock for the real economy. Against this backdrop, it looks relevant to explore how risk aversion tends to affect global market valuations, especially if this exercise helps make the promotion of more optimal portfolio rebalancing procedures in periods of fierce flight to quality. Ultimately, research initiatives in this field could contribute to reduce the systemic impact of financial distress in general.

In this dissertation, we investigated different dimensions of risk aversion, with a focus on European Sovereign debt instruments, including CDS spreads, asset swap spreads and zero coupon bonds. The period we cover offers a wide exploration over many years (2000-2016), including periods of stable market sentiment, as well as periods of recognized financial crises (namely the Global Financial Crisis in 2008, and the European debt crisis in 2011-2012). For a given sovereign bond, the (quoted) yield to maturity has to reflect the underlying risk that the borrowing entity (ie. the Treasury) would default on its debt, before maturation of the bond. This is sovereign risk. Since financial crises engender wide-spread price deteriorations in financial markets, they usually occasion an upward correction in bond yields. And logically, higher yields mean growing sovereign risk. A continued move in yields would thus eventually be perceived by investors as an implicit deterioration of the credit quality of the sovereign entity. An escalation in risk aversion then, eventually encourages the emergence of a confidence crisis, thereby inflating pressure on yields further. As the self-feeding mechanism is taking over, risk propagation ultimately has tremendous implications at the State level, especially in developed economies where the State machinery is much reliant on consistent demand from financial markets. From a Treasury point of view, there is therefore a natural incentive to get a deeper understanding of how sovereign risk could evolve under the influence of uncontrolled risk aversion. This is one of the goals we seek to achieve in this report.

In the first two chapters, we considered a probabilistic approach to sovereign risk exploration, with the main purpose of illustrating the non-linear reaction ensuing from a gradual deterioration in market sentiment. First, we noted the need to consider heavy-tailed distributions as the backbone of the analysis. Then, we had to pick-up an adequate model to capture the volatility momentum, notoriously erratic in times of financial crisis. The GAS method proved particularly efficient from that point of view, and we took advantage of its agility to calibrate the model over an extended period of time, incorporating periods of hefty variations in market sentiment. In the end, we were amazed by the quality of fit provided by Generalised Hyperbolic distributions assorted with GAS-estimated volatility. Plus, we were able to derive an empirical formulation of the un-temporal volatility, for each security. This estimator offered an interesting view on the dynamics of the intrinsic volatility, with the obtained profile suggesting that volatility tends to accelerate in a quadratic manner when it is expressed against the cumulative distribution function of the price variations.

In a second step, we extended this approach to a problem of larger dimension and we explored the dynamics of risk aversion from a bivariate point of view. While our multivariate model is not a copula per se, both have in common the fact that time series are adjusted by their own intrinsic volatility before the multivariate exploration. This proved especially convenient in our analysis, making the

estimation of multivariate correlations particularly straightforward. Unexpectedly, a proper calibration of the model also required a few adjustments to the initial formulation of the GAS method, which proved in the end fairly accommodative to our needs. This time again, we were positively surprised by the outstanding robustness of the multivariate calibration. As a general observation, results suggest that heavy-tailed distributions are effectively extremely efficient to replicate the empirical distribution of times-series affected by distorted volatility and erratic price variations. Following the multivariate calibration, we derived a preliminary picture of the multivariate dependencies, mostly based on an empirical interpretation of financial contagion. The profile we obtained illustrates very well the sharply non-linear acceleration in bivariate connections, that materializes when risk aversion exceeds a certain level of intensity.

While Chapter I focuses on the calibration of the multivariate model, Chapter II explores different ways to extract information from the model, about contagion and how it impacts sovereign risk. First, we have rationalised the dynamics of the deterioration, in terms of credit quality, that arises from the emergence of shocks. Our approach involves two different definitions of the shock: one, temporal, is based on the market-implied probability of default; this formulation involves the GAS volatility estimator. A second definition investigates the relevance of time-invariant stress tests and finally delivers an estimator of the expected market reaction, from a more general standpoint than the temporal approach. We considered a series of many shocks with gradual intensity. The analysis offers a high degree of granularity in the results, and this proved particularly helpful to extrapolate empirical rules on the general behaviour of 1) the intrinsic volatility, 2) the market response to shocks, 3) the expected frailty hitting the credit quality.

On a cross country basis, our analysis also shows that there exists a linear trajectory amongst the different sovereigns (Graph 163), that relates the maximum market reaction to what we consider as a measure of the frailty induced by financial distress. This linear behaviour is insightful information, which was unexpected.

Then, in a second part, we focused on multivariate dependencies and how these are affected by shocks. Our analysis shows that the general acceleration of the joint market reaction to shocks admits a logarithmic behaviour, when expressed as a function of the shock intensity. Results also suggest that a univariate-only exploration of sovereign risk tends to sharply underestimate the market reaction to shocks, hence there is a visibile benefit in considering a multivariate framework instead.

Finally, we explored an application of the model in the context of portfolio optimisation. First we investigated the relevance of incorporating our own estimators of volatility and market reaction (to shocks) into some popular portfolio optimisation procedures (GMV, ERC, MDP). Results indicate that the modified version, involving our own risk-estimators, consistently outperform the more standard formulations found in the literature. Involving our measure of intrinsic volatility $\hat{h}$ or the volatility forecast $\hat{\sigma}_{t+1}$ in particular, greatly enhanced the robustness of returns. Portfolios based on $\hat{\sigma}_{t+1}$ also showed an interesting performance when rebalancing happens on a bimonthly basis. This reaffirms the forecasting capability of the GAS model, which is a valuable dimension of the methodology.

In the last part of the chapter, we designed an in-house methodology for optimal portfolio rebalancing, based on mean reversion. This approach offers outstanding results, overall demonstrating that the allocation strategy is able to fit many different market environments. In

particular, a back-test over the full period shows that reallocation out of risk-on strategies and into a more prudent positioning takes place as soon as there are palpable signs of mounting risk aversion. This is a sign of robustness. While mean-reverting approaches offer simplicity, they usually prove more hazardous when financial markets are very directional. We address this issue via sensible adjustments; overall results suggest that mean reversion can effectively be used for risk management purposes.

In Chapter III, we explored different ways to quantify the behaviour of sovereign securities, with a particular emphasis on how sovereign risk tends to affect the price of financial derivatives in a risk-off environment. We consider that risk aversion and the ensuing volatility, now favour the emergence of sizeable discontinuities in market prices, that we model with stochastic jumps. This is in contrast with the probabilistic framework explored in Chapter I and Chapter II, where there is an implicit constraint that risk aversion induces a continuous transformation of the price dynamics.

The different approaches we investigate, extensively rely on Hawkes processes. These stochastic processes seek to estimate the durable impact of risk aversion onto the dynamics of jumps, via the introduction of dedicated self-exciting loops. Empirical observations suggest that jumps are more frequent when market sentiment markedly deteriorates. And effectively, our model corroborates this assertion in full, with calibration indicating that a repeated occurrence of jumps at a given time literally increases the likelihood and the amplitude of jumps, in the future. As the strength of any self-excitation is described by at least four different variables (ie. $\delta_{1,1}$, $\delta_{1,2}$, $\delta_{2,1}$, $\delta_{2,2}$, and up to eight coefficients in more complex versions), the model also quantifies the strength of any latent cross-excitation (via $\delta_{1,2}$, and $\delta_{2,1}$). Our approach, on that basis, looks particularly versatile. Results overall, suggest that there is sizeable risk transmission through all these different channels. In the multivariate framework as well, contagion from the risk-index is significant.

Calibrating the model has been a real challenge, for different reasons. First, there is a notable complexity rising from the fact that none of the jump intensity and the jump amplitude is observable in our framework. Plus, we did not have any reliable data on implied volatility. This made common approaches available in the literature inapplicable, as methodologies exploring the pricing of financial derivatives most frequently involve a reference dataset of implied volatilities, which greatly simplifies the calibration. We therefore developed an original approach to the calibration, different from conventional procedures found in the literature.

Results from the calibration look consistent from one country to another, and our estimated implied volatility remains in the vicinity of the empirical realised volatility. Jumps seem to play an active role in the shape of the resulting time series. While this translates into a somewhat jumpy implied volatility, there is evidence that our model is capable to jump as soon as from the early stages of a volatile period. This is a sign of robustness, suggesting that risk premium coefficients were successfully estimated.

A visible limitation with jump-based stochastic processes, is the relatively large number of unknowns involved into the calibration. Our unsuccessful attempt to replicate the sophisticated model of Ait-Sahalia (2010) is an illustration that too many latent variables is a risk to make the calibration remarkably unstable. Even in the alternative approach inspired by Hainaut (2016), we were left with as much as twelve unknowns in the univariate case, and sixteen in the multivariate analysis. This is significant, but thankfully convergence during the calibration was achievable.

We identify different directions for further research. First, our multivariate analysis only explores bivariate risk transmission. The tests we made suggest that there is enough tractability to increase the dimension of the calibration significantly, up to 5 bonds in our simulations. While the computational burden is significantly heightened, a quick view indicates that calibrations were successful, although they were not as stable as in the bivariate case. Results could improve the performance of our own portfolio optimisation procedure, especially as cross-asset correlations would be more accurately estimated in a high-dimensional probabilistic model.

There is also ample room for further exploration in sovereign bond options. While this market is very modest in terms of traded volumes, the greater financial stability ensuing from more efficient regulations could help increase the popularity of these products in the future. Our option model delivered an interesting estimate of the implied volatility, but it is not able to replicate the natural skewness visible in volatility smiles. Skewness is a key component when pricing financial derivatives; further investigation and any improvement on that front could make this jump model very useful for market participants.

Appendix

Proofs of propositions.

Proposition 1. Consider the functions $g^i = \lambda_t^i$ for $i = 1,2,P1,P2$. Based on eq. (180) and eq. (169), their expectations are such that:

$$\begin{aligned}\mathbb{E}\left(\mathcal{A}g^1|\mathcal{F}_{t_0}\right) &= \kappa_1\left(c_1 - \mathbb{E}\left(\lambda_t^1|\mathcal{F}_{t_0}\right)\right) + \mathbb{E}\left(\lambda_t^1|\mathcal{F}_{t_0}\right)\int_{-\infty}^{+\infty}\delta_{1,1}z\,d\nu_1(z) + \mathbb{E}\left(\lambda_t^2|\mathcal{F}_{t_0}\right)\int_{-\infty}^{+\infty}\delta_{1,2}z\,d\nu_2(z)\\ &+ \mathbb{E}\left(\lambda_t^{P1}|\mathcal{F}_{t_0}\right)\int_{-\infty}^{+\infty}\delta_{1P,1}z\,d\nu_{P1}(z) + \mathbb{E}\left(\lambda_t^{P2}|\mathcal{F}_{t_0}\right)\int_{-\infty}^{+\infty}\delta_{1P,2}z\,d\nu_{P2}(z)\\ &= \kappa_1\left(c_1 - \mathbb{E}\left(\lambda_t^1|\mathcal{F}_{t_0}\right)\right) + \mathbb{E}\left(\lambda_t^1|\mathcal{F}_{t_0}\right)\delta_{1,1}\mu_1 + \mathbb{E}\left(\lambda_t^2|\mathcal{F}_{t_0}\right)\delta_{1,2}\mu_2 + \mathbb{E}\left(\lambda_t^{P1}|\mathcal{F}_{t_0}\right)\delta_{1P,1}\mu_{P1}\\ &+ \mathbb{E}\left(\lambda_t^{P2}|\mathcal{F}_{t_0}\right)\delta_{1P,2}\mu_{P2}\end{aligned}$$

And similarly:

$$\begin{aligned}\mathbb{E}\left(\mathcal{A}g^2|\mathcal{F}_{t_0}\right) &= \kappa_2\left(c_2 - \mathbb{E}\left(\lambda_t^2|\mathcal{F}_{t_0}\right)\right) + \mathbb{E}\left(\lambda_t^1|\mathcal{F}_{t_0}\right)\delta_{2,1}\mu_1 + \mathbb{E}\left(\lambda_t^2|\mathcal{F}_{t_0}\right)\delta_{2,2}\mu_2 + \mathbb{E}\left(\lambda_t^{P1}|\mathcal{F}_{t_0}\right)\delta_{2P,1}\mu_{P1}\\ &+ \mathbb{E}\left(\lambda_t^{P2}|\mathcal{F}_{t_0}\right)\delta_{2P2,2}\mu_{P2}\end{aligned}$$

$$\mathbb{E}\left(\mathcal{A}g^{P1}|\mathcal{F}_{t_0}\right) = \kappa_{P1}\left(c_{P1} - \mathbb{E}\left(\lambda_t^{P1}|\mathcal{F}_{t_0}\right)\right) + \mathbb{E}\left(\lambda_t^{P1}|\mathcal{F}_{t_0}\right)\delta_{P1,1}\mu_{P1} + \mathbb{E}\left(\lambda_t^{P2}|\mathcal{F}_{t_0}\right)\delta_{P1,2}\mu_{P2}$$

$$\mathbb{E}\left(\mathcal{A}g^{P2}|\mathcal{F}_{t_0}\right) = \kappa_{P2}\left(c_{P2} - \mathbb{E}\left(\lambda_t^{P2}|\mathcal{F}_{t_0}\right)\right) + \mathbb{E}\left(\lambda_t^{P1}|\mathcal{F}_{t_0}\right)\delta_{P2,1}\mu_{P1} + \mathbb{E}\left(\lambda_t^{P2}|\mathcal{F}_{t_0}\right)\delta_{P2,2}\mu_{P2}$$

Then if we refer to eq. **Error! Reference source not found.**, the moments are solution of a system of ordinary differential equations (ODEs) with respect to time:

$$\frac{\partial}{\partial t}\begin{pmatrix} m_1 \\ m_2 \\ m_{P1} \\ m_{P2}\end{pmatrix} = \begin{pmatrix} \kappa_1 c_1 \\ \kappa_2 c_2 \\ \kappa_{P1} c_{P1} \\ \kappa_{P2} c_{P2}\end{pmatrix} + \begin{pmatrix} (\delta_{1,1}\mu_1 - \kappa_1) & \delta_{1,2}\mu_2 & \delta_{1P,1}\mu_{P1} & \delta_{1P,2}\mu_{P2} \\ \delta_{2,1}\mu_1 & (\delta_{2,2}\mu_2 - \kappa_2) & \delta_{2P,1}\mu_{P1} & \delta_{2P,2}\mu_{P2} \\ 0 & 0 & (\delta_{P1,1}\mu_{P1} - \kappa_{P1}) & \delta_{P1,2}\mu_{P2} \\ 0 & 0 & \delta_{P2,1}\mu_{P1} & (\delta_{P2,2}\mu_{P2} - \kappa_{P2})\end{pmatrix}\begin{pmatrix} m_1 \\ m_2 \\ m_{P1} \\ m_{P2}\end{pmatrix} \quad (213)$$

Finally m_i are obtained by solving the system in eq. (213).

Proposition 2. Let define:

$$f\left(t,\lambda_t^1,J_t^1,\lambda_t^2,J_t^2,\lambda_t^{P1},J_t^{P1},\lambda_t^{P2},J_t^{P2}\right) = \mathbb{E}\left(e^{\omega_0 X_T - \omega_1\int_t^T X_s ds + \begin{pmatrix}\omega_2\\ \omega_3\\ \omega_4\\ \omega_5\end{pmatrix}^T\begin{pmatrix}\lambda_T^1\\ \lambda_T^2\\ \lambda_T^{P1}\\ \lambda_T^{P2}\end{pmatrix}}|\mathcal{F}_t\right)$$ and let f_t, f_{λ^1}, f_{λ^2}, $f_{\lambda^{P1}}$, $f_{\lambda^{P2}}$ denote the partial derivatives of f with respect to time and intensities. According to the Feynman-Kac formula, f is solution of the next partial integro differential equation:

$$\begin{aligned}\omega_1(\alpha_1 L_t^1 - \alpha_2 L_t^2)f \\ &= f_t + \kappa_1(c_1 - \lambda_t^1)f_{\lambda^1} + \kappa_2(c_2 - \lambda_t^2)f_{\lambda^2} + \kappa_{P1}(c_{P1} - \lambda_t^{P1})f_{\lambda^{P1}} \\ &+ \kappa_{P2}(c_{P2} \\ &- \lambda_t^{P2})f_{\lambda^{P2}} + \lambda_t^1 \int_{-\infty}^{+\infty} \left[f\left(t, \lambda_t^1 + \delta_{1,1}z, J_t^1 + (Z,1)^T, \lambda_t^2 + \delta_{2,1}z, J_t^2, \lambda_t^{P1}, J_t^{P1}, \lambda_t^{P2}, J_t^{P2}\right)\right. \\ &- \left. f(t, K_t)\right] dv_1(z) \\ &+ \lambda_t^2 \int_{-\infty}^{+\infty} \left[f\left(t, \lambda_t^1 + \delta_{1,2}z, J_t^1, \lambda_t^2 + \delta_{2,2}z, J_t^2 + (Z,1)^T, \lambda_t^{P1}, J_t^{P1}, \lambda_t^{P2}, J_t^{P2}\right) - f(t, K_t)\right] dv_2(z) \\ &+ \lambda_t^{P1} \int_{-\infty}^{+\infty} \left[f\left(t, \lambda_t^1 + \delta_{1P,1}z, J_t^1, \lambda_t^2 + \delta_{2P,1}z, J_t^2, \lambda_t^{P1} + \delta_{P1,1}z, J_t^{P1} + (Z,1)^T, \lambda_t^{P2} + \delta_{P2,1}z, J_t^{P2}\right)\right. \\ &- \left. f(t, K_t)\right] dv_{P1}(z) \\ &+ \lambda_t^{P2} \int_{-\infty}^{+\infty} \left[f\left(t, \lambda_t^1 + \delta_{1P,2}z, J_t^1, \lambda_t^2 + \delta_{2P,2}z, J_t^2, \lambda_t^{P1} + \delta_{P1,2}z, J_t^{P1}, \lambda_t^{P2} + \delta_{P2,2}z, J_t^{P2} + (Z,1)^T\right)\right. \\ &- \left. f(t, K_t)\right] dv_{P2}(z)\end{aligned} \tag{214}$$

f also satisfies the following limit condition:

$$f\left(\lambda_T^1, J_T^1, \lambda_T^2, J_T^2, \lambda_T^{P1}, J_T^{P1}, \lambda_T^{P2}, J_T^{P2}\right) = \exp\left(\omega_0(\alpha_1 L_T^1 - \alpha_2 L_T^2) + \begin{pmatrix}\omega_2 \\ \omega_3 \\ \omega_4 \\ \omega_5\end{pmatrix}^T \begin{pmatrix}\lambda_T^1 \\ \lambda_T^2 \\ \lambda_T^{P1} \\ \lambda_T^{P2}\end{pmatrix}\right) \tag{215}$$

Let us assume that f has an exponential form:

$$f = \exp\left(A(T,t) + \begin{pmatrix}B_1(T,t) \\ B_2(T,t) \\ B_3(T,t) \\ B_4(T,t)\end{pmatrix}^T \begin{pmatrix}\lambda_t^1 \\ \lambda_t^2 \\ \lambda_t^{P1} \\ \lambda_t^{P2}\end{pmatrix} + \begin{pmatrix}C_1(T,t) \\ C_2(T,t) \\ C_3(T,t) \\ C_4(T,t)\end{pmatrix}^T \begin{pmatrix}L_t^1 \\ L_t^2 \\ L_t^{P1} \\ L_t^{P2}\end{pmatrix}\right) \tag{216}$$

Under this assumption, eq. (214) becomes:

$$\begin{aligned}\omega_1(\alpha_1 L_t^1 - \alpha_2 L_t^2) \\ &= \left(\frac{\partial}{\partial t}A + \lambda_t^1 \frac{\partial}{\partial t}B_1 + \lambda_t^2 \frac{\partial}{\partial t}B_2 + \lambda_t^{P1} \frac{\partial}{\partial t}B_3 + \lambda_t^{P2} \frac{\partial}{\partial t}B_4 + L_t^1 \frac{\partial}{\partial t}C_1\right. \\ &+ \left. L_t^2 \frac{\partial}{\partial t}C_2 + L_t^{P1} \frac{\partial}{\partial t}C_3 + L_t^{P2} \frac{\partial}{\partial t}C_4\right) + \lambda_t^1\left[\psi_1\left(B_1\delta_{1,1} + B_2\delta_{2,1} + C_1\right) - 1\right] \\ &+ \lambda_t^2\left[\psi_2\left(B_1\delta_{2,1} + B_2\delta_{2,2} + C_2\right) - 1\right] \\ &+ \lambda_t^{P1}\left[\psi_{P1}\left(B_1\delta_{1P,1} + B_2\delta_{2P,1} + B_3\delta_{P1,1} + B_4\delta_{P2,1} + C_3\right) - 1\right] \\ &+ \lambda_t^{P2}\left[\psi_{P2}\left(B_1\delta_{1P,2} + B_2\delta_{2P,2} + B_3\delta_{P1,2} + B_4\delta_{P2,2} + C_4\right) - 1\right] \\ &+ \kappa_1(c_1 - \lambda_t^1)B_1 + \kappa_1(c_2 - \lambda_t^2)B_2 + \kappa_{P1}(c_{P1} - \lambda_t^{P1})B_3 + \kappa_{P2}(c_{P2} - \lambda_t^{P2})B_4\end{aligned} \tag{217}$$

Since the relationship holds for any λ_t^i and L_t^i, it is also verified when their multiplicative coefficients are null. This is achieved only if:

$$\begin{cases} 0 = \dfrac{\partial}{\partial t}B_1 - \kappa_1 B_1 + \psi_1\left(B_1\delta_{1,1} + B_2\delta_{2,1} + C_1\right) - 1 \\ 0 = \dfrac{\partial}{\partial t}B_2 - \kappa_2 B_2 + \psi_2\left(B_1\delta_{2,1} + B_2\delta_{2,2} + C_2\right) - 1 \\ 0 = \dfrac{\partial}{\partial t}B_3 - \kappa_3 B_3 + \psi_{P1}\left(B_1\delta_{1P,1} + B_2\delta_{2P,1} + B_3\delta_{P1,1} + B_4\delta_{P2,1} + C_3\right) - 1 \\ 0 = \dfrac{\partial}{\partial t}B_4 - \kappa_4 B_3 + \psi_{P2}\left(B_1\delta_{1P,2} + B_2\delta_{2P,2} + B_3\delta_{P1,2} + B_4\delta_{P2,2} + C_4\right) - 1 \\ 0 = \dfrac{\partial}{\partial t}A + \kappa_1 c_1 B_1 + \kappa_2 c_2 B_2 + \kappa_{P1} c_{P1} B_3 + \kappa_{P2} c_{P2} B_4 \\ \omega_1\alpha_1 = \dfrac{\partial}{\partial t}C_1 \quad -\omega_1\alpha_2 = \dfrac{\partial}{\partial t}C_2 \quad \begin{cases} C_3 = 0 \\ C_4 = 0 \end{cases} \end{cases}$$

And as a result:

$$\begin{cases} C_1(t,T) = \omega_0\alpha_1 - \omega_1\alpha_1(T-t) \\ C_2(t,T) = -\omega_0\alpha_2 + \omega_1\alpha_2(T-t) \end{cases}$$

We also deduce that: $A(T,T) = 0$, $B_1(T,T) = \omega_2$, $B_2(T,T) = \omega_3$, $B_3(T,T) = \omega_4$, $B_4(T,T) = \omega_5$.

Proposition 3. Let us denote by Y_t the exponent of M_t:

$$Y_t = \begin{pmatrix} a_1(\theta_1,\theta_2,\theta_3,\theta_4) \\ a_2(\theta_1,\theta_2,\theta_3,\theta_4) \\ a_3(\theta_1,\theta_2,\theta_3,\theta_4) \\ a_4(\theta_1,\theta_2,\theta_3,\theta_4) \end{pmatrix}^T \begin{pmatrix} \lambda_t^1 \\ \lambda_t^2 \\ \lambda_t^{P1} \\ \lambda_t^{P2} \end{pmatrix} + (\theta_1,\theta_2,\theta_3,\theta_4) \begin{pmatrix} L_t^1 \\ L_t^2 \\ L_t^{P1} \\ L_t^{P2} \end{pmatrix} - \varphi(\theta_1,\theta_2,\theta_3,\theta_4)t \tag{218}$$

According to eq. (178) and (179), its infinitesimal dynamics is given by:

$$\begin{aligned} dY_t = {} & a_1\kappa_1\left(c_1 - \lambda_t^1\right)dt + a_2\kappa_2\left(c_2 - \lambda_t^2\right)dt + a_3\kappa_{P1}\left(c_{P1} - \lambda_t^{P1}\right)dt \\ & + a_4\kappa_{P2}\left(c_{P2} - \lambda_t^{P2}\right)dt + \left(a_1\delta_{1,1} + a_2\delta_{2,1} + \theta_1\right)dL_t^1 \\ & + \left(a_1\delta_{2,1} + a_2\delta_{2,2} + \theta_2\right)dL_t^2 \\ & + \left(a_1\delta_{1P,1} + a_2\delta_{2P,1} + a_3\delta_{P1,1} + a_4\delta_{P2,1} + \theta_3\right)dL_t^{P1} \\ & + \left(a_1\delta_{1P,2} + a_2\delta_{2P,2} + a_3\delta_{P1,2} + a_4\delta_{P2,2} + \theta_4\right)dL_t^{P2} - \varphi(\theta_1,\theta_2,\theta_3,\theta_4)dt \end{aligned} \tag{219}$$

Zhang et al. (2009) explore the formulation of Ito's lemma in the context of generalised Hawks processes. Based on Protter (2005) (Chapter 2), they show that when the amplitude of the jumps is time invariant and takes the value of 1, the Ito's formula is expressed as:

$$dM_t = M_t dY_t + \frac{1}{2}M_t d[Y_t,Y_t]_t^c + \left(e^{a(\theta)\delta+\theta} - 1 - (a(\theta)\delta + \theta)\right)M_t dJ_t \tag{220}$$

Let us now consider a time-varying jump amplitude O (like in the univariate case); and let us denote the corresponding random measure χ so that $O = \int_{-\infty}^{+\infty}\chi(dz)$. In this case, the generalized form in eq. (220) becomes:

$$dM_t = M_t dY_t + \frac{1}{2}M_t d[Y_t,Y_t]_t^c + \int_{-\infty}^{+\infty}\left(e^{(a(\theta)\delta+\theta)z} - 1 - (a(\theta)\delta + \theta)z\right)M_t dJ_t\,\chi(dz) \tag{221}$$

Back to our problem, we adjust this generalised expression to our definition that incorporates a series of jumps with time-varying amplitude O^i ($i = 1,2,P1,P2$). Let us denote the associated random measure χ^i so that $O^i = \int_{-\infty}^{+\infty} \chi^i(dz)$. Then we obtain:

$$
\begin{aligned}
dM_t = M_t dY_t + \frac{1}{2} M_t d[Y_t, Y_t]_t^c \\
&+ M_t \int_{-\infty}^{+\infty} \left(e^{(a_1\delta_{1,1}+a_2\delta_{2,1}+\theta_1)z} - 1 - \left(a_1\delta_{1,1} + a_2\delta_{2,1} + \theta_1\right)z\right)\chi^1(dz)dN_t^1 \\
&+ M_t \int_{-\infty}^{+\infty} \left(e^{(a_1\delta_{2,1}+a_2\delta_{2,2}+\theta_2)z} - 1 - \left(a_1\delta_{2,1} + a_2\delta_{2,2} + \theta_2\right)z\right)\chi^2(dz)dN_t^2 \\
&+ M_t \int_{-\infty}^{+\infty} \left(e^{(a_1\delta_{1P,1}+a_2\delta_{2P,1}+a_3\delta_{P1,1}+a_4\delta_{P2,1}+\theta_3)z} - 1\right. \\
&\left. - \left(a_1\delta_{1P,1} + a_2\delta_{2P,1} + a_3\delta_{P1,1} + a_4\delta_{P2,1} + \theta_3\right)z\right)\chi^{P1}(dz)dN_t^{P1} \\
&+ M_t \int_{-\infty}^{+\infty} \left(e^{(a_1\delta_{1P,2}+a_2\delta_{2P,2}+a_3\delta_{P1,2}+a_4\delta_{P2,2}+\theta_4)z} - 1\right. \\
&\left. - \left(a_1\delta_{1P,2} + a_2\delta_{2P,2} + a_3\delta_{P1,2} + a_4\delta_{P2,2} + \theta_4\right)z\right)\chi^{P2}(dz)dN_t^{P2}
\end{aligned}
\tag{222}
$$

with $\frac{1}{2} M_t d[Y_t, Y_t]_t^c = 0$ (see Zhang et al. (2009))

Or equal to:

$$
\begin{aligned}
dM_t = M_t(a_1\kappa_1 c_1 + a_2\kappa_2 c_2 + a_{P1}\kappa_{P1} c_{P1} - \varphi)dt - M_t\lambda_t^1\left(a_1\kappa_1 - \int_{-\infty}^{+\infty}\left(e^{(a_1\delta_{1,1}+a_2\delta_{2,1}+\theta_1)z} - 1\right)\nu_1(dz)\right)dt \\
- M_t\lambda_t^2\left(a_2\kappa_2 - \int_{-\infty}^{+\infty}\left(e^{(a_1\delta_{2,1}+a_2\delta_{2,2}+\theta_2)z} - 1\right)\nu_2(dz)\right)dt \\
- M_t\lambda_t^{P1}\left(a_{P1}\kappa_{P1} - \int_{-\infty}^{+\infty}\left(e^{(a_1\delta_{1P,1}+a_2\delta_{2P,1}+a_3\delta_{P1,1}+a_4\delta_{P2,1}+\theta_3)z} - 1\right)\nu_{P1}(dz)\right)dt \\
- M_t\lambda_t^{P2}\left(a_{P2}\kappa_{P2} - \int_{-\infty}^{+\infty}\left(e^{(a_1\delta_{1P,2}+a_2\delta_{2P,2}+a_3\delta_{P1,2}+a_4\delta_{P2,2}+\theta_4)z} - 1\right)\nu_{P2}(dz)\right)dt \\
+ M_t\int_{-\infty}^{+\infty}\left(e^{(a_1\delta_{1,1}+a_2\delta_{2,1}+\theta_1)z} - 1\right)[\chi^1(dz)dN_t^1 - \lambda_t^1\nu_1(dz)dt] \\
+ M_t\int_{-\infty}^{+\infty}\left(e^{(a_1\delta_{2,1}+a_2\delta_{2,2}+\theta_2)z} - 1\right)[\chi^2(dz)dN_t^2 - \lambda_t^2\nu_2(dz)dt] \\
+ M_t\int_{-\infty}^{+\infty}\left(e^{(a_1\delta_{1P,1}+a_2\delta_{2P,1}+a_3\delta_{P1,1}+a_4\delta_{P2,1}+\theta_3)z} - 1\right)[\chi^{P1}(dz)dN_t^{P1} - \lambda_t^{P1}\nu_{P1}(dz)dt] \\
+ M_t\int_{-\infty}^{+\infty}\left(e^{(a_1\delta_{1P,2}+a_2\delta_{2P,2}+a_3\delta_{P1,2}+a_4\delta_{P2,2}+\theta_4)z} - 1\right)[\chi^{P2}(dz)dN_t^{P2} - \lambda_t^{P2}\nu_{P2}(dz)dt]
\end{aligned}
\tag{223}
$$

Since the integrals with respect to $\chi^i(dz)dN_t^i - \lambda_t^i\nu_i(dz)dt$ are local martingales, M_t is also a martingale if and only if the following relationship holds:

$$\begin{cases} a_1\kappa_1 c_1 + a_2\kappa_2 c_2 + a_{P1}\kappa_{P1} c_{P1} - \varphi = 0 \\ a_1\kappa_1 - \int_{-\infty}^{+\infty} \left(e^{(a_1\delta_{1,1}+a_2\delta_{2,1}+\theta_1)z} - 1\right)\nu_1(dz) = 0 \\ a_2\kappa_2 - \int_{-\infty}^{+\infty} \left(e^{(a_1\delta_{2,1}+a_2\delta_{2,2}+\theta_2)z} - 1\right)\nu_2(dz) = 0 \\ a_{P1}\kappa_{P1} - \int_{-\infty}^{+\infty} \left(e^{(a_1\delta_{1P,1}+a_2\delta_{2P,1}+a_3\delta_{P1,1}+a_4\delta_{P2,1}+\theta_3)z} - 1\right)\nu_{P1}(dz) = 0 \\ a_{P2}\kappa_{P2} - \int_{-\infty}^{+\infty} \left(e^{(a_1\delta_{1P,2}+a_2\delta_{2P,2}+a_3\delta_{P1,2}+a_4\delta_{P2,2}+\theta_4)z} - 1\right)\nu_{P2}(dz) = 0 \end{cases} \quad (224)$$

This is equivalent to eq. (187) and (188).

Proposition 4. If Y_t is the exponent of M_t as defined by equation (150), the moment generating function of X_T under the risk neutral is then equal to:

$$\mathbb{E}^Q(e^{\omega X_T}|\mathcal{F}_t) = \mathbb{E}\left(e^{Y_T - Y_t + \omega X_T}|\mathcal{F}_t\right) = e^{-Y_t}\mathbb{E}\left(e^{Y_T+\omega X_T}|\mathcal{F}_t\right) \quad (225)$$

If $f\left(t, \lambda_t^1, J_t^1, \lambda_t^2, J_t^2, \lambda_t^{P1}, J_t^{P1}, \lambda_t^{P2}, J_t^{P2}\right) = \mathbb{E}\left(e^{Y_T+\omega X_T}|\mathcal{F}_t\right)$, according to the Ito's lemma, it solves the following equation:

$$\begin{aligned} 0 = {} & f_t + \kappa_1(c_1 - \lambda_t^1)f_{\lambda^1} + \kappa_2(c_2 - \lambda_t^2)f_{\lambda^2} + \kappa_{P1}(c_{P1} - \lambda_t^{P1})f_{\lambda^{P1}} \\ & + \kappa_{P2}(c_{P2} \\ & - \lambda_t^{P2})f_{\lambda^{P2}} + \lambda_t^1 \int_{-\infty}^{+\infty} \left[f\left(t, \lambda_t^1 + \delta_{1,1}z, J_t^1 + (Z,1)^T, \lambda_t^2\right.\right. \\ & \left.\left. + \delta_{2,1}z, J_t^2, \lambda_t^{P1}, J_t^{P1}, \lambda_t^{P2}, J_t^{P2}\right) - f(t,K)\right]d\nu_1(z) \\ & + \lambda_t^2 \int_{-\infty}^{+\infty} \left[f\left(t, \lambda_t^1 + \delta_{1,2}z, J_t^1, \lambda_t^2 + \delta_{2,2}z, J_t^2 + (Z,1)^T, \lambda_t^{P1}, J_t^{P1}, \lambda_t^{P2}, J_t^{P2}\right)\right. \\ & \left. - f(t,K)\right]d\nu_2(z) \\ & + \lambda_t^{P1} \int_{-\infty}^{+\infty} \left[f\left(t, \lambda_t^1 + \delta_{1P,1}z, J_t^1, \lambda_t^2 + \delta_{2P,1}z, J_t^2, \lambda_t^{P1} + \delta_{P1,1}z, J_t^{P1}\right.\right. \\ & \left.\left. + (z,1)^T, \lambda_t^{P2} + \delta_{P2,1}z, J_t^{P2}\right) - f(t,K)\right]d\nu_{P1}(z) \\ & + \lambda_t^{P2} \int_{-\infty}^{+\infty} \left[f\left(t, \lambda_t^1 + \delta_{1P,2}z, J_t^1, \lambda_t^2 + \delta_{2P,2}z, J_t^2, \lambda_t^{P1} + \delta_{P1,2}z, J_t^{P1}, \lambda_t^{P2}\right.\right. \\ & \left.\left. + \delta_{P2,2}z, J_t^{P2} + (z,1)^T\right) - f(t,K)\right]d\nu_{P2}(z) \end{aligned} \quad (226)$$

Furthermore given that

$$\begin{aligned} Y_T + \omega X_T = {} & a_1\lambda_T^1 + a_2\lambda_T^2 + a_3\lambda_T^{P1} + a_4\lambda_T^{P2} + \theta_1 L_T^1 + \theta_2 L_T^2 + \theta_3 L_T^{P1} + \theta_4 L_T^{P2} \\ & - (a_1\kappa_1 c_1 + a_2\kappa_2 c_2 + a_3\kappa_{P1}c_{P1} + a_4\kappa_{P2}c_{P2})T + \omega(\alpha_1 L_T^1 - \alpha_2 L_T^2) \\ = {} & a_1\left(\lambda_T^1 - \kappa_1 c_1 T\right) + a_2\left(\lambda_T^2 - \kappa_2 c_2 T\right) + a_3\left(\lambda_T^{P1} - \kappa_{P1}c_{P1}T\right) \\ & + a_4\left(\lambda_T^{P2} - \kappa_{P2}c_{P2}T\right) + (\theta_1 + \alpha_1\omega)L_T^1 + (\theta_2 + \alpha_2\omega)L_T^2 + \theta_3 L_T^{P1} \\ & + \theta_4 L_T^{P2} \end{aligned} \quad (227)$$

f satisfies the following terminal condition at time $t = T$:

$$f\left(T,\lambda_T^1,J_T^1,\lambda_T^2,J_T^2,\lambda_T^{P1},J_T^{P1},\lambda_T^{P2},J_T^{P2}\right) = \exp\Big((\theta_1+\alpha_1\omega)L_T^1+(\theta_2+\alpha_2\omega)L_T^2+a_1(\lambda_T^1-\kappa_1c_1T) + a_2(\lambda_T^2-\kappa_2c_2T)+a_3(\lambda_T^{P1}-\kappa_{P1}c_{P1}T)+a_4(\lambda_T^{P2}-\kappa_{P2}c_{P2}T)\Big) \quad (228)$$

Then we assume that f is an exponential affine function:

$$f=\exp\left(A(t,T)+B(t,T)^T\begin{pmatrix}\psi_1(a_1\delta_{1,1}+a_2\delta_{2,1}+\theta_1)\lambda_t^1\\ \psi_2(a_1\delta_{2,1}+a_2\delta_{2,2}+\theta_2)\lambda_t^2\\ \psi_{P1}(a_1\delta_{1P,1}+a_2\delta_{2P,1}+a_3\delta_{P1,1}+a_4\delta_{P2,1}+\theta_3)\lambda_t^{P1}\\ \psi_{P2}(a_1\delta_{1P,2}+a_2\delta_{2P,2}+a_3\delta_{P1,2}+a_4\delta_{P2,2}+\theta_4)\lambda_t^{P2}\end{pmatrix}+C(t,T)^T\begin{pmatrix}L_t^1\\ L_t^2\\ L_t^{P1}\\ L_t^{P2}\end{pmatrix}\right) \quad (229)$$

With: $B(t,T)^T=\big(B_1(t,T),B_2(t,T),B_3(t,T),B_4(t,T)\big)^T$ and $C(t,T)^T=\big(C_1(t,T),C_2(t,T),C_3(t,T),C_4(t,T)\big)^T$

Under this assumption the partial derivatives of f are given by:

$$f_t=\Big(\frac{\partial}{\partial t}A+\psi_1\lambda_t^1\frac{\partial}{\partial t}B_1+\psi_2\lambda_t^2\frac{\partial}{\partial t}B_2+\psi_{P1}\lambda_t^{P1}\frac{\partial}{\partial t}B_3+\psi_{P2}\lambda_t^{P2}\frac{\partial}{\partial t}B_{P2}+L_t^1\frac{\partial}{\partial t}C_1+L_t^2\frac{\partial}{\partial t}C_2 + L_t^{P1}\frac{\partial}{\partial t}C_{P1}+L_t^{P2}\frac{\partial}{\partial t}C_{P2}\Big)f$$

$$f_{\lambda^1}=\psi_1B_1f \quad f_{\lambda^2}=\psi_2B_2f \quad f_{\lambda^{P1}}=\psi_{P1}B_3f \quad f_{\lambda^{P2}}=\psi_{P2}B_4f$$

Where ψ_1, ψ_2, ψ_{P1}, ψ_{P2}, abusively denote $\psi_1(a_1\delta_{1,1}+a_2\delta_{2,1}+\theta_1)$, $\psi_2(a_1\delta_{2,1}+a_2\delta_{2,2}+\theta_2)$, $\psi_{P1}(a_1\delta_{1P,1}+a_2\delta_{2P,1}+a_3\delta_{P1,1}+a_4\delta_{P2,1}+\theta_3)$, $\psi_{P2}(a_1\delta_{1P,2}+a_2\delta_{2P,2}+a_3\delta_{P1,2}+a_4\delta_{P2,2}+\theta_4)$.

Integrands in eq. (226) are equal to:

$$f\big(t,\lambda_t^1+\delta_{1,1}z,J_t^1+(Z,1)^T,\lambda_t^2+\delta_{2,1}z,J_t^2,\lambda_t^{P1},J_t^{P1},\lambda_t^{P2},J_t^{P2}\big)-f(t,K_t) = f\Big[\exp\Big((B_1\psi_1\delta_{1,1}+B_2\psi_2\delta_{2,1}+C_1)z\Big)-1\Big]$$

$$f\big(t,\lambda_t^1+\delta_{1,2}z,J_t^1,\lambda_t^2+\delta_{2,2}z,J_t^2+(Z,1)^T,\lambda_t^{P1},J_t^{P1},\lambda_t^{P2},J_t^{P2}\big)-f(t,K_t) = f\Big[\exp\Big((B_1\psi_1\delta_{1,2}+B_2\psi_2\delta_{2,2}+C_2)z\Big)-1\Big]$$

$$f\big(t,\lambda_t^1+\delta_{1P,1}z,J_t^1,\lambda_t^2+\delta_{2P,1}z,J_t^2,\lambda_t^{P1}+\delta_{P1,1}z,J_t^{P1}+(Z,1)^T,\lambda_t^{P2}+\delta_{P2,1}z,J_t^{P2}\big)-f(t,K_t) = f\Big[\exp\Big((B_1\psi_1\delta_{1P,1}+B_2\psi_2\delta_{2P,1}+B_3\psi_3\delta_{P1,1}+B_4\psi_4\delta_{P2,1}+C_3)z\Big)-1\Big]$$

$$f\big(t,\lambda_t^1+\delta_{1P,2}z,J_t^1,\lambda_t^2+\delta_{2P,2}z,J_t^2,\lambda_t^{P1}+\delta_{P1,2}z,J_t^{P1},\lambda_t^{P2}+\delta_{P2,2}z,J_t^{P2}+(Z,1)^T\big)-f(t,K_t) = f\Big[\exp\Big((B_1\psi_1\delta_{1P,2}+B_2\psi_2\delta_{2P,2}+B_3\psi_3\delta_{P1,2}+B_4\psi_4\delta_{P2,2}+C_4)z\Big)-1\Big]$$

Then injecting these equations in eq. (226) yields a system of ODEs for A, B, C:

$$\begin{cases} 0 = \lambda_t^1\left[\frac{\partial}{\partial t}B_1 - \kappa_1 B_1 + \frac{1}{\psi_1}\left(\psi_1\left(B_1\psi_1\delta_{1,1} + B_2\psi_2\delta_{2,1} + C_1\right) - 1\right)\right] \\ 0 = \lambda_t^2\left[\frac{\partial}{\partial t}B_2 - \kappa_2 B_2 + \frac{1}{\psi_2}\left(\psi_2\left(B_1\psi_1\delta_{1,2} + B_2\psi_2\delta_{2,2} + C_2\right) - 1\right)\right] \\ 0 = \lambda_t^{P1}\left[\frac{\partial}{\partial t}B_{P1} - \kappa_{P1}B_{P1} + \frac{1}{\psi_{P1}}\left(\psi_{P1}\left(B_1\psi_1\delta_{1P,1} + B_2\psi_2\delta_{2P,1} + B_3\psi_{P1}\delta_{P1,1} + B_4\psi_{P2}\delta_{P2,1} + C_3\right) - 1\right)\right] \\ 0 = \lambda_t^{P2}\left[\frac{\partial}{\partial t}B_{P2} - \kappa_{P2}B_{P2} + \frac{1}{\psi_{P2}}\left(\psi_{P2}\left(B_1\psi_1\delta_{1P,2} + B_2\psi_2\delta_{2P,2} + B_3\psi_{P1}\delta_{P1,2} + B_4\psi_{P2}\delta_{P2,2} + C_4\right) - 1\right)\right] \\ 0 = \frac{\partial}{\partial t}C_1 \quad 0 = \frac{\partial}{\partial t}C_2 \quad 0 = \frac{\partial}{\partial t}C_3 \quad 0 = \frac{\partial}{\partial t}C_4 \end{cases} \tag{230}$$

With the terminal condition:

$$A(T,T) + B(T,T)^T\begin{pmatrix}\psi_1\lambda_t^1\\ \psi_2\lambda_t^2\\ \psi_{P1}\lambda_t^{P1}\\ \psi_{P2}\lambda_t^{P2}\end{pmatrix} + C(T,T)^T\begin{pmatrix}L_T^1\\ L_T^2\\ L_T^{P1}\\ L_T^{P2}\end{pmatrix} = Y_T + \omega X_T$$

And from what we deduce that:

$$\begin{cases} C_1(T,T) = \theta_1 + \alpha_1\omega \\ C_2(T,T) = \theta_2 + \alpha_2\omega \\ C_3(T,T) = \theta_3 \\ C_4(T,T) = \theta_4 \end{cases} \quad \begin{cases} B_1(T,T) = a_1/\psi_1 \\ B_2(T,T) = a_2/\psi_2 \\ B_3(T,T) = a_3/\psi_3 \\ B_4(T,T) = a_4/\psi_4 \end{cases}$$

And $A(T,T) = -a_1\kappa_1 c_1 T - a_2\kappa_2 c_2 T - a_3\kappa_{P1}c_{P1}T - a_4\kappa_{P2}c_{P2}T$

We also obtain: $C_1(t,T) = \theta_1 + \alpha_1\omega$; $C_2(t,T) = \theta_2 + \alpha_2\omega$; $C_3(t,T) = \theta_3$; $C_4(t,T) = \theta_4$.

Finally the moment generating function of X_t is equal to:

$$\begin{aligned}\mathbb{E}^Q(e^{\omega X_T}|\mathcal{F}_t) &= e^{-Y_t}\mathbb{E}\left(e^{Y_T+\omega X_T}|\mathcal{F}_t\right) \\ &= \exp\Big(A + a_1\kappa_1 c_1 t + a_2\kappa_2 c_2 t + a_3\kappa_{P1}c_{P1}t + a_4\kappa_{P2}c_{P2}t + \left(B_1\psi_1 - a_1\right)\lambda_t^1 \\ &+ \left(B_2\psi_2 - a_2\right)\lambda_t^2 + \left(B_3\psi_{P1} - a_3\right)\lambda_t^{P1} + \left(B_4\psi_{P2} - a_4\right)\lambda_t^{P2} + \omega X_t\Big)\end{aligned}$$

In the remainder of this proof, this expectation is restated in a form similar to the moment generating function of X_T under P. To achieve this, the following change of variable is done:

$$A' = A + a_1\kappa_1 c_1 t + a_2\kappa_2 c_2 t + a_3\kappa_{P1}c_{P1}t + a_4\kappa_{P2}c_{P2}t$$

$$\begin{cases} B_1' = B_1 - \frac{a_1}{\psi_1} \\ B_2' = B_2 - \frac{a_2}{\psi_2} \\ B_3' = B_3 - \frac{a_3}{\psi_{P1}} \\ B_4' = B_4 - \frac{a_4}{\psi_{P2}} \end{cases} \quad \begin{cases} B_1'(T,T) = 0 \\ B_2'(T,T) = 0 \\ B_3'(T,T) = 0 \\ B_4'(T,T) = 0 \end{cases}$$

And based on eq. (151), the following relationship holds as well:

$$\begin{cases} \kappa_1 \dfrac{a_1}{\psi_1} = \left(1 - \dfrac{1}{\psi_1}\right) \\ \kappa_2 \dfrac{a_2}{\psi_2} = \left(1 - \dfrac{1}{\psi_2}\right) \\ \kappa_{P1} \dfrac{a_3}{\psi_{P1}} = \left(1 - \dfrac{1}{\psi_3}\right) \\ \kappa_{P2} \dfrac{a_4}{\psi_{P2}} = \left(1 - \dfrac{1}{\psi_4}\right) \end{cases}$$

Then the system of ODEs in eq. (230) becomes:

$$\begin{cases} 0 = \dfrac{\partial}{\partial t} B_1' - \kappa_1 B_1' + \dfrac{1}{\psi_1}\psi_1 \left(B_1'\psi_1\delta_{1,1} + B_2'\psi_2\delta_{2,1} + \left(\theta_1 + \delta_{1,1}a_1 + \delta_{2,1}a_2\right)\right) - 1 \\ 0 = \dfrac{\partial}{\partial t} B_2' - \kappa_2 B_2' + \dfrac{1}{\psi_2}\psi_2 \left(B_1'\psi_1\delta_{1,2} + B_2'\psi_2\delta_{2,2} + \left(\theta_2 + \delta_{1,2}a_1 + \delta_{2,2}a_2\right)\right) - 1 \\ 0 = \dfrac{\partial}{\partial t} B_3' - \kappa_{P1} B_3' + \dfrac{1}{\psi_{P1}}\psi_{P1} \left(B_1'\psi_1\delta_{1P,1} + B_2'\psi_2\delta_{2P,1} + B_3'\psi_{P1}\delta_{P1,1} + B_4'\psi_{P2}\delta_{P2,1} + \left(\theta_3 + \delta_{1P,1}a_1 + \delta_{2P,1}a_2 + \delta_{P1,1}a_3 + \delta_{P2,1}a_4\right)\right) - 1 \\ 0 = \dfrac{\partial}{\partial t} B_4' - \kappa_{P2} B_4' + \dfrac{1}{\psi_{P2}}\psi_{P2} \left(B_1'\psi_1\delta_{1P,2} + B_2'\psi_2\delta_{2P,2} + B_3'\psi_{P1}\delta_{P1,1} + B_4'\psi_{P2}\delta_{P2,1} + \left(\theta_4 + \delta_{1P,2}a_1 + \delta_{2P,2}a_2 + \delta_{P1,2}a_3 + \delta_{P2,2}a_4\right)\right) - 1 \\ 0 = \dfrac{\partial}{\partial t} A' + \psi_1\kappa_1 c_1 B_1' + \psi_2\kappa_2 c_2 B_2' + \psi_{P1}\kappa_{P1} c_{P1} B_3' + \psi_{P2}\kappa_{P2} c_{P2} B_4' \end{cases} \quad (231)$$

If we consider $O^{1,Q}$, $O^{2,Q}$, $O^{P1,Q}$, $O^{P2,Q}$ with moment generating functions defined as eq. (155), the moment generating function of X_T under Q is given by:

$$\mathbb{E}^Q\left(e^{\omega X_T}|\mathcal{F}_t\right) = \exp\left(\omega X_t + A'(t,T) + \begin{pmatrix} B_1'(t,T) \\ B_2'(t,T) \\ B_3'(t,T) \\ B_4'(t,T) \end{pmatrix} + \begin{pmatrix} \lambda_t^{1,Q} \\ \lambda_t^{2,Q} \\ \lambda_t^{P1,Q} \\ \lambda_t^{P2,Q} \end{pmatrix}\right) \quad (232)$$

Where $A', B_1', B_2', B_3', B_4'$, solve a system identical to the one proposed in Proposition 2.4.

Corollary 1. If we denote $\beta_1 = \delta_{1,1}a_1 + \delta_{2,1}a_2 + \theta_1$, by construction the moment generating function under the risk-neutral measure Q is:

$$\psi_1^Q(z) = \frac{\psi_1(z+\beta_1)}{\psi_1(\beta_1)} = \frac{\rho_1}{\rho_1 - z - \beta_1}\frac{\rho_1 - \beta_1}{\rho_1} \quad (233)$$

And we conclude that the amplitude O^1 is also exponential under Q. The same reasoning holds for O^2, O^{P1}, O^{P2}.

Corollary 2. Change of numeraire:

$$\mathbb{E}^S\left(e^{\omega Y(T,S)}|\mathcal{F}_t\right) = \frac{\mathbb{E}^Q\left[\dfrac{\partial F^S}{\partial Q} \times e^{\omega Y(T,S)}|\mathcal{F}_t\right]}{\mathbb{E}^Q\left[\dfrac{\partial F^S}{\partial Q}|\mathcal{F}_t\right]} = \frac{\mathbb{E}^Q\left(\left(e^{\int_0^S r_s ds}\mathbb{E}^Q\left(e^{-\int_0^S r_s ds}|\mathcal{F}_0\right)\right)^{-1} e^{\omega Y(T,S)}|\mathcal{F}_t\right)}{e^{-\int_0^S r_s ds}\left(\mathbb{E}^Q\left(e^{-\int_0^S r_s ds}|\mathcal{F}_0\right)\right)^{-1}}$$

And because the risk-neutral measure Q is martingale we get:

$$\mathbb{E}^Q\left(e^{-\int_0^S r_s ds}|\mathcal{F}_t\right) = e^{-\int_0^t r_s ds}\mathbb{E}^Q\left(e^{-\int_t^S r_s ds}|\mathcal{F}_t\right)$$

while $\mathbb{E}^Q\left(e^{-\int_0^S r_s ds}|\mathcal{F}_0\right)$ cancels each other as $\mathcal{F}_0 \subset \mathcal{F}_t$.

So finally we have:

$$\mathbb{E}^S\left(e^{\omega Y(T,S)}|\mathcal{F}_t\right) = \frac{\mathbb{E}^Q\left(e^{-\int_t^T r_s ds}\mathbb{E}^Q\left(e^{-\int_T^S r_s ds+\omega Y(T,S)}|\mathcal{F}_T\right)|\mathcal{F}_t\right)}{\mathbb{E}^Q\left(e^{-\int_t^S r_s ds}|\mathcal{F}_t\right)}$$

Based on eq. (163) and eq. (207):

$$\mathbb{E}^Q\left(e^{-\int_T^S r_s ds+\omega Y(T,S)}|\mathcal{F}_T\right)$$

$$= \exp\left(\left(\frac{\omega}{S-T}-1\right)\left(\int_S^T \varphi(s)ds - A^S(T,S)\right)\right)$$

$$\times \exp\left(\left(\frac{\omega}{S-T}-1\right)\times\left(X_T(S-T) - \begin{pmatrix} B_1^S(T,S) \\ B_2^S(T,S) \\ B_3^S(T,S) \\ B_4^S(T,S) \end{pmatrix}^T \begin{pmatrix} \lambda_T^{1,Q} \\ \lambda_T^{2,Q} \\ \lambda_T^{P1,Q} \\ \lambda_T^{P2,Q} \end{pmatrix}\right)\right)$$

Then because $\int_t^T -r_s ds = \int_t^T (-\varphi(s) - X_s)ds$ we obtain:

$$\mathbb{E}^Q\left(e^{-\int_t^T r_s ds}\mathbb{E}^Q\left(e^{-\int_T^S r_s ds+\omega Y(T,S)}|\mathcal{F}_T\right)|\mathcal{F}_t\right)$$

$$= \mathbb{E}^Q\left[\exp\left(\int_t^T -\varphi(s)ds + \left(\frac{\omega}{S-T}-1\right)\left(\int_S^T \varphi(s)ds - A^S(T,S)\right) + \int_t^T X_s ds\right.\right.$$

$$\left.\left. + \left(\frac{\omega}{S-T}-1\right)\times\left(X_T(S-T) - \begin{pmatrix} B_1^S(T,S) \\ B_2^S(T,S) \\ B_3^S(T,S) \\ B_4^S(T,S) \end{pmatrix}^T \begin{pmatrix} \lambda_T^{1,Q} \\ \lambda_T^{2,Q} \\ \lambda_T^{P1,Q} \\ \lambda_T^{P2,Q} \end{pmatrix}\right)\right)\right]$$

We recognise here the general form of the process in Proposition 2.4 with:

$$\omega_0 = \omega - (S-T) \quad \omega_1 = 1 \quad \omega_2 = B_1^S(T,S) \quad \omega_3 = B_2^S(T,S) \quad \omega_4 = B_3^S(T,S) \quad \omega_5 = B_4^S(T,S)$$

Finally using Proposition 2.4 we deduce that:

$$\mathbb{E}^Q\left(e^{-\int_t^T r_s ds}\mathbb{E}^Q\left(e^{-\int_T^S r_s ds+\omega Y(T,S)}|\mathcal{F}_T\right)|\mathcal{F}_t\right)$$

$$= \exp\left(\int_t^T -\varphi(s)ds + \left(\frac{\omega}{S-T}-1\right)\int_t^S \varphi(s)ds + (\omega - S + t)X_t + A^T(t,T)\right.$$

$$\left. + \begin{pmatrix} B_1^T(t,T) \\ B_2^T(t,T) \\ B_3^T(t,T) \\ B_4^T(t,T) \end{pmatrix}^T \begin{pmatrix} \lambda_t^{1,Q} \\ \lambda_t^{2,Q} \\ \lambda_t^{P1,Q} \\ \lambda_t^{P2,Q} \end{pmatrix}\right)$$

With the terminal conditions $A^T(T,T) = \left(1 - \frac{\omega}{S-T}\right) A^S(T,S)$, $B_1^T(T,T) = \left(1 - \frac{\omega}{S-T}\right) B_1^S(T,S)$, $B_2^T(T,T) = \left(1 - \frac{\omega}{S-T}\right) B_2^S(T,S)$, $B_3^T(T,T) = \left(1 - \frac{\omega}{S-T}\right) B_3^S(T,S)$, $B_4^T(T,T) = \left(1 - \frac{\omega}{S-T}\right) B_4^S(T,S)$.

Then the denominator is:

$$\mathbb{E}^Q\left(e^{-\int_t^S r_s ds}|\mathcal{F}_t\right) = \exp\left(-X_t(S-t) - \int_t^S \varphi(s)ds + A^S(t,S) + \begin{pmatrix} B_1^S(t,S) \\ B_2^S(t,S) \\ B_3^S(t,S) \\ B_4^S(t,S) \end{pmatrix}^T \begin{pmatrix} \lambda_t^{1,Q} \\ \lambda_t^{2,Q} \\ \lambda_t^{P1,Q} \\ \lambda_t^{P2,Q} \end{pmatrix}\right)$$

Finally we obtain:

$$\begin{aligned} \varphi^{M,t,S}(\omega) &= \mathbb{E}^S\left(e^{\omega Y(T,S)}|\mathcal{F}_t\right) \\ &= \exp\left(\left(\frac{\omega}{S-T}\right)\int_T^S \varphi(s)ds + \omega X_t\right) \\ &\times \exp\left(A^T(t,T) - A^S(t,S) + \begin{pmatrix} B_1^T(t,T) - B_1^S(t,S) \\ B_2^T(t,T) - B_2^S(t,S) \\ B_3^T(t,T) - B_3^S(t,S) \\ B_4^T(t,T) - B_4^S(t,S) \end{pmatrix}^T \begin{pmatrix} \lambda_t^{1,Q} \\ \lambda_t^{2,Q} \\ \lambda_t^{P1,Q} \\ \lambda_t^{P2,Q} \end{pmatrix}\right) \end{aligned}$$

References

Abergel, F., Jedidi A. (2015). Long time behaviour of a Hawkes process-based limit order book. SIAM J. Financial Math. 6, 1026-1043.

Ait-Sahalia, Y. and Lo, A. W. (1998). Nonparametric estimation of state-price densities implicit in financial asset prices. Journal of Finance, 53(2):499–547.

Ait-Sahalia, Y., and Jacod, J. (2009a). Estimating the Degree of Activity of Jumps in High Frequency Data, Annals of Statistics, 37, 2202–2244.

Ait-Sahalia, Y., and Jacod, J. (2009b). Testing for jumps in a discretely observed process. Annals of Statistics, 37, 184–222.

Aït-Sahalia, Yacine & Cacho-Diaz, Julio & Laeven, Roger J.A. (2010). Modeling financial contagion using mutually exciting jump processes, Journal of Financial Economics, Elsevier, vol. 117(3), pages 585-606.

Ait-Sahalia, Y., and Jacod, J. (2011). Testing Whether Jumps Have Finite or Infinite Activity. Annuals of Statistics, 39, 1689–1719.

Ait-Sahalia, Y., and Jacod, J. (2012). Identifying the successive BlumenthalGetoor indices of a discretely observed process, Annuals of Statistics, 40, 1430–1464.

Ait-Sahalia, Y., Jacod J., Li, J. (2012). Testing for jumps in noisy high frequency data, Journal of Econometrics, 168(2), 207–222.

Ait-Sahalia, Y., Laeven, R. J. and Pelizzon, L. (2014). Mutual Excitation in Eurozone Sovereign CDS. SAFE Working Paper No. 51. Available at SSRN: https://ssrn.com/abstract=2438625 or http://dx.doi.org/10.2139/ssrn.2438625

Alfonsi, A. ,Blanc, P. (2016). Dynamic optimal execution in a mixed-market-impact Hawkes price model. Finance and Stochastics. 20, 183-218.

Andersen, T. G., Benzoni, L., and Lund, J. (2002). An empirical investigation of continuoustime equity return models. Journal of Finance, 57(3):1239–1284.

Andersen, T. G., Fusari, N., and Todorov, V. (2015a). Parametric inference and dynamic state recovery from option panels. Econometrica, 83(3):1081–1145.

Andersen, T. G., Fusari, N., and Todorov, V. (2015b). The risk premia embedded in index options. Journal of Financial Economics, 117(3):558–584.

Arai, T. (2005). An extension of mean-variance hedging to the discontinuous case, Finance and Stochastics, 9, pp. 129–139.

Bachelier, L. (1900). Théorie de la Speculation, Paris, see also: http://www.numdam.org/en/

Bachelier, L. (1912). Calcul de Probabilités, Paris, Les Grands Classiques Gauthier-Villars, Editions Jacques Gabay 1992.

Bacry, E, Delattre, S., Hoffmann, M., Muzy J. F. (2013). Scaling limits for Hawkes processes and application to financial statistics. Stochastic Processes and their Applications 123, 2475-2499.

Bacry, E., Delattre, S., Hoffmann, M., and Muzy, J.-F. (2013). Modelling microstructure noise with mutually exciting point processes. Quantitative Finance, 13(1):65–77.

Bakshi, G. and Madan, D. (2000). Spanning and Derivative-Security Valuation. Journal of Financial Economics 55, 205-238.

Bakshi, G., Cao, C., and Chen, Z. (1997). Empirical performance of alternative option pricing models. Journal of Finance, 52(5):2003–2049.

Barndorff-Nielsen, O. E., Shephard, N. (2006). Econometrics of Testing for Jumps in Financial Economics Using Bipower Variation, Journal of Financial Econometrics, 4(1), 1–30.

Basawa, I. V. ; Brockwell, P. J. (1982). Nonparametric estimation for nondecreasing Levy processes. J. Roy. Statist. Soc. Ser. B 44, 262-269.

Bates, D. S. (2000). Post-'87 crash fears in the S&P 500 futures option market. Journal of Econometrics, 94(1-2):181–238.

Bauwens, L. and Hautsch, N. (2009). Handbook of financial time series: modelling financial high frequency data using point processes. Springer, Berlin.

Bhar, R. and Chiarella, C. (1997). Transformation of Heath-Jarrow-Morton Models to Markovian Systems, European Journal of Finance 3, 1–26.

Black, F. (1976). Studies of stock price volatility changes. In Proceedings of the 1976 Meetings of the Business and Economics Statistics Section. American Statistical Association.

Black, F. and Scholes, M. (1973). The pricing of options and corporate liabilities. Journal of Political Economy, 81(3):637–654.

Bollerslev, T. and Todorov, V. (2011). Tails, fears, and risk premia. Journal of Finance, 66(6):2165–2211.

Bollerslev, T., Todorov, V. (2011). Estimation of Jump Tails, Econometrica, 79(6), 1727–1783.

Bollerslev, T., Todorov, V., and Xu, L. (2015). Tail risk premia and return predictability. Journal of Financial Economics, 118(1):113–134.

Bouleau, N. and Lamberton, D. (1989). Residual risks and hedging strategies in Markovian markets, Stochastic Process. Appl., 33, pp. 131–150.

Broadie, M., Chernov, M., and Johannes, M. (2007). Model specification and risk premia: evidence from futures options. Journal of Finance, 62(3):1453–1490.

Broadie, M., Chernov, M., and Johannes, M. (2009). Understanding index option returns. Review of Financial Studies, 22(11):4493–4529.

Buchmann, B. and Grubel, R. (2003). Decompounding: an estimation problem for Poisson random sums. Ann. Statist. 31 1054-1074.

Burger, P., Kliaras, M. (2013). Jump Diffusion Models for Option Pricing vs. the Black Scholes Model; Working Paper Series by the University of Applied Sciences bfi Vienna (81/2013).

Carr, P. and Madan, D. (1999). Option valuation using the Fast Fourier Transform. Journal of Computational Finance, 2(4):61–73.

Carrasco, M. and Florens, J.-P. (2000). Generalization of GMM to a continuum of moment conditions. Econometric Theory, 16(06):797–834.

Carrasco, M. and Florens, J.-P. (2002). Efficient GMM estimation using the empirical characteristic function. IDEI Working paper, 140.

Carrasco, M. and Kotchoni, R. (2015). Efficient estimation using the characteristic function. Working paper.

Carrasco, M., Chernov, M., Florens, J.-P., and Ghysels, E. (2007a). Efficient estimation of 53 general dynamic models with a continuum of moment conditions. Journal of Econometrics, 140(2):529–573.

Carrasco, M., Florens, J.-P., and Renault, E. (2007b). Linear inverse problems in structural econometrics estimation based on spectral decomposition and regularization. Handbook of Econometrics, 6:5633–5751.

Carverhill, A. (1994). When is the Short Rate Markovian?, Mathematical Finance 4(4), 305–312.

CBOE (2009). The CBOE volatility index – VIX. White Paper.

Chen, K., Poon, S.-H. (2013). Variance swap premium under stochastic volatility and self-exciting jumps, Manchester Business School, University of Manchester, January 2013, Working paper, p.1-50.

Chen, S. X., Delaigle, A. and Hall, P. (2010). Nonparametric estimation for a class of Levy processes. J. Econometrics 157, 257-271.

Chiarella, C. and Kwon, O. (2001b). Forward Rate Dependent Markovian Transformations of the Heath-Jarrow-Morton Term Structure Model, Finance and Stochastics 5(2), 237–257.

Christoffersen, P., Jacobs, K., and Ornthanalai, C. (2012). Dynamic jump intensities and risk premiums: Evidence from S&P500 returns and options, Journal of Financial Economics, 106(3), 447–472.

Collin. P, Dufresne, R.S (2002). Pricing swaptions in an affine framework. Journal of Deivatives, 10:9–26.

Comte, F. and Genon-Catalot (2009). Nonparametric estimation for pure jump Levy processes based on high frequency data. Stochastic Processes and their Applications 119, 4088-4123.

Comte, F. and Genon-Catalot, V. (2010). Nonparametric adaptive estimation for pure jump Levy processes. Ann. Inst. Henri Poincaré Probab. Stat. 46, 595-617.

Comte, F. and Genon-Catalot, V. (2011). Estimation for Levy processes from high frequency data within a long time interval. Ann. Statist. 39, 803-837.

Cont, R. and Da Fonseca, J. (2002). Dynamics of implied volatility surfaces. Quantitative Finance, 2(1):45–60.

Cont, R. and Tankov, P., (2004). Financial Modelling with Jump Processes, Chapman & Hall/CRC Financial Mathematics Series.

Cont, R., Tankov, P., Voltchkova, E. (2007) Hedging with Options in Models with Jumps. In: Benth F.E., Di Nunno G., Lindstrøm T., Øksendal B., Zhang T. (eds) Stochastic Analysis and Applications. Abel Symposia, vol 2. Springer, Berlin, Heidelberg

Cox, J. C., Ingersoll, J. E., and Ross, S. A. (1985). A theory of the term structure of interest rates. Econometrica, 53(2):385–407.

Cremers, M., Driessen, J., Maenhout, P. (2008). Explaining the Level of Credit Spreads: Option-implied jump risk premia in a firm value model Review of Financial Studies, Vol. 21, No. 5, (September 2008), pp. 2209-2242.

Dai Q, Singleton, K (2002). Expectation Puzzles, Time-varying Risk Premia, and Affine Models of the Term Structure. Journal of Financial Economics 63: 415-41.

Dai, Q. and Singleton, K. (2000). Specification Analysis of Affine Term Structure Models. Journal of Finance 55, 1943-1978.

Duffie, D. and Kan, R. (1996). A Yield Factor Model of Interest Rates, Mathematical Finance 6(4), 379–406.

Duffie, D. and Singleton, K. J. (1993). Simulated moments estimation of Markov models of asset prices. Econometrica, 61(4):929–952.

Duffie, D., Pan, J., and Singleton, K. J. (2000). Transform analysis and asset pricing for affine jump-diffusions. Econometrica, 68(6):1343–1376.

Egloff, D., Leippold, M., and Wu, L. (2010). Valuation and optimal investing in variance swaps. Journal of Financial and Quantitative Analysis, 45(5):1279–1310.

Embrechts, P., Kluppelberg, C. and Mikosch, T. (1997). Modelling extremal events. Berlin: Springer. MR1458613.

Eraker, B. (2004). Do stock prices and volatility jump? Reconciling evidence from spot and option prices. Journal of Finance, 59(3):1367–1404.

Eraker, B., Johannes, M., and Polson, N. (2003). The impact of jumps in volatility and returns. Journal of Finance, 58(3):1269–1300.

Errais, E., Giesecke, K., and Goldberg, L. R. (2010). Affine point processes and portfolio credit risk. SIAM Journal on Financial Mathematics, 1(1):642–665.

Fan, Y., Pastorello, S., and Renault, E. (2015). Maximization by parts in extremum estimation. The Econometrics Journal, 18(2):147–171.

Feller, W. (1951). Two singular diffusion problems. Annals of Mathematics, 54(1):173–182.

Figueroa-Lopez, J. E. (2009). Nonparametric estimation of Levy models based on discrete-sampling. Optimality, 117-146, IMS Lecture Notes Monogr. Ser., 57, Inst. Math. Statist., Beachwood, OH.

Figueroa-Lopez, J. E. and Houdré, C. (2006). Risk bounds for the non-parametric estimation of Levy processes. High dimensional probability, 96-116, IMS Lecture Notes Monogr. Ser., 51, Inst. Math. Statist., Beachwood, OH.

Fulop, A., Li, J., Yu, J., (2014). Self-exciting jumps, learning, and asset pricing implications, Singapore Management University, Working paper, June, 2014, No.02, p.1-54.

Gallant, A. R. and White, H. (1988). A unified theory of estimation and inference for nonlinear dynamic models. Basil Blackwell New York.

Goutte, S. (2013). Pricing and Hedging in Stochastic Volatility Regime Switching Models, Journal of Mathematical Finance, Vol. 3 No. 1, 2013, pp. 70-80. doi: 10.4236/jmf.2013.31006.

Gugushvili, S. (2009). Nonparametric estimation of the characteristic triplet of a discretely observed Levy process. J. Nonparametr. Stat. 21, 321-343.

Gugushvili, S. (2012). Nonparametric inference for discretely sampled Levy processes. Ann. Inst. Henri Poincar´e Probab. Stat. 48, 282-307.

Hansen, L. P. (1985). A method for calculating bounds on the asymptotic covariance matrices of generalized method of moments estimators. Journal of Econometrics, 30(1):203–238. 54

Harrison, M. and D. Kreps (1979). Martingales and Arbitrage in Multiperiod Securities Markets. Journal of Economic Theory 20, 381-408.

Hawkes, A. G. (1971). Point spectra of some mutually exciting point processes. Journal of the Royal Statistical Society. Series B (Methodological), 33(3):438–443.

Hawkes, A.G., Oakes, D. (1974). A cluster process representation of a self-exciting process. Journal of Applied Probability 493–503.

Heath, D., Jarrow, R. and Morton, A. (1992). Bond Pricing and the Term Structure of Interest Rates: A New Methodology for Contingent Claims Valuation. Econometrica, 60(1):77-105. doi:10.2307/2951677

Heston, S. L. (1993). A closed-form solution for options with stochastic volatility with applications to bond and currency options. Review of Financial Studies, 6(2):327–343.

Ho T., and Lee, S. (1986). Term Structure Movements and Pricing Interest Rate Contingent Claims, Journal of Finance, 41, 1011-1029.

Inui, K. and Kijima, M. (1998). A Markovian Framework in Multi-Factor Heath-Jarrow-Morton Models, Journal of Financial and Quantitative Analysis 33(3), 423–440.

Jamshidian, F. (1989). "An exact bond option pricing formula," Journal of Finance, Vol 44, pp 205-209.

Jing, B.-Y., Kong, X.-B., Liu, Z., and Mykland, P. (2012). On the jump activity index for semimartingales, Journal of Econometrics, 166(2), 213–223.

Johannes, M. S., Polson, N. G., and Stroud, J. R. (2009). Optimal filtering of jump diffusions: extracting latent states from asset prices. Review of Financial Studies, 22(7):2759–2799.

Jong, F. and Santa-Clara, P. (1999). The Dynamics of the Forward Interest Rate Curve: A Formulation with State Variables, Journal of Financial and Quantative Analysis 34(1), 131–157.

Jongbloed, G., van der Meulen, F. H. and van der Vaart, A. W. (2005). Nonparametric inference for Levy-driven Ornstein-Uhlenbeck processes. Bernoulli 11, 759-791.

Katz, R. W. (2002). Stochastic modeling of hurricane damage. J. Appl. Meteorol. 41, 754-762.

Kita, A. (2012). CDS Spreads Explained with Credit Spread Volatility and Jump Risk of Individual Firms. SSRN Electronic Journal. 10.2139/ssrn.2157505.

Li, G. and Zhang, C. (2013). Conditional jump intensity, conditional expected jump size, and relative stock price level. Working paper.

Liebscher, E. (2005). Towards a unified approach for proving geometric ergodicity and mixing properties of nonlinear autoregressive processes. Journal of Time Series Analysis, 26(5):669– 689.

Litterman, R. and Scheinkman, J. (1991). Common Factors Affecing Bond Returns, Journal of Fixed Income, (June 1991), 54-61.

Lord, R., Koekkoek, R., and Dijk, D. V. (2010). A comparison of biased simulation schemes for stochastic volatility models. Quantitative Finance, 10(2):177–194.

Lucas, R. E. (1978). Asset prices in an exchange economy. Econometrica, 46(6):1429–1445.

Matsuda, K., (2004). Introduction to Option Pricing with Fourier Transform: Option Pricing with Exponential Lévy Models, Working Paper, Graduate School and University Center of the City University of New York.

Merton, R. C. (1976). Option pricing when underlying stock returns are discontinuous. Journal of Financial Economics, 3(1):125–144.

Merton, R. C., (1971). “Optimum Consumption and Portfolio Rules in a Continuous-Time Model,” Journal of Economic Theory, 3, 373-413.

Meyn, S. P. and Tweedie, R. L. (2009). Markov chains and stochastic stability. Cambridge University Press.

Neumann, M. H. and Reiss, M. (2009). Nonparametric estimation for Levy processes from low-frequency observations. Bernoulli 15, 223-248.

Oakes, D. (1975). The markovian self-exciting process. Journal of Applied Probability 69–77.

Pan, J. (2002). The jump-risk premia implicit in options: evidence from an integrated timeseries study. Journal of Financial Economics, 63(1):3–50.

Park K, Kim S, Shaw WT, (2014). Estimation and Simulation of Bond Option Pricing on the Arbitrage Free Model with Jump. Journal of Applied Computational Math 3:155. doi: 10.4172/2168-9679.1000155

Pastorello, S., Patilea, V., and Renault, E. (2003). Iterative and recursive estimation in structural nonadaptive models. Journal of Business & Economic Statistics, 21(4):449–509.

Peng, C., Scaillet, O. (2007). Linear-Quadratic Jump-Diffusion Modeling. Mathematical Finance 17: 575-598.

Politis, D. N. and Romano, J. P. (1994). The stationary bootstrap. Journal of the American Statistical Association, 89(428):1303–1313.

Protter, P. E. (2005). Stochastic integration and differential equations. Springer.

Ritchken, P. and Sankarasubramanian, L. (1995). Volatility Structures of Forward Rates and the Dynamics of the Term Structure, Mathematical Finance 5(1), 55–72.

Sandmann, K. and Sondermann, D. (1997). A Note on the Stability of Lognormal Interest Rate Models and the Pricing of Eurodollar Futures. Mathematical Finance 7 (2), 119-125.

Scalas, E. (2006). The application of continuous-time random walks in finance and economics. Physica A 362, 225-239.

Schneider, P. G. and Trojani, F. (2015). Fear trading. Working paper.

Singleton, K. J. (2001). Estimation of affine asset pricing models using the empirical characteristic function. Journal of Econometrics, 102(1):111–141.

Singleton, K., Umantsev, L. (2002). Pricing Coupon Bond Options and Swaptions in Affine Term Structure Models, Math. Finance 12, 427–446.

Tankov, P. (2010). Pricing and hedging gap risk, The Journal of Computational Finance, Vol. 13 (3), (2010).

Tankov, P., Kohatsu-Higa, A. (2010). Jump-adapted discretization schemes for Levy-driven SDEs, Stochastic Processes and their Applications, Vol. 120, 2258-2285.

Taylor, R. L. (1978). Stochastic convergence of weighted sums of random elements in linear spaces. Springer.

Todorov, V., (2009). Variance risk premium dynamics: The role of jumps, The Review of Financial Studies, 2010, Vol.23, No.1, p.345-383.

Ueltzhofer, F. A. J. and Kluppelberg, C. (2011). An oracle inequality for penalised projection estimation of Levy densities from high-frequency observations. J. Nonparametr. Stat. 23, 967-989.

Vasicek, O. (1977). An Equilibrium Characterisation of the Term Structure, Journal of Financial Economics 5, 177–188.

Whaley, R. E. (2009). Understanding the VIX. The Journal of Portfolio Management, 35(3):98– 105.

Wilmott, P., (1998). Derivatives, John Wiley & Sons.

Zhao, Z. and Wu, W. B. (2009). Non-parametric inference of discretely sampled stable Levy processes. J. Econometrics 153, 83-92.

Résumé

Les périodes marquées par une aversion au risque intense sont souvent l'origine de distorsions notables dans les prix de marché, et de pertes substantielles pour les investisseurs. Chaque épisode de crise financière montre que les mouvements de ventes généralisées sur les marchés ont des conséquences très négatives sur l'économie réelle. Ainsi, explorer le phénomène d'aversion au risque et la dynamique de propagation du sentiment de panique sur les marchés financiers peut aider à appréhender ces périodes de forte volatilité.

Dans ce rapport de thèse, nous explorons différentes dimensions du phénomène d'aversion au risque, dans le cadre de portefeuilles d'obligations souveraines Européennes. Chapitre I explore le risque souverain dans le cadre d'un modèle probabiliste impliquant des distributions à queues lourdes, ainsi que la méthode GAS qui permet de capturer la dynamique de la volatilité. L'ajustement obtenu avec les distributions Hyperboliques Généralisées est robuste, et les résultats laissent penser que notre approche est particulièrement efficace durant les périodes marquées par une volatilité erratique.

Chapitre II décrit différentes manières d'exploiter ce modèle probabiliste. Afin d'illustrer le phénomène de contagion nous analysons la réaction attendue du marché à une série de chocs financiers. Ceci nous permet d'identifier des lois empiriques supposées généraliser le comportement de la réaction de marché lorsque l'aversion au risque s'intensifie.

Chapitre III est dédié au pricing de produits dérivés de taux. Nous considérons maintenant que l'aversion au risque cause l'émergence de discontinuités dans les prix de marché, que nous simulons par le biais de processus à sauts.

Mots Clés

crise souveraine, probabilité de défaut, contagion, risque souverain, aversion au risque / appétit pour le risque, CDS, obligations souveraines.

Abstract

Periods of deep risk aversion are usually marked by sizeable distortions in market prices, and substantial losses in portfolios. As observed during financial crises, a generalized debacle in financial markets is a very negative shock for the real economy. Against this backdrop, it looks relevant to explore how risk aversion tends to affect global market valuations, especially if this exercise helps make the promotion of more optimal portfolio rebalancing procedures.

In this dissertation, we investigate different dimensions of risk aversion, with a focus on European Sovereign debt securities. In Chapter I, we consider a probabilistic approach to sovereign risk exploration, with the main purpose of illustrating the non-linear reaction ensuing from a gradual deterioration in market sentiment. We consider heavy-tailed distributions, and we use the Generalised Autoregressive Score method as a means to capture the volatility momentum. The goodness of fit provided by Generalised Hyperbolic distributions is compelling, and results suggest that our approach is particularly relevant to fit periods or erratic volatility, typical of financial crises.

Chapter II explores different ways to extract information from the model, about financial contagion and how it is supposed to propagate through sovereign securities. In particular, we explore the market reaction to a series of many shocks with gradual intensity. Results offer a high degree of granularity and we extrapolate empirical rules on the expected market dynamics, when risk aversion intensifies.

In Chapter III, we explore how sovereign risk tends to affect the price of financial derivatives in a risk-off environment. We consider that risk aversion now favours the emergence of sizeable discontinuities in market prices, that we model with stochastic jumps.

Keywords

sovereign crisis, default probability, financial contagion, credit risk, risk aversion / risk appetite, CDS spreads, sovereign bonds